I hereby certify that this submission is my own work. Any quotation from, or description of, the work of others is acknowledged herein by reference to the sources, whether published or unpublished.

Giovanni Tomei

Acknowledgments

I would like to thank Prof. Patrizia Piro for the opportunity to undertake this research and for her direction and assistance throughout the development of the thesis.

I would like to express my sincere gratitude to Prof. Ćedo Maksimovic and Prof. Vito Copertino whose guidance, recommendations and suggestions have been invaluable for the development of this research project.

I would like to thank my Italian colleagues and friends who accompanied and supported me during these three years of hard work.

Special thanks to my colleagues from Imperial College London and Londoner friends who helped me in many ways.

I wish to sincerely express my gratitude to all those who provided support to me during the course of this project. Without you it would have not been possible to achieve these results.

Finally, words alone cannot express the thanks I owe to my fianceè Lucia for her encouragement and assistance and to my parents, brothers and relatives for having been always close to me.

Abstract

Currently cities and communities are experiencing ever growing problems related to urban pluvial flooding. This is due primarily to inefficient drainage inlets and overloaded sewer systems. In fact, existing drainage systems rapidly reach their maximum capacity and tend to work pressurized even in the case of medium-entity storms.

Damage and losses caused by flood events in urban areas, primarily life and economic losses and traffic disruption, can be significant. Moreover, this situation is destined to worsen in the immediate future due to the fervent urbanization process and the ongoing climate changes.

This research is therefore aimed at investigating this type of event, because to guarantee an efficient working of the drainage systems is a prerequisite in modern societies. Specifically the broader objective of the study is to contribute to an improvement of urban flood management by enhancing urban drainage modeling and storm motion forecasting. In order to achieve such scope the following detailed tasks were performed:

1. Investigation of the various LiDAR Digital Terrain Models (DTMs) available for the drainage modeling of a study area.

   From literature review it is evident that a great effort has been made to improve existing hydraulic models and to develop new ones. Nevertheless, little interest has been devoted to evaluate the effects of the use of different available LiDAR DTMs on hydraulic modeling. The research is therefore motivated by the need to know how LiDAR DTMs with different detail scale (LiDAR DSM *first*, LiDAR DSM *last* and LiDAR DTM bare earth with overlapped building) can affect the hydraulic modeling of drainage networks. Every DTM is in fact characterized by a variable presence of non-ground surface features, such as cars, buildings or vegetation, that will influence surely the hydraulic response of the urban catchment differently. Consequently every data set was studied by GIS-based analysis methods, such as calculation of surface depressions, in order to evaluate whether the consideration of all the non-ground features is necessary for

hydraulic modeling purposes, or whether the use of a less detailed LiDAR DTM, adequately improved, could be an approachable solution.

2. Analysis of improvements brought by a dual drainage approach in simulating the behavior of a drainage network during extreme rain events, compared to the use of a conventional methodology.

   Another question that justifies the work carried out by the author and presented in the thesis is related to the need of improving available urban drainage modeling. Most of these models are in fact based on process simplifications that are far removed from reality, such as assuming that when water leaves the sewer it is stored in a virtual reservoir and does not follow the natural flow paths, i.e. the effect of local topography is neglected. This approach provides a very biased image of flooding process. Consequently the research was aimed at quantifying capabilities and limits of two urban drainage modeling with diverse sophistication level. The first one was based on the classical hypothesis according to which the drainage system is composed only of the sewer system, that is to consider that stormwater, once entered the sewer system, can no longer leave this system coming back to the surface. Instead the second one was based on the dual drainage approach, i.e. it was assumed that the urban drainage system was composed of a surface network and the sewer network. The evaluation of the best approach was performed by comparing the water volume distributions in the sewer network and the number of surcharged sewer trunks resulting from hydraulic simulations. Specifically the issues relative to the development of the most complicated model, that is the dual drainage one, were studied in more detail: the influence of buildings and DTM resolution on the surface network definition, and the introduction of criteria to be taken into account for pond filtering parameters were the topics deepened through the use of an innovative methodology, the AOFD tool (Automatic Overland Flow Delineation).

3. Study of the potentials of a dense network of rain gauges in forecasting storm movements for flood prevention purposes.

   This research was performed because, currently, methods for rainfall prediction are mainly based on radar measurements. However rain gauge data are often

available whereas radar data are not. Furthermore radar instruments enable the investigation of convective cells motion, whereas rain gauges data allow the analysis of the movement of rainfall patterns recorded on the ground, that is more important for hydraulic modeling. Consequently storm movement parameters, velocity and direction, were derived by analyzing rainfall data trough available storm tracking procedures. The method proposed by Diskin was tested and, in particular, the extent to which the choice of the reference feature in the hyetograph and the location of the recording stations inside the catchment can affect the results of the methodology was studied in detail. The quality of the elaborations was estimated by comparing the results obtained with other physical phenomena which are related to storm movement, such as wind movement data. In particular statistical analysis, based on the computation of the correlation coefficient and root mean square deviation between storm and wind data sets, were performed.

With the results from the research presented herein, it is expected that:

1. DTM enhancement methods generate hydraulically corrected DTMs that can potentially lead to improvements in urban pluvial flood modeling.
2. more realistic simulations of the drainage system are performed by developing dual drainage models. In this way engineers could aim at minimizing both the costs of construction of new works and maintenance of existing structures by evaluating systematically the effectiveness of all the possible design solutions. Actually, the use of such a modeling will have to push them to optimize the working conditions of both the surface and sewer networks when evaluating flood control and mitigation measures.
3. rain gauges are considered as valid alternatives in rainfall movement prediction, to be taken into account in areas where radar measurements cannot be obtained yet. In fact the results of the elaborations will demonstrate how such instruments, that are more approachable than radar ones for economical and practical reasons, are very useful in forecasting the movements that future storm events can make in a monitored area. Similar information could be also used in connection with hydraulic models, previously calibrated for the same study area,

in order to evaluate in advance the possible flood-prone areas. In addition the analysis of the results, obtained by considering an ever decreasing number of recording stations, will give interesting information to municipalities having limited budget for equipping themselves with an adequate number of such instruments.

Sommario

Il fervente processo di urbanizzazione unitamente ai cambiamenti climatici in corso stanno favorendo il susseguirsi di fenomeni di allagamento sempre più frequenti e gravosi in tutto il mondo.

Storicamente l'attenzione dei media e delle istituzioni è stata rivolta principalmente alle inondazioni causate dai corsi d'acqua attraversanti i centri urbani o alle inondazioni delle zone costiere, mentre sono stati trascurati i fenomeni innescati da condizioni di sovraccarico della rete fognaria o da inefficienza delle caditoie, noti anche come *sewer flooding*. In maniera analoga, anche nel campo della ricerca, diversi studi sono stati rivolti verso la simulazione degli allagamenti fluviali in ambito urbano, mentre poco interesse è stato mostrato nei riguardi degli allagamenti prodotti da inefficienze del sistema di drenaggio, presumibilmente a causa della loro maggiore variabilità spaziale e temporale.

Tuttavia una simile problematica non può essere ulteriormente ignorata a causa delle precarie condizioni di funzionamento in cui versano i sistemi di drenaggio esistenti. Infatti tali strutture raggiungono rapidamente la loro massima capacità e tendono a funzionare in pressione anche in concomitanza di eventi meteorici non particolarmente intensi.

I danni associati a simili episodi possono essere ragguardevoli: disturbi nel traffico, danni economici, e nei casi peggiori anche perdite di vite umane. Questa situazione, inoltre, peggiora drammaticamente nei paesi in via di sviluppo a causa della maggiore violenza degli eventi meteorici e dalla minore affidabilità delle infrastrutture di drenaggio presenti.

Il presente progetto di dottorato è stato pertanto rivolto ad approfondire le problematiche inerenti il *sewer flooding* in quanto garantire un efficiente funzionamento dei sistemi di drenaggio è una condizione indispensabile per il corretto svolgimento delle attività di una comunità. A tal fine la ricerca è stata rivolta a migliorare la gestione degli allagamenti urbani attraverso il potenziamento dei modelli esistenti di simulazione idraulica e di previsione dello spostamento delle piogge. In particolare le seguenti problematiche sono state affrontate:

1. Analisi dei differenti LiDAR Digital Terrain Model (DTM) disponibili per la modellazione idraulica della rete di drenaggio di un'area di studio.

   È evidente come grossi sforzi siano stati spesi per migliorare gli approcci di modellazione idraulica esistenti e per svilupparne di nuovi. Tuttavia, poco interesse è stato mostrato nel valutare le conseguenze che l'uso dei vari LiDAR DTM può determinare sugli stessi modelli idraulici. Ciascuno di questi DTM (LiDAR DSM *first*, LiDAR DSM *last* e LiDAR DTM relativo al suolo nudo con edifici sovrapposti) presenta, infatti, un numero diverso di oggetti fuori terra, come autovetture, edifici o alberi, che sicuramente influenzeranno la risposta del bacino urbano in maniera diversa. Di conseguenza, tali set di dati sono stati studiati mediante procedure di analisi basate su GIS, come il calcolo delle depressioni superficiali, di modo da valutare se la considerazione di tutti gli oggetti fuori terra sia necessaria ai fini della modellazione idraulica, o se l'impiego di un LiDAR DTM meno dettagliato, ma opportunamente migliorato, possa essere una soluzione percorribile.
2. Valutazione dei miglioramenti apportati dall'impiego di una modellazione idraulica di tipo duale nella simulazione del funzionamento delle reti di drenaggio urbano durante eventi meteorici estremi.

   Un'altra problematica, che giustifica la ricerca affrontata dall'autore e riportata nella tesi, è legata alla necessità di migliorare gli approcci di modellazione esistenti. La maggior parte di questi modelli, infatti, è ancora basata su semplificazioni dei processi come ad esempio la considerazione di serbatoi virtuali al di sopra dei chiusini sovraccarichi, all'interno dei quali si ipotizza di invasare il volume idrico in eccesso scaricato dalla rete fognaria. Per quanto tali procedure possano portare a dei risultati accettabili, tuttavia è importante mettere in evidenza come non risultino adatte a simulare in maniera realistica gli allagamenti urbani in quanto ignorano il concetto fondamentale su cui si basa l'idrologia urbana tradizionale, cioè l'interazione tra la struttura del drenaggio superficiale (vincolata dalle strade, dai marciapiedi e dalle ulteriori caratteristiche della morfologia del paesaggio urbano) con il sistema di drenaggio sub – superficiale (canali e condotte).

Di conseguenza la ricerca è stata indirizzata a valutare i pregi ed i difetti di due modellazioni idrauliche con diverso livello di dettaglio. Il primo modello è stato realizzato sulla base dell'ipotesi classica secondo la quale il sistema di drenaggio sia costituito dalla sola rete fognaria: cioè si è assunto che le acque meteoriche, convogliate in fognatura, non possano più abbandonare tale sistema ritornando in superficie. Invece il secondo modello è stato sviluppato sulla base dell'approccio del drenaggio duale, secondo il quale il sistema di drenaggio urbano può ritenersi composto da una rete di deflusso superficiale, veicolata per lo più dalle strade, e dalla rete fognaria sottostante. La valutazione della metodologia più realistica è stata effettuata, successivamente, mettendo a confronto la distribuzione dei volumi idrici nelle reti fognarie ed il numero di tronchi fognari sovraccarichi risultanti dalle simulazioni eseguite.

Le problematiche relative allo sviluppo del modello idraulico più complesso, cioè quello duale, sono state opportunamente approfondite. In particolare l'influenza degli edifici e della risoluzione del DTM sulla definizione della rete superficiale, e l'introduzione di criteri, di cui tener conto nel processo di filtraggio delle depressioni superficiali, sono stati gli argomenti affrontati attraverso l'impiego di uno strumento innovativo, l'AOFD (Automatic Overland Flow Delineation).

3. Studio delle potenzialità di una fitta rete di pluviometri nel prevedere lo spostamento di eventi meteorici, ai fini della prevenzione dal rischio di allagamento.

   Questa ricerca è stata affrontata in quanto, attualmente, i metodi di previsione delle piogge sono basati principalmente su misurazioni radar. Tuttavia i dati pluviometrici risultano spesso più accessibili rispetto alle misurazioni radar. Inoltre, mentre le misurazioni radar permettono di studiare il movimento delle celle convettive generanti le piogge, i dati pluviometrici consentono di analizzare lo spostamento dei volumi idrici, generati dalle piogge, registrato al suolo, che è più importante ai fini delle modellizzazioni idrauliche.

   Di conseguenza parametri di movimento degli eventi meteorici, quali velocità e direzione, sono stati stimati impiegando metodi di storm tracking esistenti. Il metodo proposto da Diskin è stato testato e, in particolare, è stata studiata in

dettaglio la misura in cui la scelta della feature di riferimento nello ietogramma e la posizione delle stazioni di registrazione all'interno del bacino possano influenzare i risultati della metodologia. La qualità delle elaborazioni è stata stabilita confrontando i risultati ottenuti con altri fenomeni fisici associati al movimento delle piogge, cioè i dati di vento. In particolare sono state effettuate analisi statistiche, basate sul calcolo dei coefficienti di correlazione e degli scarti quadratici medi, tra i dati di vento ed i corrispondenti dati di pioggia.

Con i risultati della ricerca qui presentata, si prevede che:

1. i metodi di miglioramento dei DTM permetteranno di generare DTM idraulicamente corretti, di modo da favorire lo sviluppo di migliori modelli di simulazione idraulica.
2. simulazioni più affidabili verranno effettuate mediante lo sviluppo di modelli di drenaggio di tipo duale. In questo modo i tecnici potranno valutare in modo sistematico l'efficacia di tutte le possibili soluzioni progettuali, e, quindi, mirare a minimizzare sia i costi di costruzione di nuove opere sia quelli di manutenzione delle strutture esistenti. In verità, l’impiego di una simile modellizzazione dovrebbe spingere gli stessi tecnici ad ottimizzare il funzionamento sia della rete di drenaggio superficiale che di quella sotterranea nella fase di progettazione.
3. l’impiego di pluviometri all’interno dei bacini urbani sia considerata una soluzione alternativa valida per la previsione dello spostamento delle piogge, di cui tener conto in aree dove i dati radar non sono ancora disponibili. Infatti i risultati delle elaborazioni eseguite dimostreranno come tali strumenti, più semplici da installare rispetto ai radar stessi per motivi pratici ed economici, siano particolarmente utili nel prevedere gli spostamenti che futuri eventi meteorici potranno effettuare nell’area monitorata.

   Simili informazioni potrebbero essere anche impiegate all’interno di modelli idraulici, precedentemente tarati per la medesima area di studio, al fine di individuare le potenziali aree allagabili con un certo anticipo e, conseguentemente, realizzare per tempo tutte le misure di sicurezza previste. Inoltre lo studio dei risultati, ottenuti considerando un numero decrescente di

stazioni di registrazione, fornirà informazioni interessanti ai comuni dotati di budget limitati per l'installazione di simili equipaggiamenti.

Table of Contents

1. Sewer flooding background

1.1 Introduction

The fervent urbanization process together with the ongoing climate change favor the succession of more frequent and intense flooding phenomena all over the world.
Historically the attention of media and institutions has been paid mainly to river or coastal floods, whereas phenomena associated with overloaded sewerage systems or inefficient drainage inlets, also known as sewer flooding (fig. 1.1), have been neglected until now (Balmforth et al., 2006).

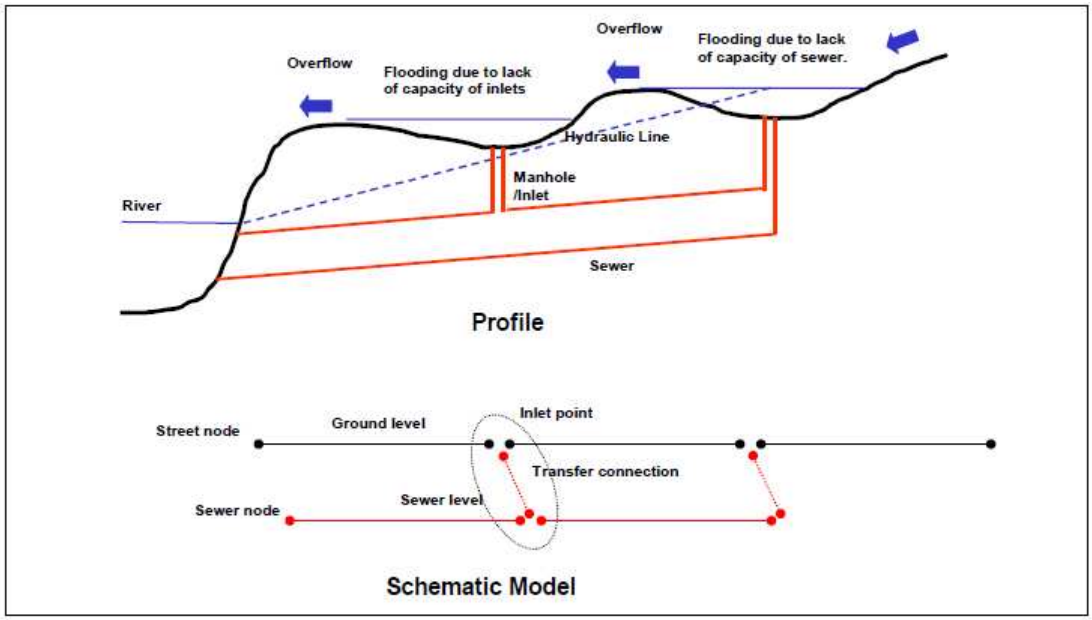

Figure 1.1 Schematic representation of the two sewer flooding situations.

Similarly, in the research field, many studies have been directed towards the simulation of river flooding in urban areas, whereas little interest has been shown with regard to flooding produced by the inefficiency of the drainage system, presumably because of its greater spatial and temporal variability. These phenomena, in fact, are closely dependent on the characteristics of the basin at the microscale, such as street gradient, sidewalks and curb height, topographic discontinuity, etc.
However, such an issue can no longer be ignored because of the precarious working conditions characterizing the existing drainage systems. In fact, these structures rapidly reach their maximum capacity and tend to work pressurized even in the case

of medium storms. Moreover, this situation worsens dramatically in developing countries due to the much heavier local rainfall and lower drainage standards, as demonstrated by the series of episodes listed below:

- 1983: Bangkok (Thailand) was inundated for nearly 6 months and the flood caused loss of life and infrastructural damage of approximately $146 million (AIT, 1985).
- September/October 1996: most of the daily activities in Dhaka city (Bangladesh) were nearly paralyzed and heavy traffic jams occurred due to stagnant water.
- 2000: nearly 17,000 telephone lines in Mumbai City ceased to function after flooding occurred and electric supply was cut off for safety purposes. The water depth reached 1.5 m at the worst inundated locations and 15 lives were lost in the flood.
- February 2002: five people were killed in Jakarta (Indonesia) as heavy rain extended floods to the city center, deepening a crisis which forced 200,000 people from their homes and killed 50 nationwide (Bangkok Post, 3rd February 2002).

1.2 Causes of sewer flooding

Such malfunctions are primarily related to the aspects reported in the following:

1. Use of simplified methods during the design phase. These procedures are not able to simulate the surface runoff realistically: thus the consequent project and location of the drainage inlets is wrong. Let us consider, for example, the situation showed in fig. 1.2: the poor inlet location or the inadequate efficiency of the surface drainage system can determine a different hydrological situation with respect to the one supposed in the design phase because the hydrological limits of catchments and sub-catchments change.

   The hydraulic behavior of the pipes involved in the catchments will also be different. A certain amount of surface runoff water produced in the first catchment by-passes to the second one and some of the flow destined to be discharged into the AB pipe, will discharge into the CD pipe. The AB and CD pipes, correctly designed according to the classical hydrological and hydraulic

procedures, will operate differently from as they were planned. Specifically, the first pipe will operate under capacity with respect to its design whereas the second one could operate with pressurized flow (Russo, 2009).

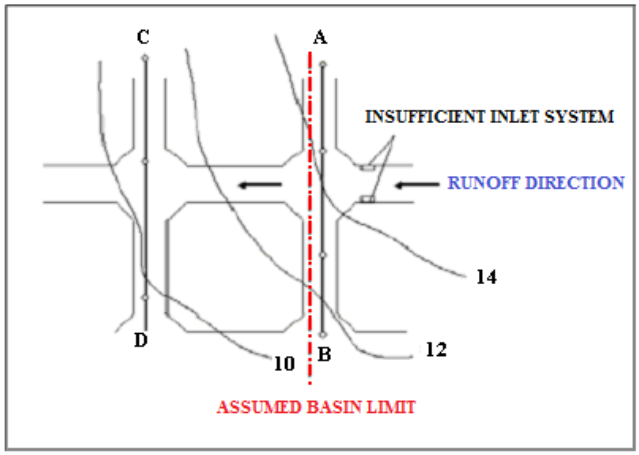

Figure 1.2 Distortion of the hydrological catchments due to the lack of an efficient system of drainage inlets (from Russo, 2009).

2. Hydrologic risk. The works are usually designed by taking as reference a synthetic rain event characterized by a given return period *T*: therefore no efficient response of the drainage system should be expected if a more intense event occurred. This assumption is in contrast with the citizens expectations who, since they pay service fees, require their urban drainage systems to operate effectively without fear of failure due to weather conditions. However, drainage systems designed to cope with the most extreme storm conditions would be too expensive to build and operate. Consequently, in establishing tolerable flood frequencies, the safety of the residents and the protection of their valuables must be balanced with the technical and economic restrictions. In this direction the instructions reported in the European Standard EN 752 are useful. In particular this standard, approved by the European Committee for Standardization (CEN, 1996, 1997), proposes two design procedures determined by the type of urban area and traffic infrastructure to be served:
   a) *Simplified procedure*. Sewer pipes are designed essentially for gravity flow by assuming rain input with return periods comprised between 1 and 10 years, depending on the area to be served (tab. 1.1);

b) *Simulation procedure.* Sewer pipes are designed by using hydraulic models that enable the resolution of the complete Saint Venant equations. Later it is necessary to verify the flood frequencies observed in the most critical sites with the values reported in tab. 1.1.

Design storm frequency[a] EN 752-2 (1 in '*n*' years)	Location	Design flooding frequency EN 752-2 (1 in '*n*' years)
1 in 1	Rural areas	1 in 10
1 in 2	Residential areas	1 in 20
1 in 2	City centers, industrial/commercial areas— with flooding check,	1 in 30
1 in 5	City centers, industrial/commercial areas— without flooding check.	–
1 in 10	Underground railway/underpasses	1 in 50

[a] For design storms no surcharge shall occur.

Table 1.1 Recommended design frequencies in EN 752.

For sub-catchments up to 200 hectares, the calculation may be limited to the simplified procedure, since the assumption of gravity flow ensures a safety margin (although not quantified), which is sufficient to guarantee acceptable flooding frequencies. In particular, in the absence of any other specific regulations, the standard suggests the rational formula for estimating the design flow, without indicating any criterion for the evaluation of the critical duration of the rainfall.

Instead, in the case of larger developments or existing drainage systems with complex hydraulic flow patterns (e.g. with loops, backwater effects, etc.), direct assessment of hydraulic performance by sewer flow simulation models is recommended thus checking flooding frequencies in accordance with tab. 1.1.

3. Errors in the execution of the works. The sewer networks are probably the civil engineering works characterized by the greatest discrepancy between the design assumptions and consequent realizations. This can be explained because, most of the time, the sewage construction is realized in difficult and dangerous situations, requiring rapid actions. Therefore few quality controls can be foreseen.

   For example the need to reduce the footprint and the impact of the construction site often force the backfilling of the excavation immediately after the conduit is laid on the ground, without permitting any control. The limited knowledge of the other existing underground networks can also determine the need to improvise

variations in order to cope with various constraints and obstacles that may occur gradually.

More generally, all these deficiencies are related to the poor consideration in which many construction companies held the sewer networks. They consider them as low-tech works and therefore ignore all the significant effects that poor construction can determine. In fact, it is important to underline that sewer network deficiencies do not cause immediate effects to the community, but chronic repercussions that appear a long time after the execution, such as obstructions in the channel sections, structural collapses or flooding (Ciaponi, 2005).

4. Lack of an adequate management and maintenance program of the works that takes into account any change occurring in the catchment. In detail such changes can be, for example, the non-stationarity of the demand that tends to reduce significantly the reliability of the works with time. For urban drainage systems, this non-stationarity is generally linked to the development rate of the urban area to be served (fig. 1.3).

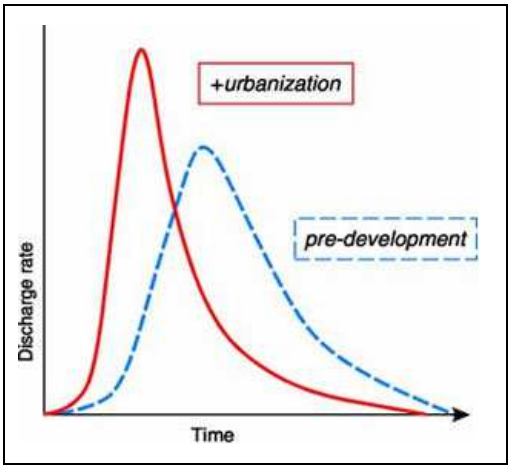

Figure 1.3 Hydrological effects due to urbanization.

In fact, it is clear how an uncontrolled urbanization process, determining the increase of the impervious areas and the reduction of the surface roughness, will produce repercussions on the sewer network performance, because of the increase in the surface runoff and the water velocities circulating over the catchment (the time of concentration decreases as showed in fig. 1.3).

Generally, the design of any sewage system should already take into account these aspects because the calculation of the design flow is based on the future scenario that can be foreseen at the moment, even referring to the existing planning acts. Nevertheless, these planning acts are usually characterized by durations that are inferior to the service life of the works. Moreover, they could be updated later based on new social, economic and political requirements, without taking into consideration the needs of the drainage network. Consequently all this determines a progressive overloading of the sewerage systems that have to face demands that were not accounted for in the design phase (Ciaponi, 2005).

The non-stationarity of the rainfall, owing to climate changes, is even more problematic. Climate change is currently the most important environmental issue: in fact, the dramatic assessments and projections by the Intergovernmental Panel on Climate Change (IPCC) are well known concerning the problem of the global warming. In particular these projections foreshadow significant implications also for the urban drainage system in both quantitative (increased frequency and intensity of extreme rain events) and qualitative terms (reduction of rainy days and consequent deterioration of the quality characteristics of the runoff, reduction of the average flow of the receptors), which should be partially taken into account in the design phase.

1.3 Consequences of flooding

Flooding in urban areas owing to the failure of drainage systems causes great damage to buildings and other public and private infrastructures. Moreover, street flooding can limit or completely stop the functioning of traffic systems and has indirect consequences such as loss of businesses and opportunities.

The perception of damage varies from person to person. Especially Konig et al. (2002) divides damages from urban flooding into three categories:

- Direct damage - typically material damage caused by water or flowing water.
- Indirect damage - e.g. traffic disruptions, administrative and labor costs, production losses, spreading of diseases, etc.

- Social consequences - negative long term effects of a more psychological character, like decrease of property values in frequently flooded areas and delayed economic development.

In addition further problems may arise from the spread of diseases such as diarrhea or Leptospirosis, which can be caused by the bacteria contained in the urine of rats. For example, in September 2000 flooding in the north east of Thailand, 6,921 cases of Leptospirosis were reported, 244 of these resulting in loss of human life (Bangkok Post, 20th September 2000). These parasites seem to thrive when urban flooding occurs regularly. In fact, moist soil provides a good environment for worm eggs to flourish, and water flooding open drains spreads eggs to new victims (Kolsky, 1998). Today antihelmintica kills parasites, but the parasites may gradually develop resistance to the drug and impose new and more severe problems. Therefore the best way to manage parasite problems is to break their life cycle, that is, to remove their natural environment by reducing the frequency and duration of flooding. In fact, Moraes (1996) found that reduced flooding limited the prevalence of roundworm and hookworm by a factor of two and hookworm alone by a factor of three.

1.4 Objectives

This PhD project is therefore aimed at investigating the sewer flooding issues since an efficient working of the drainage system is a prerequisite in the modern societies. Specifically the broader objective of the study is to contribute to an improvement of urban flood management by enhancing urban drainage modeling and storm motion forecasting. In order to achieve such scope the following detailed tasks were performed:

1. Investigation of the various LiDAR Digital Terrain Models (DTMs) available for the drainage modeling of a study area.

   From literature review it is evident that a great effort has been made to improve existing hydraulic models and to develop new ones. Nevertheless, little interest has been devoted to evaluate the effects of the use of different available LiDAR DTMs on hydraulic modeling. The research is therefore motivated by the need to know how LiDAR DTMs with different detail scale (LiDAR DSM *first*, LiDAR

DSM *last* and LiDAR DTM bare earth with overlapped building) can affect the hydraulic modeling of drainage networks. Every DTM is in fact characterized by a variable presence of non-ground surface features, such as cars, buildings or vegetation, that will influence surely the hydraulic response of the urban catchment differently. Consequently every data set was studied by GIS-based analysis methods, such as calculation of surface depressions, in order to evaluate whether the consideration of all the non-ground features is necessary for hydraulic modeling purposes, or whether the use of a less detailed LiDAR DTM, adequately improved, could be an approachable solution.

2. Analysis of improvements brought by a dual drainage approach in simulating the behavior of a drainage network during extreme rain events, compared to the use of a conventional methodology.

   Another question that justifies the work carried out by the author and presented in the thesis is related to the need of improving available urban drainage modeling. Most of these models are in fact based on process simplifications that are far removed from reality, such as assuming that when water leaves the sewer it is stored in a virtual reservoir and does not follow the natural flow paths, i.e. the effect of local topography is neglected. This approach provides a very biased image of flooding process. Consequently the research was aimed at quantifying capabilities and limits of two urban drainage modeling with diverse sophistication level. The first one was based on the classical hypothesis according to which the drainage system is composed only of the sewer system, that is to consider that stormwater, once entered the sewer system, can no longer leave this system coming back to the surface. Instead the second one was based on the dual drainage approach, i.e. it was assumed that the urban drainage system was composed of a surface network and the sewer network. The evaluation of the best approach was performed by comparing the water volume distributions in the sewer network and the number of surcharged sewer trunks resulting from hydraulic simulations. Specifically the issues relative to the development of the most complicated model, that is the dual drainage one, were studied in more detail: the influence of buildings and DTM resolution on the surface network definition, and the introduction of criteria to be taken into

account for pond filtering parameters were the topics deepened through the use of an innovative methodology, the AOFD tool (Automatic Overland Flow Delineation (Maksimović et al., 2009)).

3. Study of the potentials of a dense network of rain gauges in forecasting storm movements for flood prevention purposes.

   This research was performed because, currently, methods for rainfall prediction are mainly based on radar measurements. However rain gauge data are often available whereas radar data are not. Furthermore radar instruments enable the investigation of convective cells motion, whereas rain gauges data allow the analysis of the movement of rainfall patterns recorded on the ground, that is more important for hydraulic modeling. Consequently storm movement parameters, velocity and direction, were derived by analyzing rainfall data trough available storm tracking procedures. The method proposed by Diskin (1987; 1990) was tested and, in particular, the extent to which the choice of the reference feature in the hyetograph and the location of the recording stations inside the catchment can affect the results of the methodology was studied in detail. The quality of the elaborations was estimated by comparing the results obtained with other physical phenomena which are related to storm movement, such as wind movement data. In particular statistical analysis, based on the computation of the correlation coefficient and root mean square deviation between storm and wind data sets, were performed.

With the results from the research presented herein, it is expected that:

1. DTM enhancement methods generate hydraulically corrected DTMs that can potentially lead to improvements in urban pluvial flood modeling.
2. more realistic simulations of the drainage system are performed by developing dual drainage models. In this way engineers could aim at minimizing both the costs of construction of new works and maintenance of existing structures by evaluating systematically the effectiveness of all the possible design solutions. Actually, the use of such a modeling will have to push them to optimize the working conditions of both the surface and sewer networks when evaluating flood control and mitigation measures.

3. rain gauges are considered as valid alternatives in rainfall movement prediction, to be taken into account in areas where radar measurements cannot be obtained yet. In fact the results of the elaborations will demonstrate how such instruments, that are more approachable than radar ones for economical and practical reasons, are very useful in forecasting the movements that future storm events can make in a monitored area. Similar information could be also used in connection with hydraulic models, previously calibrated for the same study area, in order to evaluate in advance the possible flood-prone areas. In addition the analysis of the results, obtained by considering an ever decreasing number of recording stations, will give interesting information to municipalities having limited budget for equipping themselves with an adequate number of such instruments.

1.5 Thesis outline

The first chapter provides the background to the present thesis, i.e. it reports the issues related to sewer flooding. It also explains the aims and the objectives of the research and, finally, provides a general methodology of how the project will be carried out.

The second chapter describes in depth the work of other researchers concerning urban drainage modeling, especially the dual drainage concept and the use of software, as GIS and AOFD, in similar applications.

The third chapter presents the elaborations performed for improving LiDAR DTM data sets available for hydraulic modeling of the drainage network of the Liguori catchment, an experimental site located in Cosenza (Italy). Moreover the comparison between the two hydraulic modeling approaches with diverse sophistication level is also reported.

The fourth chapter is a review of the principal storm tracking methods available in the literature. Moreover the various fields of application of such models and the rainfall data collection requirements are also presented.

The fifth chapter exposes the methodology used to estimate the speed and direction of movement of rainfall events recorded by the dense network of rain gauges placed

in London. In particular the analysis performed, concerning the extent to which the choice of the reference feature in the hyetograph and the location of the recording stations inside the catchment can affect the results of the methodology, are reported. Finally, a summary of the conclusions is presented in the sixth chapter.

References

- AIT. (1985). *Flood routing and control alternatives of Chayo Praya River for Bangkok*. A report submitted to The National Economical and Social Development Board of Thailand.
- Balmforth D., Digman C., Butler D. & Shaffer P. (2006). *Scoping Study, DEFRA.*
- Ciaponi C. (2005). *Conoscenza ed affidabilità dei sistemi fognari.* Primo Convegno Nazionale di Idraulica Urbana, Sorrento 28 – 30 Settembre 2005.
- CEN, 1996. Drain and sewer systems outside buildings - Part 2: Performance Requirements, European Standard, European Committee for Standardization CEN, Brussels, Belgium 1996.
- CEN, 1997. Drain and sewer systems outside buildings - Part 4: Hydraulic design and environmental considerations, European Standard, European Committee for Standardization CEN, Brussels, Belgium 1997.
- Diskin M.H. (1987). *On the Determination of the Speed of Moving Rainfall Patterns*, Hydrological Sciences Journal, Vol32, No. 1, pp. 1-14.
- Diskin M.H. (1990). *The Speed of Two Moving Rainfall Events in Lund*, Nordic Hydrology, 21, 1990, 153-164.
- Kolsky, P. (1998). *Storm drainage*. Intermediate Technology Publications, London.
- Konig A., Sægrov S., Schilling W. (2002). *Damage assessment for urban flooding*. Ninth International Conference on Urban Drainage, Portland, Oregon, USA.
- Maksimović Č., Prodanović D., Boonya-aroonnet S., Leitão J.P., Djordjević S, Allitt R. (2009). *Overland flow and pathway analysis for modelling of urban pluvial flooding*. Journal of Hydraulic Research, 47(4):512-523.
- Moraes, L.R.S. (1996). *Health impacts of drainage and sewerage in poor urban areas in Salvador Brazil*. PhD Thesis, London School of Hygiene and Tropical Medicine, London, UK.
- Russo B. (2009). *Design of surface drainage systems according to hazard criteria related to flooding of urban areas*. PhD Thesis, University Of Calabria, Cosenza, Italy.

2. Literature review concerning urban drainage modeling

2.1 Introduction

In the first part of the chapter conventional urban drainage modeling will be described in order to highlight their limitations, particularly as concerns the simulation of sewer flooding.

Such limits, usually the cause of the wrong design of the hydraulic works, have prompted several researchers to deepen these studies in recent years. In fact, it is possible to observe that the presentation of new models has increased recently, especially after the introduction of innovative tools such as Geographical Information Systems (GIS). In detail, GIS tools were initially employed to derive urban terrain descriptions and to define parameters of existing urban hydrologic models. Along the way, new models based on such elements and using automatically defined urban flow paths were developed.

Among these procedures a more detailed report will concern the *dual drainage* concept, according to which the urban drainage system is composed of two components: a surface or *major system*, linked by streets, ditches, and various natural and artificial channels, and a subsurface sewer network or *minor system*. Such an approach enables the limitations of the classical modeling to be overcome, which assumes the drainage system to be composed only of the sewer system, that is to consider that stormwater, once entered the sewer system, can no longer leave this system by coming back to the surface.

Although the dual drainage approach is simple from the conceptual point of view, its implementation is quite complex: in fact, the sewer system is generally known, whereas the surface network must be defined by taking into account the geometric characteristics of the study area such as road slopes, dimensions of sidewalks, buildings, etc.

All these issues will be treated in more detail in the following paragraphs.

2.2 Conventional urban drainage modeling

From the 19th century, the larger cities of America and Europe started to consider the necessity of planning their drainage systems, because the provision of piped sewerage and flood-free streets was regarded as essential for the quality of urban life. Especially, the design of storm drainage systems for urban areas was dominated by the rational formula reported in eq. 2.1 (Mulvaney, 1850; Kuichling, 1889; Lloyd-Davis, 1906):

$$Q_c = \phi \cdot i_c \cdot S = \phi \cdot a \cdot t_c^{n-1} \cdot S \qquad (2.1)$$

where

- Q_c is the peak flow;
- S is the draining catchment area ;
- ϕ is the non-dimensional runoff coefficient, taking into account all the rainfall abstractions;
- i_c is the average rainfall intensity, evaluated by considering a storm duration equal to the time of concentration of the catchment t_c.

This flow rate must be later considered for designing the cross section of the generic sewer trunk by assuming uniform flow conditions in order to guarantee a correct gravity flow operation.

The widespread application of this methodology was justified by its simplicity and the dimensions of the sewers obtained from the calculations, which were affordable, given the fact that the proportion of impermeable area was still within reasonable limits. Nevertheless, since the beginning of the 20th century, the use of the procedure started to determine the estimation of very large sewer dimensions due to the increase of the runoff associated with the urbanization process. This prompted designers and researchers to assess the need to incorporate other physical aspects in the design process, such as storage routing and surcharged flow. This need was intensified after the Second World War, when European cities had to be reconstructed and optimization in the design was necessary in order to accommodate investment within public expenditure.

Various criticisms have often been expressed on the applicability of the rational formula to the complex interaction of social and structural city development with the urban flow processes. Especially the principal limit consists in the calculation of only the peak flow, whereas no additional information concerning the time distribution of the volume, i.e. the hydrographs, can be obtained.

Its simplifications are so excessive that they do not enable certain affirmation that the return period associated with the rainfall is the same as the derived flow rates (Artina et al.,1994). In fact, numerous researches have shown that the return periods of the flow rates are appreciably smaller than the return periods of the intensity - duration curves considered for the same flow calculations. This is primarily owing to the fact that conventional values were attributed to the parameters of the models, because of the lack of available experimental data (Ciaponi and Papiri, 2000). Also the estimation of the same intensity - duration curves was not usually correct: the limited quantity of sub-hourly rainfall data obliged these relationships to be derived by extrapolating the function interpolating the maximum yearly values of rain depths recorded over a range of hourly timescales (1, 3, 6, 12 and 24 hours), for the short durations. Similar approaches have been criticized by various researchers (Piga et al., 1990; Barbero and Papiri, 2000) who reported how the hourly intensity – duration expression cannot be applied for durations inferior to 15-20 minutes (Ciaponi, 2005).

Other issues concern the hydraulic analysis carried out by assuming uniform flow conditions. It is well known that such an approach means that flow conditions do not change with position in the stream or with time. In fact, it can be applied, strictly speaking, only in cylindrical riverbeds that are sloped (but not too much) in the direction of the current and are sufficiently long. Nevertheless, such situations are far from being verified in the sewer networks, which are instead characterized by frequent temporal and spatial changes of the geometry and flow rates.

Moreover, the uniform flow is not able to take into account the geometric sewer singularities, such as manholes or junction nodes, where particular hydraulic phenomena occur. In detail, if such elements are designed in order to minimize the energy losses (for example by realizing direction changes with sufficiently large curvature radii) the associated local head losses will be small and could be considered by increasing adequately the frictional energy losses (Ciaponi and Papiri,

1997). Otherwise these local energy losses will have to be taken into account with appropriate modeling (Ciaponi and Papiri, 2000).

Consequently, sometimes, the calculation was carried out by assuming steady flow conditions in order to overcome the limitations mentioned. A steady flow is one in which the conditions (velocity, pressure and cross-section) may differ from point to point but do not change with time. This approach has certainly the merit of treating the sewer network as a "system" whose components mutually interact. Subsequently, in this way, it is possible to take into account the backwater effects and the presence of the geometric sewer singularities. Moreover, this procedure, together with the representation of the piezometric profiles of the surcharged trunks, enables also the localization of the potential flooded areas.

Nevertheless, sewer flows are generally unsteady, i.e. time-varying, as reported by many authors (Cunge et al., 1980; Mignosa, 1987). In fact, during intense storm events, sewer conditions change with time and the following situations can occur:

- sewer flow routing against the slope of the conduit;
- passage from subcritical to critical flow;
- passage from free-surface to surcharged flow;
- backwater effects due to the presence of obstacles in the conduit;
- particular hydraulic phenomena due to the presence of pumping stations, detention storages or overflow weirs.

Moreover, the steady flow approach proves to be inadequate because it assumes that the peak flows are present simultaneously in every sewer trunk. This supposition is unreal and it would determine an oversizing of the works, which can also be relevant depending on the rainfall input assumed in the calculations (Ciaponi and Papiri, 2000).

Accordingly, afterwards, new approaches were introduced (Mignosa, 1987; Artina et al., 1997): in particular, the most widespread software used are EPA SWMM, InfoWorks CS and DHI Mouse. These tools enable modeling of the response of the sewer system to any rainfall input, which can also be spatially distributed over the catchment. In this way the uniform and steady assumptions are rejected, whereas sophisticated numerical methods are implemented in order to solve the unsteady flow

equations. The limit relative to the calculation of only the peak flow is overcome because these models enable estimation of the hydrographs associated with a certain storm event for every sewer trunk. Moreover, the computation of the rainfall losses is carried out with more complex methodologies rather than through the simple evaluation of the runoff coefficient ϕ.

Such urban drainage models are normally characterized or classified to help describe and discuss their capabilities, strengths, and limitations. There is no universal method to characterize them, therefore models have been classified in several ways depending on the criteria of interest. Examples of classifications are given by Anderson and Burt (1985); Dooge (1977); Larson et al. (1982); Shafer and Skaggs (1983); and Todini (1988).

In this case the classification by Vernon Knapp at al. (1991) is reported: especially this review focused on the following four categories: 1) Event and Continuous Simulation Models, 2) Conceptual and Hydrodynamic Models, 3) Lumped and Distributed Parameter Models, and 4) Models with Fitted, Physically Determined, or Empirically Derived Parameters.

1) Event and Continuous Simulation Models

Rainfall-runoff models are either event models or continuous simulation (CS) models. Event models typically estimate the runoff from an individual storm event, i.e., describing a relatively short period within the hydrologic record. Event models ordinarily evaluate a partial set of the hydrologic processes that affect the watershed: infiltration, overland and channel flow, and possibly interception and detention storage. Most event models use a constant time interval, whose value may typically range from minutes to several hours.

Continuous simulation models operate for a sustained period that includes both rainfall events and interstorm conditions. To legitimately evaluate the streamflow during interstorm periods, CS models should include additional hydrologic properties such as evapotranspiration, shallow subsurface flow, and ground-water flow. Also crucial to these models is an accounting of the soil moisture and how it relates to changes in infiltration. The CS time interval can be daily, hourly, subhourly, or

variable. Models that provide only daily simulation are not ordinarily useful for stormwater applications.

When using a CS model, the initial conditions are normally set for a time well in advance of any storm under consideration. The antecedent conditions for a storm are calculated analytically as a part of the normal model operation and are sensitive to the input series of climatological data, not to the initial conditions. The calculation of antecedent conditions using a CS model is normally considered advantageous because it does not require subjective evaluations by the model user.

For an event model, the initial conditions (antecedent soil moisture, stream and reservoir levels, etc.) must either be subjectively assigned by the user, calibrated with some type of error-reduction procedure, or approximated by an external procedure. Of these three approaches, the first two are common. In the third approach, an external approximation of the antecedent conditions may be obtained using the preceding climatological time series and applying either a simple empirical procedure or a more complex, explicit accounting of hydrologic conditions. When an explicit accounting procedure and the past climatological record are used to estimate the initial conditions, the function of the event model can approach that of a CS model. Feldman (1979) suggests that an accounting of antecedent conditions for use in a detailed event model can be obtained by using a relatively simple CS model. The authors note that the reliability of any estimate of the antecedent condition is a function of the appropriateness of the moisture accounting procedures, not whether these procedures are accomplished internally (as with CS models), or calculated independently of the model.

In modeling a long period that contains a number of floods of various magnitudes, the application of CS models provides more opportunities to compare model results with observed runoff. A long calibration period with a variety of hydrological conditions increases confidence in model results (James and Burges, 1982). Event models are typically applied to fewer storms, but increased confidence can be gained by calibrating the model to as many storms as possible.

2) Conceptual and Hydrodynamic Models

The categorization describes the types of equations used in the model to describe the hydrologic processes. These categories of models are identified as: 1) "black-box" or

transfer functions, 2) conceptual models, and 3) hydrodynamic models. Black-box models rely upon a statistical correspondence between the model input (rainfall) and model output (runoff) without relation to any underlying physical processes. Conceptual models are described by Dooge (1977) as "models which are formulated on the basis of a simple arrangement of a relatively small number of elements, each of which is itself a simple representation of a physical relationship." This definition is sufficiently broad enough to include hydrodynamic models, but conceptual models usually represent an intermediate level of component sophistication. Hydrodynamic models - sometimes also termed physically based models (Beven, 1989) - are also simplifications of reality and have a certain amount of empiricism (Haan, 1988). However, these models are generally based on the most recent physics-based understanding of the hydrologic processes that control the runoff response in the watershed. One of the attributes of the physics-based processes, as explained by Beven (1985), is that they involve laws and principles that can be validated independently of the model.

In reality, the boundaries between conceptual and hydrodynamic models are fuzzy. Individual models will normally combine both conceptual and hydrodynamic components. Not all hydrologic properties can be represented by hydrodynamic components, which forces all models to have some conceptual and empirical aspects. The predominant manner in which the components are modeled results in the overall classification. For the above reasons, any discussion of differences between conceptual and hydrodynamic models is not absolute but falls along a continuum. Comments related to hydrodynamic models may also be attributed to a hydrodynamic component that is contained within a "conceptual" model.

3) Lumped and Distributed Parameter Models

The hydrologic parameters used in the rainfall-runoff models can be represented in either a lumped or distributed manner. The lumping method averages the total rainfall, its distribution over space, soil characteristics, overland flow conditions, etc. for the entire watershed, ignoring all flow-routing mechanisms that exist within it. The expectation is that any minor details of the rainfall-runoff process will be inconsequential, resulting in an "average" flood condition. Although certain lumped

parameters may implicitly represent physical attributes of the hydrologic system, they cannot be expected to have any direct physical interpretation (Delleur, 1982; Troutman, 1985). Lumped models can be made to behave more like distributed parameter models by adopting a detailed database and dividing a watershed into very small sub-watersheds (Nix, 1991).

Distributed parameters both describe the geographical variation of parameters across the watershed and discriminate between changes in the hydrologic processes that occur throughout the watershed. In a fully distributed model, the hydrology of each small element of the watershed is distinctly simulated to include the hydrologic interactions with bordering elements. In reality, parameters in the distributed models have to be lumped to a small degree to match the grid scale used for computations (Troutman, 1985). In addition, the fitting of distributed, hydrodynamic models to observed streamflow at present is usually accomplished through the simplification and calibration of certain parameters (Bathurst, 1986). Therefore, without a sufficiently detailed database, a distributed model effectively may deteriorate into a lumped system model (McPherson and Zuidema, 1977; Beven, 1989).

A third approach simulates the hydrologic processes for a discrete number of land use and soil types. A land use and soil type combination, termed a hydrologic response unit (HRU), may occur in numerous locations in the same watershed; however, the hydrologic response is modeled for this combination only once, and this response is assumed to be homogeneous for all locations having that HRU. The HRU parameter approach is used in many rainfall-runoff models (for example, HSPF, SWMM, and PRMS) that are commonly considered distributed parameter models. Depending on how the watershed is partitioned, either the hydrologic response from each HRU is assigned to individual elements throughout the watershed, or the responses from several HRUs are prorated and aggregated to represent the lumped response from a sub-watershed.

Within the framework of any individual model, the level of distribution can be user-controlled. James and Robinson (1985) state that the appropriate extent to which a modeler chooses to distribute the parameters should depend upon the objectives of the study and the available data, time, and money.

Many studies (Larson et al., 1982; Beven, 1985; Wilcox et al., 1990) suggest that distributed parameter models are desirable because they have the greatest potential for use in describing land use change, water-quality modeling, and forecasting on ungaged watersheds. These advantages assume that the parameters of distributed models are more physically realistic than the lumped model parameters, which should be the case when the model is well designed (Troutman, 1985). Distributed parameters have the potential to be physically interpreted and, when this is the case, greater confidence can be placed in the use of the model for prediction of flows (James and Burges, 1982; Troutman, 1985). One reason that distributed parameter models have not seen widespread use is the availability of detailed databases. Future improvements in data acquisition, including the application of GIS, will likely lead to more extensive use of distributed and HRU parameter models (Toms, 1989).

4) Models with Fitted, Physically Determined, or Empirically Derived Parameters

Parameters for rainfall-runoff models can be 1) fitted through calibration, 2) determined from field measurements, or 3) empirically fixed. Fitted parameters, set in the calibration process, typically have no little or no physical interpretation. Physically determined parameters are derived from measurable watershed characteristics such as slope, channel width, hydraulic conductivity of soils, etc. Measured values may not always produce the best results when used directly in a model. Thus, some physically determined parameters may be adjusted during the calibration process and are not necessarily equal to the measured variables. But to maintain the physical relationship these parameters should be similar in magnitude and behavior to the measured values.

The use of fitted versus physically determined parameters is a major issue in the application of rainfall-runoff models. Fitted parameters are less likely to be consistent from one data set to another, and models that use these parameters are less appropriate for extrapolation (Larson, 1973; Gan and Burges, 1990). In general, lumped models and most conceptual models use fitted parameters. However, Larson et al. (1982) indicate that fitted parameters cannot reliably be transferred for use on ungaged watersheds. Thus, empirically derived parameter methods (described below) are often used with the lumped conceptual models for ungaged sites. Distributed and

quasi-distributed conceptual models can use a combination of fitted, physically determined, and empirical parameters. Distributed hydrodynamic models primarily use measured or physically determined parameters, with some empirically derived parameters.

Empirically derived parameters are developed by the regression analysis of either fitted or physically determined parameters. Empirically derived parameters may vary in the amount of physical interpretation that can be associated with their values. This category of parameters includes the Soil Conservation Service (SCS) runoff curve numbers that were developed for estimating rainfall losses on ungaged watersheds. Many of these empirically fixed relationships are required for parameterization of selected components in all models, including the models that are more physically based.

Generally, all these urban drainage models analyze the following processes (fig. 2.1): watershed precipitation; rainfall losses; overland surface runoff; sewer network flow.

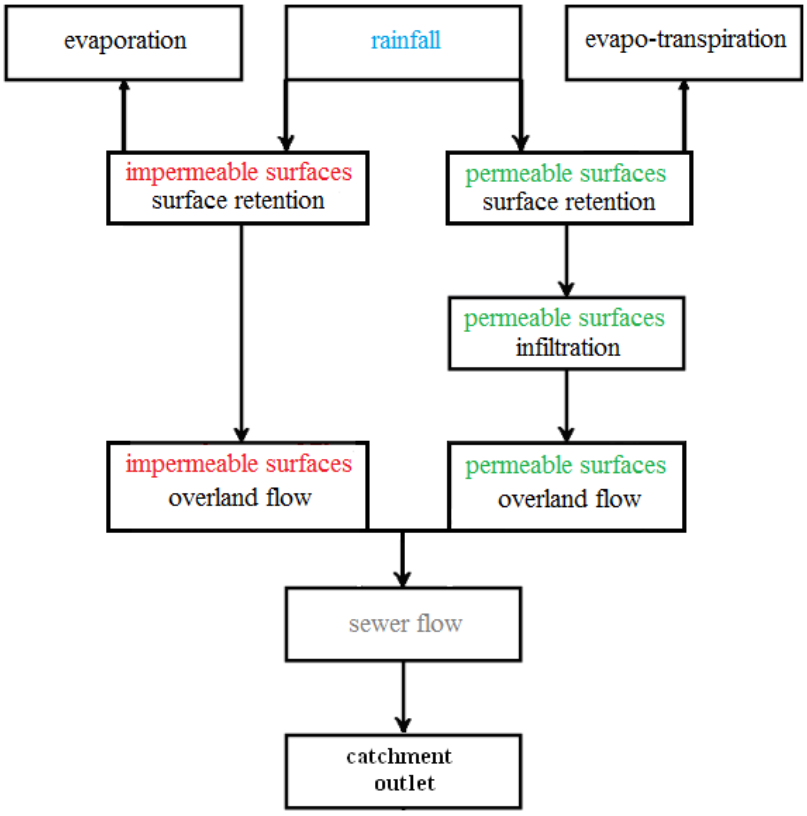

Figure 2.1 Common urban drainage modeling procedure.

2.2.1 Watershed precipitation

Two basic classes of precipitation inputs can be used in rainfall-runoff models: 1) historical precipitation; 2) synthetic precipitation.

1) Historical Precipitation

Historical precipitation is commonly used in CS models to extend the total runoff record, which includes the annual series of peak flows. In this procedure, simultaneous rainfall and runoff records are used to calibrate the model. The rainfall record from an extended period is then used as model input, and the model simulates a corresponding sequence of runoff.

The greatest advantage in the use of historical precipitation to analyze stormwater response is that it presents a variety of scenarios of both antecedent conditions and precipitation intensity within the storm. This helps provide an understanding of the types of storms that are likely to result in severe flooding.

2) Synthetic Precipitation / Design Storms

Design storms are synthetic rainstorms of a predetermined quantity, duration, temporal distribution, and frequency. They are usually based on either a geometric function of rainfall versus time (for example, the uniform and triangular distributions), or on temporal patterns based on the intensities of observed precipitation (fig. 2.2).

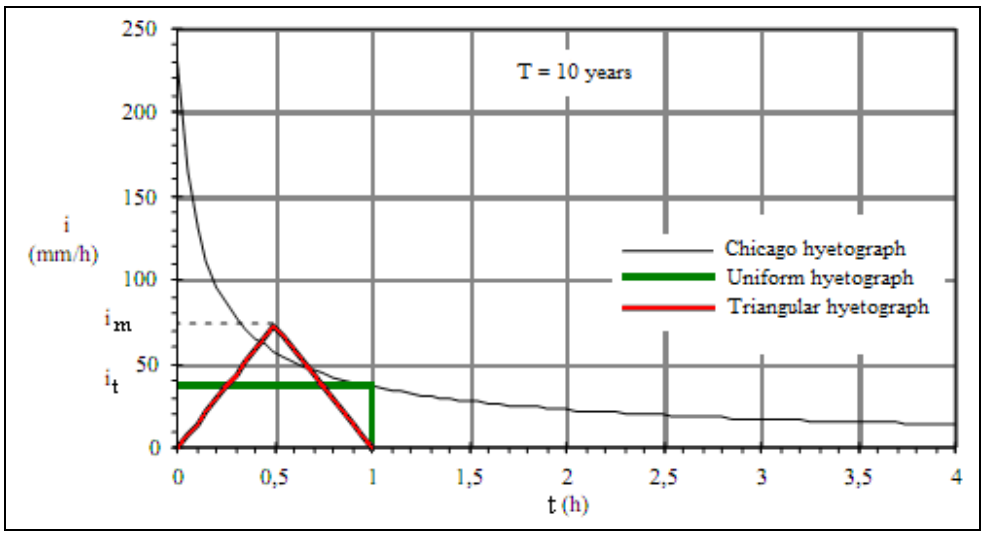

Figure 2.2 Different kinds of hyetographs evaluated for the Moie rain gauge (from AA.VV., 2004).

The synthetic design-storm hyetographs that are developed using observed rainfall intensities can be representative of either "average" or "extreme" storm events. Most of the rainfall distributions based on observed heavy rainfall - such as the HEC-1 Standard Project Storm (U.S. Army Corps of Engineers, 1990), SCS Type-II storm (U.S. Soil Conservation Service, 1972), and Chicago method (Keifer and Chu, 1957) - arrange the periods of most intense rainfall so that they are nested in the center (or other portion) of the storm.

In both synthetic and historical precipitations the rainfall input is normally considered as spatially uniform (from one rain gauge only or as the average of the values recorded by the available rain gauges) because, currently, it is difficult, or at least expensive, to obtain reliable rainfall records in urban scales due to the high-density of rain gauges required and/or the investment required to install a weather radar. However it is important to underline that spatial variability affects modeling results in both large and small (urban) catchments, as stated by many researchers (Faures et al., 1995; Goodrich et al., 1995; Woods and Sivapalan, 1999; Lau and Sharpe, 2004; Pechlivanidis et al., 2008). Such aspects will be treated in more detail in Chapter 4, where storm tracking methods will be presented.

2.2.2 Rainfall losses

The term rainfall loss refers to that portion of the total rainfall that fails to directly result in storm runoff. The rainfall losses are the primary determinant of the amount and distribution of runoff that result from an individual storm.

The estimation of the rainfall loss is considered by many to be the most complex, and possibly least studied, component in the rainfall-runoff process. Aron (1982) has considered rainfall losses to be the weakest link in the proper estimation of runoff; and others, such as Yen (1982), have stressed that the study of rainfall losses should be given considerably more attention.

Rainfall losses can be divided into three processes: 1) the interception of rainfall by plants, 2) the retention and storage of water in depressions, and 3) infiltration of water into the ground. Together, interception and depression storage are significant factors in the overall water budget. However, infiltration is frequently the only process of the three to be simulated in rainfall-runoff models, especially with event

models. There are two reasons for this type of treatment: 1) infiltration is the major rainfall loss during heavy accumulations of rainfall, and 2) the interactions between the various rainfall loss processes are not easily separated except through the use of detailed field studies.

In the following the infiltration and depression storage processes will be treated in more detail because of their widespread impact on all types of modeling.

2.2.2.1 Infiltration

- *Horton model*

The Horton equation models a decreasing rate of infiltration over time, which implies that the rate of infiltration decreases as the soil becomes more saturated (fig. 2.3).

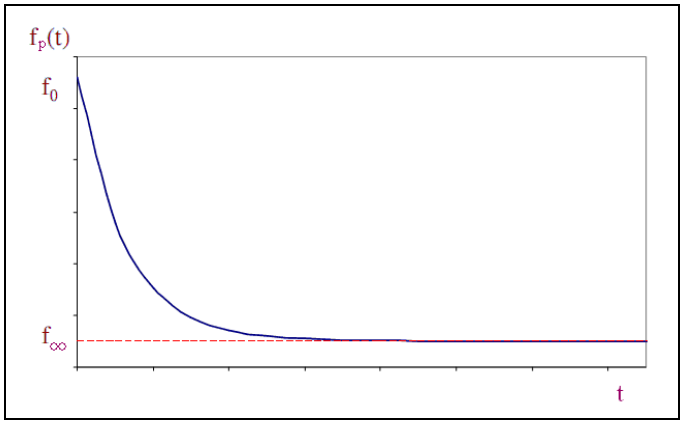

Figure 2.3 Horton's infiltration model

For conditions in which the rainfall intensity is always greater than the infiltration capacity (that is, the rainwater supply for infiltration is not limiting), this method expresses the infiltration rate as:

$$f_p = f_\infty + (f_0 - f_\infty) \cdot e^{-\alpha \cdot t} \qquad (2.2)$$

where:

- f_p is the infiltration rate at time t [mm/h];
- f_∞ is the constant or equilibrium infiltration rate after the soil has been saturated ($t = \infty$), also known as minimum infiltration rate [mm/h];
- f_0 is the initial infiltration rate ($t = 0$) or maximum infiltration rate [mm/h];

- α is the decay constant specific to the soil. [s^{-1}] ;
- t is the time [s].

The parameters of the Horton's equation depend on the soil type and the relative cover. In the literature there are several available tables based on soil characteristics. Especially, in this case, the values proposed by ILLUDAS model (tab. 2.2) and ASCE handbook (tab. 2.3) are given. The first ones are referred to the soil classification by the Soil Conservation Service (tab. 2.1).

Group	Meaning	Saturated Conductivity [in/hr]
A	Low runoff potential. Soils having high infiltration rates even when thoroughly wetted and consisting chiefly of deep, well to excessively drained sands or gravels.	$\geq$ 0.45
B	Soils having moderate infiltration rates when thoroughly wetted and consisting chiefly of moderately deep to deep, moderately well to well-drained soils with moderately fine to moderately coarse textures. E.g., shallow loess, sandy loam.	0.30 - 0.15
C	Soils having slow infiltration rates when thoroughly wetted and consisting chiefly of soils with a layer that impedes downward movement of water, or soils with moderately fine to fine textures. E.g., clay loams, shallow sandy loam.	0.15 - 0.05
D	High runoff potential. Soils having very slow infiltration rates when thoroughly wetted and consisting chiefly of clay soils with a high swelling potential, soils with a permanent high water table, soils with a clay-pan or clay layer at or near the surface, and shallow soils over nearly impervious material.	0.05 - 0.00

Table 2.1 Hydrologic Soil Group Definitions by Soil Conservation Service (SCS, 1972).

soil type	f_0 (mm/h)	f_∞ (mm/h)	k (h^{-1})
A	*250*	*25*	*2*
B	*200*	*12,5*	*2*
C	*125*	*6,5*	*2*
D	*75*	*2,5*	*2*

Table 2.2 Values of the Horton's parameter by ILLUDAS.

permeability level of the soil	f_0 (mm/h)	f_∞ (mm/h)	k (h^{-1})
high	117	17	5,34
medium	76	13	4,14
poor	76	6	4,14

Table 2.3 Values of the Horton's parameter by ASCE.

It is possible to note that the trends of the Horton's equation are clearly discordant for the two groups of parameters (fig. 2.4): especially, in most cases, the ILLUDAS values are higher than ASCE ones. The difference might be justified by the fact that the values proposed by ASCE are relative to design conditions, therefore they tend to be conservative. Whereas the values recommended by a simulation model, such as ILLUDAS, should refer to average conditions.

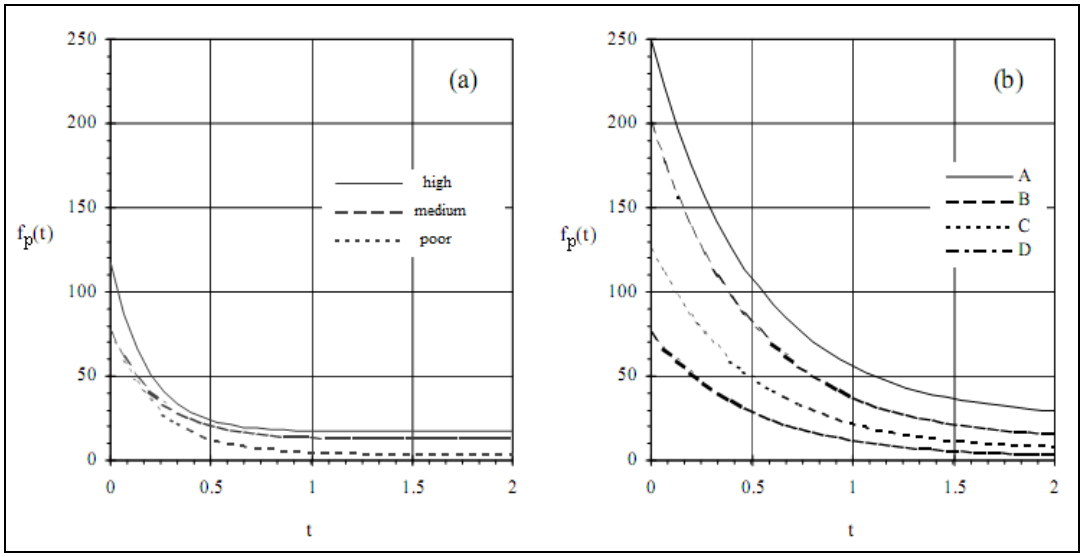

Figure 2.4 Different trend of the Horton's equation between ASCE (a) and ILLUDAS (b).

- *Green – Ampt model*

This method assumes that a sharp wetting front exists in the soil column, separating soil with some initial moisture content below from saturated soil above.

The infiltration rate f (mm/h) can be calculated as follows:

$$f(t) = f_c \cdot \left(1 + \frac{\phi \cdot \delta}{F(t)}\right) \tag{2.3}$$

where

- f_c is the saturated hydraulic conductivity [mm/h];
- ϕ is the suction head at wetting front [mm];
- δ is the moisture or water deficit, that is the difference between the saturated moisture content θ_s and the initial moisture content θ_i [-];
- F is the total infiltrated volume between the surface of the soil and the wetting front [mm].

Also the parameters of the Green – Ampt model depend on the characteristics of the soil (tab. 2.4).

Soil Texture Class	f_c [in]	ϕ [in]	θ_s [-]	θ_i [-]
Sand	4.74	1.93	0.437	0.062
Loamy Sand	1.18	2.40	0.437	0.105
Sandy Loam	0.43	4.33	0.453	0.190
Loam	0.13	3.50	0.463	0.232
Silt Loam	0.26	6.69	0.501	0.284
Sandy Clay Loam	0.06	8.66	0.398	0.244
Clay Loam	0.04	8.27	0.464	0.310
Silty Clay Loam	0.04	10.63	0.471	0.342
Sandy Clay	0.02	9.45	0.430	0.321
Silty Clay	0.02	11.42	0.479	0.371
Clay	0.01	12.60	0.475	0.378

Table 2.4 Green - Ampt parameters by Rawls et al. (1983).

- *SCS Curve Number*

The Curve Number Method was originally developed by the Soil Conservation Service (Soil Conservation Service 1964; 1972) for conditions prevailing in the United States. Since then, it has been adapted to conditions in other parts of the world.

The Curve Number Method is based on the following phenomena. The initial accumulation of rainfall represents interception, depression storage, and infiltration before the start of runoff and is called initial abstraction. After runoff has started, some of the additional rainfall is lost, mainly in the form of infiltration; this is called actual retention. With increasing rainfall, the actual retention also increases up to some maximum value: the potential maximum retention. To describe these curves mathematically, SCS assumed that the ratio of actual retention to potential

maximum retention was equal to the ratio of actual runoff to potential maximum runoff, the latter being rainfall minus initial abstraction. In mathematical form, this empirical relationship is

$$\frac{Q}{P - I_a} = \frac{F}{S} \tag{2.4}$$

where

- F is the actual retention [mm];
- S is the potential maximum retention [mm];
- Q is the accumulated runoff depth [mm];
- P is the accumulated rainfall depth [mm];
- I_a is the initial abstraction [mm].

Figure 2.5 shows the above relationship for certain values of the initial abstraction and potential maximum retention.

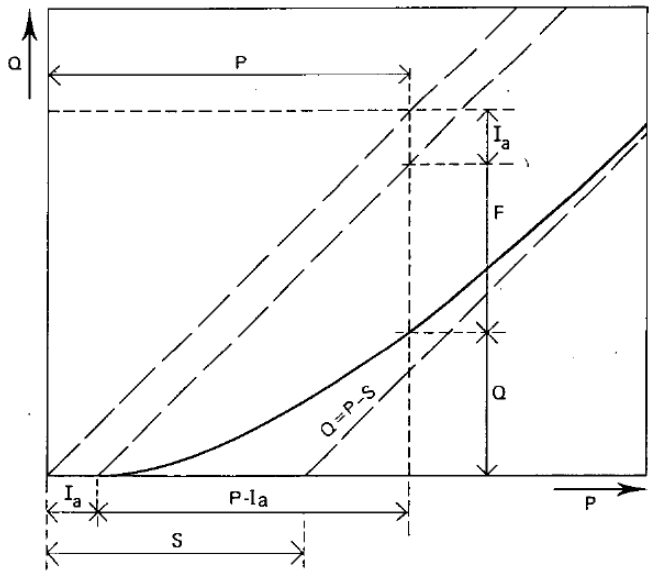

Figure 2.5 Accumulated runoff Q versus accumulated rainfall P according to the Curve Number Method.

After runoff has started, all additional rainfall becomes either runoff or actual retention (i.e. the actual retention is the difference between rainfall minus initial abstraction and runoff).

$$F = P - I_a - Q \tag{2.5}$$

Combining equations (2.4) and (2.5) yields

$$Q = \frac{\left(P - I_a\right)^2}{P - I_a + S} \tag{2.6}$$

To eliminate the need to estimate the two variables I_a and S in eq. (2.6), a regression analysis was made on the basis of recorded rainfall and runoff data from small drainage basins. The data showed a large amount of scatter (Soil Conservation Service, 1972). The following average relationship was found

$$I_a = 0.2 \cdot S \tag{2.7}$$

Combining equations (2.6) and (2.7) yields

$$Q = \frac{\left(P - 0.2 \cdot S\right)^2}{P + 0.8 \cdot S} \quad \text{for } P > 0.2 \cdot S \tag{2.8}$$

Equation (2.8) is the rainfall-runoff relationship used in the Curve Number Method. It allows the runoff depth to be estimated from rainfall depth, given the value of the potential maximum retention *S*. Such parameter mainly represents infiltration occurring after runoff has started. This infiltration is controlled by the rate of infiltration at the soil surface, or by the rate of transmission in the soil profile, or by the water-storage capacity of the profile, whichever is the limiting factor.

The potential maximum retention *S* has been converted to the Curve Number *CN* in order to make the operations of interpolating, averaging, and weighting more nearly linear. This relationship is

$$CN = \frac{25400}{254 + S} \tag{2.9}$$

As the potential maximum retention *S* can theoretically vary between zero and infinity, equation (2.9) shows that the Curve Number *CN* can range from one hundred to zero depending on the land use, land treatment, hydrological condition, hydrological soil group, and antecedent soil moisture condition in the drainage basin (tab. 2.5).

Description	Average % Impervious	Curve Number by Hydrologic Soil Group				Typical Land Uses
		A	B	C	D	
Residential (High Density)	65	77	85	90	92	Multi-family, Apartments, Condos, Trailer Parks
Residential (Med. Density)	30	57	72	81	86	Single-Family, Lot Size ¼ to 1 acre
Residential (Low Density)	15	48	66	78	83	Single-Family, Lot Size 1 acre and Greater
Commercial	85	89	92	94	95	Strip Commercial, Shopping Ctrs, Convenience Stores
Industrial	72	81	88	91	93	Light Industrial, Schools, Prisons, Treatment Plants
Disturbed/Transitional	5	76	85	89	91	Gravel Parking, Quarries, Land Under Development
Agricultural	5	67	77	83	87	Cultivated Land, Row crops, Broadcast Legumes
Open Land – Good	5	39	61	74	80	Parks, Golf Courses, Greenways, Grazed Pasture
Meadow	5	30	58	71	78	Hay Fields, Tall Grass, Ungrazed Pasture
Woods (Thick Cover)	5	30	55	70	77	Forest Litter and Brush adequately cover soil
Woods (Thin Cover)	5	43	65	76	82	Light Woods, Woods-Grass combination, Tree Farms
Impervious	95	98	98	98	98	Paved Parking, Shopping Malls, Major Roadways
Water	100	100	100	100	100	Water Bodies, Lakes, Ponds, Wetlands

Table 2.5 Curve Numbers for Hydrological Soil-Cover Complexes for Antecedent Moisture Condition Class II and I_a = 0.2 S (after Soil Conservation Service 1972).

2.2.2.2 Depression storage

In most cases, runoff is caught in small terrain depressions which play an important role in flood dynamics (Maksimović and Radojković, 1986). Nevertheless the determination and quantification of depression storage is not an easy task, because

infiltration and surface water storage occur simultaneously (Kamphorst and Duvai, 2001), as already stated. Additionally, depression shapes can be complex and the uncertainties of terrain representation should be not neglected.

However, according to Maksimović and Radojković (1986), the depression storage supply can be commonly defined by the equation as

$$s = (i - f) \cdot e^{-\frac{(I_e - F_e)}{S_d}} \tag{2.10}$$

where

- s is the depression storage at time t;
- i is the rainfall intensity;
- f is the infiltration capacity (determined by Horton's equation);
- I_e is the total accumulated rainfall up to time t;
- F_e is the total accumulated infiltration up to time t;
- S_d is the depression storage capacity parameter.

The values of S_d for different types of overland surfaces can also be found in Maksimović and Radojković (1986). These values have to be corrected for impervious surfaces due to wetting.

2.2.3 Overland surface runoff

After subtraction of the losses, the net rainfall is transported on the surface until it enters the sewer system. In particular, initially, rain water starts to accumulate on the surface. When the amount of water is small and the surface tension effect is predominant, the water may be held as isolated pots without occurrence of flow. As rain water supply continues, the surface tension can no longer overcome the gravity force and the momentum input of the raindrops along the slope of the surface. Consequently the individual water pots merge and flow starts downslope (Yen 1986). According to Akan and Houghtalen (2003), such overland flow is a special type of open-channel flow with very shallow depth; all equations developed for open-channel flow remain valid, however there are a few additional considerations that need to be addressed. *Reynolds number* (the ratio between inertial and viscous forces) values are usually small due to the shallow water depths: consequently the regime should be classified as laminar. Nevertheless, there are other phenomena that

affect this process, such as the impact of rainfall drops and flow obstructions (rocks, grass, and litter) which introduce flow disturbances continuously. Moreover, afterwards, overland flow tends to converge to surface preferential flow paths, increasing the flow depth. Accordingly, for the depth range encountered in urban surface runoff, this flow can be laminar or turbulent, subcritical or critical, stable or unstable.

Mathematically such unsteady flow can be accurately described by the Saint Venant equations. This pair of equations of the hyperbolic type, also known as shallow water wave equations, consist of the mass (2.11) and momentum conservative equations (2.12):

$$\frac{\partial Q}{\partial x}+\frac{\partial A}{\partial t}=q \tag{2.11}$$

$$\frac{\partial Q}{\partial t}+\frac{\partial}{\partial x}\left(\frac{Q^2}{A}\right)+gA\cdot\frac{\partial y}{\partial x}=gA\cdot\left(i-J\right) \tag{2.12}$$

where

- $\frac{\partial Q}{\partial t}$ is the local acceleration term;
- $\frac{\partial}{\partial x}\left(\frac{Q^2}{A}\right)$ is the convective acceleration term;
- $g\frac{\partial y}{\partial x}$ is the pressure force term;
- $g\cdot i$ is the gravity force term ;
- $g\cdot j$ is the friction force term;
- x is the longitudinal distance;
- t is the time;
- Q is the flow rate;
- A is the cross-sectional area of channel segment;
- q is the lateral inflow per unit length;
- y is the channel depth;
- i is the slope of the land surface;
- j is the friction slope;

- g is the gravity acceleration.

In detail such equations are based on the following assumptions (Havlik 1996):

- unsteady flow in open channels is one dimensional;
- the fluid is homogenous and incompressible;
- the pressure distribution is hydrostatic;
- the longitudinal axis of the channel is approximated as a straight line. The channel is prismatic, i.e. the channel cross-section and the channel bottom slope do not change with distance. The variations in the cross-section or bottom slope may be taken into consideration by approximating the channel as a series of several prismatic reaches;
- the average channel slope is small and the channel bed is fixed, that is the effects of scour and deposition are assumed to be negligible (for flow routing);
- friction can be described by using the steady-state resistance laws, such as the Manning equation.

The solution of the mass and momentum conservative equations can be obtained numerically. Conventionally the finite difference approach or the method of characteristics are employed. Especially finite difference methods can be divided into explicit and implicit schemes, of which the former are easier to program, but may require very small time steps for numerical stability - Courant condition (Chow et al 1988, Havlik 1996).

However, in practical sense, the use of the full Saint Venant equations to solve individual cases of urban overland surface flow is seldom justifiable. Computational cost is far less a constraint for the use of these equations as compared to the requirements on the detailed catchment and rainfall data. Thus simplification of the equations is required in runoff simulation applications. These are based on certain assumptions that allow simpler approximations of the momentum equation for modeling unsteady flow. If local and convective acceleration can be neglected, then the diffusion wave simplification is valid. If backwater effects are also negligible, then omission of the pressure force term in equation 2.12 is justified and the kinematic wave simplification becomes valid (Schutze et al., 2002).

Table 2.6 presents the simplified flow routing models based on the simplification of the Saint Venant equations.

Flow routing model	Force terms				
	Local acceleration term $\frac{\partial Q}{\partial t}$	Convective acceleration term $\frac{\partial\left(\frac{Q^2}{A}\right)}{\partial x}$	Pressure force term $g\frac{\partial y}{\partial x}$	Gravity force term gS_o	Friction force term gS_f
Full dynamic (DM)	x	x	x	x	x
Convective dynamic	-	x	x	x	x
Diffusive (NM)	-	-	x	x	x
Kinematic (KM)	-	-	-	x	x

Table 2.6 Flow routing models based on the Saint Venant equations (from Leitão, 2009).

In overland flow analysis, kinematic and diffusion models are those with most practical application, among the simplified flow routing models (Maksimović and Radojković, 1986). The kinematic model is the simplest model, which can be used to simulate uniform flow and steady conditions. This model assumes that gravity and friction forces balance each other, ignoring all other terms of the momentum conservative equation. In this way it is possible to model only the translation of a travelling wave. Instead the diffusion model neglects the local and convective acceleration terms but incorporates the pressure term, so can take into account the effects of non-uniform flow. This simplified model can be used to calculate translation, wave attenuation and backwater effects.

Radojkociv and Maksimović (1987), based on the works by Morris and Viera (1981) and Viera (1983), carried out a statistical analysis to assess the applicability of the kinematic and diffusion models for shallow overland flow. The results obtained by these simplified models were compared with the results calculated using the dynamic model (i.e. the full Saint Venant equations). The statistical analysis was carried out using a dimensionless form of the Saint Venant equations based on the values of F^* (eq. 2.13) and G^* (eq. 2.14), known as the dimensionless Froude and Geometric numbers, respectively.

$$F^* = \frac{q_0}{x_0 \cdot \sqrt{g \cdot h_0}} \tag{2.13}$$

$$G^* = \frac{h_0}{q_0 \cdot i / i_c} \tag{2.14}$$

where

- h_0 is the maximum depth;
- x_0 is the reference length;
- q_0 is the maximum lateral inflow;
- i_c is the normal effective rainfall intensity;
- i is the slope surface;
- g is the gravity acceleration.

The results obtained, presented in fig. 2.6, demonstrated that simplified models can be used in a large number of flow conditions.

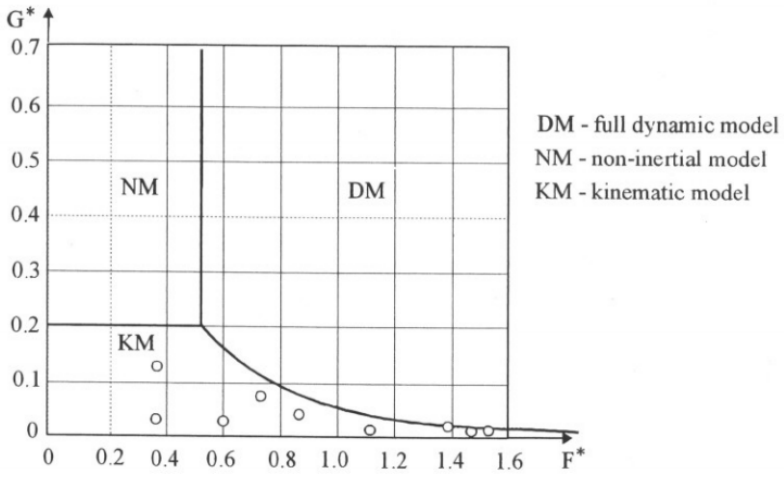

Figure 2.6 Regions of applicability of the kinematics (KM), diffusive (NM) and dynamic (DM) models for computation of overland flow (reproduced from Maksimović, 1996).

More recently other researchers reported similar results. In detail, Ball e Alexander (2006) carried out experimental works in two road catchments in Sidney (Australia) to model street surface runoff. They also found that the results obtained using the kinematic wave simplification to model runoff on road surfaces matched many of the recorded flows.

Alternatively, the modeling of the overland surface runoff can be also carried out by conceptual or hydrologic models, that are based on the principle of conservation of mass and a second function, which usually defines a relationship between stage,

storage, and discharge. Such approaches were particularly applied in the past since the lack of powerful calculation tools forced the use of less detailed models for similar applications.

The most used conceptual routing methods are 1) unit-hydrograph model, 2) time-area model, 3) reservoir model.

1) Unit Hydrograph model

It is based on the premise that a unique and time-invariant hydrograph results from effective rain falling over a particular catchment. Formally, it represents the outflow hydrograph from a unit depth (generally 10 mm) of effective rain falling uniformly over a catchment at a constant rate for a unit duration *D*.

Once derived, the unit hydrograph can be used to construct the hydrograph response to any rainfall event based on three guiding principles:

- Constancy: the time base of the unit hydrograph is constant, regardless of the intensity of the rain;
- Proportionality: the ordinates of the runoff hydrograph are directly proportional to the volume of effective rain;
- Superposition: the response to successive blocks of effective rainfall, each starting at particular times, may be obtained by summing the individual runoff hydrographs starting at the corresponding times.

2) Time-Area model

The time-area diagram is a special case of unit hydrograph (Butler and Davies, 2006). Especially it can be obtained:

- by delineating lines of equal flow ‘travel time’ (isochrones) to the catchment outfall. It is clear that the maximum travel time represents the time of concentration of the catchment itself (t_c).
- by summing the areas between the isochrones so that the response of the catchment can be defined to any rain input.

3) Reservoir model

The flow is modeled by conceptually routing it through a series of linear reservoirs, thereby achieving attenuation of the wave (Viessman et al., 1989).

The stage-discharge relationship is usually computed from information on the channel control, such as by estimating spillway coefficients. In most natural channels, this relationship must usually be calibrated from observed discharge. An exception is the Muskingum-Cunge method, whose parameters are physically based values.

2.2.4 Sewer network flow

The hydraulic processes of the sewer networks can be simulated in more detail rather than catchment processes because the sewer geometry is or should be completely known and the hydraulic phenomena occurring, although abundant and complex, are undoubtedly less numerous. This means that overland surface runoff is usually simulated by conceptual models, whereas the routing of the sewer flow is commonly analyzed by physical-based approaches, i.e. by using the mass and momentum conservative equations.

Nevertheless it is important to underline that such detailed procedures find difficulties in modeling the transition phase between open-channel and surcharged flow. In fact, in similar conditions:

- the discharge-depth relationship is not unique. Let us consider the relatively simple case of steady flow in a circular pipe as an example. The dimensionless discharge-depth relationship for steady, uniform, open-channel flow and the discharge-piezometric pressure gradient relationship for steady uniform flow in a closed conduit is shown schematically in fig. 2.7. In the open-channel flow regime, the maximum discharge does not occur at the depth h equal to the pipe diameter D. It occurs at approximately $h = 0.94\ D$, varying slightly depending on the Reynolds number of the flow. This decrease in discharge when the pipe is nearly filled is due to the rapid increase in wetted perimeter as h approaches D, and the consequent increase in the pipe boundary resistance to the flow. As shown in fig. 2.7, the relationship between the discharge and depth or piezometric

gradient is unique above point E or below point J. Between points J and E a given discharge can have different depths or piezometric gradient.

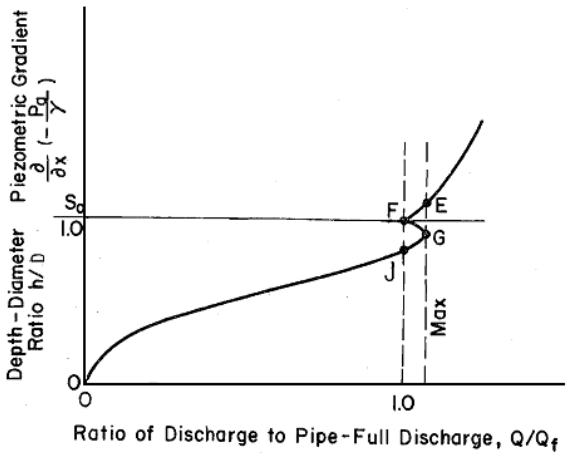

Figure 2.7 Discharge rating curve for steady flow in a circular pipe (from Yen and Pansic, 1980).

- rapid changes of the physical parameters occur. They require the use of very short time steps in order to solve the process equations: consequently the calculation becomes more computationally demanding.

Almost all the models overcome these issues by adopting the "Preissmann slot" technique (Preissmann and Cunge, 1961). In this method the surcharged pipe flow is artificially converted into open-channel flow by assuming the existence of a slot on top and along the full length of the pipe (fig. 2.8).

However the slot width, l, has to be sufficiently narrow so that its volume is negligible, but without generating computational stability problems. In particular the following condition must be respected:

$$l \le l_0 = \frac{g \cdot \Omega}{a^2} \tag{2.15}$$

where

- a is the sound celerity in the water, depending on the features of the liquid and conduit;
- Ω is the cross-sectional area of the pipe;
- g is the gravity acceleration.

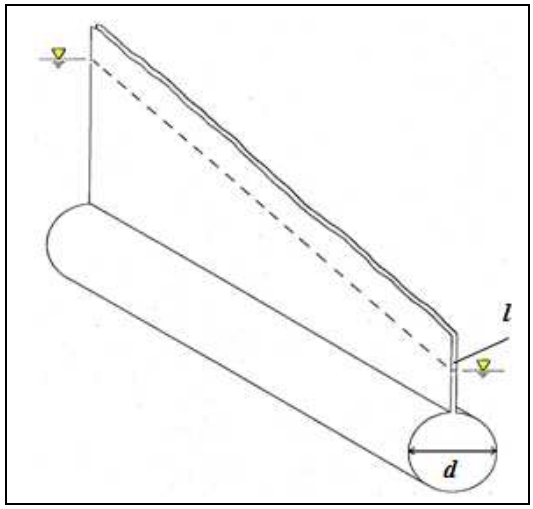

Figure 2.8 Preismann slot (from Yen and Pansic, 1980).

2.3 Limits of conventional urban drainage models in sewer flooding analysis

The use of the rainfall-runoff methods described above is common in the majority of urban drainage modeling software. However, these approaches are far too simple to appropriately model the behavior of an urban drainage system during flood conditions, as stated by Allitt (2001) and Maksimović and Prodanović (2001). In fact they ignore the fundamental concept on which the traditional urban hydrology is based on, i.e. the interaction between the surface network (linked by roads, sidewalks and other features of the urban landscape) with the buried drainage system (Butler e Davis, 2000). For example, in previous versions of MOUSE (DHI, 2000) and Infoworks CS (Wallingford Software, 2006), floodwater is treated as a stagnant volume which is temporarily stored in a virtual reservoir above the surcharged model node (manhole or sewer inlet). Especially, as shown in fig. 2.9, this water will then return to the sewer system when the system has again enough capacity to carry out the stored volume (Mark and Djordjević, 2006). In this way the surface inundation depth is finally determined by conceptual volume-depth rating curves.

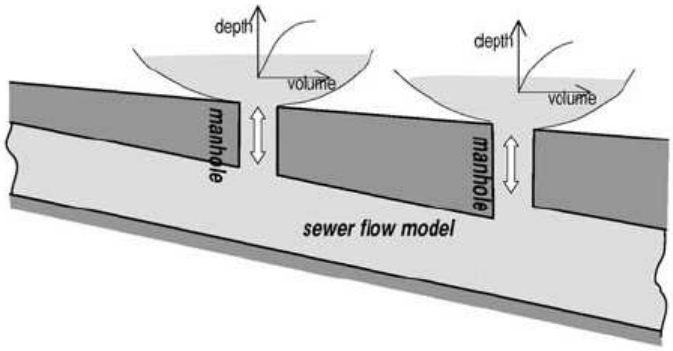

Figure 2.9 Simulating approach followed by conventional urban drainage models (from Hsu et al., 2002).

Although such a modeling of the drainage system can yield acceptable outcomes, it is inadequate during heavy storms because the overland flow occurs not only from direct runoff (i.e. rainfall) but also from surcharged sewer networks, that is it is unthinkable that stormwater, once entered the sewer system, cannot leave this system and return to the surface. For this reason, the water cycle processes illustrated in fig. 2.1 are not suitable to represent realistically the sewer flooding.

Accordingly, afterwards, further modeling approaches were developed. In detail, initially, such procedures treated the water in the sewer system and on the ground surface separately, i.e. they assumed that the surcharge-induced overland-flow could not return to the sewers, as shown in fig. 2.10

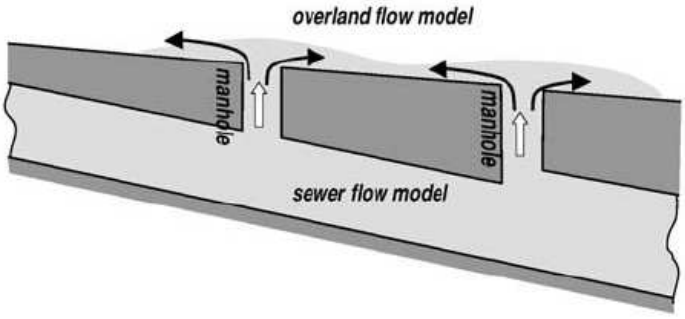

Figure 2.10 Simulating approach based on the separation of the surcharge-induced overland-flow and sewer flow (from Hsu et al., 2002).

A typical example is the model developed by Hsu et al. (2000) that will be briefly reported in the following. The authors linked a complex 2D diffusive-wave surface flow model to components of the EPA SWMM model and a pumping station model

to generate detailed dynamic information of surcharge-induced surface flooding in Taipei, Taiwan.

The parameters of the model were calibrated and verified for discrete storms, in particular the storm event relative to the typhoon Zeb (15th October 1998) was studied in more detail. This rainfall event, recorded by two rain gauges located inside the Taipei basin plain, was characterized by a total rainfall of 400 mm, a duration of 30 h, and a peak rainfall intensity of 41 mm/h.

There were no precise records of inundation areas and depth changes during the event. However, inundation zones in Downtown Taipei, which are plotted in fig. 2.11 (a), were established by the Taipei Government after the event.

The simulation results are also shown in fig. 2.11 (b).

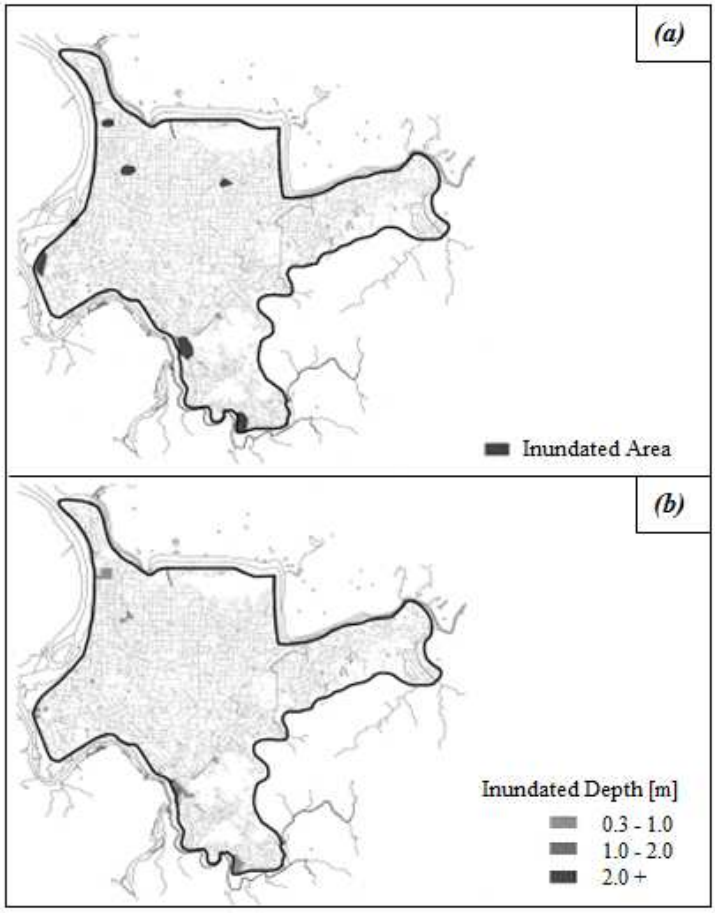

Figure 2.11 (a) Surveyed inundation zones of Downtown Taipei for Typhoon Zeb. (b) Simulated inundation zones of Downtown Taipei for Typhoon Zeb.

The comparison between the simulation results and the surveyed inundation zones reveals that most inundation situations were well simulated, consequently such a modeling should be assumed correct. Nevertheless these results are right because the Taipei basin is flat, in fact the average elevation of the area is only four meters above the mean sea level and its ground elevation decreases mildly northward with a slope of approximately 0.1%. In similar situations it is still acceptable to consider that the surcharge-induced overland-flow could not return to the sewers, because it has little influence on the simulation accuracy. Instead, for regions with local depressions, a bidirectional interaction between surface runoff and sewer flow must be considered, i.e. the water does not only overflow from the surcharged sewers but may also flow back to the sewers (fig. 2.12). Otherwise, if these processes are neglected, the surcharged water would be shown as accumulating in the depressions and unable to drain, and the flood extent would be overestimated.

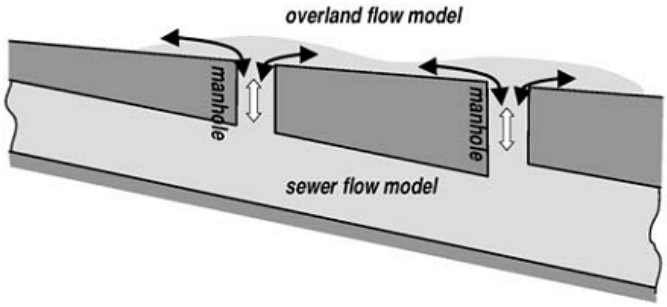

Figure 2.12 Bidirectional interaction between surface runoff and sewer flow (from Hsu et al., 2002).

Just Hsu et al. expressed such considerations in another research faced in 2002: in particular this study improved on the previous inundation model by coupling the overland and sewer flow models. As shown in fig. 2.12, the improved urban inundation model allowed for the surcharged water to reenter the sewer system through manholes which were unsurcharged.

In this case the model was tested by simulating the floods occurring in Mucha area, located in the southern part of Taipei City, as a result of the Typhoon Xangsane (November 2000). This rainfall event was characterized by a total rainfall of 504.5 mm, a duration of 24 h, and a peak rainfall intensity of 68 mm/h.

There was no measuring equipment to record the inundation area or water depth during the flood. However, also for this situation, the inundation zones were

surveyed and delineated by the Taipei City Government after the event. The flood extent established by the post-event survey is illustrated in fig. 2.13 (a) and the simulated result by the improved model is shown in fig. 2.13 (b).

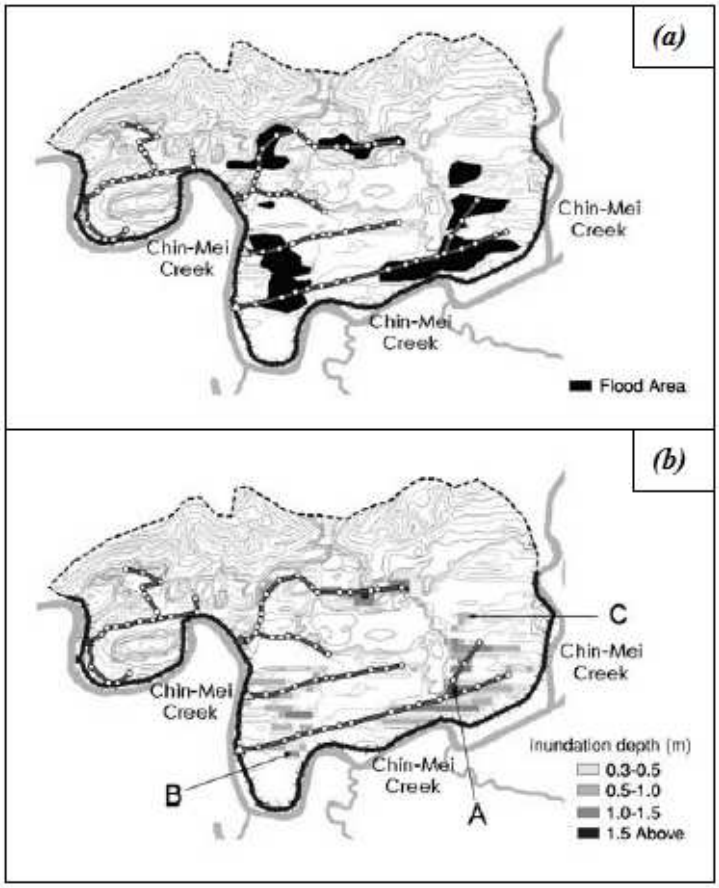

Figure 2.13 (a) Surveyed flood extent from the Typhoon Xangsane event. (b) Simulated flood extent and depth during the Typhoon Xangsane event.

The inspection of simulation results and surveyed inundation zones revealed that most of inundation situations were properly simulated by the model.

The authors compared also the temporal variations of total inundation volumes predicted by the two developed models in order to evaluate if there were differences between the findings. Figure 2.14 shows that the earlier model's failure to simulate surcharged water reentering the sewer system resulted in over estimation of total inundation and flood duration.

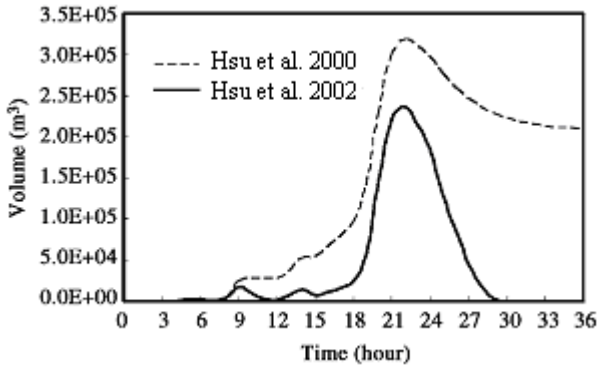

Figure 2.14 Comparison of total cumulative inundation volume of Mucha area during the Typhoon Xangsane event.

In particular, by using the improved model, the maximum inundation depths were predicted to be shallower in upstream local depressions. Instead, in depressions with upstream manholes, the surcharge could be increased by the flow that reentered the sewers at upstream inlets which were unsurcharged. An example of this behavior is reported in fig. 2.15, which compares the inundation depth hydrographs calculated by the two models for a local depression, marked as *A* in fig. 2.13 (b).

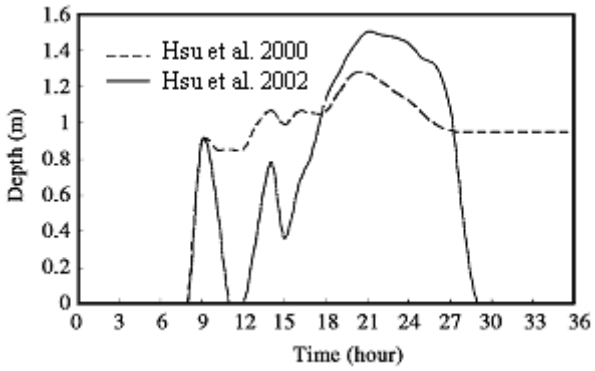

Figure 2.15 Comparison of the inundation depth variation at point *A* during the Typhoon Xangsane event.

The figure shows that the improved model predicted smaller inundation depth than the earlier model during all the storm duration, due to the fact that water could be drained out through inlets when the sewer capacity was available, except for the time range comprised between the 18th and 27th hour. As already stated, this strange result was justified by the sewer system interaction. In fact the upstream conduit discharge increased due to the runoff that flowing back to sewers at upstream unsurcharged inlets from overland flow caused by other surcharged manholes, thus

the surcharge increased and caused more serious inundation at point *A*. Consequently the maximum inundation depths would have been underestimated without taking the dynamic water interaction into consideration.

Accordingly, in conclusion, it is evident as the consideration of a bidirectional interaction between the sewer network and the overland flow is an indispensable condition for modeling reliably sewer flooding processes. Just this principle is at the bottom of the *dual drainage* approach, that will be deepened in the following.

2.4 Dual drainage concept

According to the definition of dual drainage put forth by AMK Associates (2004) and others (Stephenson, (1987); Stephenson, (1989); McBean et al., (1985); Wisner et al., (1981); Wisner and Kassem, (1982); Ellis et al., (1982)), urban stormwater drainage systems can be described by two distinct but linked flow systems (fig. 2.16):

4. the overland flow network, also referred as *major system*, which comprises terrain depressions or ponds, streets, ditches and various natural and artificial channels;
5. the sewer network, also called the *minor system*.

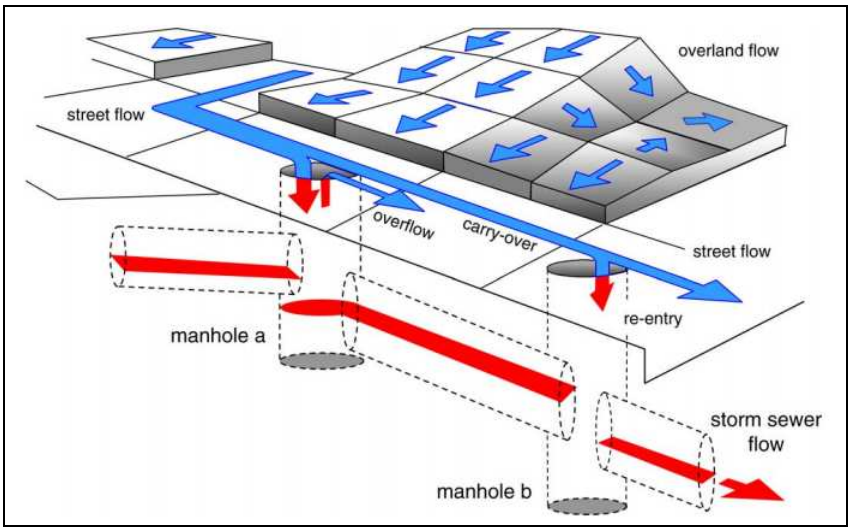

Figure 2.16 Schematic representation of the dual drainage concept (from Smith, 1993).

The minor system is normally designed to carry the runoff from a storm of 2–10 year return frequency, whereas the surface system is designed to handle events of 25–100 year return frequency. These systems are modeled as two dynamically interconnected networks. In fact manholes and sewer inlets function as points of flow exchange between sewer and overland systems (fig. 2.16).

According to Smith (2006) the dual drainage concept started to be discussed, developed and implemented before 1980s in various countries. In fact Heaney et al. (1975) and later AMK Associates (2004) report that perhaps the first mention of dual drainage for urban areas is found in the design manuals of the city of Denver, Colorado (Denver, 1969). These design criteria described the linkage of the major and minor systems. However, the major system criteria were limited to providing proper street flow gradients and capacities for the safe conveyance of surface flows.

Discussing similar criteria, McBean et al. (1985) noted that design manuals in Canada (Environment Canada, 1976) recognized that dual drainage system responses could not be easily modeled within a single simulation run. The greatest difficulties blocking this capability in a single model run were the inability of then-current techniques to handle the mismatch of flow directions between the surface and subsurface systems, and that surcharged storm sewers could create lags and increased flow durations.

Instead Kidd and Helliwell (1977) pointed out the complexities related to the interactions modeling between the surface and the sub-surface phases by stating that, unfortunately, “there is no clear-cut interface between the two phases”.

Given this deficiency, the traditional approach to model the complex interactions between the major and minor systems consisted of two stages (Ellis et al., 1982). In the first stage of designing an urban drainage system for say, a 100 year event, the minor system was designed to convey the discharge from a five-year event. Sewer pipes were sized until an acceptable level of performance was achieved. Next, the five-year hyetographs were subtracted from a 100-year design event hyetographs and the subsequent rainfall was input to the hydrologic model. The resultant surface flows were used to design the components of the major drainage system. Assuming a common outfall point, the flows from the major and minor systems were added to produce a total system response.

It is evident how this approach led to incorrect responses, such as excessive infiltration and evaporation volumes, because the input regimes were not designed to recognize each other's presence (Ellis et al., 1982). Consequently, later, further researches have been focused on the study of the interactions between the two systems (fig. 2.17): in particular several efforts have been directed at improving numerical solutions for existing hydraulic models and at developing new ones, whereas other researches have examined the definition of the surface flow paths in urban areas.

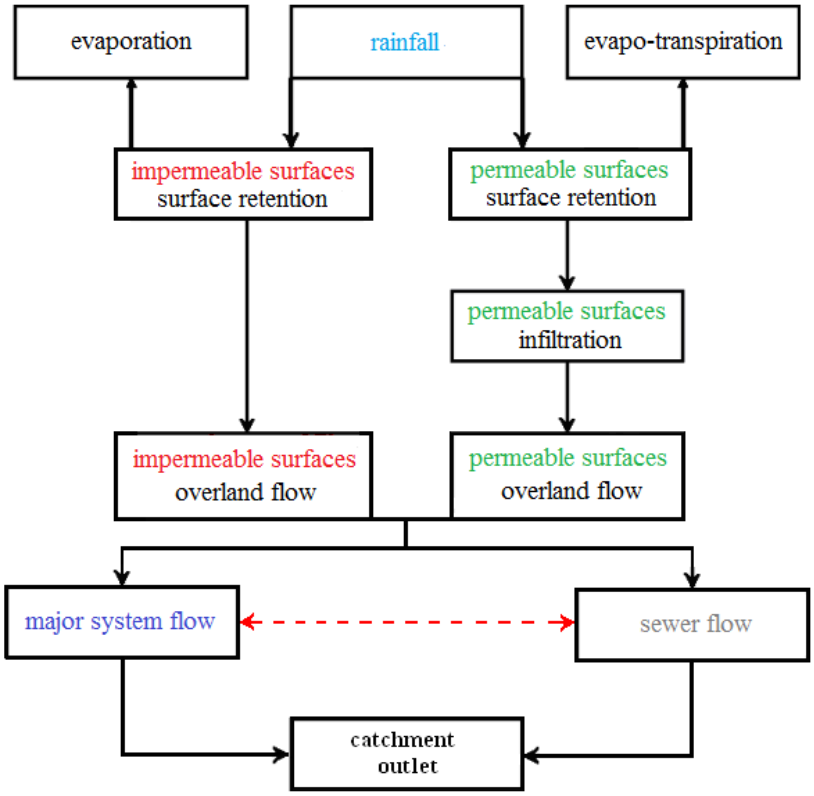

Figure 2.17 Dual drainage modeling procedure.

2.4.1 Studies on dual drainage concept

The late 1970s and early 1980s saw the beginning of significant advances in the hydrologic and hydraulic modeling of urban drainage systems. In fact, in some models, the complete equations of motion were solved for free-surface and surcharged flow in the storm sewer system.

Kassem (1982) developed a comprehensive mathematical algorithm for the simultaneous modeling of the major and minor drainage systems. His approach

contained a finite-difference formulation of the kinematic wave approach for unsteady free surface sewer flow, and a full solution of the Saint Venant equations for surcharged storm sewer flow.

That same year, Roesner and Shubinski (1982) showed that updated versions of EXTRAN could be used for integrated surface and storm sewer flow routing, given that the problem is properly specified. They provided example simulations showing surcharge and surface flooding conditions. During surface flooding, the excess amounts were allowed to exit the manhole and flow along the street channel to the next down-hill inlet to the sewer system. Kinematic routing was used to convey the surface flooding volumes.

Jacobsen and Harremoes (1984) presented a comparison of two storm sewer models for the computation of surcharge. They were able to test these two models on a well-instrumented storm sewer line that frequently surcharged and produced street flooding. They concluded that the head loss parameters are very important and are model specific rather than universal. In a related research, Guo and Song (1990) investigated surge in urban storm sewers and in-line storage elements, a phenomena that can lead to manhole-cover blow-offs and street flooding. They used a mixed transient flow model to simulate the surge movements in the main sewer line in Chicago, Illinois.

In an important development, Djordjević et al.(1991) developed a method to simultaneously solve the equations of storm sewer and street flows. They used the diffusive wave approximation of the full Saint Venant equations to model both flow phases. Their work showed that the flows in the storm sewers can be significantly affected if the excess volumes are allowed to flow along the street rather than being stored in a fictitious basin above the surcharging manhole.

Takanishi et al. (1991) reported on the development of two models that account for surface, river, and storm sewer flows in urban environments. Sewer flows were treated as one-dimensional, while overland flows were modeled as two-dimensional (2D). The authors were able to simulate surcharge at various system points and subsequent inundation.

Pankrantz et al. (1995) compared three dual drainage modeling approaches to solve complex street flooding situations in the city of Edmonton, Canada. The authors

computed runoff volumes using three hydrologic models: the SWMM Runoff Block, the OTTHYMO-89 model, and the PC OTTSWM model. EXTRAN was used in all three cases to rout flows through the storm sewer network. They concluded that after calibration, all three models provided adequate simulations of street flooding in low areas.

Afterwards, further models were introduced, such as those developed by Hsu et al. (2000), already reported above, and the SIPSON model (acronym for Simulation of Interaction between Pipe flow and Surface Overland flow in Networks) by Djordjević et al. (2005). In detail, this last one simulated simultaneously the sewer and overland flow systems as an horizontally and vertically looped network. The simulation model applied the Preissmann four-point implicit finite difference method for flow in pipes and surface channels and the conjugate gradient method as the node matrix solver. The most questionable assumption of the SIPSON model was that the surface flow was one-dimensional. However, the modeling approach was justifiable as long as the surface flow was within the street cross-section and the street profile was approximately prismatic. Otherwise, higher-dimensional models were required (Gourbesville 2001).

At the same time, while significant advances were being made in the mathematical linkage of surface and sewer hydraulic models, other researches were engaged in introducing adequate criteria for defining realistic surface flow paths in urban areas. Such issue was initially pointed out by Huber (1984) in his commentary on the work of Pethick (1984): in fact he stated that great effort had often to be made to identify the surface flow pathway when using dual drainage technique.

Djordjević et al. (1991) expressed an important point in this regard, stating that “the present models make sense only if reliable input data are available. Therefore, in this context, the use of GIS seems to be inevitable in order to realize their full potential”.

Therefore GIS tools and terrain analysis algorithms ushered in a new era of watershed modeling, and gradually impacted the analysis of urban storm water drainage with all its complexities. These new tools paved the way for more comprehensive solutions to dual drainage problems, since one of the major issues was that storm sewer systems did not always follow the surface drainage patterns

(Hsu et al., 2000; McBean et al., 1985) and overland flow paths were modified by man-made features (Djokic and Maidment, 1991).

Initial efforts looked at GIS tools to derive urban terrain descriptions and to define parameters of existing urban hydrologic models. Along the way, new models based on GIS elements and using automatically defined urban flow paths were developed.

In an early effort to do urban dual drainage runoff modeling using GIS-type computational elements, Ichikawa and Sakakibara (1984) developed a gridded rainfall-runoff model using 10 m cells. Storm sewers were linked to the surface system via manholes at specified cell locations. All surface flows were assumed to enter the sewer system at the manhole locations with no by-pass or carryover flow. Flow simulations on small urban watersheds agreed will with observed data. Their use of very small computational elements is significant in that it set the stage for the 1 m to 5 m grid size recommended years later by Prodanovic et al. (1998) and Mark et al. (2004).

Bergmann and Richtig (1990) continued the theme of Ichikawa and Sakakibara (1984) by developing a gridded overland flow model linked to both a channel routing capability and a storm sewer model. They used a hydraulic channel routing model and a simple hydraulic sewer model.

Djokić (1991) and Djokić and Maidment (1991) interfaced an expert system and the Arc/INFO GIS to evaluate the connectivity and capacity of the storm sewer network for a local jurisdiction. They reported that individual drainage areas for each inlet were too complex to be defined automatically by terrain analysis procedures. Instead, manual methods were used given the complexity of the urban flow paths and the imprecise terrain information.

Huber et al. (1991) attempted the integration of the rainfall-runoff model of the EPA SWMM with the Arc/INFO GIS and AUTOCAD. Their purpose was to assess the ability of both systems to define input variables such as flow lengths and drainage areas as needed by SWMM. The authors noted that either package could be used to derive input to SWMM, and that user familiarity would probably be the deciding factor in the choice of the software to be used.

Smith (1992) and Smith (1993) developed a simultaneous solution of the equations for rainfall-runoff conversion, overland flow, street flow, and storm sewer flow in the

context of a gridded GIS data structure. Runoff volumes in excess of the storm sewer system were allowed to flow downhill to other inlets. Time shift routing was used as a simple method to route sewer flows. Soon after, Smith and Vidmar (1994) derived automatic GIS based procedures for defining small drainage basins and surface flow paths for urban areas. They modified natural-basin terrain analysis techniques to account for man-made low-relief features such as streets which can intercept and redirect surface flows apart from the dominant topographic gradient as described by Djokić and Maidment (1991). A 12 m grid size was used to describe the land use and urban topography.

Elgy et al (1993) reported on progress to use GIS to define the input necessary for two complex, physically based storm drainage models. The study recognized the need to account for the flow diversion effects of streets and buildings. To accomplish this, a gridded terrain model with 1x1m resolution was used to describe the dominate terrain gradients, agreeing with the spatial resolution suggested by Mark et al. (2004). All terrain cells covered by building foot prints were artificially raised by five meters and all streets were lowered by 0.5 m. Flow simulations based on GIS derived model parameters agreed well with simulations based on manually derived parameters.

Prodanović et al. (1998) reported on their approach to solve the problem of full interaction between the surface and subsurface flow components. They presented a detailed description of the GIS processing steps required to implement a dual drainage model. Such studies were at the bottom of the AOFD methodology (acronym for Automatic Overland Flow Delineation), developed later by the Urban Water Research Group (UWRG) of Imperial College London (ICL) in cooperation with the University of Belgrade and the University of Exeter (Maksimović et al., 2009). The concept is based on GIS analysis of Digital Terrain Model (DTM) so that features crucial to the identification of flood vulnerable areas (pond) and preferential overland flow paths and their geometric characteristics are computed. This representation of overland flow networks can then be coupled with physically-based sewer network model in order to model pluvial urban flooding realistically.

Currently this approach seems to be one of the most accurate methodologies for the automatic definition of the major system. For this reason it was adopted for the

experimental applications reported in chapter 3, where two different hydraulic modeling of the drainage system of a same monitored catchment were performed. The first model was developed by following the classical hypothesis according to which the drainage system is composed only of the sewer system, that is to consider that stormwater, once entered the sewer system, can no longer leave this system coming back to the surface. Instead the second model was based on the dual drainage approach, i.e. it was assumed that the urban drainage system was composed of a surface network and the sewer network.

Accordingly, in order to better understand the applications carried, the following paragraphs were addressed to describe in more detail the AOFD procedure.

2.5 One-dimensional DTM-based overland flow network delineation: AOFD concepts

The surface overland flow network can be generated through the following operations (fig. 2.18):

1. preparation of DTM data: DTM has to be "hydraulically" appropriate, i.e. without large numbers of unnecessary flat areas and sinks and also with the correct alignment of slopes.
2. identification of ponds and flood vulnerable areas: the modified DTM is subsequently used to identify the location of depressions or ponds, and to define their depth (elevation)-volume relation. These ponds define possible flood candidates of vulnerable areas.
3. connectivity analysis: the DTM which also includes urban (man-made) features such as streets and buildings is used with an algorithm for defining surface pathways. These pathways connect the previously identified ponds in order to form a "surface flow network".
4. assessment of pathway geometry: suitable prismatic shapes, representative of channel cross sections are determined from the DTM in the vicinity of the pathway. The cross-section quantifies hydraulic capacity of surface flow paths.

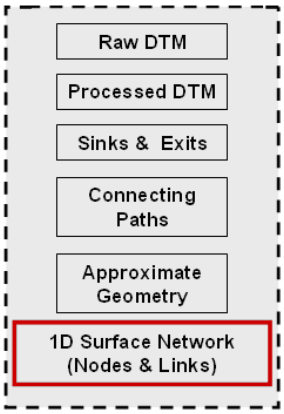

Figure 2.18 Schematic representation of the steps to be followed in order to define the overland flow network by AOFD.

In particular only the last three steps can be faced through the AOFD tool, whereas the enhancement of the DTM is an external analysis that must be carried out in a precedent phase.

1) Preparation of DTM data

In a broad sense, a DTM can be understood as a computerized ground elevation model consisting of a set of elevation points defined by x and y (location), and z (elevation) coordinates (fig. 2.19).

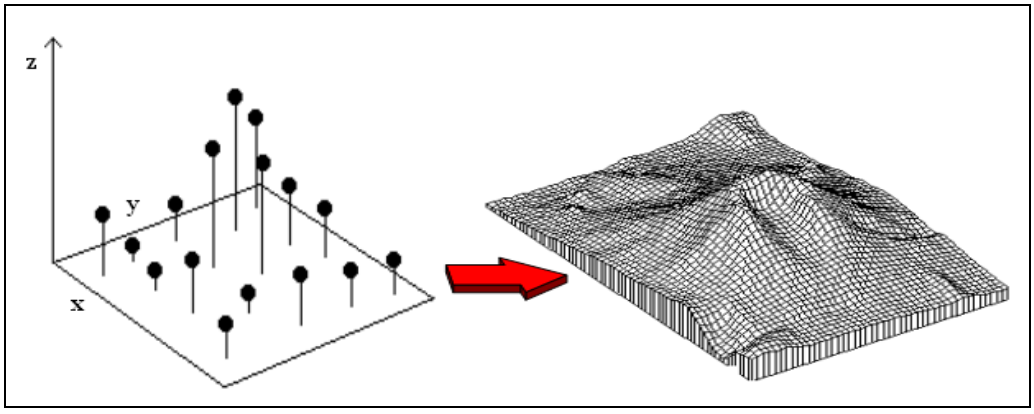

Figure 2.19 DTM definition.

Especially DTMs are generally stored in one of the two data structures: TIN or rectangular grid format.

TIN is basically a network of triangles generated by connecting elevation points available for the area of interest; the face of each triangle represents a small area of the surface (fig. 2.20).

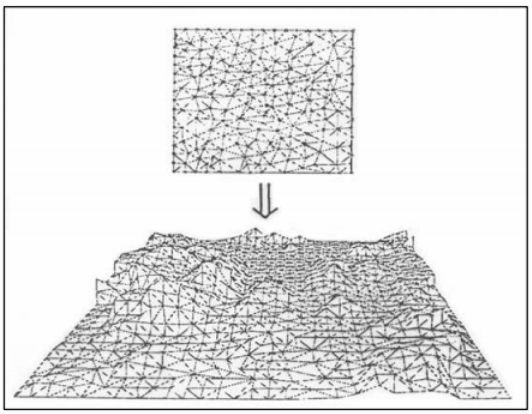

Figure 2.20 TIN representation.

The generation of TIN, called triangulation, must follow the Delaunay criterion (Delaunay, 1934), as the criterion optimizes surface representation. The Delaunay triangulation specifies that any circle around three points in a triangle will not include any other point.

According to Burrough and McDonnel (1988) and Robinson (1994), TINs are better suited to hydrology application than raster DTMs because they have the ability to accommodate more realistically the sudden variations of terrain. However, the computational performance of spatial analysis using TIN models is significantly slower and more complex when compared to regular grid DTM.

For this reason regular grid (or raster) DTM is preferred in hydrologic modeling (fig. 2.21).

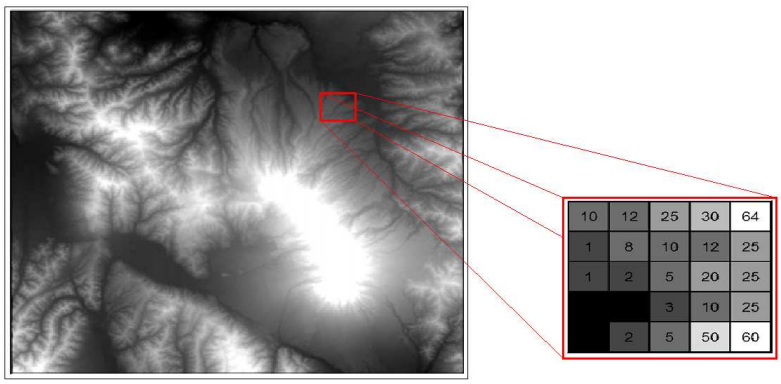

Figure 2.21 Raster DTM representation.

In fact use of regular grids offers the advantage of speed of the process and precision and reproducibility of the results (Tribe, 1992; Wilson and Gallant, 2000). Another advantage is the possibility of interpolation values in the case of data scarcity. However, also in this case, there are some disadvantages to report (Rousseaux, 2004; Vazquez and Feyen, 2007):

- DTM resolution (the size of the grid mesh) affects the storage requirements, hence computational efficiency and the quality of results;
- spatial resolution is fixed, and square grids cannot handle abrupt changes in elevation easily;
- the computed flow lines (or computed boundaries) tend to zig-zag across the landscape and increase the difficulty of calculating pathways length (and areas) accurately.

In particular raster DTMs can be present in different forms: DSM, DTM and DTM_b. The DSM is the acronym for Digital Surface Model and represents the surface elevation with terrain features represented, such as vegetation, buildings and other man made features.

DTM is often referred to as the bare earth representation: in fact they are generated from DSMs using filtering algorithms (Sithole and Vosselman, 2004). Such methods have their own advantages and drawbacks which depend on how they identify the points that belong to the bare earth and those that not. Sithole and Vosselman (2004) presented the results obtained by comparing several DTM filtering methods. They concluded that some methods produce better results than others on specific situations; however, no filtering method is better than others overall.

DTM_b (Digital Terrain Modeling with buildings) stands for the bare Earth (DTM) representation including the representation (elevation) of buildings. Zhilin (1992) and Li (1994) showed that using these elements to create DTMs increase the adequacy of terrain surface for hydrologic studies (fig. 2.22). Instead this representation can be ignored in the cases where it is possible to believe that the water flowed into most of the houses during flooding.

Figure 2.22 A 3D view of the DTM for Ballerup, Denmark, with streets and houses (from Mark et al., 2004).

Mark et al. (2004) reported as major roads must also be included in such DTMs, as the streets act as drains the surface flooding (fig. 2.23). In fact the maximum simulated water levels tend to be reduced by up to 60 cm when streets are considered.

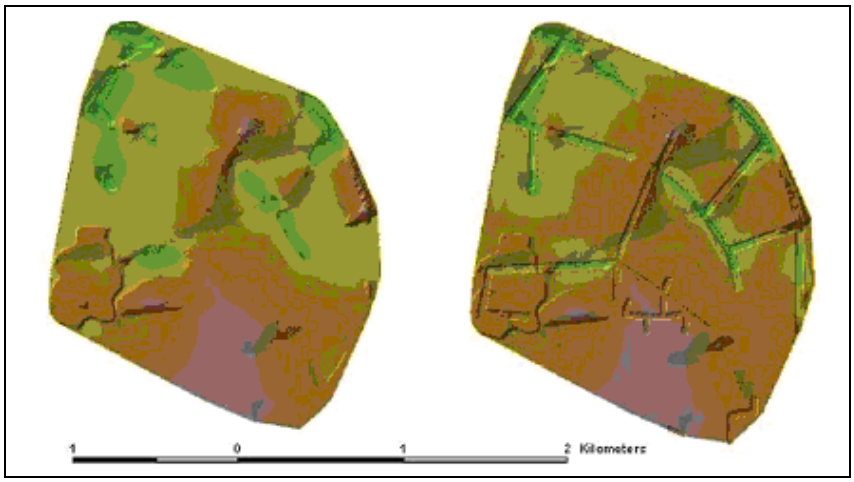

Figure 2.23 The DTM for Dhaka City, without and with the road system (from Mark et al., 2004).

A different approach to take into account such aspects is to assign different roughness coefficients to the areas occupied by buildings. However, various studies concluded that this approach is not very effective (Haile and Rientjes, 2005; Tsubaki et al., 2006). Instead Chen et al. (2008) developed a methodology based on the ratios of building area and grid cell area to include the effect of buildings in 2D overland flow simulations. The relative position of the buildings in the grid cells is also taken

into account by their method; especially they found that the use of these ratios allows the use of coarser grids in simulations without losing the accuracy usually obtained using finer grids.

In this thesis all spatial operations involving DTMs were implemented for the rectangular grid format. In particular the presence of the buildings was taken into account by adding a 10 m elevation directly to the areas really occupied by the buildings themselves in the DTM, as described in more detail in chapter 3.

It is evident how the performance and reliability of surface overland flow models are highly dependent on DTM quality in terms of accuracy and resolution (Maksimović et al., 2009). Physical processes such as surface flow, surface retention, and surface conveyance along preferential pathways require in fact high quality terrain representation data, e.g. DTM with horizontal resolution smaller or equal to 5 m, in order to properly describe the urban features (streets preferably +/- 5 cm vertical resolution). Therefore the best approach would be to produce a custom tailored DTM with a pre-specified resolution (Garbrecht and Martz, 2000). However, in the majority of the cases this solution is cost prohibitive, thus the usual procedure is to correct the DTM data set that is already available.

In fortunate circumstances one can have the DTM of the same area from two sources: the first one from LiDAR measurements (for example) and the second one generated from the contour lines. If both data sets cover the study area it is always appropriate to use the highest detailed data, i.e. the LiDAR DTMs. Instead if the area of interest is only partly covered by a high resolution data set (LiDAR for example) but completely covered by a low resolution DTM, different options can be chosen. One option is to use only the low resolution data set. In this way no discrepancies are identified, however the high resolution data set, which are of paramount importance in surface flow modeling, is not used. A second option is to merge the two data sets: (*a*) a simple merge, (*b*) averaging DTM elevations on the overlapping areas, (*c*) a weighted average over a specified buffer along the boundary, or (*d*) change only the low resolution data set based on the information of the high resolution. In this last case, only the low resolution data set is changed and adapted to the high resolution data set.

Nevertheless it is important to emphasize that the use of very detailed DTMs, such as LiDAR ones, favors the presence of a greater number of errors inherent to the acquisition and interpolation processes of the elevation data, such as pits or flat areas (Lindsay and Creed, 2006). Pits are cells that have no lower adjacent cells. Consequently, there is no downslope flow path to an adjacent cell. On the other hand, flat areas are characterized by a set of adjacent cells with the same elevation.

These errors can hamper automatic flow path delineation algorithms, and subsequently compromise the urban drainage system hydraulic simulations. Therefore they need to be solved by keeping to a minimum changes and smoothing techniques within the DTM, such as depression filling and artificial sloping of flat terrain. In particular Freeman (1991) presented two main approaches in dealing with depressions and flat areas in DTM processing. The first is to assume depressions and flat areas in a DTM as real terrain features that need to be considered as such during drainage analysis. The second considers them as spurious features that should be corrected or removed prior to drainage analysis, so a "depressionless" DTM has to be created. An approach in between these two views, the pond filtering procedure, has been developed in the AOFD and will be reported in more detail in the following paragraph.

2) Identification of ponds and flood vulnerable areas

In most cases, flood events occur during extreme rainfall when surface runoff is combined with surcharged water from the sub-surface drainage system. This exceedance flow is routed along the natural preferential overland flow paths and can subsequently accumulate in local depressions (ponds). These ponds are dynamic features (the amount of water changes in time) as they can be isolated or mutually connected, and the flow pattern into and out of ponds may change quickly during and after a major storm.

In detail the AOFD utilizes the DTM raster image in order to identify and analyze such flood vulnerable areas. The algorithm developed for this purpose searches the entire DTM and identifies the local points with elevation lower than surrounding areas. Based on the DTM, the pond boundary and storage for each low point is

delineated using an iterative “grow-up” routine. The natural exit point is identified as the termination criterion for the pond delineation (fig. 2.24).

During the pond delineation step, potential flow exchange points between overland and sewer systems are also identified to enable bidirectional flow link (Prodanović, 1999); these points are sewer inlets located within ponds.

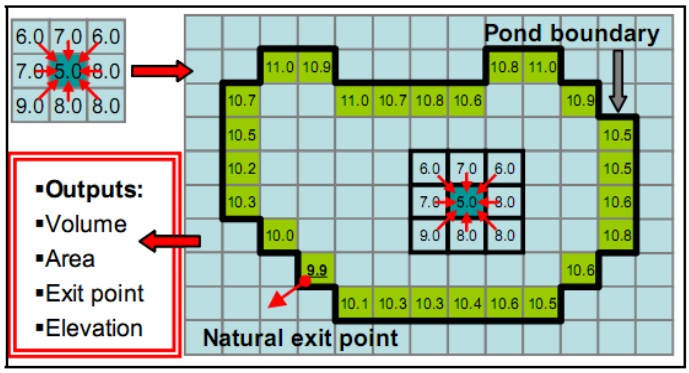

Figure 2.24 DTM-based process of identification of flood prone areas (from Maksimović et al., 2009).

In particular three types of pond delineation were developed within the AOFD methodology (fig. 2.25): (*i*) considering the DTM total area, (*ii*) considering only the area within the catchment boundary, and (*iii*) considering only the area within the catchment boundary and taken into account the sewer network. The main difference between the option (*ii*) and option (*iii*) is the inclusion of the existing underground network. With option (*iii*) ponds can have multiple exchange flow points: one natural output point as identified in option (*ii*) which represents the overland pond exit point, and one flow exchange point per sewer inlet (or manhole) within pond area.

When analyzing a high resolution DTM (e.g. 1x1m) it is very likely that a large number of small ponds will be generated. They result either from existing pit cells or errors in the DTM. Consequently statistical analysis of small pond removal is needed in order to reduce computational burden. However such removal has to be kept under control, otherwise large amounts of storage will be ignored in the simulation.

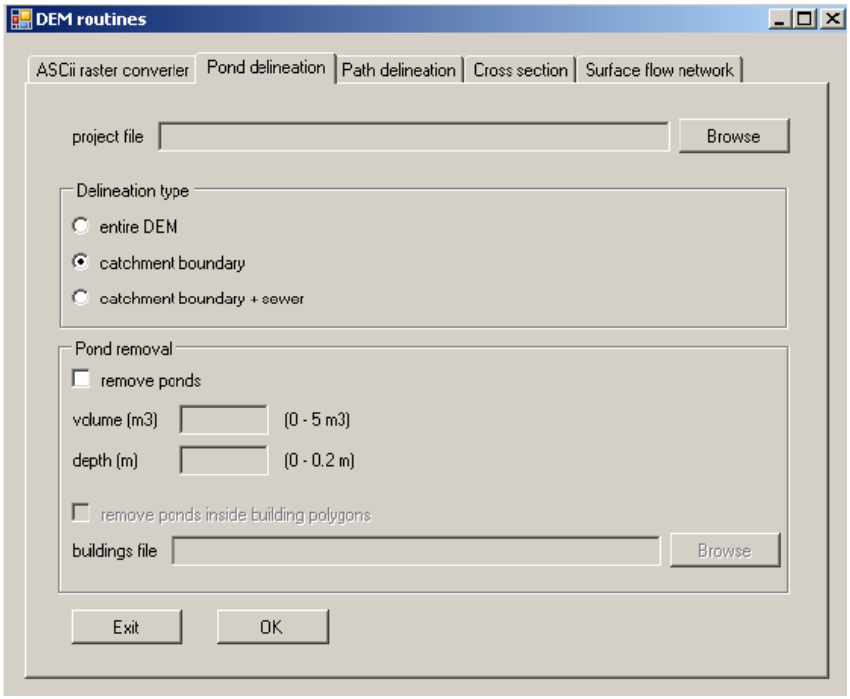

Figure 2.25 Interface of the pond delineation procedure.

The conventional method for pit cells removal in GIS is to fill all little ponds (sink) in the DTM with a threshold depth. Nonetheless, filling DTM will create flat areas which are unfavorable for determination of flow direction, as discussed previously. Instead the AOFD enables to select a combination of threshold volume and depth of delineated storages (fig. 2.25). Ponds smaller and shallower than the thresholds are taken out and the DTM remains untouched to keep slope features required for the pathway delineation procedure. An example of the pond removal is shown in fig. 2.26.

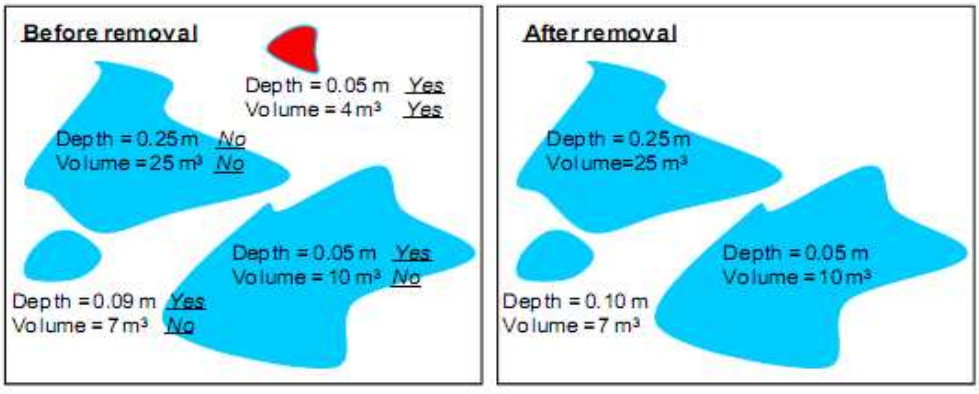

Figure 2.26 The pond removal with 0.10 m depth and 5 m^3 volume thresholds.

The ponds to be discarded have to satisfy both thresholds of depth and volume to ensure that shallow pond with big storage and deep pond with small surface area are not excluded.

Finally, in this phase, the tool enables also to remove the ponds located inside a building area. This particular case occurs when there are gardens or roof storage features constructed inside the building boundary. These storages can be modeled as initial losses from the effective rainfall surface retention, but in this model consideration they have no surface linkage to the overland drainage network. Therefore they have to be discarded from the surface runoff network.

3) Connectivity analysis

The urban surface is a complex array of different types of permeable and impermeable surfaces, but typically comprises roadways and footpaths that are lower than the surrounding areas. Such features can transfer flow over significant distances. Thus flooding can occur at locations that are remote from the source of the flood water.

Overland flow accumulates in depressions and once the top level of the depression is reached, it will overtop and generates a new surface flow. This flow can overflow directly into an adjacent depression (overflow case), flow along a connecting (preferential) pathway until it enters another depression or enter into the sewer network via gulley inlet or manhole (or even reach the catchment boundary).

The AOFD methodology delineates all these overland flow paths starting at the pond's natural exit points or at sewer inlets and manholes in the case of surcharged sewers. Especially the flow path delineation method was originally developed by Prodanović (1999). This algorithm is an adaptation of the *rolling ball* algorithm (Lea, 1992) and delineates overland flow paths by preferential flow directions based on terrain aspect, taking into account the presence of buildings and other features of urban fabric which are represented within the DTM.

In particular, in the AOFD methodology, two overland flow path delineation options are available (fig. 2.27).

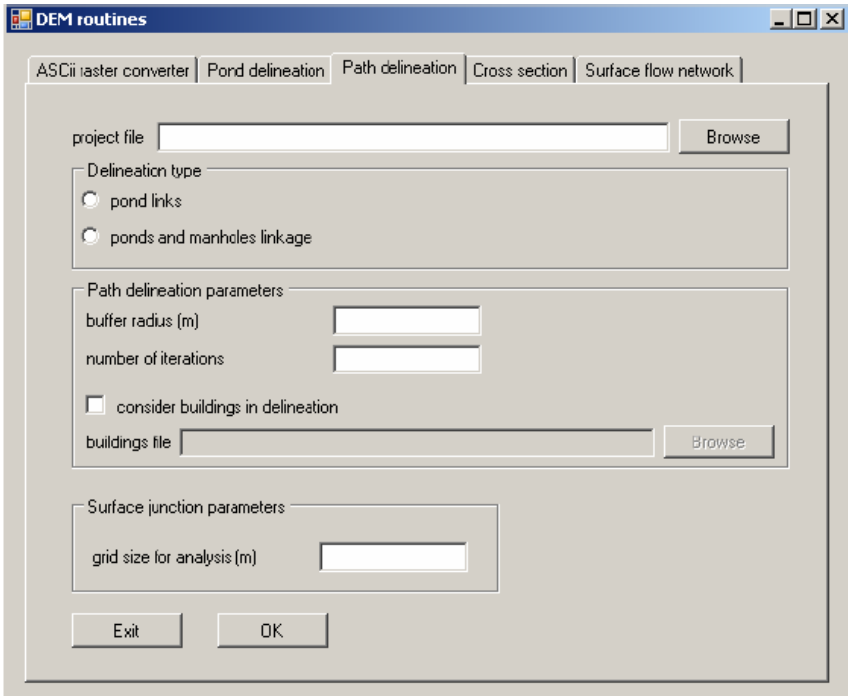

Figure 2.27 Interface of the path delineation procedure.

The first one takes only into account ponds as flow paths' starting points; the second considers also manholes and sewer inlets as possible starting points for the delineation of flow paths. With the first option the flow path delineation process terminates if the flow path enters another pond of if it reaches the end of the raster DTM. Instead, when also the sewer system is taken into account, ponds and manholes (and sewer inlets) inside the catchment boundary and outside a pond take part in the delineation process. In this case, starting points for overland flow paths are pond exit points and the manholes (and sewer inlets) locations, and the termination criteria to flow path delineation are as follows (fig. 2.28):

- flow path enters a downstream pond;
- flow path enters a downstream manhole;
- flow path reaches the catchment boundary.

Nevertheless, sometimes, the overland flow path delineation procedure stops without satisfying one of the defined terminating conditions, for example when a pathway enters a pit cell or a flat area. This problem is common for raster-based algorithms and can be severe in low quality DTM.

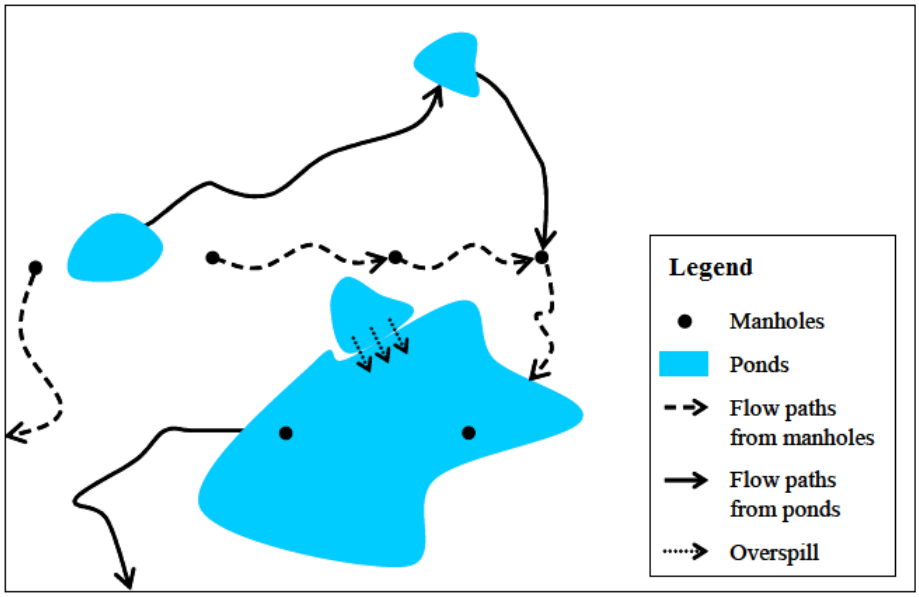

Figure 2.28 Flow path delineation options (from Leitão, 2009).

Consequently, in the AOFD, an automatic method has been developed so that an "exit" from the problematic point can be traced and the pathway delineation can be carried on. The criteria to determine the exit are elevation, distance and presence of buildings. The algorithm selects an exit by comparing the heights between the stop and potential exit points within a user defined surrounding area (buffer radius). The exit point must be lower with height difference greater than the elevation threshold, usually 1-2 cm for a fine DTM or depending on the decimal precision of the height data. Accordingly, in this phase, the tool requires the definition of the buffer radius and the number of iterations to be carried out in searching new paths (fig. 2.27).

Finally, during the automatic flow pathway delineation procedure, there is also the possibility that two or more pathways come close and then flow parallel or coincident to each other. In reality these pathways will merge themselves and will flow in single paths from the point they meet. In the simulation model this situation must be recognized and properly dealt with.

Therefore, in the AOFD, the proximity of pathways is analyzed in this way: if two or more pathways are close than the specified parameter (grid size for analysis), they will be merged (fig. 2.27). Figure 2.29 gives an example of this procedure: path 1 and path 2 come close and a new path way (path 1001) replaces the downstream

parts of the original paths. Eventually, a new set of computational nodes (called "break nodes") will be created.

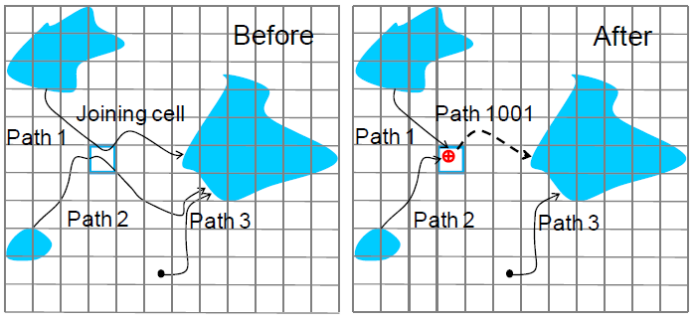

Figure 2.29 Procedure of merging pathways at joining grid cell.

4) Assessment of pathway geometry

Surface pathways are approximated by open channels. To model flow in such pathways, the following information are required: the geometry of the open-channel, upstream/downstream elevations, roughness and the actual length between two ponds or surface nodes. These information can be evaluated by the AOFD through the sequence of processes reported in fig. 2.30.

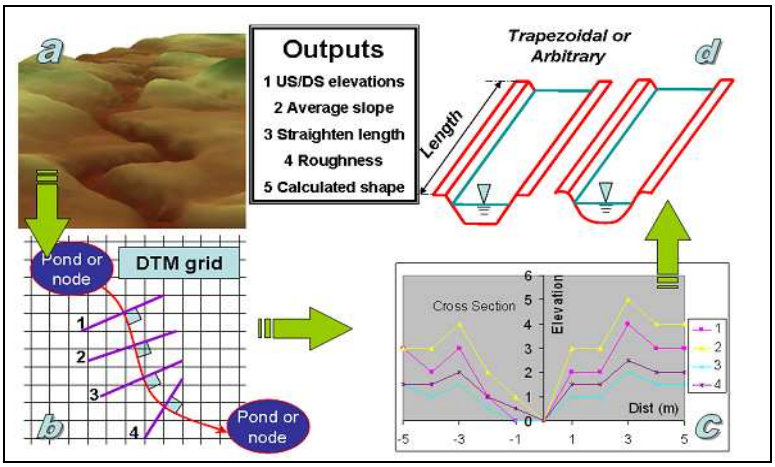

Figure 2.30 Estimation of pathways geometry: *a*) 3D DTM showing identified flow path, *b*) a number of cross-sectional lines drawn perpendicularly to the path, *c*) the arbitrary shapes of cross sections plotted as found from DTM, and *d*) averaged output with two choices – trapezoidal or arbitrary shapes.

The tool uses the previously identified pathways and draws equi-distant cross-sections along each pathway length (fig. 2.30 b). Next it uses the surrounding

DTM to estimate the flow areas of each cross section (fig. 2.30 c). Finally, the algorithm allows users to select the form of the output which may be either an arbitrary (user-defined) set of points or pre-defined (trapezoidal) cross-sections (fig. 2.30 d). If the user-defined arbitrary shape is selected, the algorithm will determine the average elevation of the entire pathway at each offset distance from the centerline (fig. 2.30 c). If the trapezoidal shape is selected, the algorithm will compute the average flow areas at different depths along the length of each pathway (so called "stage-flow area" curve) and then will find the geometry of a trapezoidal shape that satisfies the stage-flow area curve. The calculation is done by recognizing that the relation between area (*A*) and depth (*H*) of trapezoidal shape is quadratic (second-order polynomial) as shown in fig. 2.31. The width (*B*) and the 1/slope (*m*) are the unknowns to be calculated. The least square for the polynomial regression is used to find these two unknown variables.

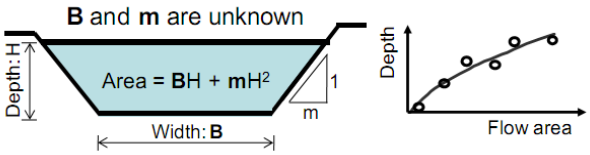

Figure 2.31 The trapezoidal shape of open channel.

In this phase users can set various parameter values for analysis as shown in fig. 2.32. The detailed explanations of four required parameters are as follows:

- the *longitudinal interval* is the distance along the pathways to locate cross section and determine its flow capacity. The value ranges in 10-50 m.
- the *maximum depth* is vertical distance between top and bottom elevations along the cross section which determines the location of building. Usually 3-5 m is recommended value.
- the *minimum depth* is vertical distance between top and bottom elevations along the cross section which determines this cross section flat. Usually 0.1-0.20 m is used.
- the *buffer radius* is the radius along cross section that will tell routine where is the boundary of analysis (left and right from centerline) to read elevation from given

DTM. Usually the value should be bigger than the averaged radius of streets (5-15 m).

- the *cross section interval* is the 'step' distance along cross section where elevations were picked up for analysis. Usually, it should be 1-3 times of the DTM cell size.

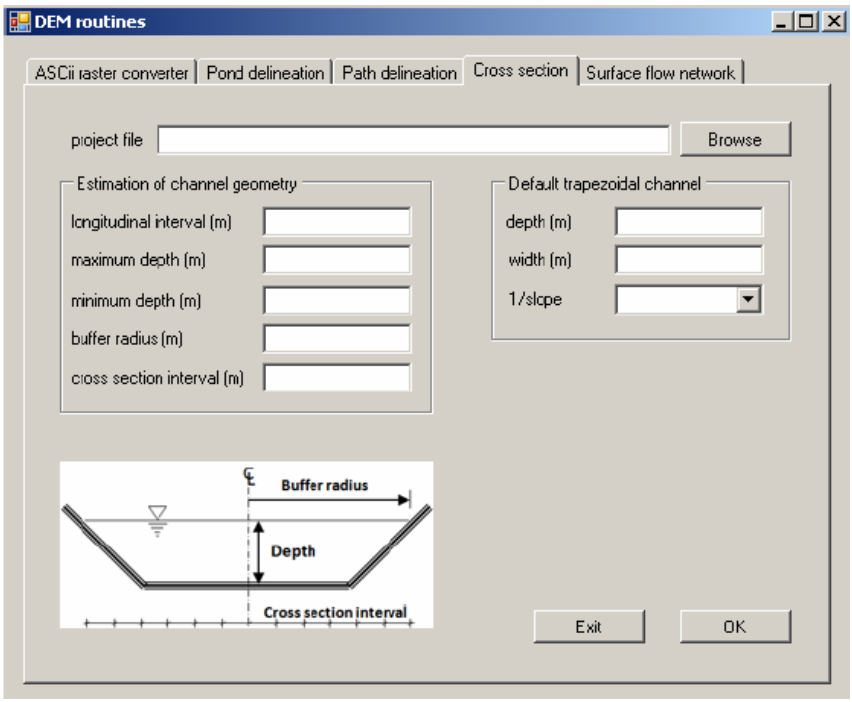

Figure 2.32 Interface of the cross sectional shape finding procedure.

Finally all the derived outputs are prepared by the current version of the tool in ArcGIS Shape file with the attributes of analyzed data such as locations, elevations, roughness, slopes, lengths etc. (fig. 2.33). This file format was selected because common software (InfoWorks CS, MOUSE, SOBEK, SWMM, SIPSON) can interpret and import the generated surface network. Consequently, in this way, the overland flow networks can then be coupled with physically-based sewer network model in order to model pluvial urban flooding realistically.

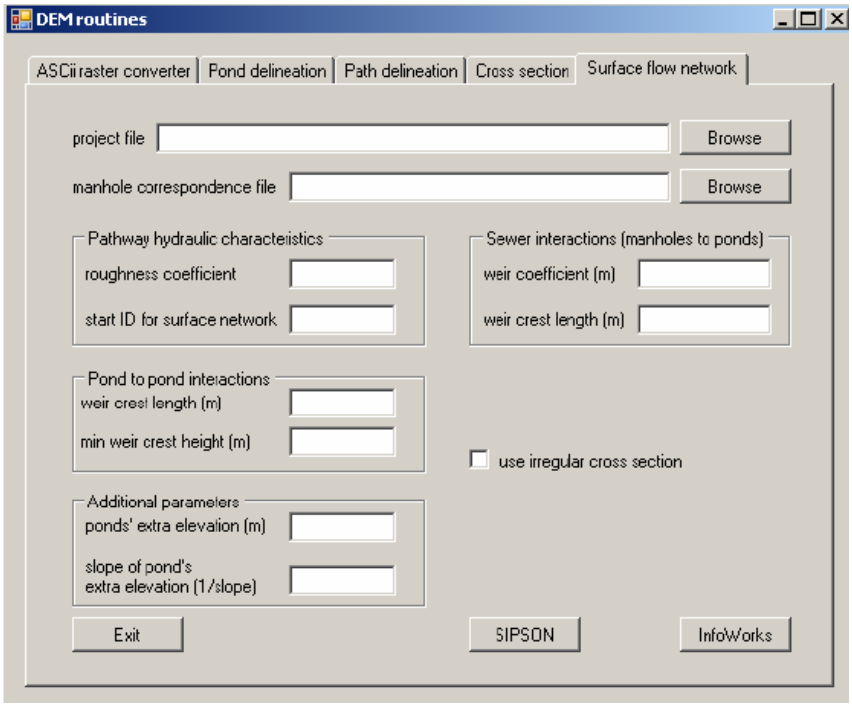

Figure 2.33 Interface of the creation of surface network files for simulation models.

2.5.1 Identification of interaction of 1D-1D model system

As already pointed out, the drainage systems are modeled as two dynamically interconnected networks, where manholes and sewer inlets function as points of flow exchange between sewer and overland systems. When flooding takes place, water from the pipe system may flow to the streets through the manhole. On the other hand, when water in the pipe system is drained, surface flooding water in the street system can flow through the manholes to the pipe system.

This bidirectional discharge can be calculated for the generic manhole based on the water level difference between sewer network and overland surface, and the crest elevation of the manhole itself (Chen at al., 2007). The upstream and downstream levels can be defined as h_u = max (h_{mh}, h_{sur}) and h_d = min (h_{mh}, h_{sur}), respectively, where h_{mh} is the hydraulic head at manhole and h_{sur} is the water surface elevation on the overland surface. Instead the crest elevation, z_{crest}, can be evaluated as follows:

$$z_{crest} = \max\left\{z_{mh,top}, z_{sur}\right\} \tag{2.16}$$

where

- $z_{mh,top}$ is the elevation of the manhole's top obtained from the sewer network dataset;
- z_{sur} is the topographic elevation of the point obtained from the DTM of the study area.

The corresponding values of $z_{mh,top}$ and z_{sur} should be equal, nevertheless inconsistency between the two datasets is often present when the manhole is located at local peak or depression inside the DTM grid, as illustrated in fig. 2.34.

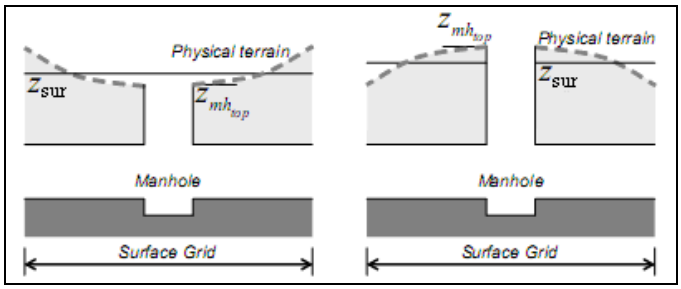

Figure 2.34 Inconsistency between top elevation of the manhole and average grid elevation (from Chen et al., 2007).

The manhole's behavior may be later described in three ways: free weir linkage, submerged weir linkage and orifice linkage.

The free weir equation is adopted when the crest elevation z_{crest} is between the values of the upstream water level h_u and the downstream water level h_d, as shown in fig. 2.35.

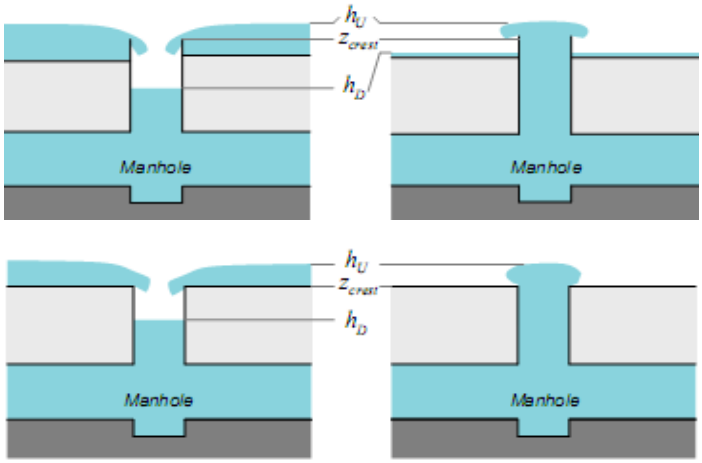

Figure 2.35 Free weir linkages (from Chen et al., 2007)..

The discharge can be then calculated as:

$$Q = sign\left[h_{mh} - h_{sur}\right] \cdot c_w \cdot w \cdot \sqrt{2 \cdot g} \cdot \left(h_u - z_{crest}\right)^{3/2} \qquad (2.17)$$

where Q is the interacting discharge, whose positive value means surcharge flow from sewer toward overland and negative value means drainage flow from surface into sewer; c_w is the weir discharge coefficient; w is the weir crest width (fig. 2.36); and g is the gravitational acceleration.

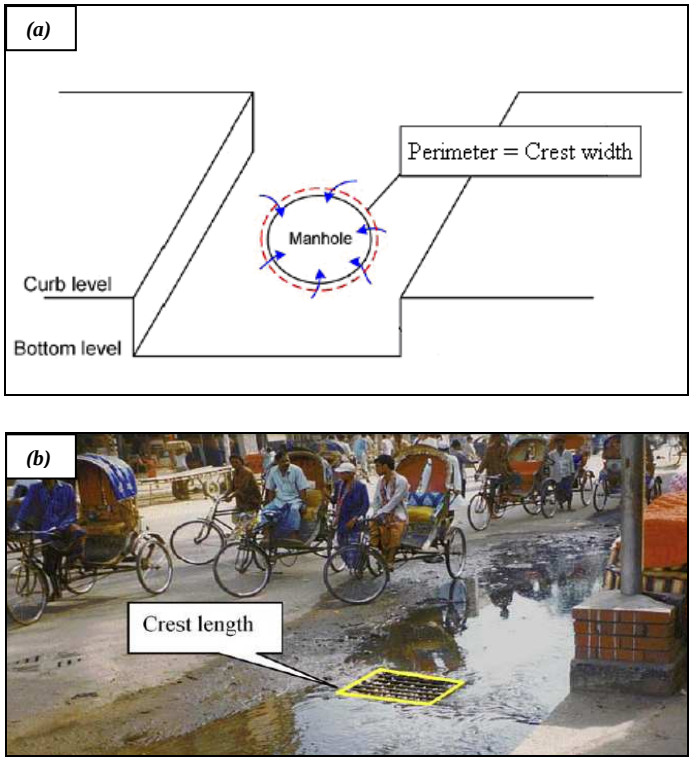

Figure 2.36 (a) The principle behind the application of a weir formula for the description of the flow exchange between pipe and street system. (b) Water flowing into a catch pit in Dhaka City. This is an illustration from real life of the principle behind the application of a Weir formula for the description of the flow exchange between pipe and street system (from Mark et al., 2004).

The submerged weir equation is used when both water levels at manhole and overland grid are greater than the crest elevation and the upstream water depth above the crest, (h_u - z_{crest}), is less than A_{mh} / w, where A_{mh} is the manhole area, shown in fig. 2.37 (a). The discharge can be then calculated as:

$$Q = sign\left[h_{mh} - h_{sur}\right] \cdot c_w \cdot w \cdot \sqrt{2 \cdot g} \cdot \left(h_u - h_d\right)^{1/2} \qquad (2.18)$$

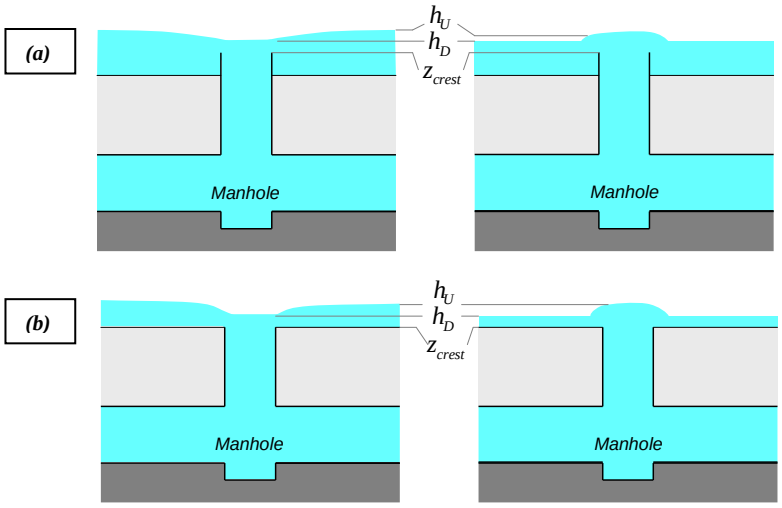

Figure 2.37 (a) Submerged weir linkage for $h_u \leq A_{mh} / w$. (b) Orifice linkage for $h_u > A_{mh} / w$ (from Chen et al., 2007).

Finally the manhole is considered fully submerged (fig. 2.37 b), when the upstream water depth above the crest, (h_u - z_{crest}), is greater than A_{mh} / w for the submerged weir linkages. In such situations the orifice equation must be used for calculating the interacting discharge:

$$Q = sign\left[h_{mh} - h_{sur}\right] \cdot c_o \cdot A_{mh} \cdot \sqrt{2 \cdot g} \cdot \left(h_u - h_d\right)^{1/2} \tag{2.19}$$

where c_o is the orifice discharge coefficient.

It is evident that the reported expressions are only approximations of the real processes, which could lead to inaccurate results. However, currently, it is complicated to include all the physical phenomena in the simulation, such as, for example, the possibility that the manhole cover can be lifted or removed by the water rising in the manhole during the outflow. Therefore, pending more reliable future updates, it is appropriate to continue adopting such approaches, by taking always into account the uncertainties related to their use.

2.5.2 Calibration

Calibration involves minimization of deviation between observed data and simulated results by adjusting parameters within the model (Mark et al., 2004).

The urban drainage model calibration can be carried out by calibration of the surface runoff model and subsequently the pipe flow model is calibrated towards measured

flow and water level at the specific locations. The surface runoff model can be calibrated by adjusting hydrological parameters, for example time of concentration, until the computed hydrograph agrees closely to observed runoff data. Next, the runoff hydrograph is used as input data for the pipe flow model to simulate discharge and water level in the pipe system by changing pipe flow parameter, such as Manning number. This step is iterated until the calculated discharge and water level outputs are agreeably close to the observed data.

Generally, in the past, the calibration process consisted in facing the sequence of operations above reported, since the capacity of the drainage system was considered normally depending only on sewer pipe sizes and pumping capacity. However, during flooding the capacity of the system is totally different because the water flows both in the pipes and on the streets. This means that, in order to calibrate an urban flood model, it is not sufficient to have only a well calibrated pipe network. Hence, measuring campaigns will have to be planned in order to collect also the flow paths, the flow extent and the flow capacity of streets so that the contribution to the drainage capacity from the street network is taken into account. In particular, if high-tech equipment is not available, the areas affected by flooding and the highest flood levels could be cheaply recorded by tools such as resident gauges and chalk gauges (Kolsky, 1998). Whenever the collection of high quality data was not carried out during a flood event, the model could be verified by comparing predicted and observed flood extent and maximum water levels, that are typically available (for example by photos).

2.5.3 Drawbacks and limitations

The greatest inaccuracy of the described approach lies in the treatment of street channels as prismatic and of flow in those channels as one-dimensional (Mark et al., 2004). In fact such a methodology is not appropriate:

- if there are irregular street geometry and/or catch pits situated in gutters on two sides of the road, that may lead to water in two parallel gutters flowing in opposite directions (fig. 2.38).

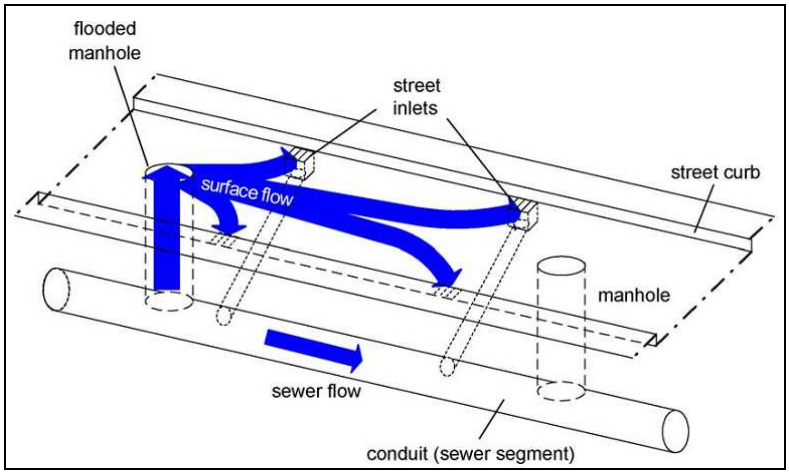

Figure 2.38 The presence of sewer inlets situated on two sides of the road may determine two parallel overland flows (from Schmitt et al., 2004).

- during extreme rain events when the curbs are overtopped. In this situation the flow is no longer 1D, moreover the water probably reaches pervious areas where roughness is significantly higher, and where infiltration may be possible.

In such situations a 1D-2D model must be used, where 1D sewer flow is integrated with 2D surface flow simulation. In particular the interactions between the two models take place between underground network nodes and surface computational grid cells (Maksimović et al., 2009). This approach enables more realistic analysis of overland flows than the 1D-1D approach, moreover treatment of buildings and other urban structures is more exact. However, 2D models require higher level of spatial details and shorter time steps, therefore they are computationally demanding and are inadequate for real-time representation or rapid forecasting of the flooding process.

Since each approach has its potential and limitations and thus it will be more adequate for certain types of analysis, it is clear that the final choice will depend on the purpose of the modeling, data availability and economic costs to set up the model (Kaushik, 2006).

Another limitation to take into account is the separation between the hydrological and hydraulic phases of the runoff (Mark et al., 2004). Such approach is absolutely acceptable for simulation of events without flooding . However, surface runoff parameters calibrated via measurements during moderate rainfall, might not be valid when the underground system cannot capture all the runoff, since the excessive

amounts of water on the surface would induce both decreased hydrological losses and quicker response (shorter concentration times).

Therefore it would be appropriate to verify if physical processes, like evaporation and infiltration, affect or not the urban flood conditions. One possible approach is described by Apirumanekul (2001) and consists in comparing the accumulated rainfall losses (evaporation for example) and the accumulated rainfall during the rain and flooding periods. If only a little rainfall abstraction takes place compared to the accumulated rainfall (the volume of flood water), the phenomenon can be ignored in the model because it does not affect the flooding processes.

References

- AA. VV., Sistemi di fognatura – Manuale di progettazione, Editore Hoepli, 2004.
- Akan A.O. and Houghtalen R.J. (2003). *Urban Hydrology, Hydraulics and Stormwater Quality: Engineering Applications and Computer Modeling*. John Wiley and Sons, Inc., Hoboken, New Jersey.
- Allit R. (2001). *Problems and pitfalls*. In WaPUG Scotland Meeting, Dunblane, UK.
- Anderson M.G. and Burt T.P. (1985). *Modeling Strategies*. In Hydrological Forecasting, M.G. Anderson and T.P. Burt (eds.), John Wiley & Sons, New York, NY, pp. 1-13.
- Apirumanekul, C. (2001). *Modeling of urban flooding in Dhaka City*. Master Thesis No. WM-00-13, Asian Institute of Technology, Bangkok.
- AMK Associates, International, Ltd, 2004.Anon., 2004. Dual Drainage Storm Water Management Model, Program Documentation and Reference Manual, Release 2.1, Ontario, Canada 2004 p. 170.
- Aron G. (1982). *Rainfall Abstractions*. In Urban Stormwater Management, D.F. Kibler (ed.), American Geophysical Union, Water Resources Monograph No. 7, Washington, D.C., pp. 69-86.
- Artina S., Calenda G., Paoletti A., Rasulo G. (1994). *Revisione dei metodi razionale e dell'invaso per il dimensionamento delle reti di drenaggio urbano*. Atti del XXIV Convegno di Idraulica e Costruzioni Idrauliche, Napoli, 20 - 22 settembre.
- Artina S., Paoletti A., (1997). *Capitolo 3: Criteri di progettazione*, Sistemi di Fognatura. Manuale di Progettazione, Centro Studi Deflussi Urbani, Hoepli, Milano.
- Ball E.J. and Alexander M. (2006). *Modeling street surface runoff*. In 7th International Conference on Hydroinformatics, Nice, France.
- Barbero G., Papiri S. (2000). *Analisi di pluviogrammi registrati a Cascina Scala (Pavia) e determinazione degli ietogrammi di progetto*. Atti del XXVII Convegno di Idraulica e Costruzioni Idrauliche, Genova.

- Bathurst J.C. (1986). *Physically-Based Distributed Modeling of an Upland Catchment Using the Systeme Hydrologique Europeen*. Journal of Hydrology 87: 79-102.
- Bergmann H. and Richtig G. (1990). *Decision Support Model for Improving Storm Drainage Management in Suburban Catchments*, Proceedings of the Fifth International Conference on Urban Storm Drainage, pp. 1429.
- Beven K.J. (1985). *Distributed Models*. In Hydrological Forecasting, M.G. Anderson and T.P. Burt (eds.), John Wiley & Sons, New York, NY, pp. 405-435.
- Beven K.J. (1989). *Changing Ideas in Hydrology - The Case of Physically-Based Models*. Journal of Hydrology 105:157-172.
- Burrough P.A. and McDonnel R.A. (1988). *Principles of Geographical Information Systems*. Oxford University Press, New York.
- Butler D., Davis J.W. (2000). *Urban Drainage*. E&FN Spon: London, 2000.
- Butler D., Davies J.W. (2006). *Urban Drainage*, 2nd edn, Spon Press, London.
- Chen A., Djordjević S., Leandro J., and Savić D. (2007). *The urban inundation model with bidirectional flow interaction between 2D overland surface and 1D sewer networks*. In (NOVATECH 2007) 6th International Conference on Sustainable Techniques and Strategies in Urban Water Management, Lyon, France.
- Chen A., Djordjević S., Leandro J., Evans B., and Savić D. (2008). *Simulation of the building blockage effect in urban flood modeling*. In 11th International Conference on Urban Drainage, Edinburgh, UK.
- Chow V.T., Maidment D.R. and Mays L.W. (1988). *Applied Hydrology*, McGraw-Hill International Editions, Singapore.
- Ciaponi C., Papiri S. (1997). *Capitolo 12: Canali e condotte: calcolo idraulico*, Sistemi di Fognatura. Manuale di Progettazione, Centro Studi Deflussi Urbani, Hoepli, Milano.
- Ciaponi C., Papiri S. (2000). *Diagnosi dei problemi funzionali di sistemi di drenaggio e definizione degli interventi correttivi ottimali*. Atti della II Conferenza Nazionale sul Drenaggio Urbano, Palermo, 10-12 maggio 2000.
- Ciaponi C. (2005). *Conoscenza ed affidabilità dei sistemi fognari.* Primo Convegno Nazionale di Idraulica Urbana, Sorrento 28 – 30 Settembre 2005.

- Cunge J.A., Holly F.M., Vervey A. (1980). *Practical Aspects of Computational River Hydraulics*, Pitman, London.
- Delaunay B. (1934). *Sur la sphère vide*. Izvestia Akademii Nauk SSSR, Otdelenie Matematicheskikh i Estestvennykh Nauk. 7:793-800.
- Delleur J.W. (1982). *Introduction to Urban Hydrology and Stormwater Management*. In Urban Stormwater Management, D.F. Kibler (ed.), American Geophysical Union, Water Resources Monograph No. 7, Washington, DC, pp. 1-34.
- Denver Council of Governments, 1969.Anon., 1969. *Urban Storm Drainage Criteria Manual*, Wright-McLaughlin Engineers 1969.
- Djokic D. (1991). *Urban Stormwater Drainage Network Assessment Using an Expert Geographical Information System*, PhD Dissertation, University of Texas at Austin. Available from UMI Dissertation Service, Order Number 9128214 1991.
- Djokic D., Maidment D.R. (1991). *Terrain analysis for urban stormwater modeling*. Hydrological Processes 5, 115-124.
- Djordjević S., Ivetic M., Maksimović Č., Rajcevic A. (1991). *An approach to the simulation of street flooding in the modeling of surcharged flow in storm sewers*. In: Maksimović Čedo (Ed.), Proceedings: New Technologies in Urban Drainage UDT '91. Elsevier Publishers, pp. 101-108.
- Djordjević S., Ivetic M., Prodanović D., Savic D., Maksimović Č. (2005). *SIPSON – Simulation of interaction between pipe flow and surface overland flow in networks*. Water Science and Technology, 52(5):275 – 283.
- Dooge J.C.I. (1977). *Problems and Methods of Rainfall-Runoff Modeling*. In Mathematical Models for Surface Water Hydrology, T.A. Cirinai, U. Maione, and J.R. Wallis (eds.), John Wiley & Sons, New York, NY, pp. 71-108.
- Elgy J., Maksimović Č., Prodanović D. (1993). *Matching Standard GIS Packages with Urban Storm Drainage Simulation Software HydroGIS 93: Applications of Geographic Information Systems in Hydrology and Water Resources*, Proceedings of the Vienna Conference, April, 1993, IAHS Publication No. 211 1993 pp.151-160.

- Ellis J.H., McBean E.A., Mulamoottil G. (1982). *Design of dual drainage systems using SWMM*. ASCE Journal of the Hydraulics Division 198 (HY10), 1222-1227.
- Environment Canada and Ontario Ministry of the Environment, 1976.Anon., 1976. *Manual of Practice on Urban Drainage* Anon., 1976. Research Report No. 10, Project 76-B-3B 1976.
- Faures J., Goodrich D., Woolhiser D.A. and Sorooshian S. (1995). *Impact of small-scale spatial rainfall variability on runoff modeling*. Journal of Hydrology, No. 173, p. 309-326.
- Feldman A.D. (1979). *Flood Hydrograph and Peak Flow Frequency Analysis*. U.S. Army Corps of Engineers, Hydrologic Engineering Center Technical Paper No. 62.
- Freeman T.G. (1991). *Calculating Catchment Area with Divergent Flow Based on Regular Grid*. Computers and Geosciences, 17(3), 413-422.
- Gan T.Y., and Burges S.J. (1990). *An Assessment of a Conceptual Rainfall-Runoff Model's Ability to Represent the Dynamics of Small Hypothetical Catchments: 2. Hydrologic Responses for Normal and Extreme Rainfall*. Water Resources Research 26 (7): 1605-1619.
- Garbrecht J., Martz L.W. (2000). *Digital elevation model issues in water resources modeling*. Hydrologic and hydraulic modeling support with geographic information systems. ESRI Press, Redlands CA, USA.
- Goodrich D., Faures J., Woolhiser D., Lane L. and Sorooshian S. (1995). *Measurements and analysis of small convective storm rainfall variability*. Journal of Hydrology, No. 173, p. 283-308.
- Gourbesville P. (2001). *2D Runoff Modeling in Urban Area with High Definition DEM*", 4th DHI Software Conf.
- Guo Q. and Song C.C.S. (1990). *Surging in Urban Storm Drainage Systems*, ASCE Journal of Hydraulic Engineering, vol. 116, no. 12, pp. 1523-1537.
- Haan C.T. (1988). *Parametric Uncertainty in Hydrologic Modeling*. In Modeling Agricultural, Forest, and Rangeland Hydrology, Proceedings of the 1988 ASAE International Symposium, ASAE Publication 07-88, Chicago, IL, pp. 330-346.

- Haile A.T. and Rientjes T.H.M. (2005). *Effects of LiDAR DEM resolution in flood modeling: a model sensitivity study for the city of Tegucigalpa, Honduras*. In ISPRS WG III/3, III/4, V/3 Workshop Laser Scanning 2005, Enschede, Netherlands.
- Havlik V. (1996). *Computational Hydraulic Modeling*, NATO-ASI on Hydroinformatics in Planning, Design, Operation and Rehabilitation of Sewer Systems.
- Heaney J.P., Huber W.C., Sheikh E., Medina M.A., Doyle J.B., Peltz W.A., Darling J.E. (1975). *Urban Stormwater Management Modeling and Decision Making*, PB-242 290, Report Prepared by University of Florida for the National Environmental Research Center, EPA Document 670/2-75-022, distributed by National Technical Information Service 1975 p. 185.
- Hsu M.H., Chen S.H. e Chang T.J. (2000). *Inundation Simulation for Urban Drainage Basin with Storm Sewer System*. Journal of Hydrology, vol. 234, pp. 21-37.
- Hsu M.H., Chen S.H., Chang T.J. (2002). *Dynamic inundation simulation of storm water interaction between sewer system and overland flows*. Journal of the Chinese Institute of Engineers, Vol. 25, No. 2, pp. 171-177.
- Huber W.C. (1984). Discussion on Papers in Session A-9 - *Special Model Studies Supplements*, Proceedings of the Third International Conference on Urban Storm Drainage, Goteborg, Sweden, June 4-8, Vol. 4 1984 pp. 1564-1577.
- Huber W.C., Zollo A.F., Tarbox T.W., Heaney J.P. (1991). *Integration of the SWMM runoff block with ARC/INFO and AUTOCAD: a case study*. Final Report to Foster-Wheeler Enviresponse, Inc., Purchase Order No. VI1-320-420000,October 1991 p. 121.
- Ichikawa A., Sakakibara T. (1984). *A Proposal of a New Simulation Model 'grid method' for Urban Storm Runoff Analysis and Design of Stormwater Systems*, Proceedings of the 3rd International Conference on Urban Storm Drainage, Goteborg, Sweden, June 4-8, Vol. 1 1984 pp. 245-253.
- Jacobsen P., Harremoes P. (1984). *The Significance of Head Loss Parameters in Surcharged Sewer Simulations Analysis and Design of Stormwater Systems*,

Proceedings of the Third International Conference on Urban Storm Drainage, Goteborg, Sweden, June 4-8, 1984, Vol. 1 1984 pp. 167-176.

- James L.D., and Burges S.J. (1982). *Selection, Calibration, and Testing of Hydrologic Models. In Hydrologic Modeling of Small Watersheds*. C.T. Haan, H.P. Johnson, and D.L. Brakensiek (eds.), American Society of Agricultural Engineers, Monograph No. 5, St. Joseph, MI, pp. 291-312.
- James W. and Robinson M.A. (1985). *Time and Space Resolution for Continuous, Dynamic Storm and Runoff Model Studies*. In Hydraulics and Hydrology in the Small Computer Age, W.R. Waldrop (ed.), Proceedings of the ASCE Specialty Conference, Lake Buena Vista, FL, pp. 1160-1165.
- Kamphorst E. C. and Duval Y. (2001). *Validation of a numerical method to quantify depression storage by direct measurement on moulded surfaces*. CATENA, 43(1):1 – 14.
- Kassem A.M.A. (1982). *Development and application of a simultaneous routing model for dual drainage*. PhD Dissertation. Civil Engineering Department, University of Ottawa, Canada.
- Kaushik C. (2006). *Urban flooding modeling. A comparative study for 1D and 2D models*. Master's thesis, UNESCO-IHE Institute for Water Education, The Netherlands.
- Keifer C.J., Chu H.H. (1957). *Syntethic storm pattern for drainage design*. Journal of Hydraulic Division, ASCE HY4, vol.83.
- Kidd C.H.R., Helliwell P.R. (1977). *Simulation of the inlet hydrograph for urban catchments*. Journal of Hydrology 35, 159–172.
- Kolsky, P. (1998). *Storm drainage*. Intermediate Technology Publications, London.
- Kuichling E. (1889). *The relationship between the rainfall and the discharge of sewers in populous areas*. Trans. ASCE, vol. 20, No. 1, p. 60.
- Larson C.L. (1973). *Hydrologic Effects of Modifying Small Watersheds - Is Prediction by Hydrologic Modeling Possible?* Transactions of the ASAE 16: 560-564, 568.
- Larson C.L., Onstad C.A., Richardson H.H. and Brooks K.N. (1982). *Some Particular Watershed Models*. In Hydrologic Modeling of Small Watersheds,

C.T. Haan, H.P. Johnson, and D.L. Brakensiek (eds.), American Society of Agricultural Engineers Monograph Number 5, St. Joseph, MI, pp. 409-434.

- Lau J. and Sharpe A. (2004). *SPRINT – spatial radar integrating tool for hydraulic models*. In 6th International Conference on Urban Drainage Modeling, UDM'04, Dresden, Germany.
- Lea N.J. (1992). *An aspect driven kinematic routing algorithm*. In Parsons A. and Abrahams A. editors, Overland Flow: Hydraulics and Erosion Mechanics, pages 393-407. Chapman and Hall, New York, USA.
- Leitão J.P.C. (2009). *Enhancement of digital elevation models and overland flow path delineation methods for advanced urban flood modeling*. Phd Thesis, Imperial College London, London, UK.
- Li Z. (1994). *A comparative study of the accuracy of Digital Terrain Models (DTMs) based on various data models*. ISPRS Journal of Photogrammetry and Remote Sensing, 49(1):2 – 11.
- Lindsay J.B. and Creed I.F. (2006). *Distinguishing actual and artefact depressions in digital elevation data*. Computer and Geosciences, 32(8):1192-1204.
- Lloyds-Davis D.E. (1906). *The elimination of storm water from sewerage systems*. Proc. ICE, No. 164, p. 41-67.
- Maksimović Č. and Radojković M. (1986) *Urban Drainage Catchments – Selected Worldwide Rainfall-Runoff Data from Experimental Catchments*, Pergamon Press,Oxford.
- Maksimović Č. (1996). *Fundamentals of physically-based rainfall / runoff models*. In Marsalek J., Maksimović Č., Zeman E. and Price R. editors, NATO Advanced Study Institute on Hydroinformatics Tools for Planning, Design, Operation and Rehabilitation of Sewer Systems. Kluwer Academic Publishers, Harrachov, Czech Republic.
- Maksimović Č. and Prodanović D. (2001). *Modeling of urban flooding – breakthrough or recycling of outdated concepts*. In Urban Drainage Modeling, Orlando, Florida, USA.

- Maksimović Č., Prodanović D., Boonya-aroonnet S., Leitão J.P., Djordjević S, Allitt R. (2009). *Overland flow and pathway analysis for modeling of urban pluvial flooding*. Journal of Hydraulic Research, 47(4):512-523.
- Mark O., Weesakul S., Apirumanekul C., Aroonnet S.B., Djordjević S. (2004). *Potential and limitations of 1D modeling of urban flooding*. Journal of Hydrology 299, 284-299.
- Mark O., Djordjević S. (2006). *While waiting for the next flood in your city…* In 7th International Conference on Hydroinformatics (HIC 2006), Nice, France.
- McBean E.A., Ellis H., Mulamoottil G. (1985). *Impact of alternative housing standards on stormwater management*. Canadian Journal of Civil Engineering 12, 192-199.
- McPherson M.B., and Zuidema F.C. (1977). *Urban Hydrological Modeling and Catchment Research: International Summary*. ASCE Urban Water Resources Research Program, Technical Memorandum No. IHP-13, New York, NY.
- Mignosa P. (1987). *Principali modelli su mainframe e microcomputer*. Atti del Seminario Nazionale " La ricerca nei deflussi urbani", Camigliatello Silano, 6-7 ottobre.
- Morris E.M. and Viera J.d.L. (1981). *Approximate forms of the Saint Venant equations for shallow surface water flow*. In International Conference on Numerical Modeling of Rivers, Channel and Overland Flow, Bratislava, Slovakia.
- Mulvaney T.J. (1850). *On the use of self registering rain and flood gauges in making observations on the relation of rainfall and of flood discharges in a given catchment*. Trans. ICE Ireland, Vol. 4, No. 2, p. 18.
- Nix S.J. (1991). *Applying Urban Runoff Models*. Water Environment and Technology: 47-49.
- Pankrantz R.H., Leblanc M.R., Newcombe A. (1995). *A comparison of dual drainage modeling techniques*. In: James, William (Ed.), Chapter 23 in Modern Methods for Modeling the Management of Stormwater Impacts, Proceedings of March 1994 Conference, p. 521.

- Pechlivanidis I., McIntyre N.R., Wheater H.S., Jackson B. and Orellana B. (2008). *Relation of spatial rainfall characteristics to runoff: an analysis of observed data*. In 10th BHS National Hydrology Symposium, Exeter, UK.
- Pethick R.W. (1984). *Runoff Models for Port of Spain,* Proceedings of the 3rd International Conference on Urban Storm Drainage, Goteborg, Sweden, June 1984 pp. 545-554 June.
- Piga E., Salis M., Passoni G. (1990). *Analisi statistica delle piogge intense di breve e brevissima durata nell'area metropolitana di Milano*, ed. Città Studi, Milano.
- Preissmann M.A., and Cunge J.A. (1961). *Calculation of Wave Propagation on Electronic machines,* Proceedings, 9th Congress, IAHR, Dubrovnik, pp. 656-664, 1961.
- Prodanović D., Djordjević S., Maksimović Č. (1998). *GIS assisted model for dual drainage simulation*. In: Vladan Babovic, Lars Christian Larsen (Eds.), Proceedings of the Third International Conference on Hydroinformatics, Copenhagen, Denmark, 24¬26 August, pp. 535-542.
- Prodanović D. (1999). *Advanced in Hydroinformatic Support to Urban Runoff*. PhD thesis, University of Belgrade, Serbia.
- Radojković M. and Maksimović Č. (1987). *On standardization of computational models for overland flow*. In Yen B.C. editor, V International Conference on Urban Storm Drainage, Lausanne, Switzerland. EPFL and WRP.
- Rawls W.J., and Brakensiek D.L. (1983). *A procedure to predict Green and Ampt infiltration parameters*. In Advances in infiltration. Proc. of the Nat'l Conference on Advances in Infiltration. Dec. 12-13. Chicago, IL.
- Robinson G.J. (1994). *The accuracy of digital elevation models derived from digitised contour data*. The Photogrammetry Record, 14(83):805 – 814.
- Roesner L.A., Shubinski R.P. (1982). *Improved Dynamic Flow Routing Model for Storm Drainage Systems*, Proceedings of the Second International Conference on Urban Storm Drainage, held in Urbana, Illinois, USA, June 14-19, pp. 164-73.
- Rousseaux F. (2004). *Detection of systematic error areas on a DTM by comparison with a high resolution LiDAR DTM*. In Geoscience and Remote Sensing Symposium, 2004, volume 6, pages 4160 – 4163.

- Schmitt T.G., Thomas M., Ettrich N. (2004). *Analysis and modeling of flooding in urban drainage systems*. Journal of Hydrology N. 299, p.300-311.
- Schutze M.R., Butler D. & Beck B.M. (2002). *Modeling, Simulation and Control of Urban Wastewater Systems*, Springer Publisher, London, Great Britain.
- Shafer J.M, and Skaggs R.L. (1983). *Identification and Characterization of Watershed Models for Evaluation of Impacts of Climate Change on Hydrology*, Battelle Memorial Institute, Technical Report.
- Sithole G. and Vosselman G. (2004). *Experimental comparison of filter algorithms for bare-Earth extraction from airborne laser scanning point clouds*. ISPRS Journal of Photogrammetry and Remote Sensing, 59(1-2):85 – 101.
- Smith M.B. (1992). *A Distributed Parameter Hydrological Model for Urban Stormwater Protection*, PhD Dissertation, University of Ljubljana, Slovenia, Department of Civil Engineering, (FAGG) Available through University Microfilms International, Order Number 9223634 1992.
- Smith M.B. (1993). *A GIS-based distributed parameter hydrologic model for urban areas*. Hydrological Processes 7, 45-61.
- Smith M.B., Vidmar A. (1994). *Data set derivation for GIS-Based Urban hydrological modeling*. Photogrammetric Engineering and Remote Sensing 60 (1), 67-76.
- Smith M.B. (2006). *Comments on 'Analysis and Modeling of Flooding in Urban Drainage Systems'*, Journal of Hydrology, vol. 317, pp. 355-363.
- Stephenson D. (1987). *The Importance of Dual Drainage*, Proceedings of the 4th International Conference on Urban Storm Drainage, Lausanne, Switzerland 1987 pp. 323-324.
- Stephenson D. (1989). *A Modular Model for Simulating Continuous or Event Runoff New Directions for Surface Water Modeling*, Proceedings of the Baltimore Symposium, IAHS Publication No. 181 1989, pp. 83-91.
- Takanishi S., Noguchi M., Nakamura T. (1991). *Simulation of Urban Stormwater by 'Numerous'*, Proceedings of the XXIV IAHR Congress held in Madrid Spain, September 9-13 1991, pp.A-99-A108.
- Todini E. (1988). *Rainfall-Runoff Modeling-Past, Present, and Future*. Journal of Hydrology 100: 341-352.

- Toms E.A. (1989). *Spatial and Temporal Variations of Precipitation Effects on Storm Hydrographs*. In Proceeding of the 1989 ASCE National Conference on Hydraulic Engineering, M.A. Ports (ed.), New Orleans, LA, pp. 559-564.
- Tribe A. (1992). *Automated recognition of valleylines and drainage networks from grid digital evolution models: a review and a new method*. Journal of Hydrology, 139:263 – 293.
- Troutman B.M. (1985). *Errors and Parameter Estimation in Precipitation-Runoff Models*. Water Resources Research 21 (8): 1195-1222.
- Tsubaki R., Fujita I. and Teraguchi H. (2006). *LiDAR data processing for detailed inundation simulation of an urbanized area*. In 7th International Conference on Hydroinformatics, Nice, France.
- U.S. Army Corps of Engineers, Hydrologic Engineering Center. (1990). HEC-1 Flood Hydrograph Package, Users Manual: July 1990.
- U.S. Soil Conservation Service (SCS). (1964). National engineering handbook, Section 4, Hydrology. Department of Agriculture, Washington, 450 p.
- U.S. Soil Conservation Service (SCS). (1972). National engineering handbook, Section 4, Hydrology. Department of Agriculture, Washington, 762 p.
- Vazquez R.F. and Feyen J. (2007). *Assessment of the effects of DEM gridding on the predictions of basin runoff using MIKE SHE and a modeling resolution of 600m*. Journal of Hydrology, 334(1-2):73 – 87.
- Vernon Knapp H., Durgunoğlu A., Terry Ortel W. (1991). *A review of rainfall-runoff modeling for stormwater management*. Prepared for the U.S. Geologic Survey, Illinois District, October 1991.
- Viera J.d.L. (1983). *Conditions governing the use of approximation for the Saint Venant equations for shallow surface water flow*. Journal of Hydrology, 60:45-58.
- Viessman W., Lewis G. and Knapp J.W. (1989). *Introduction to Hydrology*, 3rd edition edn, Harper&Row, New York.
- Wilcox B.P., Rawls W.J., Brakensiek D.L., and Wight J.R. (1990). *Predicting Runoff from Rangeland Catchments: A Comparison of Two Models*. Water Resource Research 26 (10): 2401-2410.

- Wilson J.P. and Gallant J.C. (2000). *Digital terrain analysis*. In Wilson J.P., Gallant J.C., editor, Terrain Analysis: principles and applications, pages 29-50. John Wiley and Sons, Inc., New York, USA.
- Wisner P.E., Kassem A.M., Cheung P.W. (1981). *Parks Against Storms Proceedings*, Second International Conference on Urban Storm Drainage, Urbana, Illinois, USA, June 14-19 1981, pp.322-330.
- Wisner P.E., Kassem A.M. (1982). *Analysis of dual drainage systems by OTTSWMM*. In: Feathersone, R.E., James, A. (Eds.), Proceedings of the First International Seminar on Urban Drainage Systems, Southhampton, England, September, pp. 2.93-2.101.
- Woods R.R. and Silvapalan R.M. (1999). *A synthesis of space-time variability in storm response: Rainfall, runoff generation, and routing*. Water Resources Research, 35(8), 2469 – 2485.
- Yen B.C., Pansic N. (1980). *Surcharge of Sewer Systems*. Final Report Project N. A-086-ILL, Department of Civil Engineering, University of Illinois.
- Yen B.C. (1982). *Some Measures for Evaluation and Comparison of Simulation Models*. In Urban Stormwater Hydraulics and Hydrology, B.C. Yen (ed.), Proceedings of the Second Conference on Urban Storm Drainage, Urbana, IL, pp. 341-349.
- Yen B.C. (1986). *Rainfall-Runoff Process on Urban Catchment and its Modeling*, Proc. of the International Symposium on Comparison of Urban Drainage Models with Real Catchment Data UDM, eds. Č Maksimović & M. Radojković, Pergamon Press, Oxford.
- Zhilin L. (1992). *Variation of the accuracy of digital terrain models with sampling interval*. The Photogrammetric Record, 14(79):113-128.

3. Hydraulic modeling of the drainage network of a monitored catchment

3.1 Introduction

This chapter was aimed at comparing two different hydraulic models of the drainage system of the same monitored catchment: the Liguori catchment located in Cosenza (Italy). Both the approaches required the use of a very detailed and hydraulically corrected DTM for the study site. Consequently, initially, the research concerned the investigation of the various available LiDAR Digital Terrain Models (DTMs) in order to assess which data set was the most appropriate for the applications to be performed.

The first hydraulic model was developed by following the classical hypothesis according to which the drainage system is composed only of the sewer system, that is, to consider that stormwater, once entered the sewer system, can no longer leave this system by coming back to the surface. This model, adequately calibrated, allowed the response of the sewer network to be simulated to design rain events and to assess its efficiency through the definition of suitable synthetic indexes. Specifically, for each sewer trunk, physical and hydraulic indicators were calculated in order to identify the sections of the network which require greater and more urgent attention and where available resources should be concentrated.

Although such a modeling can lead to acceptable results, it is important to emphasize that this approach is not adequate to simulate sewer flooding realistically, since it ignores the fundamental concept on which traditional urban hydrology is based, i.e. the interaction between the surface network (linked by roads, sidewalks and other features of the urban landscape) with the buried drainage system (Butler and Davis, 2000). Therefore the second model was based on the dual drainage approach, i.e. it was assumed that the urban drainage system was composed of a surface network and the sewer network.

Although this method is simple from the conceptual point of view, its implementation is quite complex: in fact, the sewer system is generally known, whereas the surface network must be defined taking into account the geometric

characteristics of the study area, such as road slopes, dimensions of sidewalks, buildings, etc. Consequently, this chapter also presents a possible definition of the surface network by using an innovative tool, the AOFD procedure (Automatic Delineation Overland Flow). In fact, this methodology, developed by the Urban Water Research Group (UWRG) of Imperial College London (ICL) in cooperation with the University of Belgrade and the University of Exeter, enabled the individuation of the potential flooded areas and the connections between these and the surcharged manholes through the use of certain GIS routines (Maksimović et al., 2009). In particular, it was studied the extent to which the resolution of the digital terrain model (DTM) and the presence of the buildings can affect the definition of the surface network.

Finally, the two hydraulic models were subjected to identical rainfall inputs, both real and synthetic, in order to verify whether different responses of the drainage network were revealed. From the performed elaborations it emerged that the dual drainage approach enables a more realistic simulation of the processes that take place in drainage networks during rainfall events. Therefore, in conclusion, this methodology is suggested for future applications.

3.2 Catchment characteristics

The research concerned the modeling of the drainage network of the Liguori catchment, an experimental site that has been studied for several years by the Department of Soil Conservation of the University of Calabria. In fact, the catchment was instrumented by installing a monitoring station, consisting of a tipping-bucket rain gauge and an ultrasonic sensor for measuring water levels (depths) at the sewer outfall. Furthermore, since 2004, sewer flow samples have been collected to characterize flow quality during wet and dry weather conditions (Piro, 2007).

The Liguori channel was originally a small tributary of the Crati river crossing the city of Cosenza (fig. 3.1).

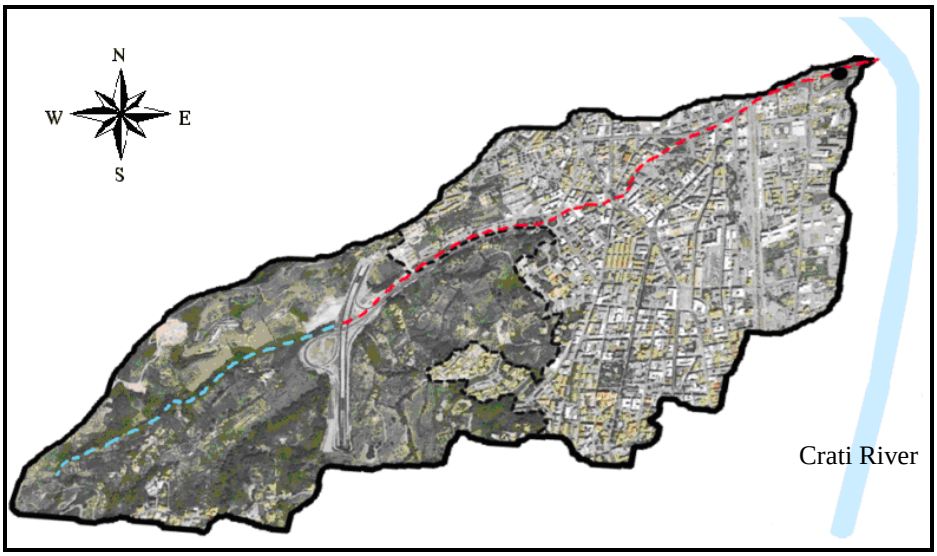

Figure 3.1 Plan view of the Liguori catchment.

Later the urban trunk of the channel was employed for conveying only storm water, through the reshaping of the riverbed in polycentric sections. However, currently, it works as a combined sewer system because of the many residential and industrial discharges. Essentially it supports a population of 50,000 inhabitants and drains a 400-ha watershed, of which about 52% consists of undeveloped agricultural or fallow area, covered mainly by vegetative soil cover, while about 48% is densely urbanized.

In the urbanized part it is possible to distinguish 42 hectares occupied by buildings, 3 hectares occupied by green areas, and 156 hectares occupied by roads and paved surfaces (tab. 3.1).

Total area [ha]	396
% Buildings	10.2
% Green areas	0.8
% Paved surfaces	37.6
% Natural area	51.4

Table 3.1 Catchment parameters.

The dry weather and the entire volume of wet weather flows are conveyed to the WWTP located in Montalto (Cosenza). During very intense rainfall events, part of the wet weather volume is discharged directly to the local receiving water, the Crati

River, through an overflow weir, without receiving any treatment.

Further physical watershed and sewershed information can be found in the literature (Piro and Sole, 2001).

3.3 DTM processing

In the hydrological analysis of urban areas an accurate definition of the sub-catchments and surface pathways require very detailed and hydraulically corrected DTMs for the study site. Consequently, in this case, LIght Detection And Ranging (LiDAR) data, characterized by an horizontal resolution of 1 m, were used thanks to the support of the Autorità di Bacino of Calabria Region. Unfortunately, this data set did not cover the Liguori catchment completely, therefore it was necessary to integrate the uncovered area with another DTM data set, obtained by digitizing the contour lines of a map with 5 m interval (DTM 5).

LiDAR technology determines the distance between ground objects and sensors by measuring the time a pulse of transmitted energy takes to return to the LiDAR sensor (fig. 3.2).

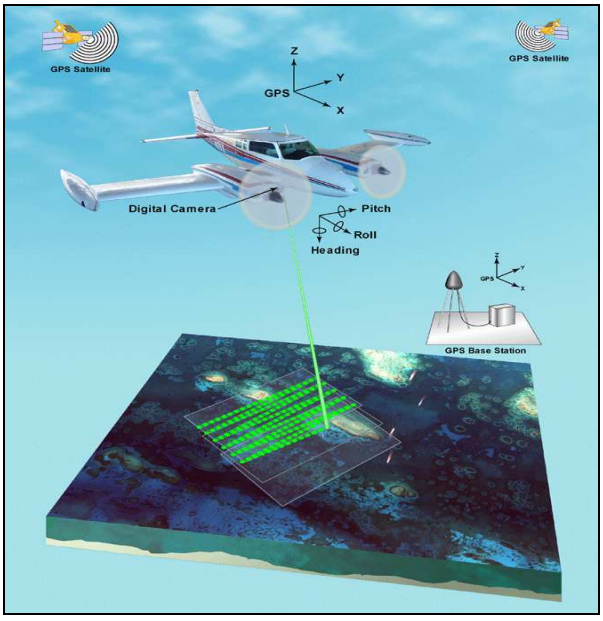

Figure 3.2 Airborne LIght Detection And Ranging (LiDAR) survey.

Currently these systems are capable to record simultaneously two echoes of the laser beam, the first and the last pulse (Ahokas et al., 2005). If the laser beam is reflected at the bare soil, first and last pulse will refer to the same object point. If the laser

beam hits a tree, a part of the light will be reflected at the canopy, resulting in the first pulse registered by the sensor. The rest will penetrate the canopy and, thus, be reflected further below, maybe even at the soil. The last pulse registered by the sensor corresponds to the lowest point where the signal was reflected (Kraus, 2002).

Therefore DTMs with different detail scale can be obtained from LiDAR surveys (fig. 3.4):

1. LiDAR DSM relative to the first pulse return (LiDAR DSM *first*), where hard vegetation (large tree boles and dense hedge lines), buildings and solid artefacts are included;
2. LiDAR DSM relative to the last pulse return (LiDAR DSM *last*), where buildings are still included whereas vegetation and solid artefacts are partly removed;
3. LiDAR DTM relative to the bare earth representation, where all vegetation, artefacts and buildings are removed.

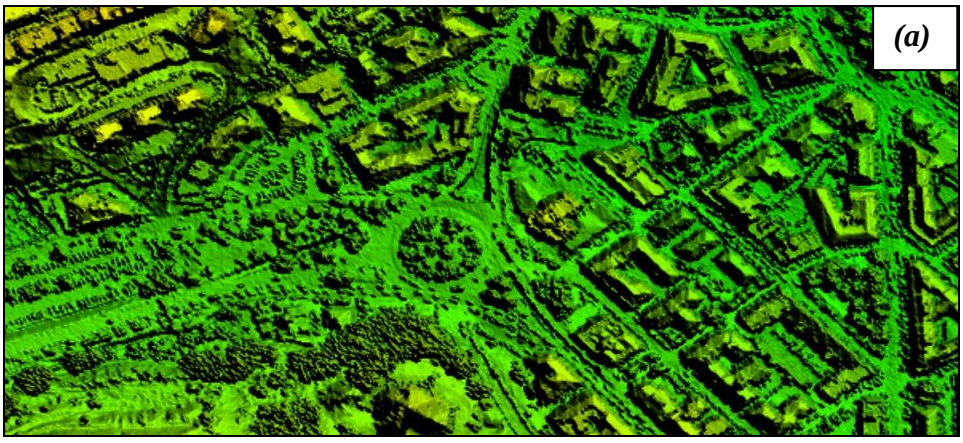

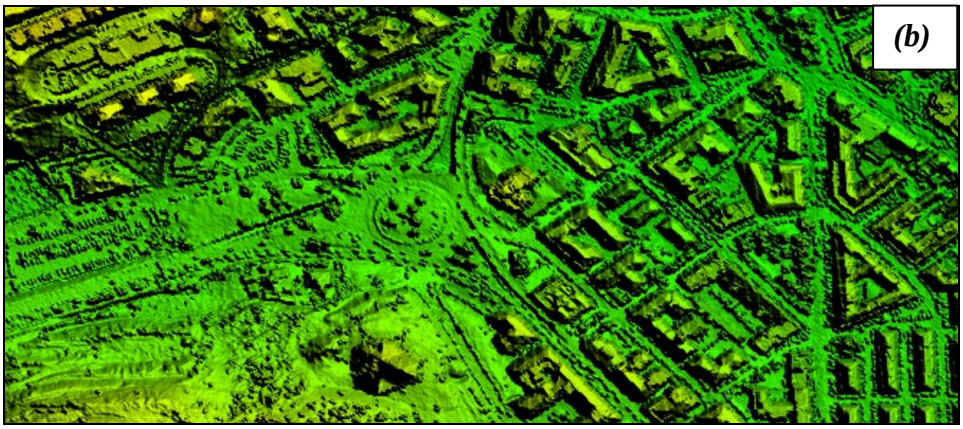

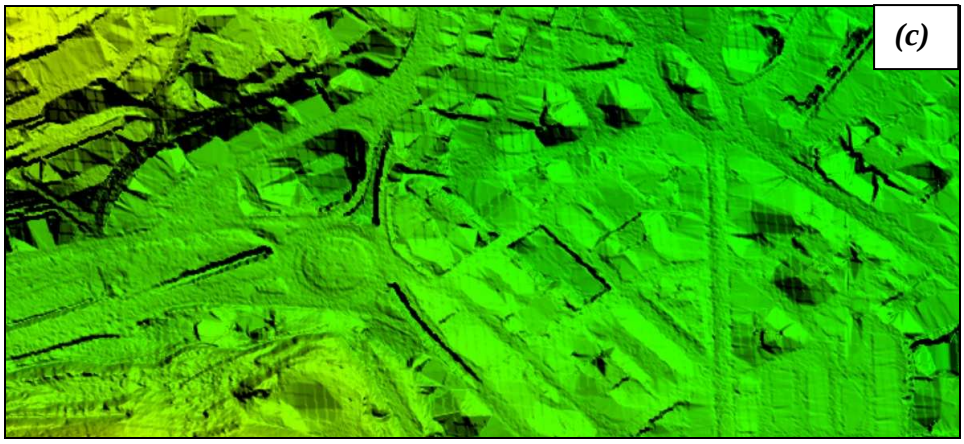

Figure 3.3 LiDAR DSM *first* (a), LiDAR DSM *last* (b) and LiDAR DTM for a same portion of the Liguori catchment.

Every LiDAR data set is characterized by a variable presence of non-ground surface features, such as cars, buildings or vegetation, that will influence surely the hydraulic response of the urban catchment differently: in fact it can be expected that a greater number of solid artefacts, included in the DTM, will determine the definition of a greater number of surface depressions, and, therefore, a bigger surface storage capacity of the catchment itself.

It is evident how the consideration of all these features would favor the development of a more realistic hydraulic model, that, however, would be also more difficult to implement. Consequently it seemed opportune to analyze the different available LiDAR DTMs in order to evaluate whether the use of a less detailed data set, adequately improved, could be an approachable solution for hydraulic modeling purposes. This topic was faced by comparing the surface depressions evaluable from the most detailed DTM, i.e. the LiDAR DSM *first*, and the simplified one proposed, that is a LiDAR DTM with overlapped buildings. In particular, the buildings were considered by adding a 10 m elevation directly to the LiDAR DTM in the areas really occupied by the buildings themselves. Nevertheless, the correct location of the buildings was not easy at all: available building layers presented perimeters that did not coincide with the contour of the buildings removed from the LiDAR DSMs, by favoring the generation of erroneous depressions close to the buildings (Fig. 3.4 a-d). It is clear that such a representation would have involved the definition of a fictitious surface network that could not be accepted for modeling purposes.

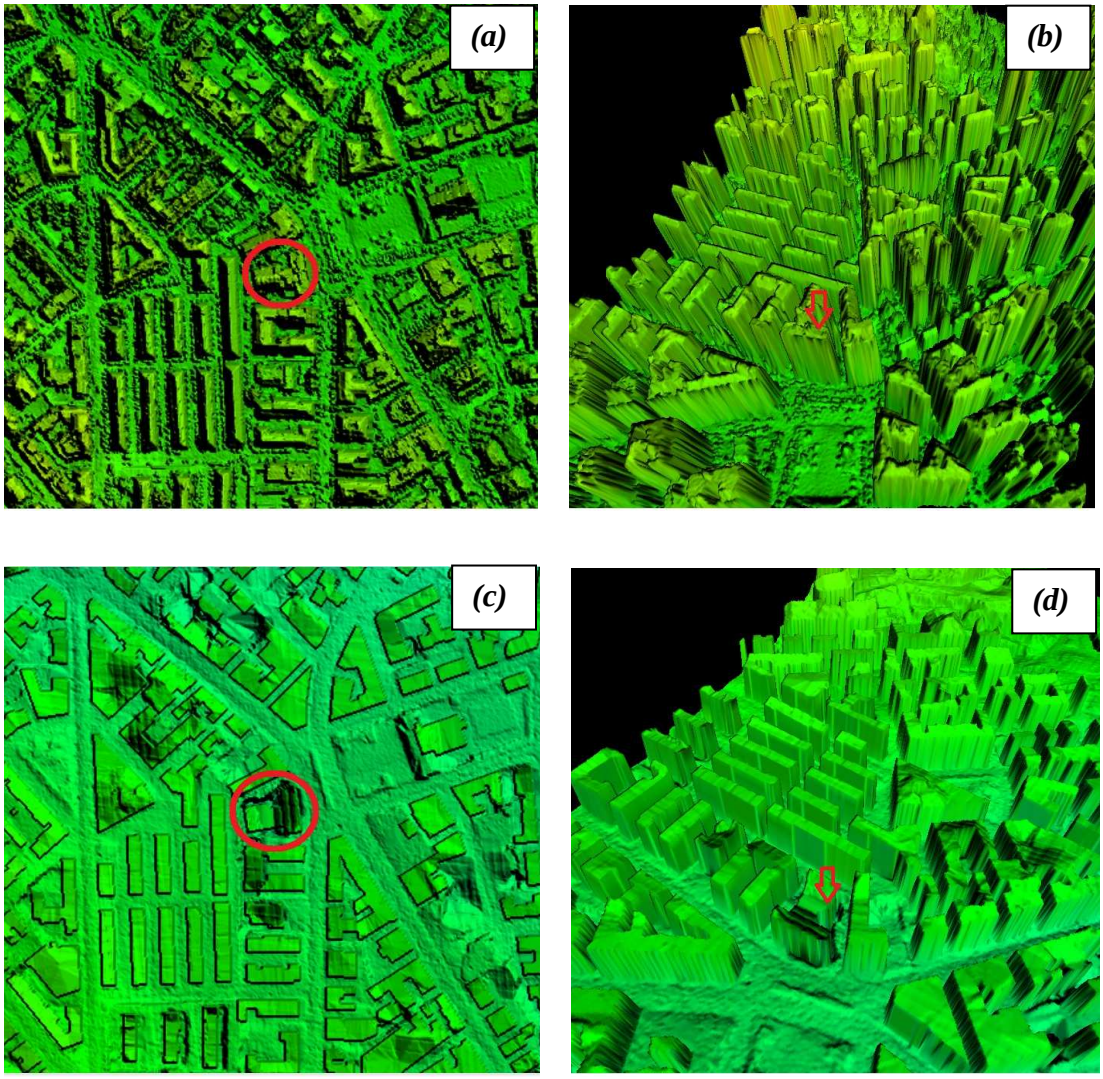

Figure 3.4 Detail of one building inside the LiDAR DSM *last* with its 3D representation (a-b); detail of the same building added wrongly inside the LiDAR DTM with its 3D representation (c-d).

Therefore, the buildings areas were derived by subtracting the LiDAR DTM to the LiDAR DSM *last*, and considering only the objects characterized by an elevation at least of 3 meters and a surface area at least of 10 m^2, assumed as minimum building properties. The accuracy of the methodology was then estimated by comparing the footprints of the original building layer and the new one obtained.

The choice of the LiDAR DSM *last*, rather than the LiDAR DSM *first*, was made because the former should contain a smaller number of objects by definition, thus the filtering process would have been simplified. This assumption was later confirmed by the results of the elaborations carried out (tab. 3.2 and fig. 3.5): in fact it is

possible to observe that the consideration of the LiDAR DSM *first* determined the definition of a greater number of non-ground surface features to be filtered in all the cases.

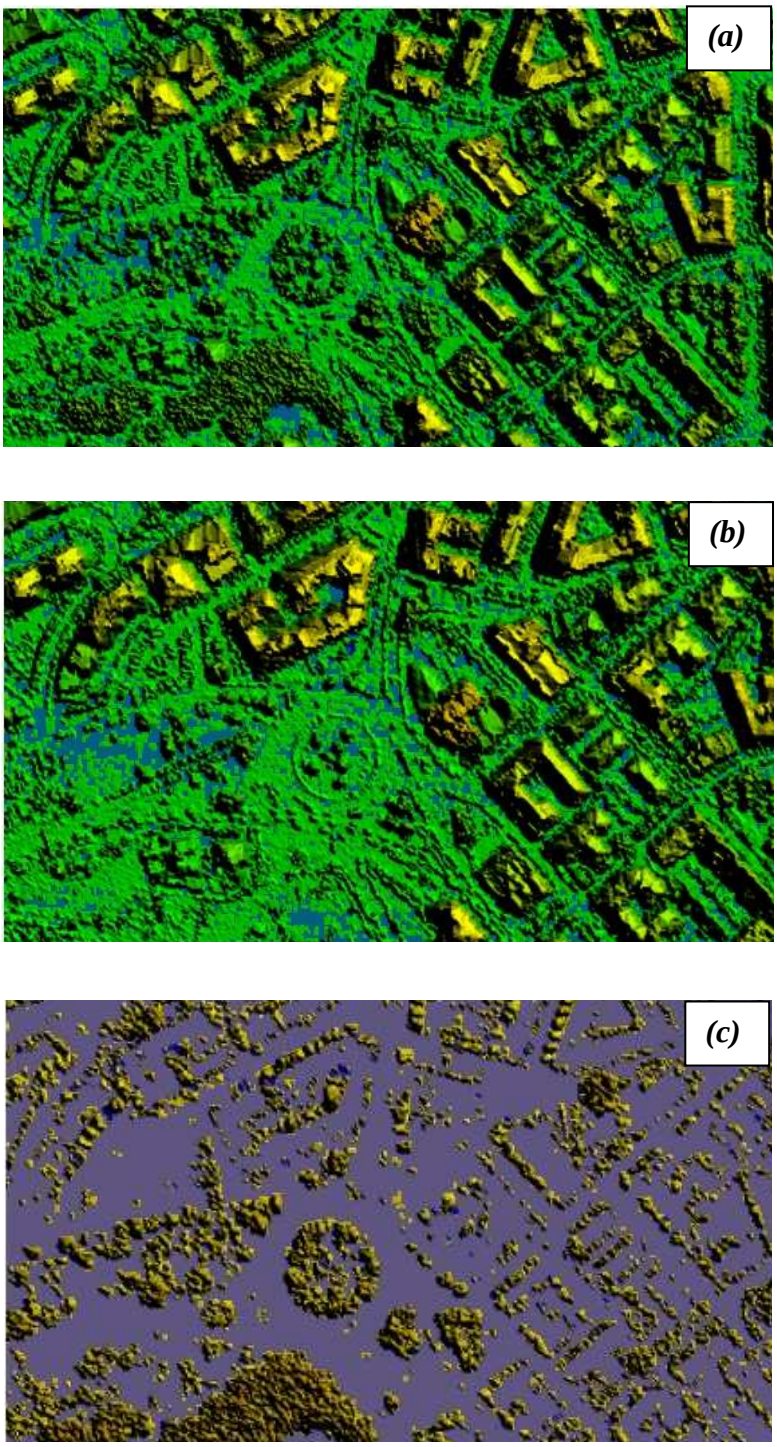

Figure 3.5 LiDAR DSM *first* - LiDAR DTM (a), LiDAR DSM *last* - LiDAR DTM (b) and LiDAR DSM *first* - LiDAR DSM *last* for the same portion of the Liguori catchment.

	% of the catchment area occupied by non-ground surface features	% of non-ground surface features to be filtered
DSM first without any filtering	42.93%	66.84%
DSM last without any filtering	40.70%	63.19%
DSM first ($z > 3$ m)	20.76%	31.94%
DSM last ($z > 3$ m)	16.62%	15.02%
DSM first ($z > 3$ m ; $A > 10$ m^2)	20.24%	30.17%
DSM last ($z > 3$ m ; $A > 10$ m^2)	16.21%	12.87%

Table 3.2 Filtering analysis results.

The proposed filtering method worked quite well because almost all the buildings were identified, also if it was not possible to distinguish vegetated areas located close to buildings, representing 12.87 % of non-ground surface features to be filtered (tab. 3.2). Consequently, later, manual editing was also necessary.

In particular the use of the new building layer in the generation of the LiDAR DTM_b was opportune because it enabled the removal of a good part of the surface depressions obtained by taking as reference the original building layer (38.90 %). A further 61.10 % of the surface depressions was still shared by the two DTMs (fig. 3.6 and 3.7).

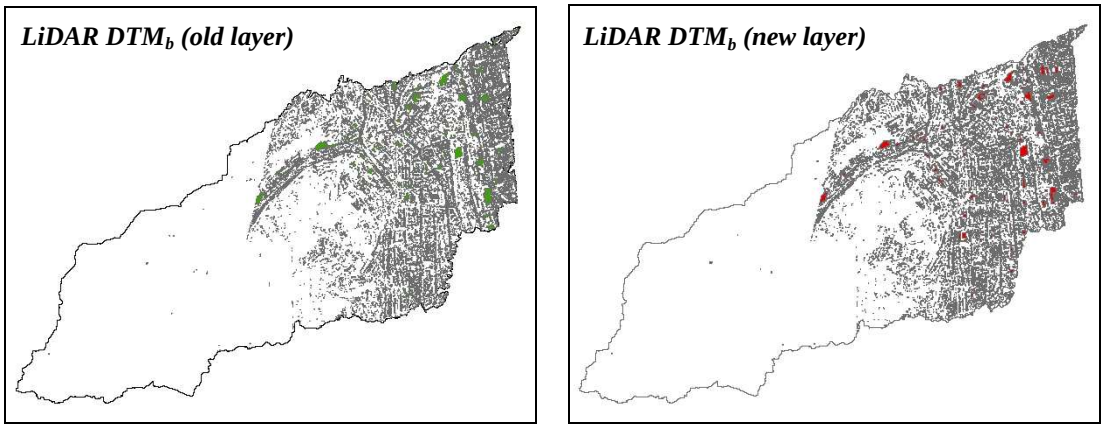

Figure 3.6 Surface depressions found inside the LiDAR DTM_bs generated by considering the two building layers.

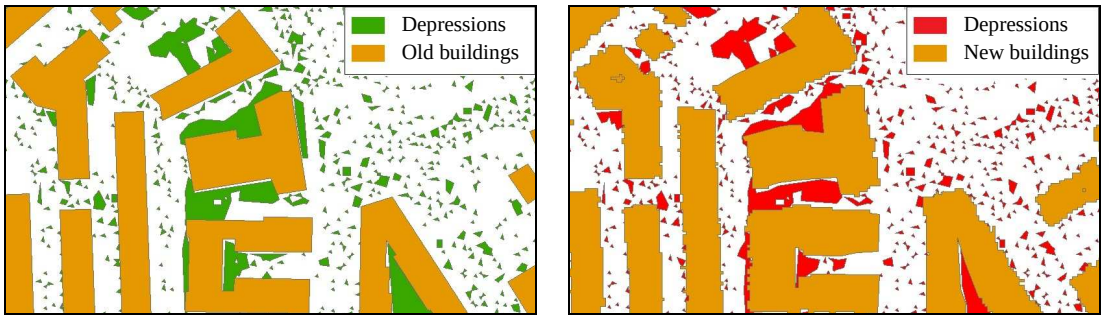

Figure 3.7 Detail of the different surface depressions found inside the LiDAR DTM_bs generated by considering the two building layers.

Afterwards the comparison between the corrected LiDAR DTM_b and the LiDAR DSM *first* was performed in terms of evaluable surface depressions, in order to verify if the former data set could be a valid approximation of the latter one. As expected, a greater number of depressions was found in the LiDAR DSM *first*, however the simplification proposed seemed acceptable since a good portion of the identified depressions was in common between the two DTMs (37 %), particularly the largest ones (tab. 3.3 and fig. 3.8).

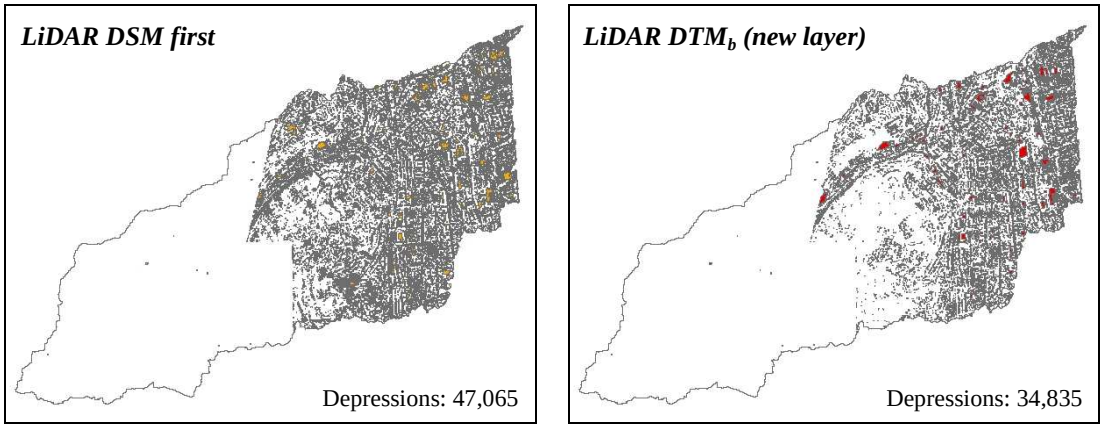

Figure 3.8 Surface depressions found inside the LiDAR DSM *first* and LiDAR DTM_b.

	depressions with surface area *A*					
	> 10 m^2	> 20 m^2	> 50 m^2	> 100 m^2	> 500 m^2	> 1000 m^2
% shared depressions between LiDAR DSM *first* and LIDAR DTM_b	4.66%	40.27%	42.01%	42.44%	45.84%	48.85%

Table 3.3 Shared surface depressions between the two LiDAR DTM data sets.

This result means that vegetation and other non-ground surface features can be neglected for hydraulic modeling purposes because they disturb the surface runoff little compared to the buildings. Similar conclusions were also reported in other researches: in particular Tsubaki et al. (2006) referred to the need to remove vegetation from the DSM in order to obtain realistic overland flow modeling results. They found in fact that if vegetation is not taken into account, flooded water will start accumulating before overflowing over the top of the vegetation itself.

However, the use of very detailed DTMs, such as LiDAR ones, favors the presence of a greater number of errors inherent to the acquisition and interpolation processes of the elevation data, such as pits or sinks, as already reported in Chapter 2. These are depressions disrupting the drainage surface, which preclude routing of flow over the surface. Sinks arise when neighboring cells of higher elevation surround a cell, or when two cells flow into each other resulting in a flow loop, or the inability for flow to exit a cell and be routed through the grid (Burrough and McDonnell, 1998).

Hydrologic parameters derived from DTMs, such as flow accumulation, flow direction and upslope contributing area, require that sinks be removed. However, just sinks could also be real components of the surface. For example, in large-scale data where surface hummocks and hollows are of importance to surface drainage flow, sinks are accurate features.

A number of methods have been described for managing depressions in DTMs (O'Callaghan and Mark, 1984; Jenson and Domingue, 1988; Hutchinson, 1989; Jenson, 1991; Rieger, 1998; Martz and Garbrecht, 1999), nevertheless, currently, there is no standard way of LiDAR data improvement (or smoothing). In this case such issue was faced by assuming that all the surface depressions found in the most realistic data set, i.e. the LiDAR DSM *first*, were correct: thus all the common depressions between LiDAR DSM *first* and the LiDAR DTM_b and between LiDAR DSM *first* and the LiDAR DTM were considered correct, whereas the remaining ones were removed by filling operations.

3.4 Traditional modeling of the drainage network

In a first phase a detailed study of the catchment was carried out through the use of the ArcGIS 9.3 software, in order to evaluate the physical characteristics of the system to insert into the hydraulic model.

Owing to the lack of information about the manhole positions, the system was modeled using "fictive manholes", whose position was obtained by considering the intersections between the sewer layout and the natural drainage network generated from the previously processed LiDAR DTM_b (fig. 3.9).

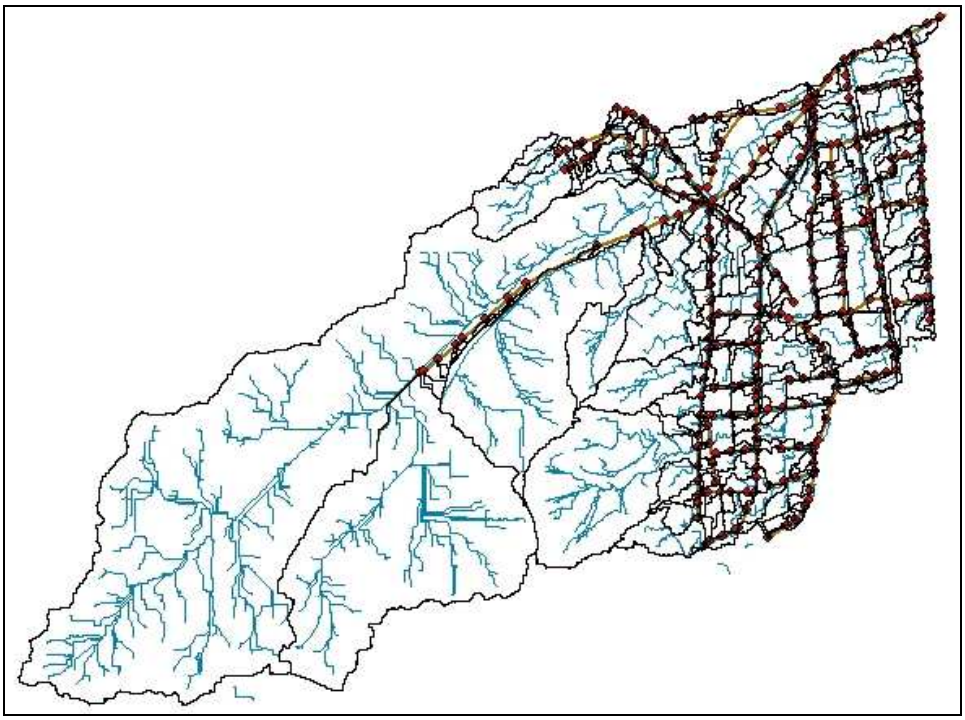

Figure 3.9 Localization of the “fictive manholes”.

Specifically, only the intersections, characterized by a Horton’s number greater than one, were considered. Later such points were assumed as outlet nodes, i.e. nodes receiving the sub-catchments runoff.

A total number of 296 sub-catchments were identified: 258 were mostly urbanized ($\%_{Imp} > 0.7$), 23 were on average urbanized ($0.3 < \%_{Imp} < 0.7$) whereas the remaining part was characterized by a natural destination. All these information together with the sewer data set, were then imported into SWMM through the use of

the inp.PINS application for the next hydraulic modeling of the drainage system (fig. 3.10) .

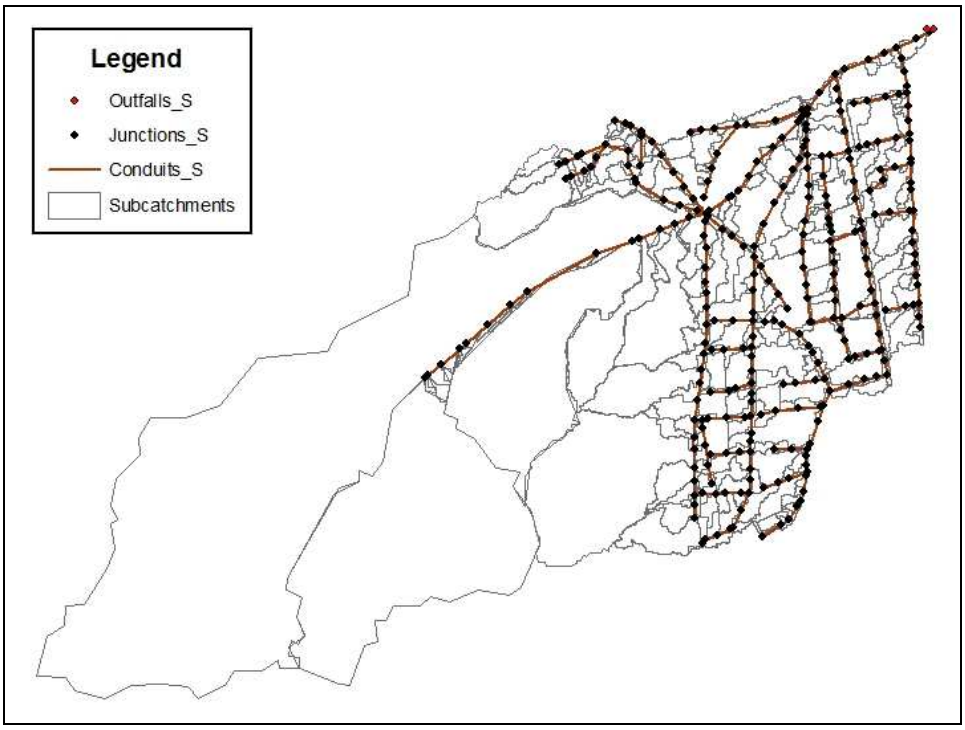

Figure 3.10 Sewer network model.

The calibration of the model was carried out on the basis of the rainfall and flow data available for eleven events, and, in particular, it concerned the following parameters:

- *Dstore_perv*, i.e. the depth of depression storage on the pervious portion of the sub-catchment [millimeters];
- *Dstore_imperv*, i.e. the depth of depression storage on the impervious portion of the sub-catchment [millimeters];
- *n*, i.e. Manning's roughness coefficient for the conduits.
- *N_perv*, i.e. Manning's coefficient for overland flow over the pervious portion of the sub-catchment;
- *N_imperv*, i.e. Manning's coefficient for overland flow over the impervious portion of the sub-catchment.

The check consisted in comparing the overall trend of the simulated and recorded hydrographs through the calculation of Pearson's coefficient. After various attempts,

it was observed that the model provided satisfactory results (Appendix A) assuming the following values for the parameters:

- *Dstore_perv* = 2.5 mm,
- *Dstore_imperv* = 0.05 mm,
- n = 0.017 s/m$^{1/3}$,
- *N_perv* = 0.22 s/m$^{1/3}$,
- *N_imperv* = 0.05 s/m$^{1/3}$.

3.4.1 Performance indicators and efficiency assessment of the drainage network

Afterwards the calibrated model was used for estimating the functioning condition of the sewer network through the calculation of two groups of synthetic indicators: physical indicators and hydraulic indicators.

This type of approach, already proposed in some previous researches (Fiorentino et al., 2005), is also recommended at the international level: in fact the International Water Association is looking to provide guidelines for the definition of optimal management procedures of networks, which are based on the use of appropriate performance indicators (Alegre et al., 2000).

The study of performance indicators is extremely useful in identifying the sections of the network which require greater and more urgent attention and where available resources should be concentrated (Di Federico, 2005). This approach also permits an evaluation of the effects that design or rehabilitation choices could have on the network behavior.

Moreover, the indicators can be calculated on the basis of diverse time intervals to evaluate the system performance evolution over the time, or they can be utilized as a common base to compare different networks in terms of performance (Ermini, 2000; Tang, 1985; Wagner et al., 1988 a,b; Billington and Allan, 1987).

In this case physical and hydraulic indicators were calculated for every sewer trunk in order to highlight which constructive defect determined the most relevant repercussion on the network performance, and then which rehabilitative interventions should be taken into account. Local geometric discontinuities, such as slope,

diameter, or direction variations, were considered through the introduction of specific slope (i_p), shape (i_f) and direction indices (i_α). In particular, some thresholds values were defined for each index, in order to distinguish three levels of criticality, which were later graphed with different colors:

• Level 1 - high criticality (red color);

• Level 2 – normal criticality (yellow color);

• Level 3 – absent criticality (green color).

The shape index (i_f) characterized the geometric discontinuity associated with changes in shape or diameter between two consecutive links. It was defined as the ratio:

$$i_f = \frac{D_d - D_u}{D_u} \tag{3.1}$$

where, respectively, D_d and D_u represented the downstream and the upstream diameters.

For the shape index the threshold value was fixed at zero: if the diameter of the downstream link was the same as the diameter of the upstream link, the level of criticality was assumed to be normal. A negative value for the shape index indicated nodes where the downstream section decreased and overflow phenomena could occur. Consequently, the associated level of criticality was high (level 1). Positive index values showed an increase in the downstream section of the link: the associated criticality level was three (table 3.4).

The slope index (i_p) expressed the criticality due to slope changes that can occur in two consecutive links:

$$i_p = \frac{j_d - j_u}{j_u} \tag{3.2}$$

where j_d and j_u were the downstream and upstream slopes.

Also for the slope index the threshold value was fixed at zero: if the slope of the downstream link was equal to the slope of the upstream link, the criticality level was assumed to be normal (level 2). Instead, negative values of the slope index localized local concave connections where deposition or accumulation of solid substances could be favored. In such situations the criticality level was high (level 1). Positive

index values indicated an increase in the slope of the downstream trunk: the associated criticality level was three (table 3.4).

The direction index (i_α) expressed the criticality due to any planimetric deviation between two consecutive links. It depended on the angle α that the prolongation of the upstream conduit defined with the downstream conduit:

$$i_\alpha = 1 - \frac{\alpha}{180} \tag{3.3}$$

Two threshold values (0.25 and 0.50) were fixed for the direction index. The value 0.25 was obtained by considering a value of α equal to 135°: if the angle α was greater than 135° ($i_\alpha < 0.25$) a high level of criticality occurred (level 1), because the insertion of the upstream conduit into the downstream conduit occurred with a significant energy loss. Instead the value 0.50 was obtained by considering a value of the angle α equal to 90°, beyond which energy losses were considered to be negligible (table 3.4).

It is evident that such singularities can determine surcharge conditions in the drainage network, and therefore outflows from manholes and consequent flooding of the surrounding area. For this reason, a volume index (i_v) was also introduced for expressing the magnitude of the node surcharge:

$$i_v = \frac{V_{flood}}{V_{in,tot}} \tag{3.4}$$

where V_{flood} is the volume discharged on the surface by the generic node and $V_{in,tot}$ is the total water volume flowing through the same node.

Two threshold levels (0 and 0.01) were fixed: when V_{flood} was zero (i_v =0), no criticality could be associated (level 3). Instead, if the flood volume was bigger than 10% of $V_{in,tot}$, the consequent level of criticality was no longer negligible (level 1). Finally, normal criticality was assumed when the volume index was comprised between 0.01 and 0 (table 3.4).

V_{flood} and $V_{in,tot}$ were deduced from the results of the simulations carried out through the previously calibrated hydraulic model. In general, it is possible to perform evaluations of the hydraulic indicators by considering both observed and synthetic hyetographs, depending on the research goals. In this case it was interesting to

evaluate the sewer network response to a design rain event with a return period of ten years.

Level of criticality	Values of i_f	Values of i_p	Values of α	Values of i_α	Values of i_v
high	$i_f < 0$	$i_p < 0$	$\alpha > 135°$	$i_\alpha < 0.25$	$i_v < 0.01$
normal	$i_f = 0$	$i_p = 0$	$90° < \alpha < 135°$	$0.25 < i_\alpha < 0.50$	$0.01 < i_v < 0$
absent	$i_f > 0$	$i_p > 0$	$\alpha < 90°$	$i_\alpha > 0.50$	$i_v = 0$

Table 3.4 Levels of criticality for the physical and hydraulic indicators.

Afterwards the computed indices were reported in GIS in order to localize immediately the most critical elements of the sewer network (fig. 3.11).

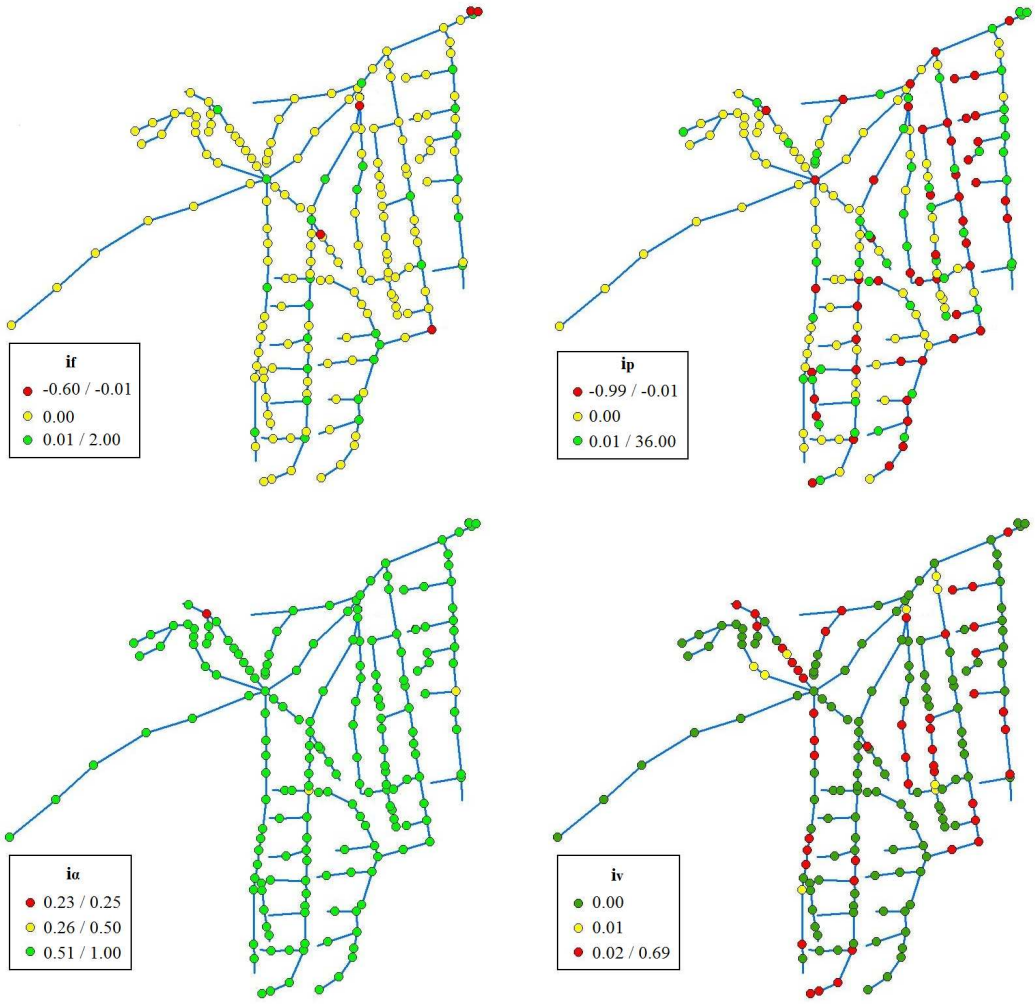

Figure 3.11 Spatial distribution of the calculated synthetic indexes.

Especially it was possible to observe that the proposed methodology detected 29 out of the 48 nodes characterized by surcharge conditions. In fact, about 60% of the points, identified by volume index values greater than 0.01, presented at least one physical criticality. In particular, the slope variation resulted the principal cause of malfunctioning of the sewer network: in fact about 86% of the nodes, characterized by physical criticalities, showed deficiencies of this nature (fig. 3.12).

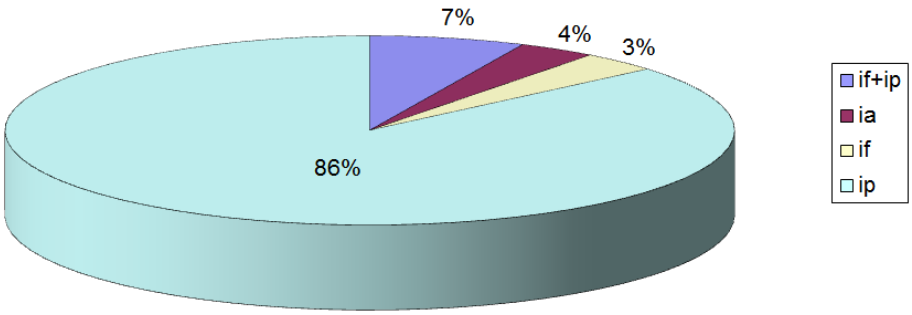

Figure 3.12 Incidence of various physical deficiencies in the performance of the sewer network.

Therefore, the network performance could be improved by adjusting the slopes of the most critical trunks, and avoiding any concave connection that could facilitate the deposit of solids transported by the flow.

Finally, it is important to underline that this methodology also showed some gaps: in fact, some surcharged nodes were not characterized by physical criticalities. These results are explained by the inability of the method to predict the consequences that the crisis of a generic node could determine on the upstream nodes. In effect, the impossibility of considering backwater effects through the simple estimation of synthetic indices is evident.

3.5 Dual drainage modeling of the drainage system

Although a traditional modeling of the drainage system can lead to acceptable results, such as the efficiency assessment of the drainage network through performance indicators, it is important to emphasize that this approach is not adequate to simulate sewer flooding realistically, since it ignores the fundamental concept on which traditional urban hydrology is based, i.e. the interaction between the surface network with the buried drainage system (*dual drainage* approach).

In reality, the flood water either fills natural surface storage (ponds) or subsequently travels across the terrain through preferential pathways by creating a surface flow network typically called the “major system,” while the “minor system” refers to the underground sewer network. The connection between the two systems is realized through the presence of inlets and manholes, through which stormwater can be channeled into the sewage system or can be discharged on the surface when the sewage system is overloaded.

Although the dual drainage method is simple from the conceptual point of view, its implementation is quite complex: in fact, the sewer system is generally known, whereas the surface network must be defined taking into account the geometric characteristics of the study area such as road slopes, dimensions of sidewalks, buildings, etc. Therefore, the definition of the major system required the use of an innovative technique: the AOFD procedure. A comprehensive data set is required to run this tool: Appendix B outlines in detail how these data can be created using ArcGIS and the likely sources of error that will prevent the AOFD tool from running successfully. After the data preparation a series of operations must be then carried out in order to derive the overland flow network. They were described adequately in Chapter 2.

It is evident that the reliability of the major system is greatly dependent on the quality of the available data, especially the DTM resolution, since the definition of the surface pathways is influenced by urban details contained in DTM itself. In the first phase precisely these issues were examined in greater depth: in particular, the extent to which the resolution of DTM and the presence of the buildings could affect the definition of the major system. Thus two different bare Earth DTMs for the same catchment were considered in order to compare the obtainable results. These DTMs were generated using different acquisition techniques and hence represented terrain with varying levels of resolution and accuracy:

- a DTM was generated by digitizing the contour lines and height points of a topographic map. The contour interval of the original map was 5 m (DTM 5);
- a LiDAR DTM was obtained from LiDAR survey and it was characterized by an horizontal resolution of 1 m (LiDAR DTM).

The buildings were also considered by adding a 10 m elevation directly to the bare Earth DTMs in the areas really occupied by the buildings themselves (fig. 3.13).

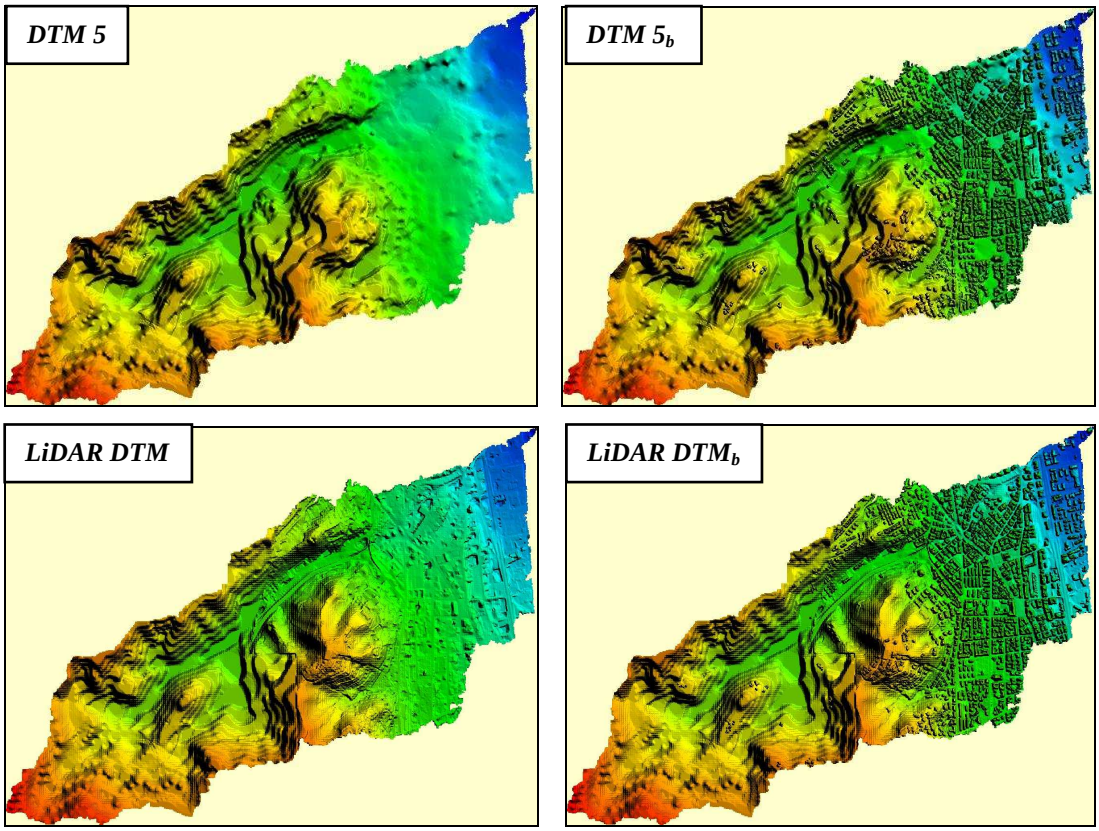

Figure 3.13 DTMs used in the case study.

The study showed that the number of surface pathways, ponds and the storage capacity of the ponds changed significantly depending on the resolution of the DTM and the consideration of the buildings inside the DTM itself (tab. 3.5 and fig. 3.14 and 3.15).

	Number of surface pathways	*Number of ponds*	*% of the catchment area occupied by the ponds*	*Ponds storage capacity [m^3]*
DTM 5	331	2	0.005%	35
DTM 5_b	1,275	924	4.50%	187,908
LIDAR DTM	1,805	1,351	4.64%	77,127
LIDAR DTM_b	2,655	2,191	5.72%	103,407

Table 3.5 Comparison of the pond and surface pathways delineation results using the four DTMs.

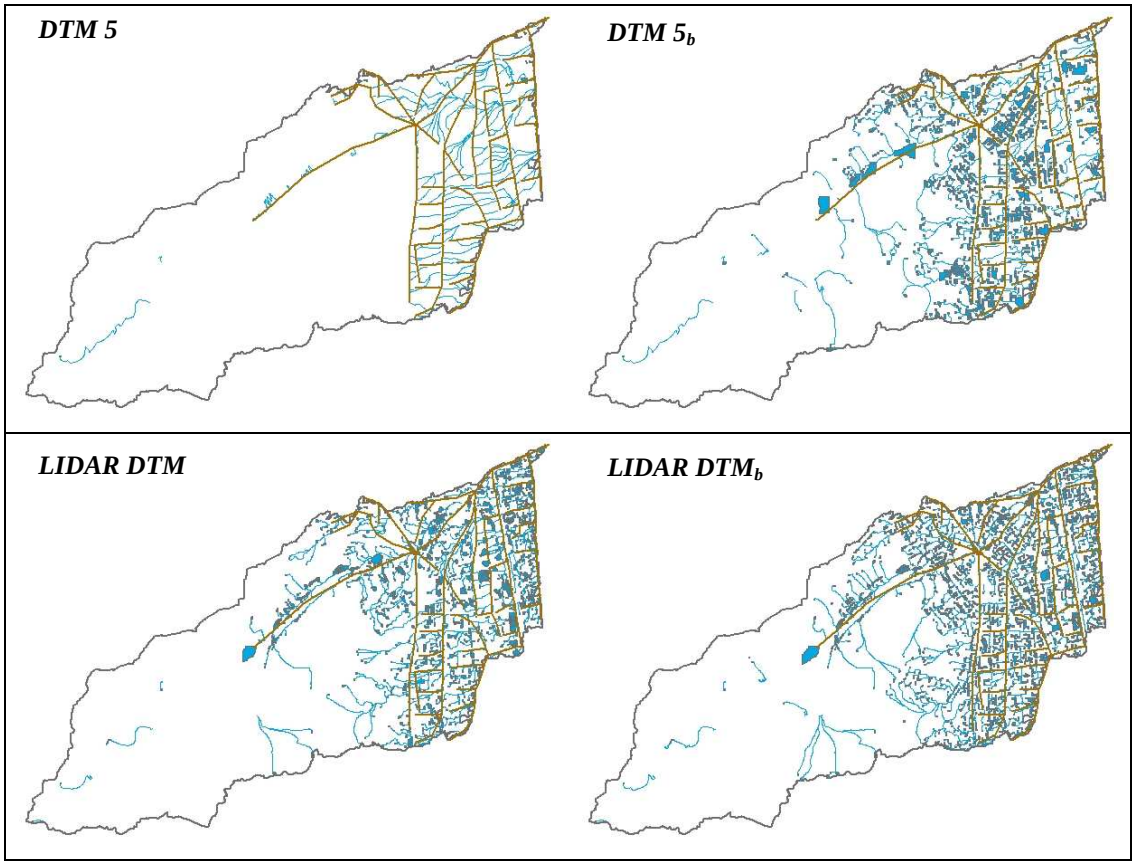

Figure 3.14 Ponds and surface pathways defined for the different DTMs considered.

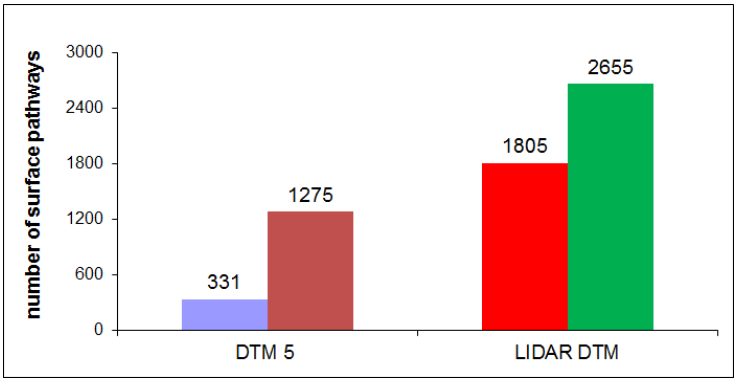

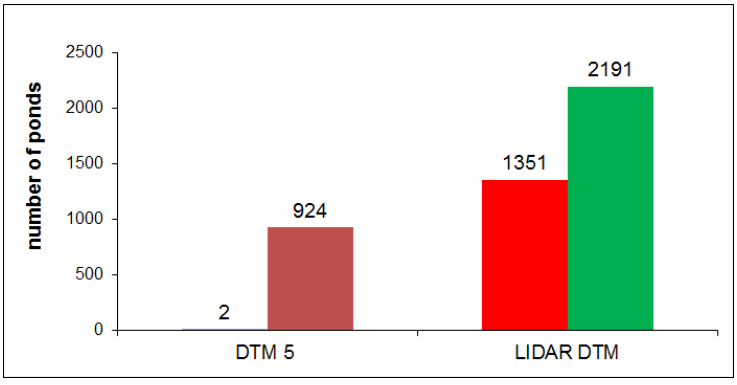

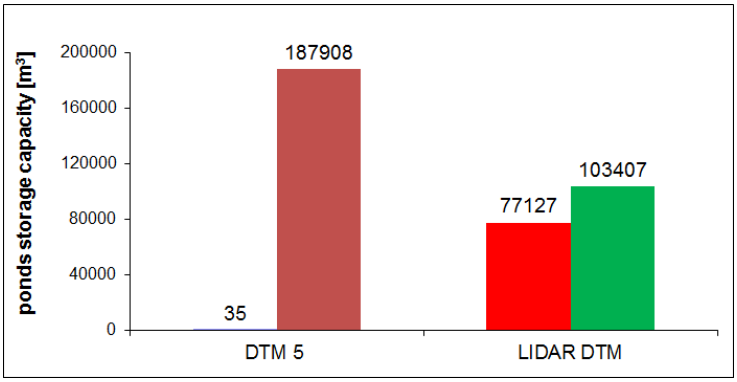

Figure 3.15 Comparison of the pond and surface pathways delineation results using the four DTMs.

It was observed that the use of more detailed DTMs enabled the definition of a greater number of ponds and surface pathways, in particular if the buildings were considered in DTM (fig. 3.15). This result was expected and can be explained by the fact that buildings act as barriers to the overland flow, hence they favor the definition of ponds with ever increasing extension and depth.

Moreover, their consideration enabled some issues to be avoided, such as ponds inside buildings and pathways crossing buildings (fig. 3.16).

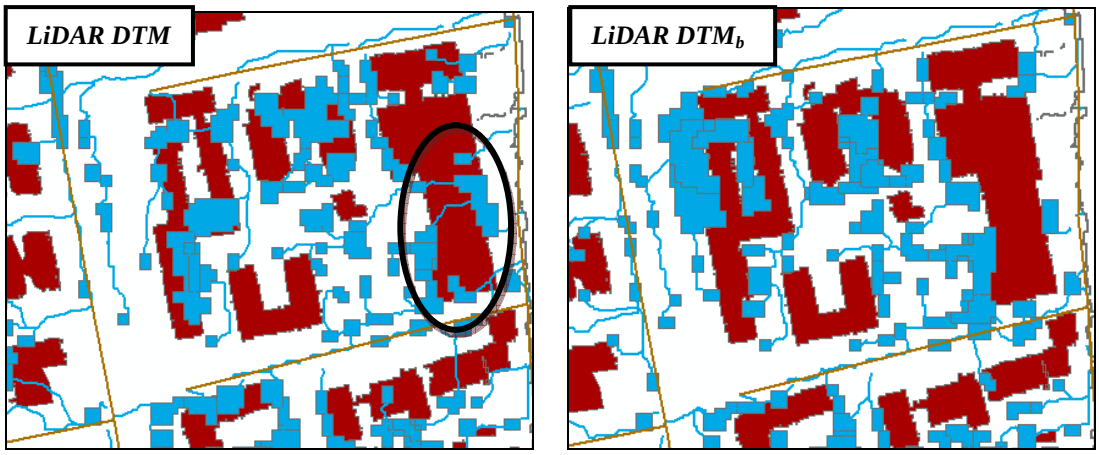

Figure 3.16 Influence of buildings on ponds identification procedure.

Nevertheless, the most interesting result was not the number of identified surface depressions, strictly speaking, but the associated storage capacity, because this feature determines the trend of the flows routing over the surface. It was observed that the increase of ponds storage capacity was significantly bigger for the DTM 5 rather than for the LiDAR DTM (187,908 m^3 for the $DTM5_b$ versus 103,407 m^3 for

the LiDAR DTM_b). This result could not be justified, principally because this increase was concentrated in a reduced number of ponds with respect to the LiDAR DTM (924 ponds for the $DTM5_b$ versus 2,191 ponds for the LiDAR DTM_b). Therefore, it was possible to conclude that the most reliable definition of the major system requires highly detailed DTMs, such as LiDAR ones.

However, the use of such data promotes the generation of a large number of small ponds, often not significant for simulation purposes, which could make heavier the computational load of the modeling. Moreover, these depressions could be also sinks that were not corrected in the previous stage of the DTM processing.

In order to overcome these drawbacks, the AOFD procedure allows all the depressions to be rejected that do not respect a series of conditions established for the depth and the volume. The ponds with smaller sizes than a threshold volume and shallower than a given depth will be removed. In this way the filtering routine removes some small ponds from the analysis, but the DTM remains unchanged. Therefore the AOFD approach to remove small ponds is different from the standard "fill" method available in the ArcGIS Toolbox. The latter method, in fact, fills all sinks (regardless of their sizes) by a user specified depth. Small ponds (or *pits*) are removed, however, big ones also lose their volume storage, and DTM is modified.

The threshold values of depth and volume can be established after a sensitivity analysis has been previously addressed: i.e. it is necessary to evaluate the optimum combination of volume and depth values that enables maximization of the number of insignificant ponds removed and minimization of the associated lost capacity. Practically, the pond removal should not affect significantly the surface storage capacity of the catchment.

Consequently, in the first stage, the maximum range of variation of the two parameters was researched (0 m < h < 9.06 m and 0 m^3 < V < 7,884 m^3), and later divided into an equal number of equidistant sub-intervals. Every time the corresponding ends of each interval were considered as threshold values in the AOFD, and two indexes were calculated:

- an accuracy index

$$i_a = 1 - \%\ lost\ volume \tag{3.5}$$

- a complexity index

$$i_c = 1 - \%\ ponds\ removed \tag{3.6}$$

The introduction of these parameters was aimed to find the condition that best balanced the two needs: accuracy and complexity of the hydraulic model. In fact, they mean that an increasing pond removal would determine an easier to implement hydraulic model, but a less accurate one because a part of the total storage capacity would be ignored.

By reporting graphically all the calculated values in a Cartesian plane with i_c on the x-axis and i_a on the y-axis, a cloud of points, well fitted by an exponential rise to maximum function with four parameters, was obtained (fig. 3.17):

$$y = a \cdot \left(1 - e^{-bx}\right) + c \cdot \left(1 - e^{-dx}\right) \tag{3.7}$$

with a = 0.21, b = 788.94, c = 0.78 and d = 12.56 (r^2 = 0.99).

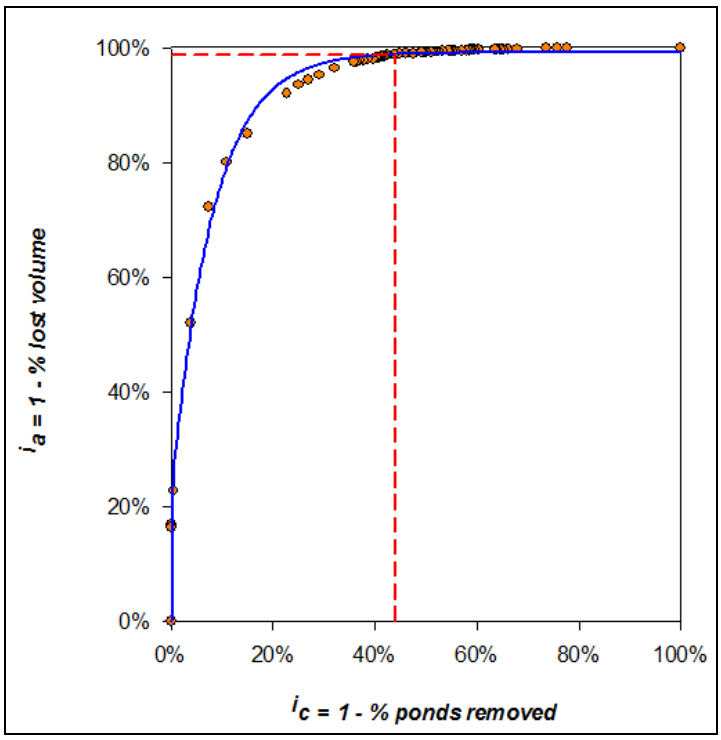

Figure 3.17 Graphical representation of i_a versus i_c values obtained from the elaborations.

The less steep branch of the curve, relative to the elaborations carried out by considering small thresholds values of volume and depth (0 m < h < 0.2 m and 0 m^3 < V < 10 m^3), demonstrated how a large number of small ponds delineated are, in most cases, the result of DTM errors (*pit cells*) because their removal did not determine any relevant change in the lost volume. In fact, i_c tended to be reduced with a higher rate than i_a. This trend was maintained until the turning point of the curve (i_c = 15.02 % and i_a = 85.09% obtained for h = 1.06 m and V = 879 m^3), beyond which every further reduction of i_c determined a significant reduction of i_a, i.e. an important loss of storage capacity.

Consequently, the analysis was later limited to the range of values relative to the first part of the curve: different threshold values of depth (comprised between 0 and 0.2 m, with a step of 0.025 m) and volume (comprised between 0 and 10 m^3, with a step of 0.5 m^3) were considered and several calculations were carried out by assuming one of the two parameters constant and by varying the other each time. All the results of the elaborations were later plotted in order to obtain:

- the constant-depth curves relative to the percentage of ponds removed (fig. 3.18 a);
- the constant-depth curves relative to the percentage of lost volume (fig. 3.18 b);
- the constant-volume curves relative to the percentage of ponds removed (fig. 3.18 c);
- the constant-volume curves relative to the percentage of lost volume (fig. 3.18 d).

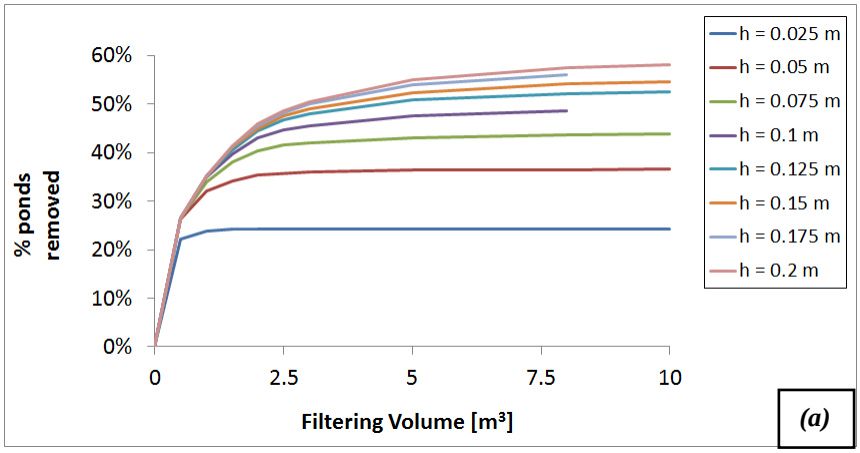

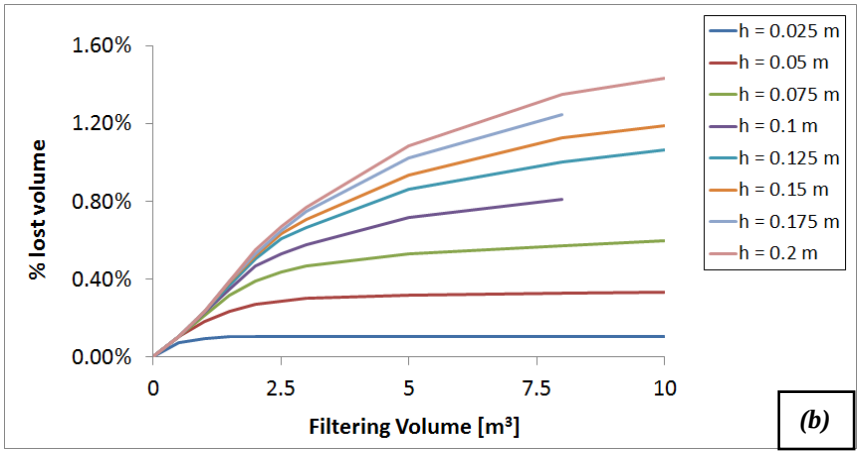

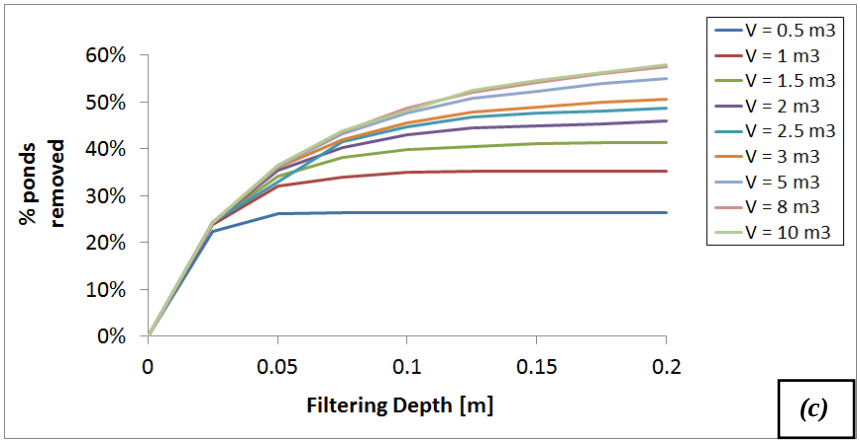

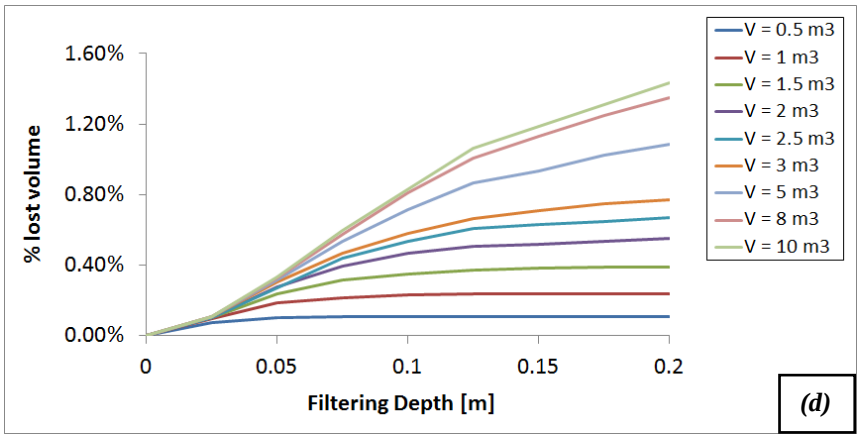

Figure 3.18 Constant-depth curves relative to % ponds removed and % lost volume (a-b); Constant-volume curves relative to % ponds removed and % lost volume (c-d).

The objective was to verify whether all the constant-depth curves presented the same point of inflection, i.e. the same optimal value of volume beyond which the further

increase of the threshold volume would not produce any variation either in the lost storage capacity or in the number of the ponds removed. Similarly the same approach would be applied for the constant-volume curves. However, the proposed methodology was not useful because it was not possible to define a unique optimal condition for both the constant-depth and constant-volume curves.

Consequently, the choice of the threshold values was later carried out by trying to find a physical explanation for these values: specifically, a value of 0.2 m was assumed for the depth, since the footpaths usually are characterized by similar height, whereas a value of 5 m^3 was chosen for the volume in order to filter all the ponds characterized by a surface area inferior to 25 m^2 (5 m^3 ÷ 0.2 m = 25 m^2). This assumption was acceptable, since the correspondent values of i_a and i_c resulted, respectively, equal to 98.92 % and 44.91 % (red line in fig. 3.17): i.e. a pond removal of 55 % determined only a lost storage capacity of 1.08% (fig. 3.19 and 3.20).

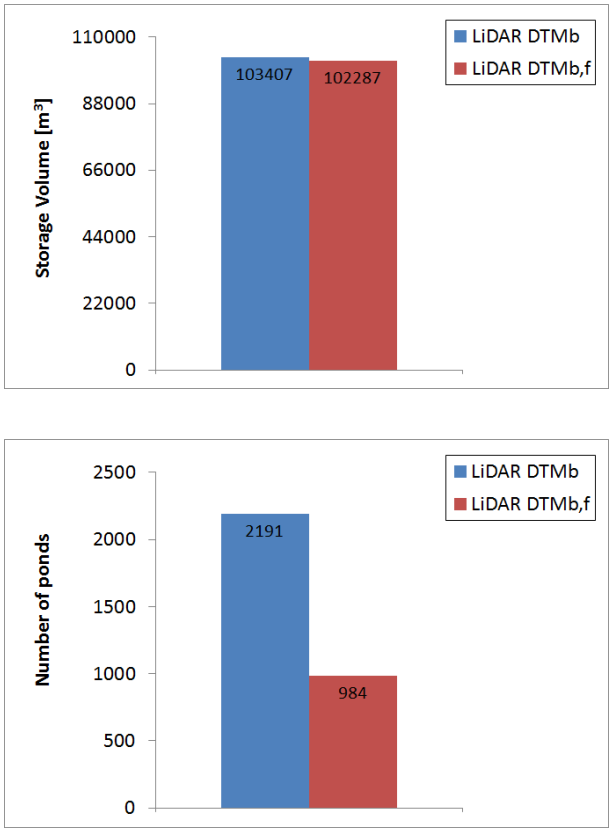

Figure 3.19 Storage volume and surface ponds in LiDAR DTM_b and LiDAR DTM_b filtered.

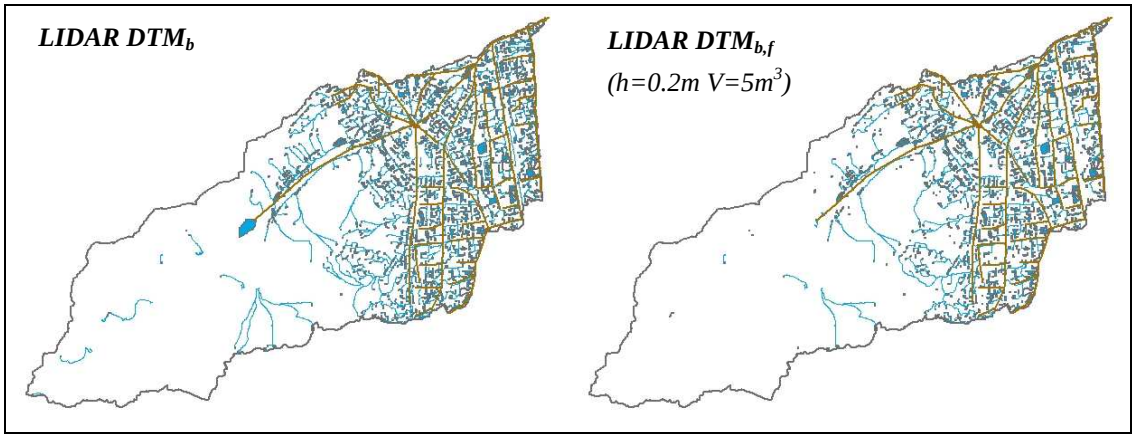

Figure 3.20 Ponds and surface pathways before and after the pond filtering process.

The obtained surface network (fig. 3.20) was later coupled with the sewer network model into SWMM, by assuming a series of 1D open channels, connecting the surcharged manholes of the sewer system with the surface depressions, schematized as storage nodes in the model (fig. 3.21).

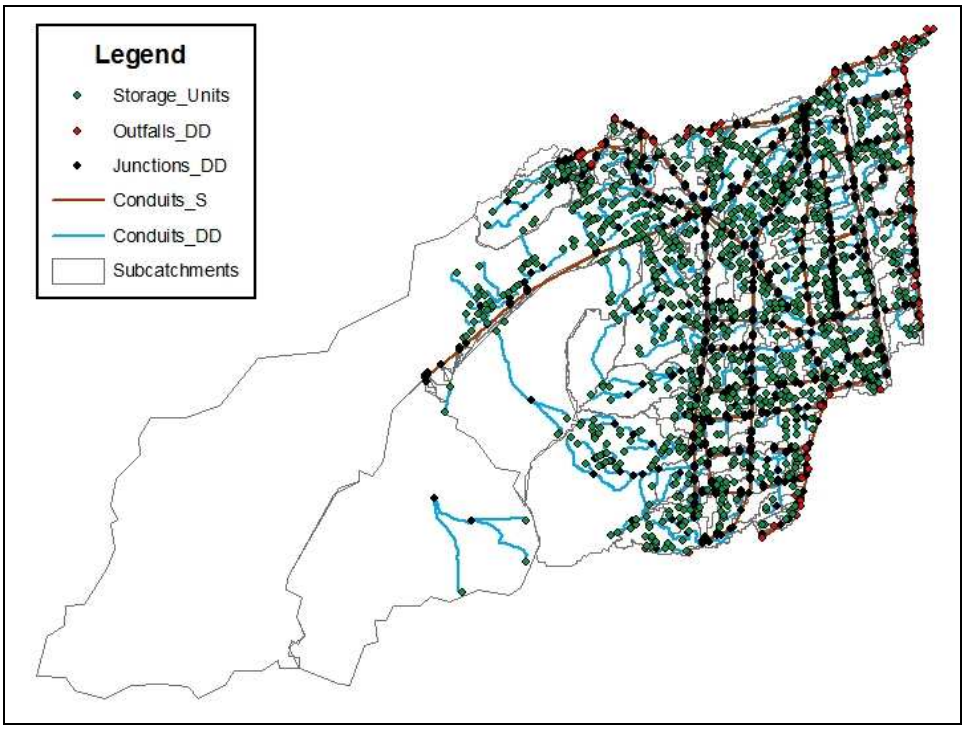

Figure 3.21 Dual drainage model.

The geometric features of ponds, such as depth - volume relations, and surface pathways were provided directly from the AOFD. In particular, the surface pathways were modeled by assuming a simple trapezoidal cross-section with:

- a width of 10 meters, equal to the usual width of the urban roads;
- a height of 1.5 meters, for taking into account the possible overcoming of the height of the curb from the surface flow;
- an inclination of the oblique sides of 45 °.

The link between the *major* and the *minor system* was realized by equipping all the surcharged sewer nodes with orifices, which had to be opened when the node started to be overloaded (in particular, in this case, when the maximum depth was reached in the node, i.e. a value of 2.5 meters). Specifically, the simulation of backwater effects to represent the surcharge of stormwater from manholes, or the rapid change of water level, required the use of dynamic wave models.

The simulation of the interaction between the surface and the sub-surface networks was thus modeled trough a 1D-1D approach. Although this methodology is less accurate than 1D-2D models, it was chosen because

1) the inferior reliability of the model was in large part compensated by the use of highly detailed topographic data, such as LiDAR DTMs;
2) a similar procedure is more adequate for real time simulation of the drainage system and rapid forecasting of the flooding processes. In fact, basically, the limitations of 1D-1D make it very difficult to simulate local conditions accurately on a small scale, whereas simulation of larger scale urban flooding gives very promising results.

The calibration of the dual drainage model would have required the availability of recorded data also for the surface network, such as flow paths, flood extent or the flow capacity of streets. The same speech is valid for the AOFD outcomes: in fact, the software gives an indication of the potential flooded areas and surface pathways based on the GIS routines developed. Then these results should be compared with all available information concerned with the past flooding processes experienced for the case study (risk maps, newspaper articles, photographs ...).

However, in this case, the lack of such information imposed the consideration of the same parameters previously adopted for the traditional modeling of the drainage network. The only new parameter was Manning's coefficient for the surface pathways, which was assumed equal to 0.013 $m^{1/3}/s$.

3.5.1 Differences between the two types of modeling

It is evident that the complexity of the hydraulic model increased by passing from a traditional approach to a dual drainage one, as it is possible to observe by comparing the two graphical representation of the networks (fig. 3.10 and fig. 3.21). In fact, the number of conduits increased from 296 to 1625, the number of junction nodes increased from 296 to 485, since further nodes, connecting the surface pathways (break nodes), had to be taken into account, and also the number of outfall nodes increased from 2 to 55, because the consideration of the surface pathways determined the generation of further outfalls inside the catchment. Moreover, it was necessary to add about 1000 storage nodes, which enabled the simulation of the ponds, and 225 orifices to be provided to the surcharged sewer nodes. Nevertheless, this complication of the model was needed in order to simulate the behavior of the drainage networks more accurately, above all during extreme rain events.

In fact, by subjecting the two hydraulic models to identical rainfall inputs (the eleven historical events above cited and three synthetic rainfall events with associated return periods of 15, 30 and 50 years), it was possible to note different water volume distributions only when the storm events surcharged the sewer network (fig. 3.22).

07/27/2006

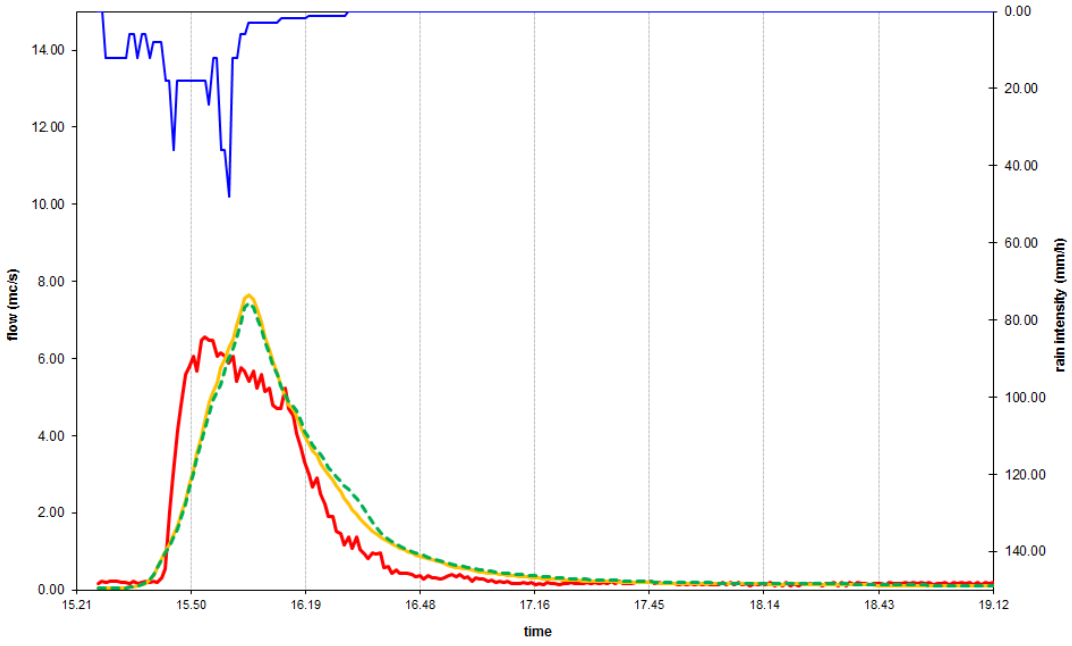

$(r_S^2 = 93.59\ \%\ ;\ r_{DD}^2 = 92.69\ \%)$

10/11/2007

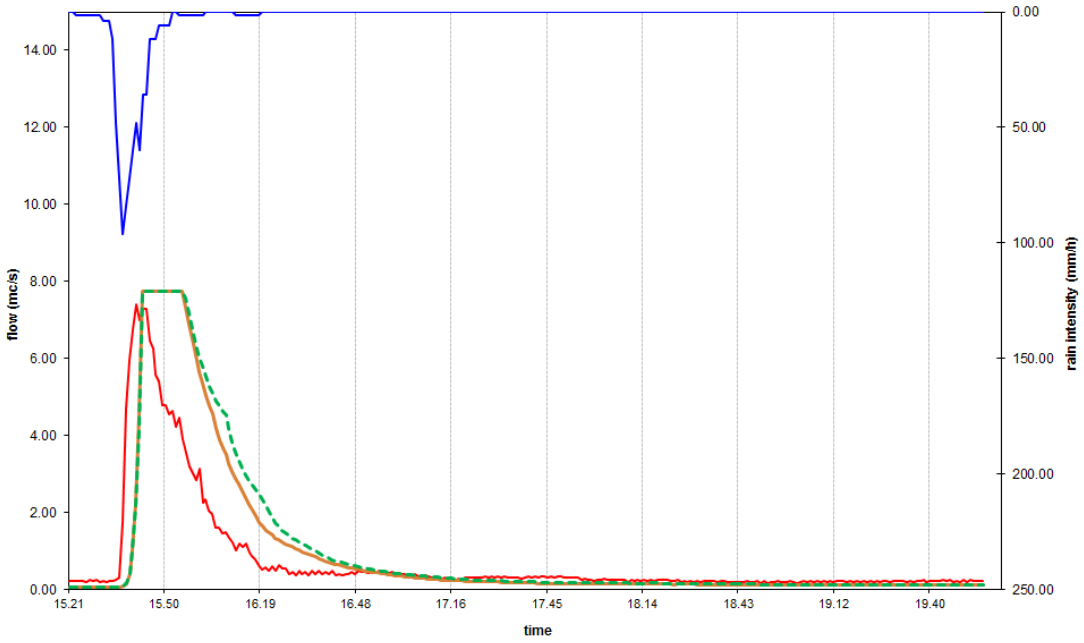

$(r_S^2 = 82.13\ \%\ ;\ r_{DD}^2 = 79.80\ \%)$

03/05/2009

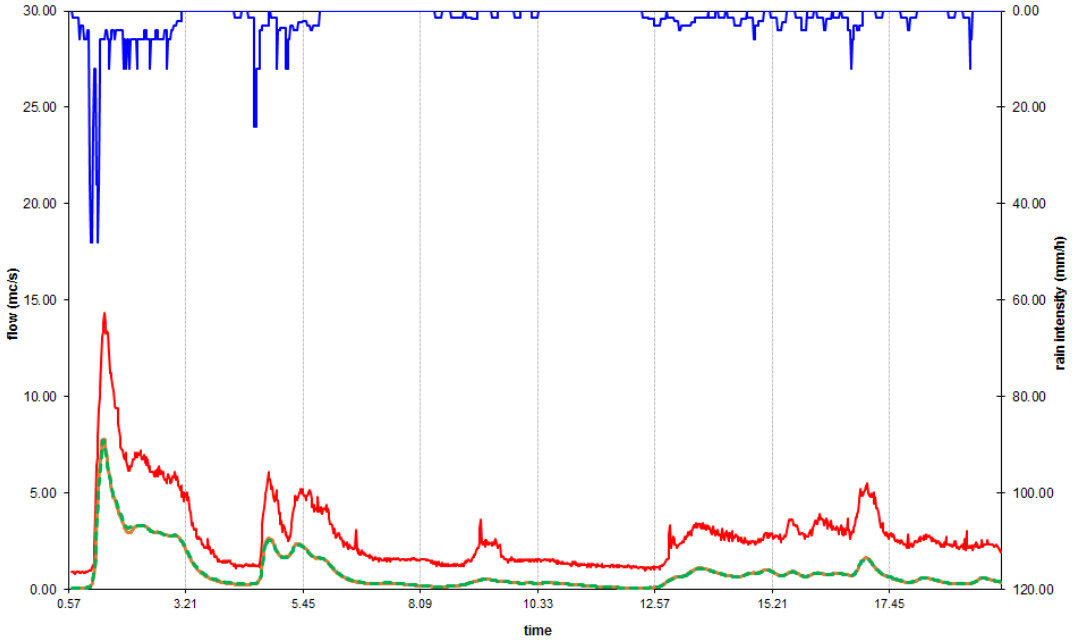

$(r_S^2 = 97.33\ \%\ ;\ r_{DD}^2 = 97.41\ \%)$

T = 15 years

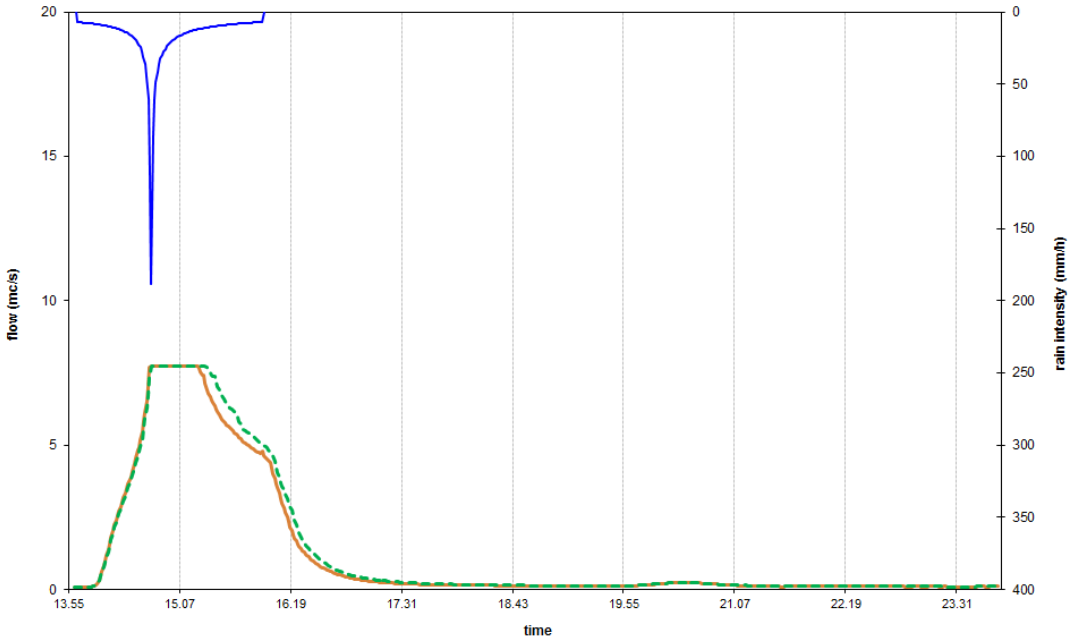

T = 30 years

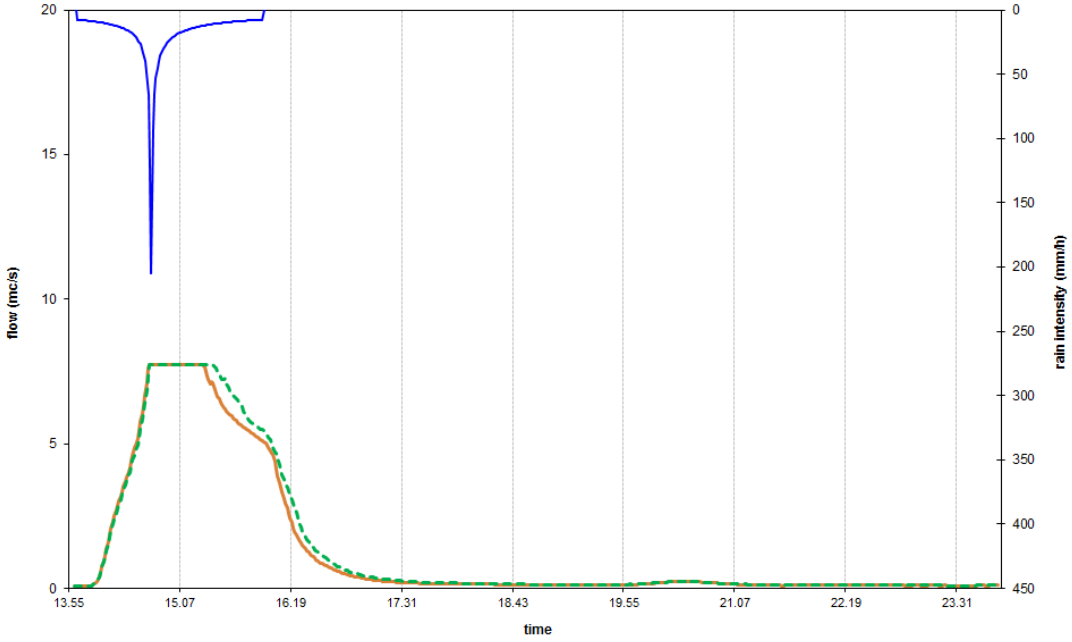

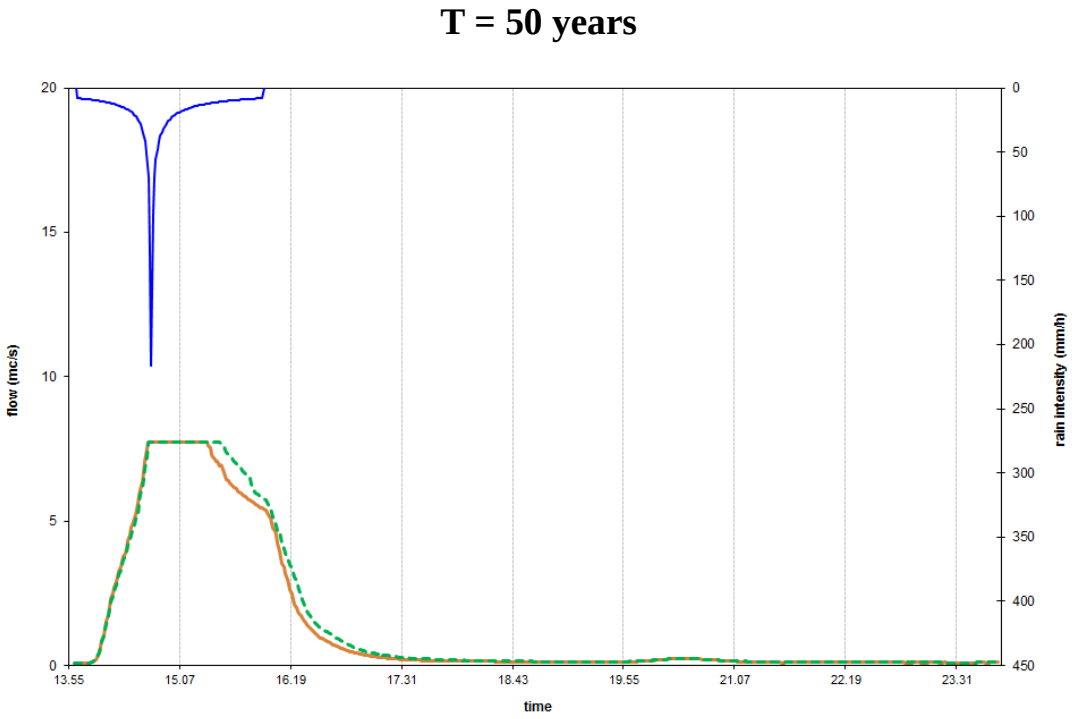

Figure 3.22 Historical and synthetic storm events where different responses from the two models were observed. In particular, for each event, the hyetograph is plotted in blue, the hydrograph simulated with traditional model is plotted in orange, and the hydrograph simulated with the dual drainage approach is plotted in green. Moreover, for the historical events, the observed hydrographs are plotted in red and the calculated Pearson's coefficients are also reported.

The above pictures, relative to the final trunk of the network, do not show clearly the diversity of the results obtained by using the two models: consequently, in order to favor a better comprehension of such aspects, these outcomes were later reported in terms of (tab. 3.6 and 3.7 and fig. 3.23 a-c):

- *Wet Weather Inflow*, i.e. the surface runoff;
- *Internal Outflow*, i.e. the flow that leaves the system through flooding at non-outfall nodes;
- *External Outflow*, i.e. the flow that leaves the system through outfall nodes (that is, the area comprised under the hydrographs reported in the previous picture 3.22);
- *Final Stored Volume*, i.e. the sum of the volumes stored in nodes and links;
- *Lost Volume*, i.e. the quantity of *Wet Weather Flow* lost during the simulation as *Internal Outflow*

$$Lost\ Volume = \frac{Internal\ Outflow}{Wet\ Weather\ Flow} \cdot 100 \qquad (3.7)$$

Recorded Rain Events	Wet Weather Inflow [m^3]	Internal Outflow [m^3]	External Outflow [m^3]	Final Stored Volume [m^3]	Lost Volume [%]
07/27/2006	16260	825	18522	96	5.07
02/15/2007	5862	0	7289	137	0
04/14/2007	3403	0	6495	97	0
04/27/2007	3073	0	9168	91	0
05/18/2007	2085	0	4006	131	0
09/19/2007	5997	0	10017	48	0
09/28/2007	5671	0	9671	46	0
10/11/2007	19491	4885	15960	112	25.06
11/15/2008	13036	0	17441	34	0
03/05/2009	59579	991	64761	100	1.66
03/29/2009	36874	0	38686	1052	0
04/28/2009	21322	0	22498	326	0

Design Rain Events	Wet Weather Inflow [m^3]	Internal Outflow [m^3]	External Outflow [m^3]	Final Stored Volume [m^3]	Lost Volume [%]
T = 15	60170	18209	45626	101	30.26
T = 30	66106	21624	48120	101	32.71
T = 50	70591	24319	49911	101	34.45

Table 3.6 Water volumes involved in the simulations carried out by considering the traditional approach.

Recorded Rain Events	Wet Weather Inflow [m^3]	Internal Outflow [m^3]	External Outflow [m^3]	Final Stored Volume [m^3]	Lost Volume [%]
07/27/2006	16260	129	18918	662	0.79
02/15/2007	5862	0	7216	225	0
04/14/2007	3403	0	6455	149	0
04/27/2007	3072	0	9135	148	0
05/18/2007	2085	0	3964	188	0
09/19/2007	5996	0	9996	91	0
09/28/2007	5671	0	9642	90	0
10/11/2007	19490	2290	17422	2074	11.75
15/15/2008	13036	0	17411	79	0
03/05/2009	59579	179	65231	712	0.30
03/29/2009	36872	0	38376	1372	0
04/28/2009	21322	0	22295	544	0

Design Rain Events	Wet Weather Inflow [m^3]	Internal Outflow [m^3]	External Outflow [m^3]	Final Stored Volume [m^3]	Lost Volume [%]
T = 15	60170	11141	48608	6500	18.52
T = 30	66106	13665	51272	7580	20.67
T = 50	70591	15929	53490	8550	22.57

Table 3.7 Water volumes involved in the simulations carried out by considering the dual drainage approach.

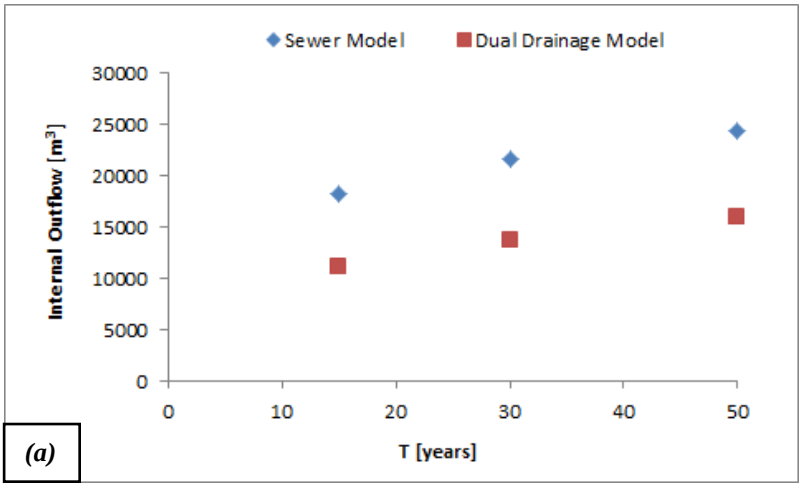

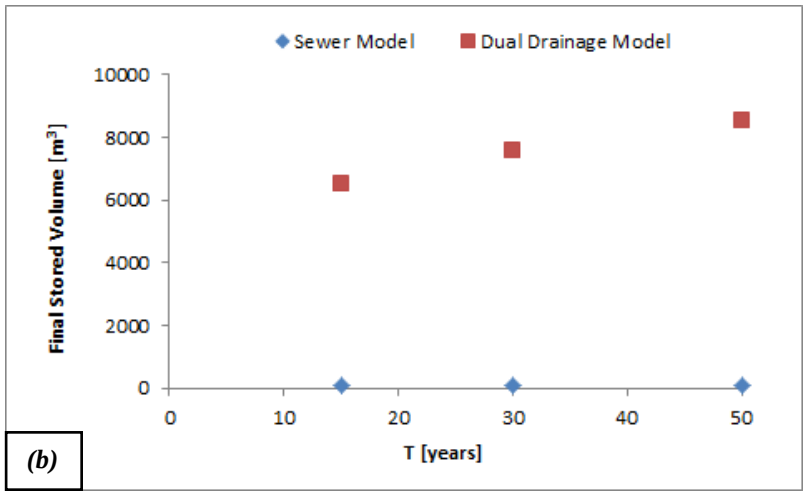

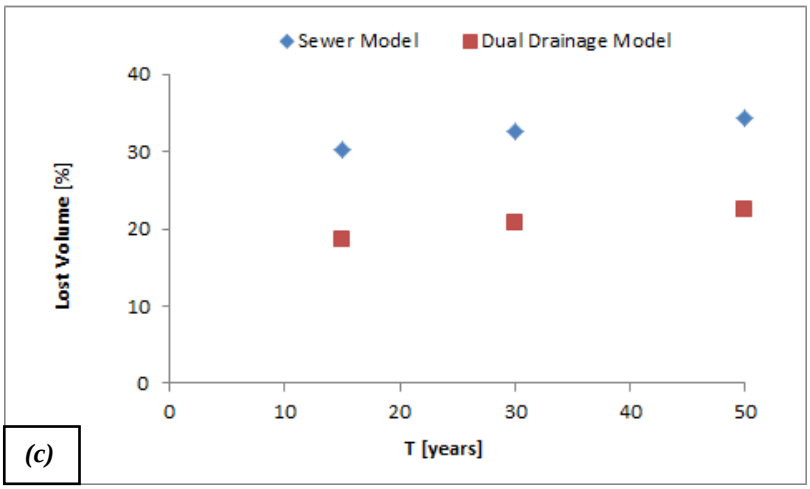

Figure 3.23 Comparison between the two models in terms of *Internal Outflow* (a), *Final Stored Volume* (b) and *Lost Volume* (c) for the design rain events considered.

The volume variations (*External Outflow*) between the two models are due to the fact that in the classical model, when the flow into a junction exceeds the capacity of the system to transport it further downstream, the excess volume overflows the system and is lost. There is the option instead of having the excess volume stored atop the junction, in a ponded fashion, and reintroduced into the system as capacity permits. In particular, under steady and kinematic wave flow routing, the ponded water can be stored simply as an excess volume. Instead, for dynamic wave routing, which is influenced by the water depths maintained at nodes, the excess volume can be assumed to pond over the node with a constant surface area, which must be defined together with the other input parameters supplied for the junction ("Allow Ponding Option"). Nevertheless, in this case, this option was rejected for two reasons:

1. it is not very clear which aspects should be taken into account in the definition of the surface area of the fictitious reservoir;
2. a similar model would be only a slight evolution of the classical approach, therefore it would not be able to solve all the negative aspects associated with such a modeling.

Therefore, from the elaborations carried out, it emerged that the classical approach is not accurate during extreme rain events because of the excessive and unjustified volume losses (*Internal Outflow* in tab. 3.6). Moreover, such methodologies would force the engineer to adopt, as unique design solution, the increasing of the cross-sections of all the sewer trunks involved by the criticality, with consequent repercussion on the costs of the structure. Therefore, the scarce accuracy of such a modeling could determine further consequences through the adoption of wrong and more expensive design solutions.

Vice versa, a dual drainage model, such as the one assumed and proposed in the research project, enabled a more realistic simulation of the sewer flooding, since it was based on a bidirectional interaction between the minor and the major system. Hence, in this way it was possible to limit the number of surcharged nodes (tab. 3.8 e fig. 3.24) and the associated volume losses (fig. 3.23 c).

	Surcharged nodes in Sewer Model	Surcharged nodes in Sewer Model, defined by the AOFD	% of surcharged nodes in Sewer Model completely corrected in Dual Drainage Model	% of surcharged nodes in Sewer Model with reduced flood volume in Dual Drainage Model	Average reduction of the flood volume
T = 15	109	86	92.66%	6.42%	63.43%
T = 30	111	84	88.29%	8.11%	61.47%
T = 50	123	96	91.06%	6.50%	60.20%

Table 3.8 Improvements in the working conditions of the sewer network realized with the dual drainage model.

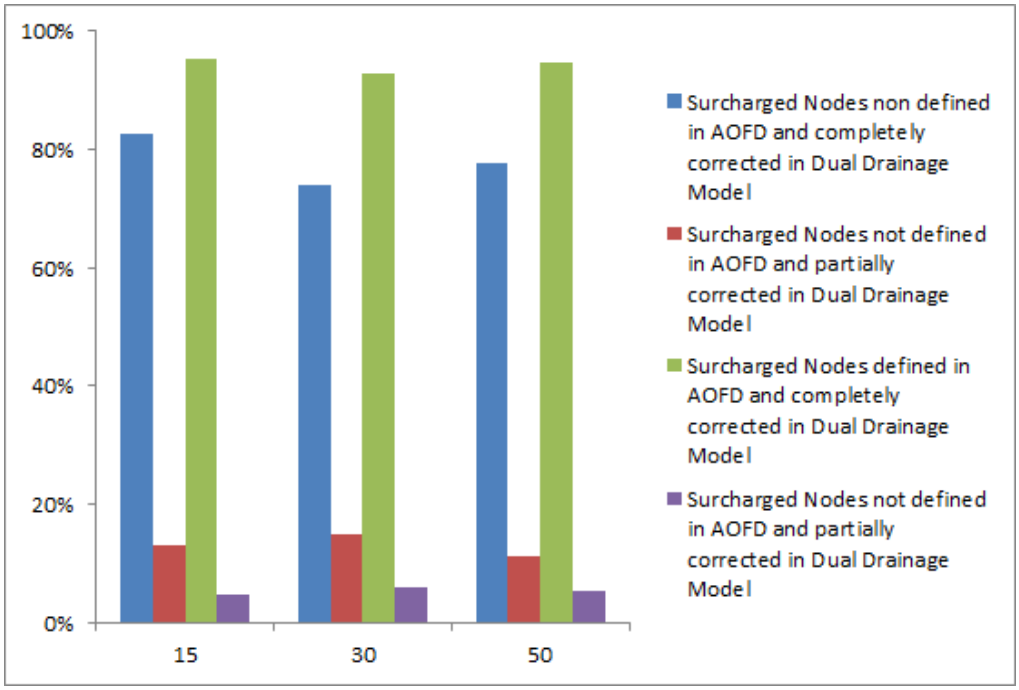

Figure 3.24 Corrections realized by the use of the dual drainage model on the surcharged nodes found in the traditional model.

In particular, it emerged that, on average, 77 % of the surcharged nodes found in the traditional model were also defined by the AOFD procedure: 94.32 % of these presented a normal behavior in the dual drainage model thanks to the connections provided with the surface network (nodes 55, 59, 60 and 61 in fig. 3.25), whereas a further 5.27 % was still overloaded, but by a volume reduced by more than 90 % (fig 3.24).

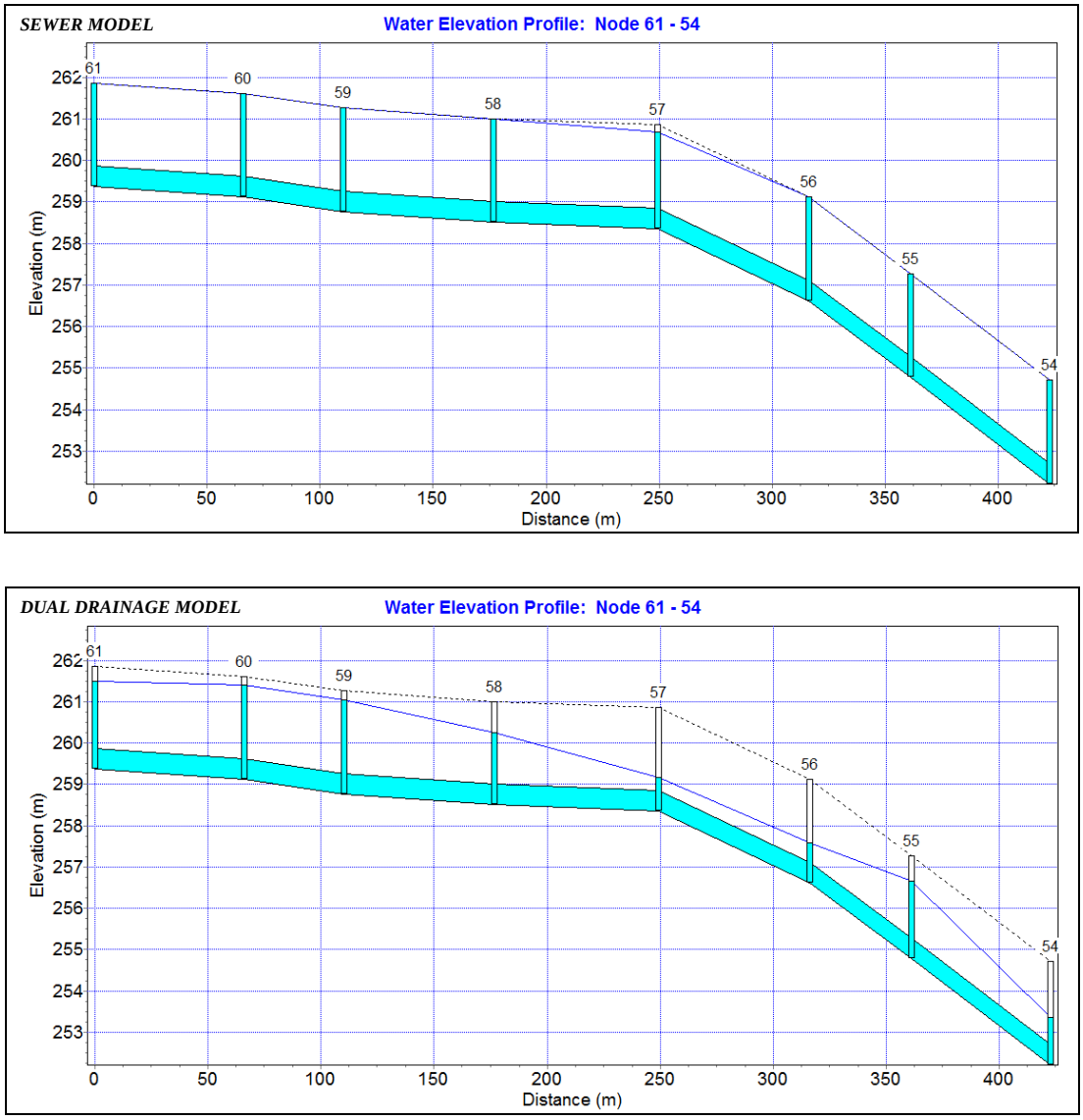

Figure 3.25 Different behavior between the two models of some surcharged nodes, localized also by the AOFD.

The dual drainage model also determined improvements in the working conditions of surcharged nodes found in the traditional model, but not defined in the AOFD procedure: on average, 78.13 % of these presented a normal behavior in the dual drainage model (node 22 in fig. 3.26), whereas a further 13 % was still overloaded, but by a volume reduced by 30 % (fig. 3.24).

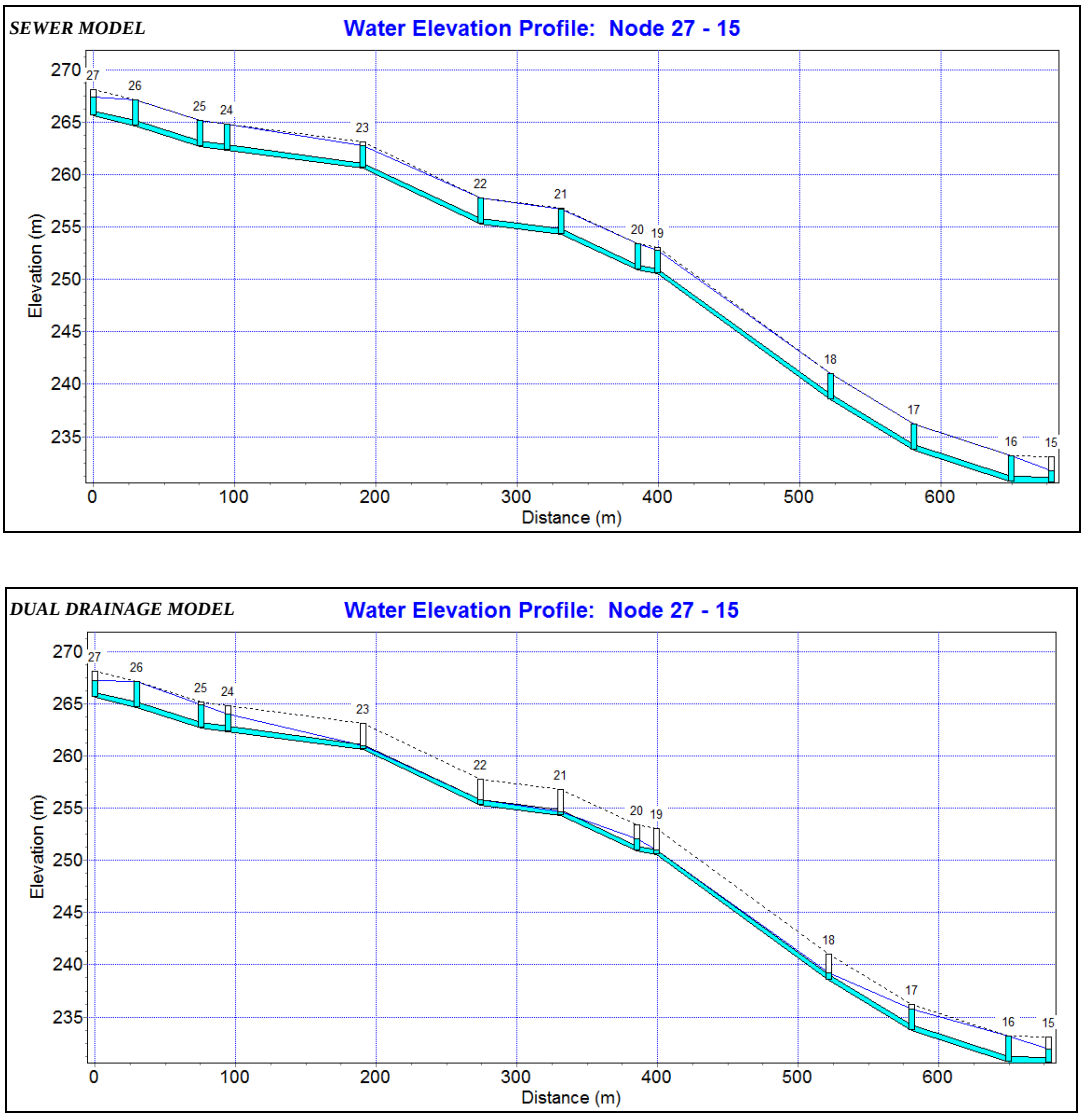

Figure 3.26 Different behavior between the two models of some surcharged nodes, not localized by the AOFD.

In conclusion, more than 90 % of the surcharged nodes found in the traditional model was completely "corrected" in the dual drainage model, whereas a further 7% was still surcharged but by a flood volume reduced by 60 % (tab. 3.8). In such situations the engineer should solve a significantly reduced number of sewer criticalities, therefore the cost of the rehabilitation works would tend surely to be decreased.

Actually, such a model should push the designer to maximize the use of the major and minor systems to manage the resulting excess runoff originated during a storm

event. It needs to be pointed out that the term “management” comprises the concepts of “conveyance”, “storage” and “infiltration” of the excess water rather than the traditional idea of developing systems to convey the runoff as fast as possible to the receiving water bodies. The development of solutions that make use of the physical aspects of both major and minor systems implies examination of the integral capacity of the underground network of assets as well as the network above ground; the latter comprising roads, inlet works, and any feature of the physical infrastructure that could interfere with (and thus alter) the movement of the water. This opens up the number of variables to be examined in a diagnostic study and at the same time widens the criteria to be used when evaluating flood control and mitigation measures. An example of this could be the Blue-Green Concept (BGC) that has been developed as a tool to integrate surface water and fluvial flood risk management with green spaces as part of the strategic spatial planning for urban environments. In fact, it incorporates the roles of sustainable urban drainage, river restoration and flood management to develop a network of blue-green components across a catchment that links green spaces with the river corridor and associated tributaries (fig. 3.27).

Figure 3.27 Example of Urban Blue Corridors.

In this way the integration between the urban waterways and the green infrastructure could improve the function of both systems through the reduction of flood risk, provision of temporary flood pathways and enhancement of biofiltration irrigation activities (White, 2008).

Precisely these urban flooding issues demonstrate, once again, how the dual drainage model is more useful than a traditional model: it is evident, in fact, that simulation

results, especially the temporal trend of the surface velocities and depth, will enable the localization of the potential flooded areas (fig. 3.28), and, consequently, the elaboration of risk map.

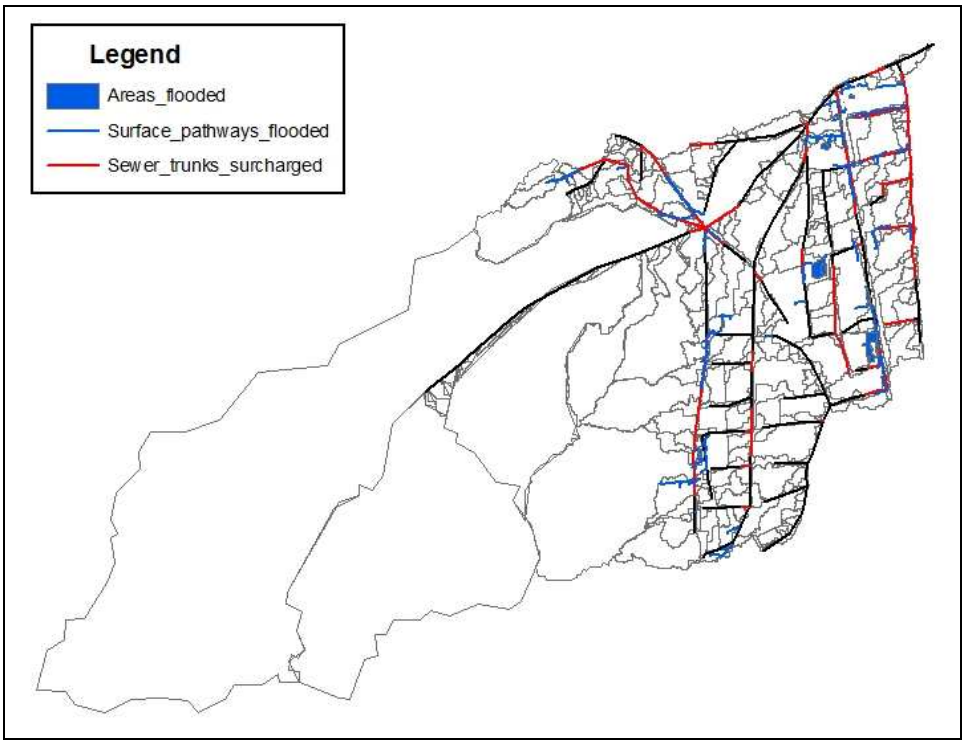

Figure 3.28 Localization of the surcharged sewer trunks and the flooded surface pathways and areas corresponding to the design rain event with return period of 50 years.

Such results will surely attract subjects, such as insurance companies and civil protection institutions. In fact, the insurance companies will find the possibility of more realistic evaluation of the damage associated with the floods advantageous; instead, the civil protection institutions could use such results for elaborating adequate emergency plans.

In particular, from this point of view, it could be very important to connect such hydraulic models, previously calibrated for a generic study area, with storm tracking methods. In fact, in this way, it could be possible to forecast the potential flooded areas with a satisfactory lead time, and, consequently, to realize all the planned safety measures in time. Exactly this aspect directed the second part of the present research towards the study of storm tracking methods in urban areas.

References

- Ahokas E., Yu X., Kaartinen H., Hyyppä J., Kaasalainen S., Matikainen L., Honkavaara E., Hyyppä H., Rönnholm P., Soininen A. (2005). *Quality of laser scanning*. In EARSeL Workshop "3-D Remote Sensing".
- Alegre E., Hirner W., Baptista J. M., and Parena R. (2000). *Performance indicators for water supply services*, Manual of Best Practice Series, IWA Publishing, London.
- Billington R., Allan R.N. (1987). *Reliability evaluation of engineering systems: concept and tecnique*. Plenum Press, NY.
- Burrough, P. and McDonnell, R. (1998). *Principles of Geographic Information Systems*, 333 pp., Oxford University Press, New York, NY, 1998.
- Butler D., Davis J.W. (2000). *Urban Drainage*. E&FN Spon: London, 2000.
- Di Federico V. (2005). *Nuovi strumenti per la gestione e manutenzione integrata delle reti idriche e fognarie: Care-W e Care-S*. Atti della Conferenza Nazionale sulla Politica energetica in Italia, Bologna, Italia, 18-19 aprile 2005.
- Ermini R. (2000). *Indici di prestazione per schemi idrici complessi*. XXVII Convegno di Idraulica e Costruzioni Idrauliche, 2000.
- Fiorentino M., Ermini R., Sole A., Di Santo G. (2005). *Tecniche GIS per la caratterizzazione dell'efficienza di funzionamento di reti di drenaggio*. Atti del I Convegno Nazionale di Idraulica Urbana, Sorrento, Italia, 28-30 settembre 2005.
- Hutchinson M. F. (1989). *A New Procedure for Gridding Elevation and Stream Line Data with Automatic Removal of Spurious Pits*, J. Hydrol., 106, 211–232, 1989.
- Jenson S. and Domingue J. O. (1988). *Extracting topographic structure from Digital Elevation Data for Geographic Information System Analysis*, Photogrammetric Eng. Remote Sensing, 54(11), 15 1593–1600, 1988.
- Jenson S. (1991). *Applications of Hydrologic Information Automatically Extracted from Digital Elevation Models*, Hydrol. Processes, 5, 31–44, 1991.
- Kraus K. (2002). *Principles of airborne laser scanning*. Journal of the Swedish Society for Photogrammetry and Remote Sensing 2002:1 (2002) 53–56.

- Maksimović Č., Prodanović D., Boonya-aroonnet S., Leitão J.P., Djordjević S, Allitt R. (2009). *Overland flow and pathway analysis for modelling of urban pluvial flooding*. Journal of Hydraulic Research, 47(4):512-523.
- Martz L. W. and Garbrecht J. (1999). *An outlet breaching algorithm for the treatment of closed depressions in a raster DEM*, Comput. Geosci., 25, 835–844, 1999.
- O'Callaghan J. F. and Mark D. M. (1984). *The extraction of drainage networks from digital elevation data*, paper presented at Computer Visualization Graph. Image Proceedings of GIS/LIS, GIS/LIS, 1984.
- Piro P. and Sole A. (2001). *Analisi di reti di drenaggio urbano mediante l'uso dei Gis. Applicazione al bacino urbano del Liguori*. Ed. Bios, Cosenza, Italia.
- Piro P. (2007). *Il bacino sperimentale urbano del Canale Liguori nella città di Cosenza. Osservazioni sperimentali quali-quantitative nel periodo 1995-2003*. Ed. Bios, Cosenza, Italia.
- Rieger W. (1998). *A phenomenon-based approach to upslope contributing area and depressions in DEMs*, Hydrol. Processes, 12, 857–872, 1998.
- Tang Y.K.(1985). *Evaluation of water distribution network reliability.* Hydraulic Division Specialty Conference. Orlando, Florida.
- Tsubaki R., Fujita I. and Teraguchi H. (2006). *LiDAR data processing for detailed inundation simulation of an urbanized area*. In 7th International Conference on Hydroinformatics, Nice, France.
- Wagner J.M., Shamir U., Marks D.H. (1988a). *Water distribution reliability: analytical methods*. Journal Water Resour. Plng. and Mgmt, ASCE, 114(3), 253-275.
- Wagner J.M., Shamir U., Marks D.H. (1988b). *Water distribution reliability: simulation methods*. Journal Water Resour. Plng. and Mgmt, ASCE, 114(3), 276-294.
- White I. (2008) *The absorbent city: urban form and flood risk management*. Urban Design and Planning. [Online] 161, 151 – 161.

4. Literature review concerning storm tracking methods based on rain gauges data

4.1 Introduction

Storm tracking procedures are employed for deriving storm movement parameters, such as velocity and direction, because, as suggested by the same name, they follow the path of storms using radar or rain gauge data. Radar has the advantage that it is sometimes possible to view an entire storm system whereas a rain-gauge network often acts only as a "window" of storm observation. However, currently, rain gauge data are often available whereas radar data are not. Moreover convective cells, cause of numerous urban floods, present dimensions sometimes close to the limit of the radar resolution, consequently they could not be accurately estimated (Shaw, 1983). For these reasons the PhD activity was limited only to the study of methods based on the rain gauges data.

In order to avoid misunderstanding, it is important that the terms rainfall velocity and rainfall direction are clearly defined, i.e. a distinction must be made between the movement of rain-producing storms and the motion of rainfall patterns (Diskin, 1987). The former is a term applied to changes occurring in the atmosphere as the region producing rainfall moves due to meteorological factors. This type of movement can be observed by radar equipment producing information about the areal extent of the rain droplets in the air at a given time and the location of the centre of this mass of droplets at successive instants of time. The second type of motion is the movement of rainfall patterns as observed by recording gauges, i.e. the velocity and direction of the water masses, generated by rainfall, occurring in a sequence on the ground (Niemczymowicz and Dahlblom, 1984). For example, stationary clouds generating rainfall in a distinct directionally oriented sequence will produce an effect on the ground which will be considered as a rainfall movement. The motion is expressed by the fact that the rainfall hyetographs recorded at the various gauges are displaced relative to one another along the time axis. Just these relative displacements will enable to derive later the speed and direction of storm movement.

Since this research is aimed at analyzing the urban flooding process, the second type of motion will be studied in detail because similar applications are more significant for distributed rainfall-runoff models. This aspect will be deepened in the first part of chapter, where the different fields of application of storm tracking models will be presented. The second part will be addressed to the description of the rainfall data collection requirements to be applied for urban hydrological elaborations in order to take into account the spatial distribution of the convective rainfall by measurements. Finally the last part will concern the description of the principal storm tracking methods available in the literature by pointing out the existing differences between them.

4.2 Application of rainfall movement

Storm tracking methods were originally developed in order to take into account the storm kinematics into rainfall input used for calculation of runoff. In fact, although considerable effort has been directed on improving rainfall – runoff models, nevertheless one important part of the modeling procedure, the generation of realistic rainfall input, has been ignored until now. In detail, due to lack of adequate data, the traditional rainfall input has been assumed to be a function of time only and uniformly distributed over entire catchment. Moreover, sometimes, if the data from several gauges were available, the data processing would have started with space averaging using suitable weighing factors. Thus, any information about spatial structure and movement, possibly present in the original data, has been lost.

During the Seventies, various researches were devoted to development of design storms with time pattern adapted to the shape of real rainfall hyetographs (Keifer and Chu, 1957; Sifalda, 1973; Desbordes, 1978; Yen and Chow, 1980; Desbordes et al., 1984; Yen, 1986). Some of these design storms proved to be useful in design of conduits. However no attention was paid to the evaluation of the statistical distribution of the direction of movement of storm rainfall patterns, their speed in a given direction and their areal extents.

All this is in a clear contradiction with the real nature of the rainfalls that is highly dynamic. In fact rainfall fields contain a complicated mixture of cloud structures

which are developing and dissipating, come close to each other and go apart, and, doing so, move across the catchment (Austin and Houze, 1972; Amorocho and Wu, 1977; Gupta and Waymyre, 1979). Moreover this wrong modeling determines also errors in the simulations, since the rainfall movement influences the runoff generation process, basically in two ways (Niemczynowicz and Jonsson, 1981; James, 1982; Shiling, 1984 a,b):

1. *direct influence*, by reinforcement of runoff in waterways or conduits geographically oriented parallel to the storm movement direction;
2. *indirect influence* on the shape of point versus areal hyetograph.

The *direct influence* of rainfall movement on the shape of runoff hydrograph, called also "the directional bias" (Niemczynowicz, 1984 a), has been recognized for a long time. Rainfall traveling downstream the catchment along the main direction of conduits produce higher peak and steeper limbs of the hydrograph than the storm moving upstream (Townson and Ong, 1974; Surkan, 1974; Niemczynowicz, 1984a, 1984b; Larson and Berndtsson, 1985). The magnitude of possible reinforcement of the peak discharge depends on several geometrical catchment and sewage network properties, as well as on rainfall pattern characteristics and velocity parameters. On conceptual catchments with geometry specially designed in order to maximize the effect of movement, maximal directional bias may reach values of several hundred percent for storms with short duration. On real catchments, using real observed rainfall events and their movement parameters, the maximal directional bias may reach values of about 20-30% in relation to the stationary storms (Niemczynowicz, 1984a). Nevertheless these values denote rainfalls with short duration, without practical importance. Therefore it is possible to conclude that the direct influence of storm movement on runoff hydrograph may be neglected in most cases for practical purposes because the maximal directional bias, for storms with practically significant magnitude, is of the order of some 5-10%.

Instead the *indirect influence* is expressed by the fact that the hyetograph, observed in one point, will change its shape if it is considered from an areal perspective. Let us consider a two-dimension case of an hypothetical uniform rain cell moving with a

constant speed of 600 m/min and a length of 6 km, over a catchment with a length of 12 km (fig. 4.1).

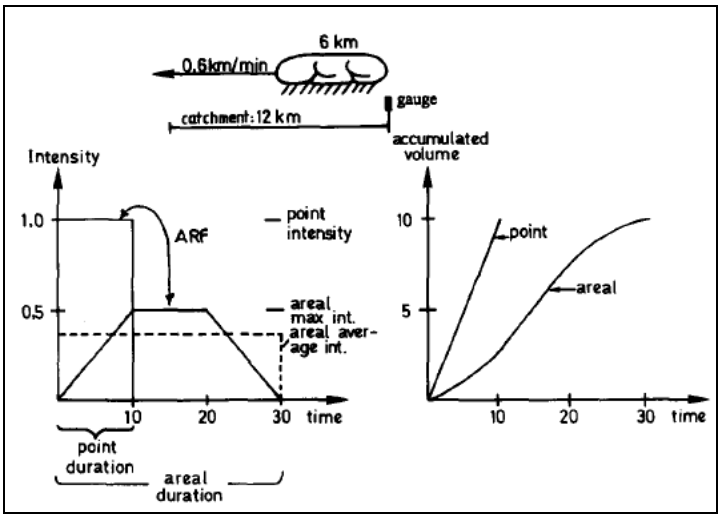

Figure 4.1 Schematic representation of point versus areal hyetographs resulting from a moving uniform rain cell (from Niemczynowicz, 1991).

In each point of the catchment the point hyetograph will be a simple block rain with a duration of l0 min (6,000 : 600). Instead the areal hyetograph will be trapezoidal with a duration of 30 min, and peak and average intensity lower than intensity observed in one point because during the first and the last 10 min only a part of the catchment is covered by incoming or passing rain cell.

Such simple example can be extended on all real storms and all real catchments. It is important to notice that the areal rainfall always differs from point rainfall by two simultaneously occurring phenomena: decrease of average areal intensity and increase of areal duration. Storm duration is longer on large catchments than on small catchments, the average areal intensity is smaller on large catchment compared with small catchments, whereas rainfall depth is the same on each point of the catchment, i.e. the total volumes are equal on both the catchments.

Consequently the *indirect influence* of rainfall movement consists in the different runoff simulated when a traditional, static input is used compared to the situation when real rainfall is moving across the catchment. In fact, in this last case, the shape of volume accumulation curve will depend on the size of the catchment and the direction from which the moving storm enters the catchment. The time of

concentration itself will be different if the moving storm enters the catchment from upstream direction compared with the case when it enters from downstream.

Therefore, in conclusion, it is evident that modern rainfall input should be based on the recognition of rainfall kinematics and it should contain the movement parameters. Such practical application may be easily achieved using any distributed model type SWMM which allow for multi-gauge input. Hyetographs from one or several gauges may be lagged in time to simulate the movement. The time and the direction of lagging is chosen so that the real velocity and the direction is simulated. The used direction and the velocity of rainfalls can, as a first approximation, be taken as the prevailing direction and averaged velocity.

4.3 Rainfall movement monitoring

The temporal and spatial distribution of convective rain cells is the result of five characteristics: (1) intensity distribution within the cell; (2) cell size; (3) intercellular distance; (4) rate of development and decay of cells; and (5) the velocity and the direction of movement. The first three characteristics may be "seen" by the single rain gauge as a two-dimensional cross section of the rainfall field as it moves above the gauge. The last two characteristics may be only observed by a dense network of gauges or by radar (Berndtsson and Niemczynowicz, 1988).

In particular such features can be considered from two different perspectives: the immobile or static perspective, which can be called the *Eulerian* point of view, and the mobile or dynamic perspective, which may be referred to as the *Lagranian* point of view.

The *Lagranian* perspective obtains when the observer follows the moving system, in our case the storm, on its path over the ground. In this perspective, the storm has an observable direction and velocity of movement. The development and decay of the rain cell will appear to the observer as a time pattern. If only one observer exists (one gauge on the moving carriage), no conclusions can be drawn about the size of the rain cell or the spacing between rain cells (fig. 4.2).

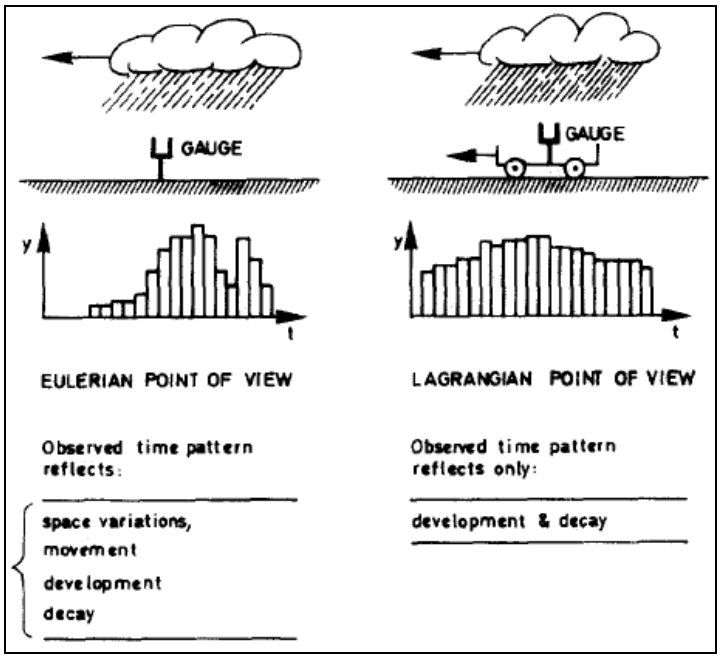

Figure 4.2 Visual representation of the Eulerian versus the Lagranian perspective on the rainfall process (from Niemczynowicz, 1991).

The *Lagranian* approach can obviously, for practical reasons, never be applied in a pure form. However, studying the rainfall pattern in a number of gauges situated along the line of movement, a *quasi-Lagranian* point of view may be obtained. Observed changes in the time pattern from one gauge to the other will tell us about the process of rainfall development and decay.

From the *Eulerian* point of view, the gauge is immobile on the ground surface while the rainfall structure is passing above. In this perspective, observed time pattern of the rainfall contains combined effects of space structure of the rain cells, their distance and size, development and decay, and the velocity of storm movement. From a point of view of an immobile observer, the rain gauge, it is not possible to separate these effects from each other. For example, it is not possible to distinguish the effects of different velocity from different size of the rain cells. The small rain cell moving slowly may produce the same time pattern as a large cell moving fast, etc.

This last approach seems the most appropriate for studying the rainfall movement, however the rain gauges must fulfill rather rigorous requirements in order to obtain data sufficiently good for successful calculation of storm parameters:

(1) the gauge network must cover an area reasonably bigger than the size of the rain cells;
(2) the distance between gauges shall be shorter than the size of the rain cells;
(3) the time resolution of registration shall be such that a number of intensity samples can be taken during the passage of a single rain cell;
(4) volume resolution shall be small enough to ensure meaningful readings during short time intervals;
(5) gauges must be synchronized in time;
(6) data shall be gathered during a period long enough to make statistical treatment possible.

The same constraints are valid for radar measurements which have also limitations concerning space and time resolution.

According to literature, the observed size of convective rain cells are comprised between 2 and 30 km^2 (Austin and Houze, 1972; Niemczynowicz, 1984 a, b). By assuming circular shape of the rain cells, cell diameter, ranging from 1.6 to 6.2 km, will be obtained. Consequently, in order to "see" the same cell in at least two gauges the distance between gauges should be about 1 km, i.e. the gauges distribution should be about of one gauge per 1 km^2.

Velocity of rain cell movement has been reported to vary between 2 and 25 m/s (Hobs and Locatelli, 1978): especially the average velocity of 400 events observed in Lund was 10 m/s (Niemczynowicz, 1984 a, b). Counting with an average velocity of 10 m/s the time of passage of rain cells above the gauge is comprised between 2.7 and 10.3 min. Therefore a time of registration about one minute is required in order to "sample" the same rain cell in the same gauge at least two times.

Finally small volume resolutions of instrument are necessary in order to have meaningful registration of small rainfall intensities (fox example tipping bucket). If the least interesting rainfall intensity is assumed to be 0.1 mm/min and the time resolution is one minute, then the reasonable volume resolution of one "tipp" of the bucket is 0.1 mm.

Therefore, counting with usual sizes and velocities of rain cells, we can arrive to the "1-1-0. l" rule of thumb: i.e. one gauge per 1 km^2, 1 min time resolution and 0.1 mm

volume resolution of registration (Krejci and Shilling, 1989; Niemczynowicz, 1989). These are the maximal rainfall data collection requirements to be applied for urban hydrological applications if the spatial distribution of the convective cells is to be resolved by measurements.

4.4 Storm tracking methods

A basic assumption, common to all storm tracking methods, is that the computations produce single values of storm speed and direction of movement for each storm event. In other words, the possibility of changes in the speed or direction as the storm sweeps over the network is ignored (Diskin, 1987). This simplification is justified since convectional storms move at a reasonably steady velocity, in fact changes occur only slowly over distances of perhaps hundreds of miles (Hindi and Kelway, 1977).

The movement of the rainfall event is therefore modeled as the motion of a wave front, defined by the single values of speed and direction to be calculated. In particular the motion is expressed by the fact the rainfall hyetographs recorded at the various gauges are displaced relative to one another along the time axis. These relative displacements depend obviously on the speed and direction of storm movement.

Since rainfall hyetographs at different stations are not identical, it is necessary to select some easily identifiable feature of the hyetograph, in order to follow it as it moves in space across the gauge network. However the results of numerous storm tracking studies reveal that the choice of the feature is a very difficult task (Hindi and Kelway, 1977; Felgate and Read, 1975; Shaw 1983) because different results were obtained depending on the nature of the feature adopted. In addition to this, there is also a significant difference in the nature of the outcomes. If the selected feature is the beginning of rainfall, the peak, the centroid of the hyetograph, etc., for any pair of stations in a given storm the difference in the times of arrival is independent of the path joining the two locations. The same result is obtained if the path is direct, or if it goes through one or more intermediate stations. For example, using such a method for three recording rainfall stations, A, B and C, it gives values that are additive, i.e.,

the time shift between stations A and C is equal to the sum of the time shift between A and B and that between B and C.

Vice versa values of the time shift computed by a method based on correlation coefficients are, on the other hand, not additive and this can lead to some difficulties if the data are used for the computation of the speed and direction of the movement of the rainfall pattern.

One of the first methods developed was simply based on the construction of the isohyetal map for every time steps running through the whole storm duration and the consequent evaluation of the movement of identifiable feature (fig. 4.3). With this method one can observe the significant change in intensity even over distances of less than a kilometer and time intervals of the order of one minute (Austin and Houze, 1972).

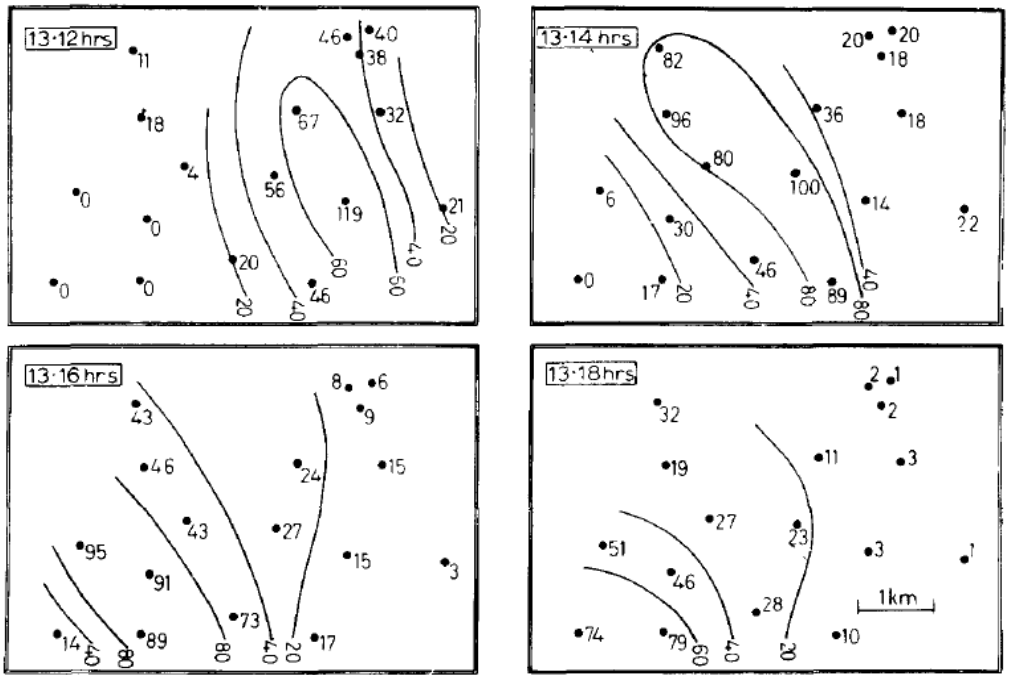

Figure 4.3 One sequences of isohyetal maps drawn at 2-min intervals showing the movements of typical cells across the gauge network. The 2-rain totals are given in units of 0.01 mm (from Felgate and Read, 1975).

Nevertheless these methods, used in manual mode, are concerned to be time consuming, moreover the final definition of the isohyetal pattern is subjective and tends to be less accurate near the edges of the catchment boundaries.

Therefore, afterwards, various efforts were made in order to overcome these limitations: in particular all these new procedures started by trying to solve the simplest case, where data were available only for three stations (fig. 4.4). The data consisted of the locations of the stations and the times of arrival of the selected feature at the stations.

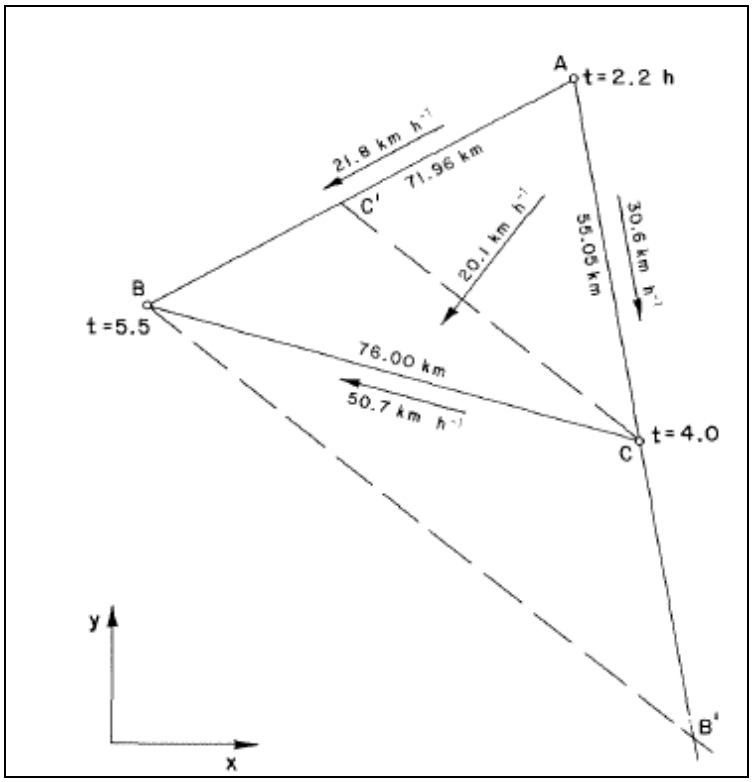

Figure 4.4 An example of the three stations graphical method (from Diskin, 1987).

An example is the graphical solution outlined in fig. 4.4, first described by Foster (1948). According to this solution, the speed of movement along the three lines joining the stations is calculated from the distances and time differences between stations. Using these speeds and starting at station A, where the arrival time is the smallest, points C' and B' are found along AB and AC, respectively, such that the time of travel along AC' is equal to that along AC and the time of travel along AB' is the same as that computed for AB. The two lines thus obtained, CC' and BB', are lines of equal time of arrival, or isochrones, for the storm considered. The speed of the storm movement can be therefore calculated from the perpendicular distance between the two isochrones and the difference between their time values, whereas

the direction of movement is parallel to this perpendicular. For the example given in fig. 4.4, the speed of storm movement is 20.1 km/h (5.58 m/s), and the direction of movement is 218 degrees clockwise from north (*y*-axis).

It should be noted that the speed along the perpendicular is smaller than the speed along any other line in the *x*, *y* plane considered. In fact, considering the isochrones as contour lines in the *x*, *y*, *t* space, the perpendicular is the line of maximum slope in the inclined plane defined by the coordinates (*x*, *y*) and time of arrival (*t*) for the three stations.

By following this geometric interpretation, Neimczynowicz and Dahlblom (1984) presented a simple program, called TRIAD, for the analytical determination of the velocity and the direction of storm movement. The method uses the time to peak as reference feature to be found on hyetographs from several gauges. In particular if only one peak for each rain gauge is observed, all time to peak values can be accepted. Occurrence of more than one peak during the same event means that more than one rain cell passed the network in some sequence (fig. 4.5).

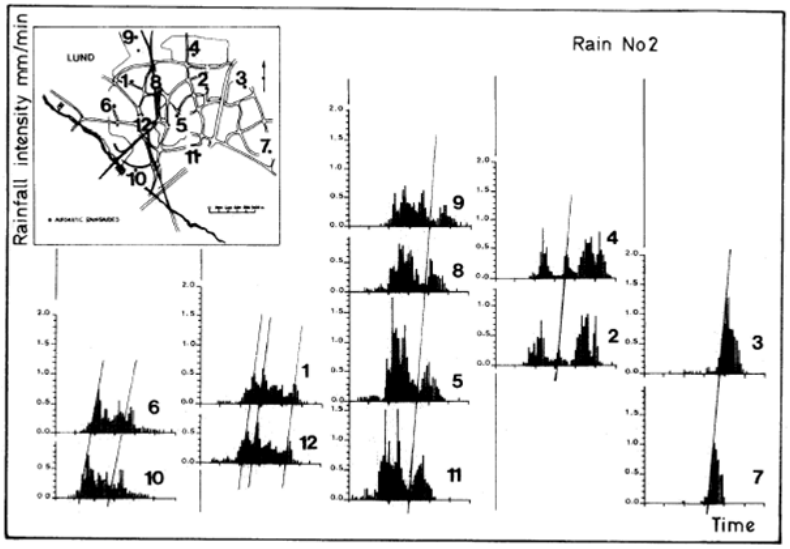

Figure 4.5 An example of multi-peak event (from Niemczynowicz, 1987).

In such cases it is often difficult to decide which of the time to peak values should be accepted as belonging to the same rain cell. Therefore a number of combinations of time to peak values have to be selected and the final velocity vector has to be taken from that combination which shows the smallest variation of velocity vectors between all triads of gauges, as it will be explained in more detail later.

Modifying the notation used by Niemczynowicz and Dahlblom, the procedure is as follows: if the time to peak values are known for three arbitrarily chosen gauges, a velocity vector V can be calculated

$$V = \left(v_x, v_y\right) \tag{4.1}$$

$$v_x = \frac{dx}{dt} \tag{4.2}$$

$$v_y = \frac{dy}{dt} \tag{4.3}$$

where (x, y) are the space coordinates for the gauges and t is the arrival time. Introducing a three dimensional space, where one axis is the time coordinate and the two others are the ordinary x and y coordinates, a plane can be placed through three points in the space:

$$t = a \cdot x + b \cdot y + c \tag{4.4}$$

where

- a is the slope of the inclined plane parallel to the x-axis and represents the inverse of v_x

$$a = \frac{dt}{dx} = \frac{1}{v_x} \tag{4.5}$$

- b is the slope of the inclined plane parallel to the y-axis and represents the inverse of v_y

$$b = \frac{dt}{dy} = \frac{1}{v_y} \tag{4.6}$$

- c is the height of the inclined plane above the origin but it has no influence on its slope.

For each combination j of three gauges, three simultaneously linear equations can be established

$$t_{i,j} = a_j \cdot x_{i,j} + b_j \cdot y_{i,j} + c_j \tag{4.7}$$

with i = 1, 2, 3 and $1 \leq j \leq m$. The number of systems, m, is equal to the number of combinations of three gauges from a number of gauges in function, n:

$$m = \binom{n}{3} \tag{4.8}$$

The solution of each of these sets of equations gives a vector R_j

$$R_j = \left(a_j, b_j\right) \tag{4.9}$$

with a length $\left\|R_j\right\|$

$$\left\|R_j\right\| = \sqrt{a_j^2 + b_j^2} \tag{4.10}$$

The absolute value of the velocity can be then calculated

$$\left\|V_j\right\| = \left\|R_j\right\|^{-1} = \frac{1}{\sqrt{a_j^2 + b_j^2}} \tag{4.11}$$

as the inverse of the steepest slope of the inclined plane, whereas the direction by the arc tangent of the velocity components in *x* and *y* directions.

$$\Theta = \arctan\left(\frac{b}{a}\right) \tag{4.12}$$

A value of the average velocity and direction for the whole area can be estimated by averaging the results obtained from all the combinations of triads of gauges:

$$\overline{V} = \frac{1}{m} \cdot \sum_{j=1}^{m} \left\|V_j\right\| \tag{4.13}$$

However, when calculating the average direction the influence of the wrong vectors has to be minimized, i.e. the influence of vectors calculated from triads of gauges for which the time of arrival does not belong to the same cell. Hence, the normalized vectors are suggested to be used:

$$R_j^* = \left\|R_j\right\|^{-1} \cdot R_j = \left\|V\right\|_j \cdot R_j \tag{4.14}$$

The sum of the normalized directions

$$R^* = \sum_{j=1}^{m} R_j^* \tag{4.15}$$

can be finally taken as the average direction of the event.

Therefore, for multi-peak events, the elimination of wrong combinations requires to be carried out by choosing only average vectors with the smallest variation between

triads. As a measure of the range of variation, the length of the average vector can be taken

$$S = \frac{1}{m} \cdot \left\| R^* \right\| \tag{4.16}$$

The value of *S* varies between 0, if velocity vectors are equally distributed over the circle, and 1, for the case when all vectors have the same direction. The direction with the smallest *S* value is taken as final storm direction for the rainfall event.

Shearman (1977) proposed a similar scheme based on pairs of stations. This method was originally developed by Marshal (1975, 1977, 1980), and is known as "lag-correlation analysis approach" because the maximum of the lag-correlation structure is assumed as reference feature.

In order to better understand what is the lag-correlation structure it is convenient to consider the figure 4.6, where the profiles of rainfall intensity versus time for three recording rain gauges are reported.

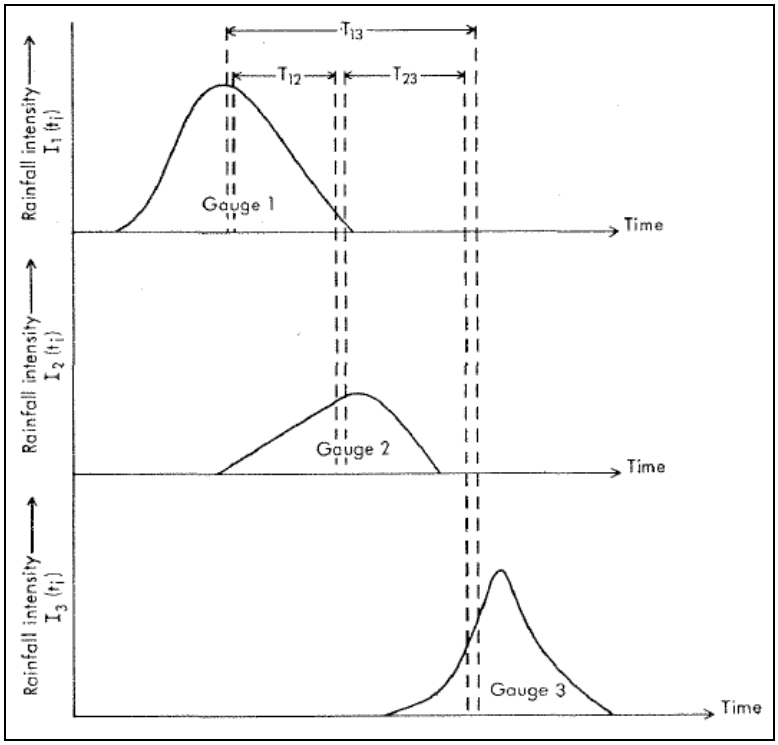

Figure 4.6 Synthetic profiles of rainfall intensity versus time showing optimum time lag (T) between pairs of rain gauges (from Shearman, 1977).

Suppose storm duration, N, is defined as the time lapse between the beginning of the storm, where any one gauge records a non-zero amount, until the cessation of the storm when all gauges are again recording no rain. In this way the time series of observations at any gauge k can be denoted $[i_k(t_i);\ i = 1, \ldots, N]$. In particular let $i_1(t_i)$ denote the rainfall intensities at rain gauges 1 at time (t_i), and $i_2(t_i + \tau)$ represent the intensity at rain gauge 2 at a time τ later. It is possible to measure the association between gauges 1 and 2 for lag τ by calculating the correlation coefficient:

$$\rho_{12} = \frac{\sigma_{12}}{\sigma_1 \cdot \sigma_2} = \frac{\sum_{i=1}^{N-\tau}\left[\left(i_1(t_i) - \bar{i_1}\right)\cdot\left(i_2(t_i+\tau) - \bar{i_2}\right)\right]}{\sum_{i=1}^{N}\left[i_1(t_i) - \bar{i_1}\right]^2 \cdot \sum_{i=1}^{N}\left[i_2(t_i) - \bar{i_2}\right]^2} \tag{4.17}$$

where

$$\bar{i_1} = \frac{1}{N}\cdot\sum_{i=1}^{N} i_1(t_i) \tag{4.18}$$

$$\bar{i_2} = \frac{1}{N}\cdot\sum_{i=1}^{N} i_2(t_i) \tag{4.19}$$

The question of interest is “what displacement of one sequence will make that sequence most similar to the other sequence, taking account of the fact that there may be differences in the total amounts of rain falling at the two gauges ?” (Graham, 2002). Therefore this calculation must be repeated with various values of τ, to give a set of correlation coefficients or a correlogram which may be represented by $\rho_{12}(\tau)$. The value of τ which corresponds to the maximum of $\rho_{12}(\tau)$ approximates to the time interval between the rainfall intensity maximums at rain gauge 1 and rain gauge 2 (fig. 4.6). This is the optimum time lag T_{12}.

A separate correlogram has to be calculated for each pair of rain gauges, and each one will yield an estimate of the optimum time lag. Thus $\rho_{13}(\tau)$ and $\rho_{23}(\tau)$ may be calculated to give values T_{13} and T_{23}.

Such values, together with the spatial coordinates of the stations, can be later inserted in eq. (4.4). In particular by subtracting the expressions from each other, it is possible to eliminate the parameter c in order to obtain the following equation:

$$\Delta t = a \cdot \Delta x + b \cdot \Delta y \tag{4.20}$$

Sets of values of Δx, Δy and Δt are obtained for each pair of rainfall stations for which the correlation coefficient between their hyetographs is above a specified threshold. The number of equations thus formed is equal to the total number of pairs that can be formed from all stations, reduced by the number of pairs producing poor correlations. Finally the resulting set of simultaneous equations can be solved for the parameters a and b by the method of least squares, and storm direction and velocity can be calculated, respectively, by eq. (4.11) and (4.12).

Instead the Marshal's method is quite different: under the assumption of spatial stationarity, the lag-τ crosscorrelation between the generic pair of stations k and w can be considered to be only a function of τ, and the relative coordinates of such stations x_{kw} ($x_{kw} = x_k - x_w$) and y_{kw} ($y_{kw} = y_k - y_w$). In this way the cross-correlations do not depend on the absolute positions of k and w but only on their relative positions.

Therefore for each pair of gauges two points can be plotted in the relative coordinate system (X, Y), representing values of $\rho_{kw,\tau}$ and $\rho_{wk,\tau}$ placed in the positions (x_{kw}, y_{kw}) and ($-x_{kw}$, $-y_{kw}$). Thus the $n \cdot (n - 1)/2$ pairs of gauges provide $n \cdot (n - 1)$ points, where n is the number of gauges in service.

Afterwards all these points will have to be interpolated by correlation isolines: consequently, for the selected τ, a "lag-τ correlation surface", denoted $\rho_\tau(X, Y)$, will be graphed in the relative coordinate system (fig. 4.7).

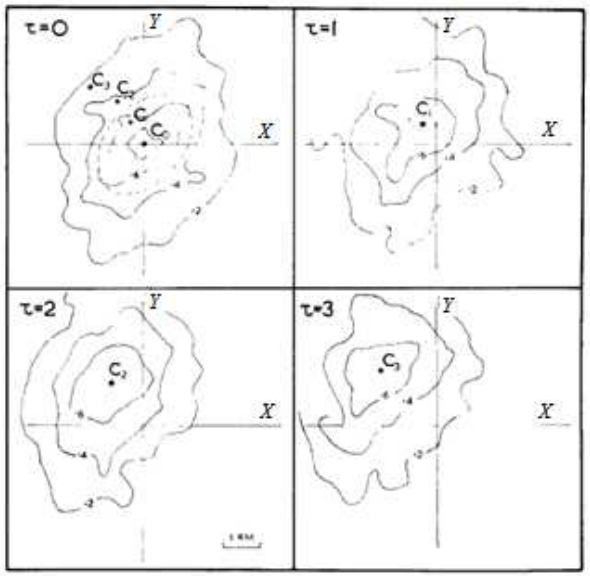

Figure 4.7 Correlation surfaces of Winchcombe storm 114 for τ = 0, 1, 2, 3 (from Marshall, 1980).

The speed and the direction can be later calculated by following the movement of the maxima of the lag correlation surfaces obtained for each lag τ (C_0, C_1, C_2 and C_3 in fig. 4.7). The direction is measured directly on the graphs, whereas the velocity is calculated manually from the time and the distance of the drift of the correlation figure. Such a model is also useful for evaluating the storm structure that can be indicated by the 0.5 contour of the fitted surfaces.

Another method, based on the correlation concept, was developed by Briggs et al. (1990), and farther extended and used by Felgate and Read (1975) and Shaw (1983). This procedure, called "full correlation analysis", assumes as reference point the maximum of the crosscorrelation function between pairs of gauges from every three-gauge group selected from the raingauge network. The time displacements between the maximum of the crosscorrelation function in three gauges are then used in order to calculate the speed and direction of storm movement.

Moreover these time displacements, in combination with the value of the average for the three-gauge autocorrelation function, give the so-called "characteristic ellipse" which is defined as the correlation contour at the 0.5 level.

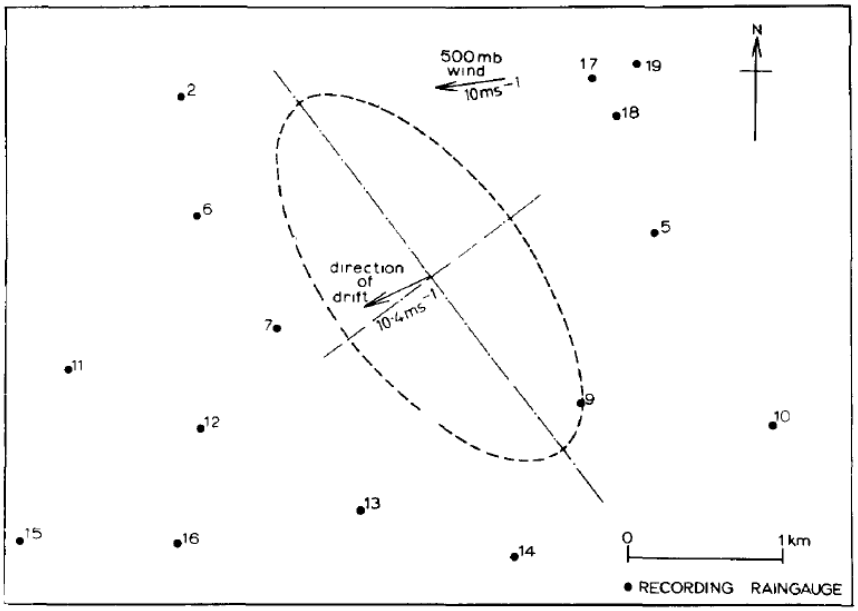

Figure 4.8 Plan of the Cardington Gauge Network showing the average "characteristic ellipse" for the storm of May 27, 1962, and the direction of movement of the cells. The 500-mbar wind direction is also shown (from Felgate and Read, 1975).

The characteristic ellipse gives indirect information about the size, the shape and the life-time of the rainfall cells.

This method was tested on six rainfall events recorded at sixteen gauges in Cardington and on three events recorded at 22 gauges in Winchcombe, England (Shaw, 1983). For seven of the nine rainfalls, the computed velocity of storm movement agreed, according to the author, well to the mean 700 mb wind velocity. Since the nine events were chosen from 280 recorded events, it is not known if the same agreement would be achieved for other events. Besides the results of a "full correlation technique" are difficult to interpret physically since the shape and size of the "characteristic ellipse" represent rather integrated effects of storm movement, cell size and the distance between gauges rather than the physical parameters of the rainfall cells.

Almost all the reported methods were later critized by Diskin (1987) because:

1. the inclusion of a large number of pairs or groups of three stations in the computations means that some stations are given more weight than others, which may not be justified by their data.
2. the accuracy of the results depends on the policy adopted for the rejection of outliers in the TRIAD method, or on the value of the correlation coefficient adopted as threshold in the “lag-correlation” and "full correlation” analysis. Moreover such rules may have to be modified for different networks of rainfall stations, or even for different storms in the same network.

Consequently the author tried to make use of all the information available but eliminating the need to set arbitrary rules for the rejection of some results. By following the geometric interpretation given by the previous approaches, the author solved the problem through the determination of the equation of the inclined plane that best fits to a given set of n points in the x, y, t space, where n is the number of stations for which data are available. The coordinates of each point are the location of the station, relative to a pair of (arbitrary) x, y axes, and the time of arrival of a specified feature at the station. In particular only features, for which the additive property was valid, are suggested to be used.

The criterion for best fit can be chosen at will, nevertheless the sum of squared deviations between observed times of arrival (T_i) and the values (t_i) predicted by the equation of the plane (eq. 4.4) is recommended.

The sum of squared deviations W is given by:

$$W = \sum_{i=1}^{n} \left[T_i - \left(a \cdot x_i + b \cdot y_i + c \right) \right]^2 \tag{4.21}$$

The values of the three parameters a, b, c that minimize this sum are found by solving the set of three simultaneous equations obtained by equating to zero the partial derivatives of eq. (4.21) with respect to these parameters. The resulting expressions for the three equations are:

$$a \cdot \sum_{i=1}^{n} x_i^2 + b \cdot \sum_{i=1}^{n} x_i \cdot y_i + c \cdot \sum_{i=1}^{n} x_i - \cdot \sum_{i=1}^{n} x_i \cdot T_i = 0 \tag{4.22}$$

$$a \cdot \sum_{i=1}^{n} x_i \cdot y_i + b \cdot \sum_{i=1}^{n} y_i^2 + c \cdot \sum_{i=1}^{n} y_i - \sum_{i=1}^{n} y_i \cdot T_i = 0 \tag{4.23}$$

$$a \cdot \sum_{i=1}^{n} x_i + b \cdot \sum_{i=1}^{n} y_i + c \cdot n - \sum_{i=1}^{n} T_i = 0 \tag{4.24}$$

The solution of these equations for the three parameters can be expressed in the following form:

$$a = \frac{A \cdot E - B \cdot C}{D \cdot E - C^2} \tag{4.25}$$

$$b = \frac{B \cdot D - A \cdot C}{D \cdot E - C^2} \tag{4.26}$$

$$c = \frac{\sum_{i=1}^{n} (T_i) - a \cdot \sum_{i=1}^{n} (x_i) - b \cdot \sum_{i=1}^{n} (y_i)}{n} \tag{4.27}$$

where the constants A, B, C, D and E are defined as follows

$$A = n \cdot \sum_{i=1}^{n} (T_i \cdot x_i) - \sum_{i=1}^{n} (T_i) \cdot \sum_{i=1}^{n} (x_i) \tag{4.28}$$

$$B = n \cdot \sum_{i=1}^{n} (T_i \cdot y_i) - \sum_{i=1}^{n} (T_i) \cdot \sum_{i=1}^{n} (y_i) \tag{4.29}$$

$$C = n \cdot \sum_{i=1}^{n}(x_i \cdot y_i) - \sum_{i=1}^{n}(x_i) \cdot \sum_{i=1}^{n}(y_i) \tag{4.30}$$

$$D = n \cdot \sum_{i=1}^{n}(x_i^2) - \sum_{i=1}^{n}(x_i) \cdot \sum_{i=1}^{n}(x_i) \tag{4.31}$$

$$E = n \cdot \sum_{i=1}^{n}(y_i^2) - \sum_{i=1}^{n}(y_i) \cdot \sum_{i=1}^{n}(y_i) \tag{4.32}$$

Finally the speed of movement is given by the inverse of the maximum slope of the plane (eq. 4.11) whereas the direction, that is parallel to that of the maximum slope, can be calculated relatively to the *x*-axis by eq. (4.12).

Nevertheless the prediction equation reported above is not the only possible model to represent the data. In fact the observed different arrival times could be also random fluctuations from an equal arrival time for all stations, that could be the average of the observed arrival times themselves.

Reverting to the geometrical interpretation, an equal arrival time is represented by a horizontal plane (parallel to the *x*,*y* axes) at the level of the average time of arrival (fig. 4.9).

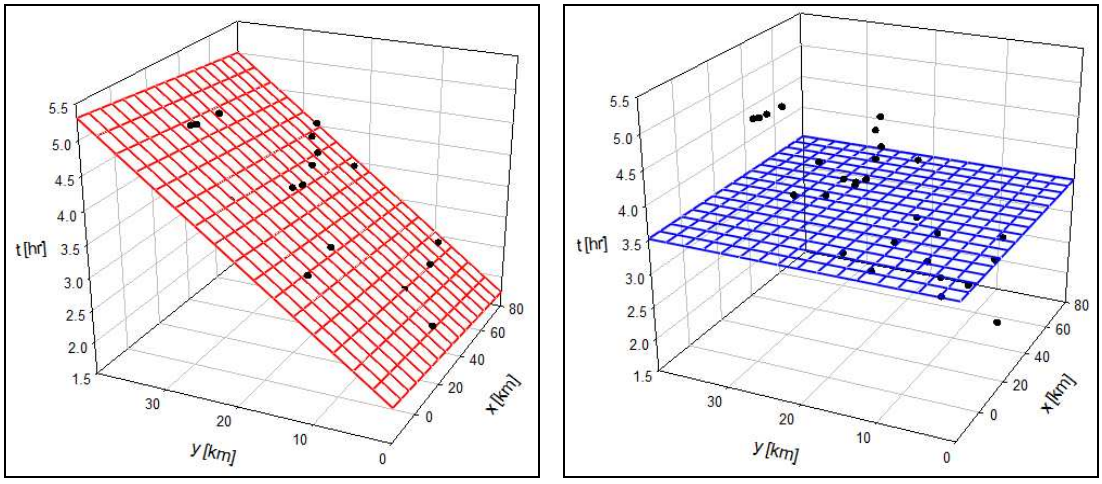

Figure 4.9 Geometrical interpretation of the movement of storms through the hypothesis of the inclined plane and the horizontal plane.

Therefore it is necessary to verify which of the planes represents better the data set. The choice can be based on the comparison between the root mean square (RMS) deviation obtained by adopting the two models (σ_I, σ_O):

$$\sigma_I = \sqrt{\frac{\sum_{i=1}^{n}\left(T_i - t_i\right)^2}{n-1}} \tag{4.33}$$

$$\sigma_O = \sqrt{\frac{\sum_{i=1}^{n}\left(T_i - \overline{T_i}\right)^2}{n-1}} \tag{4.34}$$

where

- T_i are the observed times of arrival;
- t_i are the predicted times of arrival computed by eq. (4.4);
- $\overline{T_i}$ is the average arrival time.

The ratio of the two values can be adopted as a measure of the significance of the results (*Significance Ratio*):

$$\textit{Significance Ratio}\ \left(S.R.\right) = \frac{\sigma_I}{\sigma_O} = \sqrt{\frac{\sum_{i=1}^{n}\left(T_i - t_i\right)^2}{\sum_{i=1}^{n}\left(T_i - \overline{T}_i\right)^2}} \tag{4.35}$$

The values of σ_I is always smaller than σ_O, therefore their ratio is expected to be comprised between zero and one. Values close to zero indicate high significance of the inclined plane hypothesis whereas values close to one poor performance of the proposed model. Some high values of the significance ratio, for example 0.85 or 0.90, may be adopted as limiting value, above which the hypothesis of equal arrival times cannot be rejected.

All the results produced by the proposed method, including the value of the significance ratio, are subject to errors (Diskin, 1990). These are due to inaccuracies in the observed data as well as disagreement between the real behavior of the storm and the assumption of constant speed and direction during the storm, on which eq. (4.4) is founded. Therefore an important part of any study of moving storms should be also the estimation of the magnitude of the errors in the results obtained.

If the number of rainfall measuring stations is relatively large, the following procedure is proposed for estimating the accuracy of the results(Diskin, 1990).

Consider a case where rainfall data is available for a number of stations (*n*). Naturally, to get the best estimate of the speed and direction of movement, data from all stations should be used in the computations. However, if the number of stations is large, a reasonable estimate could also be obtained by omitting one station and basing the computations on data from only *n*-1 stations. The results, based on data for *n*-1 stations, will obviously depend on the location of the station omitted and, in general, be different from the corresponding results for all *n* stations.

Computing the speed and direction of storm movement for all possible groups of *n*-1 stations, obtained by omitting one station at the time, will result in a set of results containing *n* values of computed speeds and *n* values of computed directions. The means of these results are expected to be very close to values of speed and direction derived with all data for the *n* stations. The standard deviations of the results give an indication of their accuracy. Strictly speaking, this is the accuracy of values derived from (*n*-1) stations, however, if *n* is large, the value obtained can also be taken as a measure of the accuracy of the results obtained with all the data.

This last method seemed the most appropriate for the research purposes, because it is practically sound and straightforward, moreover it overcomes the limitations characterizing the other available procedures. Consequently it was selected for the further applications reported in chapter 5.

References

- Amorocho J. and Wu B. (1977). *Mathematical models for the simulation of cyclonic storm sequences and precipitation fields*. J. Hydrol., 32: 329-345.
- Austin P.M. and Houze R.A. (1972). *Analysis of the structure of precipitation patterns in New England*. J. Appl. Meteorol., 11: 926-934.
- Berndtsson R. and Niemczynowicz J. (1988). *Spatial and temporal scales in rainfall analysis some aspects and future perspectives*. J. Hydrol., 100: 293-313.
- Briggs B.H., Phillips G.J. and Shinn D.H. (1950). *The analysis of observations on spaced receivers of the fading of radio signals*. Proc. Phys. Soc.. London, Set. B, 63: 106-121.
- Desbordes M. (1978). *Urban runoff and design storm modeling*. In" Proc. Urban Storm Drainage, Univ. Southampton. Pentech, London, pp. 353-361.
- Desbordes M., Raous P. and Trevisiol Y. (1984). *Areal reduction factors on short time and space intervals*. In: P. Harremoes (Editor), Rainfall as the Basis for Urban Drainage and Analysis. Proc. Spec. Seminar, Copenhagen. Pergamon, Oxford, pp. 189-198.
- Diskin M.H. (1987). *On the Determination of the Speed of Moving Rainfall Patterns*, Hydrological Sciences Journal, Vol32, No. 1, pp. 1-14.
- Diskin M.H. (1990). *The Speed of Two Moving Rainfall Events in Lund*, Nordic Hydrology, 21, 1990, 153-164.
- Felgate D.G. and Read D.D. (1975). *Correlation analysis of the cellular structure of storms observed by raingauges*. J. Hydrol., 24:191-200.
- Foster E.E. (1948). *Rainfall and Runoff*. The Macmillan Company, New York, NY.
- Graham J.G. Upton. (2002). *A correlation – regression method for tracking rainstorms using rain gauge data*. Journal of Hydrology, 261 (2002), 60 – 73.
- Gupta V.K. and Waymyre E.C. (1979). *A stochastic kinematic study of subsynoptic space-time rainfall*. Water Resour. Res.. 3(15): 637-644.
- Hindi W.N.A. and Kelway P.S. (1977). *Determination of storm velocities as an aid to the quality control of recording raingauge data*. J. Hydrol., 32: 115-137.

- Hobs P.V. and Locatelli J.D. (1978). *Rainbands, precipitation cores and generating cells in a cyclonic storm*. J. Atmos. Sci., 35: 230-241.
- James W. and Schackenberger R. (1982). *Application of kinematic storm model to runoff modeling*. Proc. Am. Geogr. Union Meeting, AGM, Philadelphia, Pa., pp. 2-18.
- Keifer,C.U. and Chu H.H. (1957). *Synthesis storm pattern for drainage system*. J. Hydrol. Div., 83.
- Krejci V. and Schilling W. (1989). *Urban hydrologists need meteorologists*. Proc. Int. Workshop Precipitation Measurement, St.Moritz, pp. 371-376.
- Larsson M. and Berdtsson R. (1985). *Simulation of the effect of rainfall movement on runoff using the complete Saint-Venant equations*. In: Proc. Int. Symp. Multivariate Analysis of Hydrologic Processes. Hsieh Wen Shen edition, Colorado State Univ., Fort Collins, CO, pp. 361-371.
- Marshall R.J. (1975). *Stochastic model to simulate moving storms*. Proc. Nat. Symp. Precipit. Anal. Hydrol. Modeling, Davis, Calif.
- Marshall R.J. (1977). *Statistical analysis of storm and daily rainfall data*. PhD. Thesis. Bristol University.
- Marshall R.J. (1980). *The estimation and distribution of storm movement and storm structure using a correlation analysis technique and rain gauge data*. J. Hydrol.. 48: 19-39.
- Niemczynowicz J. and Jonsson O. (1981). *Extreme rainfall events in Lund 1979-1980*. Nord. Hydrol., 12: 129 - 142.
- Niemczynowicz J. and Dahlblom P. (1984). *Dynamic properties of rainfall in Lund*. Nordic Hydrol., 15: 9-24.
- Niemczynowicz J. (1984 a). *An investigation of the areal and dynamic properties of rainfall and its influence on runoff generating processes*. Dep. Water Resour. Eng., Univ. Lund, Rep., 1005, 215 pp.
- Niemczynowicz J. (1984b). *Investigation of the influence of rainfall movement of runoff hydrograph*. Part 1 Simulation on conceptual catchment; Part 2. Simulation on real catchments in the city of Lund. Nord. Hydrol., 15: 57-70; 71-84.

- Niemczynowicz J. (1987). *Storm tracking using rain gauge data*. J. Hydrol., 93: 135-152.
- Niemczynowicz J. (1989). *On the rainfall data for urban hydrological applications*. In: Proc. Int. Workshop on Precipitation Measurement, St.Moritz, pp. 377-383.
- Niemczynowicz J. (1991). *On storm movement and its applications*. Atm. Res., 27: 109-127.
- Shaw S.R. (1983). *An investigation of the cellular structure of the storm using correlation techniques*. J. Hydrol., 62: 63-79.
- Shearman R.J. (1977). *The speed and direction of movement of storm rainfall patterns*. Meteorological Office, Bracknel, Berkshire, UK, Report UDC 551.515.43.
- Shilling W. (1984 a). *Short-term flow forecasting for real time stormwater control*. Proc. Third Int. Conf. Urban Storm Drain., Goteborg, pp. 1111-1119.
- Shilling W. (1984 b). *A quantitative assessment of uncertainties in stormwater modeling*. Proc. Third Int. Conf. Urban Storm Drain., Goteborg, pp. 625-633.
- Sifalda V. (1973). *Entwicklung eines Berechnungsregens fur die Bemessung yon Kanalenetzen*. GWF Wasser/Abwasser, 114: 435-440.
- Surkan A.J. (1974). *Simulation of storm velocity effects on flow from distributed channel networks*. Water Resour. Res., 10 (6).
- Townson J.M. and Ong H.S. (1974). *A laboratory study of runoff caused by line storm moving over a conceptual catchment*. Water Serv. USA.
- Yen B.C. and Chow V.T. (1980). *Design hyetographs for small drainage structures*. J. Hydrol. Div., 6: 1055-1076.
- Yen B.C. (1986). Rainfall-runoff process on urban catchments and its modeling. In: Proc. Int. Symp. on Urban Drainage Modelling, Dubrovnik. Pergamon, pp. 1-26.

5. Storm tracking study based on rain gauges data of a monitored catchment

5.1 Introduction

This chapter exposes the methodology used to estimate the speed and direction of movement of rainfall events recorded by the dense network of rain gauges placed in London. In detail rainfall data were provided by Imperial College London in order to deepen the knowledge of rainfall characteristics in view of their critical effects in causing regular flash floods. In fact it is evident how information, such as the rate and direction of movement of storms relative to the orientation of the catchment, is relevant to flood studies. Moreover, in this way, it will be also possible to enhance decision making by urban planners, engineers and policy makers (Desa and Niemczymowicz, 1997).

The lack of an adequate instrumental equipment for the Liguori catchment did not allow the possibility of performing a similar study for this site, for which the drainage model was previously developed. Therefore it was not possible to prove how the linkage between storm tracking procedures and hydraulic modeling could enable the identification in advance of potential flooded areas. However the elaborations carried out demonstrated how rain gauges may be considered as valid alternatives in rainfall movement prediction, to be taken into account in areas where radar measurements cannot be obtained yet.

In particular the speed and direction of movement of rainfall patterns, assumed constant during any given storm, were derived from data sets comprised of the coordinates (x, y) of the rainfall recording stations and the times of arrival (t) of some prominent feature of the recorded hyetographs. The results of numerous storm tracking studies reveal that the choice of the feature is a very difficult task (Hindi and Kelway, 1977; Felgate and Read, 1975; Shaw 1983). Consequently, in this case, three features were used for the definition of arrival times: t_{cent}, the time to the centroid of the hyetograph, t_{Imax}, the time of highest rainfall intensity and t_{onset}, the time of start of rainfall.

Different results were obtained depending on the nature of the feature adopted. The relative merits of selecting one feature or another were explored by comparing the various results obtained with other physical phenomena which are related to the storm movement, such as wind movement.

Finally, the research was also aimed at evaluating the extent to which the location of the rain gauges inside the catchment could condition the results of the methodology. These further elaborations are also important because some municipalities do not have the funds for equipping themselves with an adequate number of rain gauges, therefore it is significant to know how the results could change if a reduced number of recording stations is employed. Consequently, four different network configurations were finally considered in order to compare the obtainable results.

5.2 Data collection system and data base

Thirty-eight automatic tipping-bucket rain gauges are placed fairly evenly over the city of London (fig. 5.1 and tab. 5.1):

- six have been operating since 2006 (*Atomwide, Carshalton, Harringay, Hayes, Kensington, New Malden*);
- seven since 2007 (*Belmont, Catford, Eltham, Hillingdon, Hornchurch N, Rainham, Southwark*);
- six since 2008 (*Clapton, Colindale, Greenwich, Hornchurch W, Newham, Walthamstow*);
- nineteen since 2009 (*Bedfont, Bow, Brent, Camden, Dagenham, Enfield, Islington, Merton, Mill-Hill, Richmond S, Southall, Stanmore, Streatham, Thornton, Twickenham, Wandsworth S, Wandsworth SW, Welling, Westminster*).

The network covers an area of about 1,600 km^2, consequently there is one gauge per 42 km^2. The registration is governed by the same clock assuring absolute time synchronization and the time resolution of the registration is fifteen minutes. Therefore, it is evident that it was not possible to respect the “1-1-0.1” rule recommended for such elaborations. However the results obtained were in agreement with findings from other previous studies performed in other parts of the world.

				Coordinate UTM		
Location	**Latitude**	**Longitude**	**LongHemi**	**Easting**	**Northing**	**Zone**
Atomwide, Orpington, SE London	51.388	0.108	E	298785.55	5696942.91	31 U
Bedfont, W London	51.457	0.431	W	678475.76	5703777.4	30 U
Belmont, S London	51.346	0.202	W	694853.73	5692019.36	30 U
Bow, London	51.528	0.027	W	706216.75	5712733.52	30 U
Brent, London	51.551	0.231	W	691972.39	5714735.29	30 U
Camden, London	51.533	0.133	W	698843.86	5712995.87	30 U
Carshalton, S London	51.366	0.167	W	697204.76	5694336.57	30 U
Catford, SE London	51.443	0.028	W	706531.3	5703280.44	30 U
Clapton, E London	51.562	0.065	W	703429.7	5716407.22	30 U
Colindale, NW London	51.6	0.247	W	690658.07	5720141.5	30 U
Dagenham, E London	51.561	0.145	E	302109.84	5716076.44	31 U
Eltham, SE London	51.451	0.039	E	294268.95	5704138.91	31 U
Enfield, London	51.657	0.083	W	701760.49	5726919.62	30 U
Greenwich, London	51.487	0.041	E	294569.72	5708135.75	31 U
Harringay, N London	51.585	0.106	W	700487.2	5718851.11	30 U
Hayes, SE London	51.382	0.004	E	291523.78	5696566.56	31 U
Hillingdon, W London	51.557	0.389	W	680996.32	5714999.42	30 U
Hornchurch (N), E London	51.584	0.22	E	307404.69	5718433.33	31 U
Hornchurch (W), E London	51.564	0.196	E	305656.98	5716273.16	31 U
Islington, London	51.538	0.114	W	700139.43	5713603.62	30 U
Kensington, Central London	51.517	0.207	W	693780.39	5711018.32	30 U
Merton, London	51.412	0.212	W	693878.25	5699330.84	30 U
Mill Hill, NW London	51.629	0.248	W	690467.34	5723363.29	30 U
New Malden, SW London	51.384	0.265	W	690309.47	5696078.77	30 U
Newham, E London	51.532	0.033	E	294217.4	5713161.34	31 U
Rainham, E London	51.515	0.204	E	306003.01	5710803.9	31 U
Richmond (S), Surrey	51.454	0.298	W	687726.47	5703776.5	30 U
Southall, W London	51.499	0.387	W	681365.36	5708555.48	30 U
Southwark, SE London	51.475	0.097	W	701596.13	5706645.86	30 U
Stanmore, Middlesex	51.617	0.332	W	684703.38	5721813.32	30 U
Streatham, London	51.445	0.121	W	700060.99	5703244.58	30 U
Thornton Heath, Surrey	51.394	0.121	W	700283.91	5697574.37	30 U
Twickenham, SW London	51.453	0.345	W	684465.62	5703545.86	30 U
Walthamstow, London	51.599	0.024	W	706103.34	5720635.8	30 U
Wandsworth (S), London	51.445	0.197	W	694780.72	5703039.67	30 U
Wandsworth (SW), London	51.446	0.203	W	694359.61	5703134.91	30 U
Welling, Kent	51.473	0.119	E	299922.59	5706363.12	31 U
Westminster, Central London	51.519	0.138	W	698558.07	5711425.73	30 U

Table 5.1 Details of rain gauges in the study area.

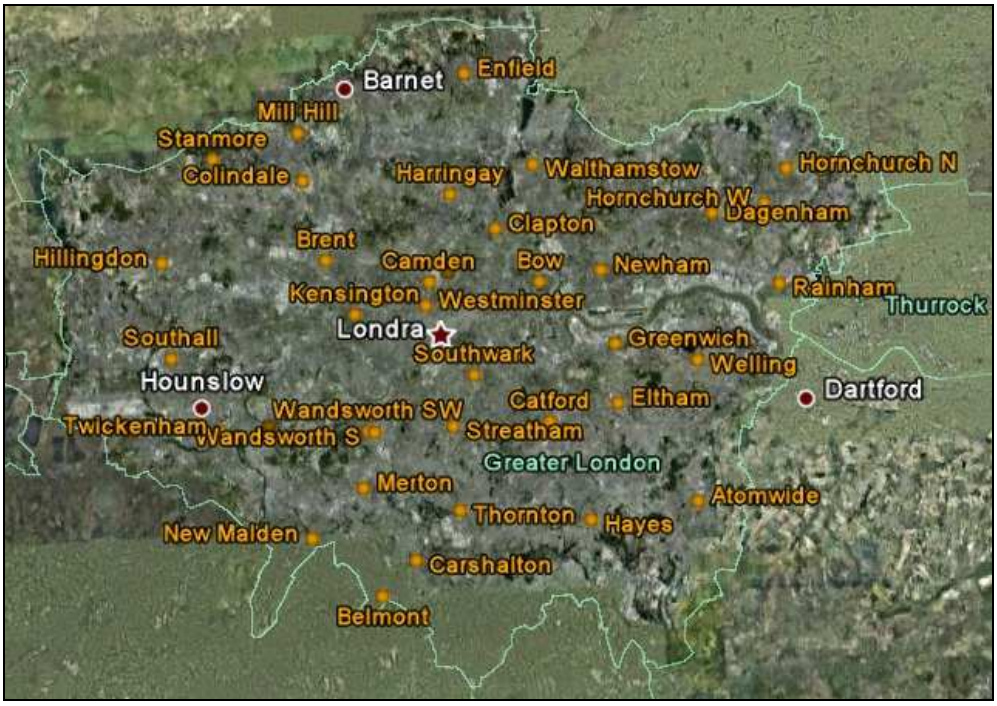

Figure 5.1 Location map of rain gauges in London.

Further information concerning the gauging system is available from the web site http://weather.lgfl.org.uk/map.aspx.

5.2.1 Storm selection

On average, from three to twenty-nine stations successfully recorded the rainfall data via data logger system set in event mode. Unfortunately a part of these data could not be analyzed because periodic malfunctioning of the gauges and data loggers were not totally avoided.

Only storms, recorded by at least three rain gauges and with a duration at least of five hours, were considered. In particular, initially, the storm rainfalls were recognized from the most operating rain gauge, i.e. *Atomwide*. Later the durations of all the storms identified were assumed as reference for determining the storms for the other rain gauges. Altogether thirty-nine rainfall events were found appropriate, as shown in Table 5.2: specifically, it can be seen that the duration of all storms ranges from 5 hours to 36.5 hours with an average duration of 12.5 hours.

Event no.	Starting Time	Final Time	Duration [hr]	Number of gauges operating
1	10/11/2006 19:45	11/11/2006 03:45	8	5
2	05/12/2006 05:15	05/12/2006 12:45	7.5	6
3	07/12/2006 01:15	07/12/2006 09:15	8	6
4	06/01/2007 09:45	06/01/2007 17:15	7.5	5
5	10/01/2007 03:15	10/01/2007 12:45	9.5	6
6	17/01/2007 06:15	17/01/2007 12:45	6.5	6
7	13/02/2007 18:15	14/02/2007 11:45	17.5	3
8	27/05/2007 14:45	28/05/2007 07:45	17	8
9	09/10/2007 07:15	09/10/2007 18:45	11.5	12
10	18/11/2007 14:45	20/11/2007 03:15	36.5	12
11	25/12/2007 04:45	25/12/2007 15:45	11	13
12	11/01/2008 04:15	11/01/2008 15:15	11	12
13	14/01/2008 22:15	15/01/2008 12:15	14	11
14	29/01/2008 23:15	30/01/2008 05:15	6	13
15	15/03/2008 15:45	16/03/2008 01:45	10	14
16	29/03/2008 13:45	30/03/2008 05:45	15	13
17	30/04/2008 07:15	30/04/2008 22:15	15	14
18	25/05/2008 01:15	25/05/2008 16:15	15	14
19	26/05/2008 02:45	27/05/2008 04:15	25.5	14
20	29/05/2008 14:15	29/05/2008 21:15	7	13
21	07/07/2008 02:45	07/07/2008 21:45	19	15
22	09/07/2008 06:15	10/07/2008 01:15	19	13
23	02/09/2008 02:15	02/09/2008 12:15	10	13
24	05/09/2008 09:15	06/09/2008 00:15	15	12
25	04/10/2008 22:45	05/10/2008 15:45	17	13
26	10/11/2008 08:15	10/11/2008 18:15	10	12
27	04/12/2008 05:15	04/12/2008 10:15	5	12
28	13/12/2008 00:45	14/12/2008 00:15	23.5	14
29	19/01/2009 03:15	19/01/2009 10:15	7	18
30	03/02/2009 09:45	03/02/2009 17:15	7.5	15
31	06/02/2009 05:15	06/02/2009 13:45	8.5	17
32	09/02/2009 07:15	10/02/2009 06:15	23	17
33	08/06/2009 22:45	09/06/2009 08:45	10	26
34	11/07/2009 21:15	12/07/2009 05:15	8	24
35	02/09/2009 16:15	03/09/2009 00:45	8.5	27
36	15/09/2009 09:45	16/09/2009 01:45	16	27
37	05/10/2009 08:15	05/10/2009 15:15	7	28
38	06/10/2009 06:45	06/10/2009 12:15	5.5	29
39	07/10/2009 13:45	08/10/2009 00:15	10.5	28

Table 5.2 List of storms used in the study.

5.3 Method of analysis

Before focusing attention on the methodology adopted, it is important to underline that a basic assumption, common to all storm tracking methods, is that the computations produce single values of storm speed and direction of movement for each storm event. In other words, the possibility of changes in the speed or direction as the storm sweeps over the network is ignored (Diskin, 1987). The movement of the rainfall event is therefore modeled as the motion of a wave front, defined by the single values of speed and direction to be calculated.

In particular, the motion is expressed by the fact the rainfall hyetographs recorded at the various gauges are displaced relative to one another along the time axis. This relative displacement obviously depends on the speed and direction of storm movement.

Since rainfall hyetographs at different stations are not identical, it is necessary to select some easily identifiable feature of the hyetograph, in order to follow it as it moves in space across the gauge network. The results of numerous storm tracking studies says that the choice of the feature is a very difficult task (Hindi and Kelway, 1977; Felgate and Read, 1975; Shaw 1983) because different results were obtained depending on the nature of the feature adopted. Consequently, in this case, three different features were used for the definition of the arrival times: t_{cent}, the time to the centroid of the hyetograph, t_{Imax}, the time of highest rainfall intensity and t_{onset}, the time of start of rainfall. The purpose was to investigate which feature gave the most reliable results, by comparing the various outcomes obtained with other physical phenomena which are related to the storm movement, such as wind movement.

The arrival times for each feature were read directly, or computed automatically, from the recorded hyetographs at the various stations. The origin of all time values was arbitrary, but it was, of course, the same for all stations in each storm.

Using each time one of the features selected for a specified storm event, a set of arrival time values (t) were derived for a number of stations. These values, together with the coordinates of the rain measuring stations (x, y values reported in tab. 5.3 and estimated with reference to the axes shown in fig. 5.2), formed the data set from which the speed and direction of rainfall were derived.

Location	x [km]	y [km]
Atomwide, Orpington, SE London	62.11	6.89
Bedfont, W London	2.22	14.56
Belmont, S London	27.67	2.22
Bow, London	47.11	22.44
Brent, London	24.44	25.00
Camden, London	35.33	23.00
Carshalton, S London	31.56	4.44
Catford, SE London	47.00	13.00
Clapton, E London	42.89	26.22
Colindale, NW London	22.67	30.44
Dagenham, E London	66.22	26.11
Eltham, SE London	54.44	13.89
Enfield, London	40.89	36.78
Greenwich, London	54.67	17.89
Harringay, N London	38.33	28.78
Hayes, SE London	50.56	6.22
Hillingdon, W London	6.89	25.67
Hornchurch (N), E London	74.56	28.67
Hornchurch (W), E London	71.89	26.44
Islington, London	37.44	23.56
Kensington, Central London	27.11	21.22
Merton, London	26.56	9.56
Mill Hill, NW London	22.56	33.67
New Malden, SW London	20.67	6.44
Newham, E London	53.78	22.89
Rainham, E London	72.78	21.00
Richmond (S), Surrey	17.00	14.22
Southall, W London	7.11	19.22
Southwark, SE London	39.33	16.56
Stanmore, Middlesex	13.22	32.33
Streatham, London	36.67	13.22
Thornton Heath, Surrey	36.67	7.56
Twickenham, SW London	11.78	14.11
Walthamstow, London	47.44	30.33
Wandsworth (S), London	28.22	13.22
Wandsworth (SW), London	27.56	13.33
Welling, Kent	63.33	16.33
Westminster, Central London	34.78	21.44

Table 5.3 Coordinates of rain gauges evaluated with reference to the axes presented in fig. 5.2.

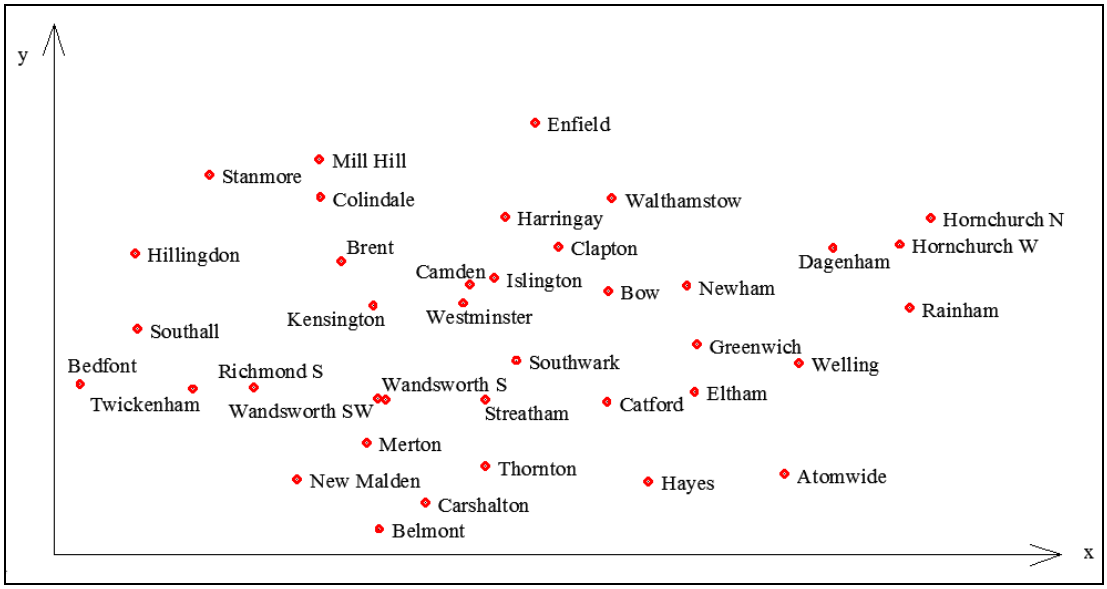

Figure 5.2 Recording rainfall stations in London

All this information was used according to the method proposed by Diskin (1990): in particular, this procedure interprets geometrically the problem of the storm movement by determining the equation of the inclined plane in the *x*, *y*, *t* space, that best fits to the set of data points (fig. 5.3).

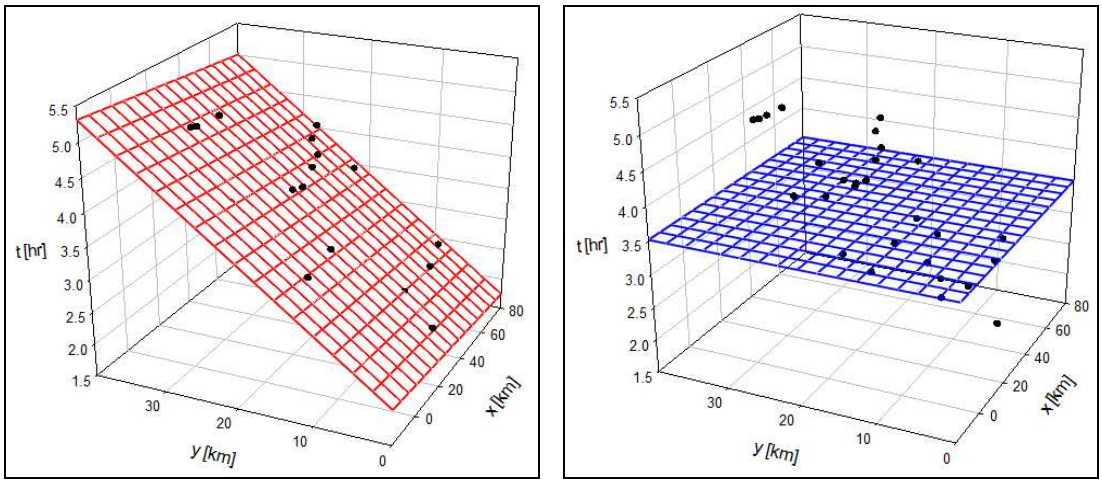

Figure 5.3 Geometrical interpretation of the movement of storms through the hypothesis of the inclined plane and the horizontal plane.

The method was selected because it is practically sound and straightforward, besides it requires “only” that all the rain gauges be fully synchronized, as verified for the case study.

The procedure is described in more detail in chapter 4, nevertheless it will be also reported, briefly, in this paragraph. In particular, it is based on the evaluation of the parameters *a*, *b* and *c* of the inclined plane that best represents the set of data points:

$$t = a \cdot x + b \cdot y + c \tag{5.1}$$

The speed of movement is given by the inverse of the maximum slope of the plane

$$V\left[\text{km/hr}\right] = \frac{1}{\sqrt{a^2 + b^2}} \tag{5.2}$$

whereas the direction, which is parallel to that of the maximum slope, can be calculated relatively to the *x*-axis by

$$\Theta\left[\text{deg.}\right] = \arctan\left(\frac{b}{a}\right) \tag{5.3}$$

It is clear that the units of measurement of the computed parameters depend on the units of measurement assumed for the input data.

The values of the parameters are obtained from data sets by minimizing the sum of the squared deviations between the observed arrival times (T_i) and the predicted values (t_i) computed by eq. (5.1) for all stations. The equations derived for the three parameters can be expressed in the following form

$$a = \frac{A \cdot E - B \cdot C}{D \cdot E - C^2} \tag{5.4}$$

$$b = \frac{B \cdot D - A \cdot C}{D \cdot E - C^2} \tag{5.5}$$

$$c = \frac{\sum_{i=1}^{n}\left(T_i\right) - a \cdot \sum_{i=1}^{n}\left(x_i\right) - b \cdot \sum_{i=1}^{n}\left(y_i\right)}{n} \tag{5.6}$$

where *n* is the number of stations for which data are available, and the constants *A*, *B*, *C*, *D* and *E* are computed from the known set of data by the following equations

$$A = n \cdot \sum_{i=1}^{n}\left(T_i \cdot x_i\right) - \sum_{i=1}^{n}\left(T_i\right) \cdot \sum_{i=1}^{n}\left(x_i\right) \tag{5.7}$$

$$B = n \cdot \sum_{i=1}^{n}\left(T_i \cdot y_i\right) - \sum_{i=1}^{n}\left(T_i\right) \cdot \sum_{i=1}^{n}\left(y_i\right) \tag{5.8}$$

$$C = n \cdot \sum_{i=1}^{n} (x_i \cdot y_i) - \sum_{i=1}^{n} (x_i) \cdot \sum_{i=1}^{n} (y_i) \tag{5.9}$$

$$D = n \cdot \sum_{i=1}^{n} (x_i^2) - \sum_{i=1}^{n} (x_i) \cdot \sum_{i=1}^{n} (x_i) \tag{5.10}$$

$$E = n \cdot \sum_{i=1}^{n} (y_i^2) - \sum_{i=1}^{n} (y_i) \cdot \sum_{i=1}^{n} (y_i) \tag{5.11}$$

Nevertheless, the prediction equation reported above is not the only possible model to represent the data. In fact, the observed different arrival times could be also random fluctuations from an equal arrival time for all stations, which could be the average of the observed arrival times themselves.

Reverting to the geometrical interpretation, an equal arrival time is represented by a horizontal plane (parallel to the *x*,*y* axes) at the level of the average time of arrival (fig. 5.3).

Therefore it is necessary to verify which of the planes better represents the data set: the choice can be based on the comparison between the root mean square (RMS) deviation obtained by adopting the two models (σ_I, σ_O)

$$\sigma_I = \sqrt{\frac{\sum_{i=1}^{n} (T_i - t_i)^2}{n-1}} \tag{5.12}$$

$$\sigma_O = \sqrt{\frac{\sum_{i=1}^{n} (T_i - \overline{T_i})^2}{n-1}} \tag{5.13}$$

where

- T_i are the observed times of arrival;
- t_i are the predicted times of arrival computed by eq. (5.1);
- $\overline{T_i}$ is the average arrival time.

The ratio of the two values can be adopted as a measure of the significance of the results (*Significance Ratio*):

$$\textit{Significance Ratio}\ \left(S.R.\right)=\frac{\sigma_I}{\sigma_O}=\sqrt{\frac{\sum_{i=1}^{n}\left(T_i-t_i\right)^2}{\sum_{i=1}^{n}\left(T_i-\overline{T}_i\right)^2}} \tag{5.14}$$

The values of σ_I is always smaller than σ_O, therefore their ratio is expected to be comprised between zero and one. Values close to zero indicate high significance of the inclined plane hypothesis whereas values close to one poor performance of the proposed model. In this case a threshold value was adopted for this parameter: in particular all the elaborations, characterized by a significance ratio bigger than 0.85, were rejected because it meant that the hypothesis of equal arrival times was the best one, and consequently no storm movement could be considered.

Finally, the accuracy of all the results produced, including the values of significance ratio, was estimated by repeating computations of the speed and direction for subsets of the data, obtained by omitting each time one of the recording station (Diskin, 1990). The average values of these results are expected to be very close to the values of speed and direction derived considering all the stations, whereas the standard deviations can be assumed as indication of their accuracy. Actually, this accuracy is derived from (*n*-1) stations, however, if *n* is large, the value obtained can also be taken as a measure of the accuracy of the results obtained with all the data.

5.4 Results and discussion

5.4.1 Storm velocity and direction

Values of the speed and direction of movement were computed, using the complete sets of data reported in Appendix D, for each of the three definitions of arrival time. Only the elaborations with significance ratios smaller than 0.85 were not rejected. In particular the values of velocity [km/hr] and directions [degrees from North], considered for the further applications, were those ones obtained by averaging the *N* values calculated by omitting each time one of the recording station (tab. 5.4). As expected, these values resulted very close to the corresponding values based on the complete set of data (Appendix D).

	Centroid			Peak			Onset		
Event no.	**V**	**θ**	S. R.	**V**	**θ**	S. R.	**V**	**θ**	S. R.
1	12.44	72.22	0.17	6.79	141.84	0.13	54.25	80.29	0.28
2	14.02	59.59	0.38	18.39	144.17	0.77	6.48	35.61	0.41
3	51.43	151.37	0.57	29.59	133.61	0.20			
4	12.97	156.47	0.21				26.41	124.08	0.22
5	10.37	141.68	0.46	10.35	59.38	0.74			
6	41.47	132.22	0.58	26.48	43.69	0.67	16.89	136.97	0.56
7	12.62	55.55	0.04	4.17	162.11	0.02			
8	17.87	163.45	0.65	7.22	105.72	0.61	4.25	163.93	0.55
9	20.16	154.38	0.41				6.45	170.28	0.53
10	8.68	154.07	0.76				11.58	18.95	0.63
11	10.06	137.51	0.39	6.65	155.32	0.62	12.31	112.91	0.77
12				34.21	166.76	0.44			
13							5.77	152.59	0.85
14	33.79	155.70	0.49	33.06	165.44	0.62	20.96	154.42	0.74
15	17.81	173.36	0.57	16.46	153.62	0.79	13.24	33.87	0.71
16	5.60	158.25	0.64	3.70	158.41	0.75			
17	5.27	164.72	0.52	4.36	19.39	0.70	27.91	153.29	0.58
18	9.10	64.54	0.48	5.87	168.38	0.69	23.97	175.64	0.28
19	8.51	159.41	0.59	5.68	26.54	0.66	18.01	26.25	0.43
20	41.39	83.86	0.54	13.92	43.01	0.53	56.56	97.54	0.81
21	19.84	100.96	0.58	9.77	165.46	0.52	5.86	160.20	0.64
22	11.34	174.62	0.41	34.73	20.27	0.84	53.64	44.66	0.34
23	21.71	135.06	0.40	31.65	140.55	0.63	26.85	129.96	0.80
24							11.47	149.35	0.63
25							19.46	131.62	0.82
26	17.54	157.74	0.79	16.91	163.83	0.66			
27	55.06	160.06	0.72	18.87	156.71	0.60	71.41	80.30	0.45
28	5.71	173.89	0.50	3.95	39.82	0.74	4.28	25.87	0.52
29	34.78	174.24	0.69	25.20	170.80	0.70	51.52	25.09	0.58
30	18.90	157.23	0.70						
31	12.16	168.77	0.38	17.85	6.03	0.79	28.62	137.14	0.52
32	19.96	142.30	0.71						
33							15.76	158.29	0.84
34	17.14	177.37	0.59						
35	37.55	103.06	0.39	31.02	103.29	0.63	10.75	155.85	0.62
36	8.06	131.72	0.57	6.01	135.95	0.78	20.60	127.17	0.43
37	12.24	177.89	0.38	9.07	176.89	0.62	9.80	7.82	0.62
38	31.72	140.77	0.68	24.16	130.37	0.80			
39	52.16	123.77	0.59				78.75	19.18	0.78

Table 5.4 Results obtained with the full set of data.

The values of velocity and direction, computed using the various definitions of arrival time, were quite different (tab. 5.4 and tab. 5.5).

	Centroid			**Peak**			**Onset**		
	V	**θ**	S. R.	**V**	**θ**	S. R.	**V**	**θ**	S. R.
Min.	5.27	55.55	0.04	3.70	6.03	0.02	4.25	7.82	0.22
Max.	55.06	177.89	0.79	34.73	176.89	0.84	78.75	175.64	0.85
Mean	20.87	139.35	0.52	16.29	116.33	0.62	24.61	103.07	0.58
S.D.	14.31	35.92	0.17	10.82	57.46	0.20	20.78	57.40	0.18
C.V.	0.69	0.26	0.33	0.66	0.49	0.33	0.84	0.56	0.31

Table 5.5 Range variation, average value, standard deviation and coefficient of variation resulted from the elaborations carried out.

Specifically, the average velocity was 20.87 km/hr (5.80 m/s) for the elaborations based on the centroid feature, 16.29 km/hr (4.52 m/s) for the elaborations based on the peak feature, 24.61 km/hr (6.84 m/s) for the elaborations based on the onset feature.

Precisely the velocity outcomes demonstrate the quality of the elaborations carried out: in fact, these values were quite in agreement with the results obtained in several studies performed in other regions. Hobs and Locatelli (1978) reported that storm velocity ranged between 2 and 25 m/s. Chaudhry et al. (1994) gave an average storm velocity of 11.67 m/s using data from radar. Marshall (1980) computed 11.4 m/s, Niemczynowicz and Dahlblom (1984) found an average velocity of storms 10.35 m/s while Shearman (1977) obtained about 15 m/s for 60% of the storms analyzed. Finally Eagleson (1970) mentioned the velocity of convective cells to be in the range between 8.94 and 13.41 m/s.

Nevertheless, also some differences emerged: in this case, in fact, computed velocity data set resulted well fitted by a normal distribution for all the three features (fig. 5.4 a-c), whereas Niemczynowicz (1987) observed that the relative frequency of storm velocities was well fitted by a two-parameter lognormal distribution.

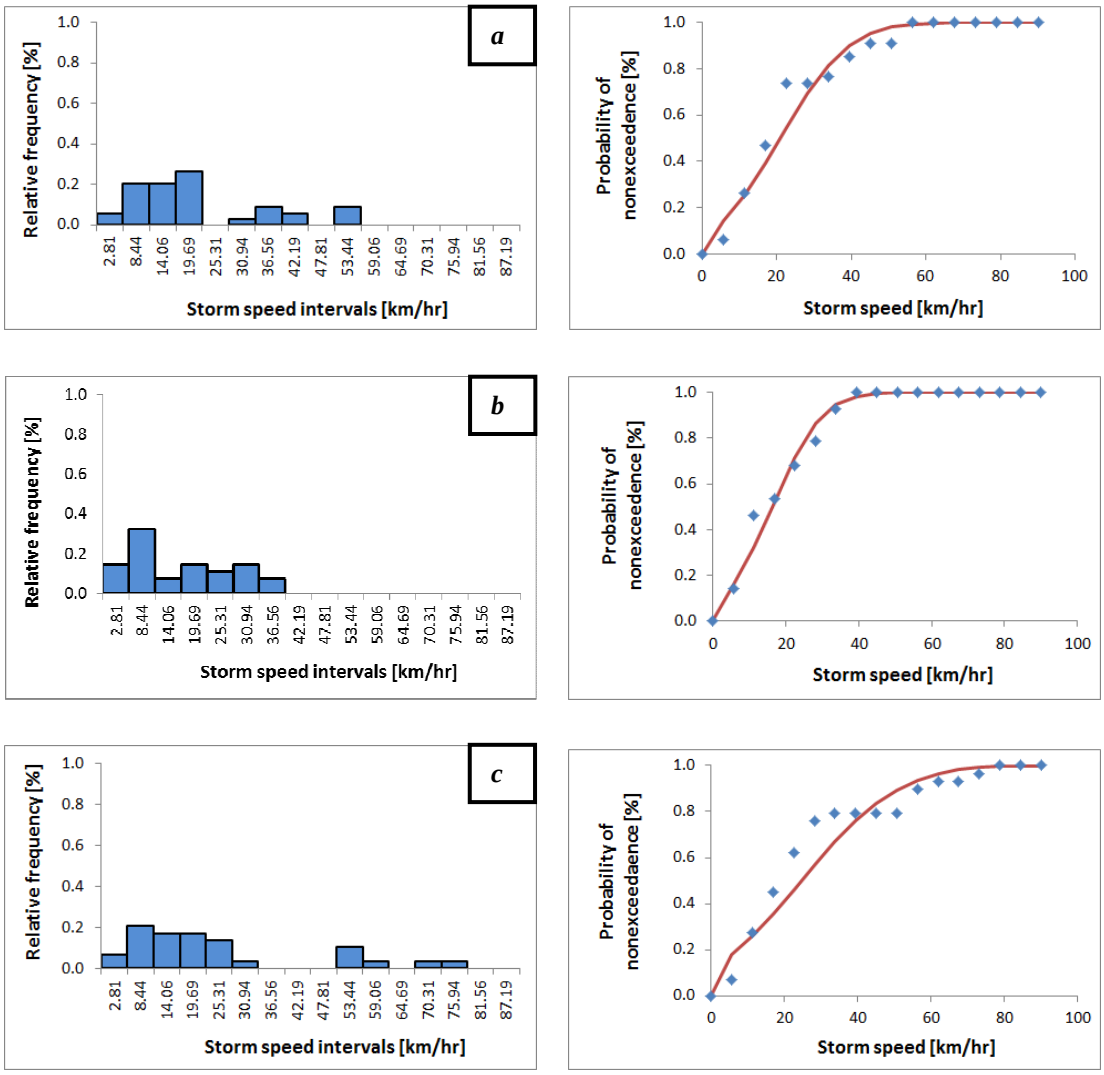

Figure 5.4 Relative frequency and probability of nonexceedence of storm velocity for the elaborations based on the centroid feature (a), the peak feature (b) and the onset feature (c).

The average storm direction calculated was 139.35 degrees counted clockwise from the North for the elaborations based on the centroid feature, 116.33 degrees for the elaborations based on the peak feature, 103.07 degrees for the elaborations based on the onset feature.

Also in this case the outcomes were well fitted by a normal distribution for all the three features (fig. 5.5 a-c).

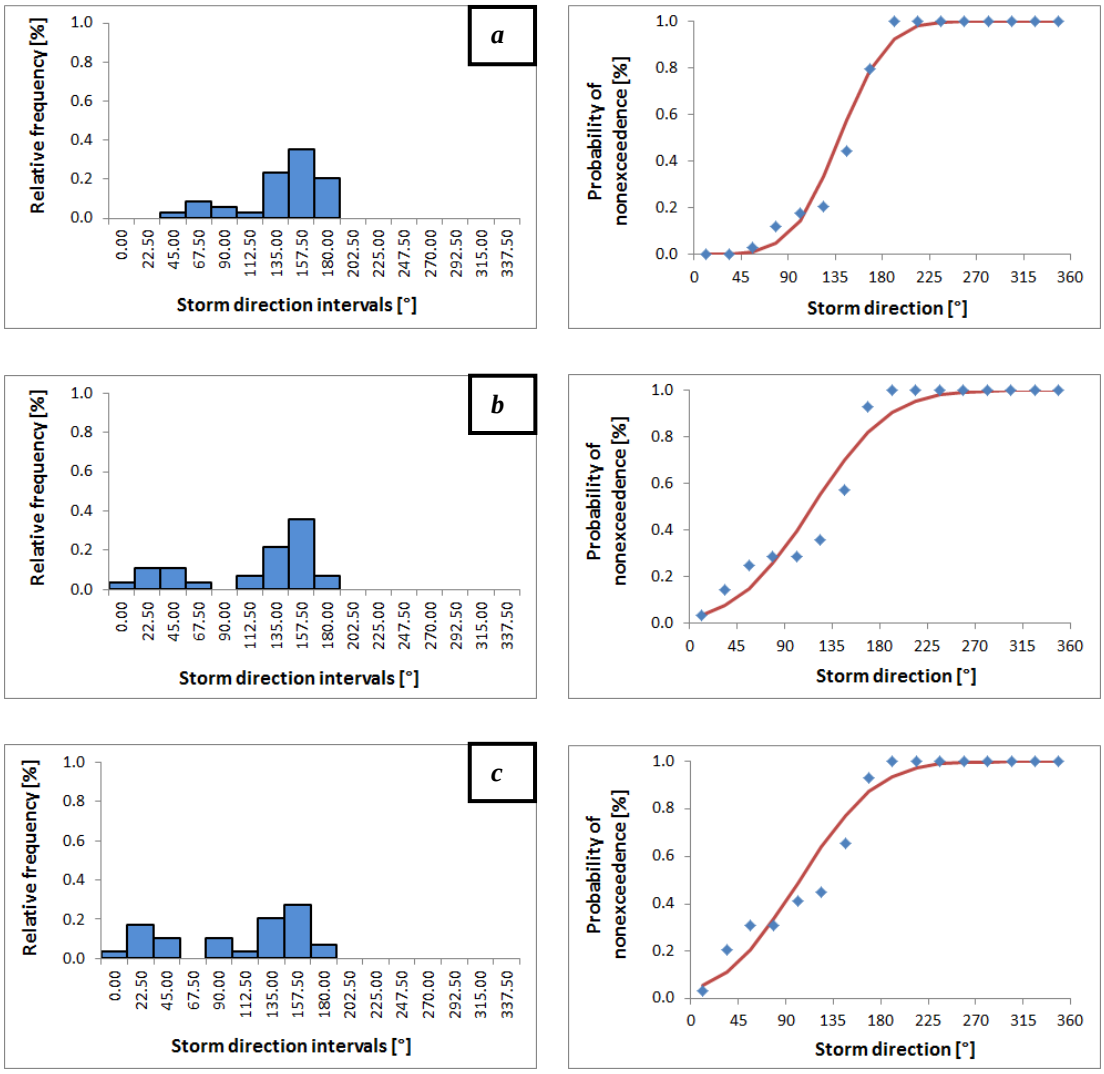

Figure 5.4 Relative frequency and probability of nonexceedence of storm direction for the elaborations based on the centroid feature (a), the peak feature (b) and the onset feature (c).

Since the influence of storm movement on runoff depends on joint effects of storm velocity and direction, it was interesting to know the relative frequency of storm velocity on different directions. Table 5.6 gives the relative frequencies of storm velocity and direction in velocity and direction classes, and the same results are plotted in fig. 5.5. It can be noticed that there is:

1. a distinct maximum of relative frequency around storm velocities 16.88 – 22.50 km/hr and storm direction towards South-East and South-South-East for the elaborations based on the centroid feature;

2. a distinct maximum of relative frequency around storm velocities 5.63 – 11.25 km/hr and storm direction towards South-East and South-South-East for the elaborations based on the peak feature;
3. a distinct maximum of relative frequency around storm velocities 5.63 – 11.25 km/hr and storm direction towards South-East and South-South-East for the elaborations based on the onset feature.

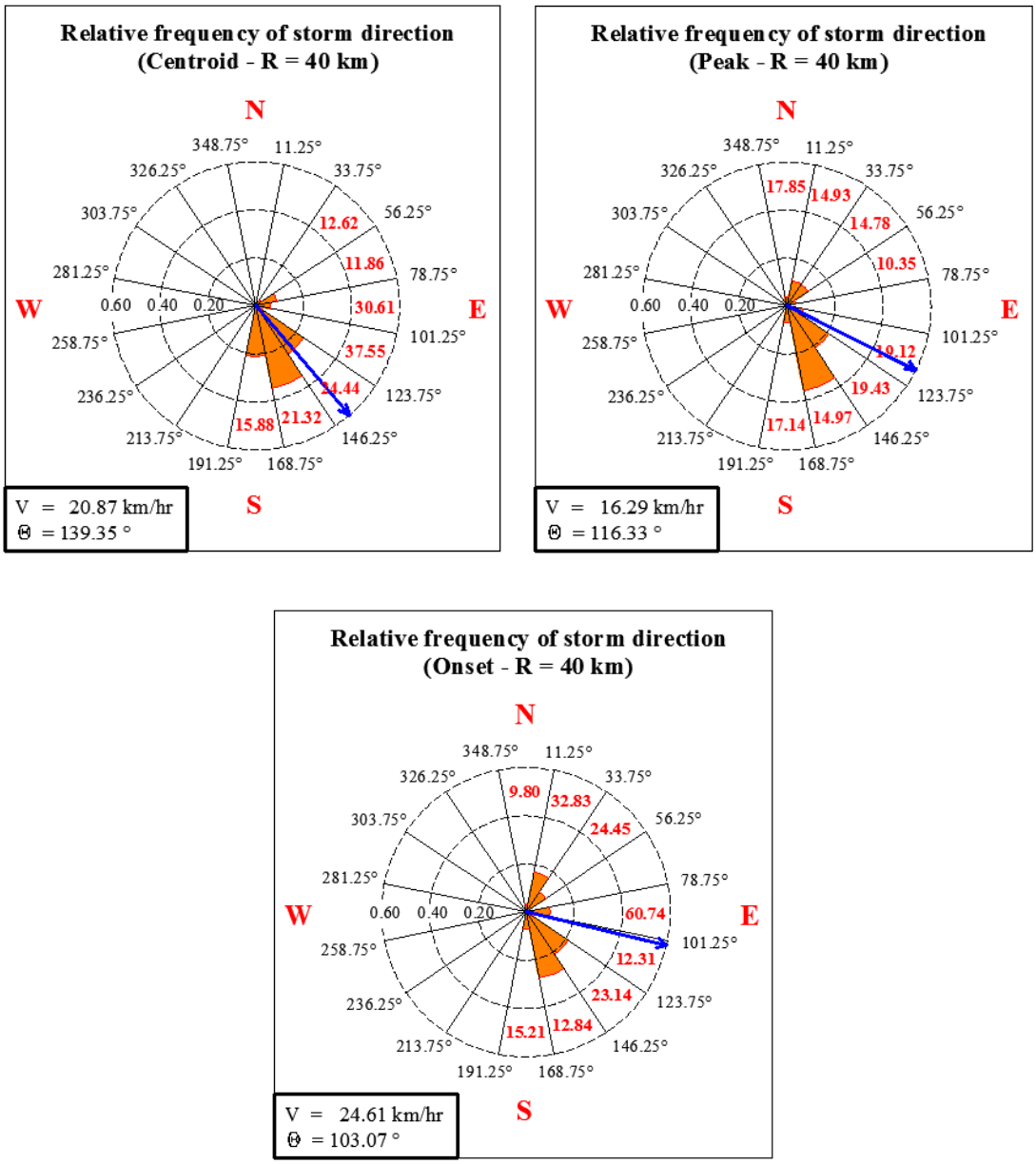

Figure 5.5 Relative frequency of storm direction for the three features considered.

CENTROID

Storm Velocity [km / hr]	Storm Direction [degrees from N]																All
	348,75° 11,25° N (0°)	11,25° 33,75° NNE (22,5°)	33,75° 56,25° NE (45°)	56,25° 78,75° ENE (67,5°)	78,75° 101,25° E (90°)	101,25° 123,75° ESE (112,5°)	123,75° 146,25° SE (135°)	146,25° 168,75° SSE (157,5°)	168,75° 191,25° S (180°)	191,25° 213,75° SSW (202,5°)	213,75° 236,25° SW (225°)	236,25° 258,75° WSW (247,5°)	258,75° 281,25° W (270°)	281,25° 303,75° WNW (292,5°)	303,75° 326,25° NW (315°)	326,25° 348,75° NNW (337,5°)	
0 - 5.63	0	0	0	0	0	0	0	2	0	0	0	0	0	0	0	0	2
5.63 - 11.25	0	0	0	1	0	0	3	2	1	0	0	0	0	0	0	0	7
11.25 - 16.88	0	0	1	2	0	0	0	1	3	0	0	0	0	0	0	0	7
16.88 - 22.50	0	0	0	0	1	0	2	4	2	0	0	0	0	0	0	0	9
22.50 - 28.13	0	0	0	0	0	0	0	0	0	0	0	0	0	0	0	0	0
28.13 - 33.75	0	0	0	0	0	0	1	0	0	0	0	0	0	0	0	0	1
33.75 - 39.38	0	0	0	0	0	1	0	1	1	0	0	0	0	0	0	0	3
39.38 - 45.00	0	0	0	0	1	0	1	0	0	0	0	0	0	0	0	0	2
45.00 - 50.63	0	0	0	0	0	0	0	0	0	0	0	0	0	0	0	0	0
50.63 - 56.25	0	0	0	0	0	0	1	2	0	0	0	0	0	0	0	0	3
56.25 - 61.88	0	0	0	0	0	0	0	0	0	0	0	0	0	0	0	0	0
61.88 - 67.50	0	0	0	0	0	0	0	0	0	0	0	0	0	0	0	0	0
67.50 - 73.13	0	0	0	0	0	0	0	0	0	0	0	0	0	0	0	0	0
73.13 - 78.75	0	0	0	0	0	0	0	0	0	0	0	0	0	0	0	0	0
78.75 - 84.38	0	0	0	0	0	0	0	0	0	0	0	0	0	0	0	0	0
84.38 - 90.00	0	0	0	0	0	0	0	0	0	0	0	0	0	0	0	0	0
All	0	0	1	3	2	1	8	12	7	0	0	0	0	0	0	0	34

V [km / hr]	0.00	0.00	12.62	11.86	30.61	37.55	24.44	21.32	15.88	0.00	0.00	0.00	0.00	0.00	0.00	0.00

Storm Velocity [km / hr]	Storm Direction [degrees from N]																All
	348,75° 11,25° N (0°)	11,25° 33,75° NNE (22,5°)	33,75° 56,25° NE (45°)	56,25° 78,75° ENE (67,5°)	78,75° 101,25° E (90°)	101,25° 123,75° ESE (112,5°)	123,75° 146,25° SE (135°)	146,25° 168,75° SSE (157,5°)	168,75° 191,25° S (180°)	191,25° 213,75° SSW (202,5°)	213,75° 236,25° SW (225°)	236,25° 258,75° WSW (247,5°)	258,75° 281,25° W (270°)	281,25° 303,75° WNW (292,5°)	303,75° 326,25° NW (315°)	326,25° 348,75° NNW (337,5°)	
0 - 5.63	0.00	0.00	0.00	0.00	0.00	0.00	0.00	0.06	0.00	0.00	0.00	0.00	0.00	0.00	0.00	0.00	0.06
5.63 - 11.25	0.00	0.00	0.00	0.03	0.00	0.00	0.09	0.06	0.03	0.00	0.00	0.00	0.00	0.00	0.00	0.00	0.21
11.25 - 16.88	0.00	0.00	0.03	0.06	0.00	0.00	0.00	0.03	0.09	0.00	0.00	0.00	0.00	0.00	0.00	0.00	0.21
16.88 - 22.50	0.00	0.00	0.00	0.00	0.03	0.00	0.06	0.12	0.06	0.00	0.00	0.00	0.00	0.00	0.00	0.00	0.26
22.50 - 28.13	0.00	0.00	0.00	0.00	0.00	0.00	0.00	0.00	0.00	0.00	0.00	0.00	0.00	0.00	0.00	0.00	0.00
28.13 - 33.75	0.00	0.00	0.00	0.00	0.00	0.00	0.03	0.00	0.00	0.00	0.00	0.00	0.00	0.00	0.00	0.00	0.03
33.75 - 39.38	0.00	0.00	0.00	0.00	0.00	0.03	0.00	0.03	0.03	0.00	0.00	0.00	0.00	0.00	0.00	0.00	0.09
39.38 - 45.00	0.00	0.00	0.00	0.00	0.03	0.00	0.03	0.00	0.00	0.00	0.00	0.00	0.00	0.00	0.00	0.00	0.06
45.00 - 50.63	0.00	0.00	0.00	0.00	0.00	0.00	0.00	0.00	0.00	0.00	0.00	0.00	0.00	0.00	0.00	0.00	0.00
50.63 - 56.25	0.00	0.00	0.00	0.00	0.00	0.00	0.03	0.06	0.00	0.00	0.00	0.00	0.00	0.00	0.00	0.00	0.09
56.25 - 61.88	0.00	0.00	0.00	0.00	0.00	0.00	0.00	0.00	0.00	0.00	0.00	0.00	0.00	0.00	0.00	0.00	0.00
61.88 - 67.50	0.00	0.00	0.00	0.00	0.00	0.00	0.00	0.00	0.00	0.00	0.00	0.00	0.00	0.00	0.00	0.00	0.00
67.50 - 73.13	0.00	0.00	0.00	0.00	0.00	0.00	0.00	0.00	0.00	0.00	0.00	0.00	0.00	0.00	0.00	0.00	0.00
73.13 - 78.75	0.00	0.00	0.00	0.00	0.00	0.00	0.00	0.00	0.00	0.00	0.00	0.00	0.00	0.00	0.00	0.00	0.00
78.75 - 84.38	0.00	0.00	0.00	0.00	0.00	0.00	0.00	0.00	0.00	0.00	0.00	0.00	0.00	0.00	0.00	0.00	0.00
84.38 - 90.00	0.00	0.00	0.00	0.00	0.00	0.00	0.00	0.00	0.00	0.00	0.00	0.00	0.00	0.00	0.00	0.00	0.00
All	0.00	0.00	0.03	0.09	0.06	0.03	0.24	0.35	0.21	0.00	0.00	0.00	0.00	0.00	0.00	0.00	1.00

V [km / hr]	0.00	0.00	12.62	11.86	30.61	37.55	24.44	21.32	15.88	0.00	0.00	0.00	0.00	0.00	0.00	0.00

PEAK

Storm Velocity [km / hr]	Storm Direction [degrees from N]																All
	348,75° 11,25° N (0°)	11,25° 33,75° NNE (22,5°)	33,75° 56,25° NE (45°)	56,25° 78,75° ENE (67,5°)	78,75° 101,25° E (90°)	101,25° 123,75° ESE (112,5°)	123,75° 146,25° SE (135°)	146,25° 168,75° SSE (157,5°)	168,75° 191,25° S (180°)	191,25° 213,75° SSW (202,5°)	213,75° 236,25° SW (225°)	236,25° 258,75° WSW (247,5°)	258,75° 281,25° W (270°)	281,25° 303,75° WNW (292,5°)	303,75° 326,25° NW (315°)	326,25° 348,75° NNW (337,5°)	
0 – 5.63	0	1	1	0	0	0	0	2	0	0	0	0	0	0	0	0	4
5.63 – 11.25	0	1	0	1	0	1	2	3	1	0	0	0	0	0	0	0	9
11.25 – 16.88	0	0	1	0	0	0	0	1	0	0	0	0	0	0	0	0	2
16.88 – 22.50	1	0	0	0	0	0	1	2	0	0	0	0	0	0	0	0	4
22.50 – 28.13	0	0	1	0	0	0	1	0	1	0	0	0	0	0	0	0	3
28.13 – 33.75	0	0	0	0	0	1	2	1	0	0	0	0	0	0	0	0	4
33.75 – 39.38	0	1	0	0	0	0	0	1	0	0	0	0	0	0	0	0	2
39.38 – 45.00	0	0	0	0	0	0	0	0	0	0	0	0	0	0	0	0	0
45.00 – 50.63	0	0	0	0	0	0	0	0	0	0	0	0	0	0	0	0	0
50.63 – 56.25	0	0	0	0	0	0	0	0	0	0	0	0	0	0	0	0	0
56.25 – 61.88	0	0	0	0	0	0	0	0	0	0	0	0	0	0	0	0	0
61.88 – 67.50	0	0	0	0	0	0	0	0	0	0	0	0	0	0	0	0	0
67.50 – 73.13	0	0	0	0	0	0	0	0	0	0	0	0	0	0	0	0	0
73.13 – 78.75	0	0	0	0	0	0	0	0	0	0	0	0	0	0	0	0	0
78.75 – 84.38	0	0	0	0	0	0	0	0	0	0	0	0	0	0	0	0	0
84.38 – 90.00	0	0	0	0	0	0	0	0	0	0	0	0	0	0	0	0	0
All	1	3	3	1	0	2	6	10	2	0	0	0	0	0	0	0	28
V [km / hr]	17.85	14.93	14.78	10.35	0.00	19.12	19.43	14.97	17.14	0.00	0.00	0.00	0.00	0.00	0.00	0.00	

Storm Velocity [km / hr]	Storm Direction [degrees from N]																All
	348,75° 11,25° N (0°)	11,25° 33,75° NNE (22,5°)	33,75° 56,25° NE (45°)	56,25° 78,75° ENE (67,5°)	78,75° 101,25° E (90°)	101,25° 123,75° ESE (112,5°)	123,75° 146,25° SE (135°)	146,25° 168,75° SSE (157,5°)	168,75° 191,25° S (180°)	191,25° 213,75° SSW (202,5°)	213,75° 236,25° SW (225°)	236,25° 258,75° WSW (247,5°)	258,75° 281,25° W (270°)	281,25° 303,75° WNW (292,5°)	303,75° 326,25° NW (315°)	326,25° 348,75° NNW (337,5°)	
0 – 5.63	0.00	0.04	0.04	0.00	0.00	0.00	0.00	0.07	0.00	0.00	0.00	0.00	0.00	0.00	0.00	0.00	0.14
5.63 – 11.25	0.00	0.04	0.00	0.04	0.00	0.04	0.07	0.11	0.04	0.00	0.00	0.00	0.00	0.00	0.00	0.00	0.32
11.25 – 16.88	0.00	0.00	0.04	0.00	0.00	0.00	0.00	0.04	0.00	0.00	0.00	0.00	0.00	0.00	0.00	0.00	0.07
16.88 – 22.50	0.04	0.00	0.00	0.00	0.00	0.00	0.04	0.07	0.00	0.00	0.00	0.00	0.00	0.00	0.00	0.00	0.14
22.50 – 28.13	0.00	0.00	0.04	0.00	0.00	0.00	0.04	0.00	0.04	0.00	0.00	0.00	0.00	0.00	0.00	0.00	0.11
28.13 – 33.75	0.00	0.00	0.00	0.00	0.00	0.04	0.07	0.04	0.00	0.00	0.00	0.00	0.00	0.00	0.00	0.00	0.14
33.75 – 39.38	0.00	0.04	0.00	0.00	0.00	0.00	0.00	0.04	0.00	0.00	0.00	0.00	0.00	0.00	0.00	0.00	0.07
39.38 – 45.00	0.00	0.00	0.00	0.00	0.00	0.00	0.00	0.00	0.00	0.00	0.00	0.00	0.00	0.00	0.00	0.00	0.00
45.00 – 50.63	0.00	0.00	0.00	0.00	0.00	0.00	0.00	0.00	0.00	0.00	0.00	0.00	0.00	0.00	0.00	0.00	0.00
50.63 – 56.25	0.00	0.00	0.00	0.00	0.00	0.00	0.00	0.00	0.00	0.00	0.00	0.00	0.00	0.00	0.00	0.00	0.00
56.25 – 61.88	0.00	0.00	0.00	0.00	0.00	0.00	0.00	0.00	0.00	0.00	0.00	0.00	0.00	0.00	0.00	0.00	0.00
61.88 – 67.50	0.00	0.00	0.00	0.00	0.00	0.00	0.00	0.00	0.00	0.00	0.00	0.00	0.00	0.00	0.00	0.00	0.00
67.50 – 73.13	0.00	0.00	0.00	0.00	0.00	0.00	0.00	0.00	0.00	0.00	0.00	0.00	0.00	0.00	0.00	0.00	0.00
73.13 – 78.75	0.00	0.00	0.00	0.00	0.00	0.00	0.00	0.00	0.00	0.00	0.00	0.00	0.00	0.00	0.00	0.00	0.00
78.75 – 84.38	0.00	0.00	0.00	0.00	0.00	0.00	0.00	0.00	0.00	0.00	0.00	0.00	0.00	0.00	0.00	0.00	0.00
84.38 – 90.00	0.00	0.00	0.00	0.00	0.00	0.00	0.00	0.00	0.00	0.00	0.00	0.00	0.00	0.00	0.00	0.00	0.00
All	0.04	0.11	0.11	0.04	0.00	0.07	0.21	0.36	0.07	0.00	0.00	0.00	0.00	0.00	0.00	0.00	1.00
V [km / hr]	17.85	14.93	14.78	10.35	0.00	19.12	19.43	14.97	17.14	0.00	0.00	0.00	0.00	0.00	0.00	0.00	

ONSET

Storm Velocity [km / hr]	Storm Direction [degrees from N]																All
	348,75° 11,25° N (0°)	11,25° 33,75° NNE (22,5°)	33,75° 56,25° NE (45°)	56,25° 78,75° ENE (67,5°)	78,75° 101,25° E (90°)	101,25° 123,75° ESE (112,5°)	123,75° 146,25° SE (135°)	146,25° 168,75° SSE (157,5°)	168,75° 191,25° S (180°)	191,25° 213,75° SSW (202,5°)	213,75° 236,25° SW (225°)	236,25° 258,75° WSW (247,5°)	258,75° 281,25° W (270°)	281,25° 303,75° WNW (292,5°)	303,75° 326,25° NW (315°)	326,25° 348,75° NNW (337,5°)	
0 - 5.63	0	1	0	0	0	0	0	1	0	0	0	0	0	0	0	0	2
5.63 - 11.25	1	0	1	0	0	0	0	3	1	0	0	0	0	0	0	0	6
11.25 - 16.88	0	1	1	0	0	1	0	2	0	0	0	0	0	0	0	0	5
16.88 - 22.50	0	1	0	0	0	0	3	1	0	0	0	0	0	0	0	0	5
22.50 - 28.13	0	0	0	0	0	0	2	1	1	0	0	0	0	0	0	0	4
28.13 - 33.75	0	0	0	0	0	0	1	0	0	0	0	0	0	0	0	0	1
33.75 - 39.38	0	0	0	0	0	0	0	0	0	0	0	0	0	0	0	0	0
39.38 - 45.00	0	0	0	0	0	0	0	0	0	0	0	0	0	0	0	0	0
45.00 - 50.63	0	0	0	0	0	0	0	0	0	0	0	0	0	0	0	0	0
50.63 - 56.25	0	1	1	0	1	0	0	0	0	0	0	0	0	0	0	0	3
56.25 - 61.88	0	0	0	0	1	0	0	0	0	0	0	0	0	0	0	0	1
61.88 - 67.50	0	0	0	0	0	0	0	0	0	0	0	0	0	0	0	0	0
67.50 - 73.13	0	0	0	0	1	0	0	0	0	0	0	0	0	0	0	0	1
73.13 - 78.75	0	1	0	0	0	0	0	0	0	0	0	0	0	0	0	0	1
78.75 - 84.38	0	0	0	0	0	0	0	0	0	0	0	0	0	0	0	0	0
84.38 - 90.00	0	0	0	0	0	0	0	0	0	0	0	0	0	0	0	0	0
All	1	5	3	0	3	1	6	8	2	0	0	0	0	0	0	0	29
V [km / hr]	9.80	32.83	24.45	0.00	60.74	12.31	23.14	12.84	15.21	0.00	0.00	0.00	0.00	0.00	0.00	0.00	

Storm Velocity [km / hr]	Storm Direction [degrees from N]																All
	348,75° 11,25° N (0°)	11,25° 33,75° NNE (22,5°)	33,75° 56,25° NE (45°)	56,25° 78,75° ENE (67,5°)	78,75° 101,25° E (90°)	101,25° 123,75° ESE (112,5°)	123,75° 146,25° SE (135°)	146,25° 168,75° SSE (157,5°)	168,75° 191,25° S (180°)	191,25° 213,75° SSW (202,5°)	213,75° 236,25° SW (225°)	236,25° 258,75° WSW (247,5°)	258,75° 281,25° W (270°)	281,25° 303,75° WNW (292,5°)	303,75° 326,25° NW (315°)	326,25° 348,75° NNW (337,5°)	
0 - 5.63	0.00	0.03	0.00	0.00	0.00	0.00	0.00	0.03	0.00	0.00	0.00	0.00	0.00	0.00	0.00	0.00	0.07
5.63 - 11.25	0.03	0.00	0.03	0.00	0.00	0.00	0.00	0.10	0.03	0.00	0.00	0.00	0.00	0.00	0.00	0.00	0.21
11.25 - 16.88	0.00	0.03	0.03	0.00	0.00	0.03	0.00	0.07	0.00	0.00	0.00	0.00	0.00	0.00	0.00	0.00	0.17
16.88 - 22.50	0.00	0.03	0.00	0.00	0.00	0.00	0.10	0.03	0.00	0.00	0.00	0.00	0.00	0.00	0.00	0.00	0.17
22.50 - 28.13	0.00	0.00	0.00	0.00	0.00	0.00	0.07	0.03	0.03	0.00	0.00	0.00	0.00	0.00	0.00	0.00	0.14
28.13 - 33.75	0.00	0.00	0.00	0.00	0.00	0.00	0.03	0.00	0.00	0.00	0.00	0.00	0.00	0.00	0.00	0.00	0.03
33.75 - 39.38	0.00	0.00	0.00	0.00	0.00	0.00	0.00	0.00	0.00	0.00	0.00	0.00	0.00	0.00	0.00	0.00	0.00
39.38 - 45.00	0.00	0.00	0.00	0.00	0.00	0.00	0.00	0.00	0.00	0.00	0.00	0.00	0.00	0.00	0.00	0.00	0.00
45.00 - 50.63	0.00	0.00	0.00	0.00	0.00	0.00	0.00	0.00	0.00	0.00	0.00	0.00	0.00	0.00	0.00	0.00	0.00
50.63 - 56.25	0.00	0.03	0.03	0.00	0.03	0.00	0.00	0.00	0.00	0.00	0.00	0.00	0.00	0.00	0.00	0.00	0.10
56.25 - 61.88	0.00	0.00	0.00	0.00	0.03	0.00	0.00	0.00	0.00	0.00	0.00	0.00	0.00	0.00	0.00	0.00	0.03
61.88 - 67.50	0.00	0.00	0.00	0.00	0.00	0.00	0.00	0.00	0.00	0.00	0.00	0.00	0.00	0.00	0.00	0.00	0.00
67.50 - 73.13	0.00	0.00	0.00	0.00	0.03	0.00	0.00	0.00	0.00	0.00	0.00	0.00	0.00	0.00	0.00	0.00	0.03
73.13 - 78.75	0.00	0.03	0.00	0.00	0.00	0.00	0.00	0.00	0.00	0.00	0.00	0.00	0.00	0.00	0.00	0.00	0.03
78.75 - 84.38	0.00	0.00	0.00	0.00	0.00	0.00	0.00	0.00	0.00	0.00	0.00	0.00	0.00	0.00	0.00	0.00	0.00
84.38 - 90.00	0.00	0.00	0.00	0.00	0.00	0.00	0.00	0.00	0.00	0.00	0.00	0.00	0.00	0.00	0.00	0.00	0.00
All	0.03	0.17	0.10	0.00	0.10	0.03	0.21	0.28	0.07	0.00	0.00	0.00	0.00	0.00	0.00	0.00	1.00
V [km / hr]	9.80	32.83	24.45	0.00	60.74	12.31	23.14	12.84	15.21	0.00	0.00	0.00	0.00	0.00	0.00	0.00	

Table 5.6 Relative frequency of storm velocity and direction for the three features considered.

Especially the graph reported in fig. 5.5, similar to a windrose map, enables assessment of all the possible movements that a future storm can make, and a certain value of probability is associated with every movement.

Such results are very important because in this way it is possible to verify whether a future storm event, recorded by one of the borderline stations within the study area, will reach the center of the catchment or not and, in the former case, how much time it will take to move towards the catchment itself.

5.4.2 Relation between storm movement and wind movement

As already pointed out before, different results were obtained depending on the nature of the feature adopted. Therefore it was necessary to check the quality of the computed results by comparing these ones with other physical phenomena which are related to the storm movement, such as wind movement (Niemczynowicz, 1991). In this way it was possible to verify the feature giving the most reliable results.

Wind data were recorded by the same rain gauges previously described: in fact, the network monitors a multitude of weather variables including temperature, humidity, barometric pressure, solar radiation, ultra-violet radiation, rainfall, and wind speed/direction. Consequently the time resolution of the registration was the same as reported above, i.e. fifteen minutes.

For every storm event analyzed, the corresponding values of wind velocity and direction were computed by averaging all the wind measurements recorded during the event itself. These values are reported in Table 5.7: in particular it can be noticed that the average velocity was 6.73 km/hr (1.87 m/s) and the average direction was 172.30 degrees counted clockwise from the North.

Also in this case the outcomes, both velocities and directions, were well fitted by a normal distribution (fig. 5.6 a-b).

Finally, by considering the relative frequencies of storm velocity and direction in velocity and direction classes (fig. 5.7 and tab. 5.8), it emerged that there was a distinct maximum of relative frequency around storm velocities 5.63 – 11.25 km/hr and storm direction towards South and South-South-West.

Event no.	**V**	**θ**
1	4.13	187.05
2	12.30	187.68
3	11.62	185.09
4	3.90	191.58
5	10.01	199.73
6	10.00	197.83
7	4.92	169.47
8	8.01	143.22
9	3.42	197.09
10	5.97	170.08
11	6.78	195.84
12	5.97	166.49
13	12.96	197.54
14	4.56	223.24
15	4.34	130.68
16	11.28	182.93
17	5.06	191.62
18	5.52	123.93
19	8.15	112.16
20	3.13	114.41
21	6.86	194.17
22	5.17	191.73
23	5.63	198.00
24	6.30	185.47
25	8.06	195.99
26	6.08	210.87
27	9.68	197.25
28	9.25	179.40
29	7.46	178.90
30	5.68	166.01
31	5.30	132.62
32	6.97	169.36
33	3.60	114.42
34	5.58	190.66
35	9.12	188.55
36	7.19	131.71
37	3.04	115.12
38	5.41	181.38
39	4.25	130.44

	V	**θ**
Min.	3.04	112.16
Max.	12.96	223.24
Mean	6.73	172.30
S.D.	2.62	30.78
C.V.	0.39	0.18

Table 5.7 On the left the wind data calculated for every storm event are listed; on the right the range variation, the average value, the standard deviation and the coefficient of variation are reported.

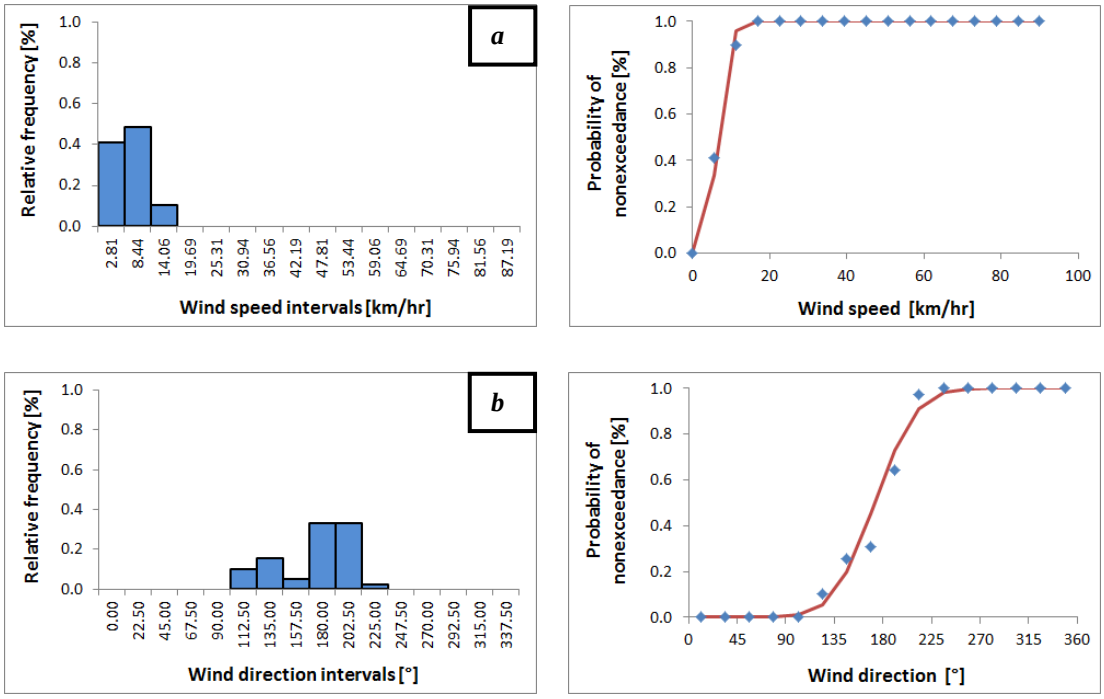

Figure 5.6 Relative frequency and probability of nonexceedence of wind velocity (a) and direction (b).

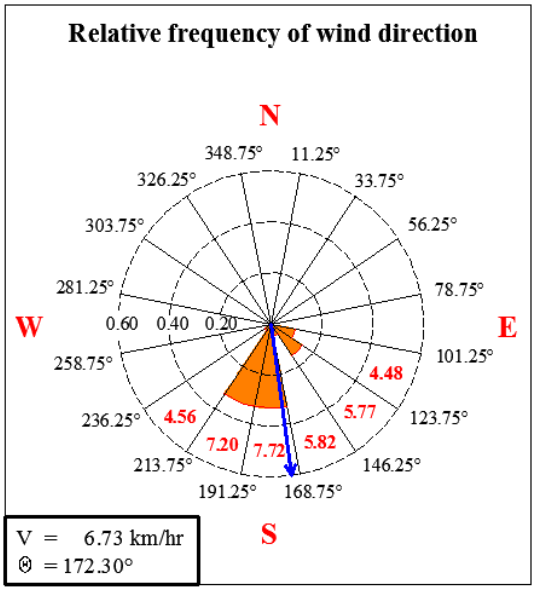

Figure 5.7 Relative frequency of storm direction for the wind data considered.

WIND

Storm Velocity [km / hr]	Storm Direction [degrees from N]																All
	348,75 - 11,25	11,25 - 33,75	33,75 - 56,25	56,25 - 78,75	78,75 - 101,25	101,25 - 123,75	123,75 - 146,25	146,25 - 168,75	168,75 - 191,25	191,25 - 213,75	213,75 - 236,25	236,25 - 258,75	258,75 - 281,25	281,25 - 303,75	303,75 - 326,25	326,25 - 348,75	
	N (0°)	NNE (22,5°)	NE (45°)	ENE (67,5°)	E (90°)	ESE (112,5°)	SE (135°)	SSE (157,5°)	S (180°)	SSW (202,5°)	SW (225°)	WSW (247,5°)	W (270°)	WNW (292,5°)	NW (315°)	NNW (337,5°)	
0 - 5.63	0	0	0	0	0	3	4	0	4	4	1	0	0	0	0	0	16
5.63 - 11.25	0	0	0	0	0	1	2	2	6	8	0	0	0	0	0	0	19
11.25 - 16.88	0	0	0	0	0	0	0	0	3	1	0	0	0	0	0	0	4
16.88 - 22.50	0	0	0	0	0	0	0	0	0	0	0	0	0	0	0	0	0
22.50 - 28.13	0	0	0	0	0	0	0	0	0	0	0	0	0	0	0	0	0
28.13 - 33.75	0	0	0	0	0	0	0	0	0	0	0	0	0	0	0	0	0
33.75 - 39.38	0	0	0	0	0	0	0	0	0	0	0	0	0	0	0	0	0
39.38 - 45.00	0	0	0	0	0	0	0	0	0	0	0	0	0	0	0	0	0
45.00 - 50.63	0	0	0	0	0	0	0	0	0	0	0	0	0	0	0	0	0
50.63 - 56.25	0	0	0	0	0	0	0	0	0	0	0	0	0	0	0	0	0
56.25 - 61.88	0	0	0	0	0	0	0	0	0	0	0	0	0	0	0	0	0
61.88 - 67.50	0	0	0	0	0	0	0	0	0	0	0	0	0	0	0	0	0
67.50 - 73.13	0	0	0	0	0	0	0	0	0	0	0	0	0	0	0	0	0
73.13 - 78.75	0	0	0	0	0	0	0	0	0	0	0	0	0	0	0	0	0
78.75 - 84.38	0	0	0	0	0	0	0	0	0	0	0	0	0	0	0	0	0
84.38 - 90.00	0	0	0	0	0	0	0	0	0	0	0	0	0	0	0	0	0
All	0	0	0	0	0	4	6	2	13	13	1	0	0	0	0	0	39
V [km / hr]	0.00	0.00	0.00	0.00	0.00	4.48	5.77	5.82	7.72	7.20	4.56	0.00	0.00	0.00	0.00	0.00	

Storm Velocity [km / hr]	Storm Direction [degrees from N]																All
	348,75 - 11,25	11,25 - 33,75	33,75 - 56,25	56,25 - 78,75	78,75 - 101,25	101,25 - 123,75	123,75 - 146,25	146,25 - 168,75	168,75 - 191,25	191,25 - 213,75	213,75 - 236,25	236,25 - 258,75	258,75 - 281,25	281,25 - 303,75	303,75 - 326,25	326,25 - 348,75	
	N (0°)	NNE (22,5°)	NE (45°)	ENE (67,5°)	E (90°)	ESE (112,5°)	SE (135°)	SSE (157,5°)	S (180°)	SSW (202,5°)	SW (225°)	WSW (247,5°)	W (270°)	WNW (292,5°)	NW (315°)	NNW (337,5°)	
0 - 5.63	0.00	0.00	0.00	0.00	0.00	0.08	0.10	0.00	0.10	0.10	0.03	0.00	0.00	0.00	0.00	0.00	0.41
5.63 - 11.25	0.00	0.00	0.00	0.00	0.00	0.03	0.05	0.05	0.15	0.21	0.00	0.00	0.00	0.00	0.00	0.00	0.49
11.25 - 16.88	0.00	0.00	0.00	0.00	0.00	0.00	0.00	0.00	0.08	0.03	0.00	0.00	0.00	0.00	0.00	0.00	0.10
16.88 - 22.50	0.00	0.00	0.00	0.00	0.00	0.00	0.00	0.00	0.00	0.00	0.00	0.00	0.00	0.00	0.00	0.00	0.00
22.50 - 28.13	0.00	0.00	0.00	0.00	0.00	0.00	0.00	0.00	0.00	0.00	0.00	0.00	0.00	0.00	0.00	0.00	0.00
28.13 - 33.75	0.00	0.00	0.00	0.00	0.00	0.00	0.00	0.00	0.00	0.00	0.00	0.00	0.00	0.00	0.00	0.00	0.00
33.75 - 39.38	0.00	0.00	0.00	0.00	0.00	0.00	0.00	0.00	0.00	0.00	0.00	0.00	0.00	0.00	0.00	0.00	0.00
39.38 - 45.00	0.00	0.00	0.00	0.00	0.00	0.00	0.00	0.00	0.00	0.00	0.00	0.00	0.00	0.00	0.00	0.00	0.00
45.00 - 50.63	0.00	0.00	0.00	0.00	0.00	0.00	0.00	0.00	0.00	0.00	0.00	0.00	0.00	0.00	0.00	0.00	0.00
50.63 - 56.25	0.00	0.00	0.00	0.00	0.00	0.00	0.00	0.00	0.00	0.00	0.00	0.00	0.00	0.00	0.00	0.00	0.00
56.25 - 61.88	0.00	0.00	0.00	0.00	0.00	0.00	0.00	0.00	0.00	0.00	0.00	0.00	0.00	0.00	0.00	0.00	0.00
61.88 - 67.50	0.00	0.00	0.00	0.00	0.00	0.00	0.00	0.00	0.00	0.00	0.00	0.00	0.00	0.00	0.00	0.00	0.00
67.50 - 73.13	0.00	0.00	0.00	0.00	0.00	0.00	0.00	0.00	0.00	0.00	0.00	0.00	0.00	0.00	0.00	0.00	0.00
73.13 - 78.75	0.00	0.00	0.00	0.00	0.00	0.00	0.00	0.00	0.00	0.00	0.00	0.00	0.00	0.00	0.00	0.00	0.00
78.75 - 84.38	0.00	0.00	0.00	0.00	0.00	0.00	0.00	0.00	0.00	0.00	0.00	0.00	0.00	0.00	0.00	0.00	0.00
84.38 - 90.00	0.00	0.00	0.00	0.00	0.00	0.00	0.00	0.00	0.00	0.00	0.00	0.00	0.00	0.00	0.00	0.00	0.00
All	0.00	0.00	0.00	0.00	0.00	0.10	0.15	0.05	0.33	0.33	0.03	0.00	0.00	0.00	0.00	0.00	1.00
V [km / hr]	0.00	0.00	0.00	0.00	0.00	4.48	5.77	5.82	7.72	7.20	4.56	0.00	0.00	0.00	0.00	0.00	

Table 5.8 Relative frequency of wind velocity and direction.

By comparing, for every event, the values of wind velocity with the corresponding storm values it was observed that storm velocities exceeded wind velocities in almost all the cases. Such result was in contrast to the findings by Niemczynowicz and Dahlblom (1984), however, it can be explained because the wind data are recorded on the ground level, therefore inferior values of this parameter should be expected because of the presence of obstacles, such as buildings.

This reason justifies also the observed weak correlations between these parameters for all the three data sets (fig. 5.8).

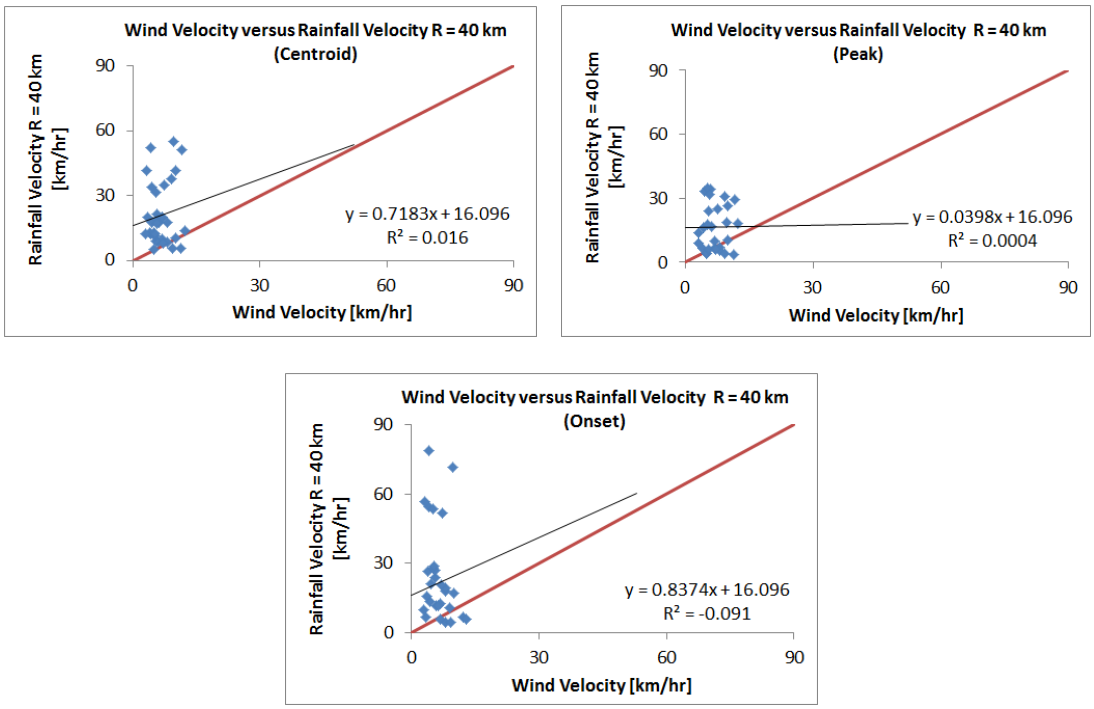

Figure 5.8 Comparison between wind and storm velocities.

The reported pictures confirm this conclusion: the points are scattered and there are virtually no relations between the variables, although a linear regression model was supposed. Similar relations were observed by other several researchers (Shearman, 1977; Marshall, 1980; Niemczynowicz and Dahlblom, 1984). Specifically, Niemczynowicz and Dahlblom (1984) reported that *there is a good correlation between storm and high-altitude wind movement parameters (registered at 800 mb, 700 mb and 600 mb height, approximately corresponding to altitudes 1,200m, 2,200 m and 4,500 m above sea level), whereas no relation exists between storm and wind velocity at ground level.*

Also the correlation coefficients between wind and storm directions were not significant, although a better agreement was observed between the two data sets (fig. 5.9).

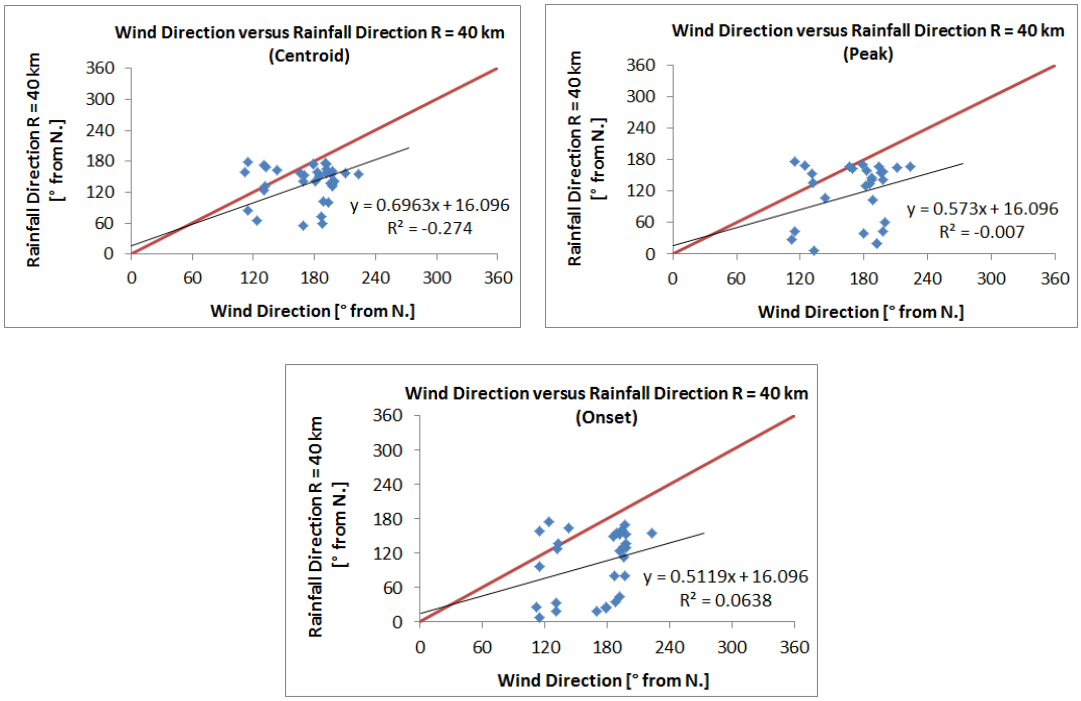

Figure 5.9 Comparison between wind and storm directions.

In this case, nevertheless, the values of wind direction resulted underestimated with respect to the corresponding storm values in almost all the cases.

In particular, both the data sets showed no rainfall moving to the West (fig. 5.7 and 5.5).

Figure 5.10 Storm movement observed for the case study.

This result is surely related to the orographic structure of the country and it is very important because it enables affirmation that, usually, storms cross the city in their movement towards the sea, i.e. it should not be expected a movement directed in the opposite direction (fig. 5.10).

Later, in order to estimate what was the best feature to consider in storm tracking methods, the root mean square deviation were calculated between the data sets of wind velocities and storm velocities predicted assuming each time one of the features. The same procedure was applied for the direction data:

$$\sigma_V = \sqrt{\frac{\sum_{i=1}^{N_f} \left(V_W - V_f\right)^2}{N_f - 1}} \tag{5.15}$$

$$\sigma_\Theta = \sqrt{\frac{\sum_{i=1}^{N_f} \left(\Theta_W - \Theta_f\right)^2}{N_f - 1}} \tag{5.16}$$

where

- V_W is the wind velocity measured for the generic rain event considered;
- V_f is the storm velocity computed for the same rain event, by considering each time one of the features selected;
- Θ_W is the wind direction measured for the generic rain event considered;
- Θ_f is the storm direction computed for the same rain event, by considering each time one of the features selected;
- N_f is the number of rain events analyzed with the storm tracking method, considering each time one of the features selected..

The values computed are reported in Table 5.9 together with the correlation coefficients.

Feature	σ_V [km/hr]	Correlation$_V$	σ_Θ [°]	Correlation$_\Theta$	N_f
Centroid	20.26	0.13	56.50	0.08	34
Peak	14.54	0.03	83.52	0.15	28
Onset	28.41	-0.27	89.10	0.26	29

Table 5.9 Root mean square deviation and correlation coefficients computed for the three features.

As already stated, a scarce agreement was found between storm and wind movement parameters because of:

- the use of wind data recorded at ground level;
- the temporal ad spatial resolution of the registration that was quite distant from the maximal rainfall collection requirements suggested for urban hydrological applications ("1-1-0.1" rule).

In particular, it emerged that the onset feature was the worst one since it presented the biggest root mean square deviation for both velocity and direction. This outcome was expected because the poor time resolution of the registration would have surely conditioned more the elaborations carried out by considering this feature. In fact, it is evident how a time resolution of fifteen minutes could favour the erroneous individuation of an equal start time of the storms from most of the stations.

Instead, the centroid provided the best approximation of the wind direction, whereas the peak gave the best estimate of the wind velocity. Specifically, in both cases, wind velocities were overestimated: the average wind velocity was 6.73 km/hr whereas the average storm velocity was 20.87 km/hr for the centroid-based elaborations and 16.29 km/hr for the peak-based elaborations. Nevertheless, this error is favourable because it means that the storm will be expected to reach the catchment in less time with respect to reality, therefore, all the safety measures provided will have to be realized in advance.

Consequently, in the end, the centroid was chosen as reference feature because the bigger mistake in the overestimation of the velocity, however advantageous for the safety measures, was compensated by the better evaluation of the direction of movement of the wind (the average wind direction was 172.30 degrees counted clockwise from the North, whereas the average storm direction was 139.35 degrees for the centroid-based elaborations and 116.33 degrees for the peak-based elaborations). Similar conclusions were also reported by other researchers: in fact, May and Julien (1998) noted that the use of the centroid of the hyetograph gives more reliable results than using time of the onset of the storm.

Therefore, the calculations developed for the centroid will have to be considered for assessing all the possible future movements of the storms. For example, a future storm event, recorded by one of the borderline stations within the study area, such as

Enfiled or Mill Hill, should reach the center of the catchment with a related probability of 80%. This consideration can be derived through the information contained inside the windrose map plotted in fig. 5.5:

- 24 % of the storms is expected to move towards South-East with an average velocity of 24.44 km/hr;
- 35 % of the storms is expected to move towards South-South-East with an average velocity of 21.32 km/hr;
- 21 % of the storms is expected to move towards South with an average velocity of 15.88 km/hr.

Thus, since the distance between the borderline stations and the center of the catchment is more or less 20 km and the average storm velocity is 20.54 km/hr, the storm should reach the center of the catchment in two hours. Later this arrival time should be considered as the starting time of the simulation to carry out with the hydraulic model developed and calibrated for the catchment itself. In this way, finally, the potential flooded areas could be assessed in advance and, therefore, all the security measures provided could be implemented in time.

5.4.3 Influence of the rain gauges location on the storm tracking results

Finally, the research was aimed to evaluate the extent to which the location of the rain gauges inside the catchment could condition the results of the methodology. These further elaborations are important because some municipalities do not have the funds for equipping themselves with an adequate number of rain gauges, therefore it is important to know how the results could change if a reduced number of recording stations is employed.

Consequently, four different measuring networks were considered in order to compare their results:

1. all the rain gauges, lying inside a circle centered in Westminster and with a 40 km radius, were considered, i.e. all the recording stations were assumed (defined later as *case R = 40 km*);
2. all the rain gauges, lying inside a circle centered in Westminster and with a 30 km radius, were considered (defined later as *case R = 30 km*);

3. all the rain gauges, lying inside a circle centered in Westminster and with a 20 km radius, were considered (defined later as *case R = 20 km*);
4. all the rain gauges, lying inside a circle centered in Westminster and with a 10 km radius, were considered (defined later as *case R = 10 km*).

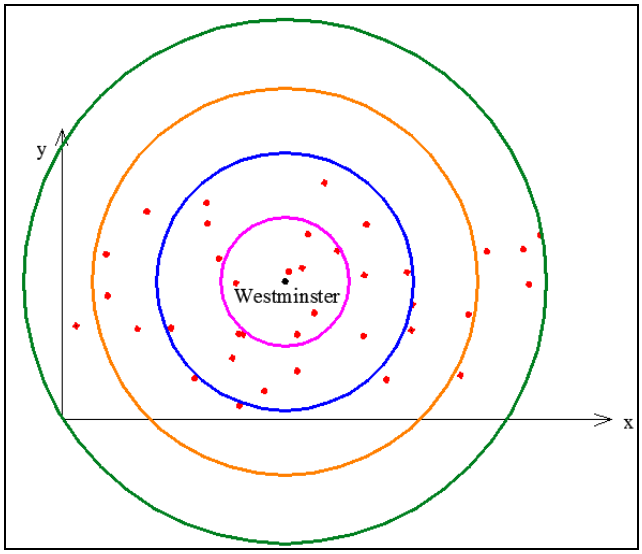

Figure 5.11 Various group of rain gauges considered for the elaborations.

All the elaborations already carried out for the *case R = 40 km*, i.e. estimation of the speed and direction of storms and consequent statistical analysis of the results, required to be repeated for the other three groups of rain gauges. The principal results obtained are reported in the following tables and figures: tab. 5.10 and fig. 5.12 for the *case R = 30 km*, tab. 5.11 and fig. 5.13 for the *case R = 20 km*, tab. 5.12 and fig. 5.14 for the *case R = 10 km*. In particular, also in this case, all the data sets were well fitted by a normal distribution.

Then, in order to verify whether the consideration of a decreasing number of rain gauges could determine errors in the evaluation of the storm parameters, the root mean square deviation and the correlation coefficients were calculated between the data sets of wind velocities and storm velocities for all the three cases (fig. 5.15, fig. 5.17 and fig. 5.19). The same procedure was applied for the direction data (fig. 5.16, fig. 5.18 and fig. 5.20).

	Centroid			Peak			Onset		
	V	**θ**	S. R.	**V**	**θ**	S. R.	**V**	**θ**	S. R.
Min.	5.36	13.00	0.00	4.10	18.35	0.00	4.04	4.36	0.00
Max.	51.04	174.12	0.80	34.86	173.84	0.82	86.70	174.85	0.85
Mean	20.87	125.51	0.48	15.58	111.43	0.59	23.45	105.02	0.58
S.D.	13.86	44.27	0.21	9.97	52.34	0.19	21.54	56.55	0.19
C.V.	0.66	0.35	0.44	0.64	0.47	0.33	0.92	0.54	0.33

Table 5.10 Range variation, average value, standard deviation and coefficient of variation for the *case R = 30 km*.

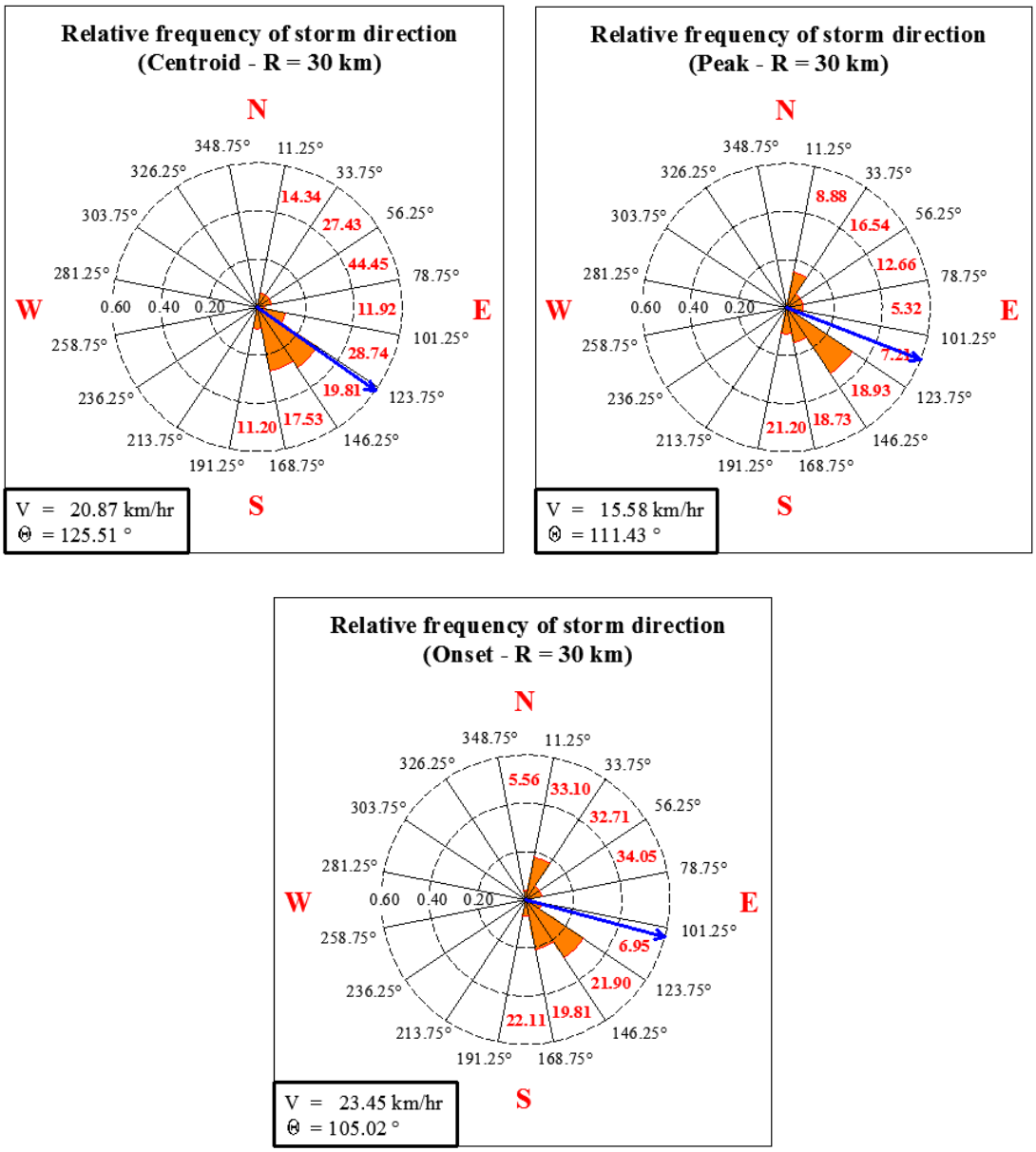

Figure 5.12 Relative frequency of storm direction for the case *R = 30 km*.

	Centroid			Peak			Onset		
	V	**θ**	S. R.	**V**	**θ**	S. R.	**V**	**θ**	S. R.
Min.	2.54	11.86	0.00	0.70	7.03	0.00	1.09	13.33	0.00
Max.	65.39	172.81	0.82	37.31	167.47	0.84	65.71	165.16	0.82
Mean	17.81	107.54	0.37	12.19	87.79	0.46	17.90	87.30	0.53
S.D.	14.62	46.98	0.25	10.43	50.86	0.27	14.62	47.84	0.24
C.V.	0.82	0.44	0.67	0.86	0.58	0.59	0.82	0.55	0.44

Table 5.11 Range variation, average value, standard deviation and coefficient of variation for the *case R = 20 km*.

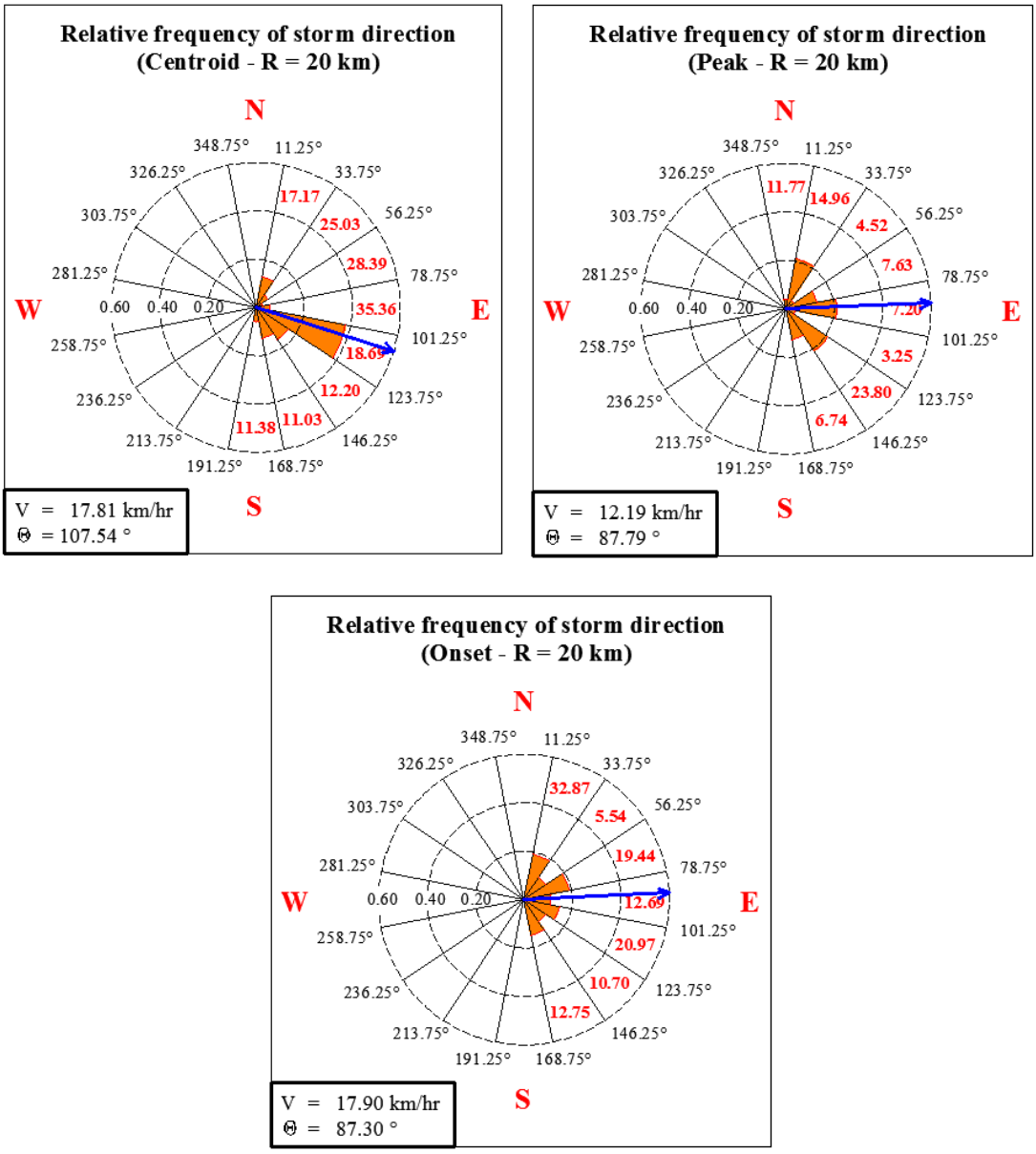

Figure 5.13 Relative frequency of storm direction for the case *R = 20 km*.

	Centroid			Peak			Onset		
	V	**θ**	S. R.	**V**	**θ**	S. R.	**V**	**θ**	S. R.
Min.	1.80	61.97	0.00	1.28	25.06	0.00	1.53	41.17	0.00
Max.	60.69	164.36	0.84	19.63	152.06	0.77	15.80	159.18	0.65
Mean	12.52	105.83	0.13	6.58	94.15	0.11	7.08	99.62	0.18
S.D.	13.57	29.20	0.25	5.43	32.82	0.24	3.73	36.23	0.27
C.V.	1.08	0.28	1.85	0.83	0.35	2.12	0.53	0.36	1.52

Table 5.12 Range variation, average value, standard deviation and coefficient of variation for the *case R = 10 km*.

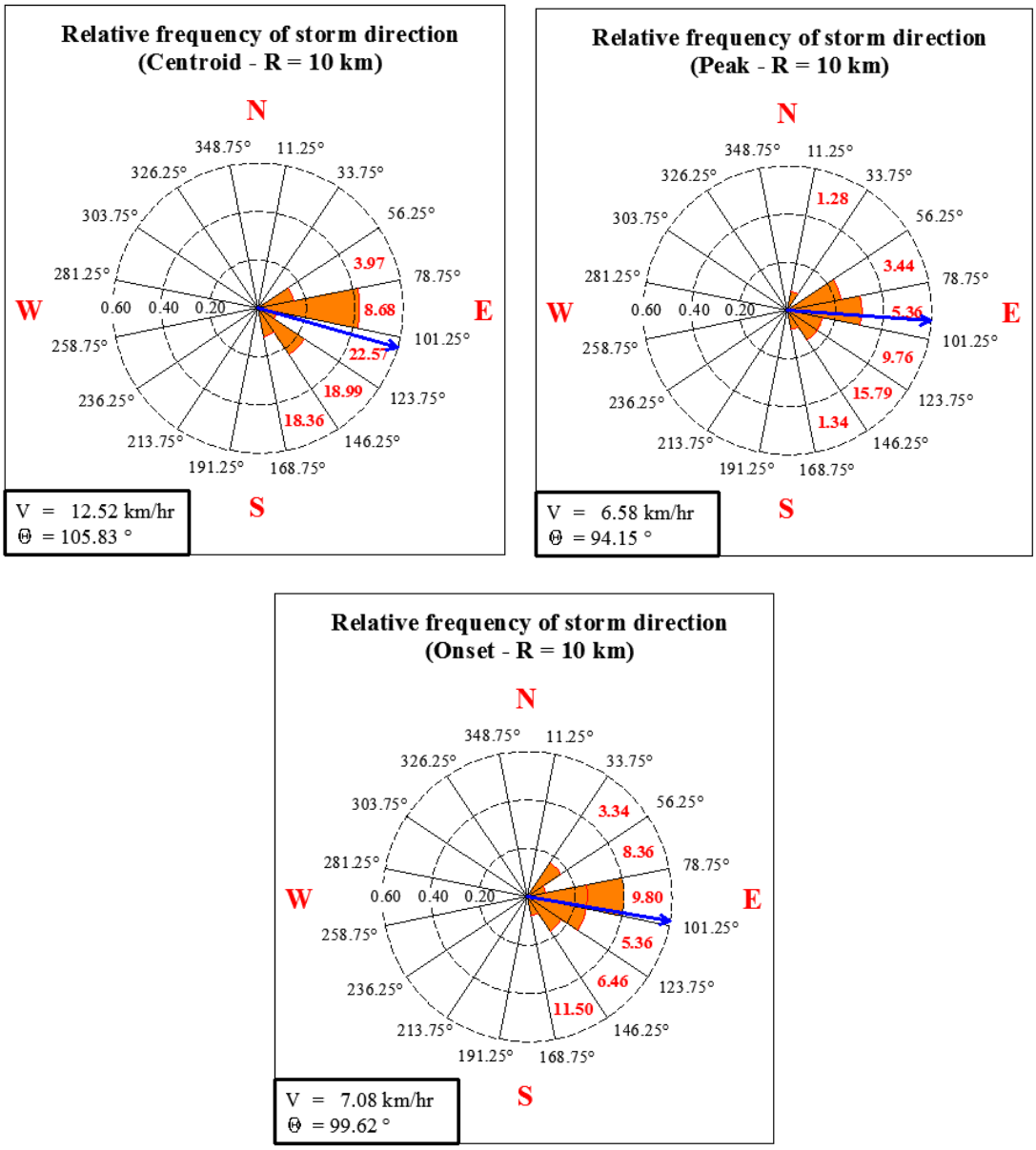

Figure 5.14 Relative frequency of storm direction for the case *R = 10 km*.

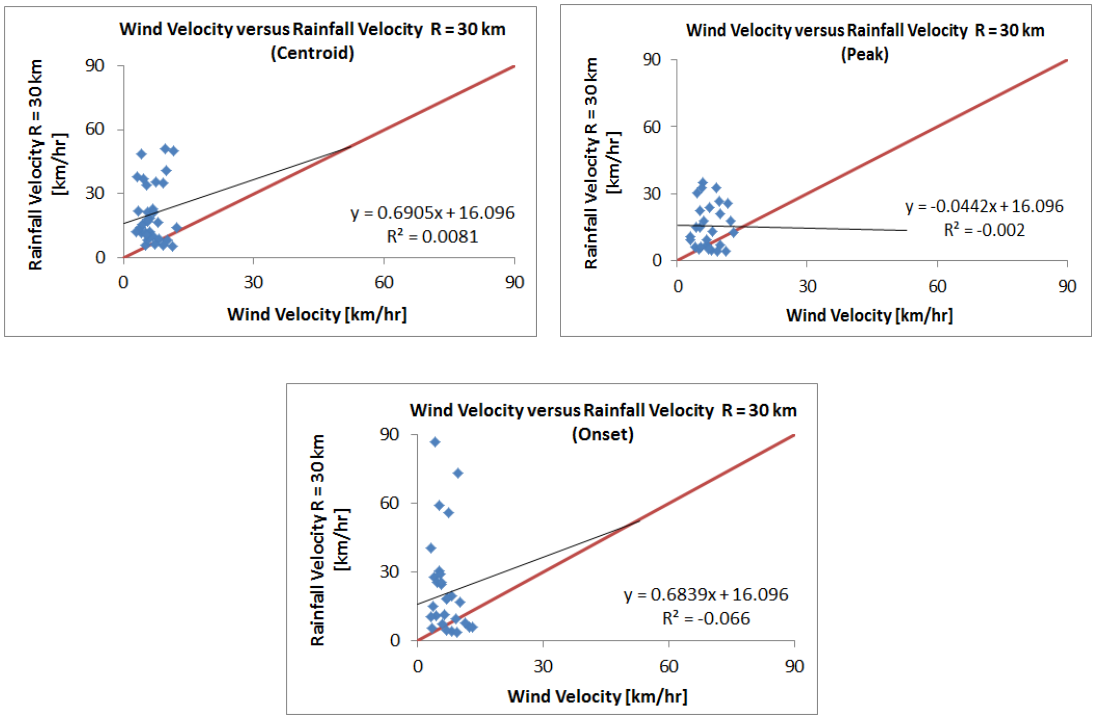

Figure 5.15 Comparison between wind and storm velocities for the *case R = 30 km*.

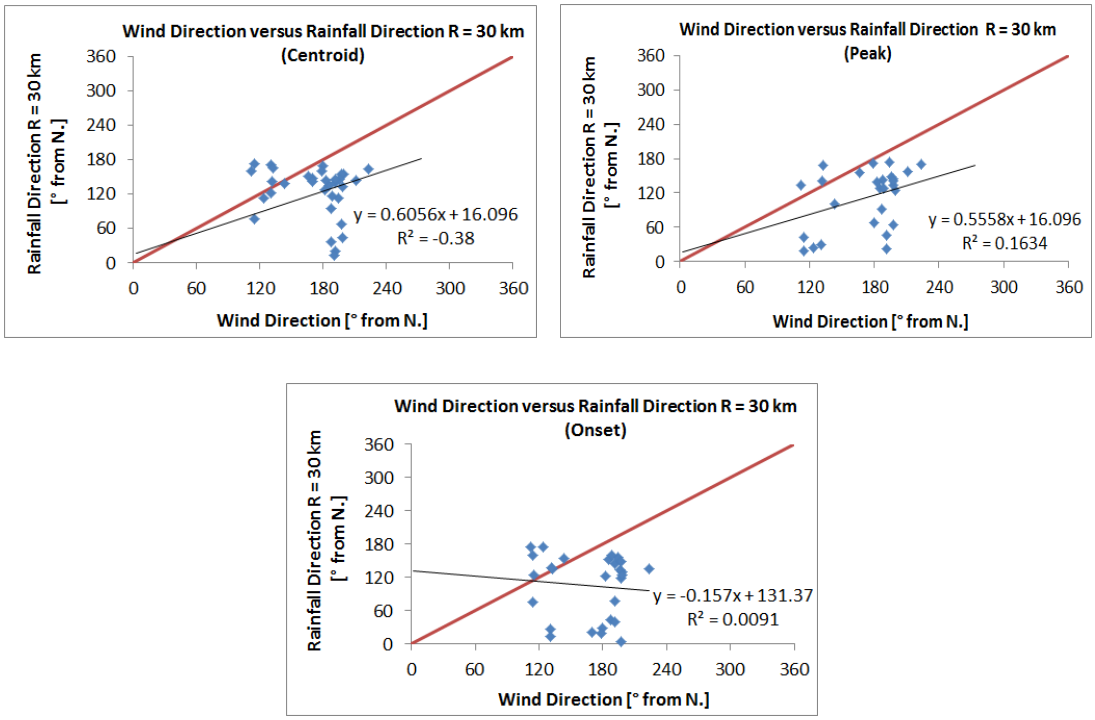

Figure 5.16 Comparison between wind and storm directions for the *case R = 30 km*.

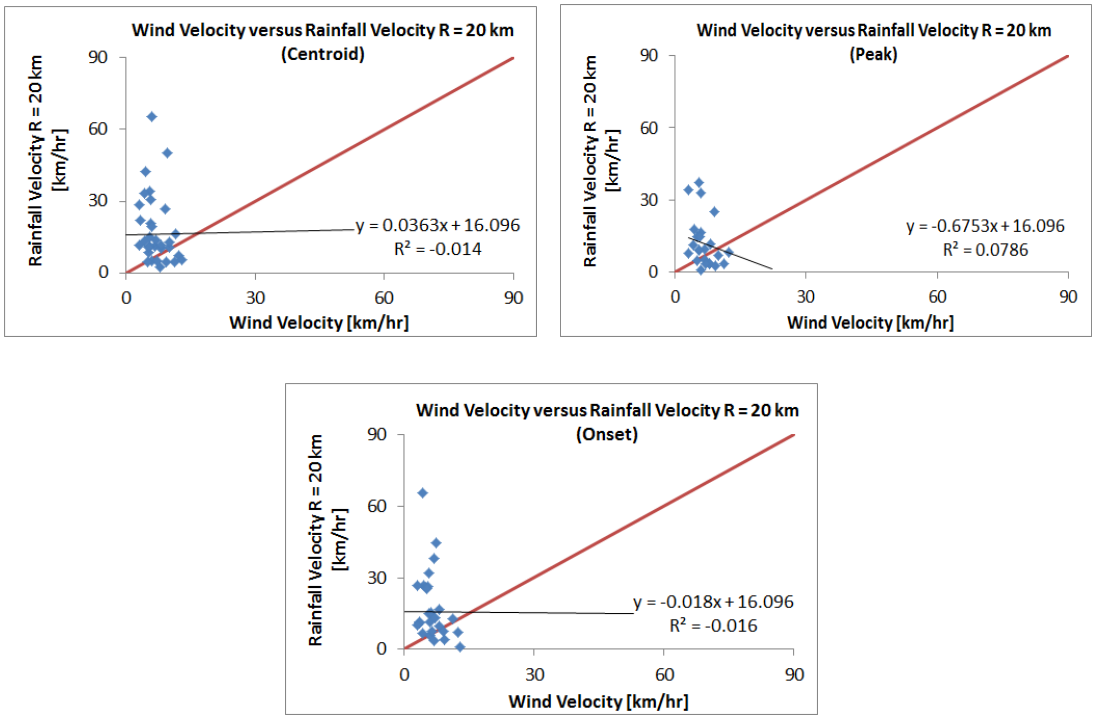

Figure 5.17 Comparison between wind and storm velocities for the *case R = 20 km*.

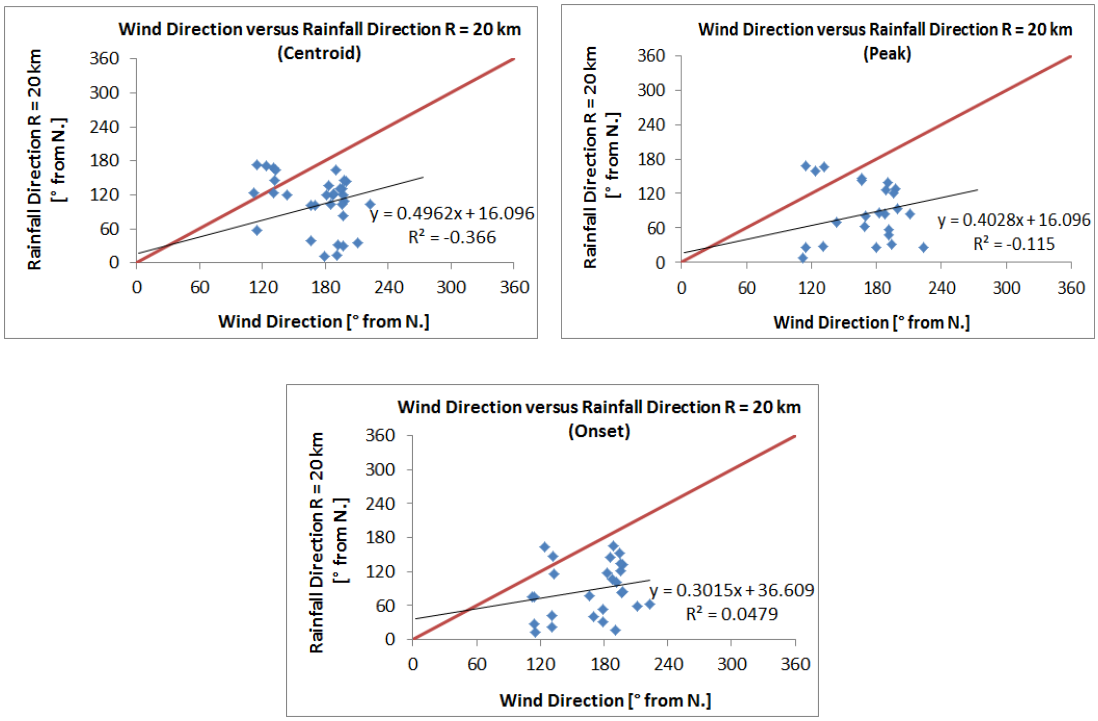

Figure 5.18 Comparison between wind and storm directions for the *case R = 20 km*.

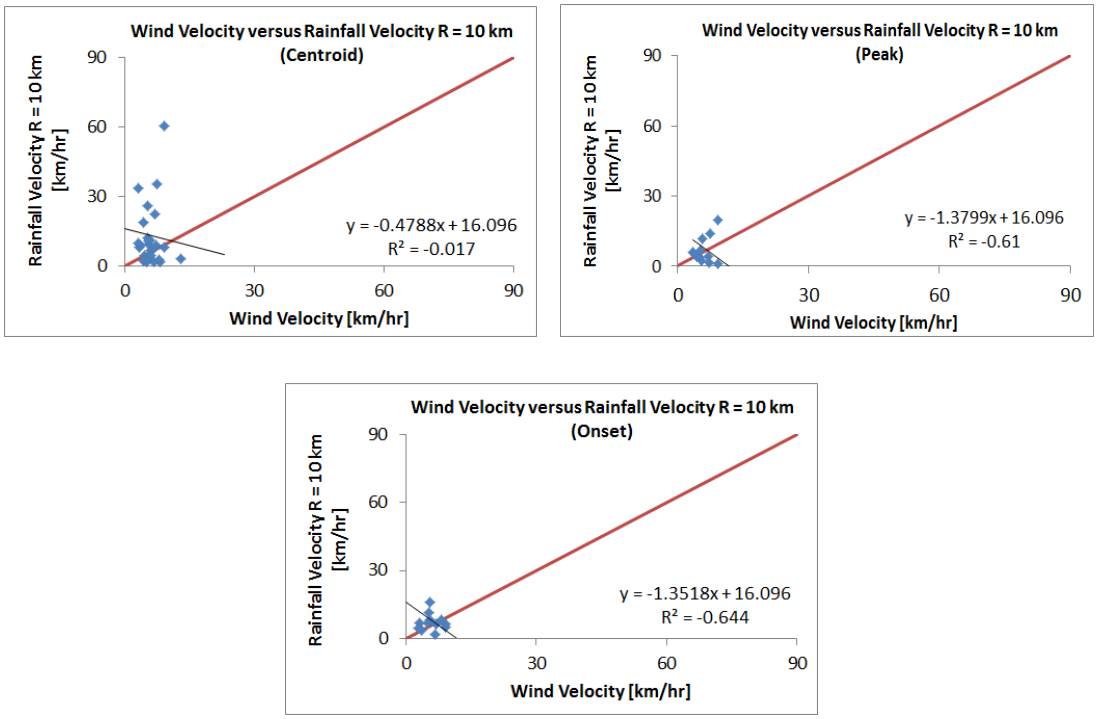

Figure 5.19 Comparison between wind and storm velocities for the *case R = 10 km*.

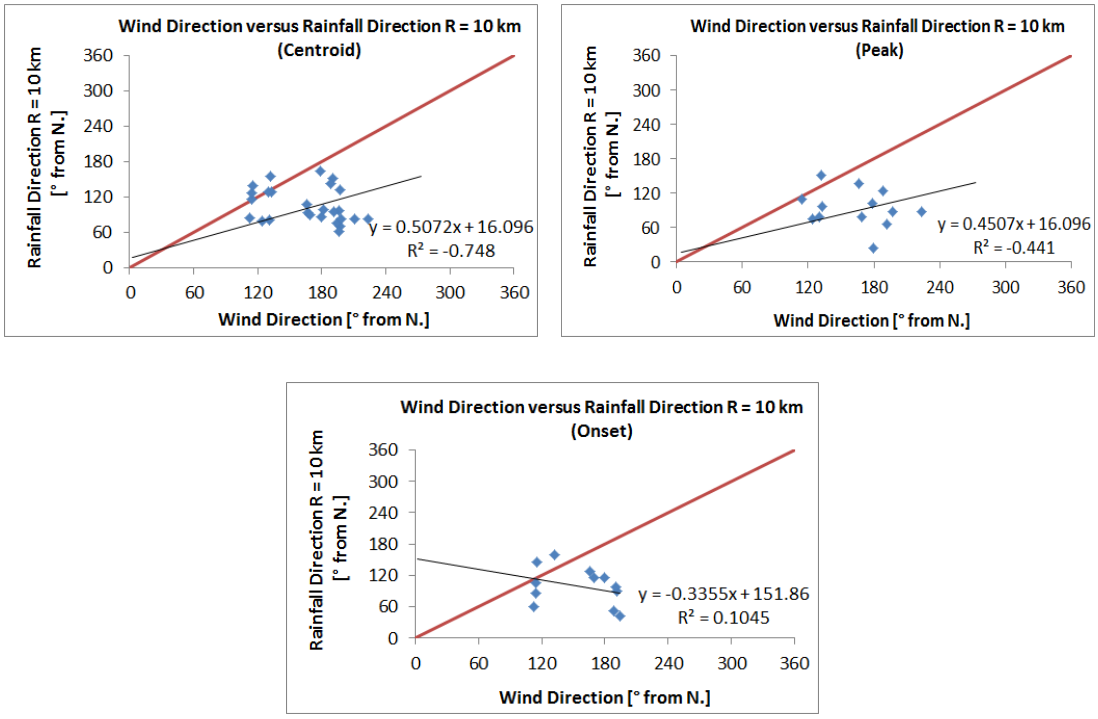

Figure 5.20 Comparison between wind and storm directions for the *case R = 10 km*.

Also these calculations were characterized by a poor correlation between wind and storm movement parameters (tab. 5.13, tab. 5.14 and tab. 5.15).

R [km]	σ_V [km/hr]	Correlation$_V$	σ_Θ [°]	Correlation$_\Theta$	N_f
40	20.26	0.13	56.5	0.08	34
30	19.98	0.1	76.17	-0.22	33
20	19.01	-0.26	93.02	-0.35	32
10	15.1	0.06	80.58	-0.28	26

Table 5.13 Root mean square deviation and correlation coefficients computed for the four types of rain gauges network (centroid feature considered).

R [km]	σ_V [km/hr]	Correlation$_V$	σ_Θ [°]	Correlation$_\Theta$	N_f
40	14.54	0.03	83.52	0.15	28
30	13.25	0.04	79.36	0.41	27
20	12.73	-0.35	104.82	-0.08	24
10	5.18	0.32	89.14	-0.22	13

Table 5.14 Root mean square deviation and correlation coefficients computed for the four types of rain gauges network (peak feature considered).

R [km]	σ_V [km/hr]	Correlation$_V$	σ_Θ [°]	Correlation$_\Theta$	N_f
40	28.41	-0.27	89.1	0.26	29
30	28.11	-0.23	93.94	-0.1	28
20	19.51	-0.34	97.75	0.22	27
10	4.5	-0.02	82.35	-0.32	12

Table 5.15 Root mean square deviation and correlation coefficients computed for the four types of rain gauges network (onset feature considered).

Specifically, it could be noted that the consideration of an ever decreasing number of recording stations determined different effects on σ_V and σ_Θ. In fact:

- the velocity error tended clearly to be reduced (fig. 5.21 a);
- the direction error showed a slightly increasing trend until R = 20 km, and a final reduction for R = 10 km (fig. 5.21 b). This last result is misleading and it should be due to the limited number of events analysed for the *case R = 10 km*. For this reason it was not considered in the following considerations.

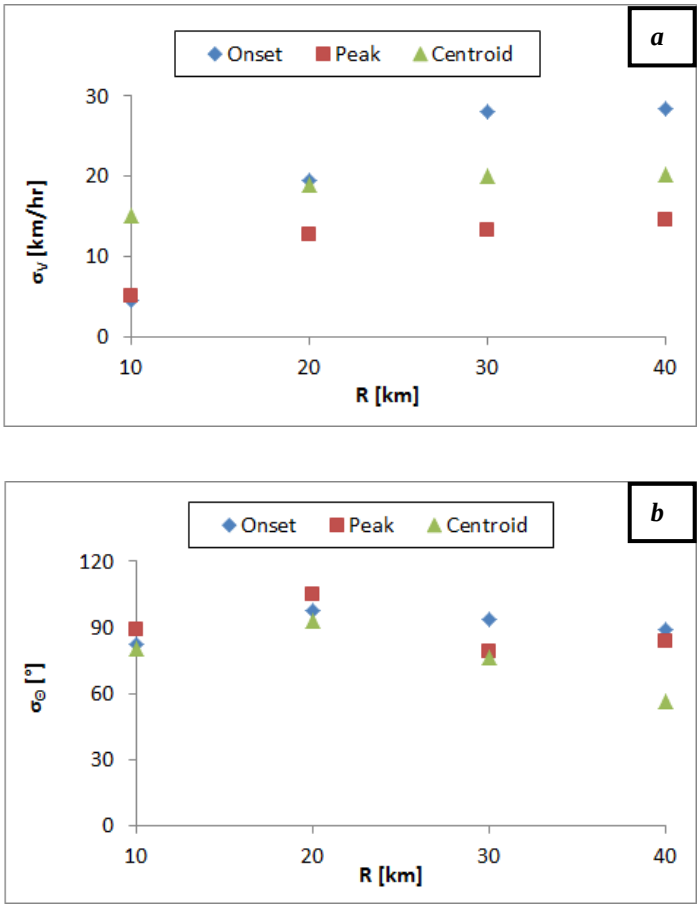

Figure 5.21 Wind data comparison: σ_V versus R for the three features considered (a); σ_Θ versus R for the three features considered (b).

Therefore, it could be noticed that the reduction of the recording stations would enable a better estimation of the velocity but a worse evaluation of the direction, i.e. the storm velocities would be less overestimated and the directions would be more underestimated. Just the further underestimation of storm direction demonstrated how a similar network configuration would not be adequate: in fact, important repercussions could happen by wrongly ignoring rainfalls that instead will effectively reach the catchment.

Thus, in conclusion, it emerged that the results obtained by considering all the stations would be changed if a limited instrumental equipment was bought by the municipalities for economic reasons. The magnitude of the error should be taken into account by the municipalities themselves before making similar decisions. This latter analysis was carried out for the case study: the results are reported in terms of σ_V

and σ_Θ, calculated between the data sets relative to the case *R = 40 km* and each of the other three cases considered in the research (tab. 5.16, tab. 5.17, tab. 5.18 and fig. 5.22).

R [km]	σ_V [km/hr]	Correlation$_V$	σ_Θ [°]	Correlation$_\Theta$	N
30	1.87	0.99	47.89	0.36	33
20	10.9	0.75	72.35	-0.18	29
10	13.46	0.65	55.23	0.14	22

Table 5.16 Root mean square deviation and correlation coefficients computed for the three types of rain gauges network (centroid feature considered).

R [km]	σ_V [km/hr]	Correlation$_V$	σ_Θ [°]	Correlation$_\Theta$	N
30	3.82	0.94	66.21	0.31	26
20	8.57	0.73	65.11	0.5	19
10	13.14	0.71	67.33	0.34	9

Table 5.17 Root mean square deviation and correlation coefficients computed for the four three of rain gauges network (peak feature considered).

R [km]	σ_V [km/hr]	Correlation$_V$	σ_Θ [°]	Correlation$_\Theta$	N
30	4.28	0.98	53.01	0.59	27
20	10.19	0.85	48.59	0.35	23
10	21.05	0.45	86.79	-0.3	9

Table 5.18 Root mean square deviation and correlation coefficients computed for the three types of rain gauges network (onset feature considered).

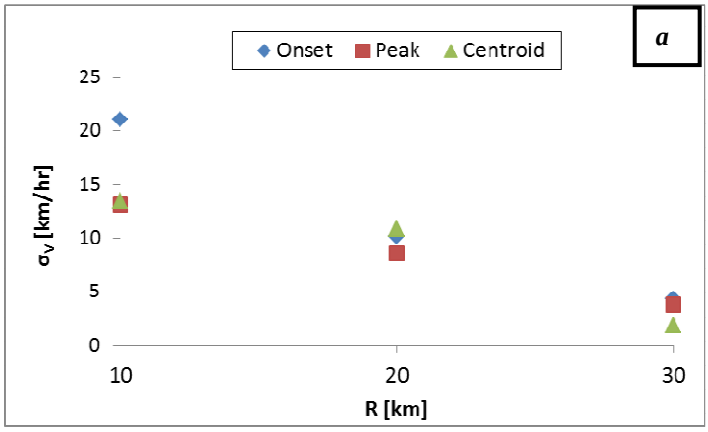

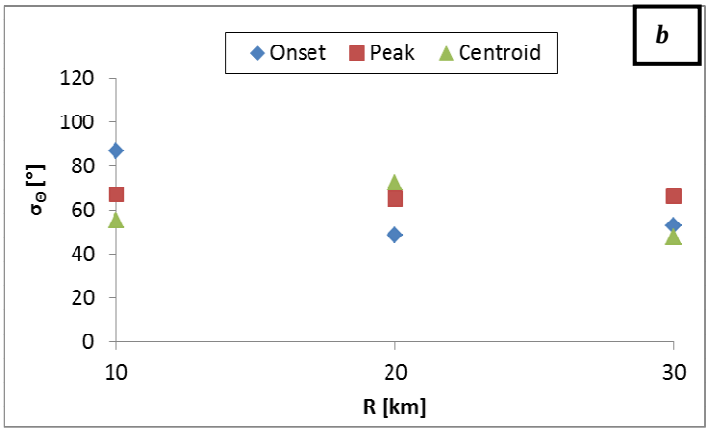

Figure 5.22 Rainfall data comparison: σ_V versus R for the three features considered (a); σ_Θ versus R for the three features considered (b).

References

- Chaudhry F.H., Andrade Filho A.G. and Cavalheiros R.V. (1994). In: ed. J. Niemczynowicz, *Statistics on Tropical Convective Storms Observed by Radar*. Proceedings of International Workshop 'Closing the Gap between Theory and Practice in Urban Rainfall Applications', St. Moritz, Switzerland, 30 Nov.-4 Dec.1994. UNESCO, WMO, IRWA, IAWQ, pp. 96-106.
- Desa M.N.M. and Niemczynowicz J. (1997). *Dynamics of short rainfall storms in a small scale urban area in Coly Limper, Malaysia*. Atmospheric Research, 44 (1997) 293 – 315.
- Diskin M.H. (1987). *On the Determination of the Speed of Moving Rainfall Patterns*, Hydrological Sciences Journal, Vol32, No. 1, pp. 1-14.
- Diskin M.H. (1990). *The Speed of Two Moving Rainfall Events in Lund*, Nordic Hydrology, 21, 1990, 153-164.
- Eagleson P.S. (1970). *Dynamic Hydrology*. McGraw-Hill, New York.
- Felgate D.G. and Read D.D. (1975). *Correlation analysis of the cellular structure of storms observed by raingauges*. J. Hydrol., 24:191-200.
- Hindi W.N.A. and Kelway P.S. (1977). *Determination of storm velocities as an aid to the quality control of recording raingauge data*. J. Hydrol., 32: 115-137.
- Hobs P.V. and Locatelli J.D. (1978). *Rainbands, precipitation cores and generating cells in a cyclonic storm*. J. Atmos. Sci., 35: 230-241.
- Marshall R.J. (1980). *The estimation and distribution of storm movement and storm structure, using a correlation analysis technique and rain-gauge data*. J. Hydrol., 48: 19-39.
- May D.R., Julien P.Y. (1998). *Eulerian and Lagrangian correlation structures of convective rainstorms*. Water Resour. Res. 34, 2671 – 2684.
- Niemczynowicz J. and Dahlblom P. (1984). *Dynamic properties of rainfall in Lund*. Nordic Hydrol., 15: 9-24.
- Niemczynowicz J. (1987). *Storm tracking using rain gauge data*. J. Hydrol., 93: 135-152.
- Niemczynowicz J. (1991). *On storm movement and its applications*. Atm. Res., 27: 109-127.

- Shaw S.R. (1983). *An investigation of the cellular structure of the storm using correlation techniques*. J. Hydrol., 62: 63-79.
- Shearman R.J. (1977). *The speed and direction of movement of storm rainfall patterns*. Meteorological Office, Bracknel, Berkshire, UK, Report UDC 551.515.43.

6. Conclusions

6.1 Overview

Currently cities and communities are experiencing ever growing problems related to urban pluvial flooding. This is due primarily to inefficient drainage inlets and overloaded sewer systems. In fact, existing drainage systems rapidly reach their maximum capacity and tend to work pressurized even in the case of medium-entity storms.

Damage and losses caused by flood events in urban areas, primarily life and economic losses and traffic disruption, can be significant. Moreover, this situation is destined to worsen in the immediate future due to the fervent urbanization process and the ongoing climate changes.

This research is therefore aimed at investigating this type of event, because to guarantee an efficient working of the drainage systems is a prerequisite in modern societies. Specifically the broader objective of the study is to contribute to an improvement of urban flood management by enhancing urban drainage modeling and storm motion forecasting. In order to achieve such scope the following detailed tasks were performed:

1. Investigation of the various LiDAR Digital Terrain Models (DTMs) available for the drainage modeling of a study area.
2. Analysis of improvements brought by a dual drainage approach in simulating the behavior of a drainage network during extreme rain events, compared to the use of a conventional methodology.
3. Study of the potentials of a dense network of rain gauges in forecasting storm movements for flood prevention purposes.

A summary of the achievements and discussion of the results obtained from the tests and comparisons carried out in this research are presented below.

6.2 Hydraulic modeling of the drainage network of a monitored catchment

The first part of the research was directed at demonstrating how conventional urban drainage modeling is inadequate to simulate realistically the behavior of the drainage system during extreme rain events. Consequently, two hydraulic models were developed for the same monitored catchment, the Liguori catchment located in Cosenza (Italy), in order to compare their performances. The first model was developed by following the classical hypothesis according to which the drainage system is composed only of the sewer system, that is, to consider that stormwater, once entered the sewer system, can no longer leave this system by coming back to the surface. Instead the second model was based on the dual drainage approach, i.e. it was assumed that the urban drainage system was composed of a surface network and the sewer network.

Both the approaches required the use of a very detailed and hydraulically corrected DTM for the study site. For this reason LiDAR data, characterized by an horizontal resolution of 1 m, were used. Nevertheless DTMs with different detail scale can be obtained from similar surveys: LiDAR DSM *first*, LiDAR DSM *last* and LiDAR DTM are in fact characterized by a variable presence of non-ground surface features, such as cars, buildings or vegetation, that will influence surely the hydraulic response of the urban catchment differently. Therefore it seemed opportune to evaluate whether the use of a less detailed data set, such as a LiDAR DTM with overlapped buildings, could be a valid approximation of the highest detailed one, i.e. the LiDAR DSM *first*, in order to make easier the successive hydraulic modeling of the drainage network.

In detail the study consisted in comparing the surface depressions evaluable from the two data sets: from the elaborations carried out it emerged that the simplification proposed was acceptable since a good portion of the identified depressions was in common between the two DTMs (37 %), particularly the largest ones. Thus the LiDAR DSM *first* could be ignored for hydraulic modeling because the consideration of vegetation and further non-ground surface features would complicate the modeling phase in vain. In fact these objects affect the overland flow less than the buildings.

Afterwards the LiDAR DTM_b was further on improved by removing errors inherent to the acquisition and interpolation processes of the elevation data, such as pits or sinks. Specifically the following methodology was employed: all the depressions shared between this DTM and the LiDAR DSM *first* were assumed real whereas the remaining ones were removed by filling operations.

Building areas were identified by subtracting the LiDAR DTM to the LiDAR DSM *last*, and considering only the objects characterized by an elevation at least of 3 meters and a surface area at least of 10 m^2, assumed as minimum building properties. This procedure was necessary because the use of the available building layer, whose perimeter did not coincide with the contour of the buildings removed from the LiDAR DSMs, determined the generation of erroneous depressions close to the buildings in the LiDAR DTM_b. The LiDAR DSM *last* was chosen because it was characterized by an inferior number of man-made features and trees than LiDAR DSM *first*, thus it made the filtering procedure easier.

The accuracy of the proposed filtering methodology was then established by comparing the footprints of the original building layer and the new one obtained. In particular it was observed that the method worked quite well because almost all the buildings were identified, also if it was not possible to distinguish vegetated areas located close to buildings, representing 12.87 % of non-ground surface features to be filtered. Consequently, later, manual editing was also necessary.

In particular the use of the new building layer in the generation of the LiDAR DTM_b was opportune because it enabled the removal of a good part of the surface depressions obtained by taking as reference the original building layer (38.90 %). A further 61.10 % of the surface depressions was still shared by the two DTMs.

Afterwards the processed LiDAR DTM_b was used to derive the hydrological information necessary for the development of the hydraulic models. In particular the position of the “fictive manholes” of the sewer network was defined by the intersections between the sewer layout and the natural drainage network generated from the LiDAR DTM_b itself.

The conventional hydraulic approach was based on the modeling of only the sewer network. This model was reliable if the sewer network was not overloaded, and it enabled also the development of interesting applications, such as the evaluation of

the drainage network efficiency through the calculation of physical and hydraulic indicators. These indices, computed for each sewer trunk, were later represented in GIS in order to estimate which constructive defect determined the most relevant repercussion on the network performance, and then which rehabilitative interventions would have to be taken into account. Specifically, from the elaborations carried out, it was possible to observe that the slope variation resulted the principal cause of sewer network malfunctioning.

Nevertheless, this procedure was not adequate to model the drainage system behavior accurately during extreme rain events, because it ignores the fundamental concept on which the traditional urban hydrology is based, i.e. the interaction between the surface network with the buried drainage system. This result emerged by the comparison with the other hydraulic model developed based on the dual drainage concept. In fact, by subjecting both the models to identical rainfall inputs (eleven historical events and three synthetic rainfall events with associated return periods of 15, 30 and 50 years), it was possible to note that different volume distributions emerged only in the cases where the storm events determined the surcharge of the sewer network. In particular, as was expected, the conventional model localized a greater number of surcharged trunks, which would have forced the engineer to increase the dimensions of the pipes involved with consequent repercussions on the cost of the works.

Vice versa, the dual drainage model enabled a more realistic simulation of the sewer flooding, since it considered a bidirectional interaction between the surface and the sewer system. Hence, in this way, it was possible to limit the number of surcharged sewer trunks: in fact more than 90 % of the surcharged nodes found in the conventional model was completely “corrected” in the dual drainage model, whereas a further 7% was still surcharged but by a flood volume reduced of 60 %.

Consequently, the dual drainage modeling was finally recommended for future applications by underlining also the issues related to the development of a similar approach. In fact, the most difficult phase is the definition of a realistic surface network to be coupled with the sewer network. In this project the use of an innovative procedure was tested: the AOFD tool. In fact, this methodology enabled the individuation of the potential flooded areas (ponds) and the connections between

these and the surcharged manholes based on GIS analysis of DTM. In particular, from the elaborations carried out, the following considerations emerged:

1. the buildings have to be considered within the DTM. In fact, their presence determined the definition of ponds with ever increasing extension and depth since they act as barriers to the overland flow. Moreover , in this way, it was possible to avoid errors, such as ponds localized inside buildings or pathways crossing buildings.
2. high-detailed DTMs, such as LiDAR ones, have to be used in similar applications. In fact, the DTM 5 was an unstable data set since it showed a remarkable increase in surface storage capacity when buildings were considered within the DTM itself. Nevertheless, the use of highly-detailed DTMs, such as LiDAR ones, promoted the definition of a large number of small ponds, often not significant for simulation purposes, which could make the computational load of the modeling heavier. Moreover, these depressions could be also sinks that were not corrected in the previous stage of the DTM processing. For these reasons a pond filtering study was faced: different threshold values of depth and volume were considered in order to evaluate the best values that maximized the ponds removal and minimized the related lost storage capacity. In this case a value of 0.2 m for the depth and 5 m^3 for the volume were assumed so that the pond removal was of 55 % whereas the lost storage capacity was of 1.08%.

6.3 Storm tracking study based on rain gauges data of a monitored catchment

The dual drainage model proved to be also suitable because simulation results, such as the temporal trend of the surface velocities and depth, enabled the localization of the potential flooded areas. These applications will surely attract subjects, such as insurance companies and civil protection institutions. In fact, the insurance companies will find the possibility of more realistic evaluation of the damage associated with the floods advantageous; instead the civil protection institutions could use such results for elaborating adequate emergency plans.

In particular, from the flood prevention point of view, it could be also very important to deepen the knowledge of rainfall characteristics in view of their critical effects in

causing regular flash floods. It is evident how information, such as the statistical distribution of the direction of movement of storm rainfall patterns and the average speed for each direction, is relevant to flood studies. In fact, in this way, it would be possible to verify whether a future storm event, recorder by one of the borderline stations within the study area, will reach the center of the catchment or not and, in the former case, how much time it will take to move towards the catchment itself. Moreover, if a calibrated and reliable hydraulic model was available for the same study area, similar information could be also used in order to evaluate in advance the possible flood-prone areas.

The speed and direction of movement of rainfall events, recorded by the dense network of rain gauges placed in London, were thus evaluated by using the storm tracking method proposed by Diskin. The lack of an adequate instrumental equipment for the Liguori catchment, for which the drainage model was previously developed, did not enable to prove how the linkage between storm tracking procedures and hydraulic modeling is an approachable methodology for forecasting potential flooded areas. However the elaborations carried out demonstrated how rain gauges may be considered as valid alternatives in rainfall movement prediction, to be taken into account in areas where radar measurements cannot be obtained yet. In fact the method of computing storm velocities and directions was sufficiently good since the calculated velocity values were in agreement with the results obtained in several studies performed in other regions. However, also some differences emerged: in this case, in fact, computed velocity and direction data sets resulted well fitted by a normal distribution, whereas other researchers observed that the relative frequency was well fitted by a two-parameter lognormal distribution.

The choice of the best hyetograph feature to be considered in the elaborations was another issue faced. Three features were used for the definition of arrival times: t_{cent}, the time to the centroid of the hyetograph, t_{Imax}, the time of highest rainfall intensity and t_{onset}, the time of start of rainfall. The feature giving the most reliable results was established by comparing, through statistical tests, the results of the elaborations performed with other physical phenomena which are related to the storm movement, such as wind movement. From the applications carried out it could be noticed that:

1. the time and spatial resolution of the recording stations affect significantly the results of the applications. In fact, in this case, the poor time resolution (15 minutes) determined that the onset was the worst feature since it favoured the erroneous individuation of an equal arrival time of the storms from most of the stations. Instead the centroid feature provided the best approximation of the wind direction, whereas the peak gave the best estimate of the wind velocity. Nevertheless, in the end, the centroid was recommended for future applications because the bigger mistake in the overestimation of the velocity, however advantageous for the safety measures, was compensated by the better evaluation of the direction of movement of the wind.
2. the use of wind data recorded at the ground level should be avoided in similar calculations because they did not enable strong correlations to be found between storm and wind movement parameters. In fact, by comparing the corresponding wind and storm parameters, it emerged that wind velocities were overestimated whereas wind directions were underestimated. This result, already reported in other studies in the literature, was expected because such measurements are affected by the presence of obstacles at ground level, such as buildings. Consequently, high altitude wind data, available in the airports, will have to be assumed for further applications.

Finally, the research was also aimed to evaluate to what extent the location of the rain gauges inside the catchment could condition the results of the methodology. These further elaborations were carried out because some municipalities do not have the funds for equipping themselves with an adequate number of rain gauges, therefore it is significant to know how the results could change if a reduced number of recording stations is employed. Consequently, other three network configurations were considered in order to compare their results. Specifically, it was noted that the reduction of the recording stations would enable a better estimation of the velocity but a worse evaluation of the direction, i.e. the storm velocities would be less overestimated and the directions would be more underestimated. Precisely the further underestimation of storm direction demonstrated how a similar network configuration would not be adequate because important repercussions could occur by ignoring wrongly rainfalls that instead will effectively reach the catchment.

Appendix A – Calibration of the conventional urban drainage model

For each rainfall event the hyetograph (blue color), the observed hydrograph (red color) and the hydrograph simulated with the traditional model (orange color) are plotted in the following pictures. The calculated Pearson's coefficient (r_S^2) is also reported.

07/27/2006

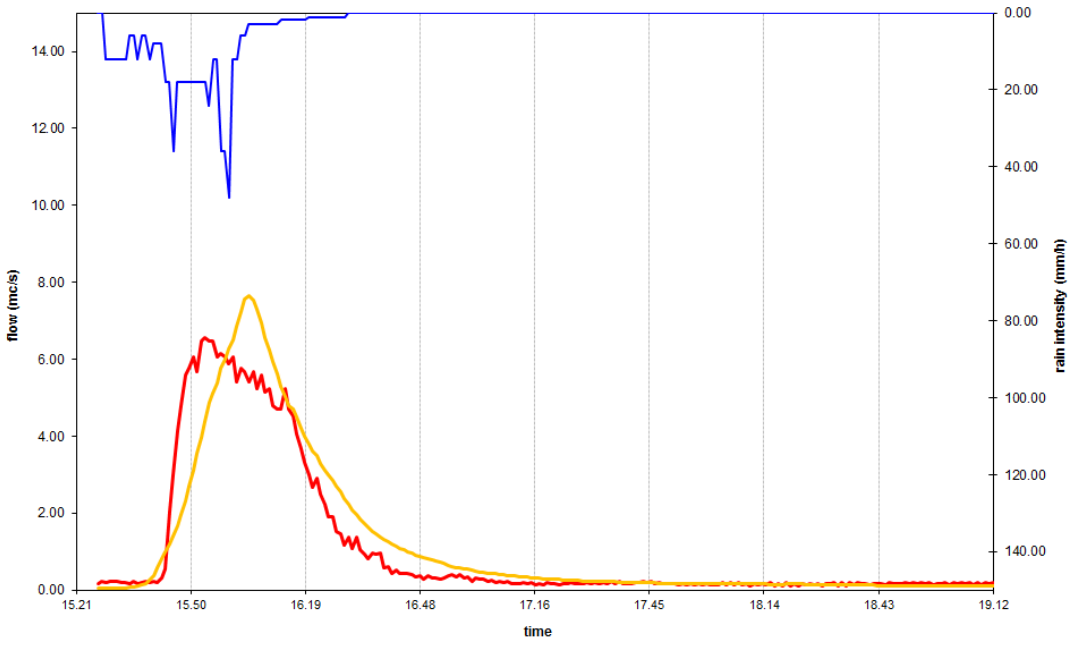

($r_S^2 = 93.59\ \%$)

02/15/2007

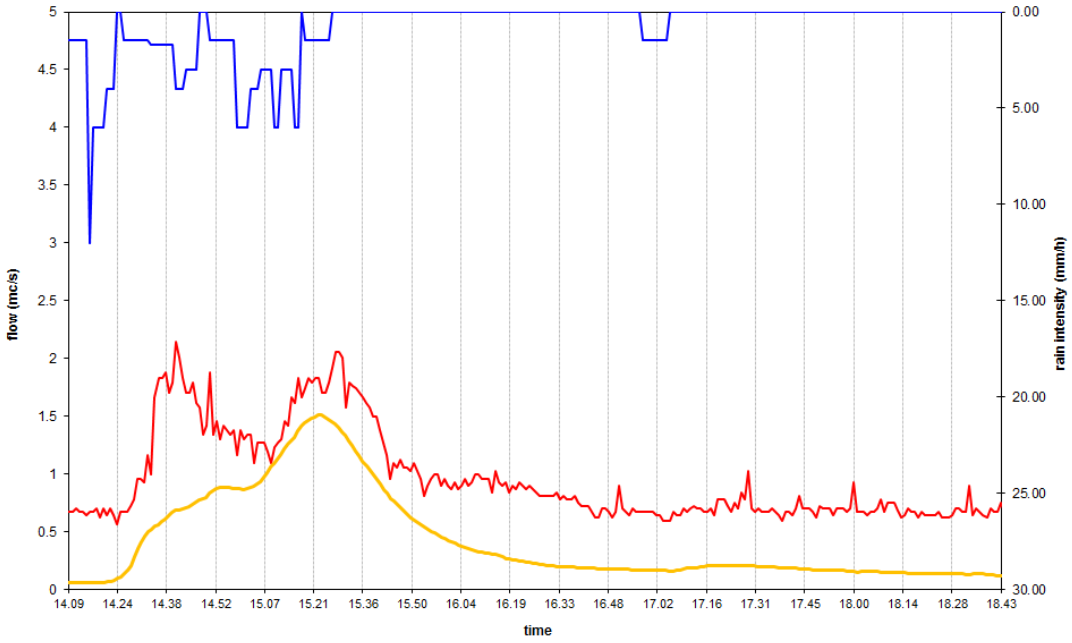

($r_S^2 = 89.63\ \%$)

04/14/2007

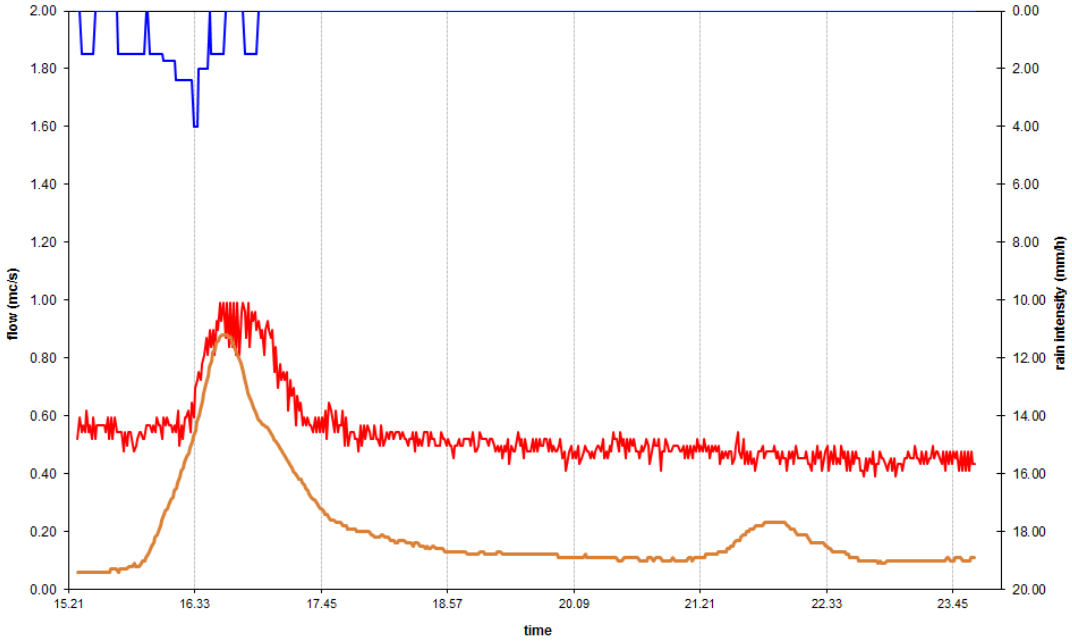

($r_S^2 = 88.81\ \%$)

05/18/2007

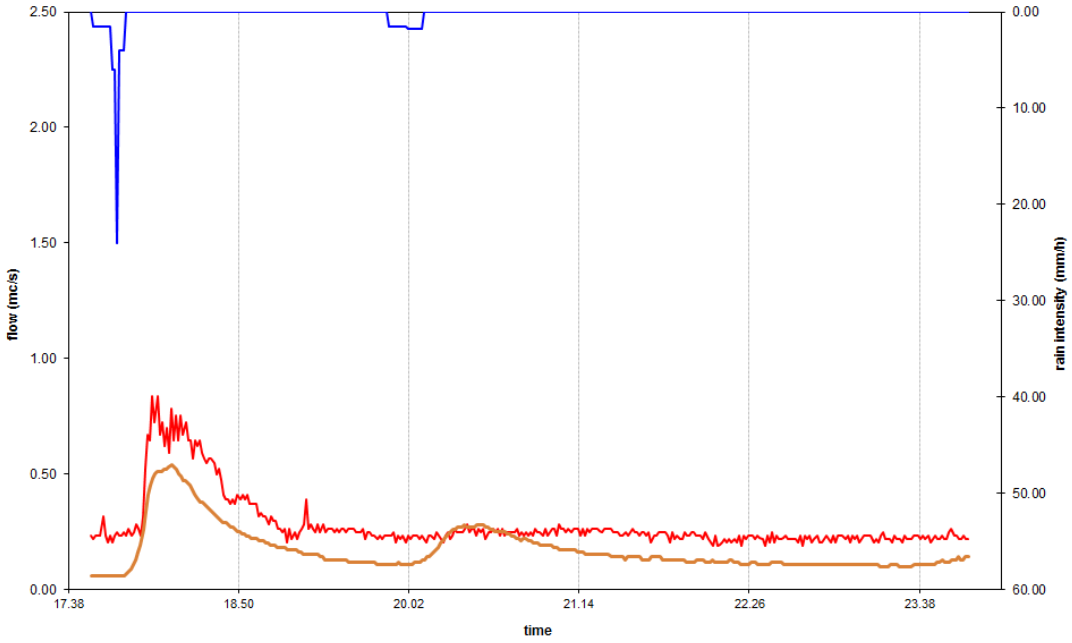

($r_S^2 = 89.07\ \%$)

09/19/2007

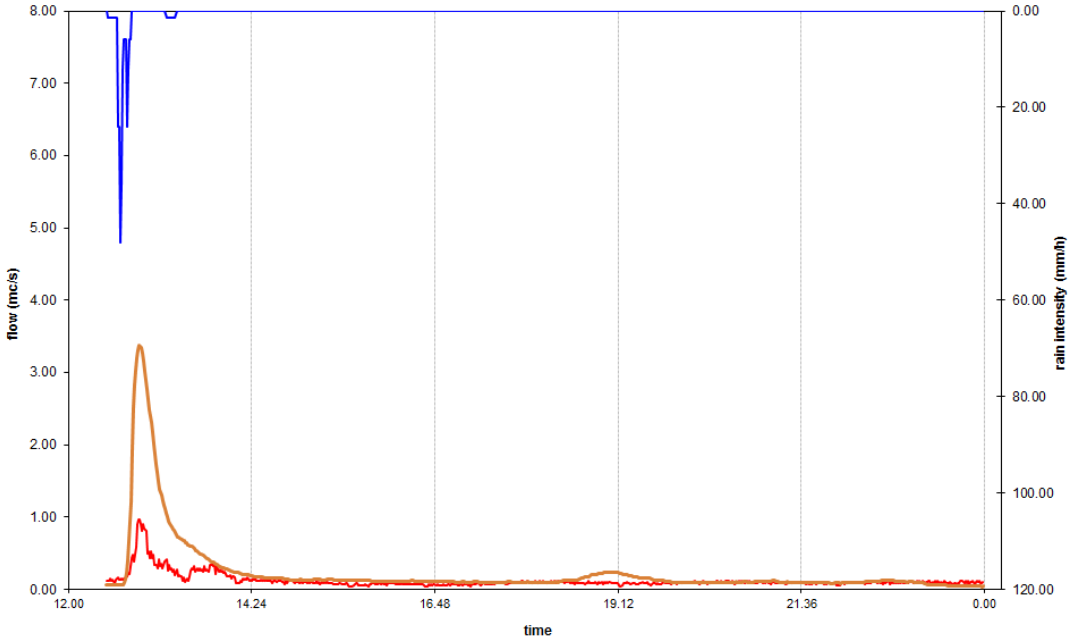

($r_S^2 = 92.40\ \%$)

09/28/2007

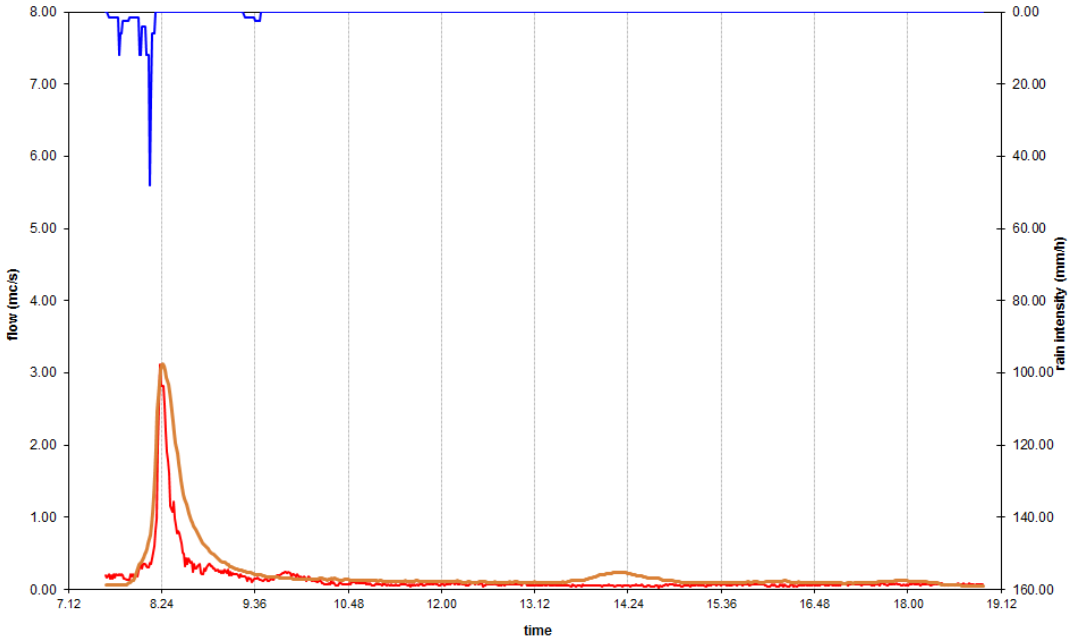

($r_S^2 = 93.20\ \%$)

10/11/2007

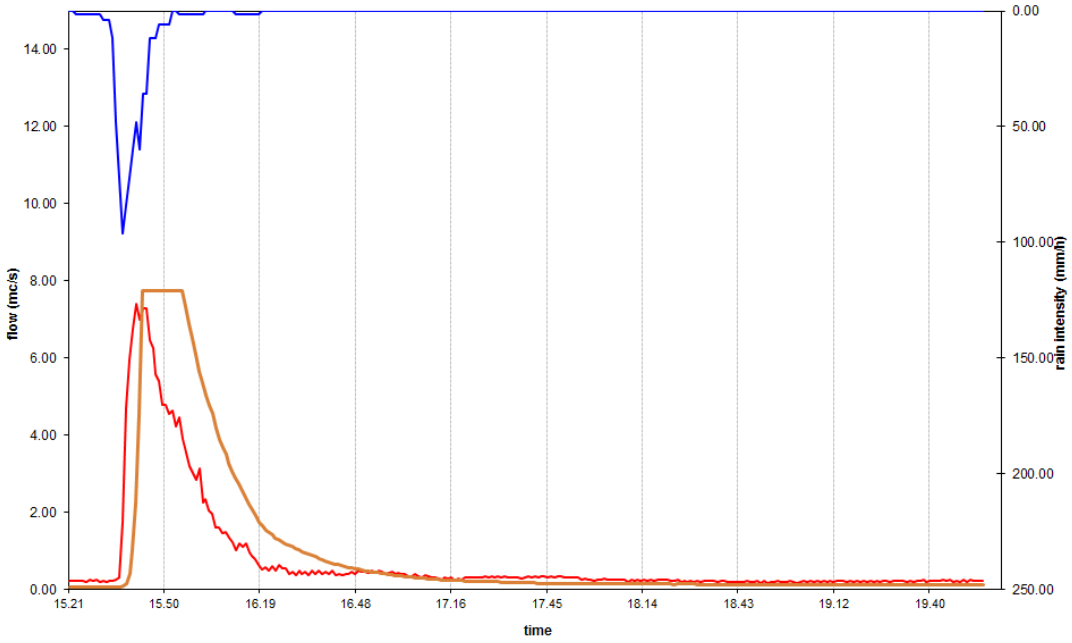

($r_S^2 = 82.13\ \%$)

11/15/2008

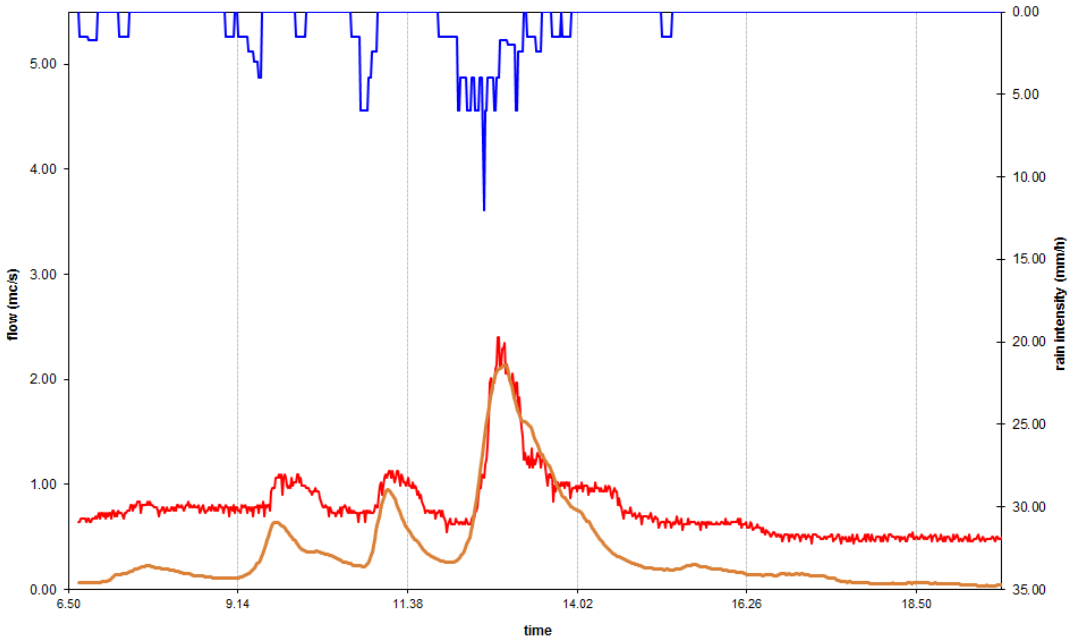

($r_S^2 = 92.36\ \%$)

03/05/2009

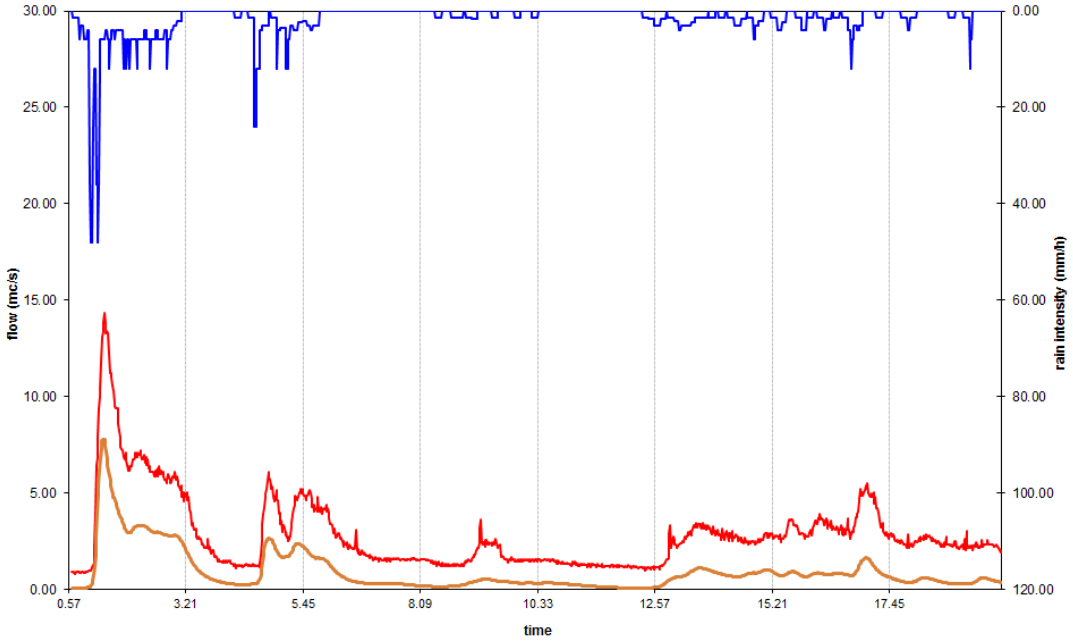

($r_S^2 = 97.33\ \%$)

03/29/2009

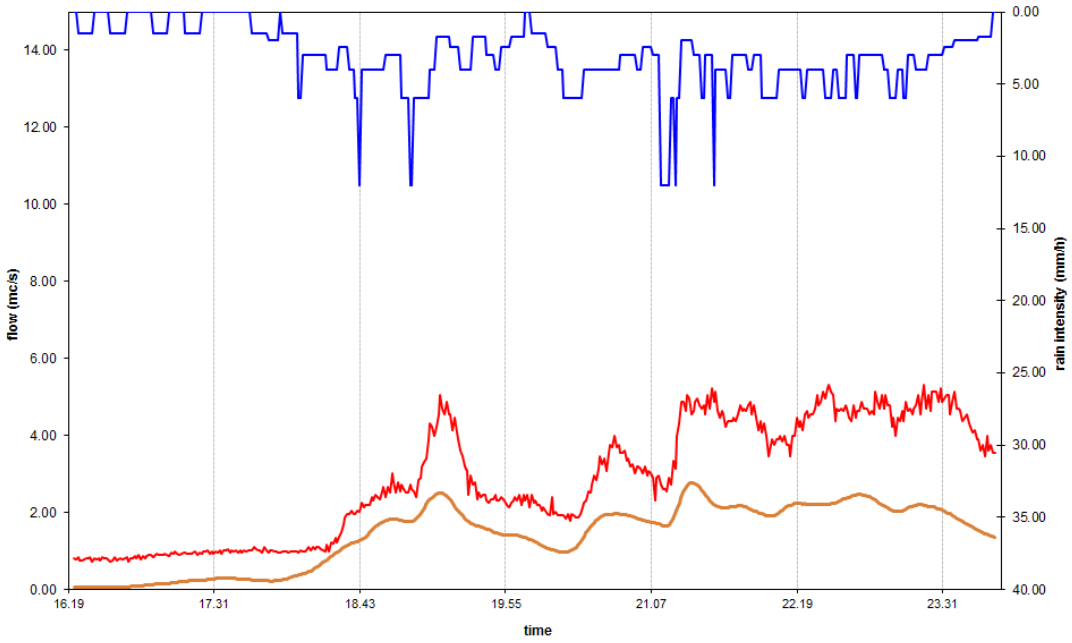

($r_S^2 = 93.85\ \%$)

04/28/2009

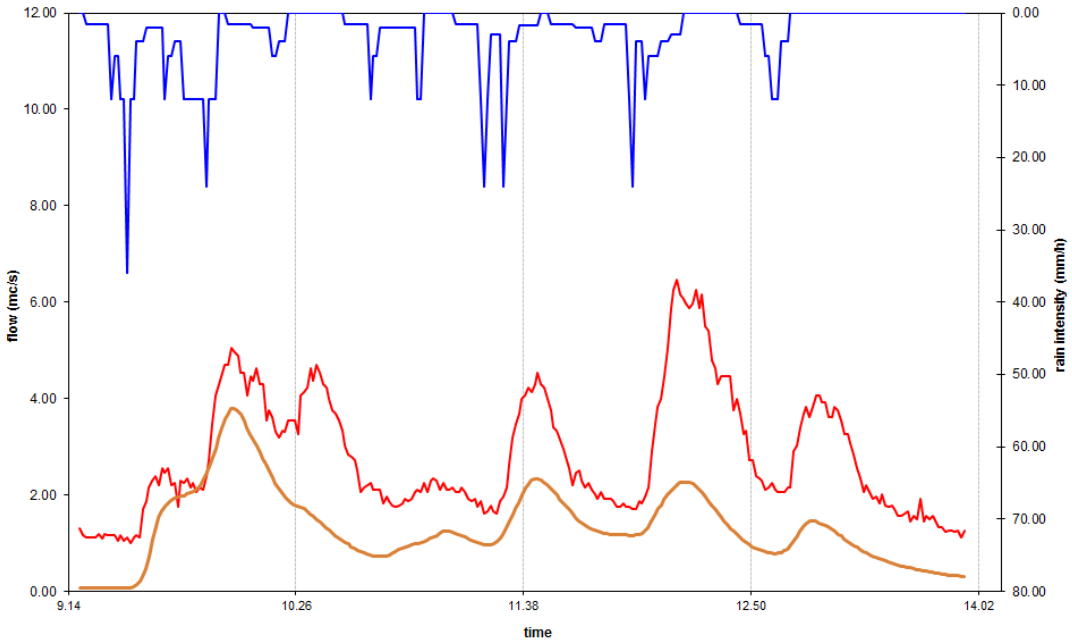

($r_S^2 = 74.37\ \%$)

Appendix B – AOFD data preparation

The flow diagram in fig. A1 shows the different procedures needed to generate the overland flow network by the AOFD.

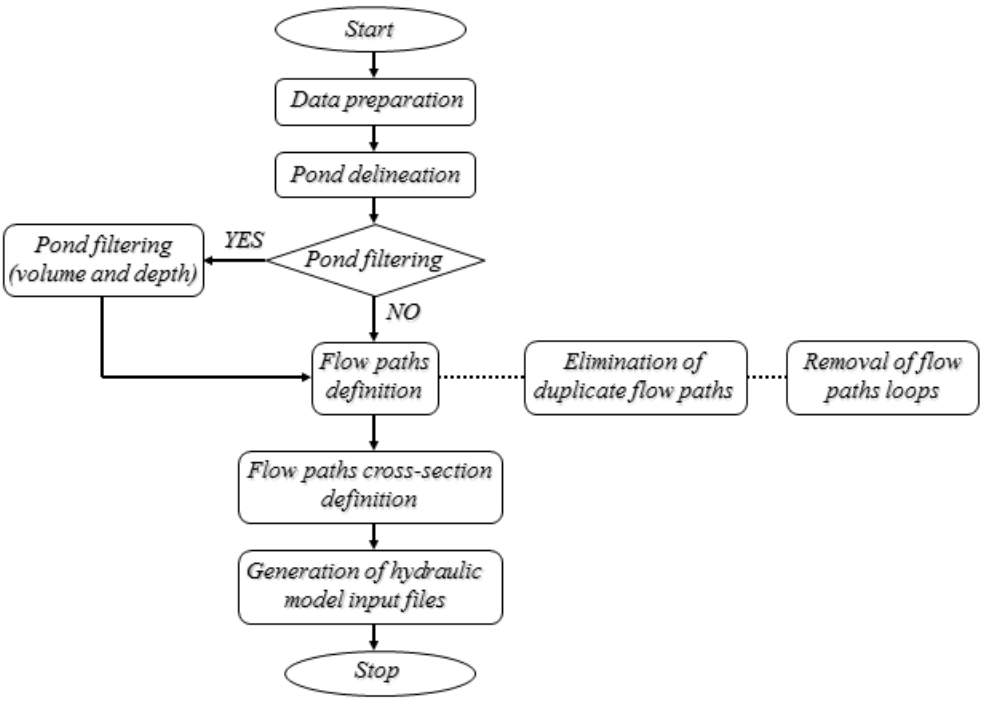

Figure A1 Flowchart of the overland flow tool (from Leitão, 2009).

The files required to run the tool have to be organized as follows (fig. A2):

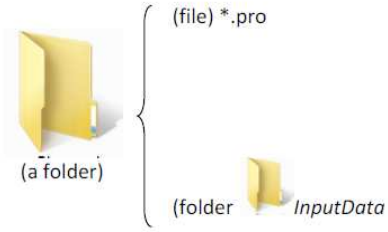

Figure A2 Working folder structure (from Leitão, 2009).

The project file (*.pro) is a text file with a description of the general parameters of the input data. It contains the names of all the input files to be used in the surface flow path generation (with no file extension), as well as information about number of columns and rows, and cell size of raster images used by the routines.

In InputData folder the following input files have to be stored:

- Digital Terrain Model (DTM)

- Slope image
- Aspect image
- Manholes
- Catchment boundary
- Cover layer (the same as catchment boundary)
- Building layer

These data have to be created according to the suggestions reported in table A1.

Input	**Output**	**Process**
Boundary Polygons	Boundary Vector	This boundary can be created using AutoCad, then opening the file in ArcGIS and exporting it, in order to obtain a shapefile (polygon type), which can afterwards be converted to the IDRISI format using the conversion tools of AOFD. When creating this boundary, be careful with coordinate system and scale of the drawing.
Boundary Vector	Boundary Raster	Create a raster layer from the polygon: 1. Conversion Tools – To Raster – Polygon to Raster.
Boundary Raster	Reclassified Raster	Reclassify raster values to those required for AOFD (Where 1 = cells inside, -1 = cells outside catchment) 1. Spatial analyst tools – reclass – reclassify. 2. Conversion Tools – From Raster – Raster to ASCII (required for AOFD tool).
Building Vector Layer	Buildings in catchment	Clip the building polygons to fit the catchment boundary 1. Analysis tools – Overlay – Intersect (input building polygon and catchment boundary polygon).
Buildings catchment vector	Buildings Raster and reclassified	1. Convert the intersected vector layer to a raster layer using the conversion tool: Conversion tool – To Raster – Polygon to raster. 2. Reclassify the building raster so that all values (those in buildings) = 1 and No Data (that outside of buildings) = 0 by using: Spatial analyst tools – reclass – reclassify. 3. Convert the reclassified raster layer to ASCII format: Conversion tool – from Raster – Raster to ASCII.
Manhole data	Manhole points	Select manholes that fall inside the catchment boundary and create a new layer from these: 1. First select the combined and stormwater sewers from the attribute table: Options – Select by attribute – Enter: "PURPOSE" = 'S' OR "PURPOSE" = 'C'. 2. With these selected, intersect the manhole layer with the catchment boundary: Analysis tools – Overlay – Intersect.
Selected manhole points	Raster manhole layer	Convert the point data to raster data 1. Use the Editor toolbar to add additional points to the clipped point layer (this is required to make sure a large enough area converts to raster) Editor – start editing – select manhole vector layer to edit – click on the sketch tool – add 4 points around the existing point area, well outside the boundary – Stop editing – save edits. 2. Conversion tools – To Raster – Point to Raster. 3. Clip the raster layer using the spatial analysis toolbar, using a raster layer with the correct size, such as the Boundary Raster layer: Spatial analyst toolbar – Options – Set 'Analysis Mask' in General to 'Raster'– Set 'Analysis Extent' in Extent to 'Same as Layer "Raster" - Set 'Analysis Cell Size' in Cell Size as 'Same as Layer "Raster" – OK – Spatial Analyst toolbar – Raster Calculator – Select Raster layer – Evaluate.
Manhole raster	Reclass manhole raster	Reclass raster layer: 1. Spatial analyst tools – reclass – reclassify. 2. Set unique values, each call should have its own value ranging from 1 to n. Make sure at this point there are the same amount of raster cells as

		manhole points. If not check that there is only one point in each raster and all points are converted. 3. Create a catchment raster (as described previously) with cell values of 0 inside the catchment and -1 outside. 4. Merge this raster layer and the manhole raster using the raster calculator: input '[New catchment later] + [Manhole Raster]' and click evaluate. 5. Make output calculation permanent: right click on layer – Data - Make permanent. 6. Reclass to ASCII format as previously described.
Manhole *.csv and *.ntt files		The AOFD needs *.csv and *.ntt files for the manhole data. 1. These can be created using Microsoft Excel, or InfoWorks CS. The format of these is given below.
ASCII DTM tiles	ASCII DTM	Convert DTM tiles: 1. Convert each tile to raster format by using: Conversion tools – To raster – ASCII to raster (Ensure output data type is 'FLOAT'). 2. Merge the new raster tiles using: Data management – Raster – Raster dataset – mosaic. 3. Clip the cells to the catchment raster layer: Spatial analyst toolbar – Options – Set 'Analysis Mask' in General to 'Raster Boundary' – Set 'Analysis Extent' in Extent to 'Same as Layer "Raster" - Set 'Analysis Cell Size' in Cell Size as 'Same as Layer "Raster" – OK – Spatial Analyst toolbar – Raster Calculator – Select Raster layer – Evaluate. 4. Incorporate the building height into the DTM by using the reclassified building layer (in this case assign a value to cells with buildings to 10) Incorporate by using the raster calculator: input [DTM] + [Reclassified Building] – click evaluate. 5. Convert the total clipped raster mosaic to ASCII using: Conversion tools – From raster – Raster to ASCII.
DTM	Slope	Use the AOFD conversion tool to create a DTM with a slope away from the catchment boundary. 1. Raster conversion – ESRI ASCII to IDRISI (16bit) file – select DTM – tick the 'assign elevation to noData values' – convert. 2. Convert the new image file back using the IDRISI 16bit file to ESRI ASCII file. 3. Using ArcInfo convert the created ASCII file to a raster: Conversion tools – ASCII to raster (ensure to select the output data type as 'FLOAT'). 4. Create the slope by: Spatial analyst – Surface – Slope (Select percentage NOT degree). 5. Use the Raster Calculator in the Spatial Analyst Toolbar to convert the slope to a gradient – Enter [Slope Layer] ÷ 100. 6. Convert to ASCII using Conversion Tools – From Raster – Raster to ASCII (required for AOFD tool).
DTM	Aspect	Use the clipped DTM layer to determine the aspect: 1. Spatial analyst – Surface - Aspect.

Table A1 AOFD layer creation methodology using ArcInfo 9.3.1.

In particular, in this phase, it is important to take care of:

- *Raster extent*. Raster layers must present the same extension. If they do not clip correctly, or to the same layer, errors will potentially occur in the AOFD process. Consequently it is opportune to use a raster layer to clip them with in order to ensure raster layers clip correctly.
- *Consistent cell size*. In this case, LiDAR data was provided with a 1m × 1m resolution, however the computational power required to compute this resolution

is considerable, thus data was converted to a 3m × 3m resolution. In similar operations it is important to be careful with the method by which the average of the cells is calculated.

- *Slope values*. These need to be expressed in a gradient, and not as a percentage or a degree. This can be achieved by using the raster calculator and dividing the slope (percentage) values by 100.
- *Manholes*. Problems may occur when converting from vector points to raster points. It is necessary to check:
    1. if more than one manhole is contained in a raster cell. In this case the manhole needs to be moved, not deleted;
    2. if manholes, located on the boundary, are converted or not to raster cells. Also in this case they need to be moved in from the boundary.

  It is also important to ensure the number of manholes in the vector, raster, *.csv and *.ntt files are the same. In particular the manhole *.csv and *.ntt files are characterized by the following formats (fig. A3), with *n* equaling the total number of manhole points in the vector and raster layers (these should be the same). The *.csv can save in excel, whereas the *.ntt file can be created by changing the file extension of the file once it has been saved.

For the *.csv	
1	1
2	2
3	3
.	.
.	.
n	n

For the *.ntt file			
1	1	FFFF	1
2	2	FFFF	1
3	3	FFFF	1
.	.	.	.
.	.	.	.
n	n	FFFF	1

Figure A3 Manhole *.csv and *.ntt file formats.

All these files have to be saved in IDRISI 16bit vector and/or raster format (tab. A2). This format was chosen because it has the advantage to be presented in ASCII text format, thus it is editable by a text editing software which (except for raster image files that are in binary format) makes manual modifications easy.

Since such format is not commonly recognized by other used software (e.g. ArcGIS or MapInfo), the AOFD tool has included an interface to convert IDRISI 16 bit format to ArcGIS format (shapefiles, ASCII files) and vice versa (fig. A4).

DTM or DTMb	IDRISI 16 bit Raster	*.doc, *.img		Double format
SLOPE	IDRISI 16 bit Raster	*.doc, *.img		Double format
ASPECT	IDRISI 16 bit Raster	*.doc, *.img		Double format
MANHOLES	IDRISI 16 bit Raster	*.doc, *.img	Manholes represented by their IDs. Cells representing catchment boundary = 0, outside = -1	Integer format
	IDRISI 16 bit Vector	*.vec, *.dvc		
	Text	*.csv, *.ntt	Creates correspondance between the integer manhole ID and in raster format and the manhole IDs in the hydraulic model	Text format
CATCHMENT BOUNDARY	IDRISI 16 bit Raster	*.doc, *.img	Cells outside catchment = 0, inside = 1	Integer format
	IDRISI 16 bit Vector	*.vec, *.dvc	Polygon type, polygon ID = 1	
COVER	IDRISI 16 bit Raster	*.doc, *.img	Copy of catchment boundary	Integer format
	IDRISI 16 bit Vector	*.vec, *.dvc		
BUILDINGS	IDRISI 16 bit Raster	*.doc, *.img	Value inside buildings = 1, outside = 0	Integer format
	IDRISI 16 bit Vector	*.vec, *.dvc		

Table A2 Input data characteristics and formats.

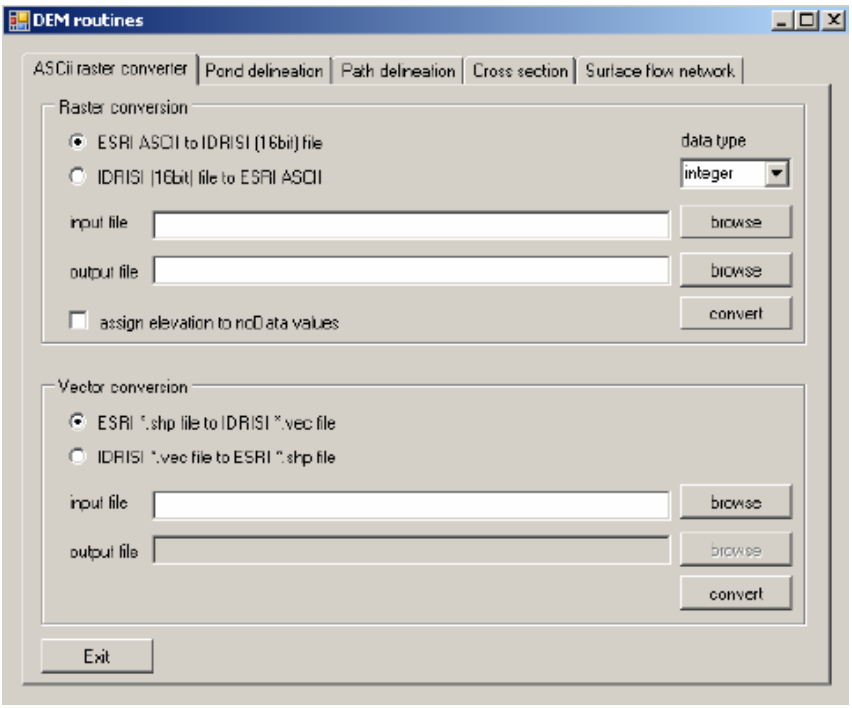

Figure A4 File conversion tab.

Other folders will be created later: after the first run of the "pond delineation" routine, results will be saved in the "Ponds" folder. Similarly the "path delineation" results will be stored in the "Paths" folder, and so on. Finally when the analysis is

completed, the final structure of files and folders will be organized in the way shown by figure A5.

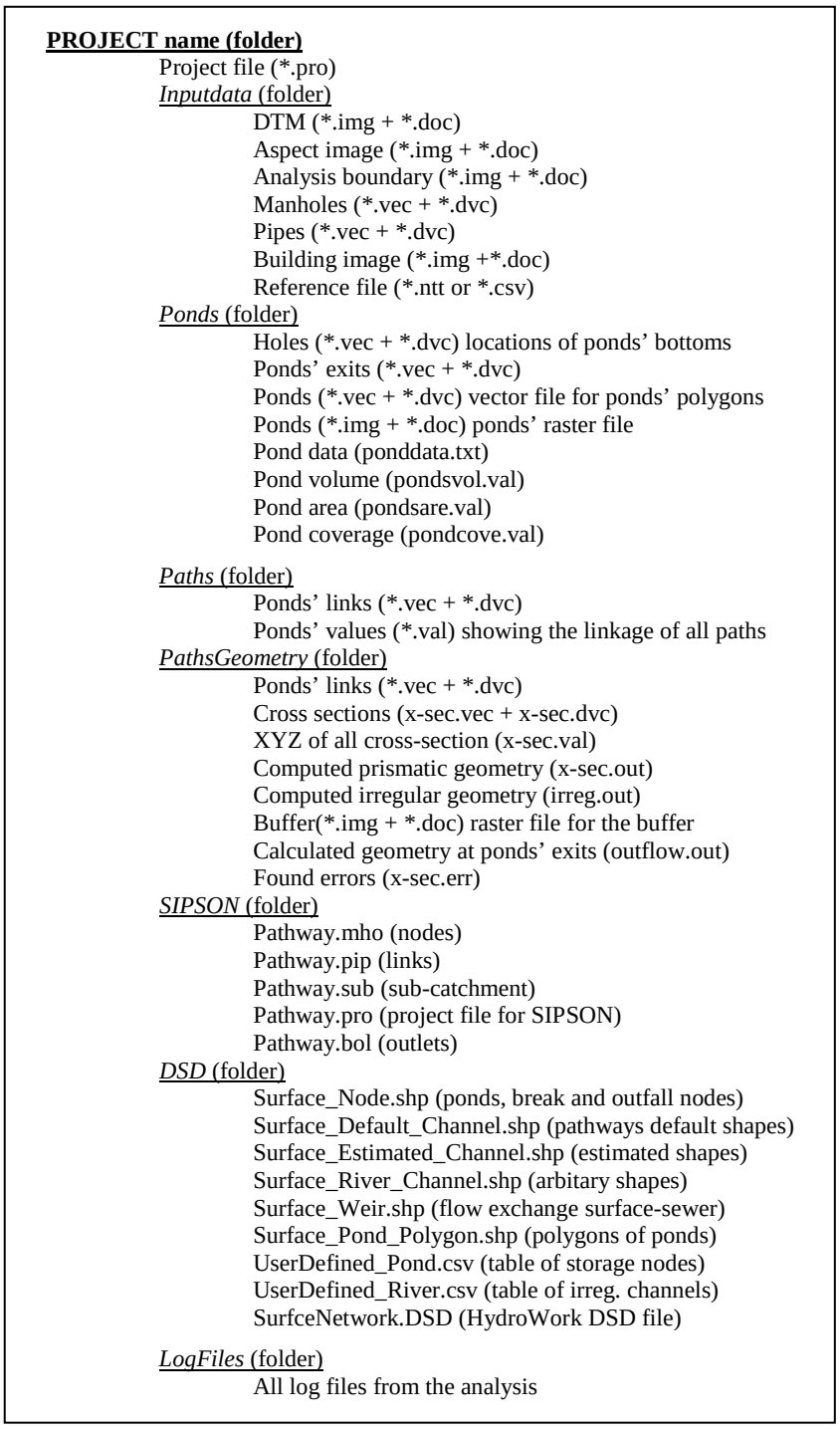

Figure A5 Folder structure when all analysis completed.

Appendix C – Comparison between the two urban drainage modeling

In the following the hydraulic simulations, where no differences were observed between the two approaches, are reported. In particular, for each rainfall event, the hyetograph (blue color), the observed hydrograph (red color), the hydrograph simulated with the traditional model (orange color) and the hydrograph simulated with the dual drainage approach (green color) are plotted. The calculated Pearson's coefficients (r_S^2 and r_{DD}^2) are also reported.

02/15/2007

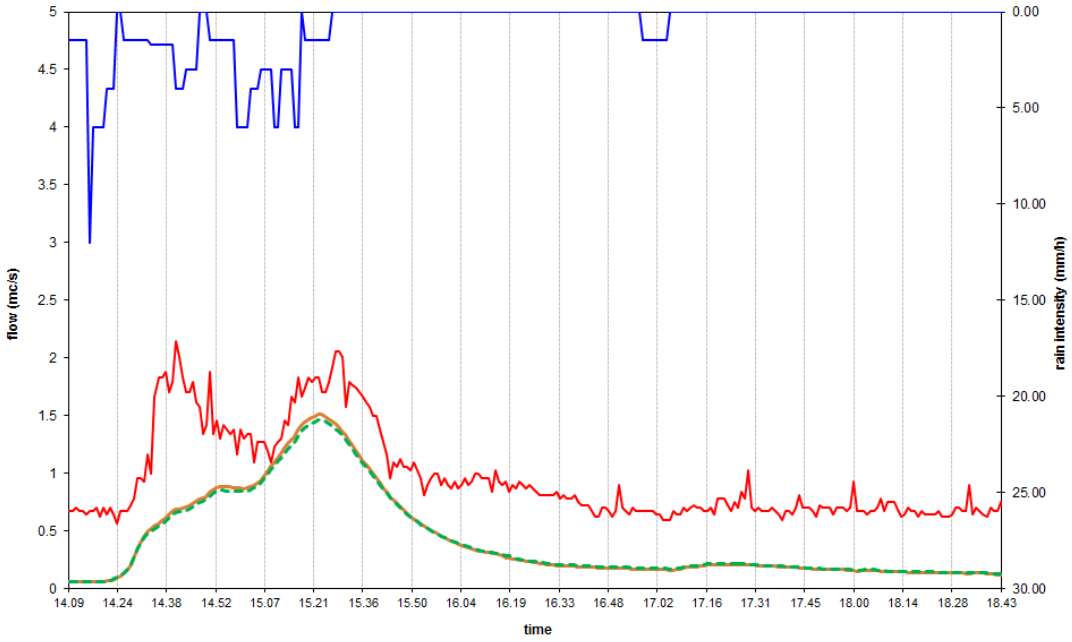

($r_S^2 = 89.63$ % ; $r_{DD}^2 = 89.29$ %)

04/14/2007

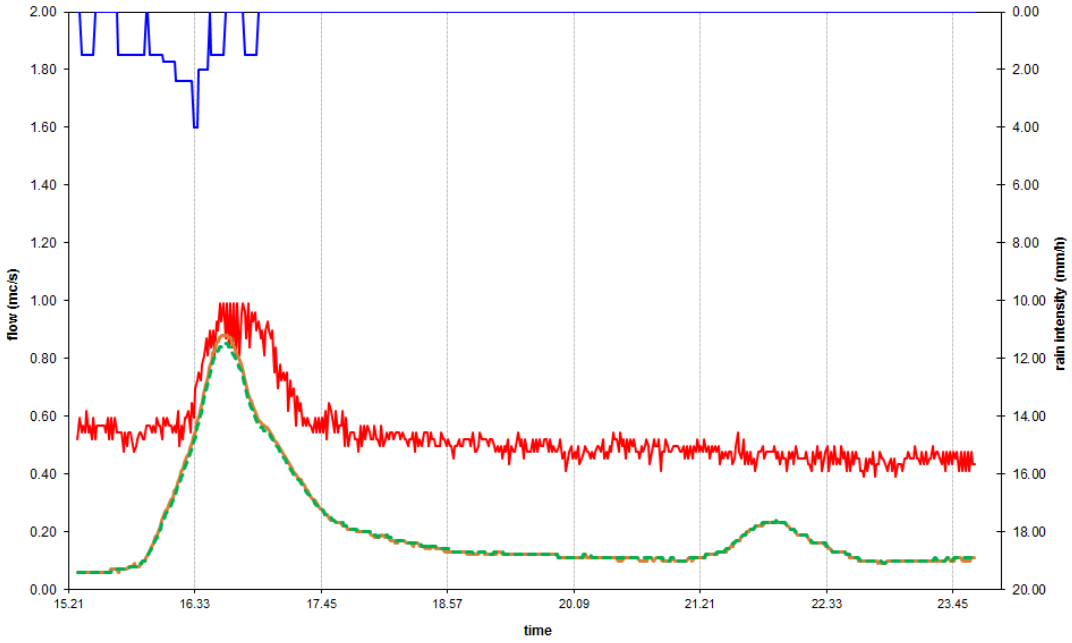

$(r_S^2 = 88.81\ \%\ ;\ r_{DD}^2 = 88.73\ \%)$

05/18/2007

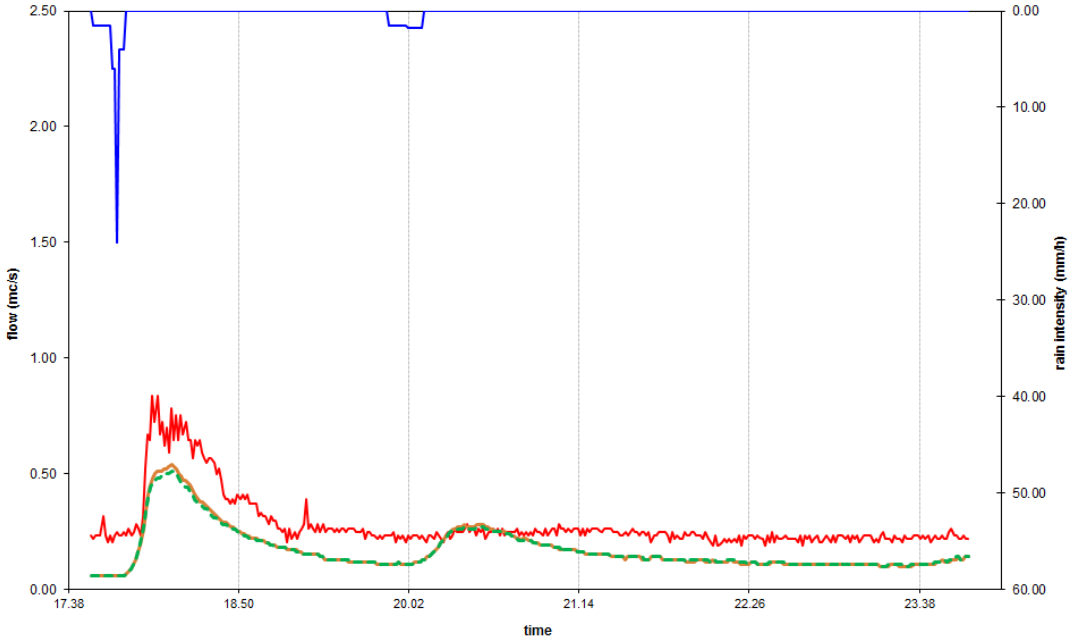

$(r_S^2 = 89.07\ \%\ ;\ r_{DD}^2 = 88.62\ \%)$

09/19/2007

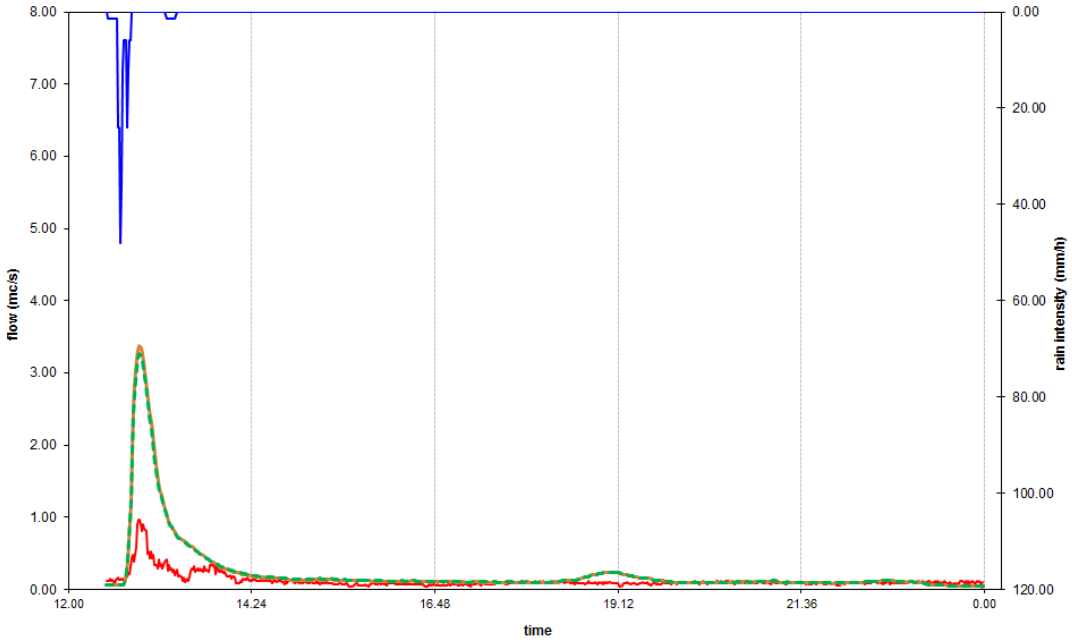

$(r_S^2 = 92.40\ \%\ ;\ r_{DD}^2 = 92.54\ \%)$

09/28/2007

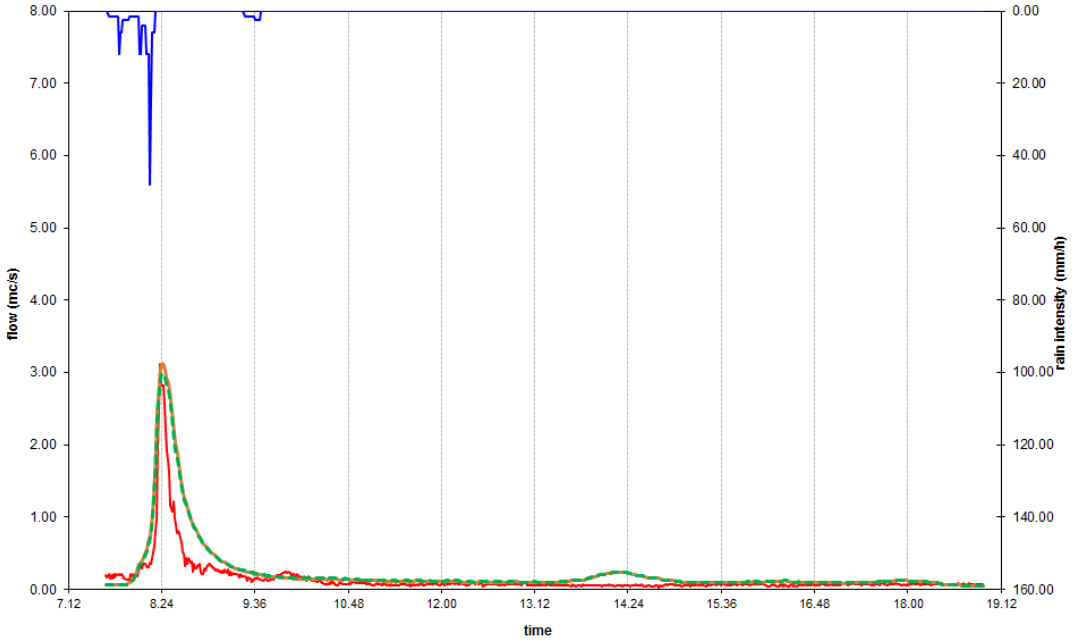

$(r_S^2 = 93.20\ \%\ ;\ r_{DD}^2 = 93.10\ \%)$

11/15/2008

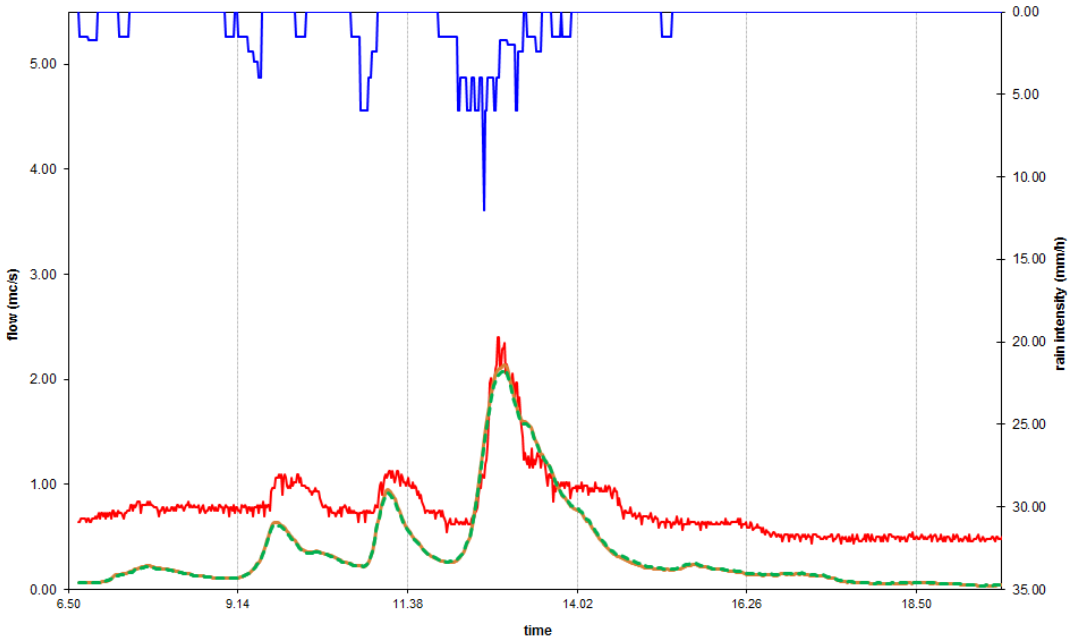

$(r_S^2 = 92.36\ \%\ ;\ r_{DD}^2 = 92.13\ \%)$

03/29/2009

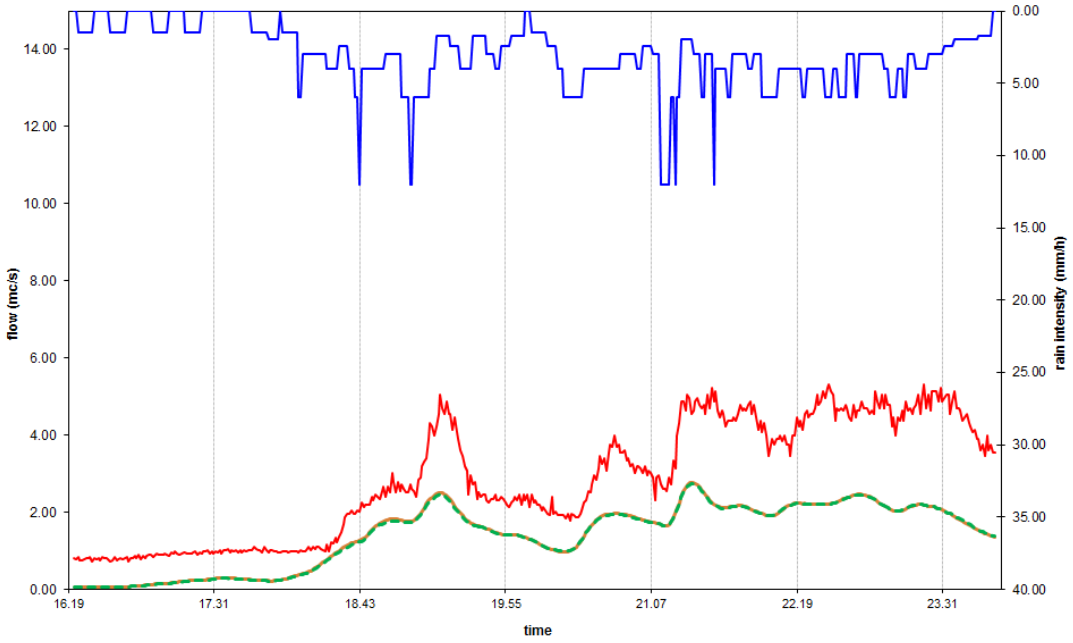

$(r_S^2 = 93.85\ \%\ ;\ r_{DD}^2 = 94.23\ \%)$

04/28/2009

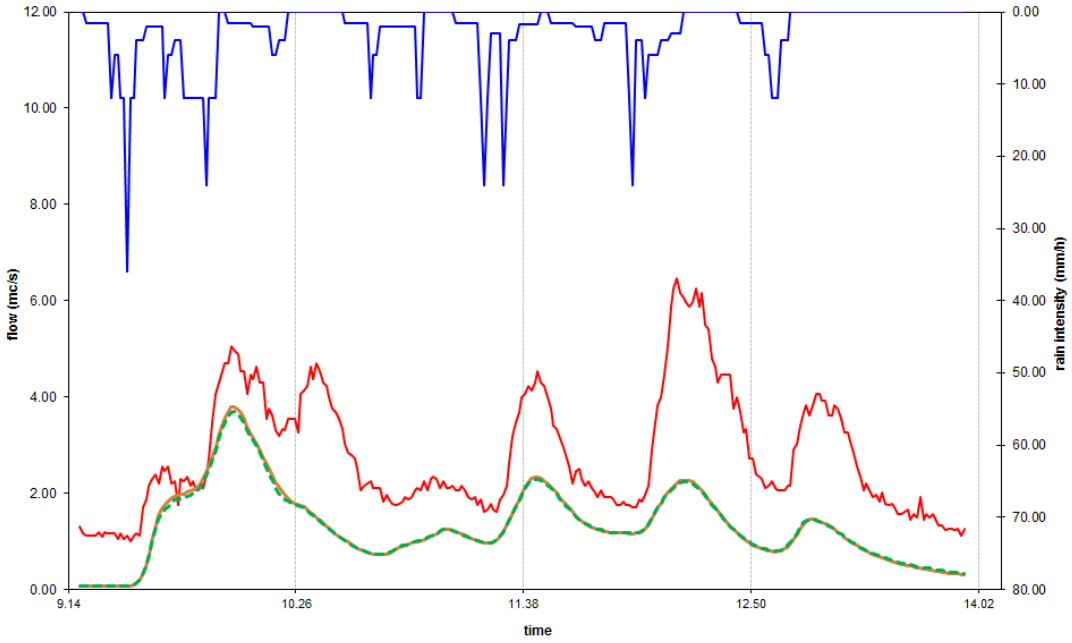

$(r_S^2 = 74.37\ \%\ ;\ r_{DD}^2 = 74.99\ \%)$

Appendix D – Storm tracking elaborations

Starting Date: 10/11/2006 19:45 – **Final Time:** 11/11/2006 03:45

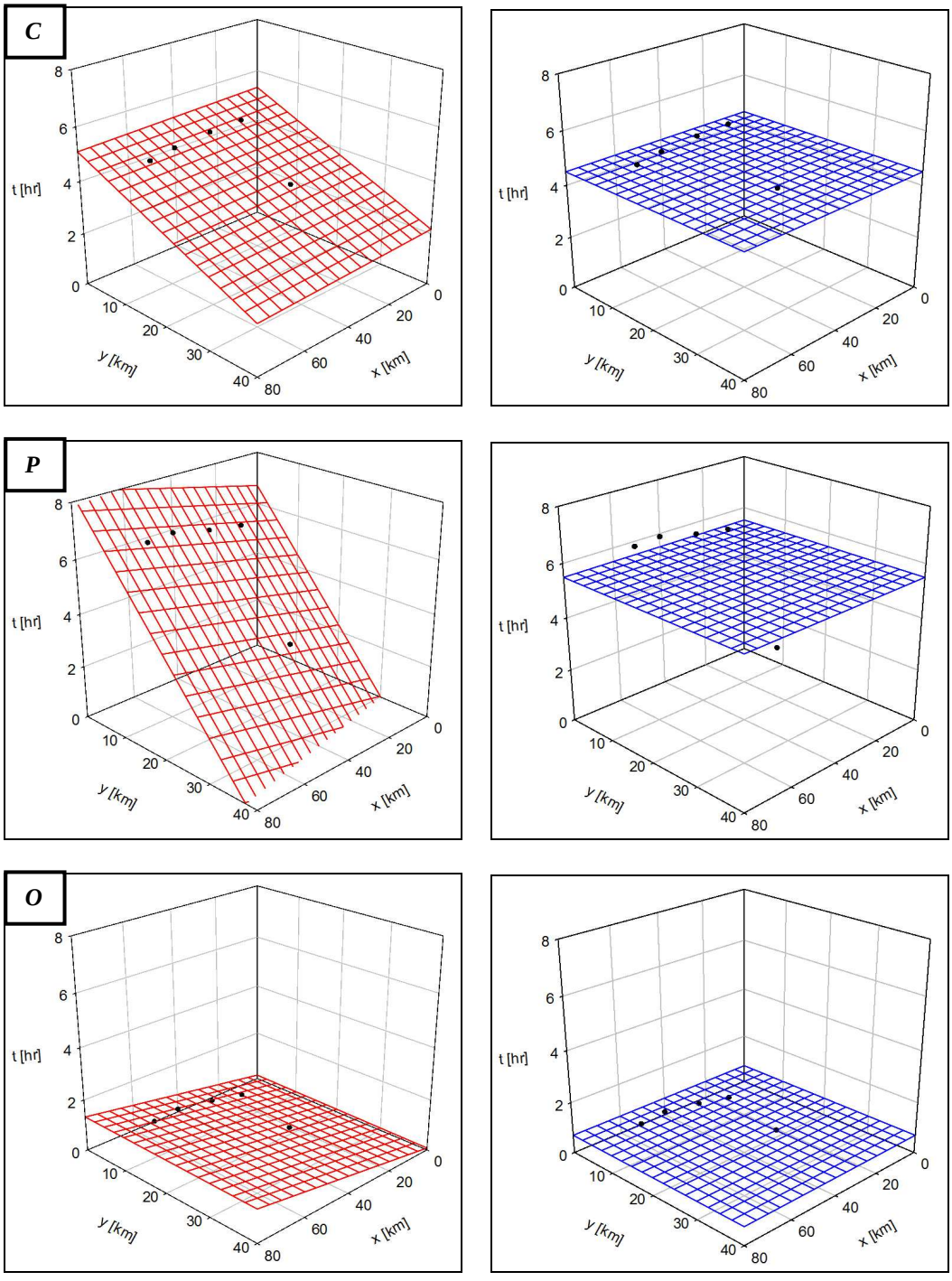

	Centroid			Peak			Onset		
	V [km / hr]	**θ** [° from N]	S. R.	**V** [km / hr]	**θ** [° from N]	S. R.	**V** [km / hr]	**θ** [° from N]	S. R.
n	12.65	2.08	0.26	4.47	174.68	0.15	67.33	97.12	0.32
n-1	12.44	72.22	0.17	6.79	141.84	0.13	54.25	80.29	0.28

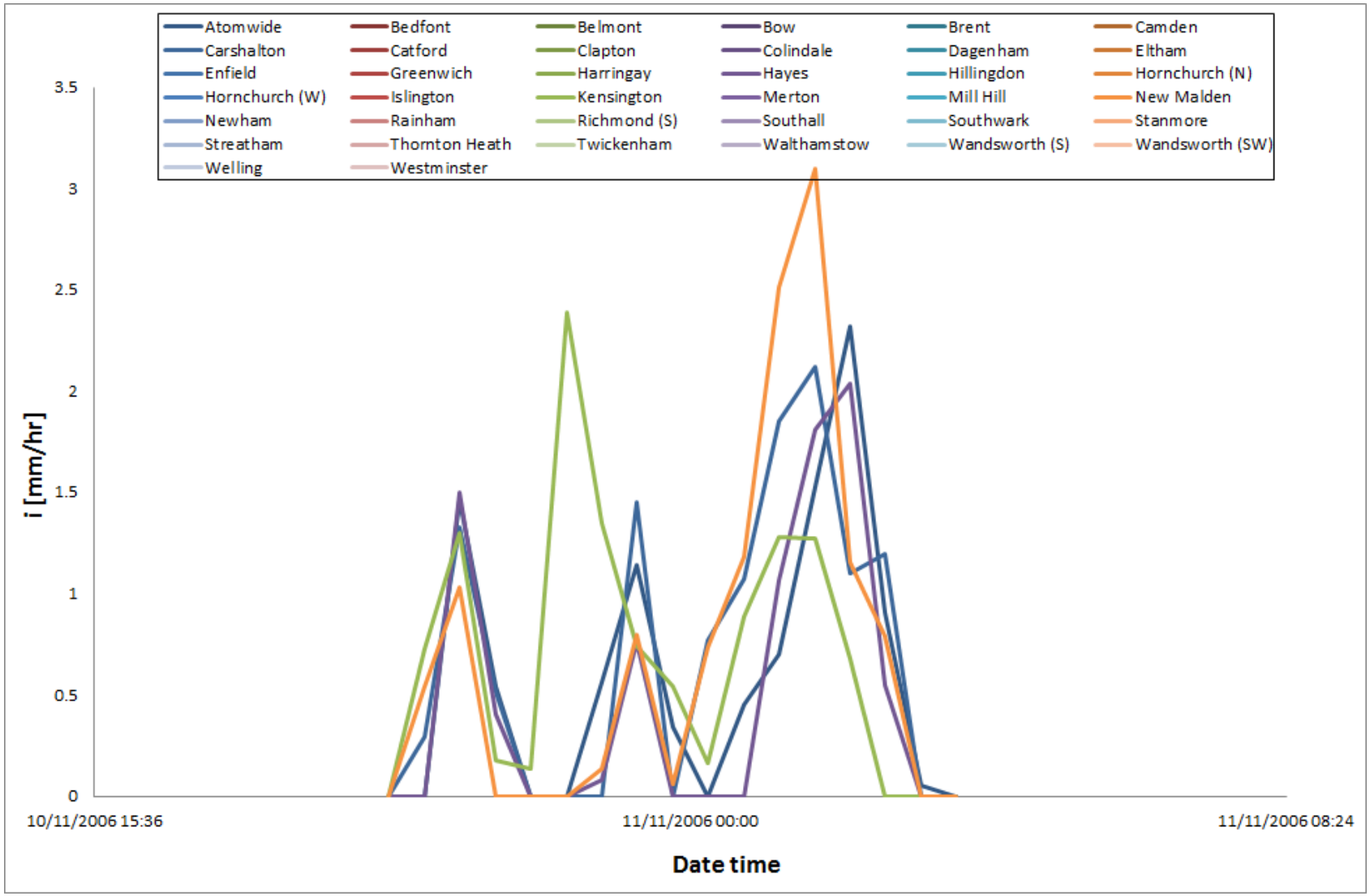
Atomwide
Bedfont
Belmont
Bow
Brent
Camden
Carshalton
Catford
Clapton
Colindale
Dagenham
Eltham
Enfield
Greenwich
Harringay
Hayes
Hillingdon
Hornchurch (N)
Hornchurch (W)
Islington
Kensington
Merton
Mill Hill
New Malden
Newham
Rainham
Richmond (S)
Southall
Southwark
Stanmore
Streatham
Thornton Heath
Twickenham
Walthamstow
Wandsworth (S)
Wandsworth (SW)
Welling
Westminster
3.5
3
2.5
2
1.5
1
0.5
0
i [mm/hr]
10/11/2006 15:36
11/11/2006 00:00
11/11/2006 08:24
Date time

Starting Date: 05/12/2006 05:15 – **Final Time:** 05/12/2006 12:45

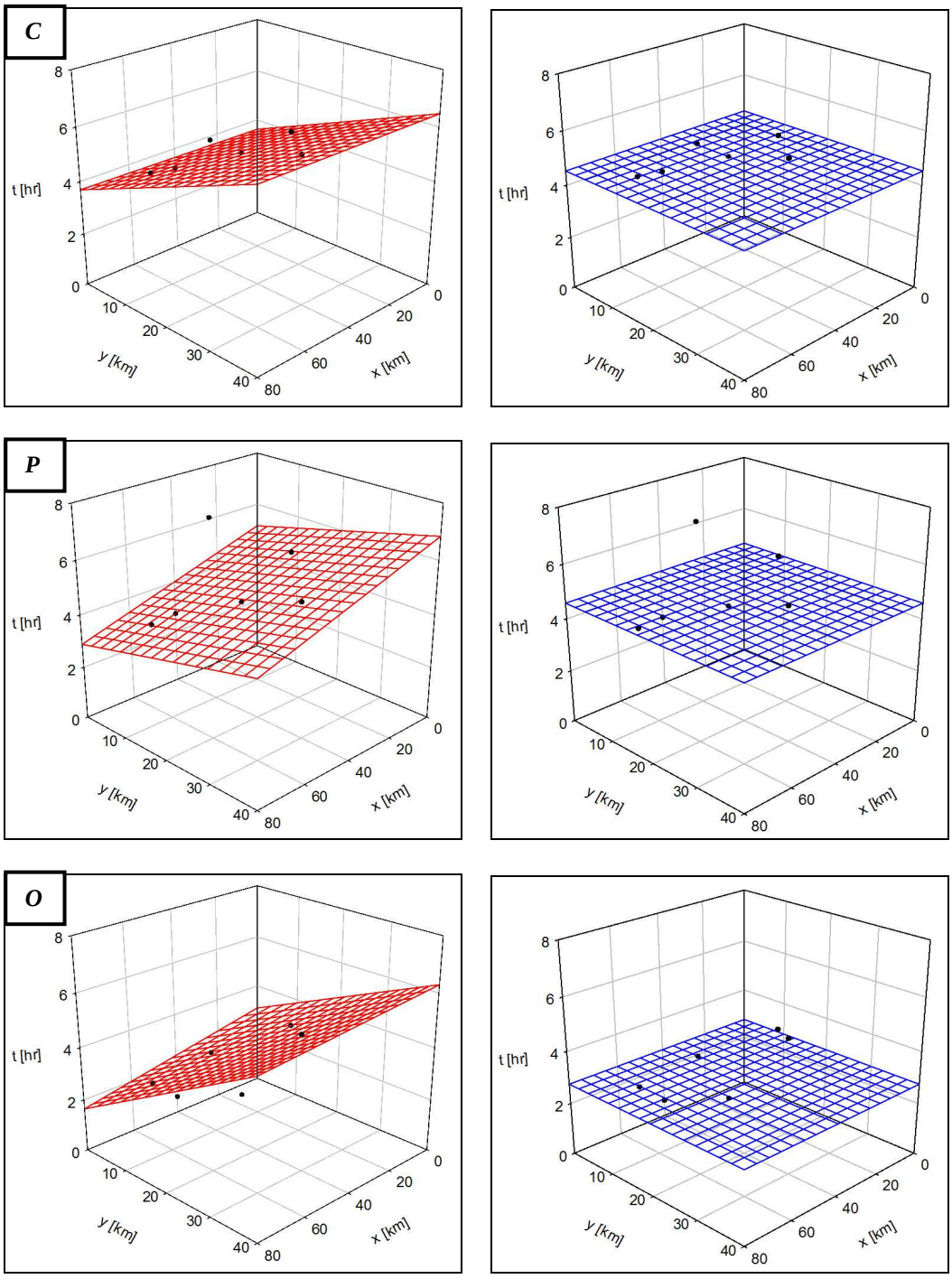

	Centroid			Peak			Onset		
	V [km / hr]	**θ** [° from N]	S. R.	**V** [km / hr]	**θ** [° from N]	S. R.	**V** [km / hr]	**θ** [° from N]	S. R.
n	13.97	0.81	0.42	19.49	146.90	0.89	6.40	7.10	0.45
n-1	14.02	59.59	0.38	18.39	144.17	0.77	6.48	35.61	0.41

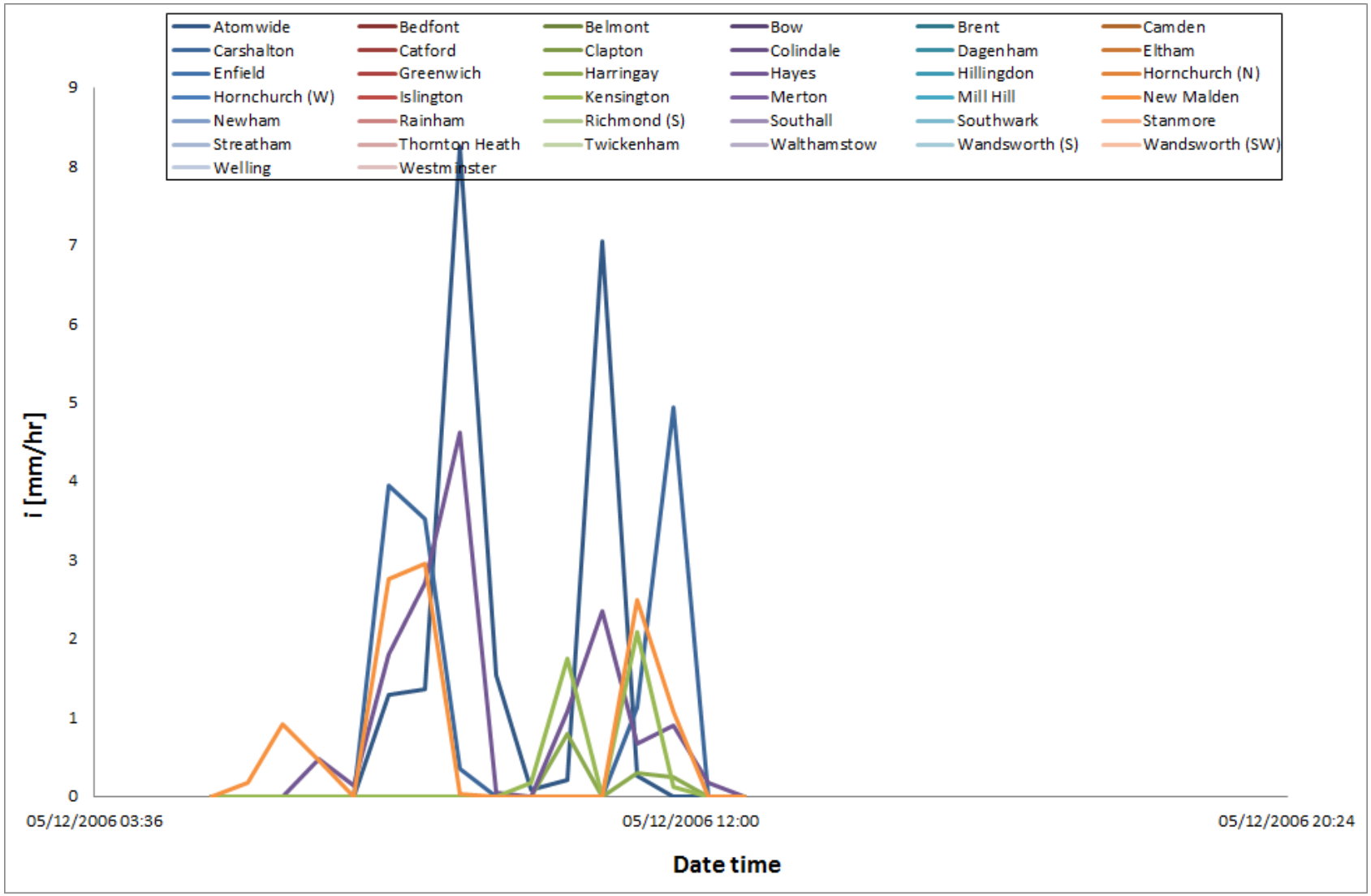
Atomwide
Bedfont
Belmont
Bow
Brent
Camden
Carshalton
Catford
Clapton
Colindale
Dagenham
Eltham
Enfield
Greenwich
Harringay
Hayes
Hillingdon
Hornchurch (N)
Hornchurch (W)
Islington
Kensington
Merton
Mill Hill
New Malden
Newham
Rainham
Richmond (S)
Southall
Southwark
Stanmore
Streatham
Thornton Heath
Twickenham
Walthamstow
Wandsworth (S)
Wandsworth (SW)
Welling
Westminster
i [mm/hr]
0
1
2
3
4
5
6
7
8
9
05/12/2006 03:36
05/12/2006 12:00
05/12/2006 20:24
Date time

Starting Date: 07/12/2006 01:15 – **Final Time:** 07/12/2006 09:15

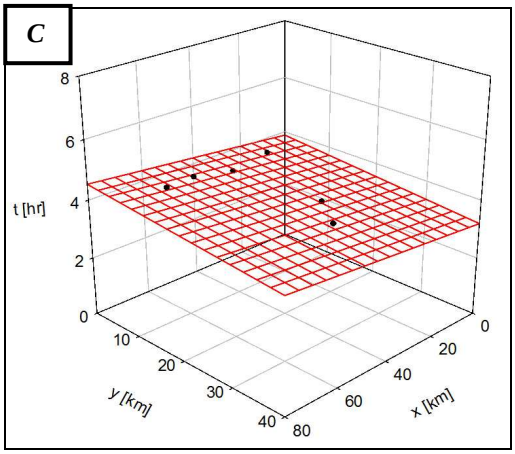

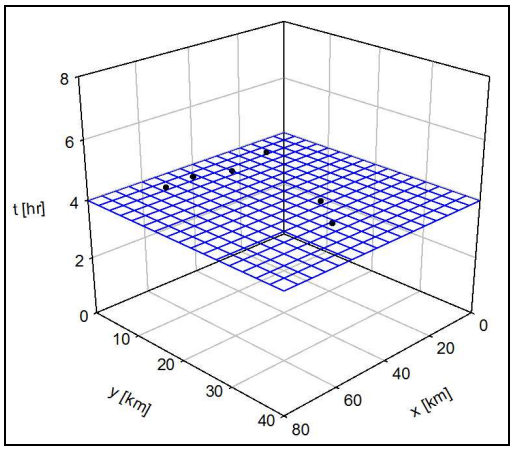

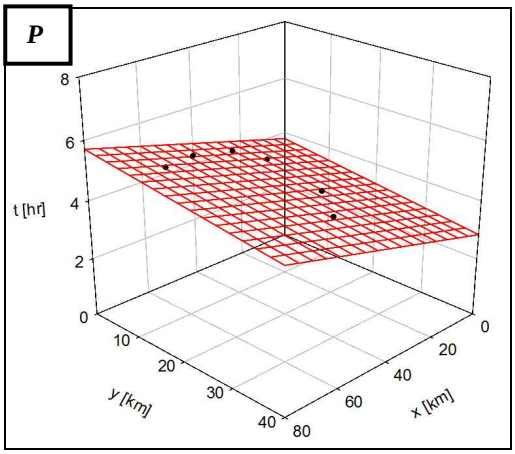

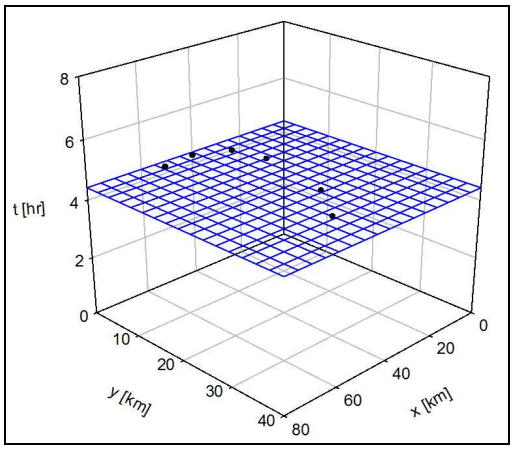

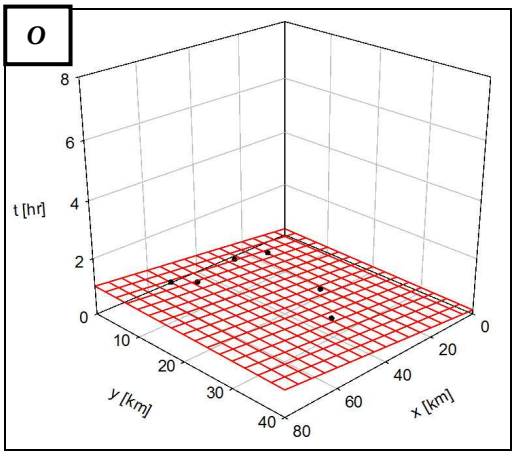

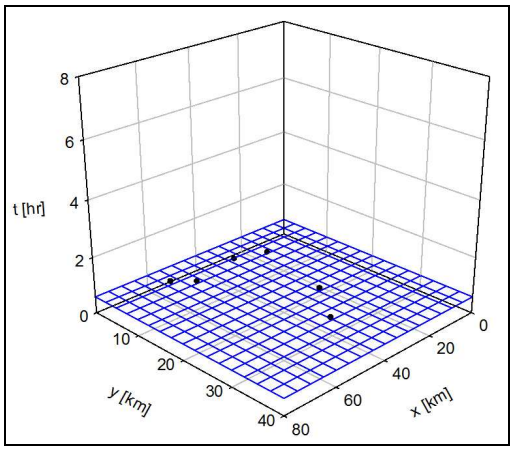

	Centroid			Peak			Onset		
	V [km / hr]	**θ** [° from N]	S. R.	**V** [km / hr]	**θ** [° from N]	S. R.	**V** [km / hr]	**θ** [° from N]	S. R.
n	53.27	153.96	0.65	29.75	133.86	0.22	100.81	105.03	0.65
n-1	51.43	151.37	0.57	29.59	133.61	0.20			

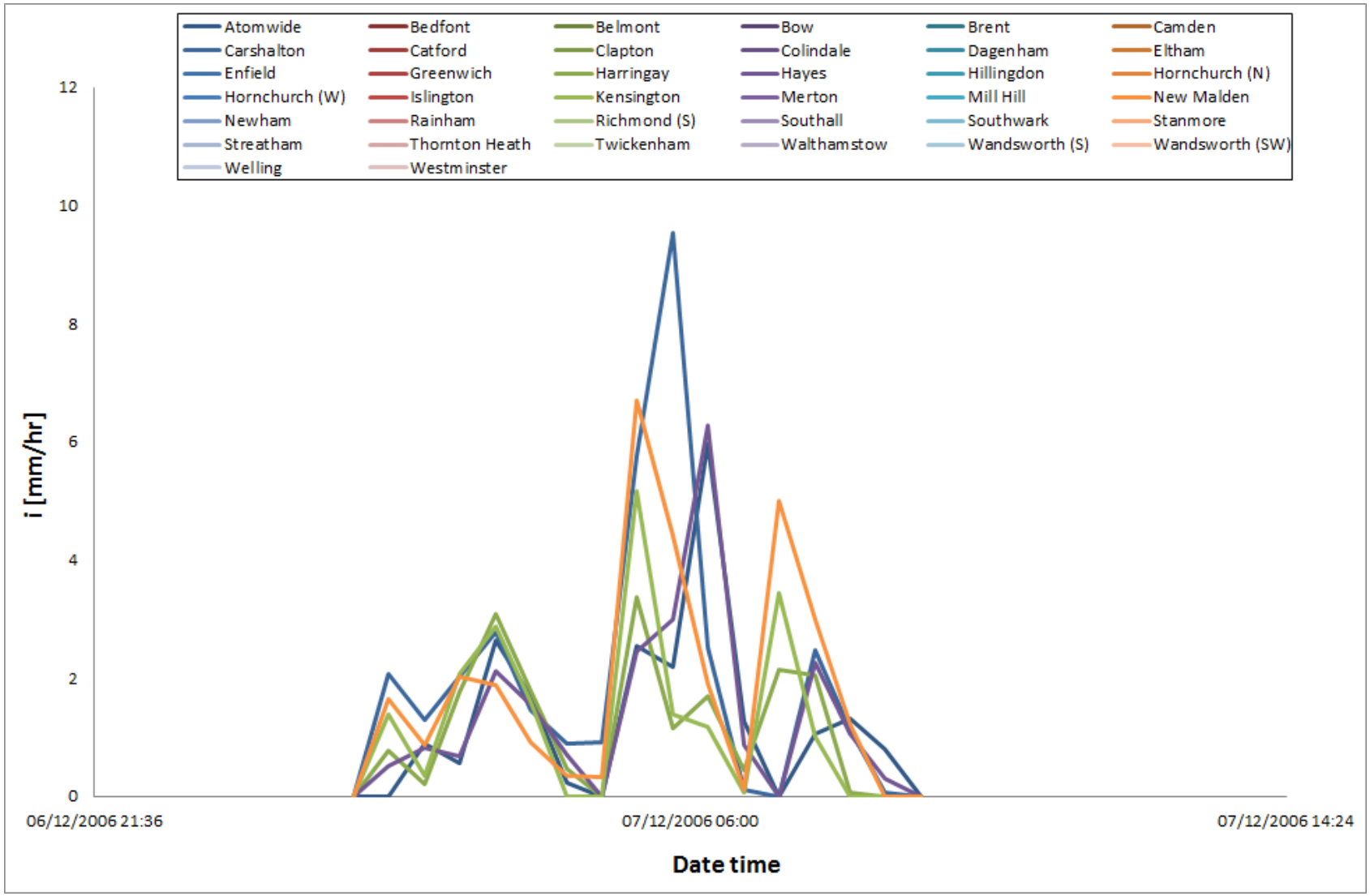
Atomwide
Bedfont
Belmont
Bow
Brent
Camden
Carshalton
Catford
Clapton
Colindale
Dagenham
Eltham
Enfield
Greenwich
Harringay
Hayes
Hillingdon
Hornchurch (N)
Hornchurch (W)
Islington
Kensington
Merton
Mill Hill
New Malden
Newham
Rainham
Richmond (S)
Southall
Southwark
Stanmore
Streatham
Thornton Heath
Twickenham
Walthamstow
Wandsworth (S)
Wandsworth (SW)
Welling
Westminster
12
10
8
6
4
2
0
i [mm/hr]
06/12/2006 21:36
07/12/2006 06:00
07/12/2006 14:24
Date time

Starting Date: 06/01/2007 09:45 – **Final Time:** 06/01/2007 17:15

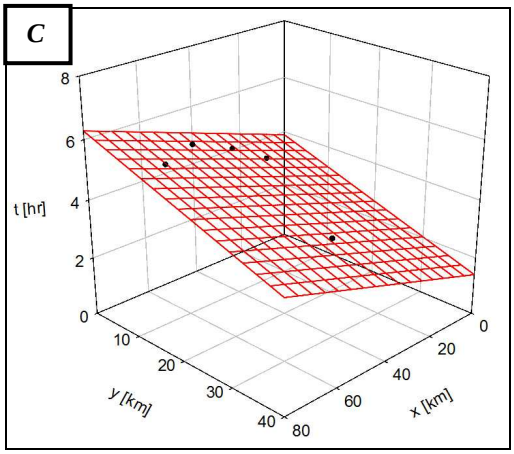

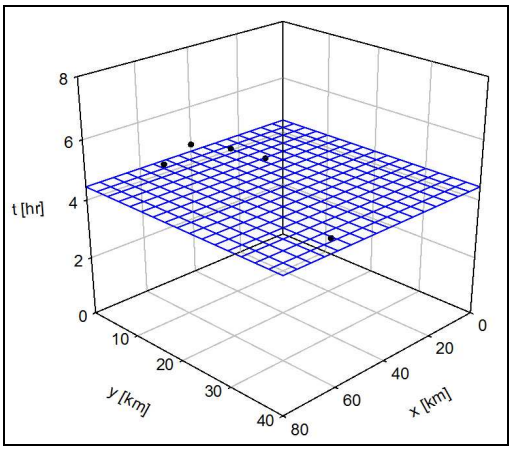

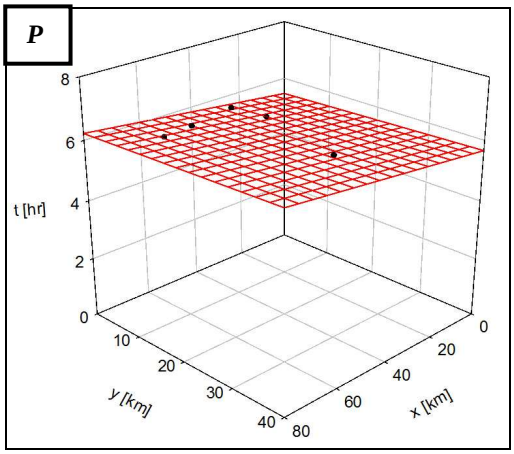

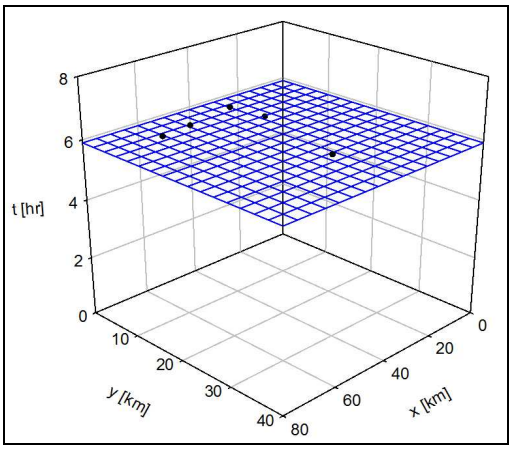

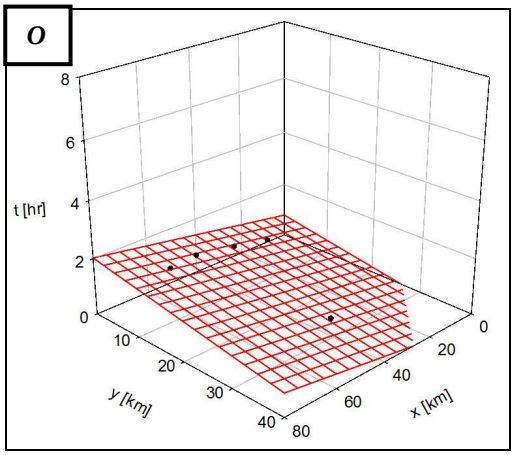

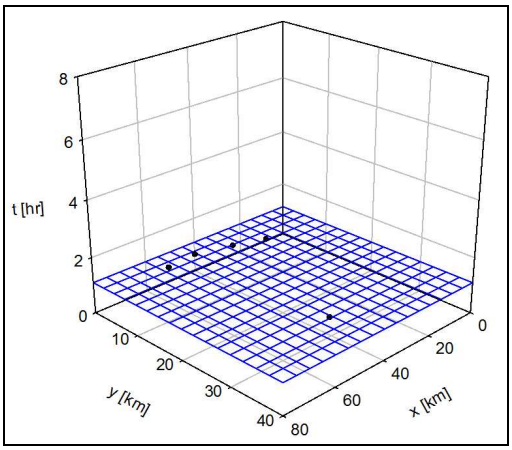

	Centroid			Peak			Onset		
	V [km / hr]	**θ** [° from N]	S. R.	**V** [km / hr]	**θ** [° from N]	S. R.	**V** [km / hr]	**θ** [° from N]	S. R.
n	14.52	154.31	0.26	89.71	60.33	0.68	29.39	153.23	0.25
n-1	12.97	156.47	0.21				26.41	124.08	0.22

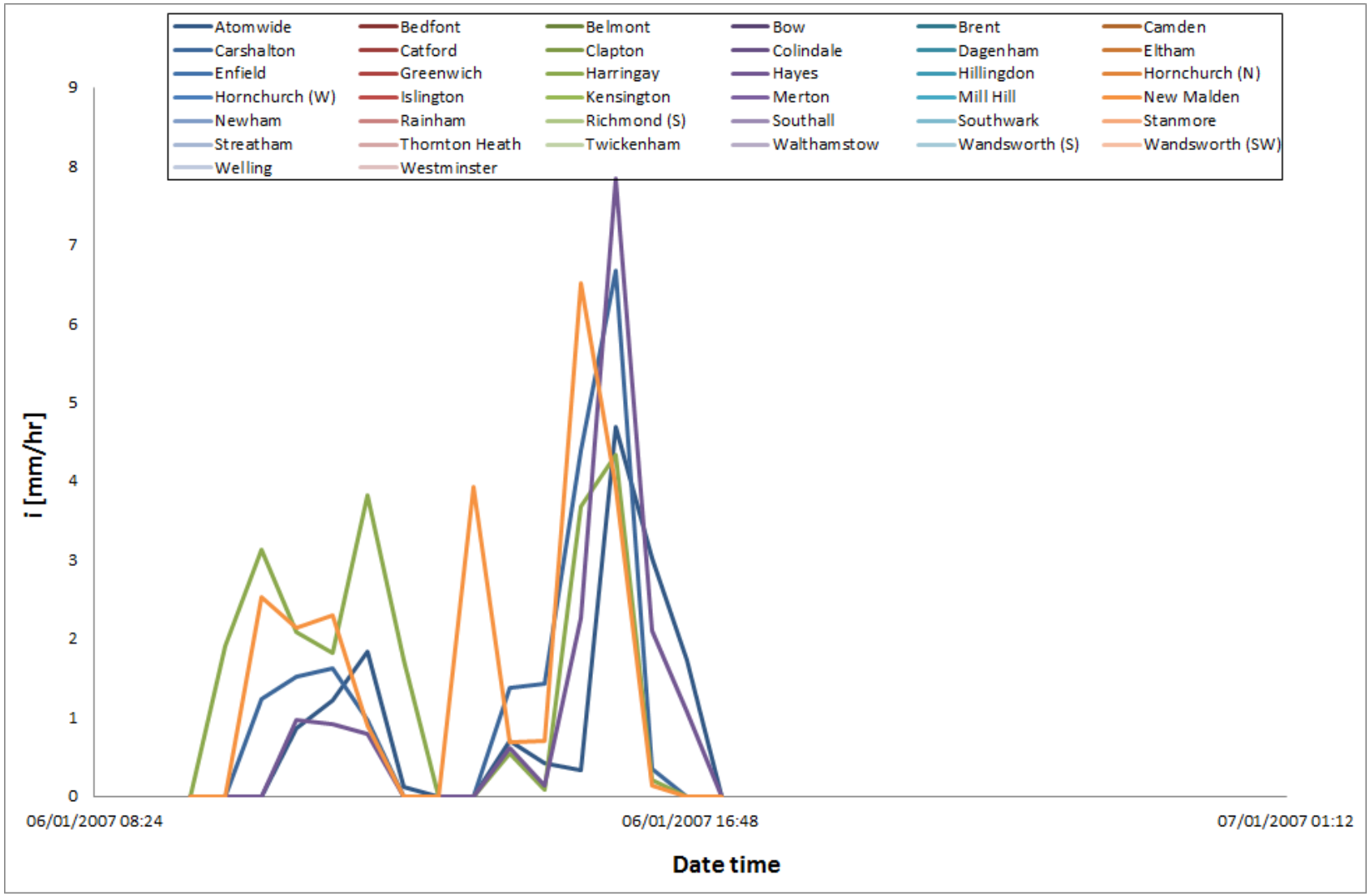
Atomwide
Bedfont
Belmont
Bow
Brent
Camden
Carshalton
Catford
Clapton
Colindale
Dagenham
Eltham
Enfield
Greenwich
Harringay
Hayes
Hillingdon
Hornchurch (N)
Hornchurch (W)
Islington
Kensington
Merton
Mill Hill
New Malden
Newham
Rainham
Richmond (S)
Southall
Southwark
Stanmore
Streatham
Thornton Heath
Twickenham
Walthamstow
Wandsworth (S)
Wandsworth (SW)
Welling
Westminster
i [mm/hr]
0
1
2
3
4
5
6
7
8
9
06/01/2007 08:24
06/01/2007 16:48
07/01/2007 01:12
Date time

Starting Date: 10/01/2007 03:15 – **Final Time:** 10/01/2007 12:45

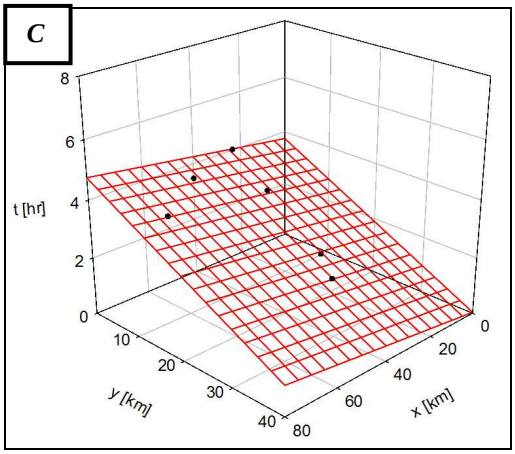

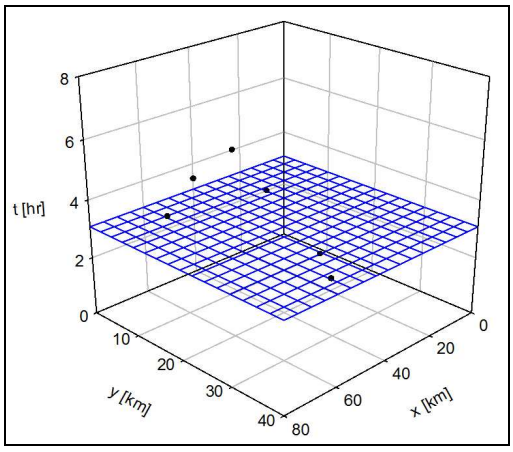

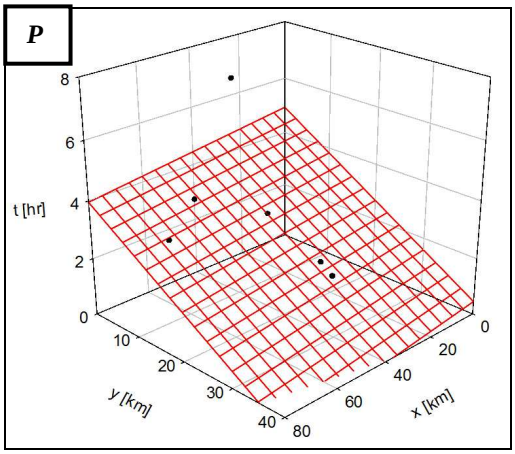

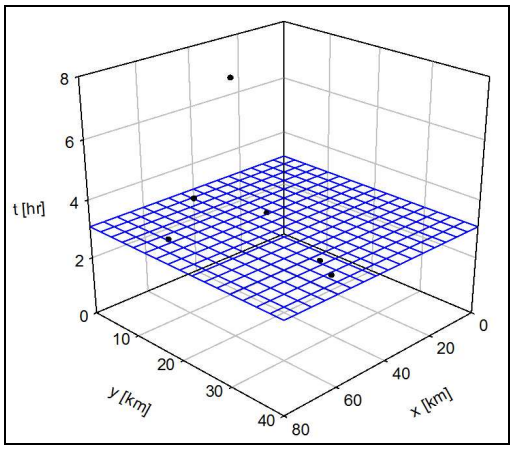

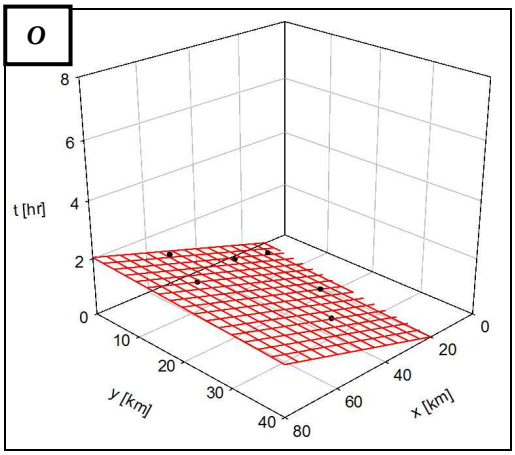

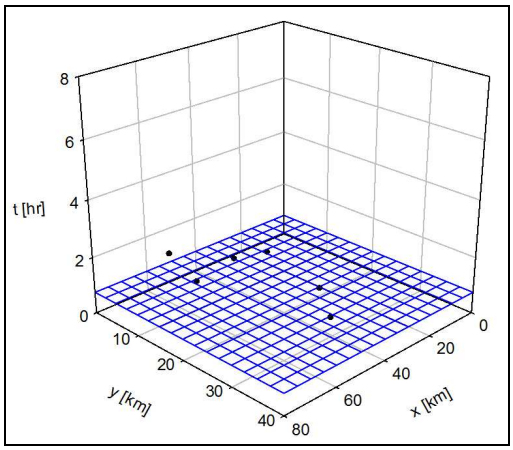

	Centroid			Peak			Onset		
	V [km / hr]	**θ** [° from N]	S. R.	**V** [km / hr]	**θ** [° from N]	S. R.	**V** [km / hr]	**θ** [° from N]	S. R.
n	10.68	172.32	0.50	8.86	6.25	0.84	33.60	105.03	0.65
n-1	10.37	141.68	0.46	10.35	59.38	0.74			

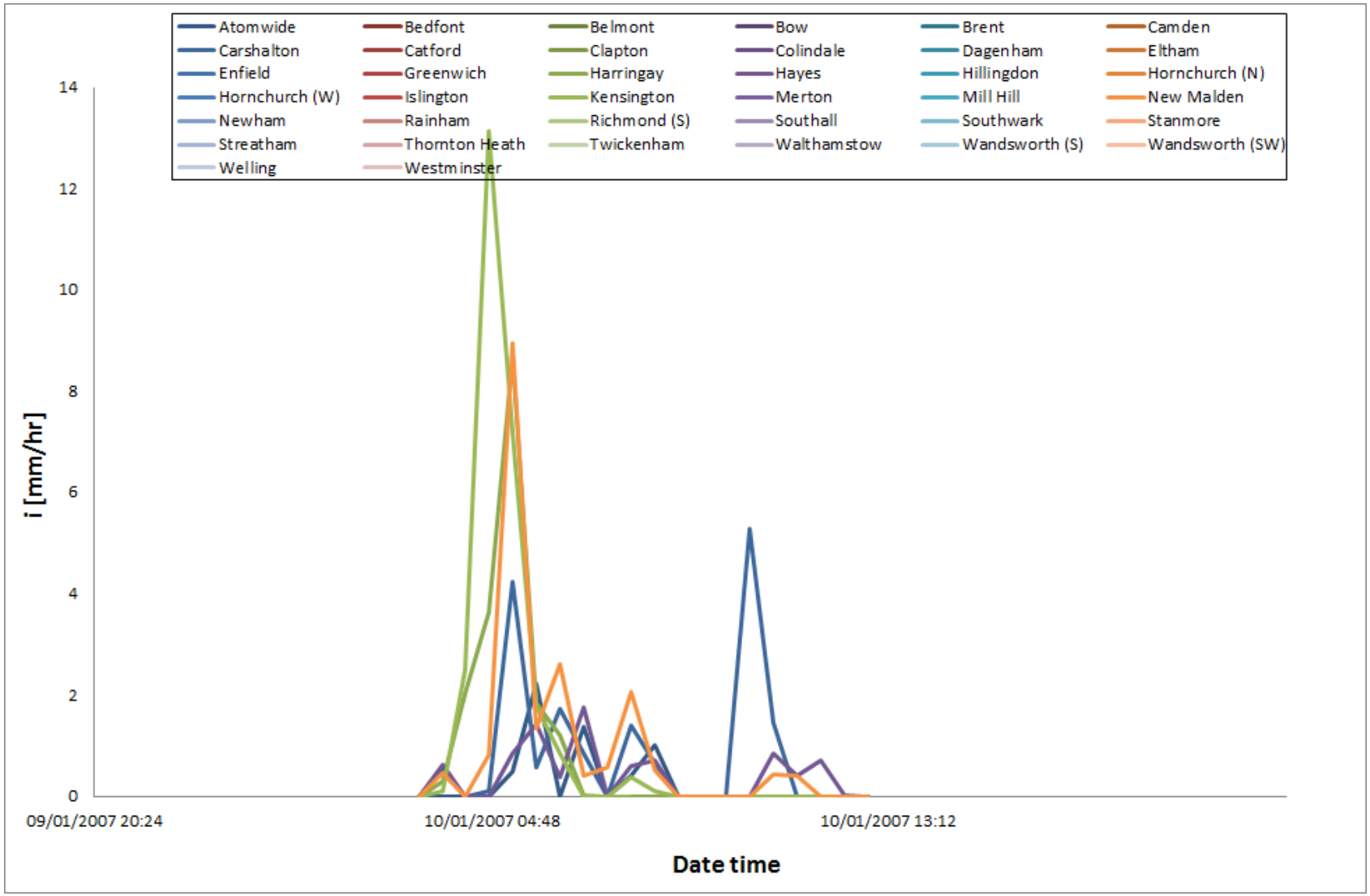
Atomwide
Bedfont
Belmont
Bow
Brent
Camden
Carshalton
Catford
Clapton
Colindale
Dagenham
Eltham
Enfield
Greenwich
Harringay
Hayes
Hillingdon
Hornchurch (N)
Hornchurch (W)
Islington
Kensington
Merton
Mill Hill
New Malden
Newham
Rainham
Richmond (S)
Southall
Southwark
Stanmore
Streatham
Thornton Heath
Twickenham
Walthamstow
Wandsworth (S)
Wandsworth (SW)
Welling
Westminster
14
12
10
8
6
4
2
0
i [mm/hr]
09/01/2007 20:24
10/01/2007 04:48
10/01/2007 13:12
Date time

Starting Date: 17/01/2007 06:15 – **Final Time:** 17/01/2007 12:45

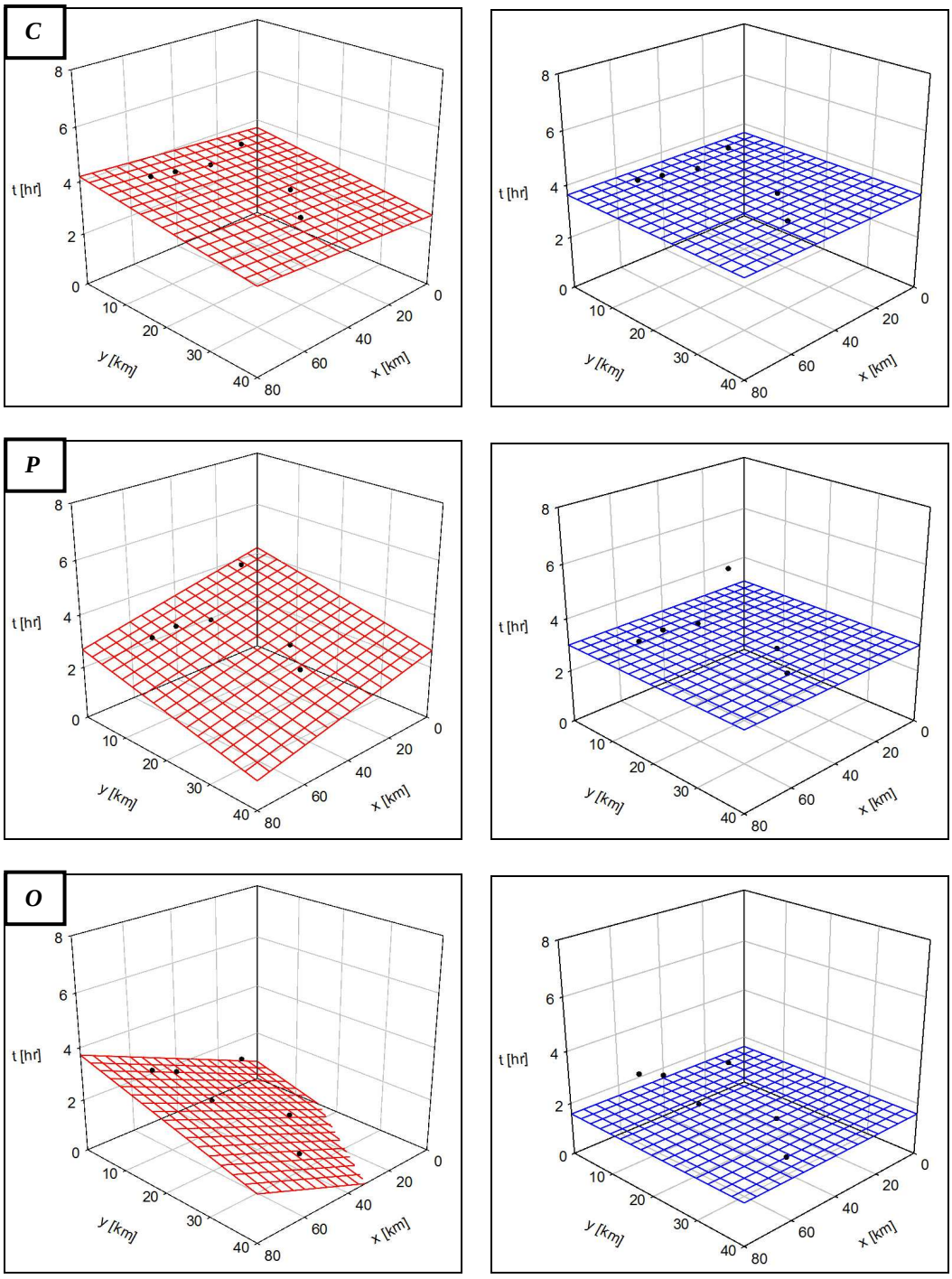

	Centroid			Peak			Onset		
	V [km / hr]	**θ** [° from N]	S. R.	**V** [km / hr]	**θ** [° from N]	S. R.	**V** [km / hr]	**θ** [° from N]	S. R.
n	40.63	165.01	0.66	22.60	26.05	0.81	16.43	142.59	0.64
n-1	41.47	132.22	0.58	26.48	43.69	0.67	16.89	136.97	0.56

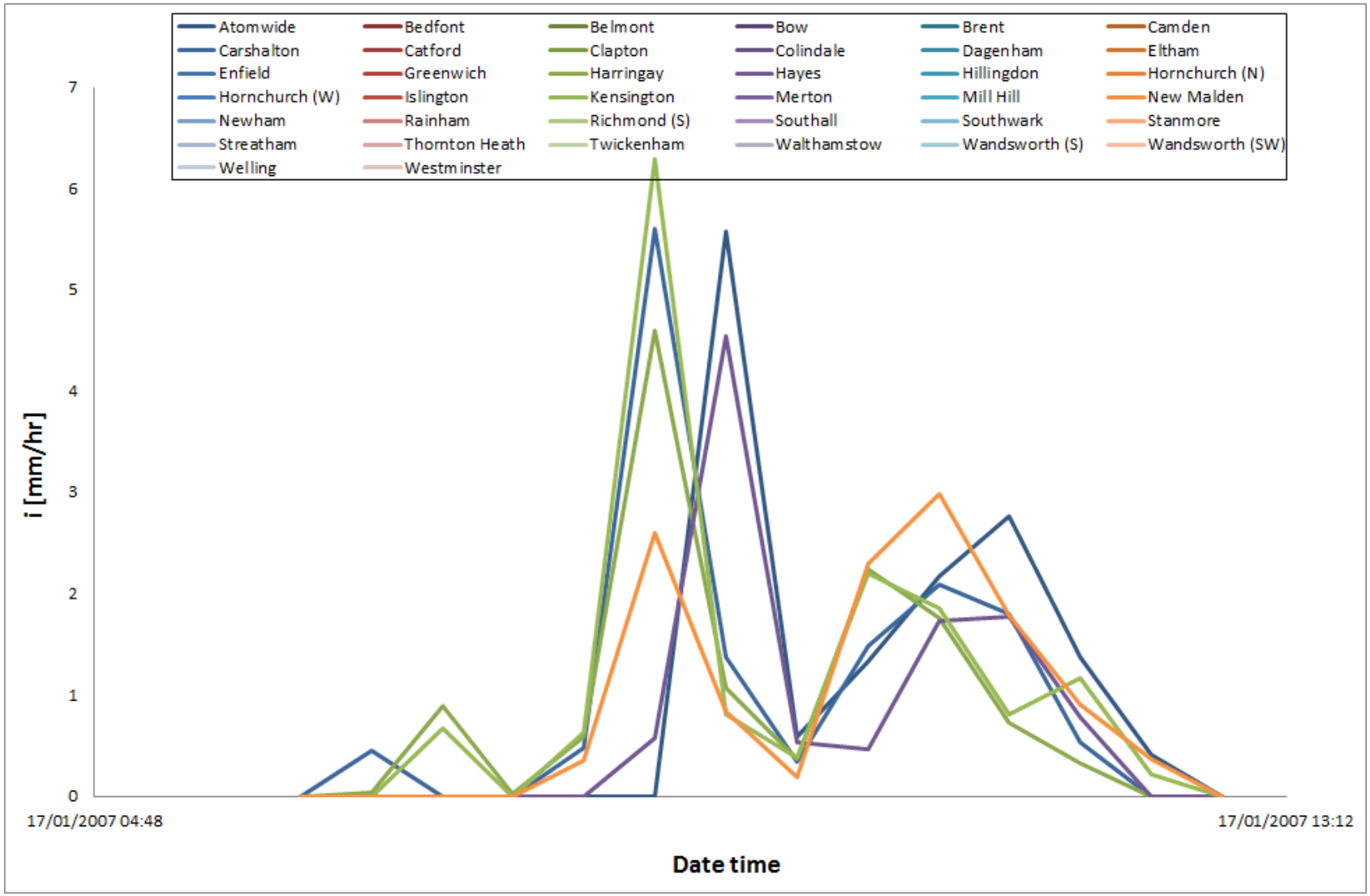
Atomwide
Bedfont
Belmont
Bow
Brent
Camden
Carshalton
Catford
Clapton
Colindale
Dagenham
Eltham
Enfield
Greenwich
Harringay
Hayes
Hillingdon
Hornchurch (N)
Hornchurch (W)
Islington
Kensington
Merton
Mill Hill
New Malden
Newham
Rainham
Richmond (S)
Southall
Southwark
Stanmore
Streatham
Thornton Heath
Twickenham
Walthamstow
Wandsworth (S)
Wandsworth (SW)
Welling
Westminster
i [mm/hr]
0
1
2
3
4
5
6
7
17/01/2007 04:48
17/01/2007 13:12
Date time

Starting Date: 13/02/2007 18:15 – **Final Time:** 14/02/2007 11:45

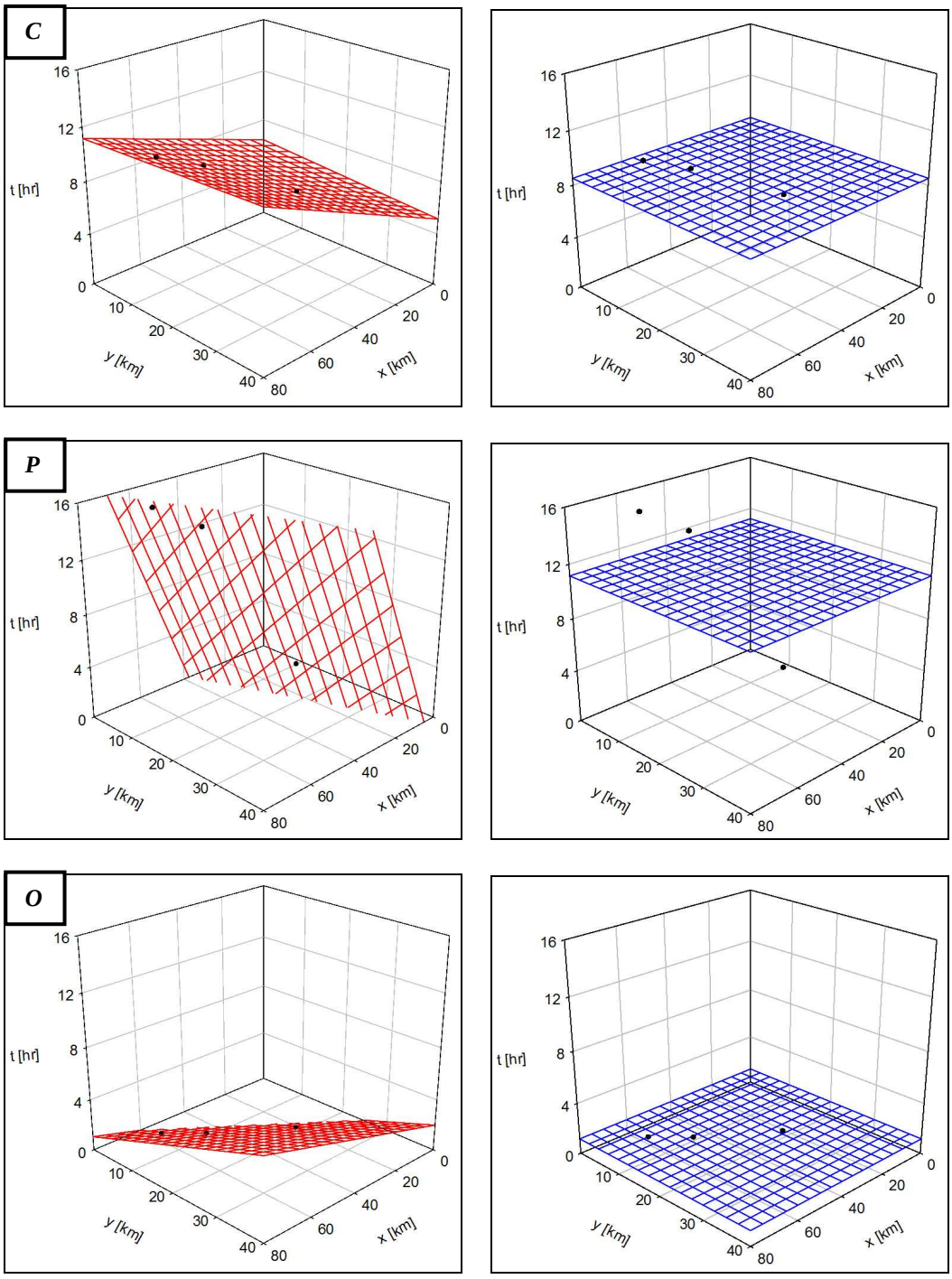

	Centroid			Peak			Onset		
	V [km / hr]	**θ** [° from N]	S. R.	**V** [km / hr]	**θ** [° from N]	S. R.	**V** [km / hr]	**θ** [° from N]	S. R.
n	5.64	48.83	0.00	1.50	50.69	0.00	7.14	22.24	0.00
n-1	12.62	55.55	0.04	4.17	162.11	0.02			

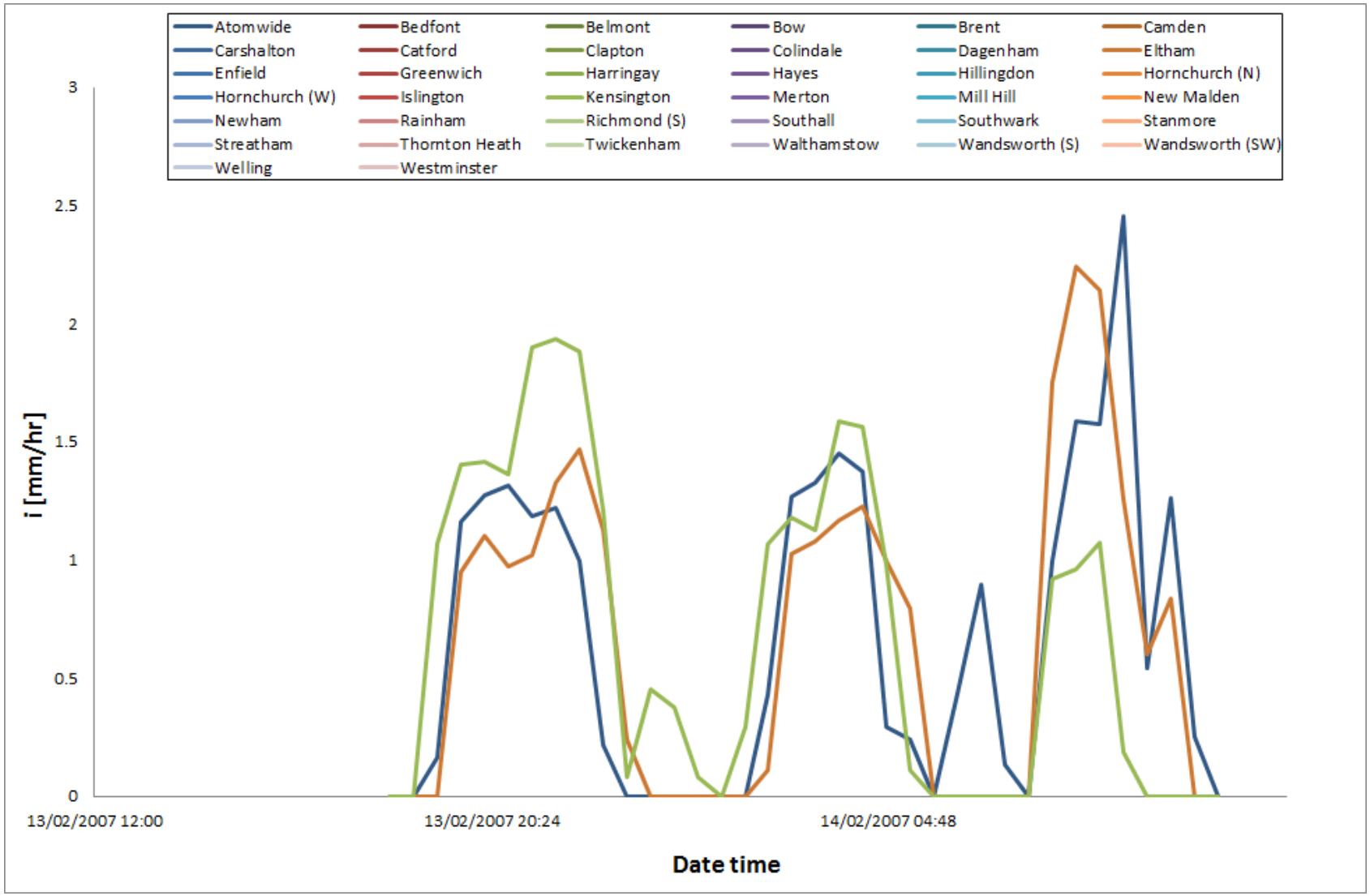
Atomwide
Bedfont
Belmont
Bow
Brent
Camden
Carshalton
Catford
Clapton
Colindale
Dagenham
Eltham
Enfield
Greenwich
Harringay
Hayes
Hillingdon
Hornchurch (N)
Hornchurch (W)
Islington
Kensington
Merton
Mill Hill
New Malden
Newham
Rainham
Richmond (S)
Southall
Southwark
Stanmore
Streatham
Thornton Heath
Twickenham
Walthamstow
Wandsworth (S)
Wandsworth (SW)
Welling
Westminster
3
2.5
2
1.5
1
0.5
0
i [mm/hr]
13/02/2007 12:00
13/02/2007 20:24
14/02/2007 04:48
Date time

Starting Date: 27/05/2007 14:45 – **Final Time:** 28/05/2007 07:45

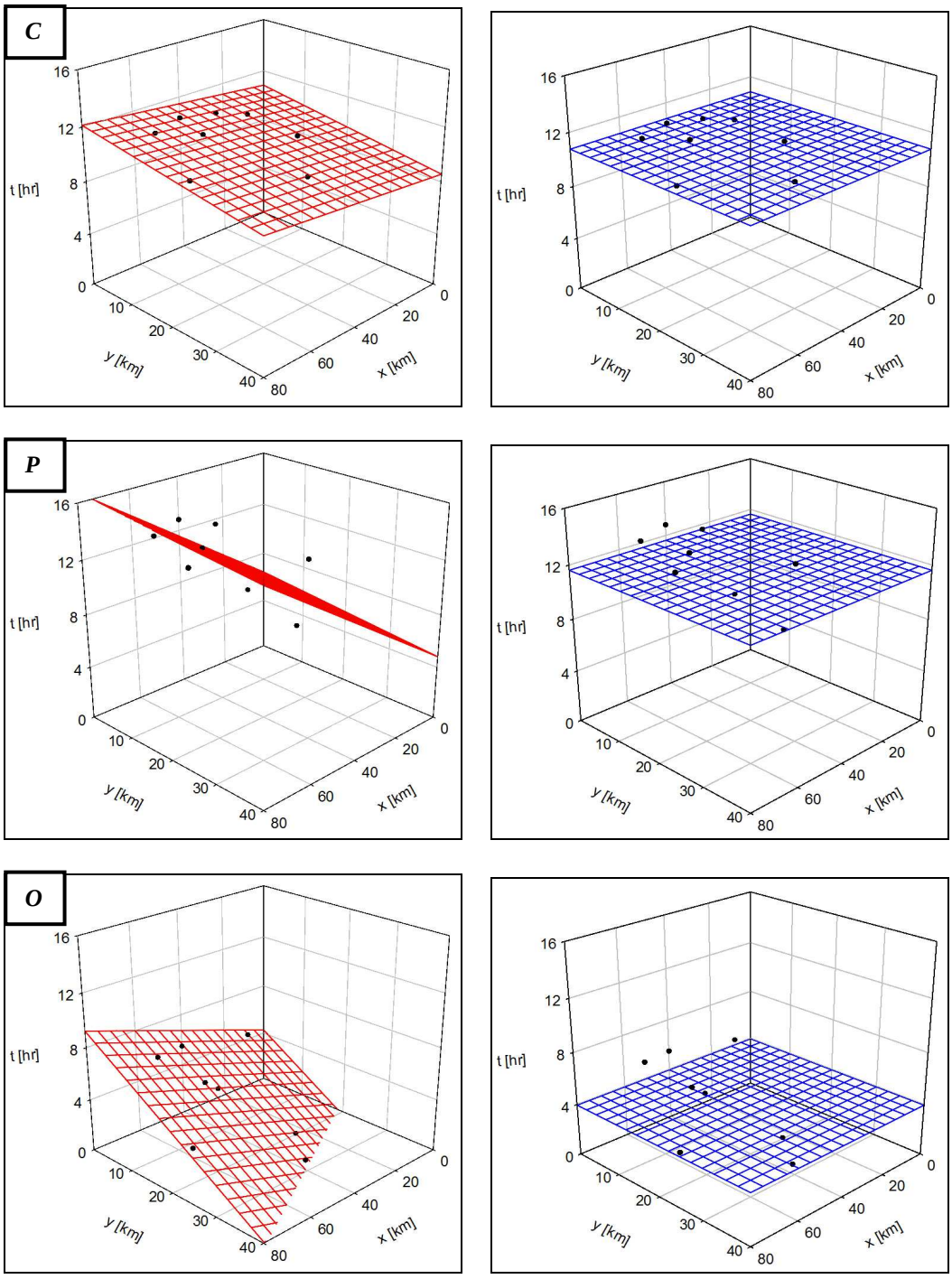

	Centroid			Peak			Onset		
	V [km / hr]	**θ** [° from N]	S. R.	**V** [km / hr]	**θ** [° from N]	S. R.	**V** [km / hr]	**θ** [° from N]	S. R.
n	16.83	164.48	0.66	7.43	107.47	0.64	4.22	164.84	0.58
n-1	17.87	163.45	0.65	7.22	105.72	0.61	4.25	163.93	0.55

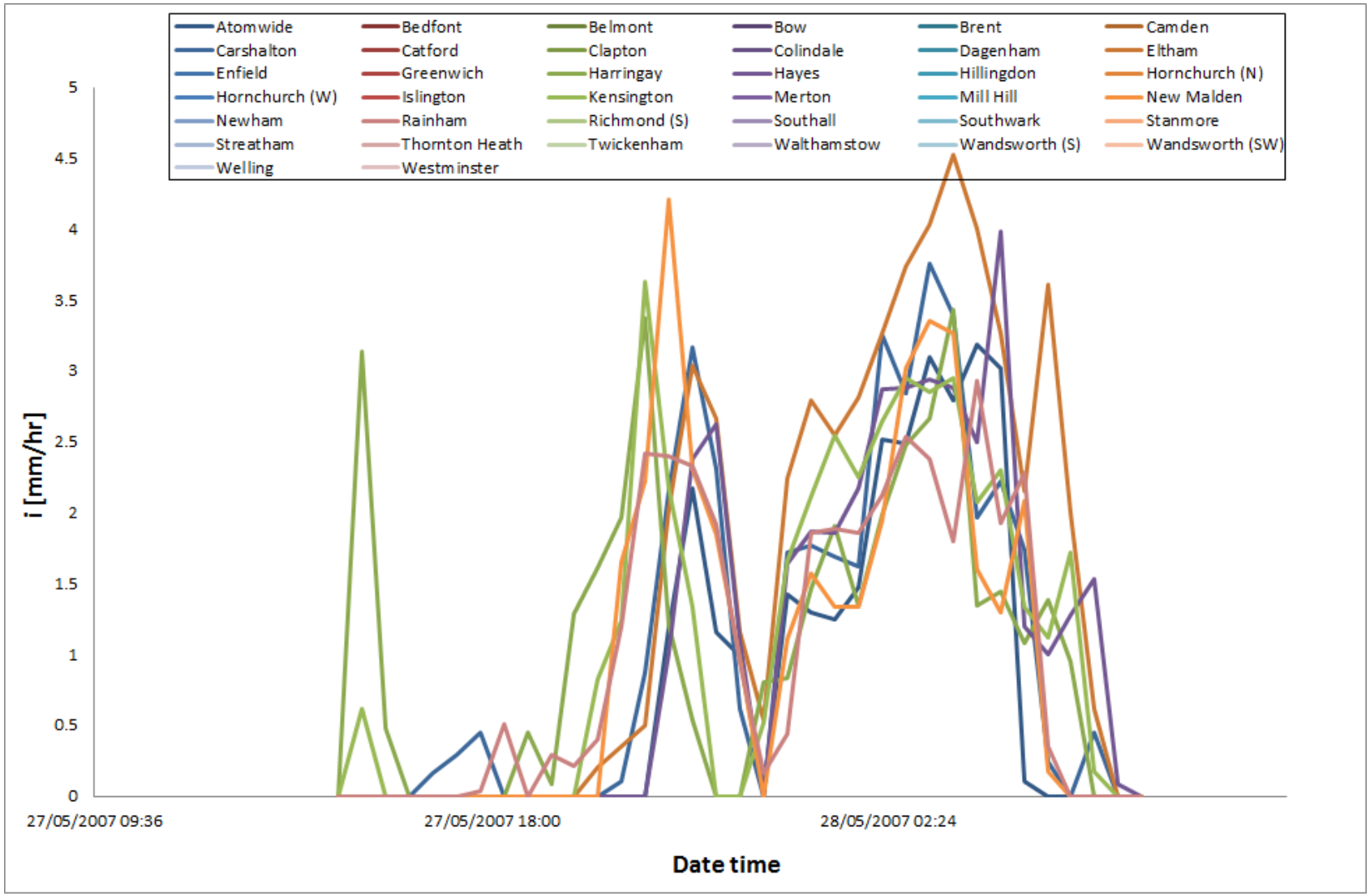
Atomwide
Bedfont
Belmont
Bow
Brent
Camden
Carshalton
Catford
Clapton
Colindale
Dagenham
Eltham
Enfield
Greenwich
Harringay
Hayes
Hillingdon
Hornchurch (N)
Hornchurch (W)
Islington
Kensington
Merton
Mill Hill
New Malden
Newham
Rainham
Richmond (S)
Southall
Southwark
Stanmore
Streatham
Thornton Heath
Twickenham
Walthamstow
Wandsworth (S)
Wandsworth (SW)
Welling
Westminster
5
4.5
4
3.5
3
2.5
2
1.5
1
0.5
0
i [mm/hr]
27/05/2007 09:36
27/05/2007 18:00
28/05/2007 02:24
Date time

Starting Date: 09/10/2007 07:15 – **Final Time:** 09/10/2007 18:45

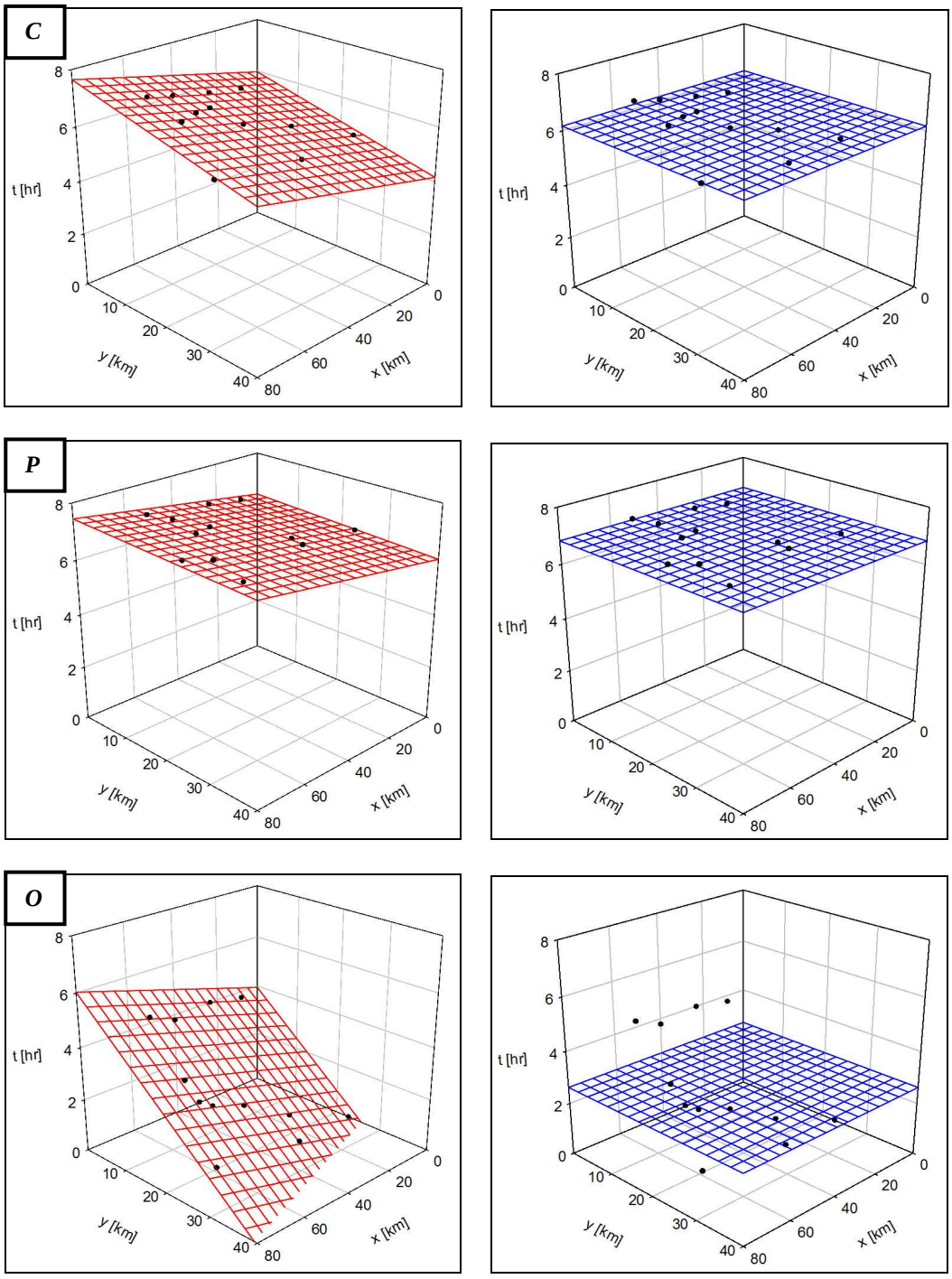

	Centroid			Peak			Onset		
	V [km / hr]	**θ** [° from N]	S. R.	**V** [km / hr]	**θ** [° from N]	S. R.	**V** [km / hr]	**θ** [° from N]	S. R.
n	20.11	154.81	0.42	62.33	125.06	0.90	6.44	170.35	0.53
n-1	20.16	154.38	0.41	61.49	124.44	0.88	6.45	170.28	0.53

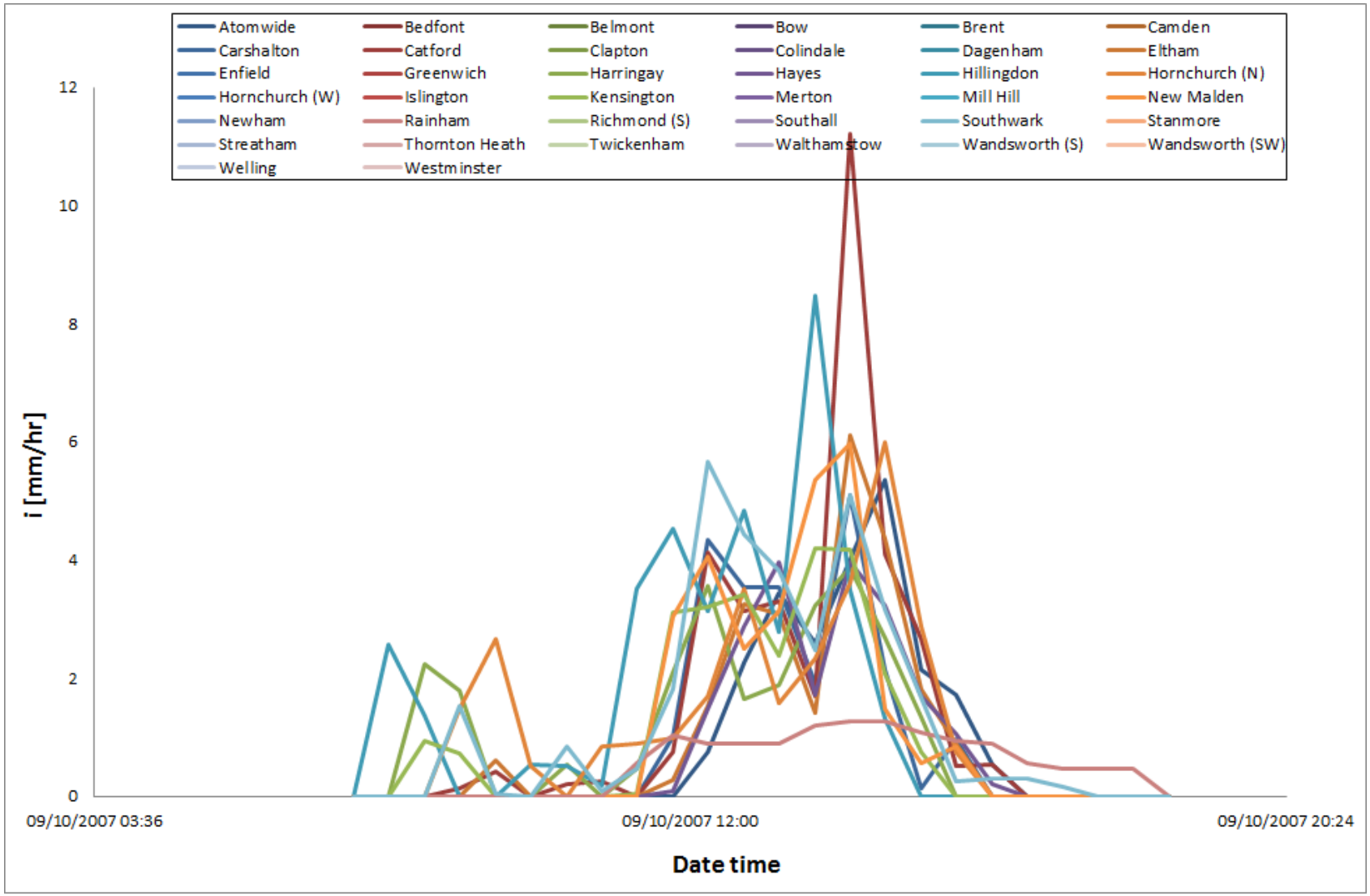
Atomwide
Bedfont
Belmont
Bow
Brent
Camden
Carshalton
Catford
Clapton
Colindale
Dagenham
Eltham
Enfield
Greenwich
Harringay
Hayes
Hillingdon
Hornchurch (N)
Hornchurch (W)
Islington
Kensington
Merton
Mill Hill
New Malden
Newham
Rainham
Richmond (S)
Southall
Southwark
Stanmore
Streatham
Thornton Heath
Twickenham
Walthamstow
Wandsworth (S)
Wandsworth (SW)
Welling
Westminster
12
10
8
6
4
2
0
i [mm/hr]
09/10/2007 03:36
09/10/2007 12:00
09/10/2007 20:24
Date time

Starting Date: 18/11/2007 14:45 – **Final Time:** 20/11/2007 03:15

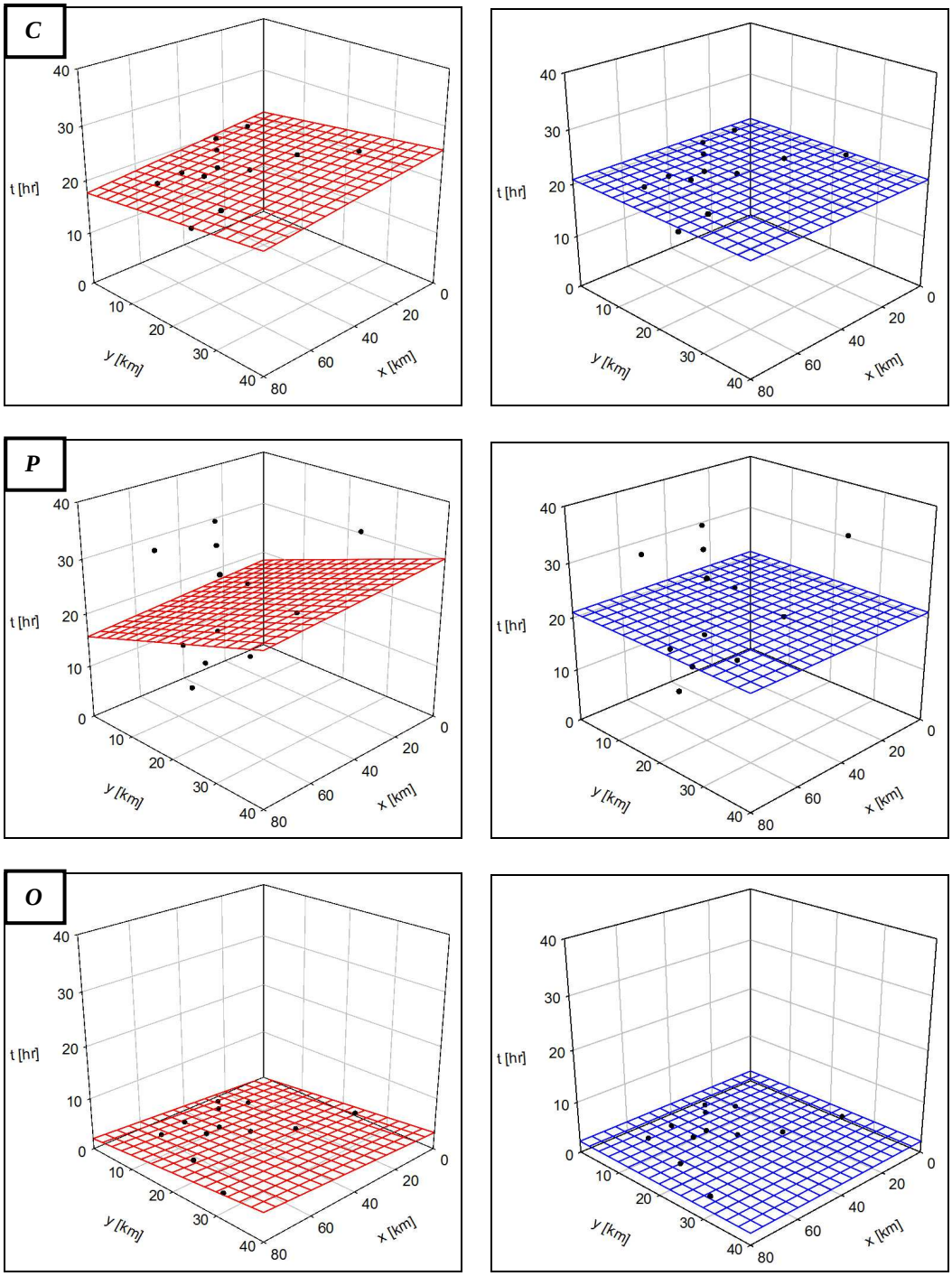

	Centroid			Peak			Onset		
	V [km / hr]	**θ** [° from N]	S. R.	**V** [km / hr]	**θ** [° from N]	S. R.	**V** [km / hr]	**θ** [° from N]	S. R.
n	8.62	156.15	0.78	3.39	173.52	0.97	11.32	17.74	0.65
n-1	8.68	154.07	0.76	4.09	129.36	0.96	11.58	18.95	0.63

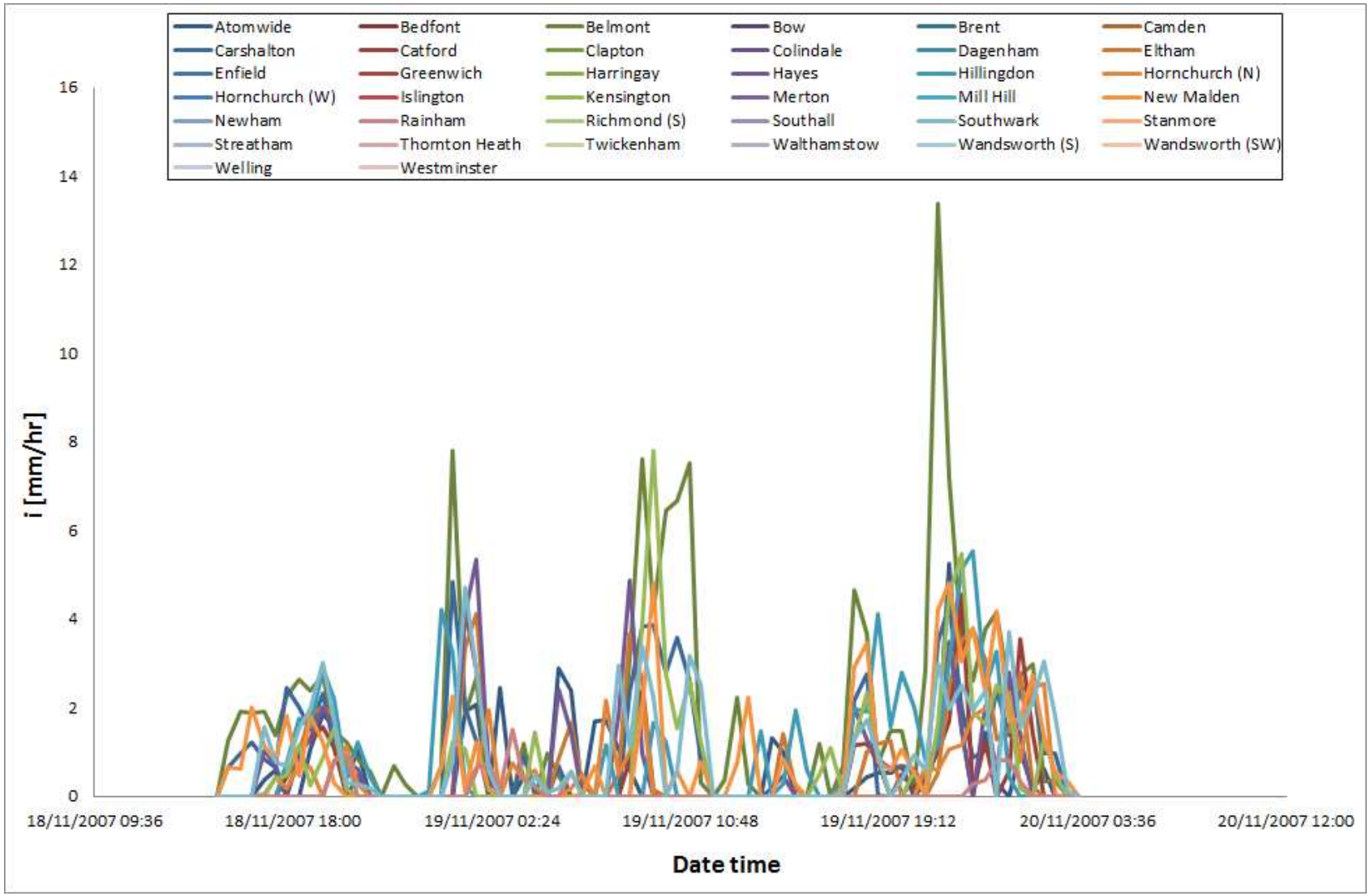
Atomwide
Bedfont
Belmont
Bow
Brent
Camden
Carshalton
Catford
Clapton
Colindale
Dagenham
Eltham
Enfield
Greenwich
Harringay
Hayes
Hillingdon
Hornchurch (N)
Hornchurch (W)
Islington
Kensington
Merton
Mill Hill
New Malden
Newham
Rainham
Richmond (S)
Southall
Southwark
Stanmore
Streatham
Thornton Heath
Twickenham
Walthamstow
Wandsworth (S)
Wandsworth (SW)
Welling
Westminster
16
14
12
10
8
6
4
2
0
i [mm/hr]
18/11/2007 09:36
18/11/2007 18:00
19/11/2007 02:24
19/11/2007 10:48
19/11/2007 19:12
20/11/2007 03:36
20/11/2007 12:00
Date time

Starting Date: 25/12/2007 04:45 – **Final Time:** 25/12/2007 15:45

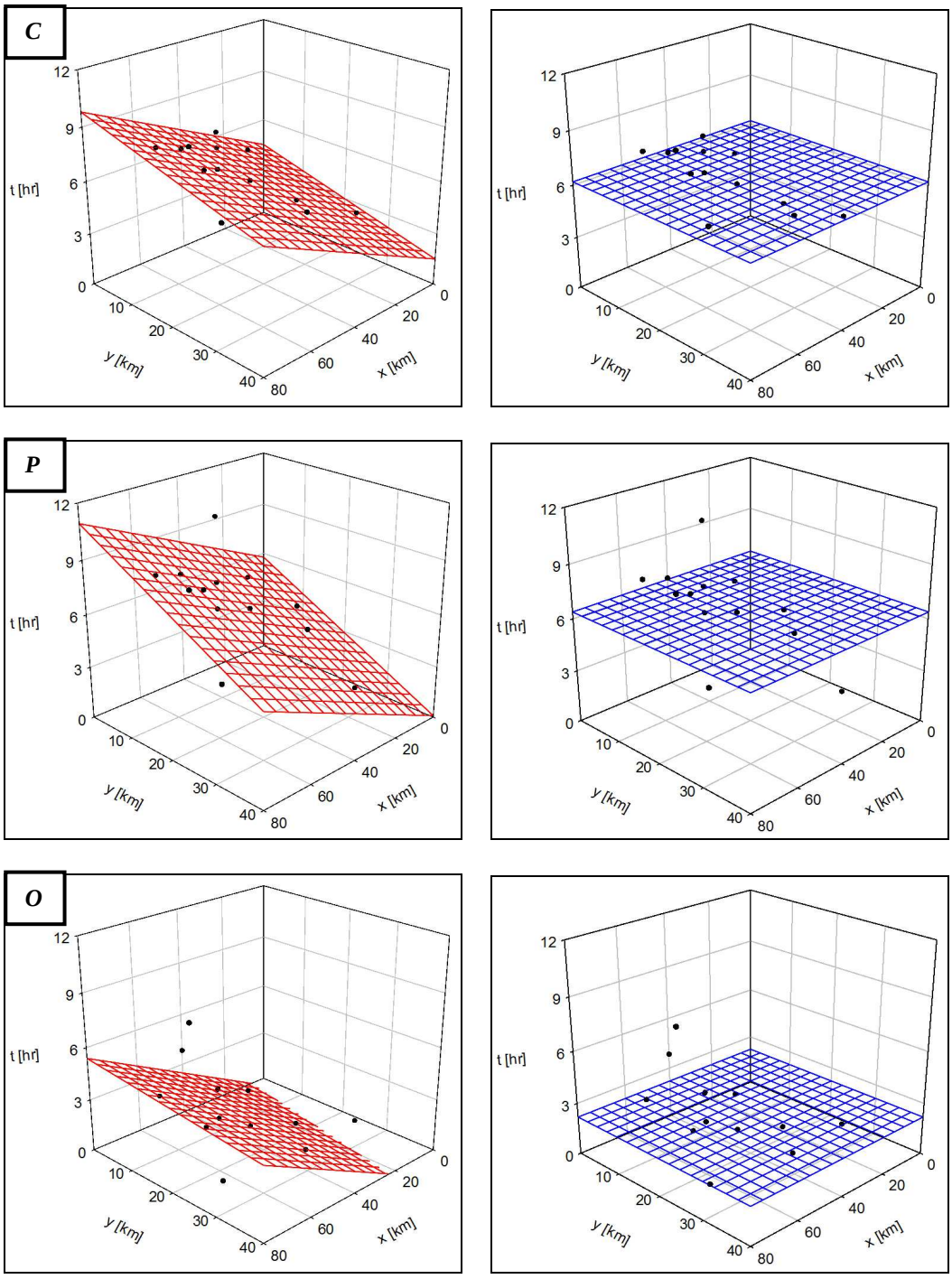

	Centroid			Peak			Onset		
	V [km / hr]	**θ** [° from N]	S. R.	**V** [km / hr]	**θ** [° from N]	S. R.	**V** [km / hr]	**θ** [° from N]	S. R.
n	10.07	137.71	0.40	6.41	155.52	0.62	12.61	112.48	0.78
n-1	10.06	137.51	0.39	6.65	155.32	0.62	12.31	112.91	0.77

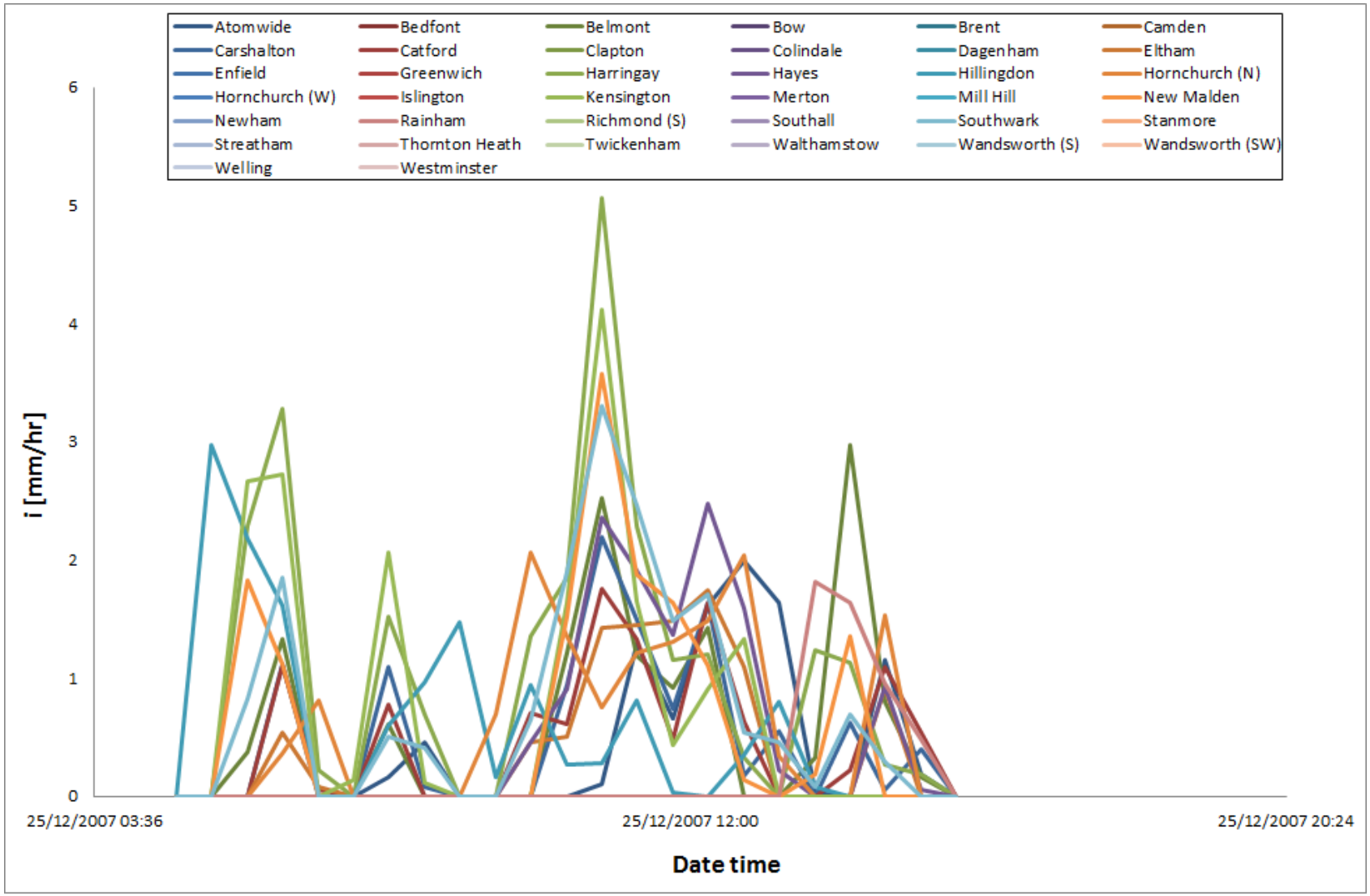
Atomwide
Bedfont
Belmont
Bow
Brent
Camden
Carshalton
Catford
Clapton
Colindale
Dagenham
Eltham
Enfield
Greenwich
Harringay
Hayes
Hillingdon
Hornchurch (N)
Hornchurch (W)
Islington
Kensington
Merton
Mill Hill
New Malden
Newham
Rainham
Richmond (S)
Southall
Southwark
Stanmore
Streatham
Thornton Heath
Twickenham
Walthamstow
Wandsworth (S)
Wandsworth (SW)
Welling
Westminster
i [mm/hr]
0
1
2
3
4
5
6
25/12/2007 03:36
25/12/2007 12:00
25/12/2007 20:24
Date time

Starting Date: 11/01/2008 04:15 – **Final Time:** 11/01/2008 15:15

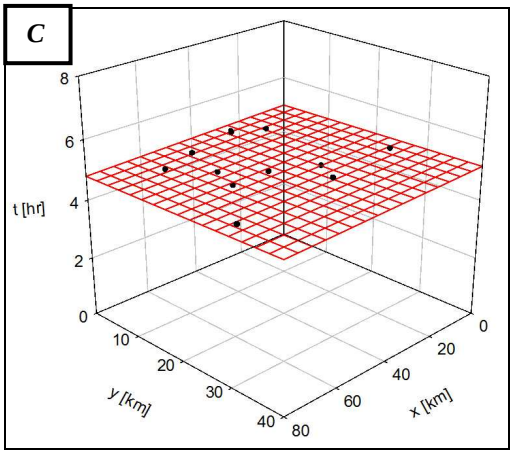

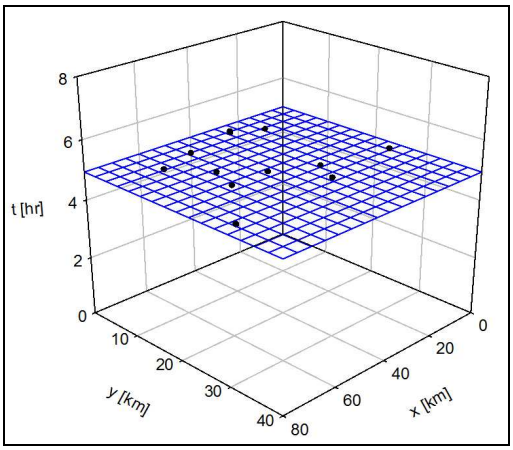

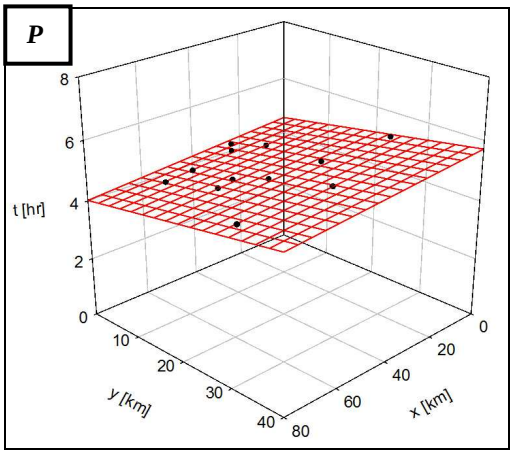

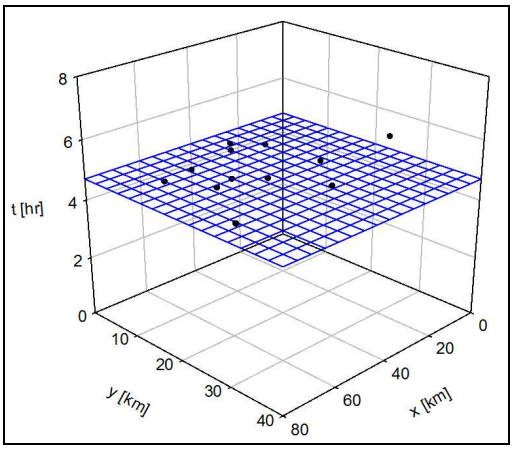

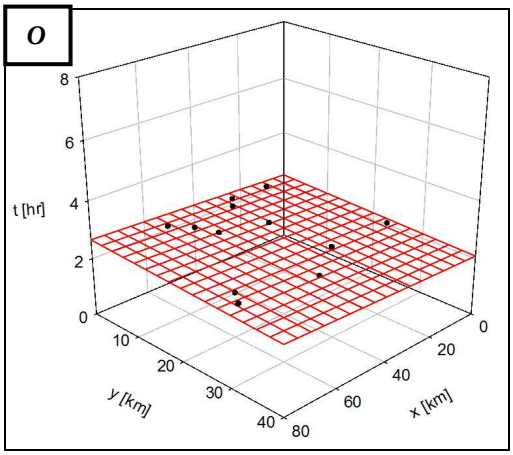

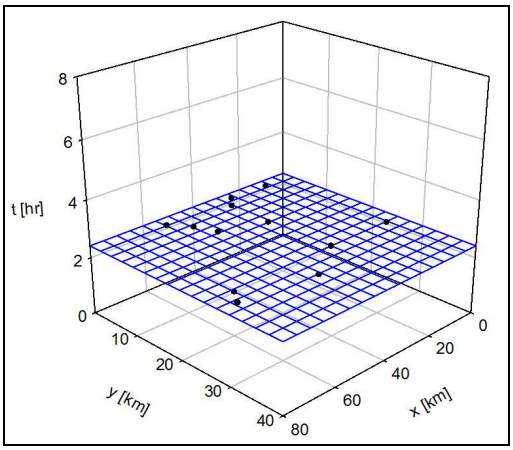

	Centroid			Peak			Onset		
	V [km / hr]	**θ** [° from N]	S. R.	**V** [km / hr]	**θ** [° from N]	S. R.	**V** [km / hr]	**θ** [° from N]	S. R.
n	241.43	143.92	0.98	33.67	166.73	0.44	123.31	154.45	0.99
n-1	243.76	136.53	0.97	34.21	166.76	0.44	143.94	139.44	0.99

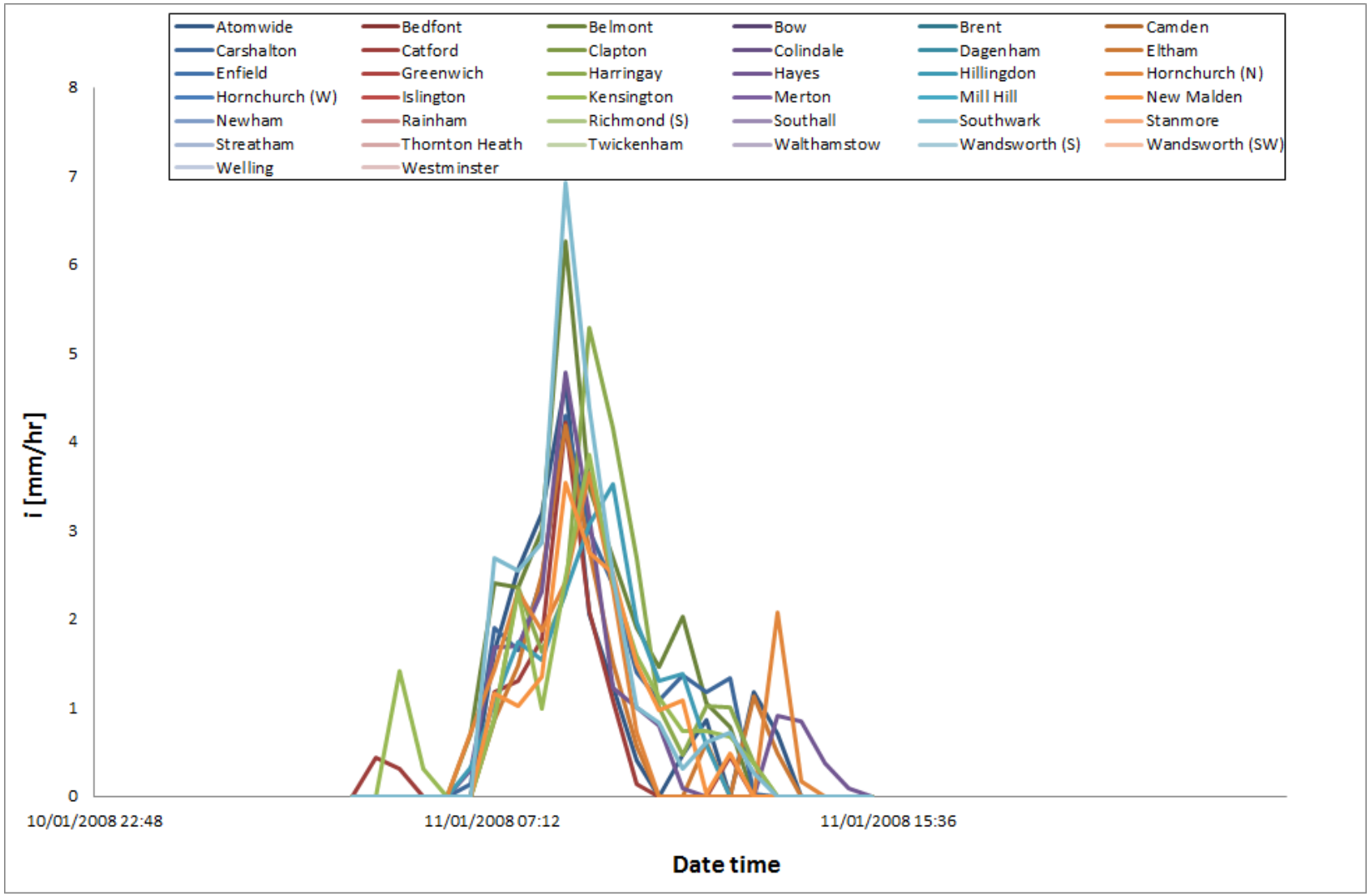
Atomwide
Bedfont
Belmont
Bow
Brent
Camden
Carshalton
Catford
Clapton
Colindale
Dagenham
Eltham
Enfield
Greenwich
Harringay
Hayes
Hillingdon
Hornchurch (N)
Hornchurch (W)
Islington
Kensington
Merton
Mill Hill
New Malden
Newham
Rainham
Richmond (S)
Southall
Southwark
Stanmore
Streatham
Thornton Heath
Twickenham
Walthamstow
Wandsworth (S)
Wandsworth (SW)
Welling
Westminster
i [mm/hr]
0
1
2
3
4
5
6
7
8
10/01/2008 22:48
11/01/2008 07:12
11/01/2008 15:36
Date time

Starting Date: 14/01/2008 22:15 – **Final Time:** 15/01/2008 12:15

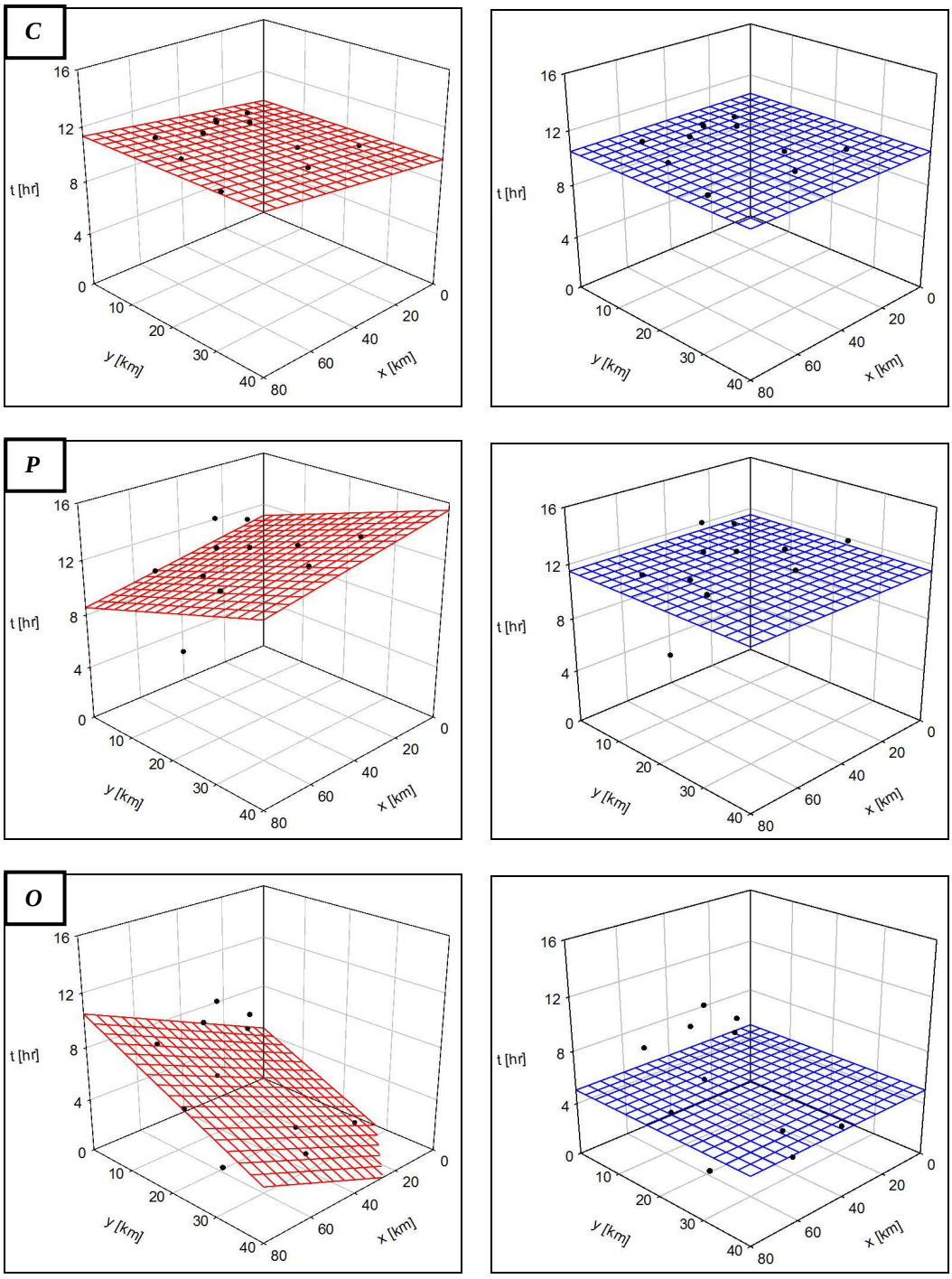

	Centroid			Peak			Onset		
	V [km / hr]	**θ** [° from N]	S. R.	**V** [km / hr]	**θ** [° from N]	S. R.	**V** [km / hr]	**θ** [° from N]	S. R.
n	46.17	87.12	0.92	8.71	163.94	0.88	5.64	154.78	0.86
n-1	44.26	82.92	0.91	10.19	162.41	0.87	5.77	152.59	0.85

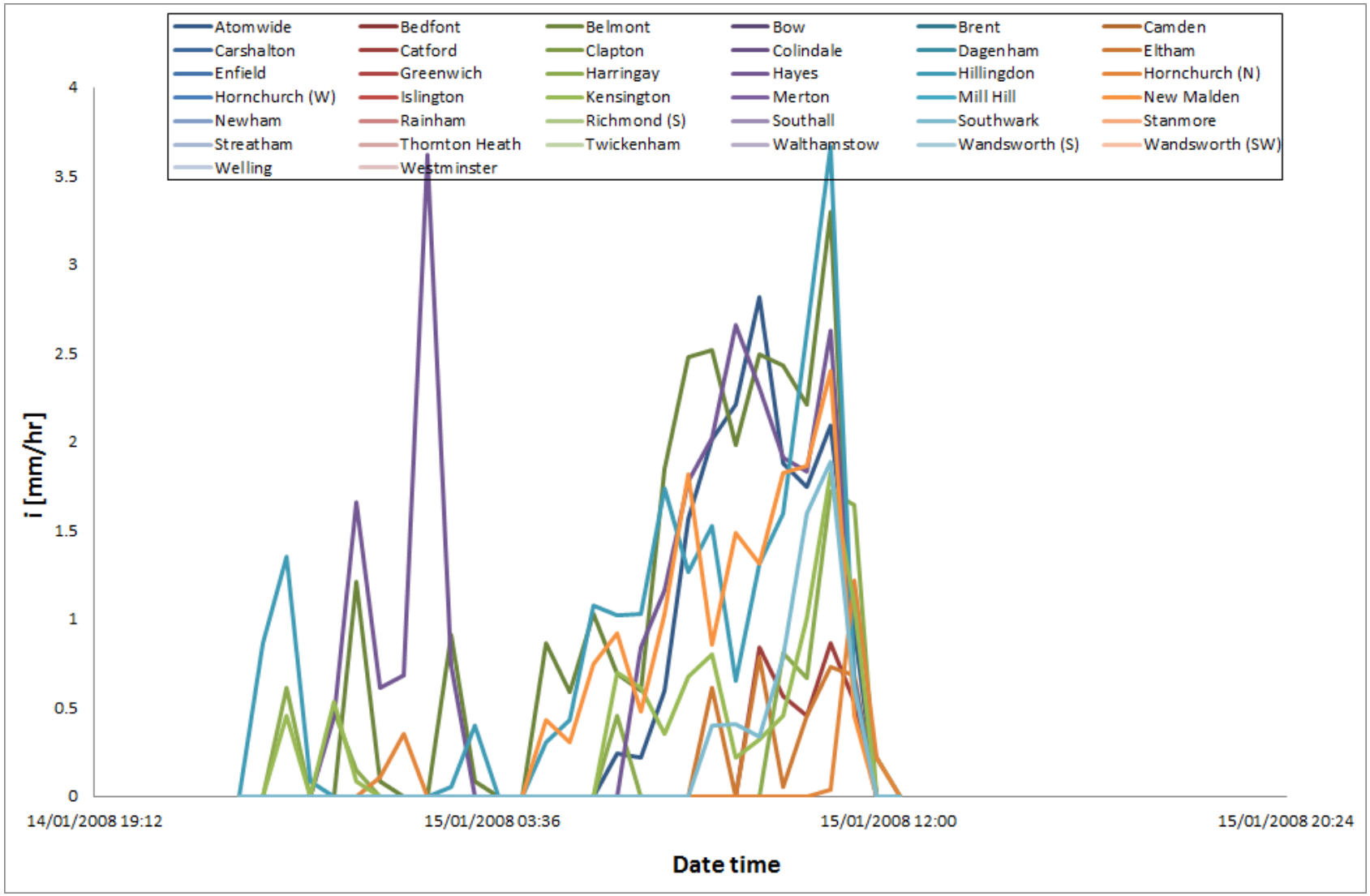
Atomwide
Bedfont
Belmont
Bow
Brent
Camden
Carshalton
Catford
Clapton
Colindale
Dagenham
Eltham
Enfield
Greenwich
Harringay
Hayes
Hillingdon
Hornchurch (N)
Hornchurch (W)
Islington
Kensington
Merton
Mill Hill
New Malden
Newham
Rainham
Richmond (S)
Southall
Southwark
Stanmore
Streatham
Thornton Heath
Twickenham
Walthamstow
Wandsworth (S)
Wandsworth (SW)
Welling
Westminster
i [mm/hr]
4
3.5
3
2.5
2
1.5
1
0.5
0
14/01/2008 19:12
15/01/2008 03:36
15/01/2008 12:00
15/01/2008 20:24
Date time

Starting Date: 29/01/2008 23:15 – **Final Time:** 30/01/2008 05:15

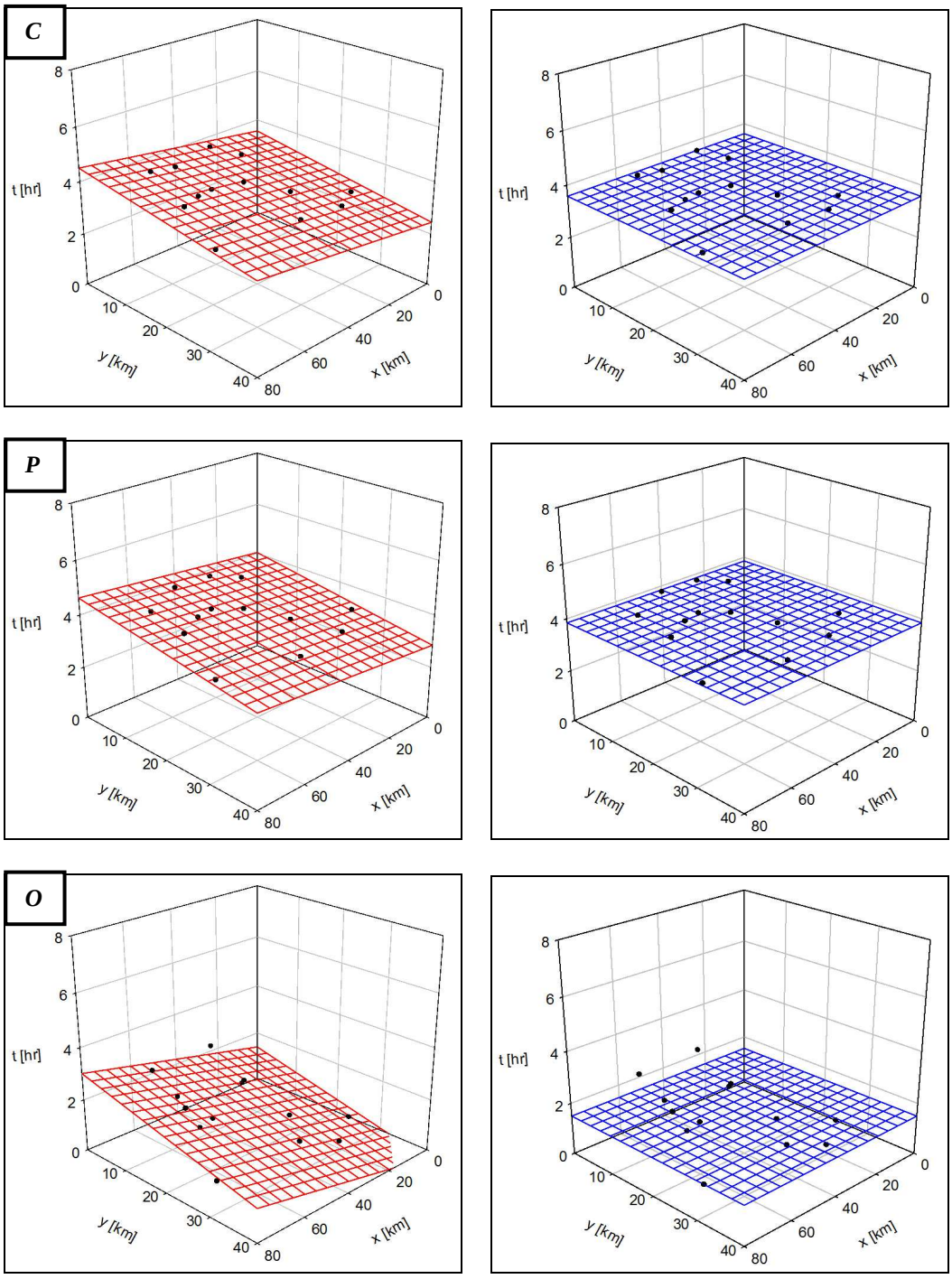

	Centroid			Peak			Onset		
	V [km / hr]	**θ** [° from N]	S. R.	**V** [km / hr]	**θ** [° from N]	S. R.	**V** [km / hr]	**θ** [° from N]	S. R.
n	33.69	155.92	0.49	32.89	165.69	0.63	20.73	155.13	0.74
n-1	33.79	155.70	0.49	33.06	165.44	0.62	20.96	154.42	0.74

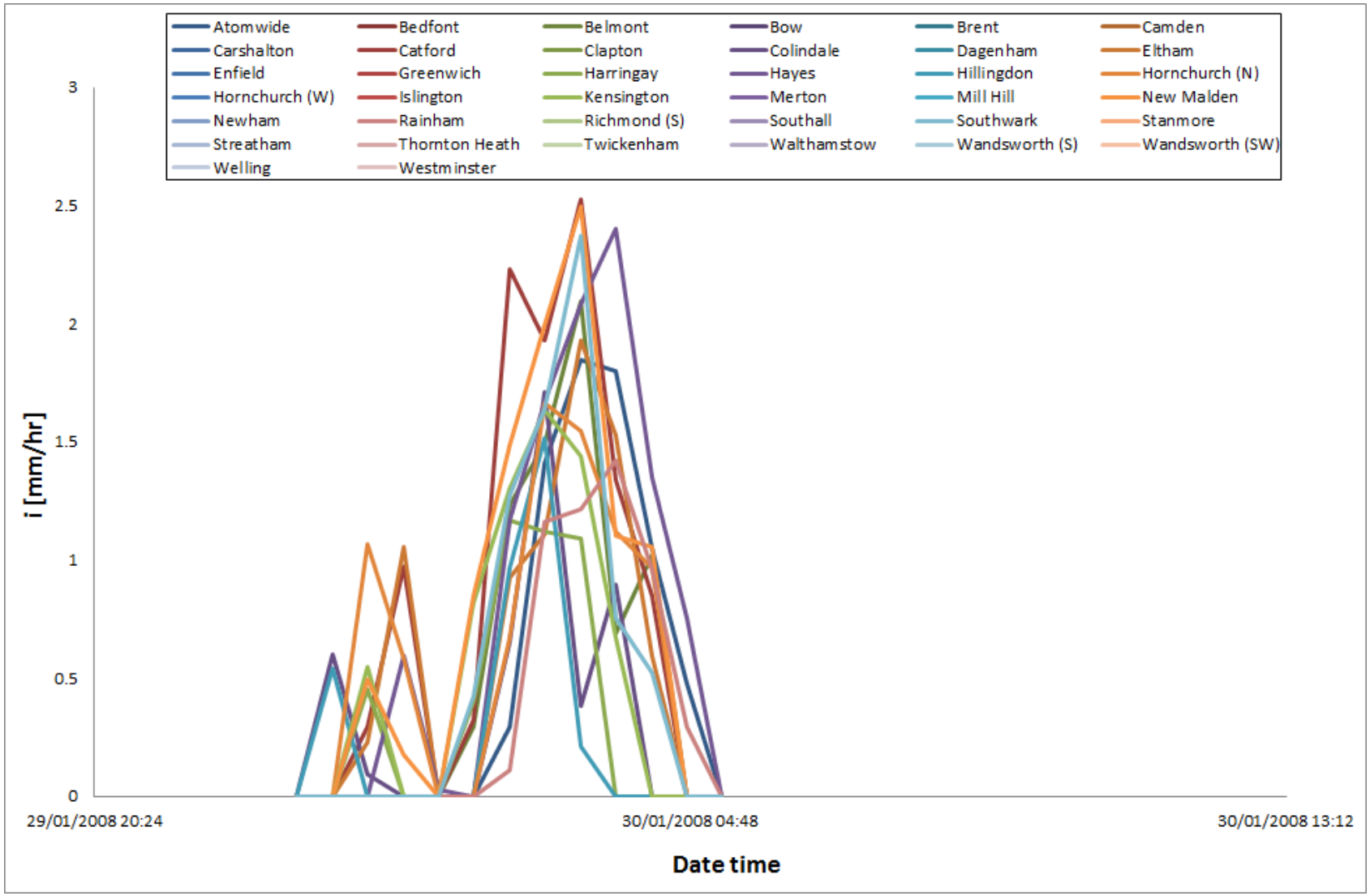
Atomwide
Bedfont
Belmont
Bow
Brent
Camden
Carshalton
Catford
Clapton
Colindale
Dagenham
Eltham
Enfield
Greenwich
Harringay
Hayes
Hillingdon
Hornchurch (N)
Hornchurch (W)
Islington
Kensington
Merton
Mill Hill
New Malden
Newham
Rainham
Richmond (S)
Southall
Southwark
Stanmore
Streatham
Thornton Heath
Twickenham
Walthamstow
Wandsworth (S)
Wandsworth (SW)
Welling
Westminster
3
2.5
2
1.5
1
0.5
0
i [mm/hr]
29/01/2008 20:24
30/01/2008 04:48
30/01/2008 13:12
Date time

Starting Date: 15/03/2008 15:45 – **Final Time:** 16/03/2008 01:45

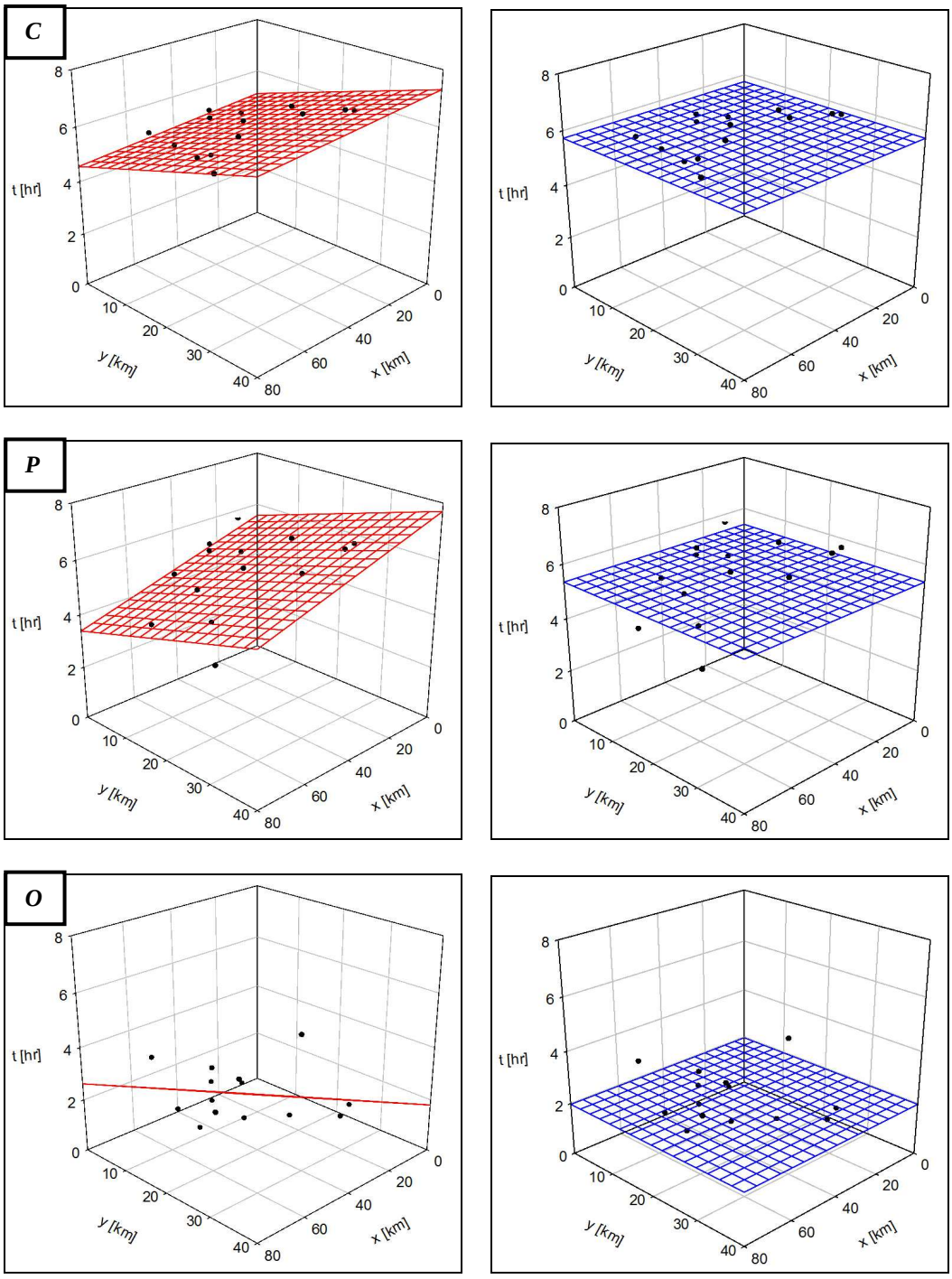

	Centroid			Peak			Onset		
	V [km / hr]	**θ** [° from N]	S. R.	**V** [km / hr]	**θ** [° from N]	S. R.	**V** [km / hr]	**θ** [° from N]	S. R.
n	17.85	173.34	0.58	16.56	153.52	0.80	13.23	33.56	0.72
n-1	17.81	173.36	0.57	16.46	153.62	0.79	13.24	33.87	0.71

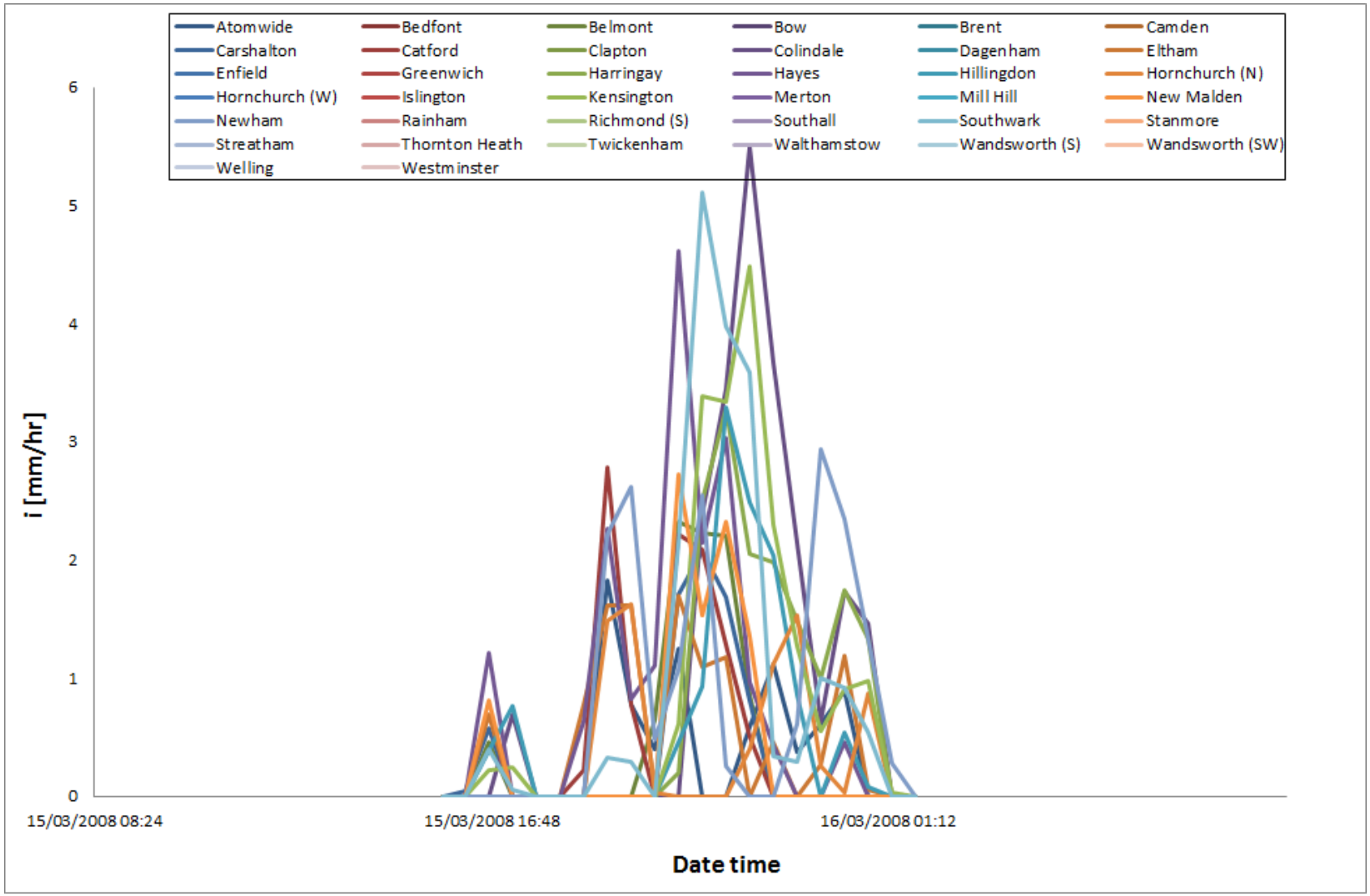
Atomwide
Bedfont
Belmont
Bow
Brent
Camden
Carshalton
Catford
Clapton
Colindale
Dagenham
Eltham
Enfield
Greenwich
Harringay
Hayes
Hillingdon
Hornchurch (N)
Hornchurch (W)
Islington
Kensington
Merton
Mill Hill
New Malden
Newham
Rainham
Richmond (S)
Southall
Southwark
Stanmore
Streatham
Thornton Heath
Twickenham
Walthamstow
Wandsworth (S)
Wandsworth (SW)
Welling
Westminster
i [mm/hr]
0
1
2
3
4
5
6
15/03/2008 08:24
15/03/2008 16:48
16/03/2008 01:12
Date time

Starting Date: 29/03/2008 13:45 – **Final Time:** 30/03/2008 05:45

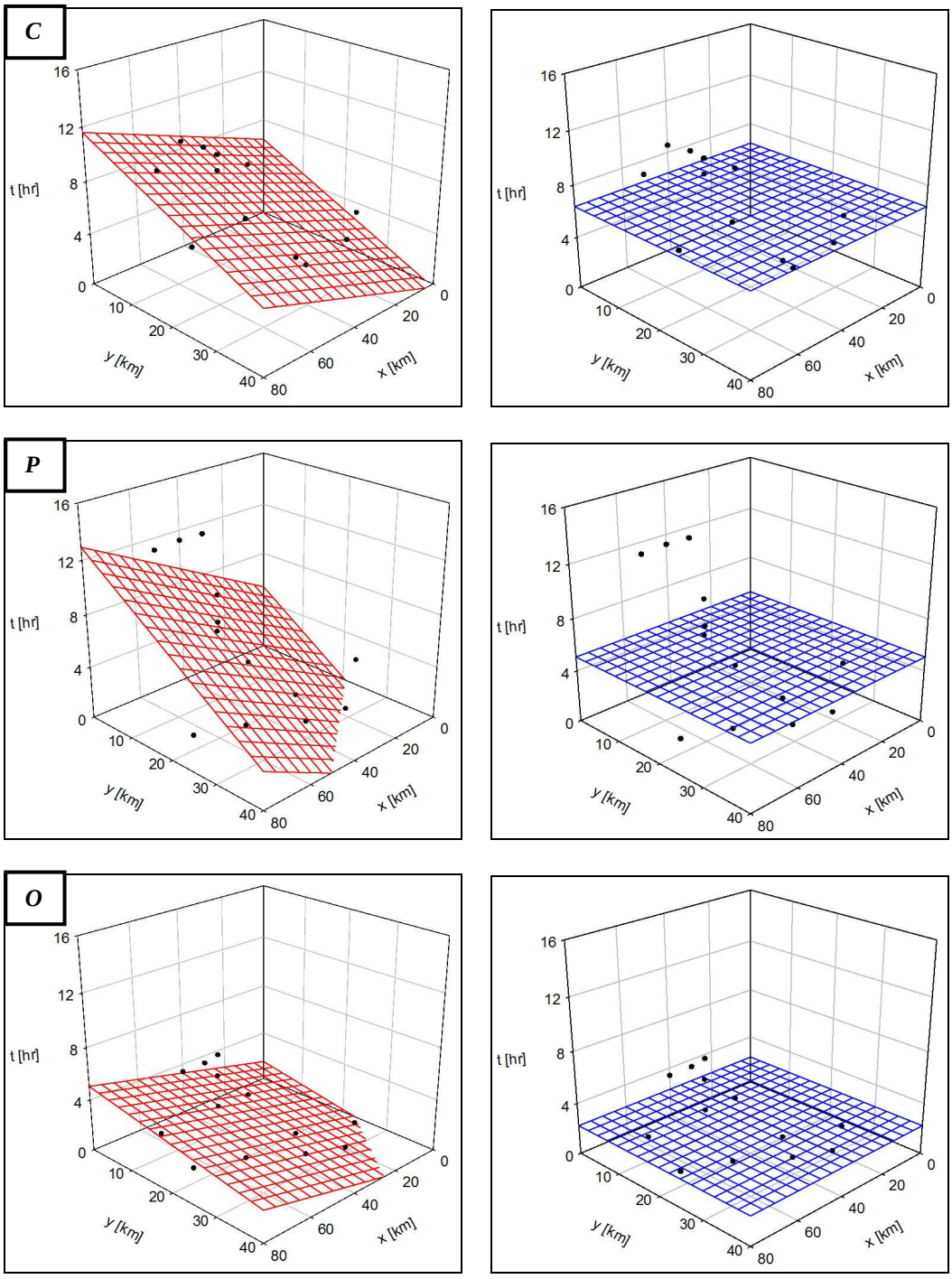

	Centroid			Peak			Onset		
	V [km / hr]	**θ** [° from N]	S. R.	**V** [km / hr]	**θ** [° from N]	S. R.	**V** [km / hr]	**θ** [° from N]	S. R.
n	5.60	158.55	0.64	3.70	159.01	0.75	12.57	146.15	0.89
n-1	5.60	158.25	0.64	3.70	158.41	0.75	12.60	145.49	0.88

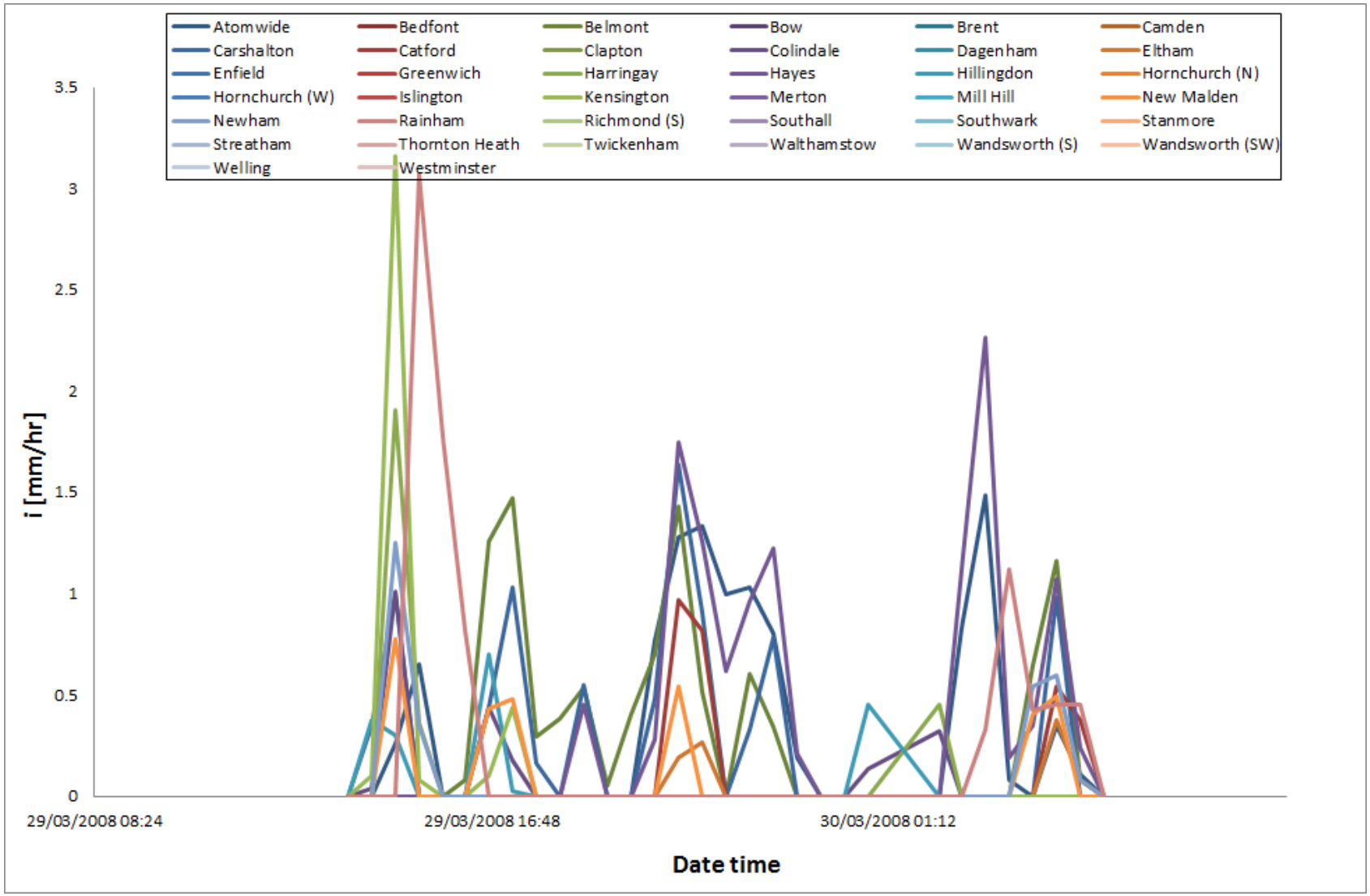
Atomwide
Bedfont
Belmont
Bow
Brent
Camden
Carshalton
Catford
Clapton
Colindale
Dagenham
Eltham
Enfield
Greenwich
Harringay
Hayes
Hillingdon
Hornchurch (N)
Hornchurch (W)
Islington
Kensington
Merton
Mill Hill
New Malden
Newham
Rainham
Richmond (S)
Southall
Southwark
Stanmore
Streatham
Thornton Heath
Twickenham
Walthamstow
Wandsworth (S)
Wandsworth (SW)
Welling
Westminster
3.5
3
2.5
2
1.5
1
0.5
0
i [mm/hr]
29/03/2008 08:24
29/03/2008 16:48
30/03/2008 01:12
Date time

Starting Date: 30/04/2008 07:15 – **Final Time:** 30/04/2008 22:15

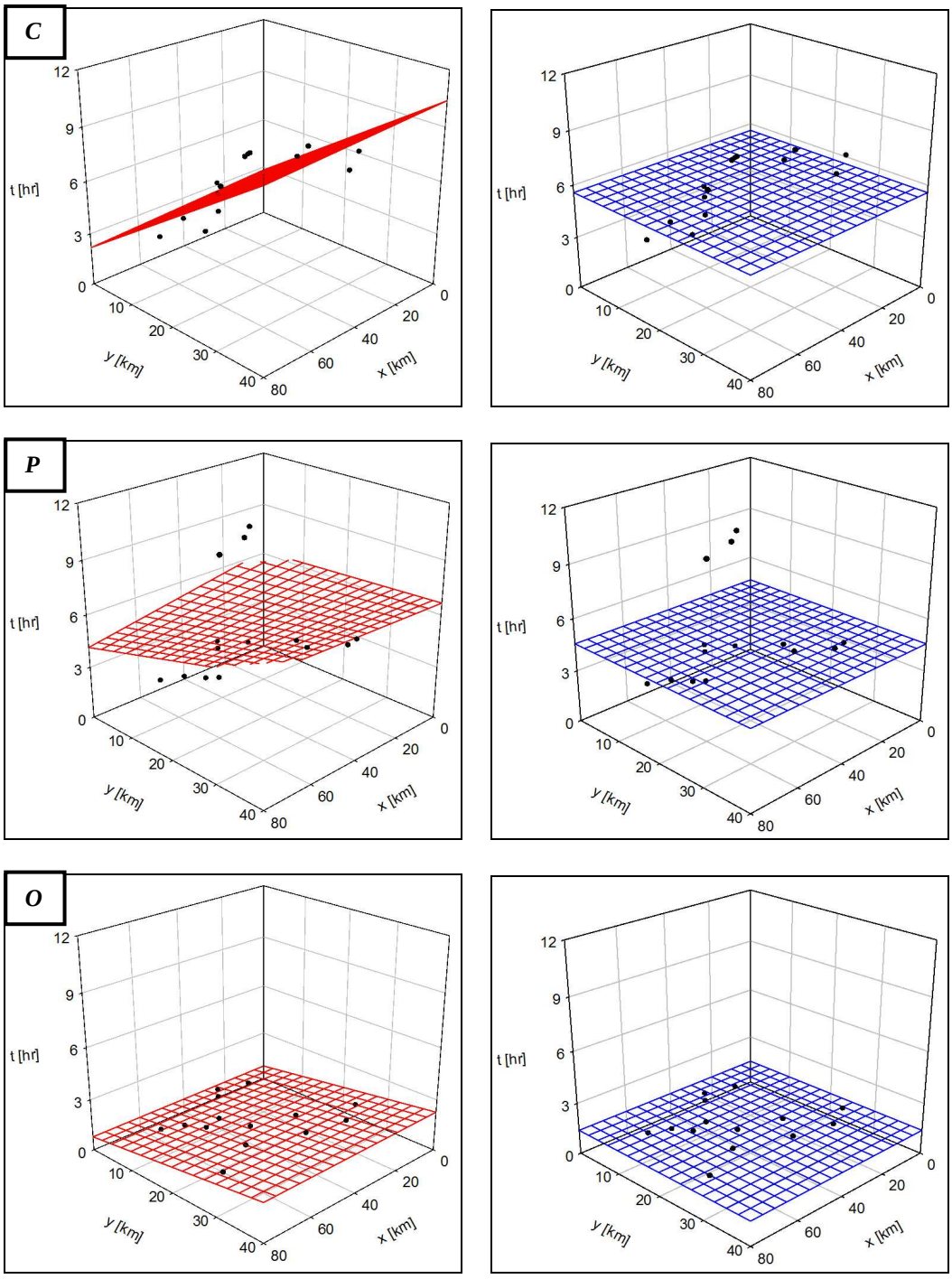

	Centroid			Peak			Onset		
	V [km / hr]	**θ** [° from N]	S. R.	**V** [km / hr]	**θ** [° from N]	S. R.	**V** [km / hr]	**θ** [° from N]	S. R.
n	5.27	177.72	0.52	4.34	19.51	0.71	27.80	179.18	0.59
n-1	5.27	164.72	0.52	4.36	19.39	0.70	27.91	153.29	0.58

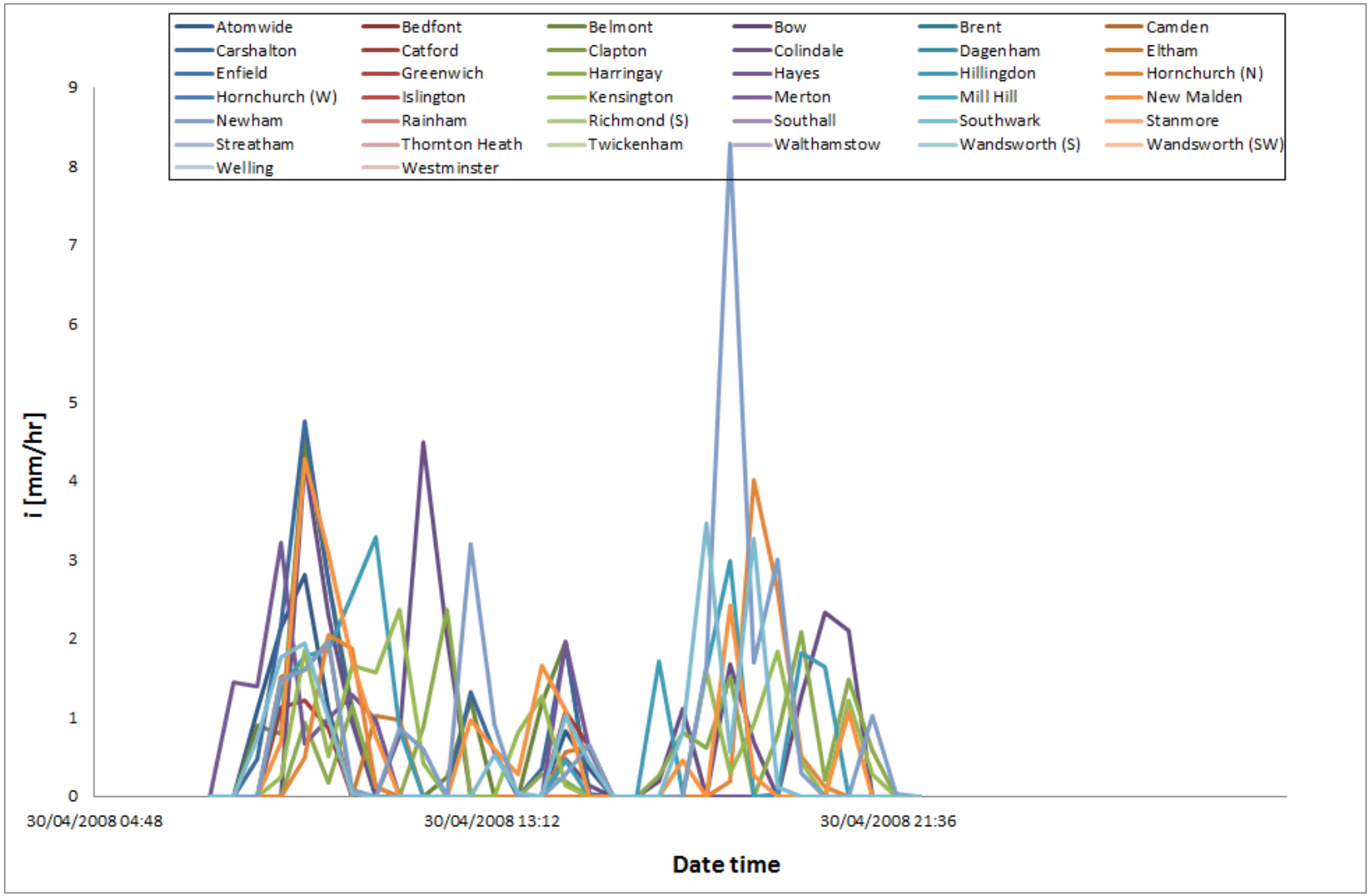
Atomwide
Bedfont
Belmont
Bow
Brent
Camden
Carshalton
Catford
Clapton
Colindale
Dagenham
Eltham
Enfield
Greenwich
Harringay
Hayes
Hillingdon
Hornchurch (N)
Hornchurch (W)
Islington
Kensington
Merton
Mill Hill
New Malden
Newham
Rainham
Richmond (S)
Southall
Southwark
Stanmore
Streatham
Thornton Heath
Twickenham
Walthamstow
Wandsworth (S)
Wandsworth (SW)
Welling
Westminster
i [mm/hr]
0
1
2
3
4
5
6
7
8
9
30/04/2008 04:48
30/04/2008 13:12
30/04/2008 21:36
Date time

Starting Date: 25/05/2008 01:15 – **Final Time:** 25/05/2008 16:15

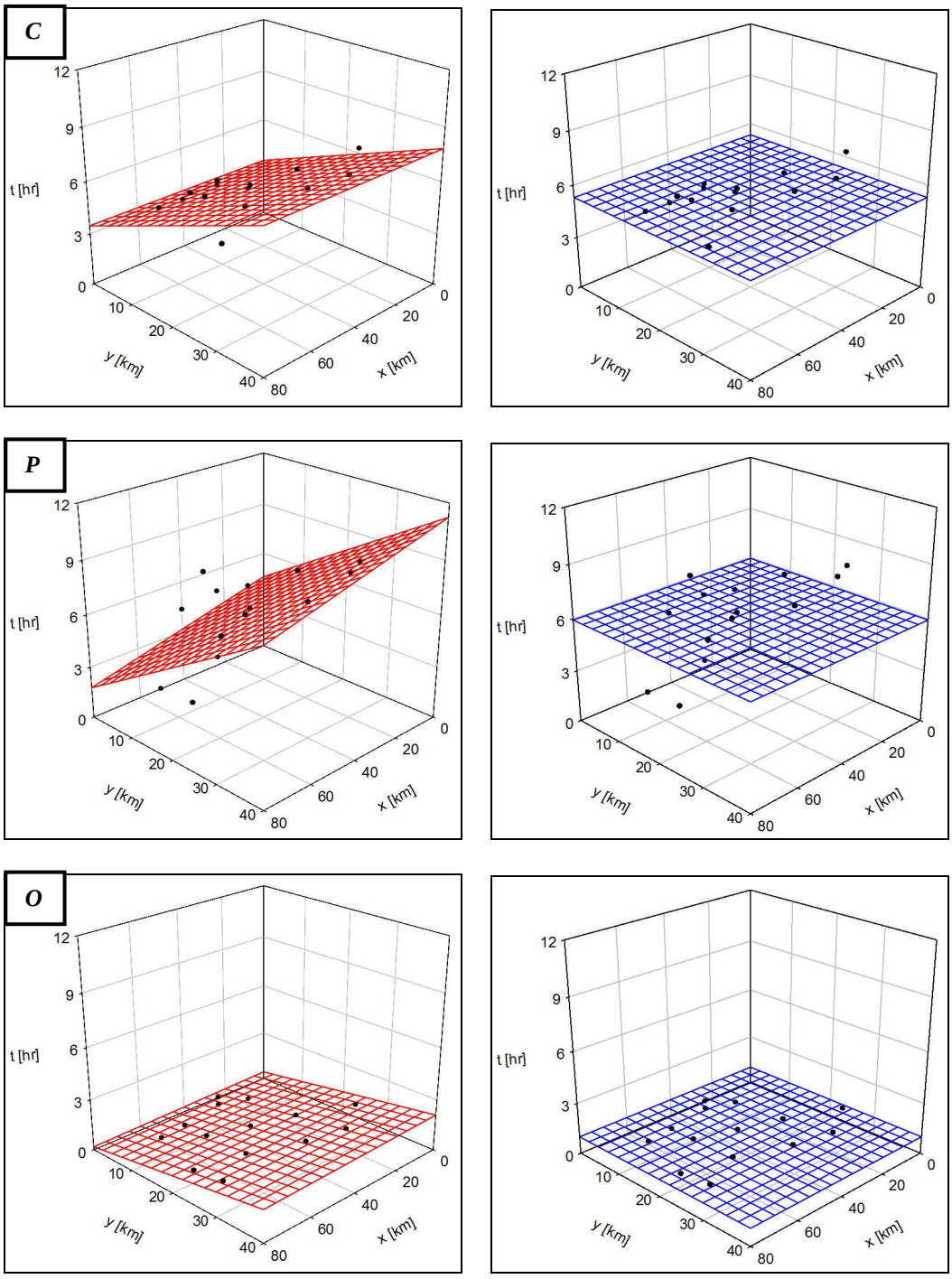

	Centroid			Peak			Onset		
	V [km / hr]	**θ** [° from N]	S. R.	**V** [km / hr]	**θ** [° from N]	S. R.	**V** [km / hr]	**θ** [° from N]	S. R.
n	9.10	0.20	0.49	5.82	168.54	0.69	23.95	175.67	0.29
n-1	9.10	64.54	0.48	5.87	168.38	0.69	23.97	175.64	0.28

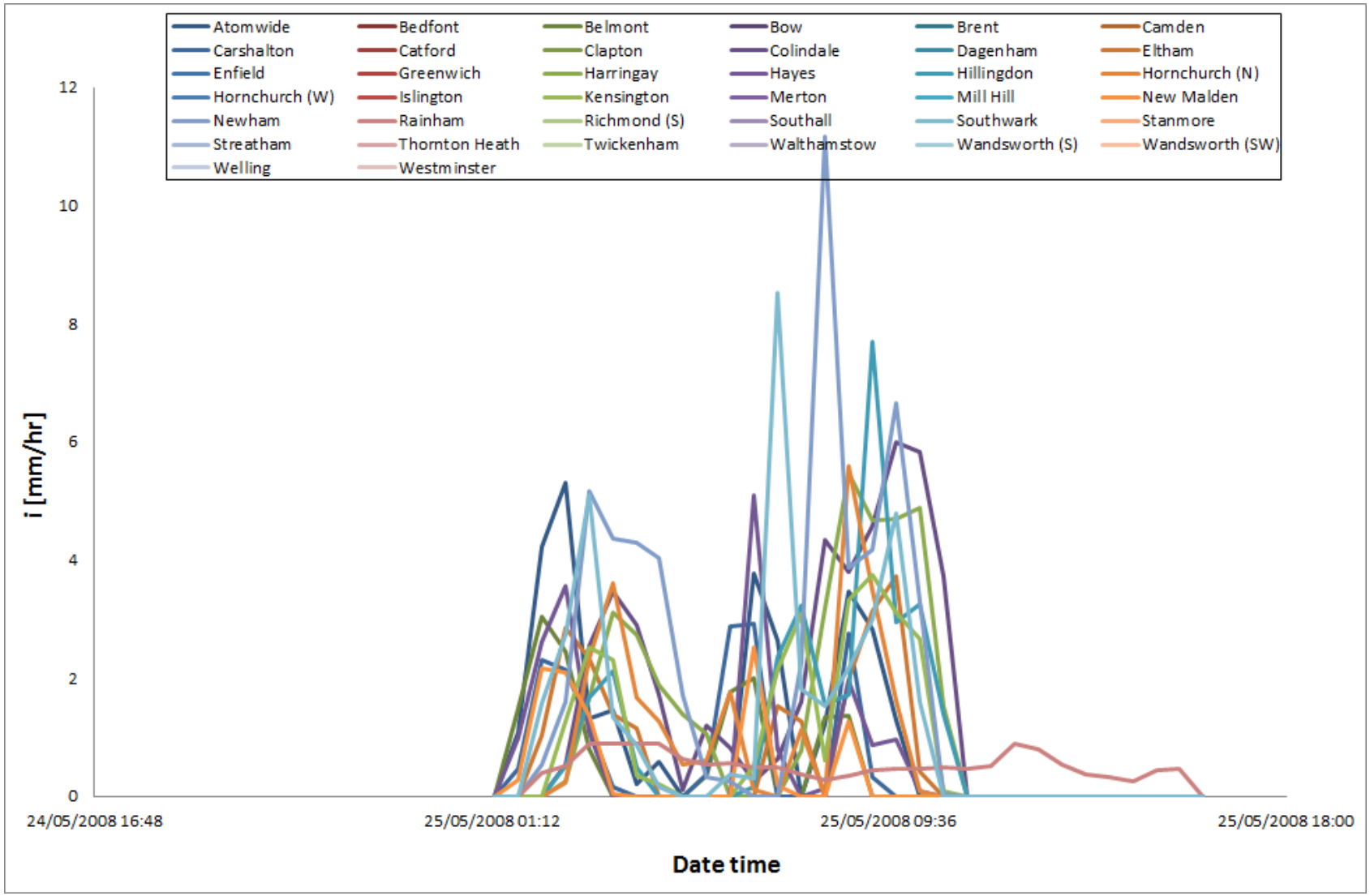
Atomwide
Bedfont
Belmont
Bow
Brent
Camden
Carshalton
Catford
Clapton
Colindale
Dagenham
Eltham
Enfield
Greenwich
Harringay
Hayes
Hillingdon
Hornchurch (N)
Hornchurch (W)
Islington
Kensington
Merton
Mill Hill
New Malden
Newham
Rainham
Richmond (S)
Southall
Southwark
Stanmore
Streatham
Thornton Heath
Twickenham
Walthamstow
Wandsworth (S)
Wandsworth (SW)
Welling
Westminster
12
10
8
6
4
2
0
i [mm/hr]
24/05/2008 16:48
25/05/2008 01:12
25/05/2008 09:36
25/05/2008 18:00
Date time

Starting Date: 26/05/2008 02:45 – **Final Time:** 27/05/2008 04:15

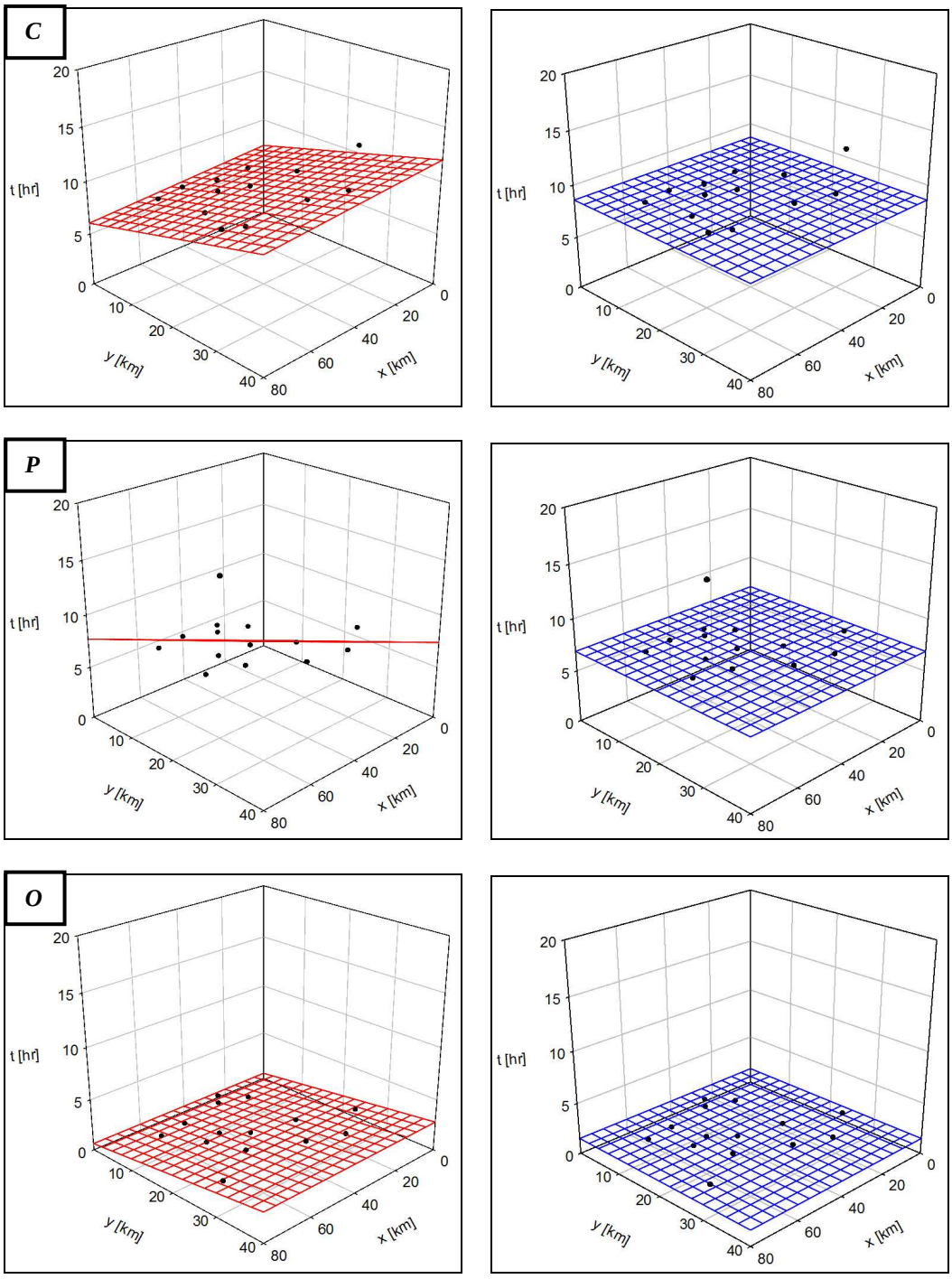

	Centroid			Peak			Onset		
	V [km / hr]	**θ** [° from N]	S. R.	**V** [km / hr]	**θ** [° from N]	S. R.	**V** [km / hr]	**θ** [° from N]	S. R.
n	8.44	172.32	0.60	5.21	27.58	0.67	17.96	0.68	0.44
n-1	8.51	159.41	0.59	5.68	26.54	0.66	18.01	26.25	0.43

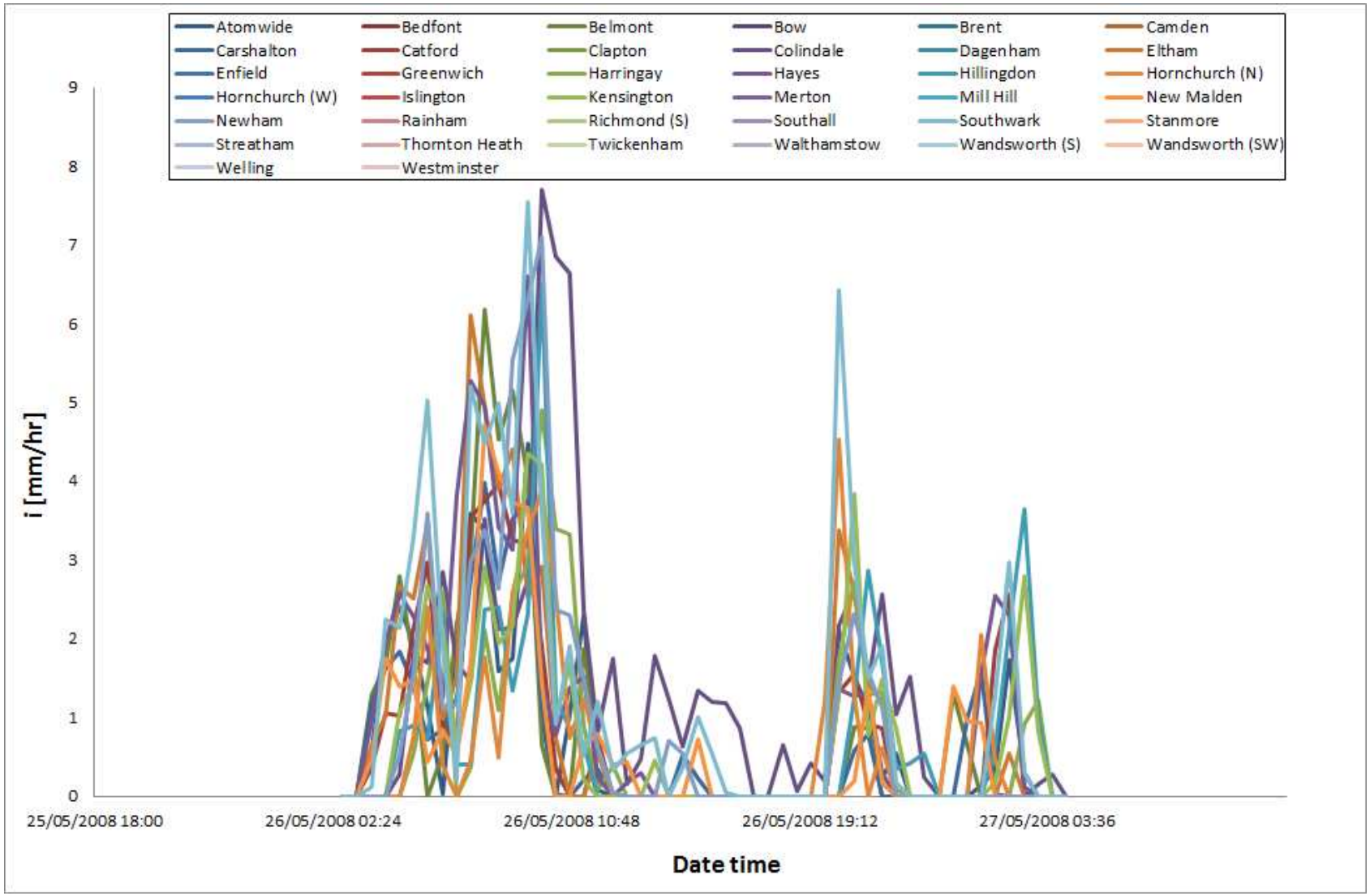
Atomwide
Bedfont
Belmont
Bow
Brent
Camden
Carshalton
Catford
Clapton
Colindale
Dagenham
Eltham
Enfield
Greenwich
Harringay
Hayes
Hillingdon
Hornchurch (N)
Hornchurch (W)
Islington
Kensington
Merton
Mill Hill
New Malden
Newham
Rainham
Richmond (S)
Southall
Southwark
Stanmore
Streatham
Thornton Heath
Twickenham
Walthamstow
Wandsworth (S)
Wandsworth (SW)
Welling
Westminster
i [mm/hr]
0
1
2
3
4
5
6
7
8
9
25/05/2008 18:00
26/05/2008 02:24
26/05/2008 10:48
26/05/2008 19:12
27/05/2008 03:36
Date time

Starting Date: 29/05/2008 14:15 – **Final Time:** 29/05/2008 21:15

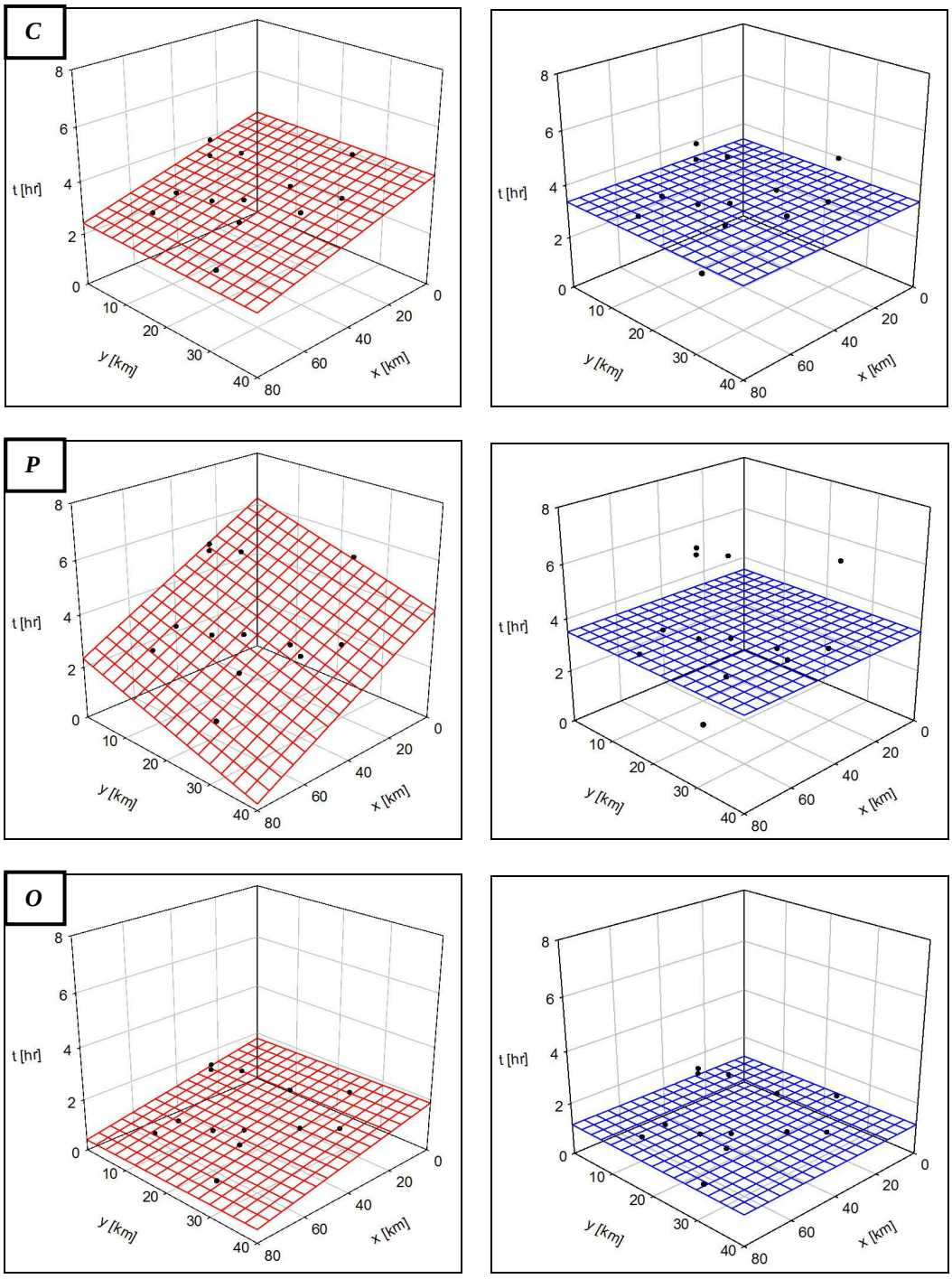

	Centroid			Peak			Onset		
	V [km / hr]	**θ** [° from N]	S. R.	**V** [km / hr]	**θ** [° from N]	S. R.	**V** [km / hr]	**θ** [° from N]	S. R.
n	41.71	84.09	0.55	13.98	43.10	0.54	57.90	98.13	0.82
n-1	41.39	83.86	0.54	13.92	43.01	0.53	56.56	97.54	0.81

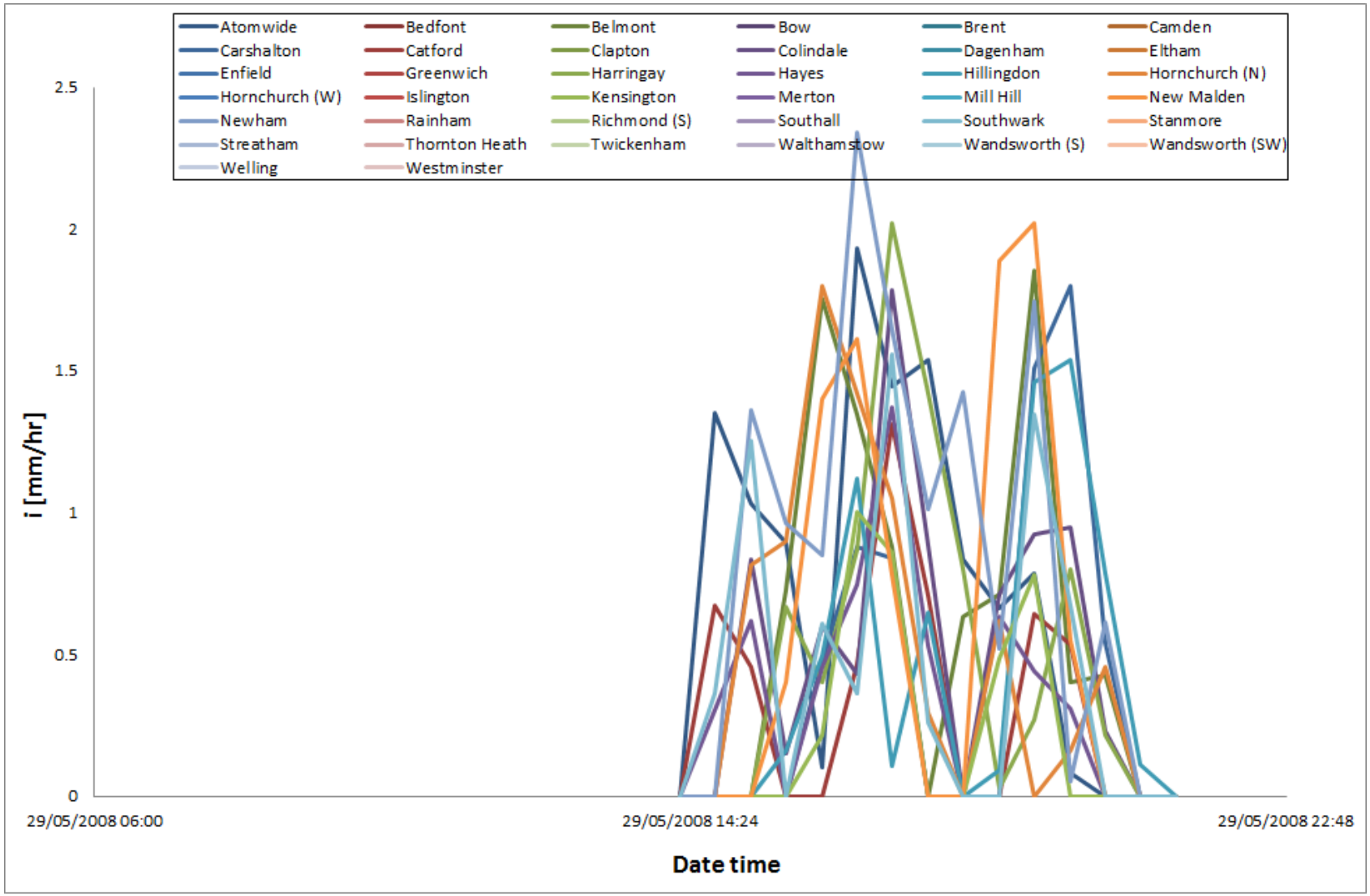
Atomwide
Bedfont
Belmont
Bow
Brent
Camden
Carshalton
Catford
Clapton
Colindale
Dagenham
Eltham
Enfield
Greenwich
Harringay
Hayes
Hillingdon
Hornchurch (N)
Hornchurch (W)
Islington
Kensington
Merton
Mill Hill
New Malden
Newham
Rainham
Richmond (S)
Southall
Southwark
Stanmore
Streatham
Thornton Heath
Twickenham
Walthamstow
Wandsworth (S)
Wandsworth (SW)
Welling
Westminster
2.5
2
1.5
1
0.5
0
i [mm/hr]
29/05/2008 06:00
29/05/2008 14:24
29/05/2008 22:48
Date time

Starting Date: 07/07/2008 02:45 – **Final Time:** 07/07/2008 21:45

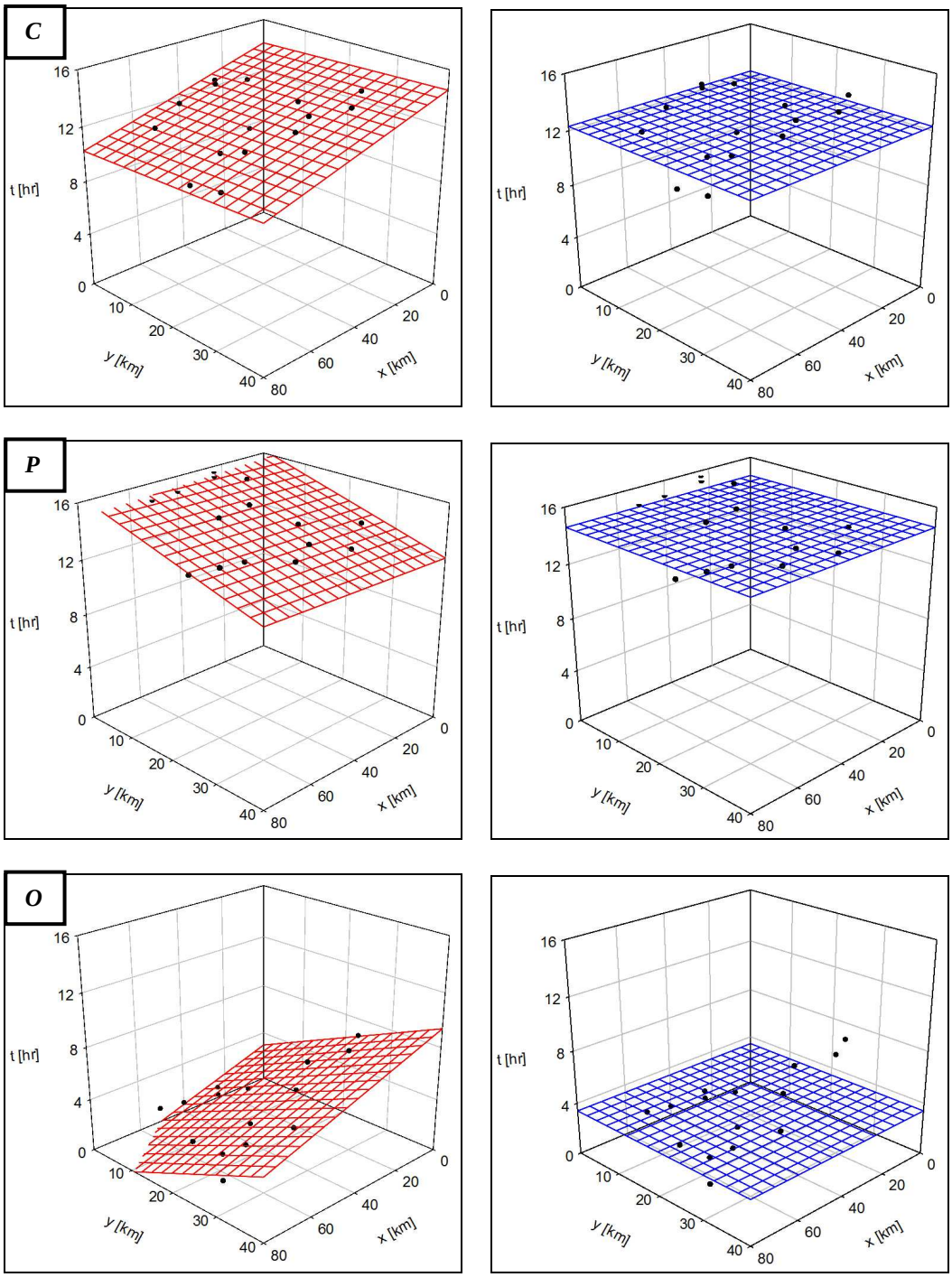

	Centroid			Peak			Onset		
	V [km / hr]	**θ** [° from N]	S. R.	**V** [km / hr]	**θ** [° from N]	S. R.	**V** [km / hr]	**θ** [° from N]	S. R.
n	19.90	100.97	0.59	9.78	177.45	0.53	5.83	160.20	0.64
n-1	19.84	100.96	0.58	9.77	165.46	0.52	5.86	160.20	0.64

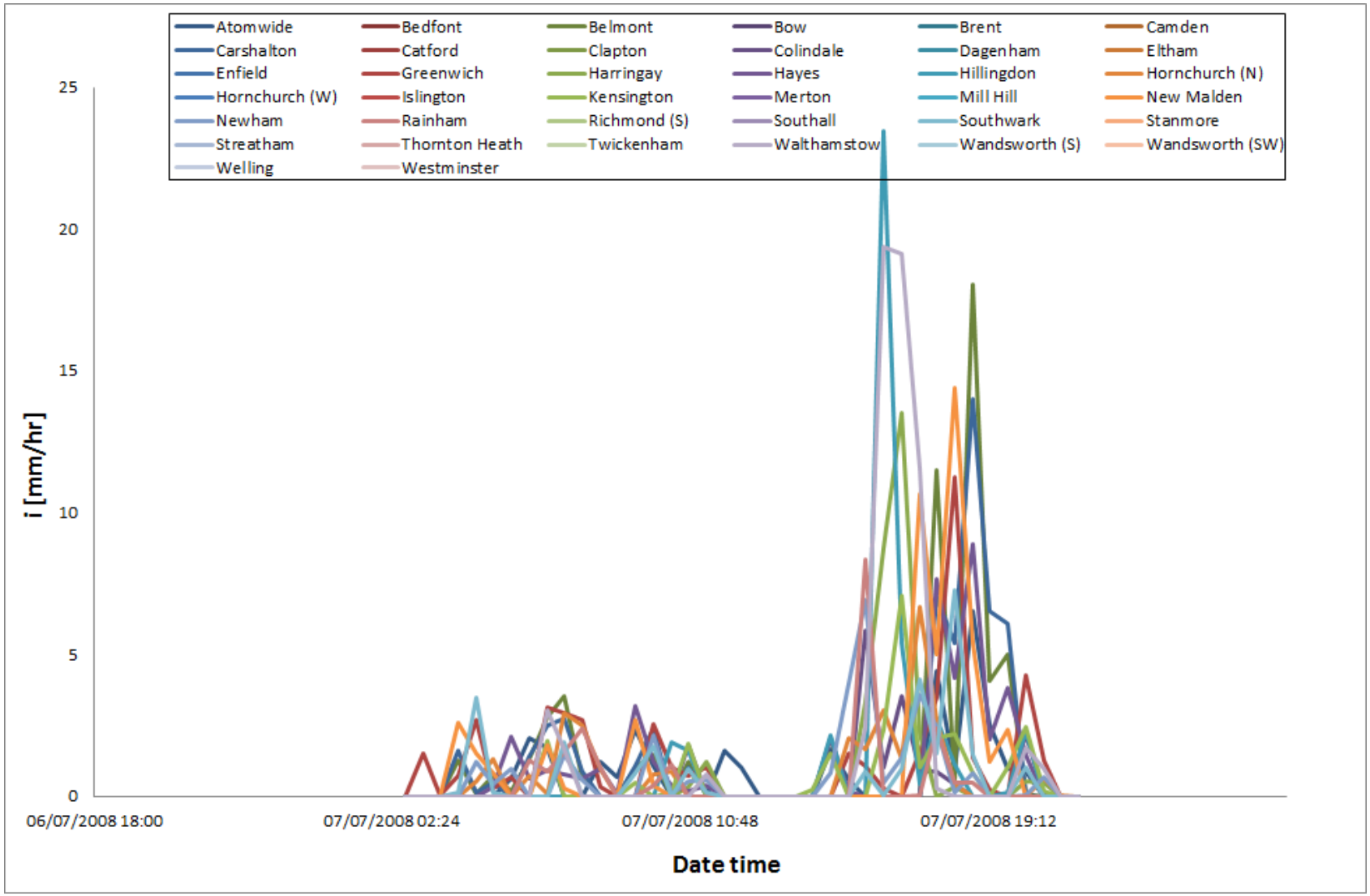
Atomwide
Bedfont
Belmont
Bow
Brent
Camden
Carshalton
Catford
Clapton
Colindale
Dagenham
Eltham
Enfield
Greenwich
Harringay
Hayes
Hillingdon
Hornchurch (N)
Hornchurch (W)
Islington
Kensington
Merton
Mill Hill
New Malden
Newham
Rainham
Richmond (S)
Southall
Southwark
Stanmore
Streatham
Thornton Heath
Twickenham
Walthamstow
Wandsworth (S)
Wandsworth (SW)
Welling
Westminster
25
20
15
10
5
0
i [mm/hr]
06/07/2008 18:00
07/07/2008 02:24
07/07/2008 10:48
07/07/2008 19:12
Date time

Starting Date: 09/07/2008 06:15 – **Final Time:** 10/07/2008 01:15

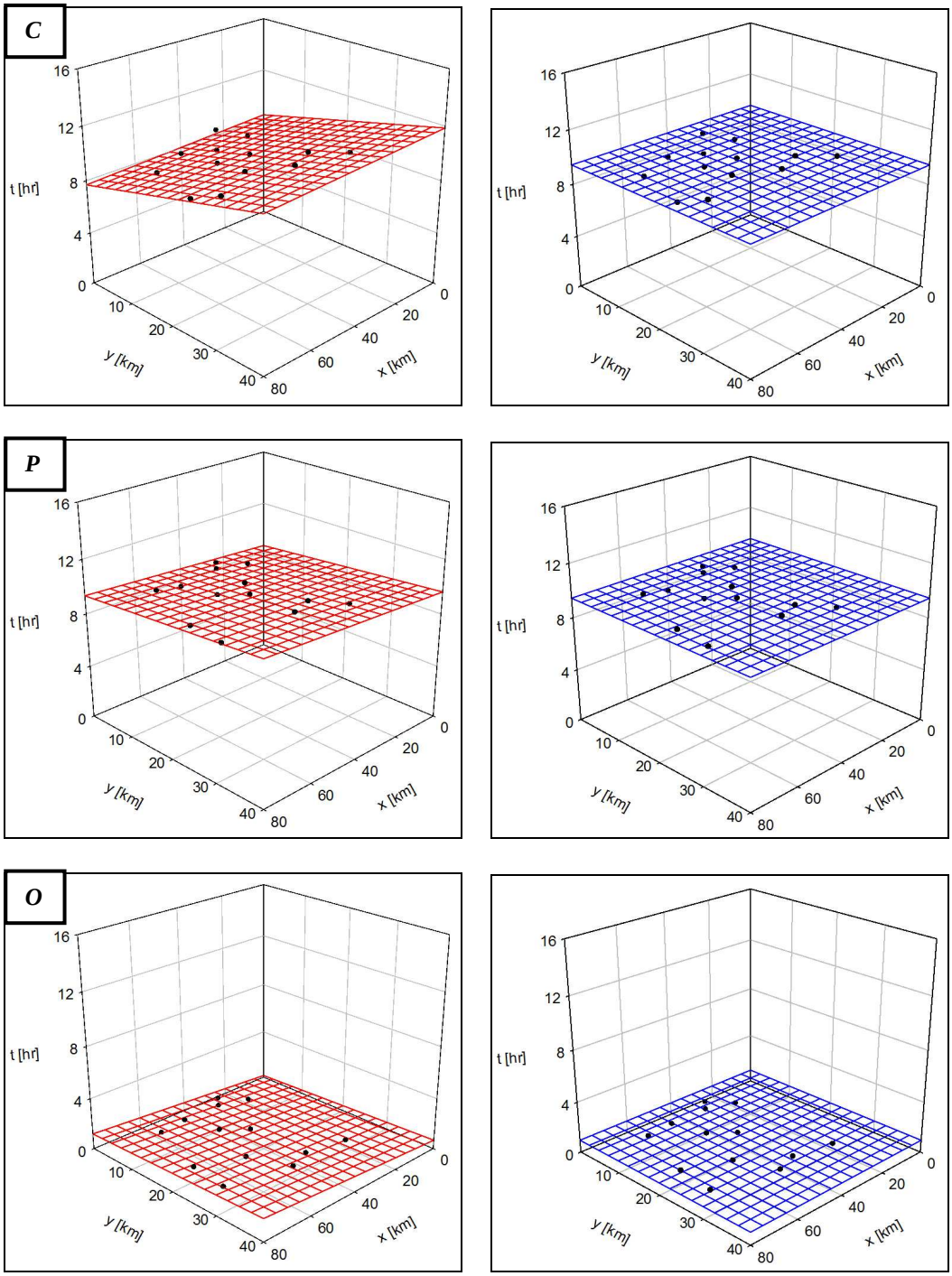

	Centroid			Peak			Onset		
	V [km / hr]	**θ** [° from N]	S. R.	**V** [km / hr]	**θ** [° from N]	S. R.	**V** [km / hr]	**θ** [° from N]	S. R.
n	11.34	174.66	0.41	34.69	20.23	0.85	53.60	44.28	0.34
n-1	11.34	174.62	0.41	34.73	20.27	0.84	53.64	44.66	0.34

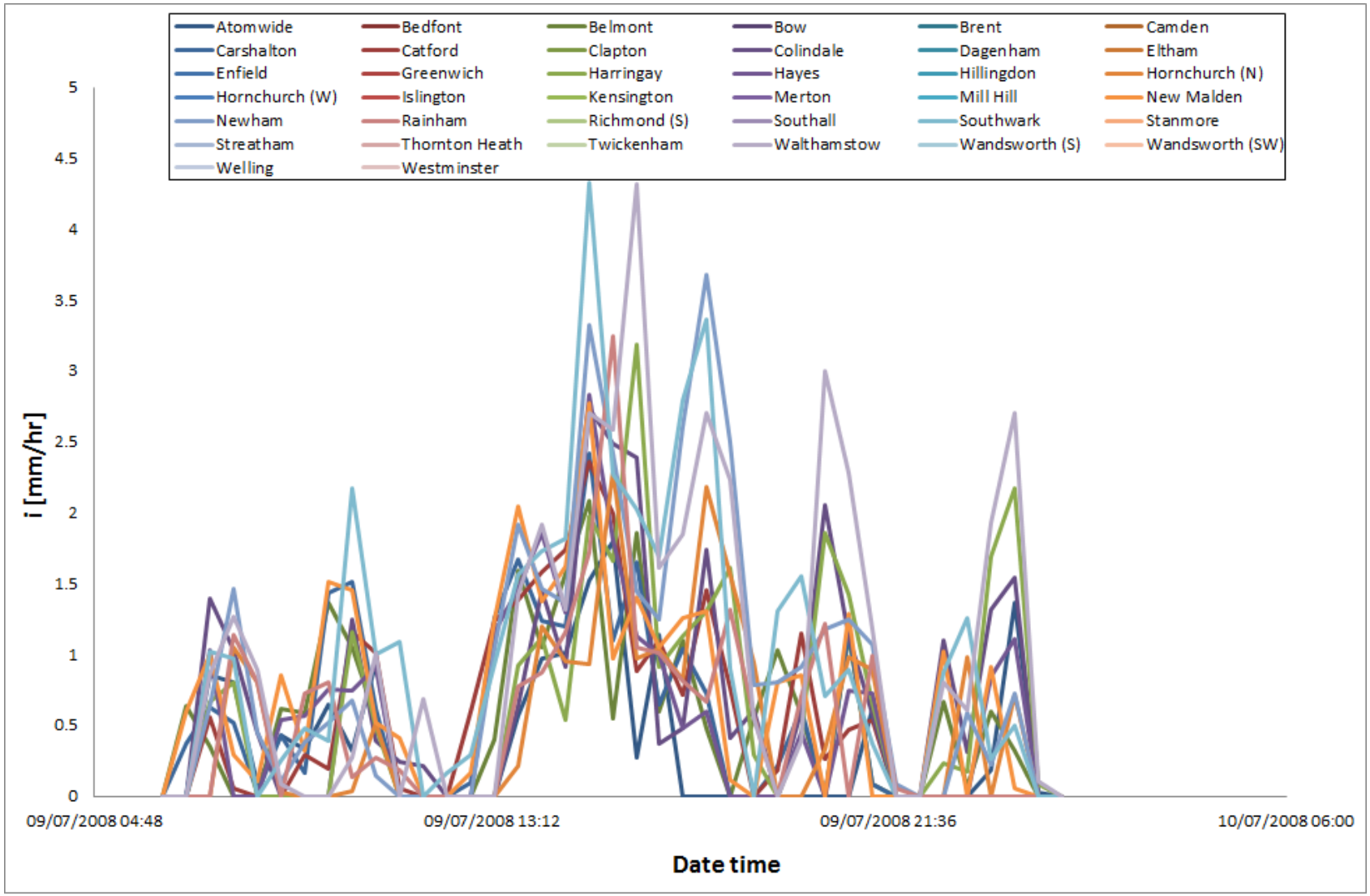
Atomwide
Bedfont
Belmont
Bow
Brent
Camden
Carshalton
Catford
Clapton
Colindale
Dagenham
Eltham
Enfield
Greenwich
Harringay
Hayes
Hillingdon
Hornchurch (N)
Hornchurch (W)
Islington
Kensington
Merton
Mill Hill
New Malden
Newham
Rainham
Richmond (S)
Southall
Southwark
Stanmore
Streatham
Thornton Heath
Twickenham
Walthamstow
Wandsworth (S)
Wandsworth (SW)
Welling
Westminster
i [mm/hr]
5
4.5
4
3.5
3
2.5
2
1.5
1
0.5
0
09/07/2008 04:48
09/07/2008 13:12
09/07/2008 21:36
10/07/2008 06:00
Date time

Starting Date: 02/09/2008 02:15 – **Final Time:** 02/09/2008 12:15

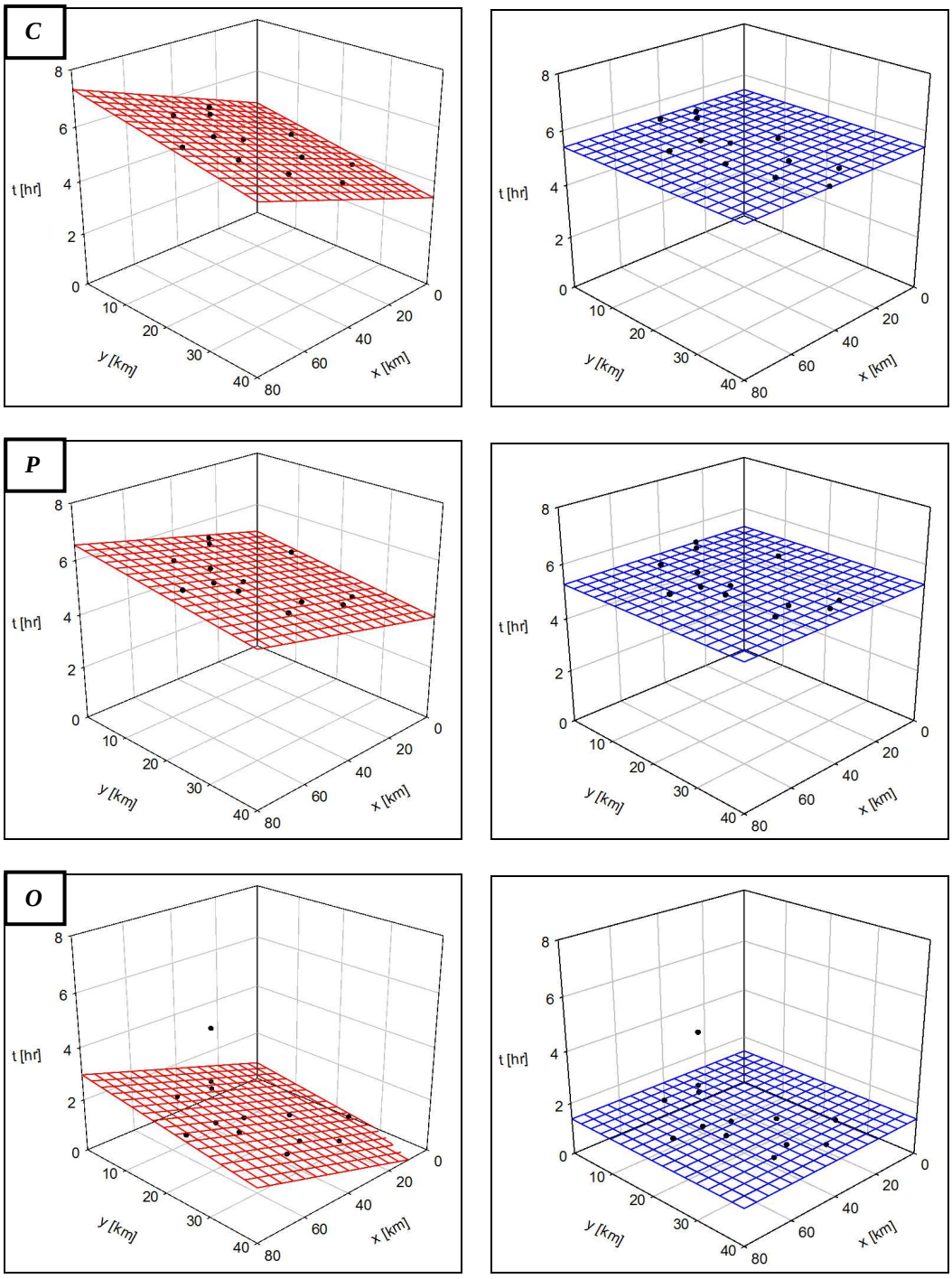

	Centroid			Peak			Onset		
	V [km / hr]	**θ** [° from N]	S. R.	**V** [km / hr]	**θ** [° from N]	S. R.	**V** [km / hr]	**θ** [° from N]	S. R.
n	21.64	135.07	0.40	31.21	140.33	0.64	26.76	130.44	0.84
n-1	21.71	135.06	0.40	31.65	140.55	0.63	26.85	129.96	0.80

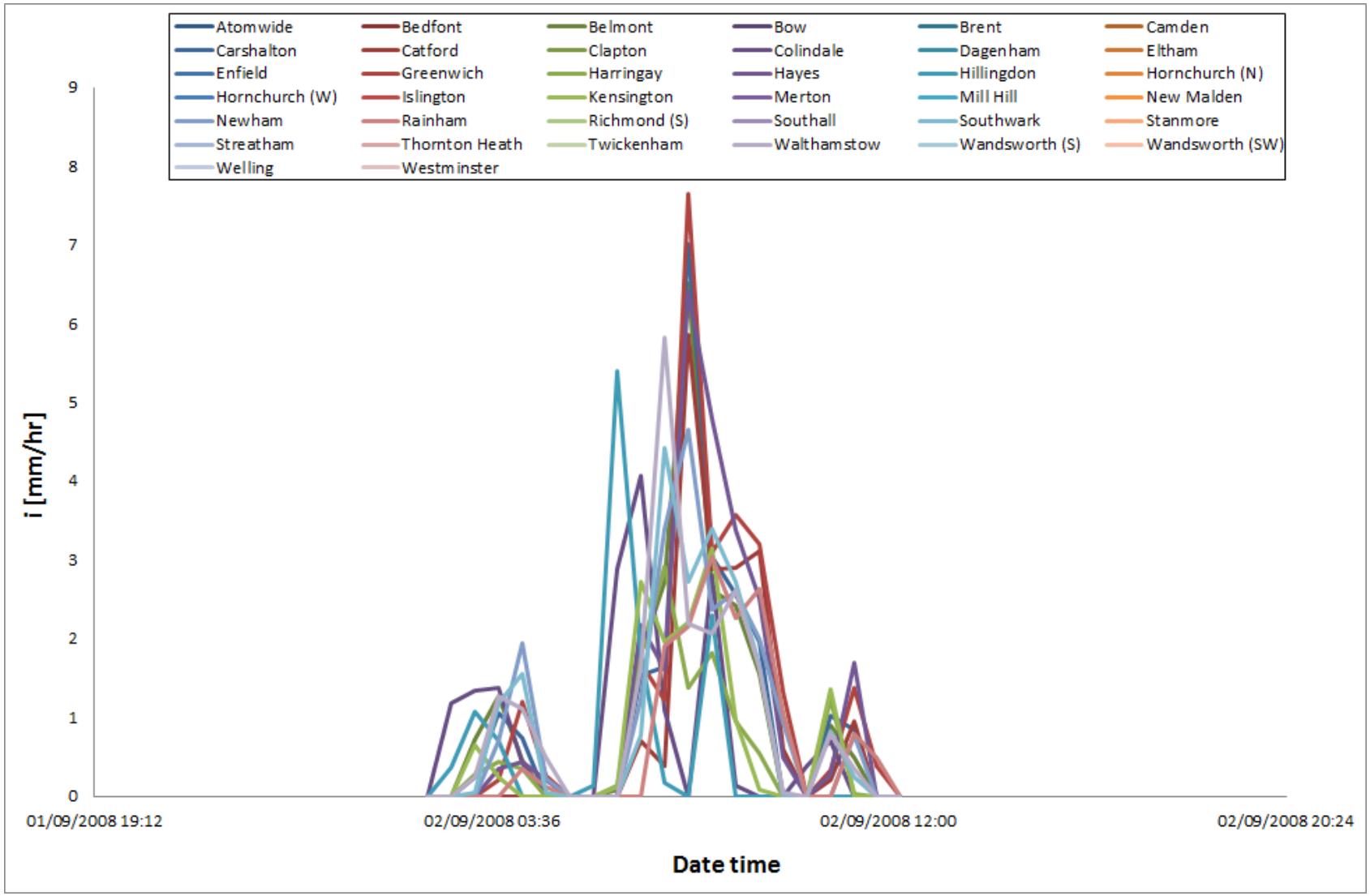
Atomwide
Bedfont
Belmont
Bow
Brent
Camden
Carshalton
Catford
Clapton
Colindale
Dagenham
Eltham
Enfield
Greenwich
Harringay
Hayes
Hillingdon
Hornchurch (N)
Hornchurch (W)
Islington
Kensington
Merton
Mill Hill
New Malden
Newham
Rainham
Richmond (S)
Southall
Southwark
Stanmore
Streatham
Thornton Heath
Twickenham
Walthamstow
Wandsworth (S)
Wandsworth (SW)
Welling
Westminster
i [mm/hr]
0
1
2
3
4
5
6
7
8
9
01/09/2008 19:12
02/09/2008 03:36
02/09/2008 12:00
02/09/2008 20:24
Date time

Starting Date: 05/09/2008 09:15 – **Final Time:** 06/09/2008 00:15

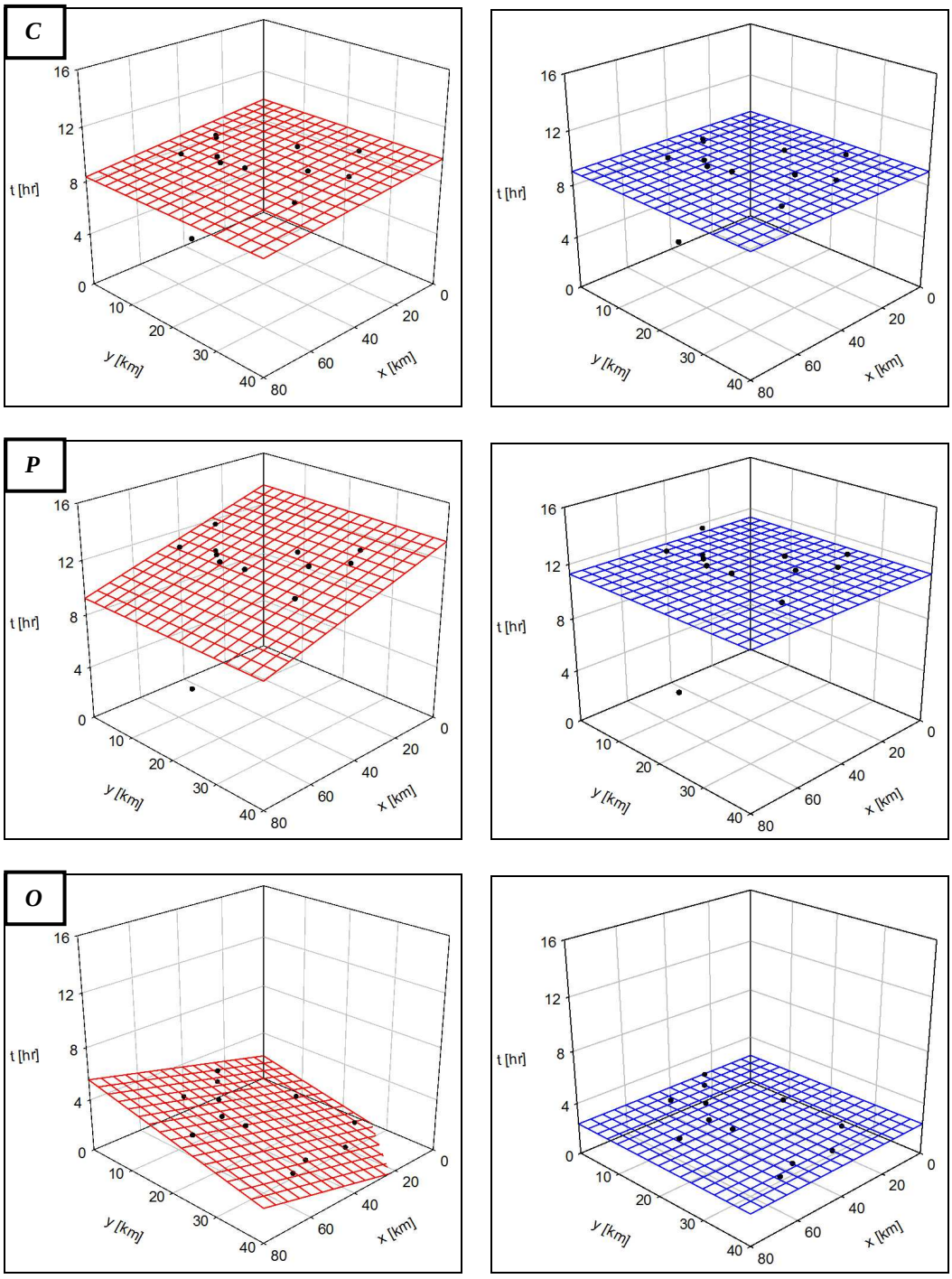

	Centroid			Peak			Onset		
	V [km / hr]	**θ** [° from N]	S. R.	**V** [km / hr]	**θ** [° from N]	S. R.	**V** [km / hr]	**θ** [° from N]	S. R.
n	59.38	88.85	0.96	18.57	84.75	0.89	11.44	149.47	0.64
n-1	49.76	84.70	0.94	18.39	81.01	0.88	11.47	149.35	0.63

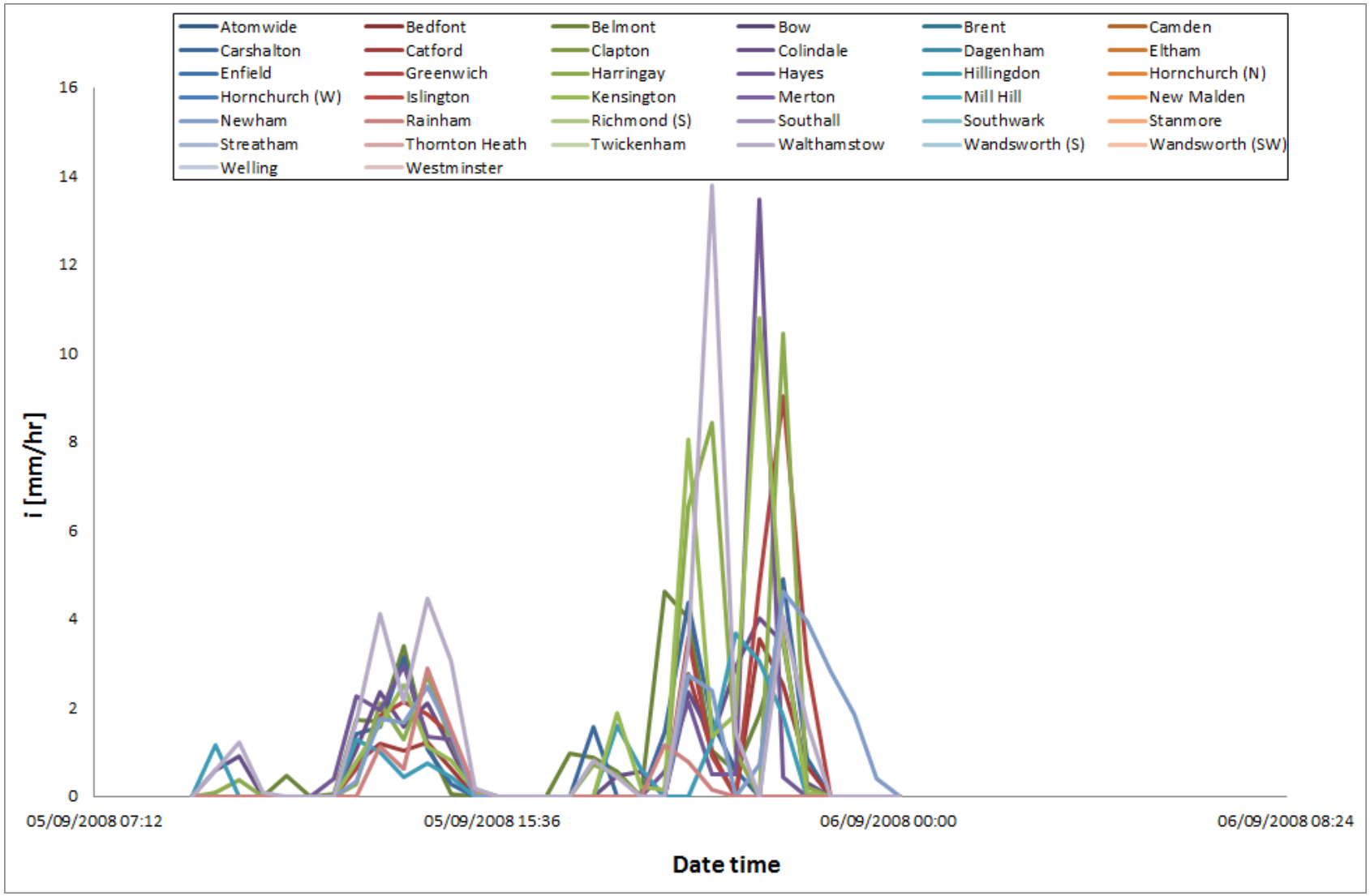
Atomwide
Bedfont
Belmont
Bow
Brent
Camden
Carshalton
Catford
Clapton
Colindale
Dagenham
Eltham
Enfield
Greenwich
Harringay
Hayes
Hillingdon
Hornchurch (N)
Hornchurch (W)
Islington
Kensington
Merton
Mill Hill
New Malden
Newham
Rainham
Richmond (S)
Southall
Southwark
Stanmore
Streatham
Thornton Heath
Twickenham
Walthamstow
Wandsworth (S)
Wandsworth (SW)
Welling
Westminster
16
14
12
10
8
6
4
2
0
i [mm/hr]
05/09/2008 07:12
05/09/2008 15:36
06/09/2008 00:00
06/09/2008 08:24
Date time

Starting Date: 04/10/2008 22:45 – **Final Time:** 05/10/2008 15:45

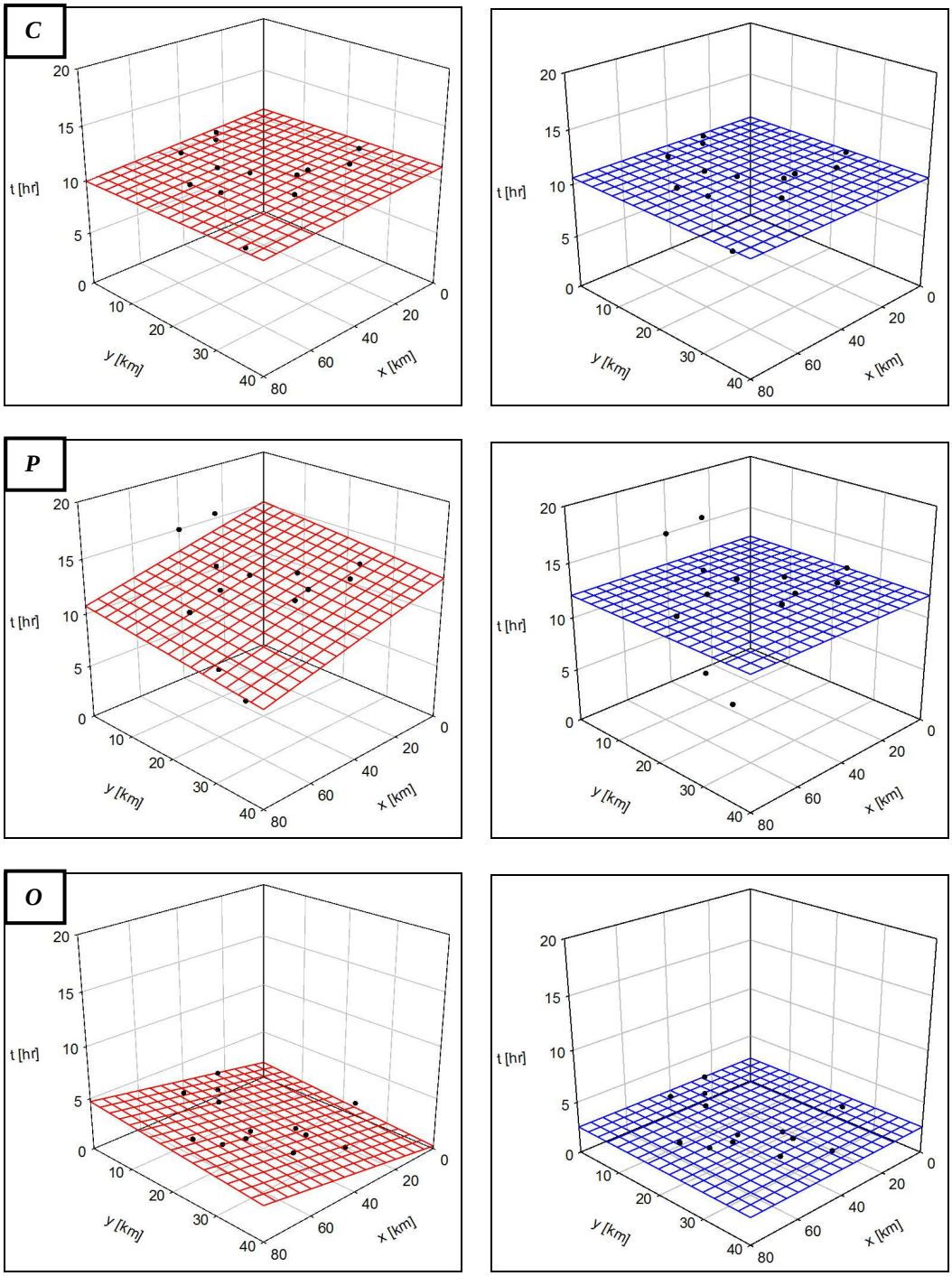

	Centroid			Peak			Onset		
	V [km / hr]	**θ** [° from N]	S. R.	**V** [km / hr]	**θ** [° from N]	S. R.	**V** [km / hr]	**θ** [° from N]	S. R.
n	67.10	114.16	0.99	13.78	49.74	0.97	19.33	132.16	0.83
n-1	58.71	94.34	0.98	15.73	55.62	0.96	19.46	131.62	0.82

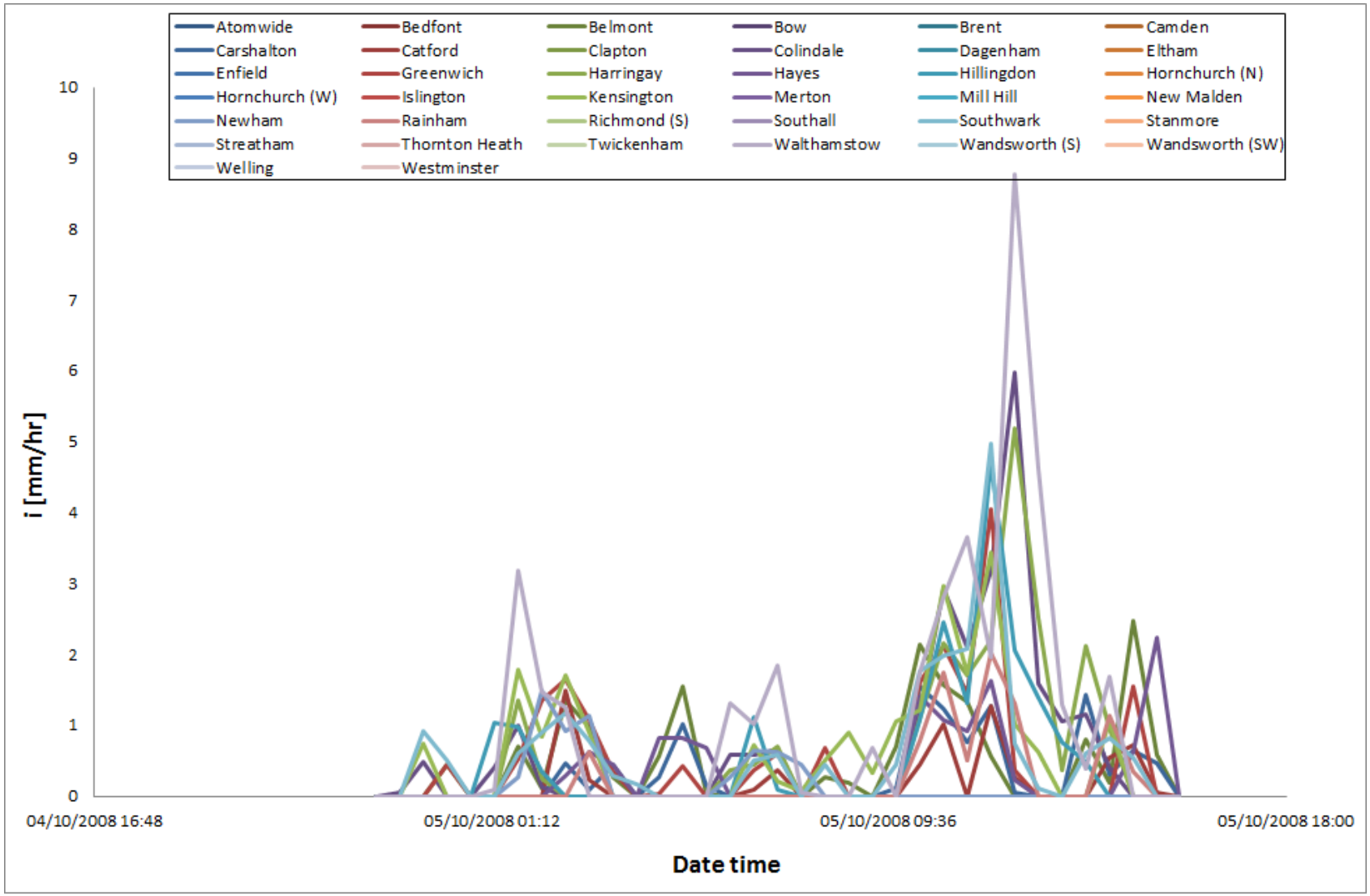
Atomwide
Bedfont
Belmont
Bow
Brent
Camden
Carshalton
Catford
Clapton
Colindale
Dagenham
Eltham
Enfield
Greenwich
Harringay
Hayes
Hillingdon
Hornchurch (N)
Hornchurch (W)
Islington
Kensington
Merton
Mill Hill
New Malden
Newham
Rainham
Richmond (S)
Southall
Southwark
Stanmore
Streatham
Thornton Heath
Twickenham
Walthamstow
Wandsworth (S)
Wandsworth (SW)
Welling
Westminster
10
9
8
7
6
5
4
3
2
1
0
i [mm/hr]
04/10/2008 16:48
05/10/2008 01:12
05/10/2008 09:36
05/10/2008 18:00
Date time

Starting Date: 10/11/2008 08:15 – **Final Time:** 10/11/2008 18:15

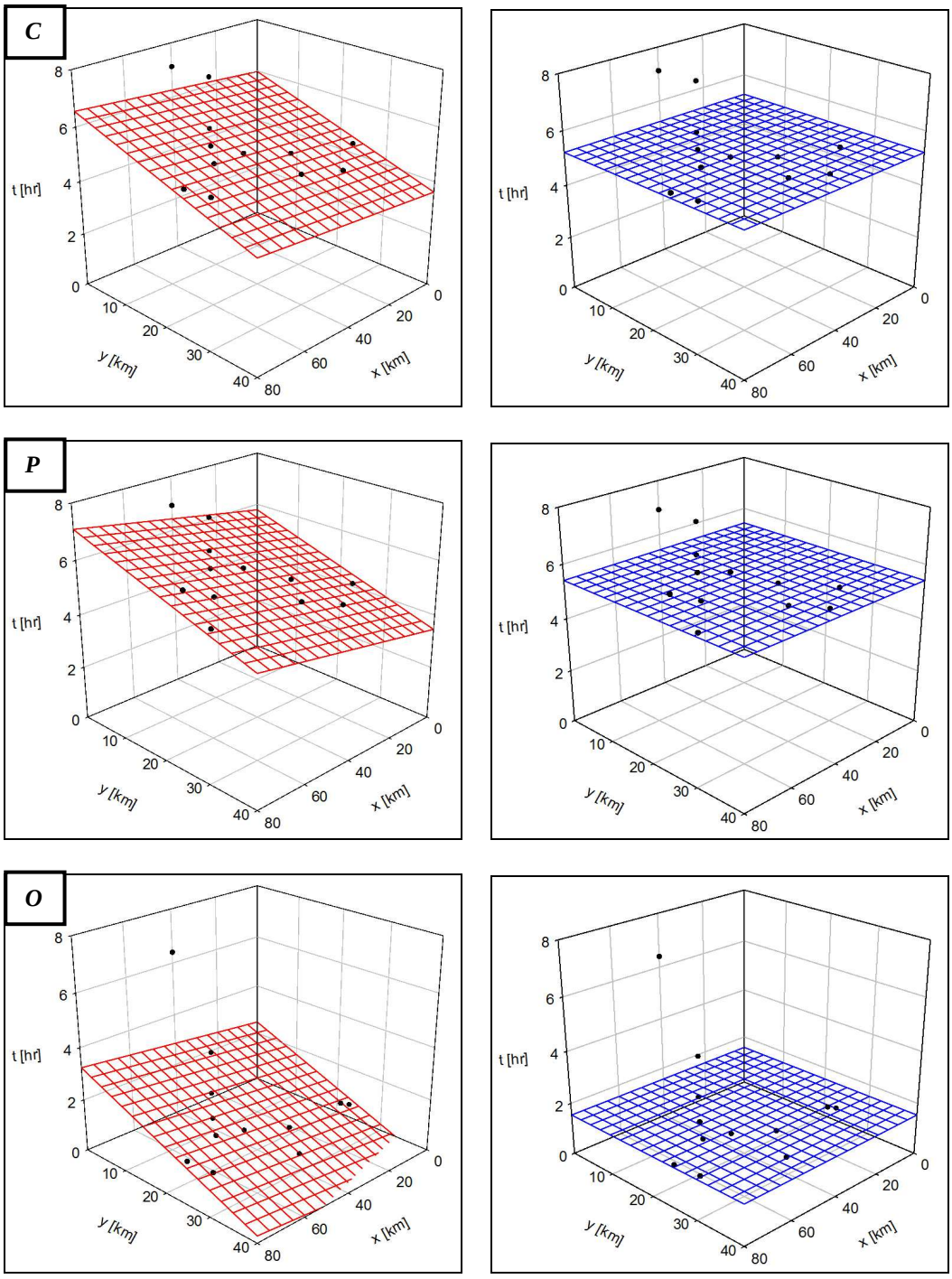

	Centroid			Peak			Onset		
	V [km / hr]	**θ** [° from N]	S. R.	**V** [km / hr]	**θ** [° from N]	S. R.	**V** [km / hr]	**θ** [° from N]	S. R.
n	16.79	173.04	0.80	16.61	164.17	0.67	13.35	172.70	0.91
n-1	17.54	157.74	0.79	16.91	163.83	0.66	21.72	144.96	0.91

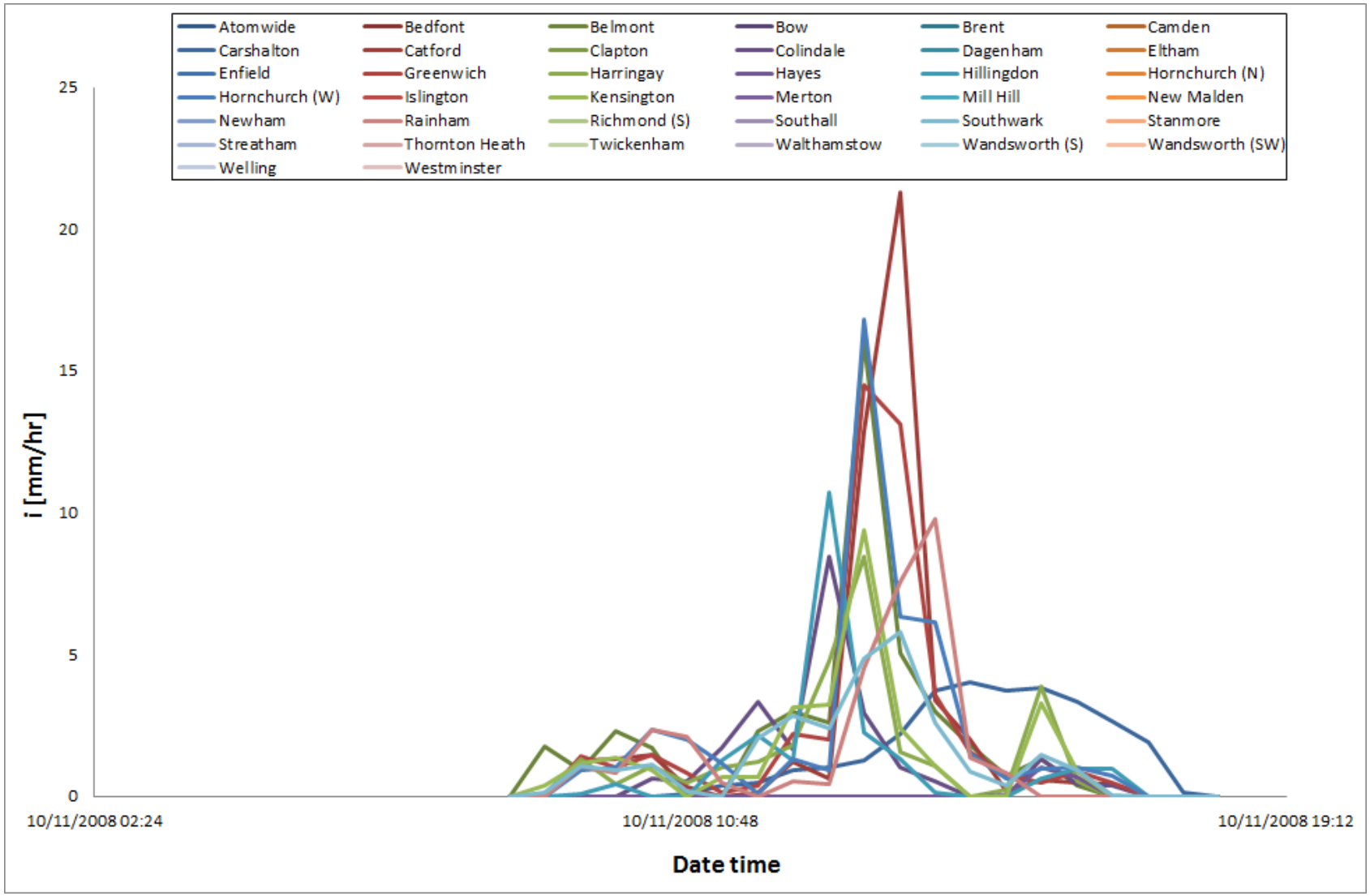
Atomwide
Bedfont
Belmont
Bow
Brent
Camden
Carshalton
Catford
Clapton
Colindale
Dagenham
Eltham
Enfield
Greenwich
Harringay
Hayes
Hillingdon
Hornchurch (N)
Hornchurch (W)
Islington
Kensington
Merton
Mill Hill
New Malden
Newham
Rainham
Richmond (S)
Southall
Southwark
Stanmore
Streatham
Thornton Heath
Twickenham
Walthamstow
Wandsworth (S)
Wandsworth (SW)
Welling
Westminster
25
20
15
10
5
0
i [mm/hr]
10/11/2008 02:24
10/11/2008 10:48
10/11/2008 19:12
Date time

Starting Date: 04/12/2008 05:15 – **Final Time:** 04/12/2008 10:15

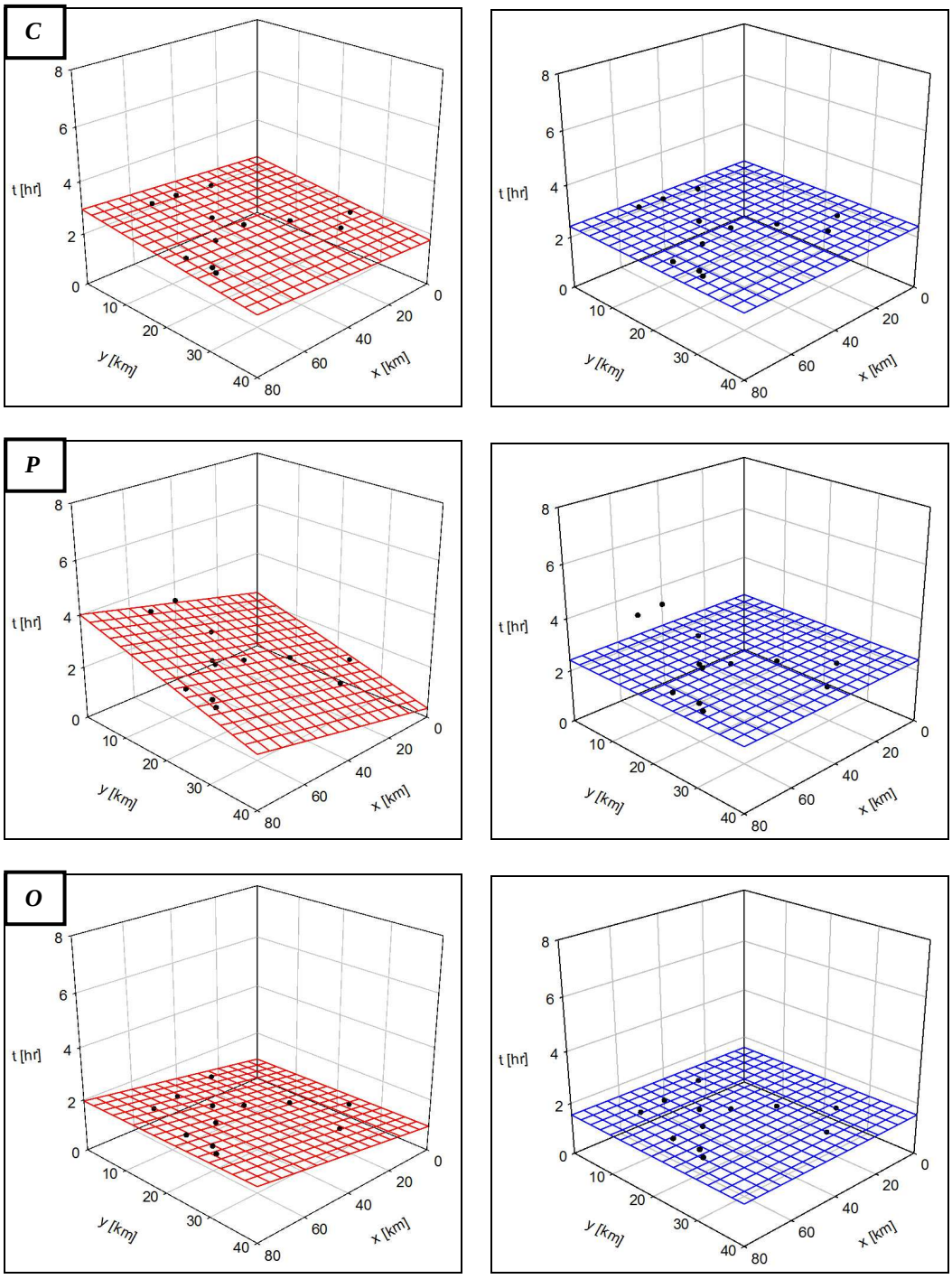

	Centroid			Peak			Onset		
	V [km / hr]	**θ** [° from N]	S. R.	**V** [km / hr]	**θ** [° from N]	S. R.	**V** [km / hr]	**θ** [° from N]	S. R.
n	54.01	160.26	0.73	18.59	157.13	0.61	72.10	80.55	0.45
n-1	55.06	160.06	0.72	18.87	156.71	0.60	71.41	80.30	0.45

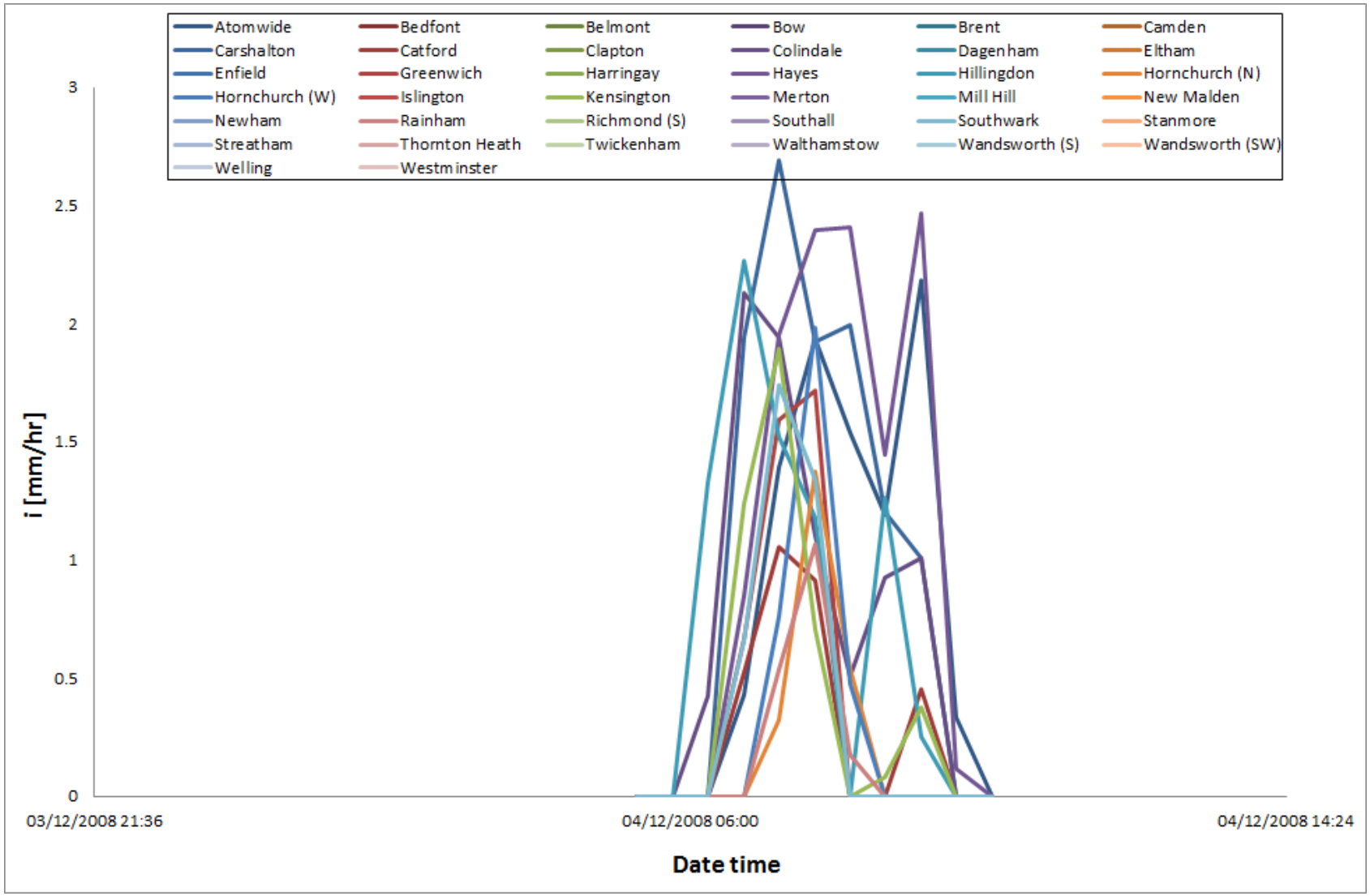
Atomwide
Bedfont
Belmont
Bow
Brent
Camden
Carshalton
Catford
Clapton
Colindale
Dagenham
Eltham
Enfield
Greenwich
Harringay
Hayes
Hillingdon
Hornchurch (N)
Hornchurch (W)
Islington
Kensington
Merton
Mill Hill
New Malden
Newham
Rainham
Richmond (S)
Southall
Southwark
Stanmore
Streatham
Thornton Heath
Twickenham
Walthamstow
Wandsworth (S)
Wandsworth (SW)
Welling
Westminster
3
2.5
2
1.5
1
0.5
0
i [mm/hr]
03/12/2008 21:36
04/12/2008 06:00
04/12/2008 14:24
Date time

Starting Date: 13/12/2008 00:45 – **Final Time:** 14/12/2008 00:15

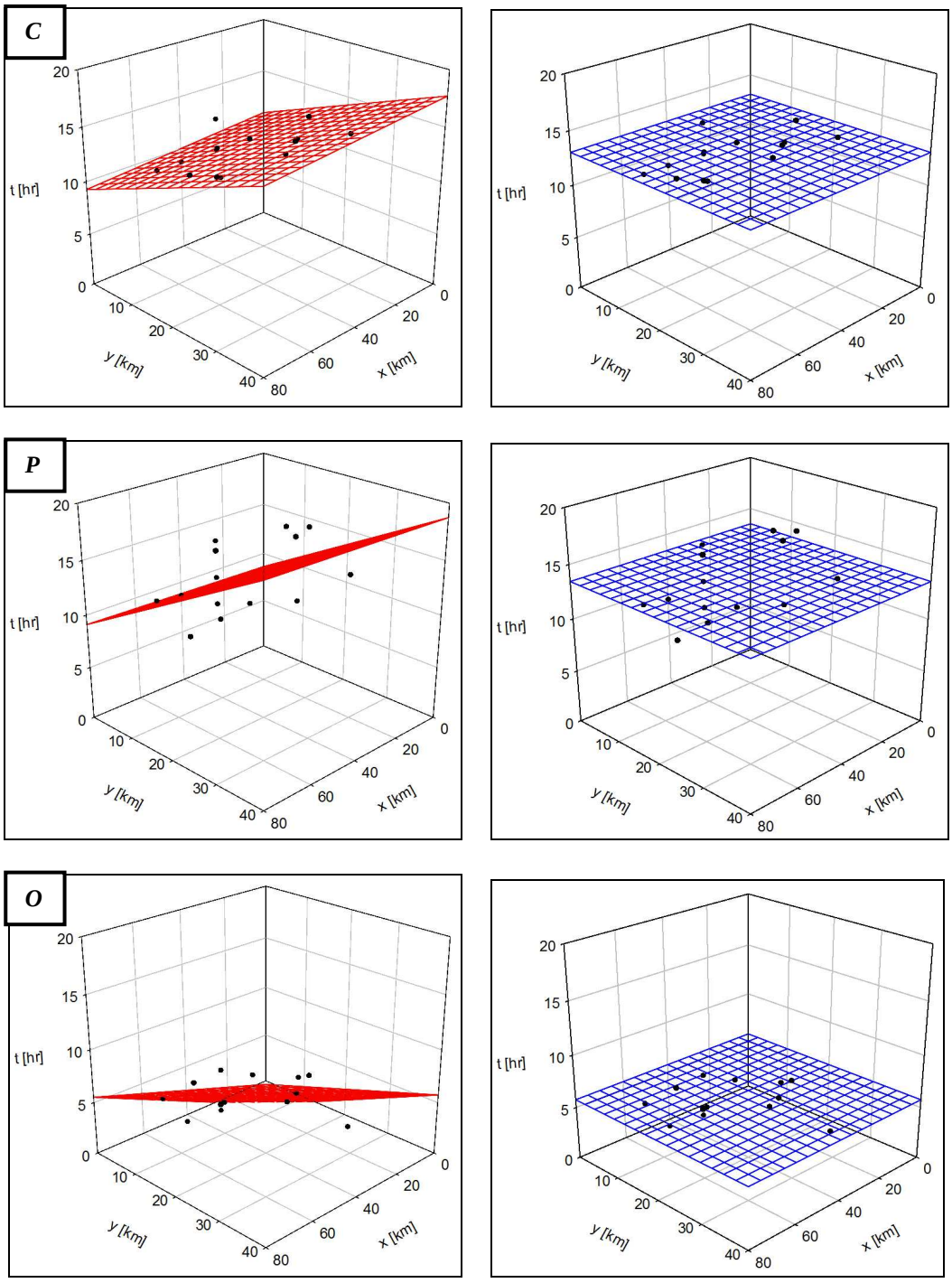

	Centroid			Peak			Onset		
	V [km / hr]	**θ** [° from N]	S. R.	**V** [km / hr]	**θ** [° from N]	S. R.	**V** [km / hr]	**θ** [° from N]	S. R.
n	5.71	173.95	0.51	3.94	1.36	0.74	4.28	25.91	0.53
n-1	5.71	173.89	0.50	3.95	39.82	0.74	4.28	25.87	0.52

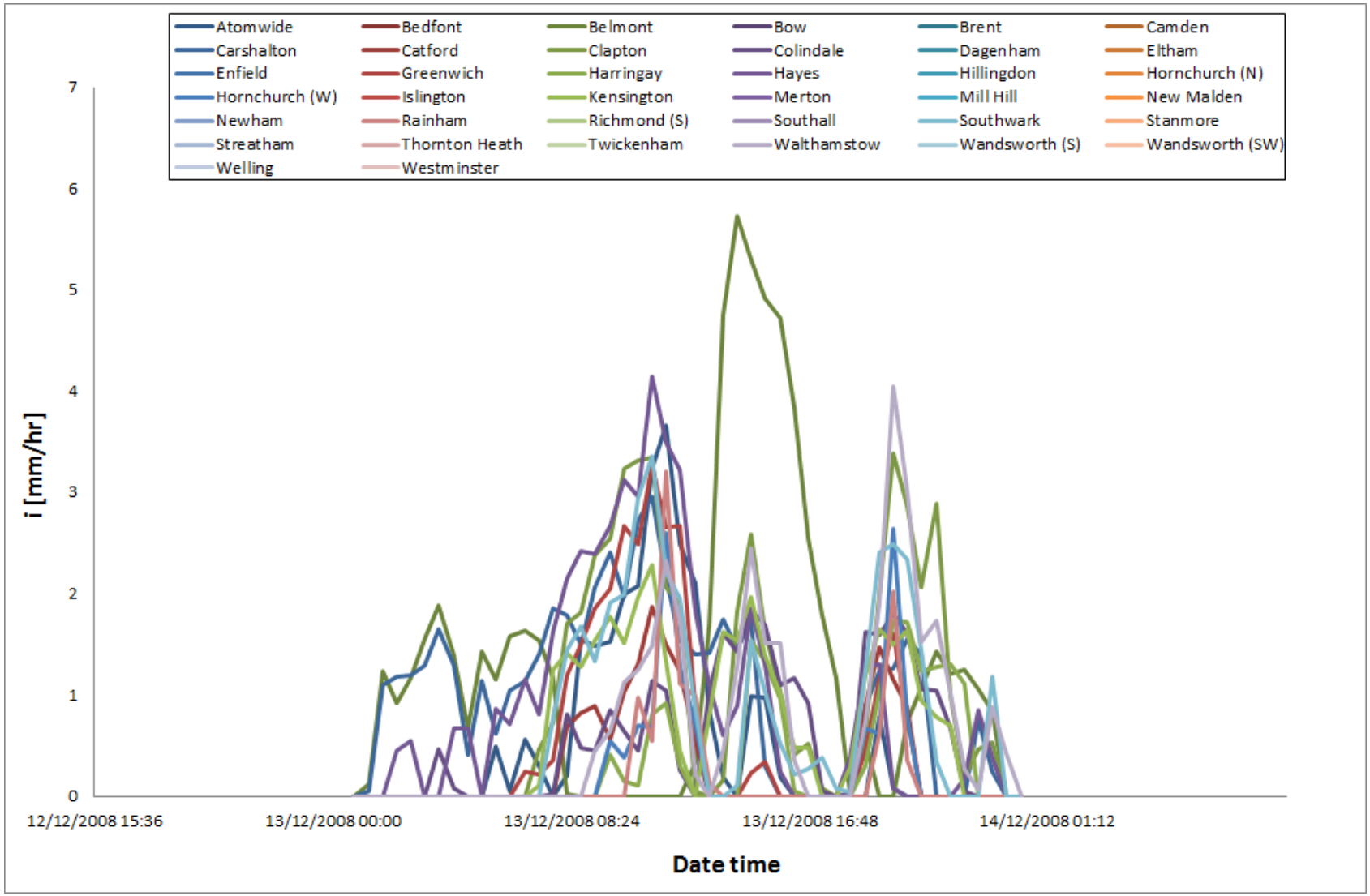
Atomwide
Bedfont
Belmont
Bow
Brent
Camden
Carshalton
Catford
Clapton
Colindale
Dagenham
Eltham
Enfield
Greenwich
Harringay
Hayes
Hillingdon
Hornchurch (N)
Hornchurch (W)
Islington
Kensington
Merton
Mill Hill
New Malden
Newham
Rainham
Richmond (S)
Southall
Southwark
Stanmore
Streatham
Thornton Heath
Twickenham
Walthamstow
Wandsworth (S)
Wandsworth (SW)
Welling
Westminster
i [mm/hr]
0
1
2
3
4
5
6
7
12/12/2008 15:36
13/12/2008 00:00
13/12/2008 08:24
13/12/2008 16:48
14/12/2008 01:12
Date time

Starting Date: 19/01/2009 03:15 – **Final Time:** 19/01/2009 10:15

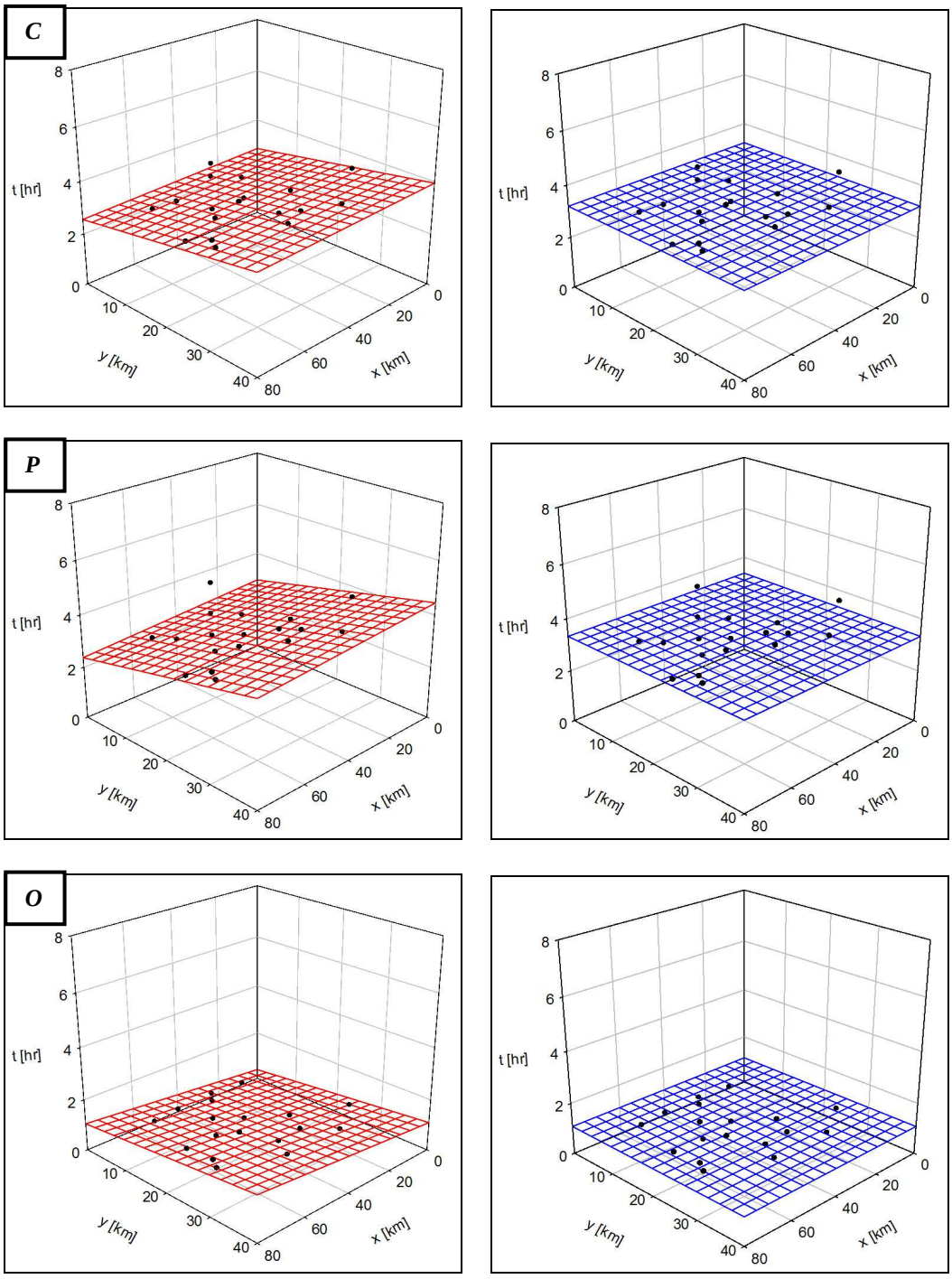

	Centroid			Peak			Onset		
	V [km / hr]	**θ** [° from N]	S. R.	**V** [km / hr]	**θ** [° from N]	S. R.	**V** [km / hr]	**θ** [° from N]	S. R.
n	34.63	174.21	0.70	25.07	170.88	0.70	51.31	24.97	0.58
n-1	34.78	174.24	0.69	25.20	170.80	0.70	51.52	25.09	0.58

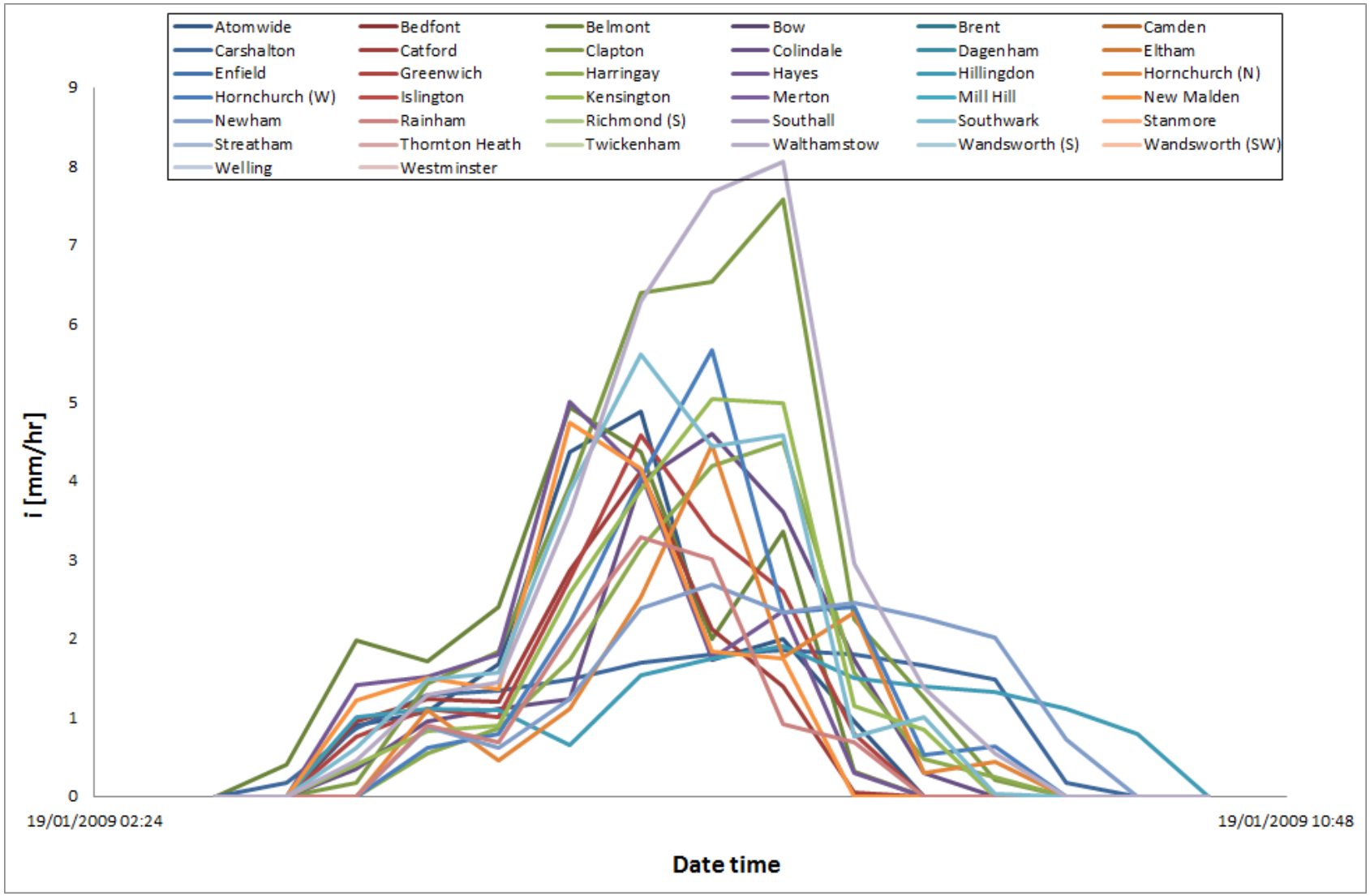
Atomwide
Bedfont
Belmont
Bow
Brent
Camden
Carshalton
Catford
Clapton
Colindale
Dagenham
Eltham
Enfield
Greenwich
Harringay
Hayes
Hillingdon
Hornchurch (N)
Hornchurch (W)
Islington
Kensington
Merton
Mill Hill
New Malden
Newham
Rainham
Richmond (S)
Southall
Southwark
Stanmore
Streatham
Thornton Heath
Twickenham
Walthamstow
Wandsworth (S)
Wandsworth (SW)
Welling
Westminster
i [mm/hr]
0
1
2
3
4
5
6
7
8
9
19/01/2009 02:24
19/01/2009 10:48
Date time

Starting Date: 03/02/2009 09:45 – **Final Time:** 03/02/2009 17:15

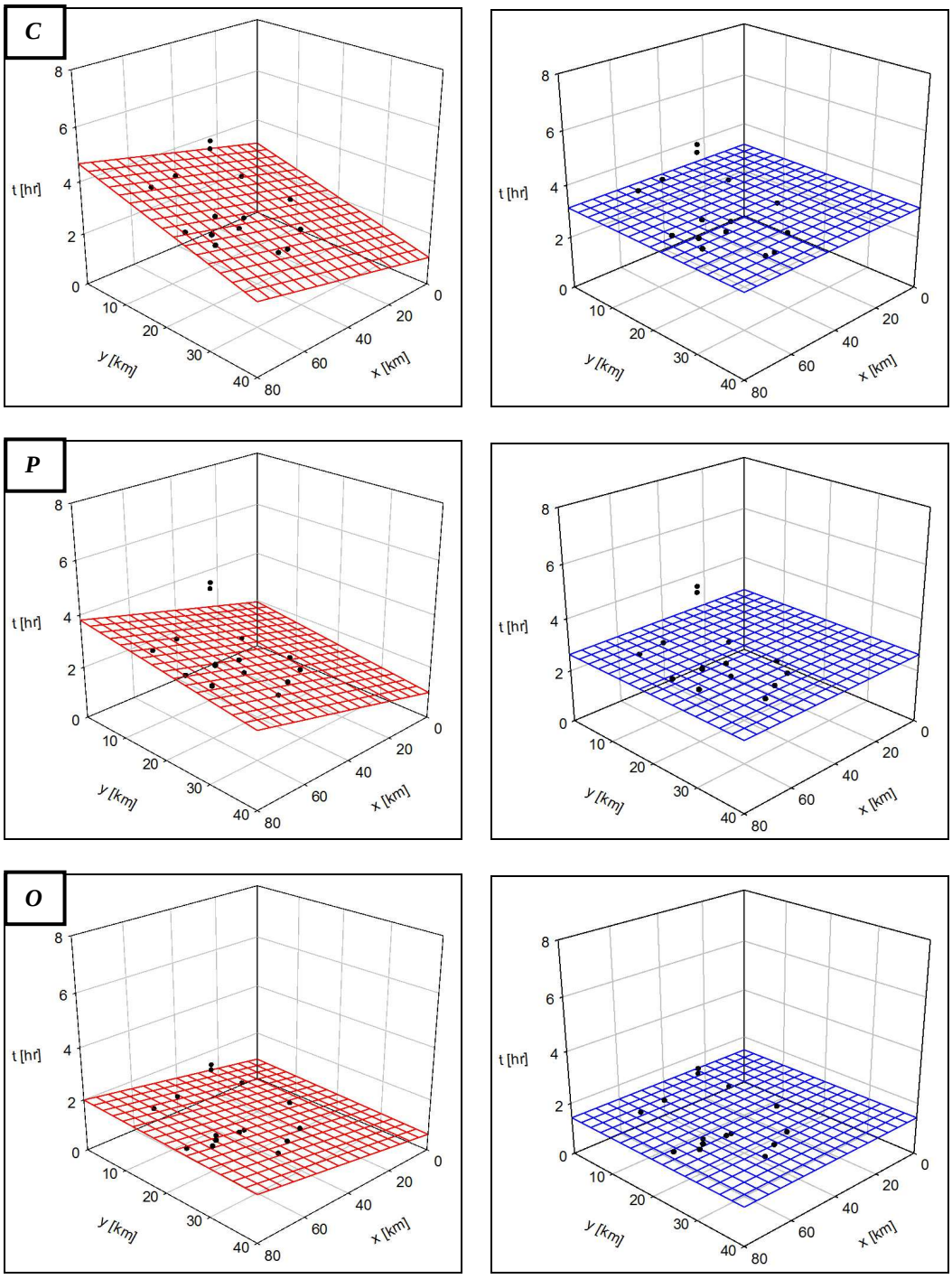

	Centroid			Peak			Onset		
	V [km / hr]	**θ** [° from N]	S. R.	**V** [km / hr]	**θ** [° from N]	S. R.	**V** [km / hr]	**θ** [° from N]	S. R.
n	18.85	157.29	0.70	30.13	135.24	0.89	65.31	112.02	0.90
n-1	18.90	157.23	0.70	30.18	134.43	0.88	64.73	111.49	0.90

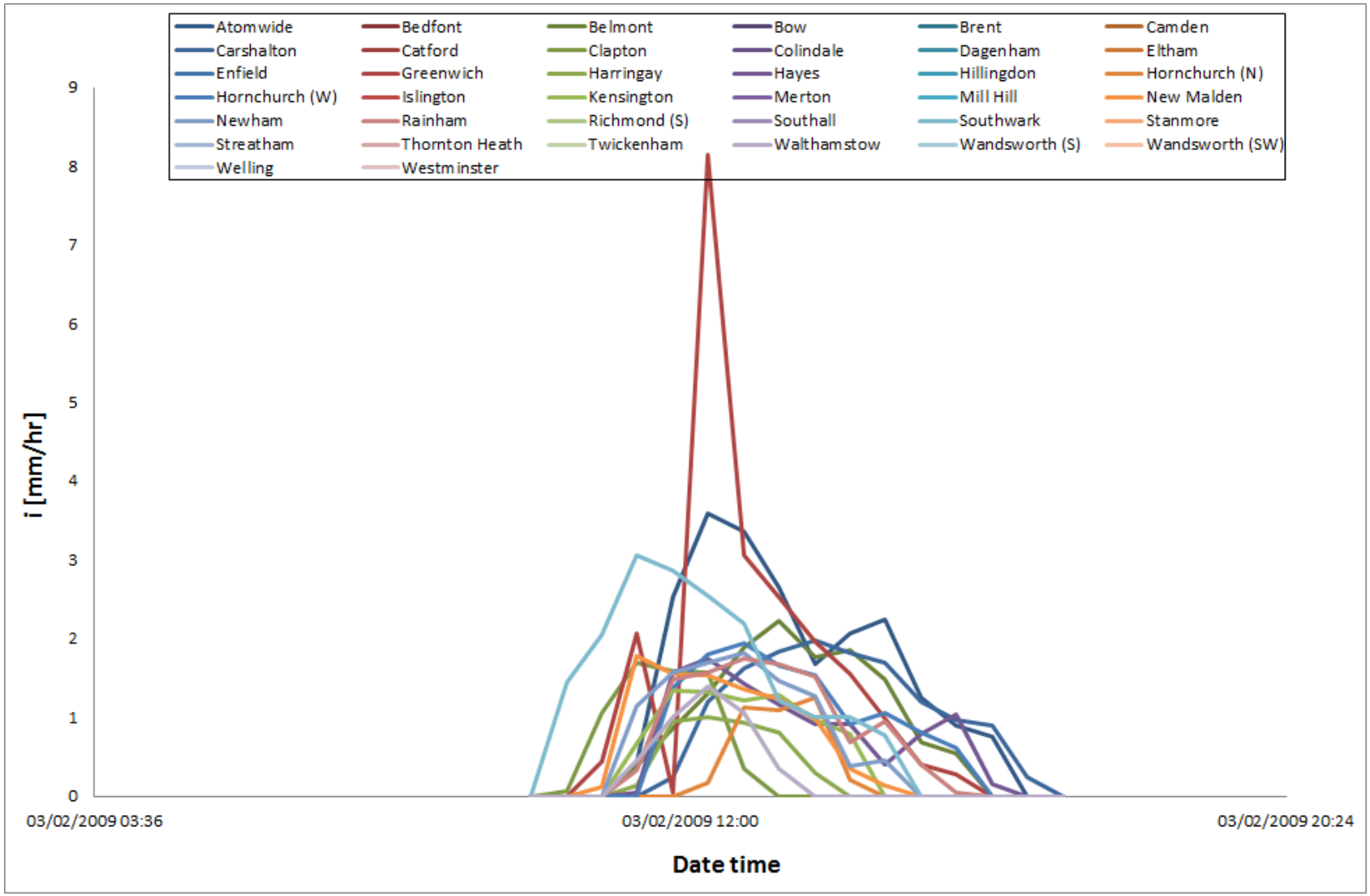
Atomwide
Bedfont
Belmont
Bow
Brent
Camden
Carshalton
Catford
Clapton
Colindale
Dagenham
Eltham
Enfield
Greenwich
Harringay
Hayes
Hillingdon
Hornchurch (N)
Hornchurch (W)
Islington
Kensington
Merton
Mill Hill
New Malden
Newham
Rainham
Richmond (S)
Southall
Southwark
Stanmore
Streatham
Thornton Heath
Twickenham
Walthamstow
Wandsworth (S)
Wandsworth (SW)
Welling
Westminster
i [mm/hr]
0
1
2
3
4
5
6
7
8
9
03/02/2009 03:36
03/02/2009 12:00
03/02/2009 20:24
Date time

Starting Date: 06/02/2009 05:15 – **Final Time:** 06/02/2009 13:45

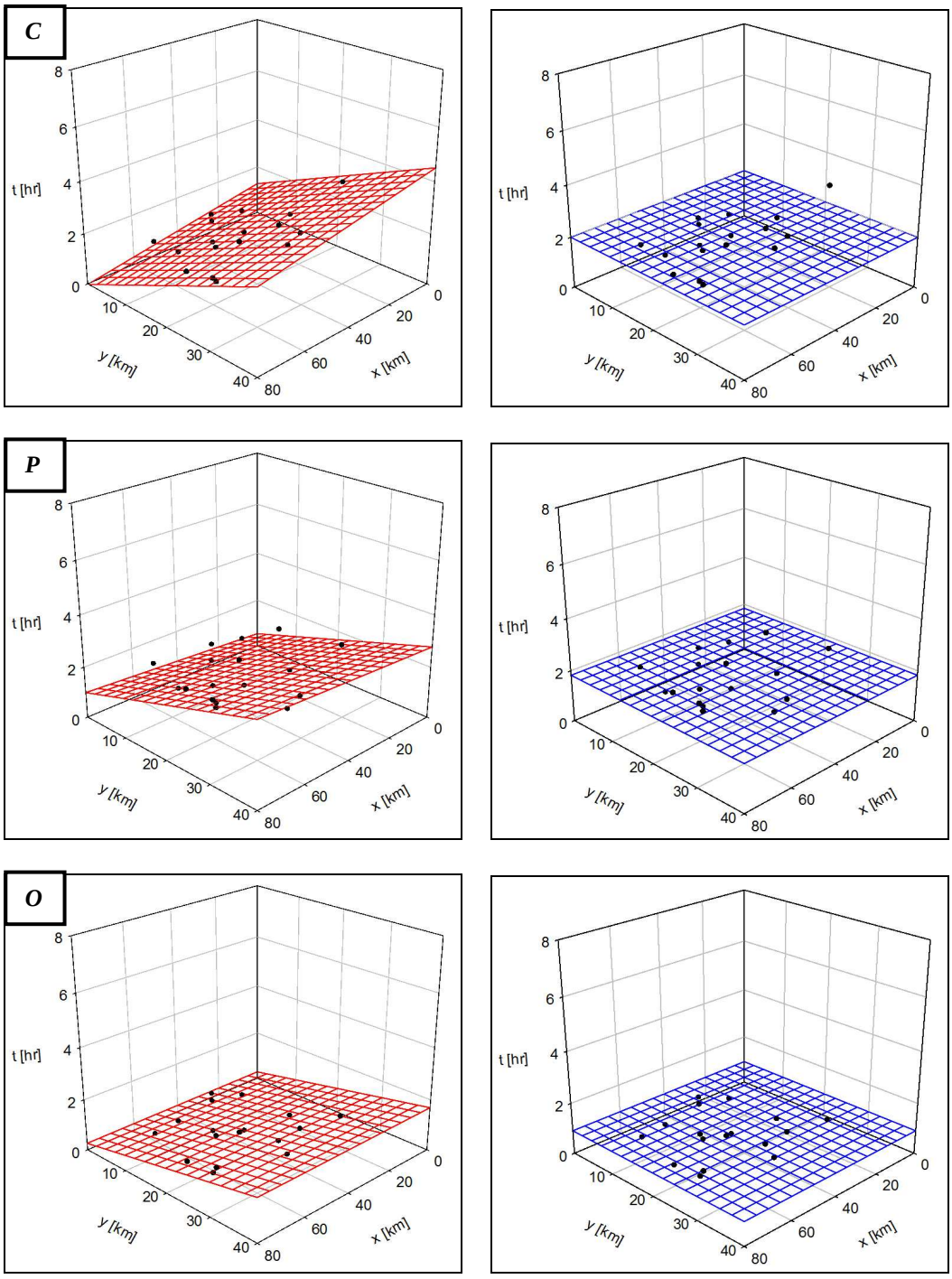

	Centroid			Peak			Onset		
	V [km / hr]	**θ** [° from N]	S. R.	**V** [km / hr]	**θ** [° from N]	S. R.	**V** [km / hr]	**θ** [° from N]	S. R.
n	12.11	168.68	0.39	17.69	5.73	0.79	28.57	179.47	0.52
n-1	12.16	168.77	0.38	17.85	6.03	0.79	28.62	137.14	0.52

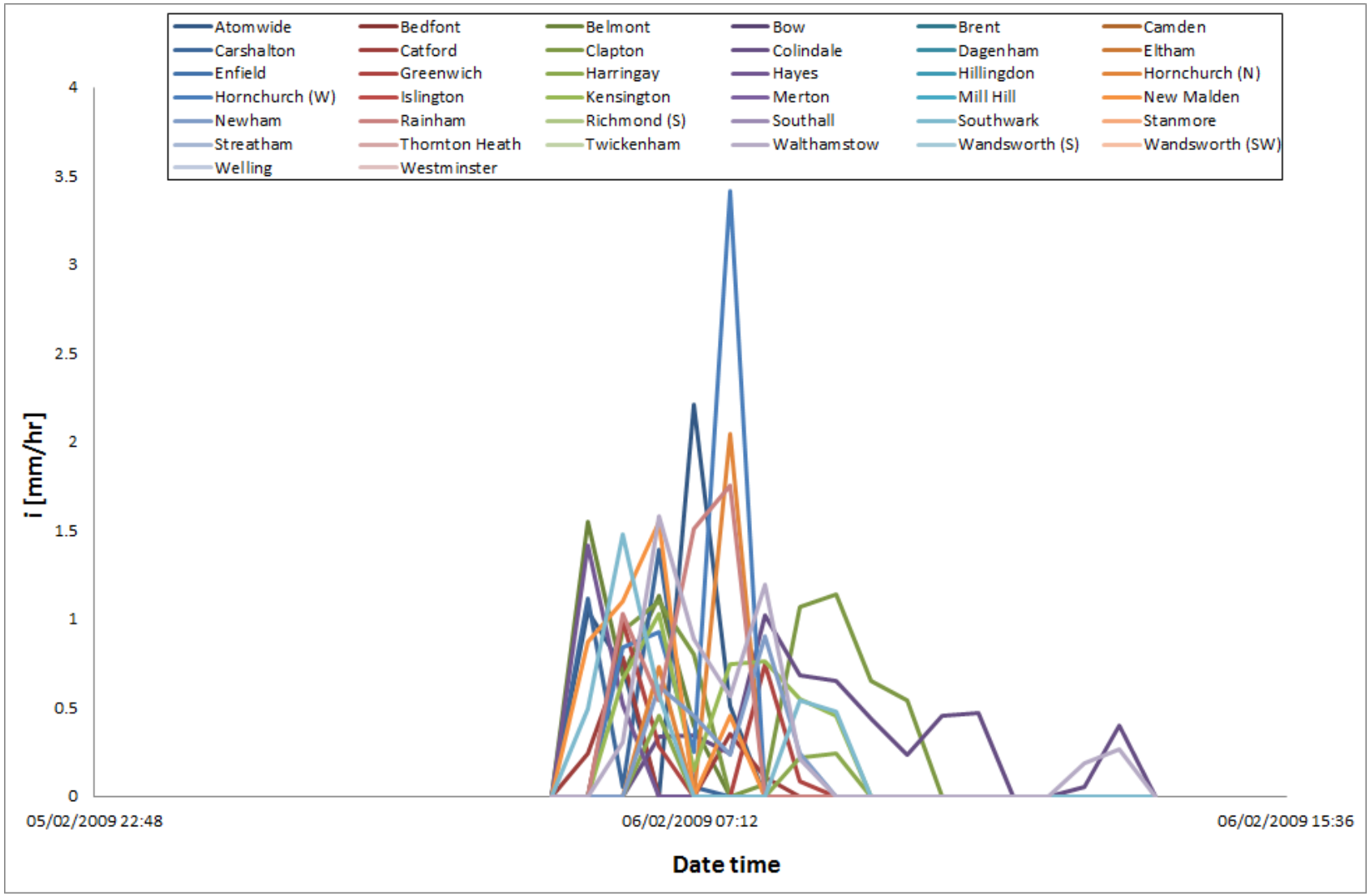
Atomwide
Bedfont
Belmont
Bow
Brent
Camden
Carshalton
Catford
Clapton
Colindale
Dagenham
Eltham
Enfield
Greenwich
Harringay
Hayes
Hillingdon
Hornchurch (N)
Hornchurch (W)
Islington
Kensington
Merton
Mill Hill
New Malden
Newham
Rainham
Richmond (S)
Southall
Southwark
Stanmore
Streatham
Thornton Heath
Twickenham
Walthamstow
Wandsworth (S)
Wandsworth (SW)
Welling
Westminster
4
3.5
3
2.5
2
1.5
1
0.5
0
i [mm/hr]
05/02/2009 22:48
06/02/2009 07:12
06/02/2009 15:36
Date time

Starting Date: 09/02/2009 07:15 – **Final Time:** 10/02/2009 06:15

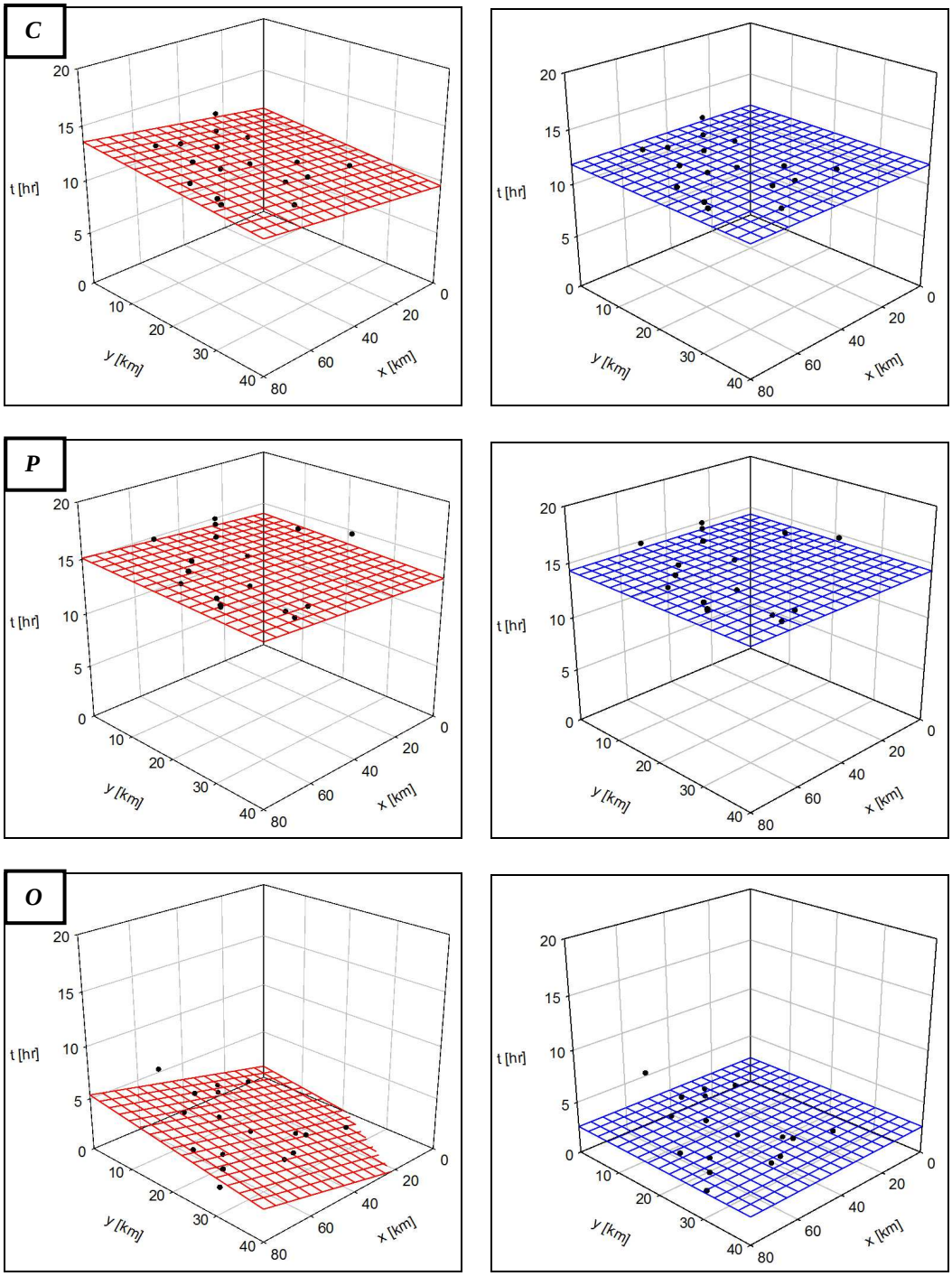

	Centroid			Peak			Onset		
	V [km / hr]	**θ** [° from N]	S. R.	**V** [km / hr]	**θ** [° from N]	S. R.	**V** [km / hr]	**θ** [° from N]	S. R.
n	19.87	142.55	0.72	44.41	141.73	0.99	12.74	138.82	0.88
n-1	19.96	142.30	0.71	62.82	127.19	0.99	13.26	138.11	0.88

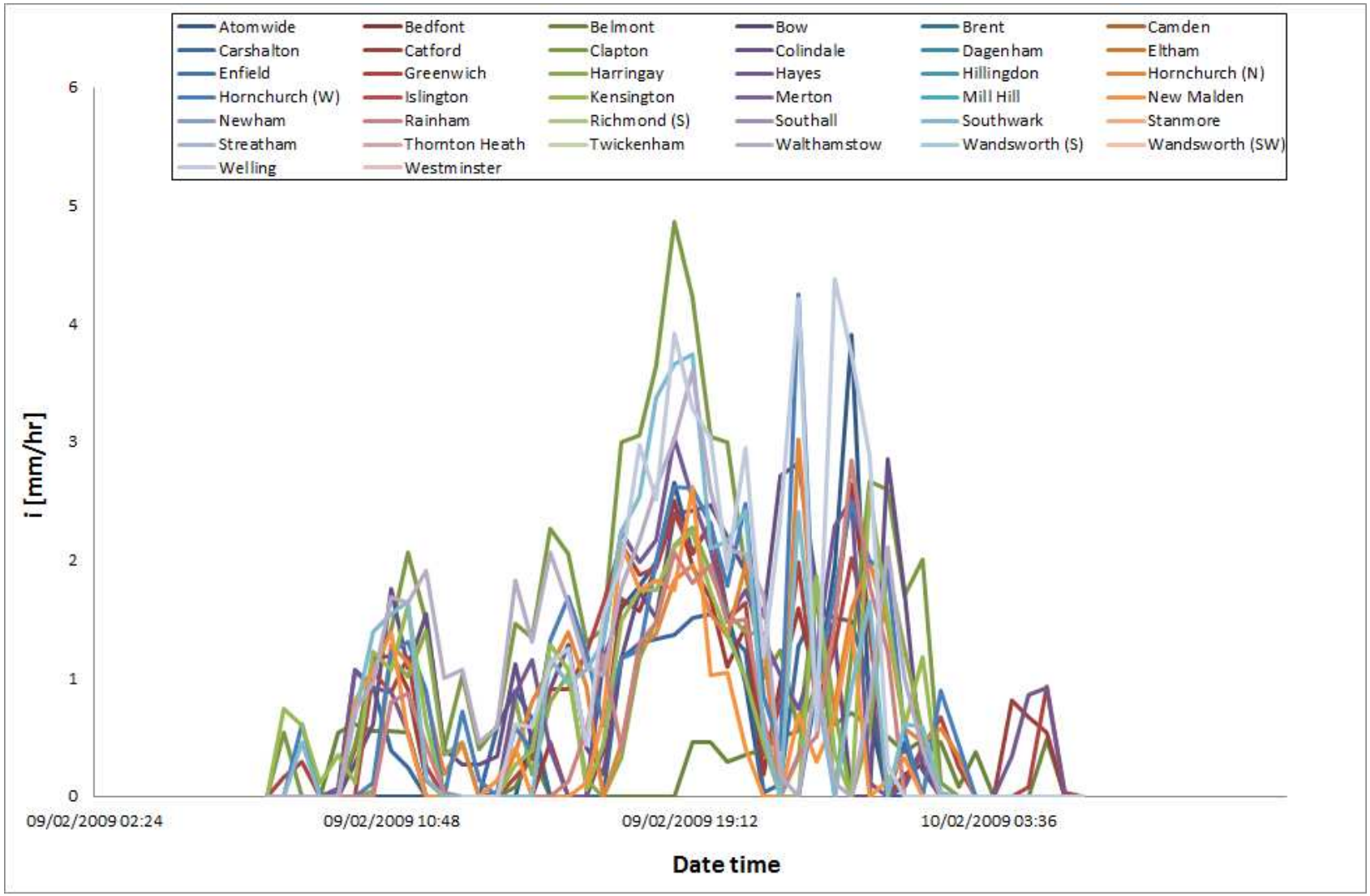
Atomwide
Bedfont
Belmont
Bow
Brent
Camden
Carshalton
Catford
Clapton
Colindale
Dagenham
Eltham
Enfield
Greenwich
Harringay
Hayes
Hillingdon
Hornchurch (N)
Hornchurch (W)
Islington
Kensington
Merton
Mill Hill
New Malden
Newham
Rainham
Richmond (S)
Southall
Southwark
Stanmore
Streatham
Thornton Heath
Twickenham
Walthamstow
Wandsworth (S)
Wandsworth (SW)
Welling
Westminster
i [mm/hr]
0
1
2
3
4
5
6
09/02/2009 02:24
09/02/2009 10:48
09/02/2009 19:12
10/02/2009 03:36
Date time

Starting Date: 08/06/2009 22:45 – **Final Time:** 09/06/2009 08:45

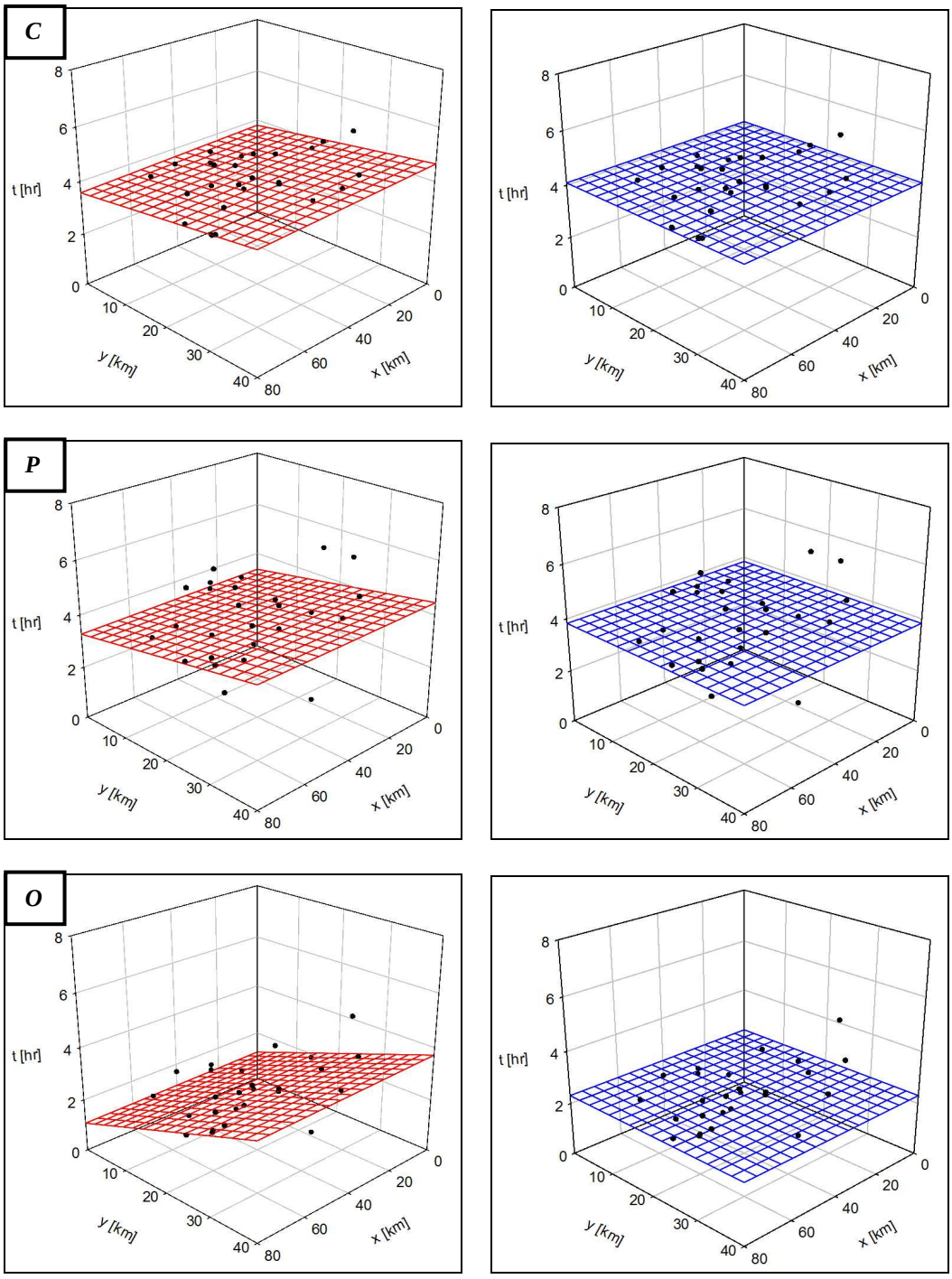

	Centroid			Peak			Onset		
	V [km / hr]	**θ** [° from N]	S. R.	**V** [km / hr]	**θ** [° from N]	S. R.	**V** [km / hr]	**θ** [° from N]	S. R.
n	45.05	173.68	0.93	35.49	178.60	0.98	15.70	178.98	0.84
n-1	45.59	166.84	0.93	36.26	130.56	0.98	15.76	158.29	0.84

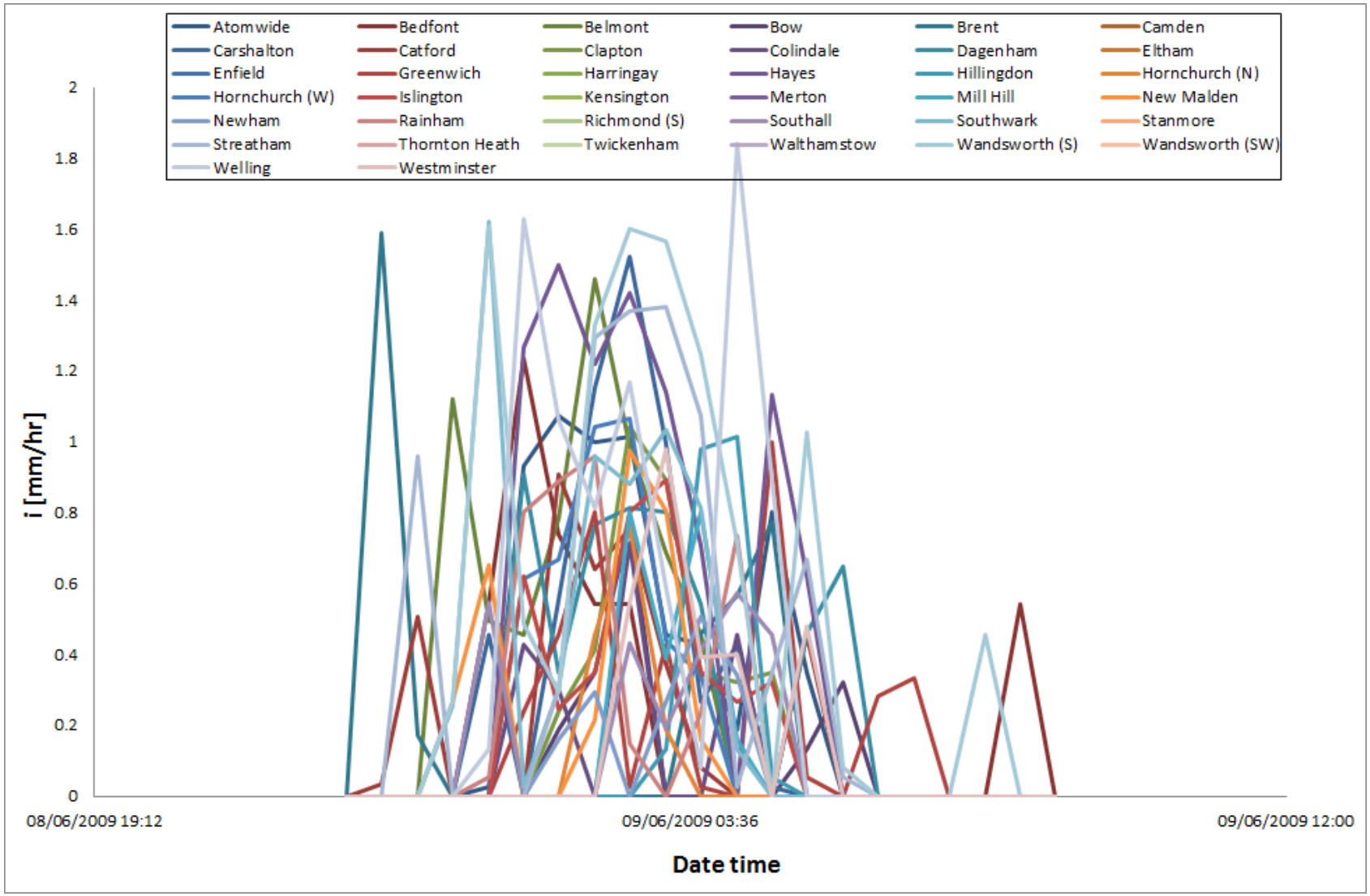
Atomwide
Bedfont
Belmont
Bow
Brent
Camden
Carshalton
Catford
Clapton
Colindale
Dagenham
Eltham
Enfield
Greenwich
Harringay
Hayes
Hillingdon
Hornchurch (N)
Hornchurch (W)
Islington
Kensington
Merton
Mill Hill
New Malden
Newham
Rainham
Richmond (S)
Southall
Southwark
Stanmore
Streatham
Thornton Heath
Twickenham
Walthamstow
Wandsworth (S)
Wandsworth (SW)
Welling
Westminster
2
1.8
1.6
1.4
1.2
1
0.8
0.6
0.4
0.2
0
i [mm/hr]
08/06/2009 19:12
09/06/2009 03:36
09/06/2009 12:00
Date time

Starting Date: 11/07/2009 21:15 – **Final Time:** 12/07/2009 05:15

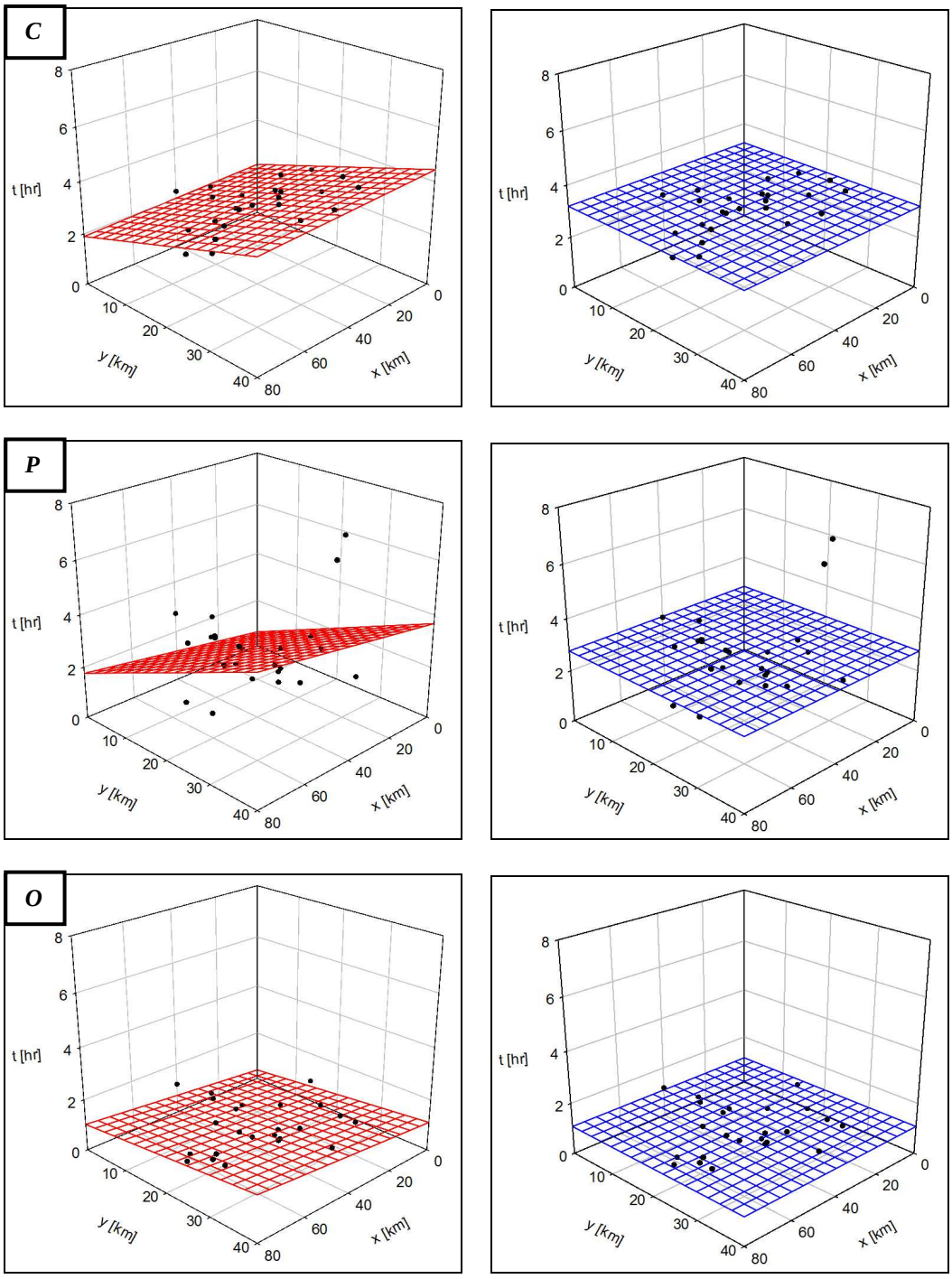

	Centroid			Peak			Onset		
	V [km / hr]	**θ** [° from N]	S. R.	**V** [km / hr]	**θ** [° from N]	S. R.	**V** [km / hr]	**θ** [° from N]	S. R.
n	17.13	177.36	0.59	12.86	10.53	0.87	49.98	23.99	0.85
n-1	17.14	177.37	0.59	13.15	11.12	0.87	50.41	24.42	0.85

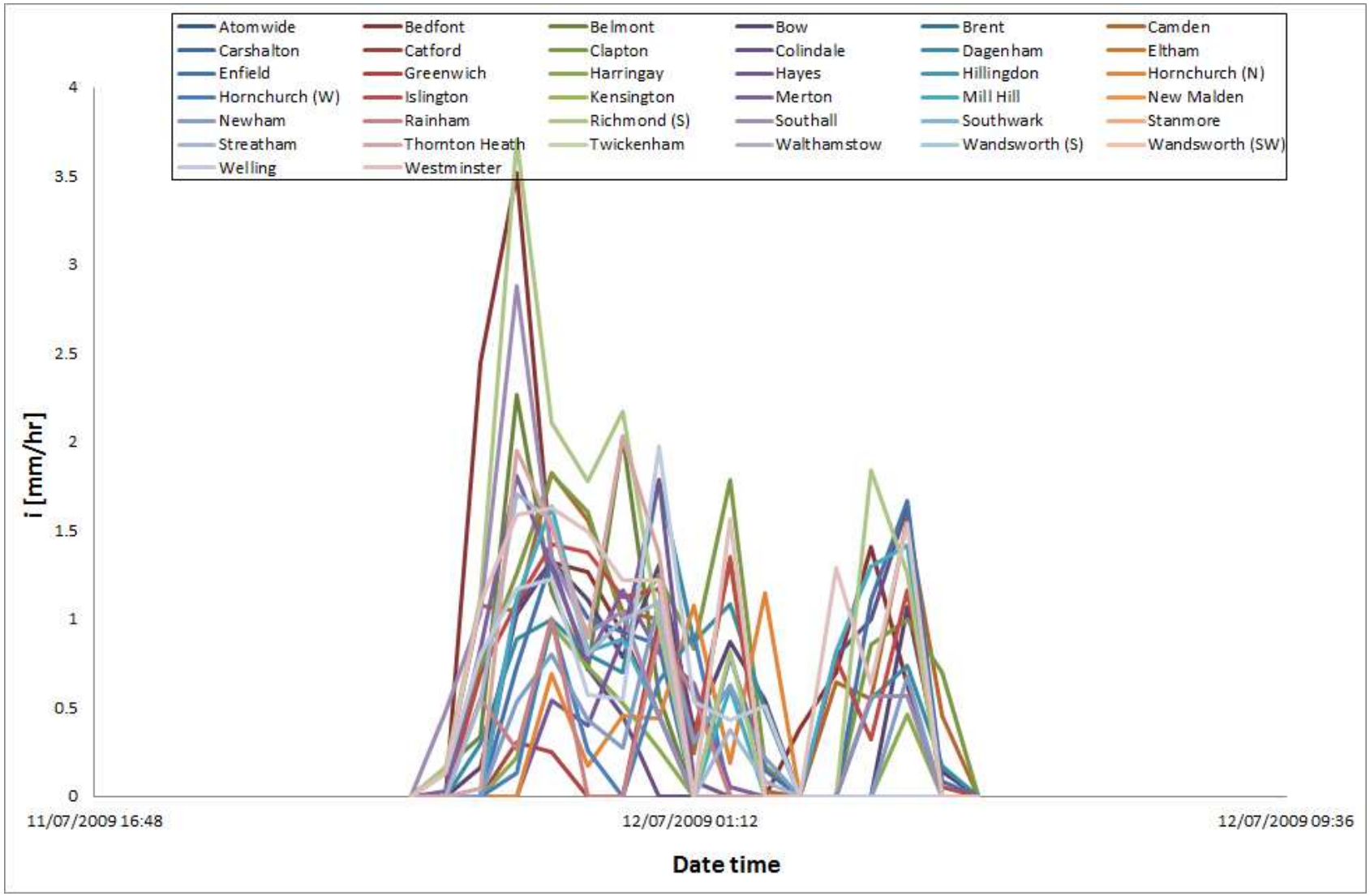
Atomwide
Bedfont
Belmont
Bow
Brent
Camden
Carshalton
Catford
Clapton
Colindale
Dagenham
Eltham
Enfield
Greenwich
Harringay
Hayes
Hillingdon
Hornchurch (N)
Hornchurch (W)
Islington
Kensington
Merton
Mill Hill
New Malden
Newham
Rainham
Richmond (S)
Southall
Southwark
Stanmore
Streatham
Thornton Heath
Twickenham
Walthamstow
Wandsworth (S)
Wandsworth (SW)
Welling
Westminster
i [mm/hr]
4
3.5
3
2.5
2
1.5
1
0.5
0
11/07/2009 16:48
12/07/2009 01:12
12/07/2009 09:36
Date time

Starting Date: 02/09/2009 16:15 – **Final Time:** 03/09/2009 00:45

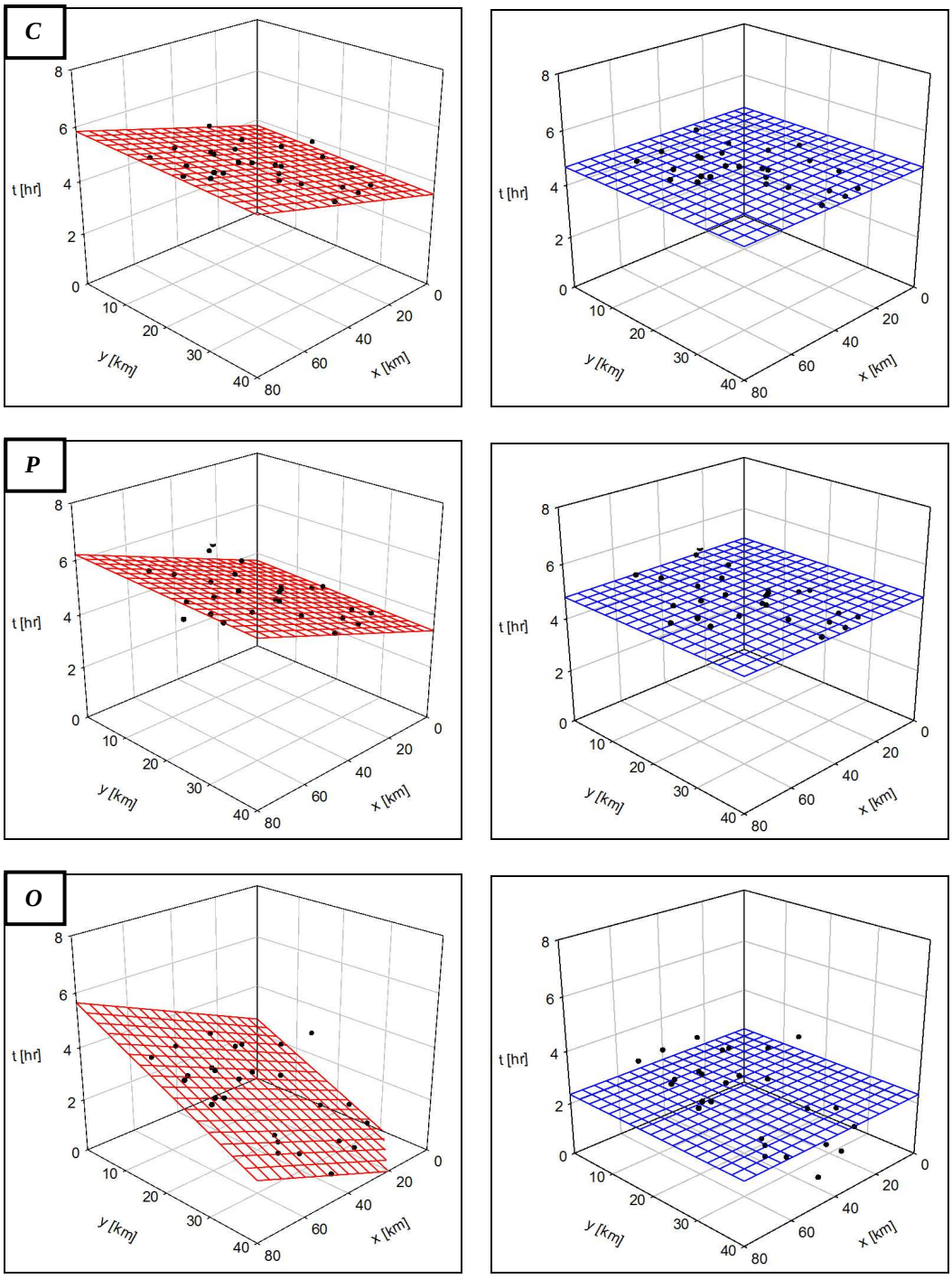

	Centroid			Peak			Onset		
	V [km / hr]	**θ** [° from N]	S. R.	**V** [km / hr]	**θ** [° from N]	S. R.	**V** [km / hr]	**θ** [° from N]	S. R.
n	37.58	103.09	0.39	31.10	103.18	0.64	10.76	155.87	0.62
n-1	37.55	103.06	0.39	31.02	103.29	0.63	10.75	155.85	0.62

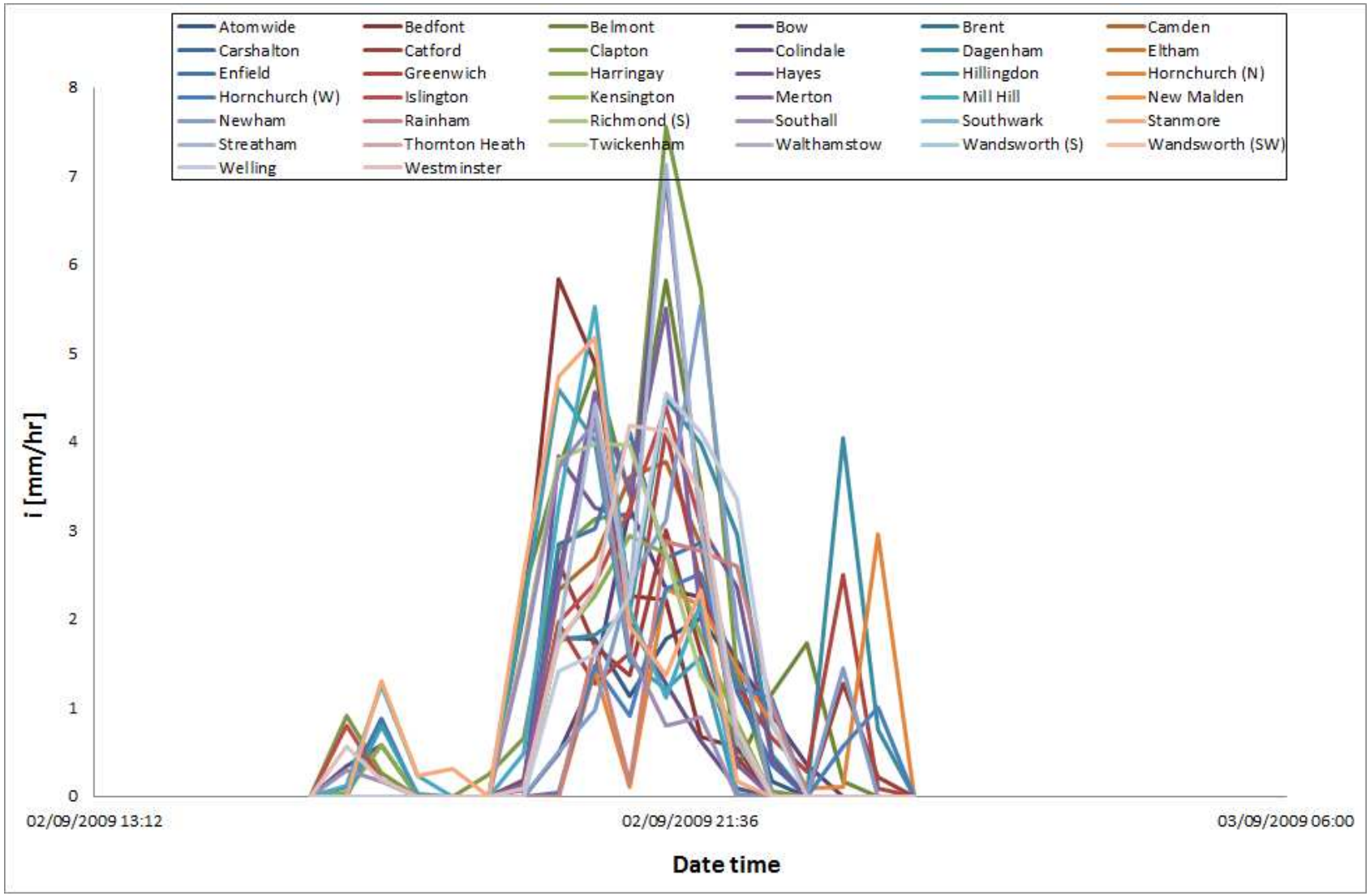
Atomwide
Bedfont
Belmont
Bow
Brent
Camden
Carshalton
Catford
Clapton
Colindale
Dagenham
Eltham
Enfield
Greenwich
Harringay
Hayes
Hillingdon
Hornchurch (N)
Hornchurch (W)
Islington
Kensington
Merton
Mill Hill
New Malden
Newham
Rainham
Richmond (S)
Southall
Southwark
Stanmore
Streatham
Thornton Heath
Twickenham
Walthamstow
Wandsworth (S)
Wandsworth (SW)
Welling
Westminster
i [mm/hr]
0
1
2
3
4
5
6
7
8
02/09/2009 13:12
02/09/2009 21:36
03/09/2009 06:00
Date time

Starting Date: 15/09/2009 09:45 – **Final Time:** 16/09/2009 01:45

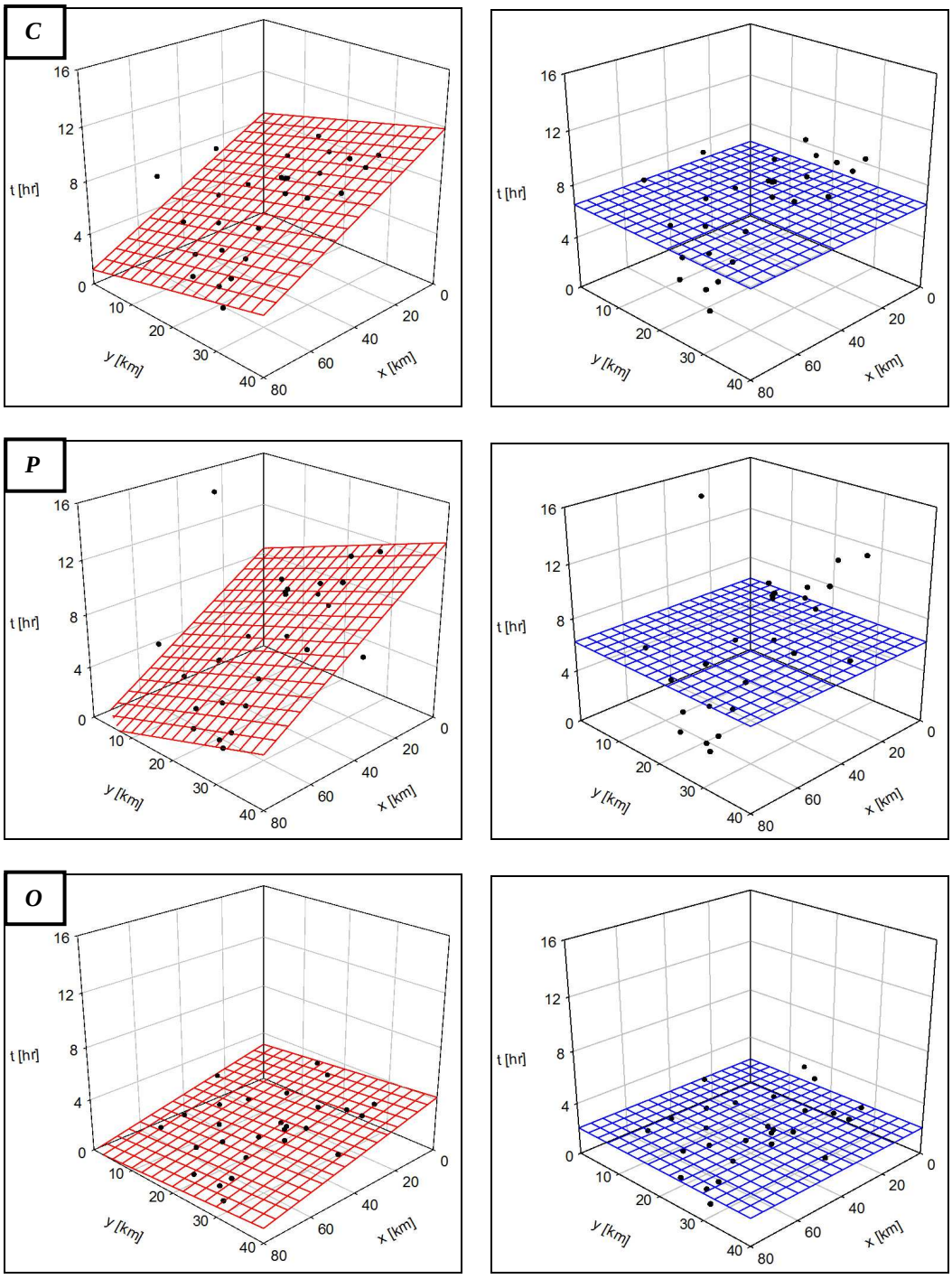

	Centroid			Peak			Onset		
	V [km / hr]	**θ** [° from N]	S. R.	**V** [km / hr]	**θ** [° from N]	S. R.	**V** [km / hr]	**θ** [° from N]	S. R.
n	8.05	131.80	0.58	5.99	136.30	0.78	20.61	127.17	0.44
n-1	8.06	131.72	0.57	6.01	135.95	0.78	20.60	127.17	0.43

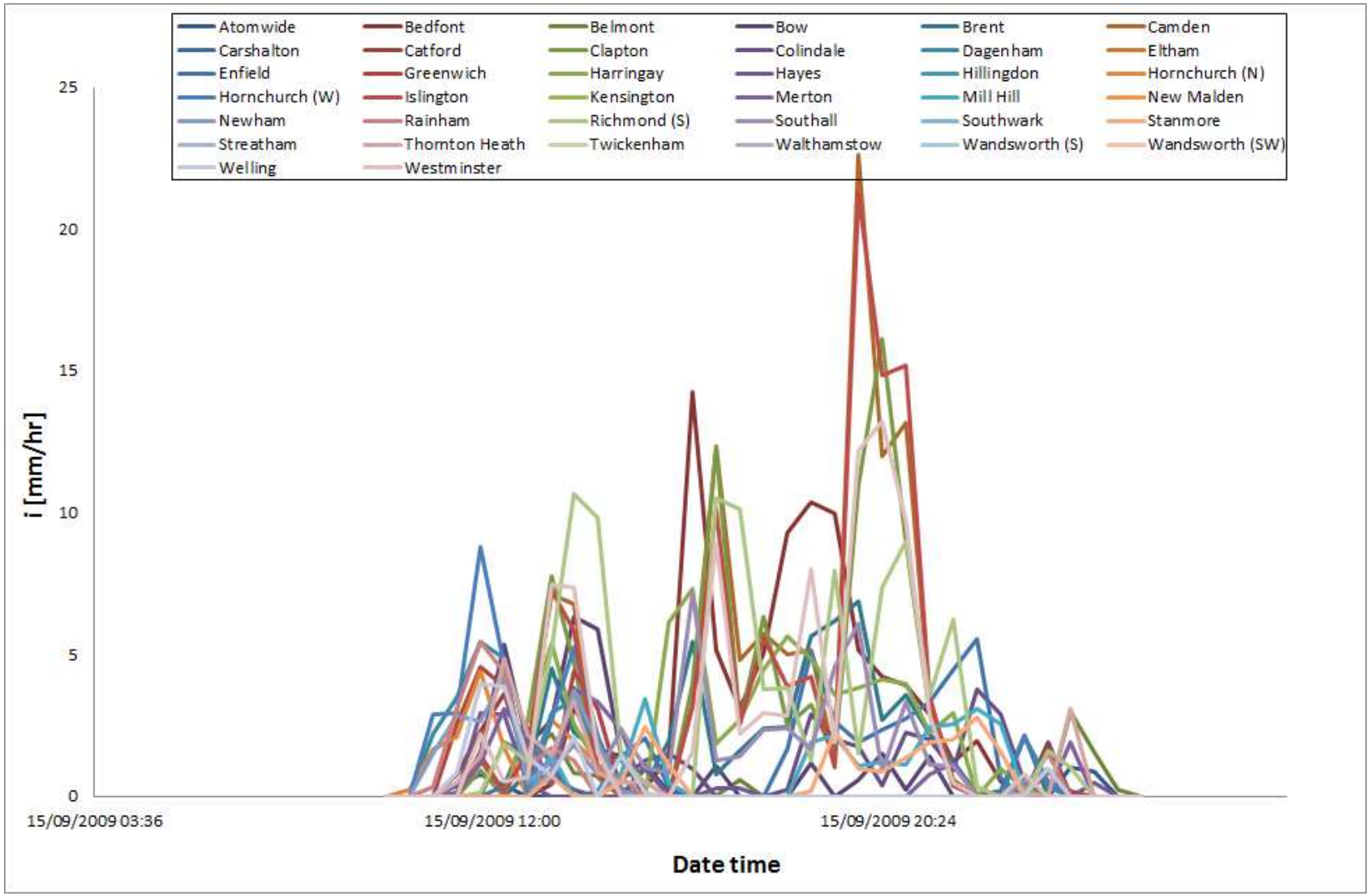
Atomwide
Bedfont
Belmont
Bow
Brent
Camden
Carshalton
Catford
Clapton
Colindale
Dagenham
Eltham
Enfield
Greenwich
Harringay
Hayes
Hillingdon
Hornchurch (N)
Hornchurch (W)
Islington
Kensington
Merton
Mill Hill
New Malden
Newham
Rainham
Richmond (S)
Southall
Southwark
Stanmore
Streatham
Thornton Heath
Twickenham
Walthamstow
Wandsworth (S)
Wandsworth (SW)
Welling
Westminster
25
20
15
10
5
0
i [mm/hr]
15/09/2009 03:36
15/09/2009 12:00
15/09/2009 20:24
Date time

Starting Date: 05/10/2009 08:15 – **Final Time:** 05/10/2009 15:15

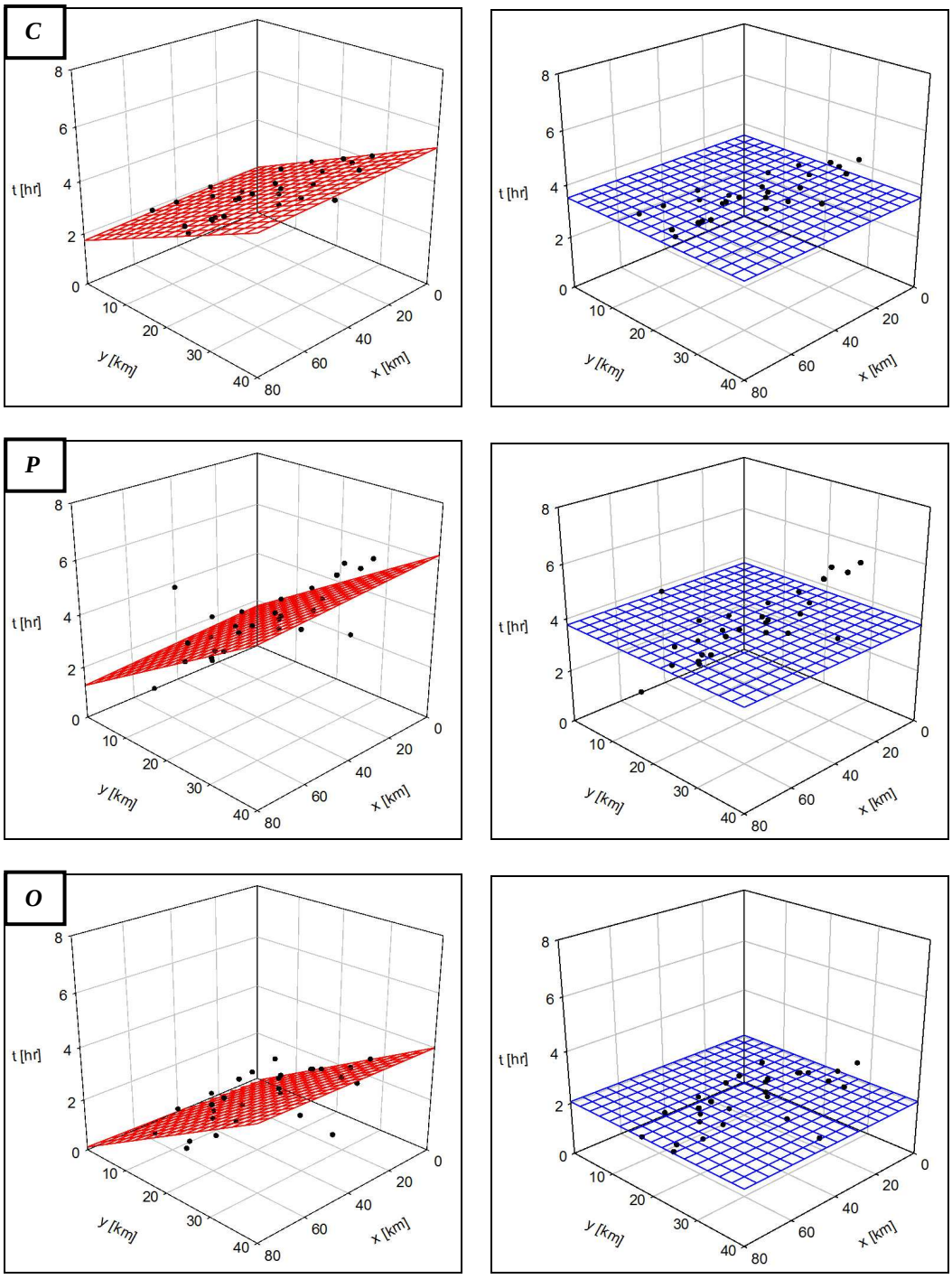

	Centroid			Peak			Onset		
	V [km / hr]	**θ** [° from N]	S. R.	**V** [km / hr]	**θ** [° from N]	S. R.	**V** [km / hr]	**θ** [° from N]	S. R.
n	12.24	177.89	0.38	9.06	176.88	0.62	9.80	1.39	0.63
n-1	12.24	177.89	0.38	9.07	176.89	0.62	9.80	7.82	0.62

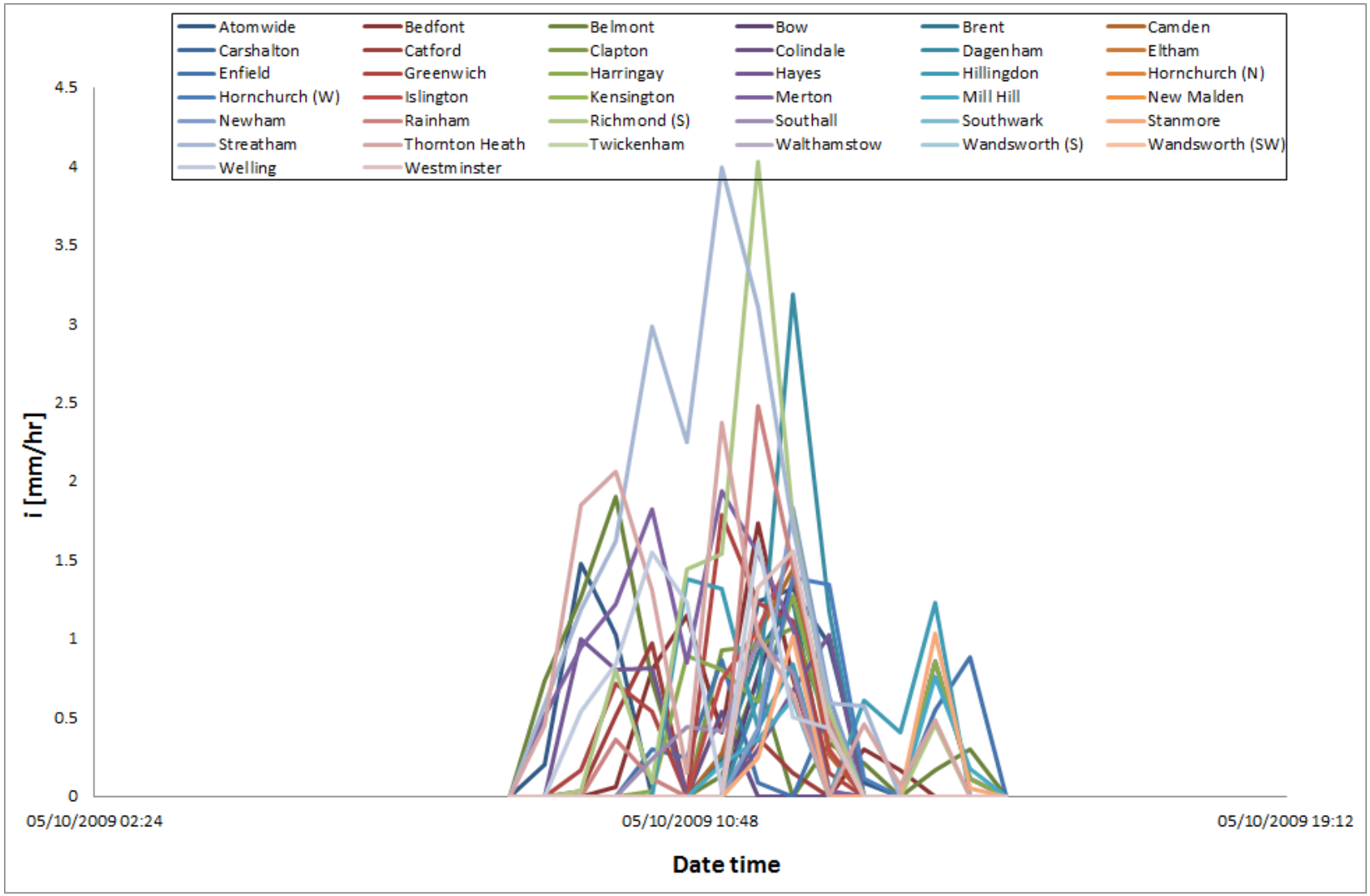
Atomwide
Bedfont
Belmont
Bow
Brent
Camden
Carshalton
Catford
Clapton
Colindale
Dagenham
Eltham
Enfield
Greenwich
Harringay
Hayes
Hillingdon
Hornchurch (N)
Hornchurch (W)
Islington
Kensington
Merton
Mill Hill
New Malden
Newham
Rainham
Richmond (S)
Southall
Southwark
Stanmore
Streatham
Thornton Heath
Twickenham
Walthamstow
Wandsworth (S)
Wandsworth (SW)
Welling
Westminster
4.5
4
3.5
3
2.5
2
1.5
1
0.5
0
i [mm/hr]
05/10/2009 02:24
05/10/2009 10:48
05/10/2009 19:12
Date time

Starting Date: 06/10/2009 06:45 – **Final Time:** 06/10/2009 12:15

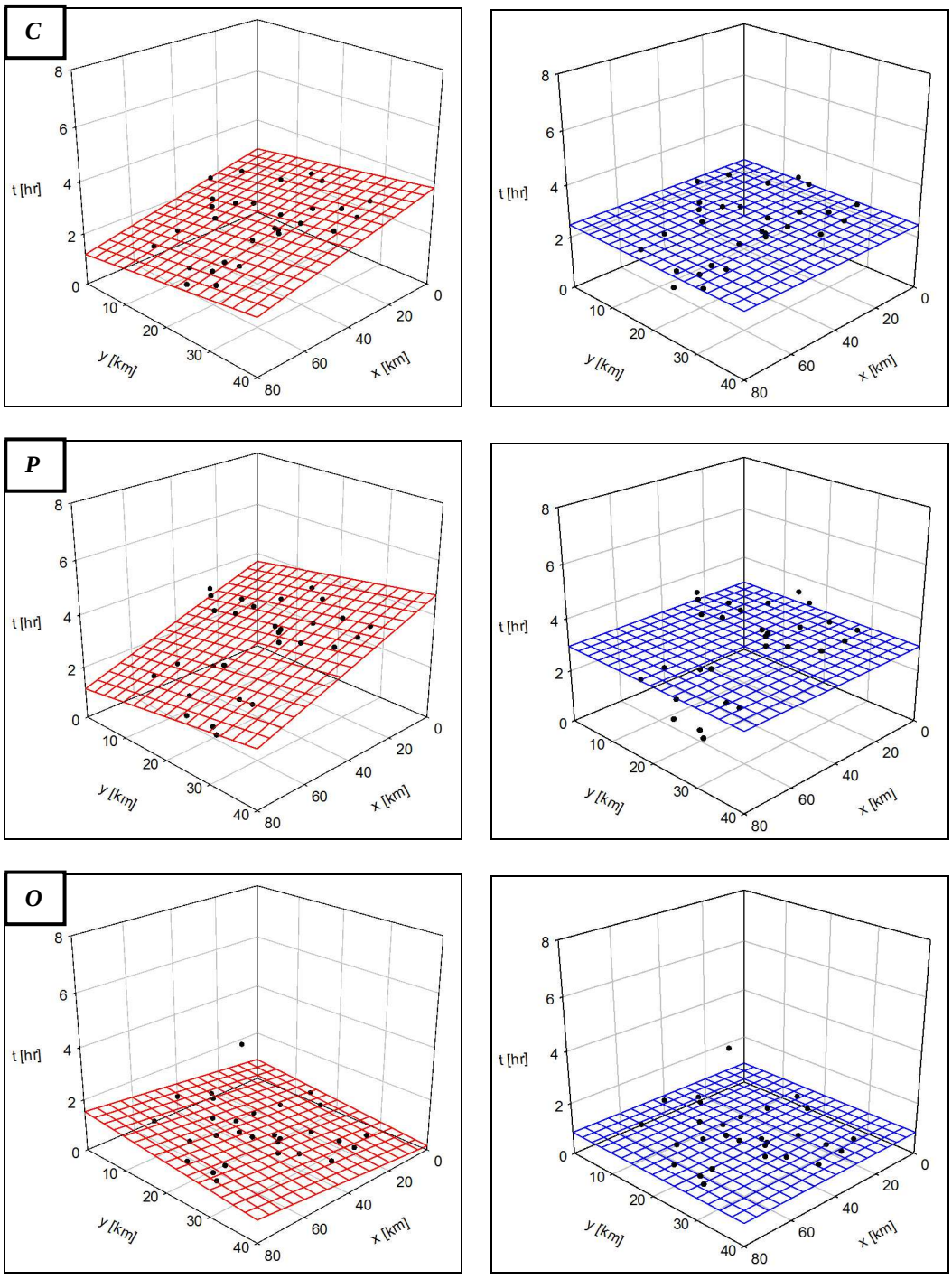

	Centroid			Peak			Onset		
	V [km / hr]	**θ** [° from N]	S. R.	**V** [km / hr]	**θ** [° from N]	S. R.	**V** [km / hr]	**θ** [° from N]	S. R.
n	31.67	140.86	0.68	24.14	130.54	0.81	52.31	153.25	0.90
n-1	31.72	140.77	0.68	24.16	130.37	0.80	52.47	152.75	0.90

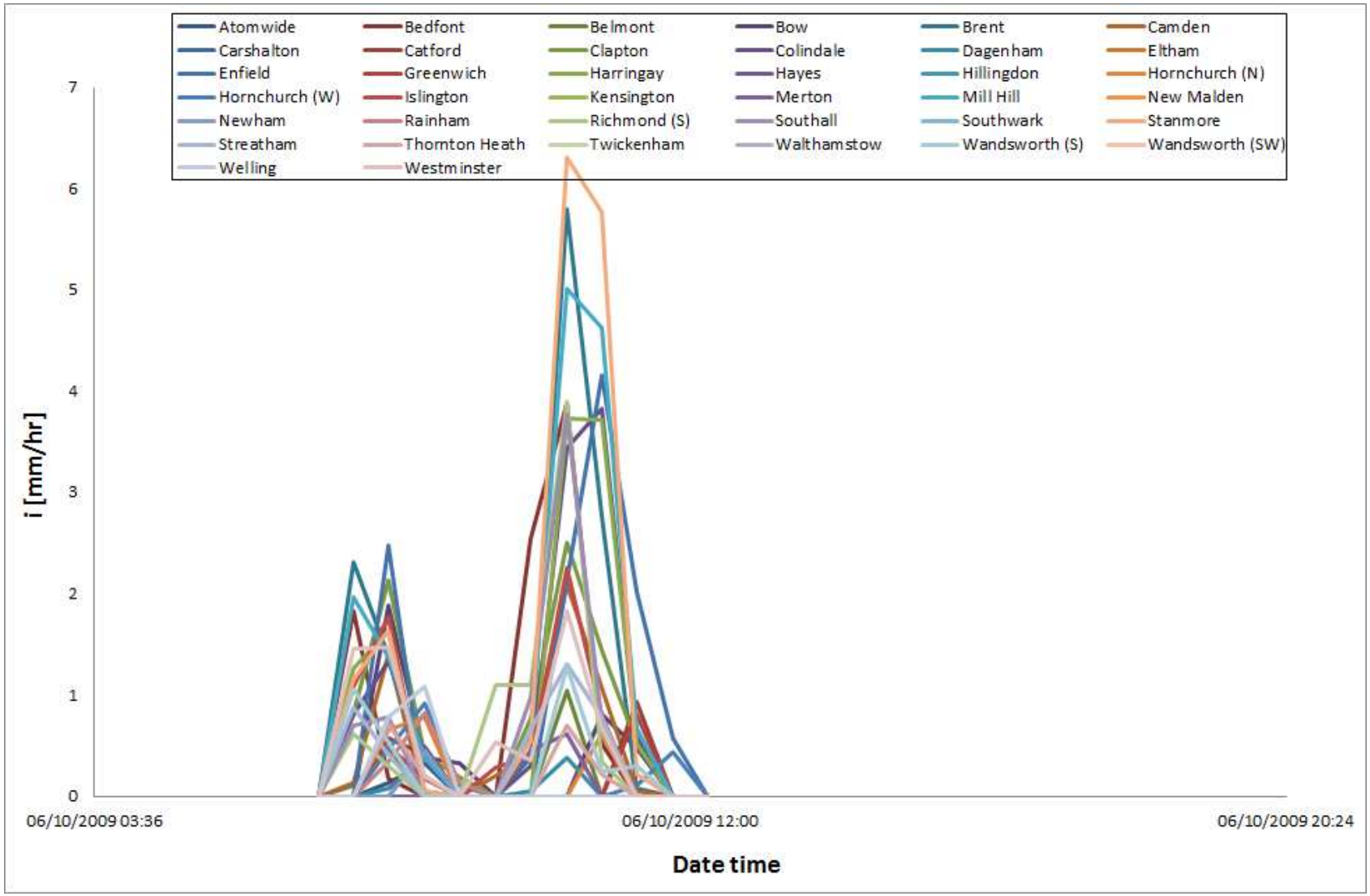
Atomwide
Bedfont
Belmont
Bow
Brent
Camden
Carshalton
Catford
Clapton
Colindale
Dagenham
Eltham
Enfield
Greenwich
Harringay
Hayes
Hillingdon
Hornchurch (N)
Hornchurch (W)
Islington
Kensington
Merton
Mill Hill
New Malden
Newham
Rainham
Richmond (S)
Southall
Southwark
Stanmore
Streatham
Thornton Heath
Twickenham
Walthamstow
Wandsworth (S)
Wandsworth (SW)
Welling
Westminster
i [mm/hr]
0
1
2
3
4
5
6
7
06/10/2009 03:36
06/10/2009 12:00
06/10/2009 20:24
Date time

Starting Date: 07/10/2009 13:45 – **Final Time:** 08/10/2009 00:15

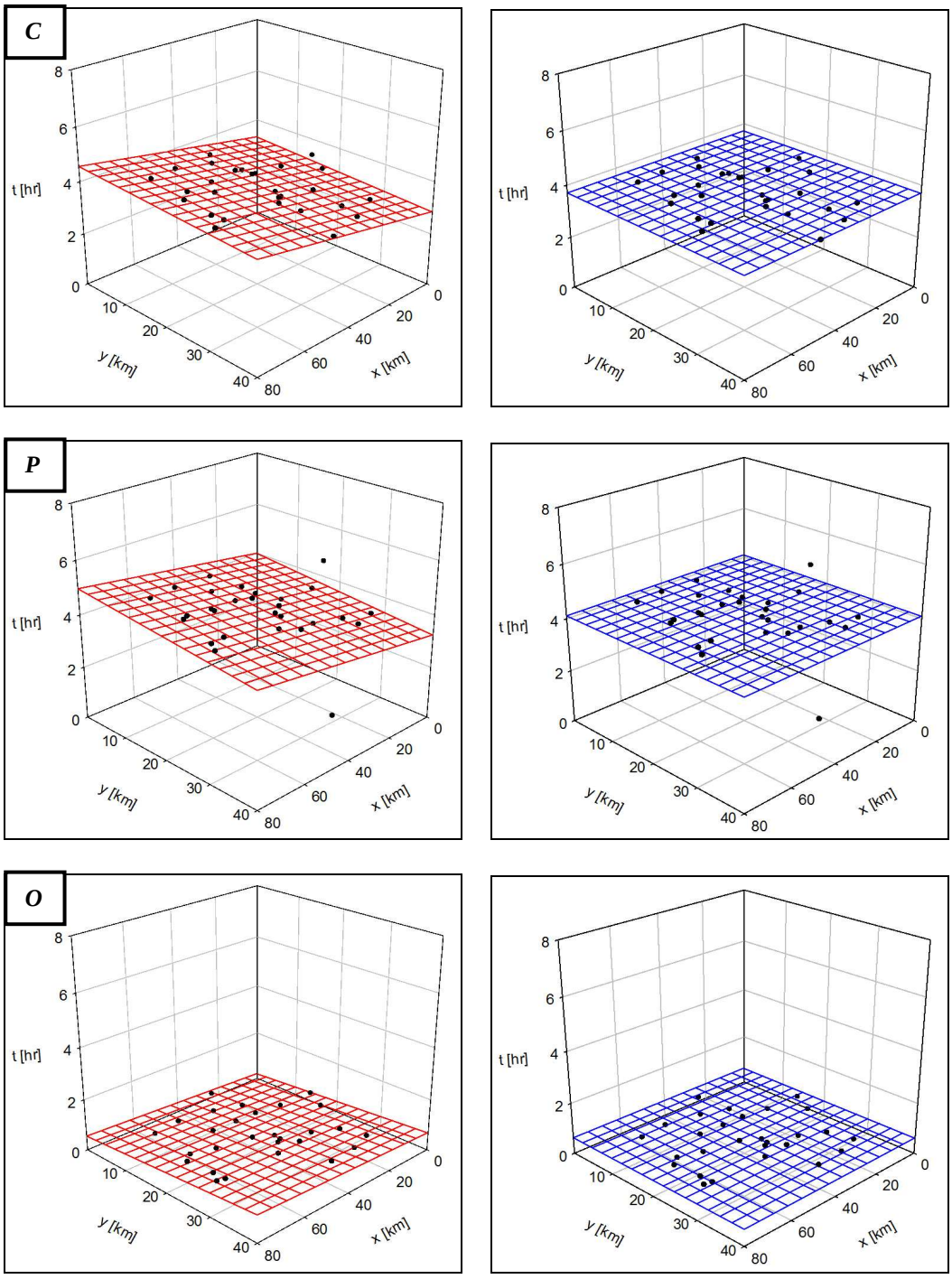

	Centroid			Peak			Onset		
	V [km / hr]	**θ** [° from N]	S. R.	**V** [km / hr]	**θ** [° from N]	S. R.	**V** [km / hr]	**θ** [° from N]	S. R.
n	52.17	123.83	0.59	44.64	147.49	0.90	78.58	19.15	0.78
n-1	52.16	123.77	0.59	44.81	146.08	0.89	78.75	19.18	0.78

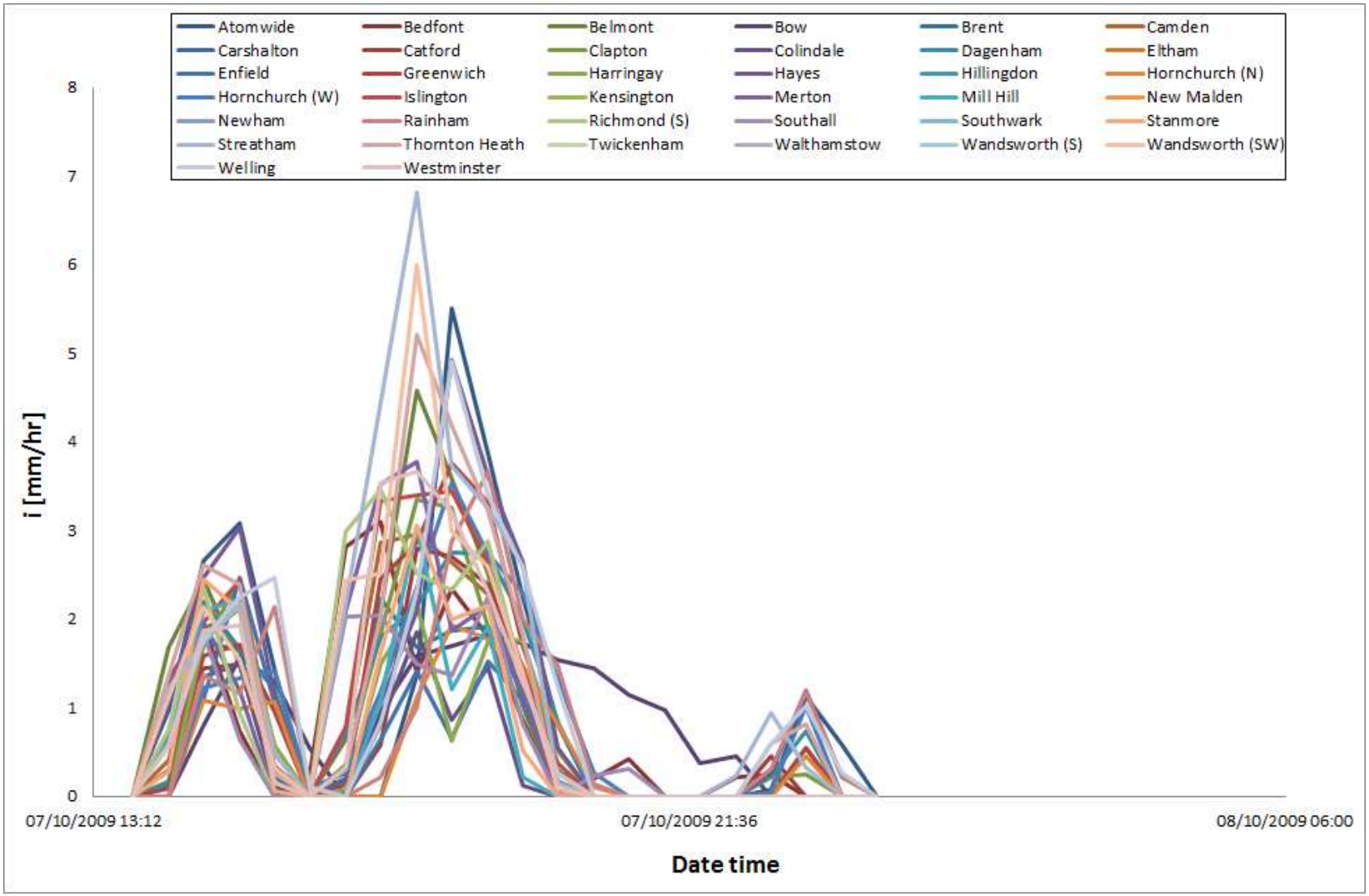
Atomwide
Bedfont
Belmont
Bow
Brent
Camden
Carshalton
Catford
Clapton
Colindale
Dagenham
Eltham
Enfield
Greenwich
Harringay
Hayes
Hillingdon
Hornchurch (N)
Hornchurch (W)
Islington
Kensington
Merton
Mill Hill
New Malden
Newham
Rainham
Richmond (S)
Southall
Southwark
Stanmore
Streatham
Thornton Heath
Twickenham
Walthamstow
Wandsworth (S)
Wandsworth (SW)
Welling
Westminster
i [mm/hr]
0
1
2
3
4
5
6
7
8
07/10/2009 13:12
07/10/2009 21:36
08/10/2009 06:00
Date time